



UNIL | Université de Lausanne

Unicentre

CH-1015 Lausanne

<http://serval.unil.ch>

Year : 2020

COMPARTMENTATION OF DEFENCES IN ARABIDOPSIS THALIANA ROOTS

Emonet Aurélia

Emonet Aurélia, 2020, COMPARTMENTATION OF DEFENCES IN ARABIDOPSIS THALIANA
ROOTS

Originally published at : Thesis, University of Lausanne

Posted at the University of Lausanne Open Archive <http://serval.unil.ch>

Document URN : urn:nbn:ch:serval-BIB_77F13BF943128

Droits d'auteur

L'Université de Lausanne attire expressément l'attention des utilisateurs sur le fait que tous les documents publiés dans l'Archive SERVAL sont protégés par le droit d'auteur, conformément à la loi fédérale sur le droit d'auteur et les droits voisins (LDA). A ce titre, il est indispensable d'obtenir le consentement préalable de l'auteur et/ou de l'éditeur avant toute utilisation d'une oeuvre ou d'une partie d'une oeuvre ne relevant pas d'une utilisation à des fins personnelles au sens de la LDA (art. 19, al. 1 lettre a). A défaut, tout contrevenant s'expose aux sanctions prévues par cette loi. Nous déclinons toute responsabilité en la matière.

Copyright

The University of Lausanne expressly draws the attention of users to the fact that all documents published in the SERVAL Archive are protected by copyright in accordance with federal law on copyright and similar rights (LDA). Accordingly it is indispensable to obtain prior consent from the author and/or publisher before any use of a work or part of a work for purposes other than personal use within the meaning of LDA (art. 19, para. 1 letter a). Failure to do so will expose offenders to the sanctions laid down by this law. We accept no liability in this respect.



UNIL | Université de Lausanne

Faculté de biologie
et de médecine

Département de Biologie Moléculaire Végétale

COMPARTMENTATION OF DEFENCES
IN *ARABIDOPSIS THALIANA* ROOTS

Thèse de doctorat ès sciences de la vie (PhD)

présentée à la

Faculté de biologie et de médecine

par

Aurélia Emonet

Master de l'Université de Lausanne

Jury

Prof. Dr. Antoine Guisan, Président

Prof. Dr. Niko Geldner, Directeur de thèse

Prof. Dr. Edward Farmer, Expert

Prof. Dr. Cyril Zipfel, Expert

Lausanne

2020

Imprimatur

Vu le rapport présenté par le jury d'examen, composé de

Président·e	Monsieur	Prof.	Antoine	Guisan
Directeur·trice de thèse	Monsieur	Prof.	Niko	Geldner
Expert·e·s	Monsieur	Prof.	Edward	Farmer
	Monsieur	Prof.	Cyril	Zipfel

le Conseil de Faculté autorise l'impression de la thèse de

Madame Aurélia Emonet

Master ès Sciences moléculaires du vivant, Université de Lausanne, Suisse

intitulée

**Compartmentation of defences
in *Arabidopsis Thaliana* roots**

Lausanne, le 30 octobre 2020

pour le Doyen
de la Faculté de biologie et de médecine

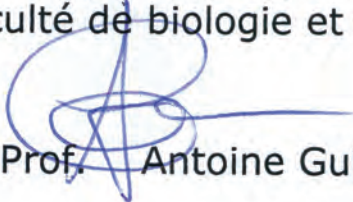

Prof. Antoine Guisan

TABLE OF CONTENT

<i>TABLE OF CONTENT</i>	1
<i>LIST OF FREQUENTLY USED ABBREVIATIONS</i>	7
<i>SUMMARY</i>	9
<i>RÉSUMÉ EN FRANÇAIS</i>	11
<i>RÉSUMÉ TOUT PUBLIC</i>	13
1 <i>GENERAL INTRODUCTION</i>	15
1.1. THE LAYERED INNATE IMMUNE SYSTEM OF LAND PLANTS	16
1.2. MAMPs AND DAMPs AS DANGER SIGNALS FOR INNATE IMMUNITY	19
1.3. MAMP-TRIGGERED IMMUNITY SIGNALLING: FLS2 AND FLG22	22
1.3.1. PRRs FORM TIGHTLY REGULATED SIGNALLING PLATFORMS	22
1.3.2. SIGNALLING AT THE PLASMA MEMBRANE UPON MAMP PERCEPTION	23
1.3.3. TRANSDUCTION OF IMMUNE SIGNAL – EARLY RESPONSES	24
1.4. DOWNSTREAM DEFENCE RESPONSES AS FINAL OUTPUT OF MTI	28
1.5. GROWTH AND DEFENCE: AIMING FOR THE EQUILIBRIUM	30
1.6. THE RHIZOSPHERE, A MELTING POT OF BIOTIC INTERACTIONS	32
1.6.1. THE RHIZOSPHERE COMMUNITY OR THE 2 ND GENOME OF THE PLANT	32
1.6.2. MICROBIOTA AS A PROVIDER OF SERVICES	34
1.7. IMMUNITY IN THE ROOT, A STORY OF COMPARTMENTATION	36
1.7.2. INTERACTION OF RHIZOSPHERE MICROBES WITH THE ROOT	37
1.7.3. MAMP-TRIGGERED IMMUNITY ALSO OCCURS IN THE ROOT	39
1.8. SCOPE OF THE PHD THESIS	42
1.9. LITERATURE	44
2 <i>CO-INCIDENCE OF DAMAGE AND MICROBIAL PATTERNS CONTROLS LOCALIZED IMMUNE RESPONSES IN ROOTS</i>	61
2.1. RATIONAL OF THE STUDY	62
2.2. CONTRIBUTIONS	63
2.3. ORIGINAL ARTICLE	63

2.4.	<i>APPENDICES</i>	97
2.4.1.	FLG22 PEPTIDE INCREASES SLIGHTLY <i>FLS2</i> EXPRESSION	97
2.4.2.	ETHYLENE TRANSCRIPTIONALLY ACTIVATES <i>FLS2</i>	98
2.4.3.	ATPEP1 SLIGHTLY INCREASES <i>FLS2</i> EXPRESSION IN THE STELE	99
2.4.4.	<i>FLS2</i> EXPRESSION IN CORTICAL CELLS AROUND LATERAL ROOTS CORRELATES WITH RESPONSIVENESS TO FLG22	100
2.5.	SUPPLEMENTARY MATERIAL AND METHODS	106
2.5.1.	PLANT MATERIAL AND GROWTH CONDITIONS	106
2.5.2.	ELICITOR AND INHIBITOR TREATMENT	106
2.5.3.	FIXATION AND STAINING	106
2.5.4.	MICROSCOPY	107
2.5.5.	QUANTIFICATION	107
2.6.	LITERATURE	108
3	<i>SPATIALLY RESTRICTED IMMUNE RESPONSES ALLOW FOR ROOT MERISTEMATIC ACTIVITY DURING BACTERIAL COLONISATION</i>	109
3.1.	RATIONAL OF THE STUDY	110
3.2.	CONTRIBUTIONS	112
3.3.	MANUSCRIPT	112
3.4.	APPENDICES	164
3.4.1.	GENERATION OF NEW TISSUE-SPECIFIC <i>PROM::FLS2-GFP</i> LINES	164
3.4.2.	INFLUENCE OF <i>FLS2</i> EXPRESSION ON MTI MARKERS	167
3.4.3.	CELL-SPECIFIC QUANTIFICATION DEVELOPMENT – TRIAL WITH DAPI STAINING	171
3.4.4.	GENERATION OF SYNTHETIC UNIVERSAL REPORTER OF DEFENCE	171
3.4.5.	LIGNIN DEPOSITION AFTER CO-INCIDENCE OF DAMAGE AND FLG22 PERCEPTION	172
3.4.6.	<i>WER::FLS2</i> RESPONDS STRONGLY TO THE PATHOGEN <i>PSEUDOMONAS SYRINGAE</i> STRAIN DC3000	173
3.4.7.	SCREEN OF COMMENSAL BACTERIAL CULTURE COLLECTION FOR DIFFERENTIAL ROOT GROWTH INHIBITION	174
3.5.	SUPPLEMENTARY MATERIAL AND METHODS	175
3.5.1.	PLANT MATERIAL AND GROWTH CONDITIONS	175
3.5.2.	BACTERIAL STRAIN AND GROWTH CONDITIONS	175
3.5.3.	PLASMID CONSTRUCTION	175
3.5.4.	PLANT GENOTYPING	176
3.5.5.	ADAPTED DAPI STAINING	176
3.5.6.	LASER ABLATION SETUP	176
3.6.	LITERATURE	177
3.7.	SUPPLEMENTAL TABLES	179

4	INTERACTIONS BETWEEN THE RHIZOSPHERE AND <i>WER::FLS2</i> IMMUNE SUPER-COMPETENT LINE	181
4.1.	CONTRIBUTIONS	182
4.2.	INTRODUCTION	183
4.2.1.	BACTERIAL MICROBIOME: KEEPING FRIENDS CLOSE	183
4.2.2.	PLANTS ACTIVELY RECRUIT THEIR BACTERIAL MICROBIOME	183
4.2.3.	PLANT GENOTYPES INFLUENCE THE MICROBIOME COMPOSITION	184
4.2.4.	MTI AS SELECTIVE PRESSURE FOR THE RECRUITMENT OF AN ADAPTED MICROBIOME	185
4.3.	RESULTS	187
4.3.1.	ECTOPIC EXPRESSION OF <i>FLS2</i> DOES NOT AFFECT GROWTH ON NATURAL SOILS	187
4.3.2.	SINGLE BACTERIA INOCULATION IN GNOTOBIOTIC SYSTEM DOES NOT INCREASE ROOT GROWTH INHIBITION OF <i>WER::FLS2</i>	188
4.3.3.	<i>MICROBIOME COMPOSITION IS NOT SIGNIFICANTLY AFFECTED BY WER::FLS2</i>	191
4.4.	DISCUSSION	193
4.4.1.	RHIZOSPHERE BACTERIA SUPPRESS MTI RESPONSES IN <i>WER::FLS2</i>	193
4.4.2.	IMPACT OF THE CULTURE SYSTEM	194
4.4.3.	THE RHIZOSPHERE COMMUNITY STRUCTURE IS HARDLY IMPACTED BY PRRs LOCALISATION	196
4.5.	MATERIAL AND METHODS	199
4.5.1.	PLANT MATERIAL AND GROWTH CONDITIONS	199
4.5.2.	SHOOT AND ROOT BIOMASS ANALYSIS	199
4.5.3.	BACTERIAL SYNTHETIC COMMUNITY PREPARATION	199
4.5.4.	FLOW-POT SYSTEM	200
4.5.5.	CALCINED CLAY	201
4.5.6.	SIX-WELL PLATE CALCINED CLAY SYSTEM	201
4.5.7.	DNA EXTRACTION AND LIBRARY PREPARATION	202
4.5.8.	16S rRNA GENE PROCESSING AND BETA-DIVERSITY ANALYSIS	202
4.5.9.	STATISTIC ANALYSES	203
4.6.	LITERATURE	204
4.7.	SUPPLEMENTAL FIGURES AND TABLES	208
5	MODULATION OF MTI BY COMMENSALS	217
5.1.	INTRODUCTION	218
5.1.1.	MECHANISMS OF MTI AVOIDANCE AND SUPPRESSION BY THE MICROBIOME	218
5.1.2.	<i>PSEUDOMONAS PROTEGENS</i> STRAIN CHA0 AS MODEL FOR COMMENSAL COLONIZATION	221
5.2.	RESULTS	222
5.2.1.	SELECTION OF CHA0 CANDIDATE MUTANTS IMPAIRED IN <i>FLS2</i> -RESPONSES SUPPRESSION	222
5.2.2.	<i>P.PROTEGENS</i> CHA0 DOES NOT INHIBIT <i>PER5</i> INDUCTION	224
5.2.3.	CHA0 MUTANTS IMPAIRED IN pH REGULATION TEND TO LOSE <i>FLS2</i> -SPECIFIC RGI SUPPRESSION	225

5.2.4.	<i>PSEUDOMONAS SIMIAE</i> WCS417R AND <i>PSEUDOMONAS CAPEFERRUM</i> WCS358 PARTIALLY INHIBIT <i>PER5</i> INDUCTION	228
5.2.5.	<i>P. SIMIAE</i> WCS417R AND <i>P. CAPEFERRUM</i> WCS358 PARTIALLY SUPPRESS RELATIVE RGI INDEPENDENTLY OF GLUCONATE SYNTHESIS	230
5.3.	DISCUSSION	231
5.3.1.	VARIABILITY OF RESULTS – NOTE OF CAUTION	231
5.3.2.	LIPOPOLYSACCHARIDE AND EXOPOLYSACCHARIDE SYNTHESIS MUTANTS	231
5.3.3.	GLUCONATE SYNTHESIS AFFECTS <i>PER5</i> INDUCTION	233
5.3.4.	IS ACIDIFICATION RESPONSIBLE FOR SUPPRESSION OF ROOT GROWTH INHIBITION?	234
5.4.	MATERIAL AND METHODS	236
5.4.1.	BACTERIAL STRAINS AND GROWTH CONDITIONS	236
5.4.2.	BACTERIAL ROOT INOCULATION ASSAYS	236
5.4.3.	QUANTIFICATION OF <i>PER5</i> SIGNALLING	236
5.5.	SUPPLEMENTAL FIGURES AND TABLES	237
5.6.	LITERATURE	241
6	<i>INTERPLAY BETWEEN FLG22, ATPEP1 AND ETHYLENE-MEDIATED IMMUNE RESPONSES</i>	247
6.1.	INTRODUCTION	248
6.1.1.	ATPEP SIGNALLING REINFORCES MAMP-TRIGGERED IMMUNITY THROUGH THE ETHYLENE PATHWAY	248
6.1.2.	RATIONAL OF THE STUDY	249
6.2.	RESULTS	251
6.2.1.	FLG22 AND ATPEP1 INDUCE IMMUNE AND ETHYLENE RESPONSES WITH DIFFERENT PATTERNS	251
6.2.2.	ETHYLENE SIGNALLING IS INVOLVED IN FLG22-DRIVEN <i>PER5</i> INDUCTION	254
6.2.3.	INHIBITION OF ETHYLENE SIGNALLING INCREASES RESPONSE TO ATPEP1 IN THE STELE	255
6.2.4.	ACC INDUCES <i>MYB51</i> BUT HAD WEAK OR NO EFFECT ON <i>PER5</i> AND <i>WRKY11</i> EXPRESSION	257
6.2.5.	<i>PR4</i> IS PARTIALLY DEPENDENT OF ETHYLENE SIGNALLING	258
6.3.	DISCUSSION	259
6.4.	MATERIAL AND METHODS	262
6.4.1.	PLANT MATERIAL AND GROWTH CONDITIONS	262
6.4.2.	ELICITOR AND INHIBITOR TREATMENTS	262
6.4.3.	MICROSCOPY ANALYSIS	262
6.5.	LITERATURE	263
6.6.	SUPPLEMENTAL FIGURES	266
7	<i>COMPARISON OF CIF2- AND FLG22-INDUCED LIGNIFICATION OF THE ENDODERMIS</i>	269
7.1.	CONTRIBUTIONS	270

7.2.	INTRODUCTION	271
7.2.1.	LIGNIN IN CASPARIAN STRIP AND ECTOPIC COMPENSATORY LIGNIN	271
7.2.2.	COMPENSATORY LIGNIN IS DEPENDENT ON THE SCHENGEN PATHWAY	272
7.2.3.	SIMILARITY BETWEEN MTI AND SCHENGEN PATHWAYS	274
7.2.4.	THE ENDODERMIS AS A MODEL TO STUDY SPECIFICITY	275
7.3.	RESULTS	277
7.3.1.	LIGNIN DEPOSITION IN RESPONSE TO CIF2 AND FLG22 HAVE UNMATCHING PATTERNS	277
7.3.2.	ROS PRODUCTION COINCIDES WITH LIGNIN DEPOSITION PATTERN IN <i>CASP1::FLS2</i>	278
7.3.3.	<i>RBOHF</i> , <i>RBOHD</i> AND <i>MYB15</i> ARE IMPLICATED IN FLG22-DRIVEN LIGNIN DEPOSITION	279
7.3.4.	COMPARISON OF MTI AND SCHENGEN UPSTREAM PATHWAYS	283
7.3.5.	FLG22 AND CIF2 INDUCES VERY SIMILAR TRANSCRIPTOMIC CHANGES	285
7.4.	DISCUSSION	290
7.4.1.	MTI AND SCHENGEN PATHWAYS TRIGGER A COMMON STRESS-INDUCED SIGNALLING MODULE	290
7.4.2.	SPECIFIC LOCALISATION OF SCHENGEN AND IMMUNE RESPONSES	292
7.4.3.	SPECIFICITY AT THE HEART OF THE ENDODERMIS	293
7.5.	MATERIAL AND METHODS	296
7.5.1.	PLANT MATERIAL	296
7.5.2.	GENERATION OF CRISPR LINES	296
7.5.3.	gDNA EXTRACTION AND SELECTION OF CRISPR-CAS9 INDUCED MUTANTS	297
7.5.4.	ELICITOR TREATMENT	297
7.5.5.	H ₂ O ₂ PRODUCTION <i>IN SITU</i> ANALYSIS USING TRANSMISSION ELECTRON MICROSCOPY	297
7.5.6.	SAMPLE PREPARATION FOR RNAseq ANALYSIS	298
7.5.7.	RNAseq LIBRARY PREPARATION AND SEQUENCING	298
7.5.8.	RNAseq DATA PROCESSING AND ANALYSIS	299
7.5.9.	qPCR	300
7.6.	LITERATURE	301
7.7.	SUPPLEMENTAL FIGURES AND TABLES	305
8	<i>CONCLUDING REMARKS AND PERSPECTIVES</i>	315
8.1.	THE LOCAL COMPONENT OF IMMUNITY	316
8.2.	REGULATION OF MTI RESPONSES IN THE ROOT IS HIGHLY DYNAMIC	319
8.3.	MAMP-TRIGGERED IMMUNE RESPONSES INFLUENCE PLANT DEVELOPMENT	321
8.4.	FINAL REMARK	323
8.5.	LITERATURE	324
	<i>ACKNOWLEDGEMENTS</i>	327

LIST OF FREQUENTLY USED ABBREVIATIONS

ACC	1-amino-cyclopropane-1-carboxylic acid
ACS	ACC SYNTHASE
BAK1	BRI1-ASSOCIATED RECEPTOR KINASE
BIK1	BOTRYTIS-INDUCED KINASE1
BIR	BAK1-INTERACTING RECEPTOR-LIKE KINASE
BR	Brassinosteroids
BRI1	BRASSINOSTEROID INSENSITIVE 1
BZR1	BRASSINAZOLE-RESISTANT 1
CaM	Calmodulin
CASP	CASPARIAN STRIP DOMAIN PROTEIN
CIF	CASPARIAN STRIP INTEGRITY FACTOR
CPK	CALCIUM DEPENDENT PROTEIN KINASE
CS	Casparian Strip
CSD	Casparian Strip Domain
CWI	Cell Wall Integrity
DAMP	Damage-Associated Molecular Pattern
eATP	extracellular Adenosine-Triphosphate
EFR	EF-Tu RECEPTOR
ET	Ethylene
ETI	Effector-Triggered Immunity
ETS	Effector-Triggered Susceptibility
FER	FERONIA
FIR	FLS2-INTERACTING RECEPTOR
FLS2	FLAGELLIN SENSING 2
FRK1	FLG22-INDUCED RECEPTOR-LIKE KINASE 1
ISR	Induced Systemic Resistance
JA	Jasmonic Acid
LAC	LACCASE
LORE	LIPOLIGOSACCHARIDE-SPECIFIC REDUCED ELICITATION

LPS	Lipopolysaccharides
LRR	Leucine-Rich Repeat
MAMP	Microbe-associated molecular pattern
MAPK	MITOGEN-ACTIVATED PROTEIN KINASE
MTI	MAMP-Triggered Immunity
MYB51	MYB DOMAIN PROTEIN 51
NLR	Nucleotide-binding and Leucine-Rich repeat domain proteins
OG	Oligogalacturonide
PEPR	PEP1 RECEPTOR
PER5	PEROXIDASE 5
PGN	Peptidoglycan
PGPR	Plant-Growth Promoting Rhizobacteria
PROPEP	ELICITOR PEPTIDE PRECURSOR
PRR	Pattern Recognition Receptor
PR4/HEL	PATHOGENESIS-RELATED 4/HEVEIN-LIKE
PRX	PEROXIDASE
RALF	RAPID ALKALINIZATION FACTOR
RBOH	RESPIRATORY BURST OXIDASE HOMOLOG
RGI	Root Growth Inhibition
RLCK	Receptor-Like Cytoplasmic Kinase
RLK	Receptor-Like Kinases
RLP	Receptor-Like Protein
ROS	Reactive Oxygen Species
SA	Salicylic Acid
SERK	SOMATIC EMBRYOGENESIS RECEPTOR-LIKE KINASE
SGN	SCHENGEN
WRKY	WRKY DNA-BINDING PROTEINS

SUMMARY

Plants rely on an adaptable immune system to regulate their intricate interactions with the many microorganisms that surround them, particularly in the soil. While roots can mount very effective defences against pathogens, they also host an extremely rich microbiota that provides beneficial functions to the plant. Surprisingly, commensal and pathogenic bacteria are recognized via the same conserved molecular patterns which induce MAMP-triggered immunity (MTI). This raises the question of how plants manage to accommodate a useful microbial community without overstimulating their immune system, which would cause growth penalties. It was recently shown that plant roots restrict their immune responses at microbial entry sites, suggesting that plants spatially control their defences. Nevertheless, MTI responses were rarely assessed with a tissue-specific resolution.

In this work, we first demonstrated that the combination of local damage and microbial molecular patterns could unlock defences in otherwise unresponsive parts of the root. This would ensure that defences are only induced when plants are threatened by aggressive microbial colonizers. We also showed that MAMP-receptor expression is induced by damage, which determines MAMP responsiveness in certain regions. Using recombinant lines expressing the FLS2 receptor ectopically, we discovered that the root central meristem is refractory to flg22 ligand perception. However, ectopic FLS2 expression in the meristematic epidermis can render this region super-competent, leading to strong root growth inhibition in the presence of commensals. Therefore, our findings revealed that the spatial regulation of defence is crucial to the flexibility of MAMP perception.

Furthermore, we explored how commensal bacteria can bypass plant defences. We found that despite the strong sensitivity of super-competent plants, their growth was not affected by either specific individual bacterial strains or by complex bacterial communities. The structure of bacterial communities was also not affected by the strong responsiveness of these lines. To understand how bacteria can overcome plant defence, we screened a population of *Pseudomonas protegens* CHA0 mutants for loss of MTI suppression and identified potential candidates with defects in lipopolysaccharides, exopolysaccharides or gluconate synthesis.

Tissue-specific expression of FLS2 revealed lignification as a downstream response of MTI. When induced specifically in the endodermis, this lignification was surprisingly akin to the response observed after external application of CIF2 endogenous peptide, which lead to stimulation of the SCHENGEN pathway ensuring the integrity of the Casparian strip. Since FLS2 and SCHENGEN signalling share several analogous components, we used the endodermal FLS2 line to investigate how specificity is achieved by two different pathways in a single cell-type. Using transcriptomic and microscopic analyses, we showed that both pathways have a large set of core responses in common, as well as specific features. Thus, the endodermis can be used as a model system to assess signalling specificity between the related CIF2 and flg22 signalling pathways.

Plant defences have long been studied as a whole, focusing on the outcome of single plant-pathogen interactions. This work shows that the use of cell-type specific immune response markers can improve our understanding of immunity at the cellular scale and reveals the complex dynamics between tissue-specific MTI responses and bacterial communities.

RÉSUMÉ EN FRANÇAIS

Les plantes interagissent constamment avec les micro-organismes qui les entourent. Les racines, en particulier, abritent une communauté bactérienne extrêmement riche qui leur fournit une vaste palette de fonctions bénéfiques. On peut toutefois constater que de nombreuses bactéries, qu'elles soient commensales ou pathogènes, sont capables d'activer l'immunité innée des végétaux. En effet, elles présentent des motifs moléculaires conservés, les MAMPs (*microbes-associated molecular patterns*), aussi nommés éliciteurs, qui vont être reconnus par des récepteurs membranaires PRRs (*pattern recognition receptors*). On peut dès lors se demander comment les plantes réussissent à héberger un microbiote sans surstimuler leur système immunitaire, ce qui ralentirait leur croissance, tout en se défendant contre les pathogènes. Il a été montré récemment que les plantes confinent leurs réponses immunitaires aux régions les plus vulnérables de la racine. Cela suggère qu'elles sont capables de contrôler localement leurs défenses. Néanmoins, l'immunité innée n'a pas encore été étudiée avec une résolution qui soit tissu-spécifique.

Dans ce projet, nous avons tout d'abord démontré qu'il suffisait de combiner un dommage localisé avec une exposition à des MAMPs pour débloquent les défenses immunitaires dans les zones racinaires qui étaient auparavant insensibles à la présence d'éliciteurs. Ce mécanisme permettrait à la plante d'induire une réponse immune uniquement en présence de bactéries agressives. Nous avons également montré que l'expression du récepteur FLAGELLIN SENSING 2 (FLS2) était activée par des lésions tissulaires, et déterminait, associée aux propriétés intrinsèques des différents tissus, les régions sensibles à l'éliciteur flg22 (flagellin peptide 22). En effet, l'utilisation de lignées exprimant le récepteur FLS2 de façon ectopique nous a permis de découvrir que la zone centrale du méristème de la racine est réfractaire à la perception de flg22. Cependant, l'épiderme entourant cette région peut être rendu hautement immunocompétent si FLS2 y est artificiellement exprimé. Cette super-immunocompétence cause ainsi une importante inhibition de la croissance racinaire en présence de flg22 ou de bactéries pourtant inoffensives. Notre analyse révèle ainsi l'importance d'une localisation contrôlée des réponses immunitaires.

Nous avons également étudié les moyens par lesquels les bactéries contournent les défenses immunitaires des plantes. En effet, nous avons montré que, malgré la forte sensibilité des plantes super-compétentes, leur croissance n'est pas affectée lorsqu'inoculées avec certaines souches bactériennes spécifiques, ou avec un microbiote complexe. De plus, ces lignées super-compétentes n'influencent pas la composition de la communauté bactérienne. Pour comprendre le mécanisme de cette suppression immune, nous avons effectué un crible génétique sur une population de mutants de la souche *Pseudomonas protegens* CHA0. Nous avons isolé des candidats, affectés dans la synthèse du gluconate, de lipopolysaccharides et d'exopolysaccharides, ayant perdus leurs propriétés immunosuppressives.

L'expression tissu-spécifique de FLS2 nous a permis d'identifier le processus de lignification comme une réponse de l'immunité innée. Lorsqu'induite spécifiquement dans l'endoderme, cette lignification est étonnamment semblable à la réponse induite par la voie de signalisation SCHENGEN (SGN). Activée par le peptide CIF2, elle contrôle l'intégrité des cadres de Caspary. Comme l'immunité et la signalisation SGN partagent nombre de composants, nous les avons comparés au sein d'un même type cellulaire pour comprendre comment elles induisent des réponses spécifiques. Grâce à des analyses microscopiques et transcriptomiques, nous avons montré que les deux voies de signalisation partagent un même set de réponses centrales, mais diffèrent dans leur localisation et leur temporalité. L'endoderme se révèle être un excellent système modèle pour étudier la spécificité des réponses induites par CIF2 et flg22.

Les défenses végétales ont longtemps été étudiées comme un tout, se concentrant principalement sur le résultat d'une interaction entre une plante et un pathogène, ou, au mieux, sur la réponse immune d'un organe spécifique. Ce projet de thèse offre à présent plusieurs exemples dans lesquels l'utilisation de marqueurs de l'immunité, spécifiques à un type cellulaire, a amélioré notre compréhension à plus petite échelle de l'immunité innée. Ces approches apporteront une nouvelle lumière sur notre conception du système immunitaire végétal.

RÉSUMÉ TOUT PUBLIC

Compartimentation des défenses dans les racines *d'Arabidopsis thaliana*

Aurélia Emonet, Département de Biologie Moléculaire Végétale (DBMV), Université de Lausanne

Tout comme les animaux, les plantes possèdent un système immunitaire inné et peuvent se défendre efficacement contre les pathogènes. Cependant, leurs racines hébergent une myriade de bactéries bénéfiques qui les aident dans de multiples fonctions, mais qui peuvent également déclencher les réponses immunitaires de la plante. Malheureusement, nous ne comprenons toujours pas comment les plantes arrivent à distinguer une bactérie bénéfique d'un pathogène virulent, et comment elles décident de la stratégie à adopter : se défendre ou accueillir le colonisateur ?

Nous commençons à comprendre que les plantes sont capables de réguler finement leurs réponses immunitaires, notamment en confinant leurs réponses immunes à certaines régions vulnérables. Nous avons pu démontrer que le reste de la racine n'est pas complètement insensible pour autant, et peut soudainement induire une réponse immune si la racine est blessée et entre en contact avec des molécules bactériennes. Ainsi, la lésion des tissus de la racine induit la production de récepteurs FLS2 qui vont détecter les éliciteurs bactériens flg22. De la sorte, la plante ignore les bactéries bénéfiques, mais s'active lorsque celles-ci font des dégâts. De plus, nous avons observé que des défenses activées au mauvais endroit pouvait passablement affecter la croissance racinaire. Ainsi, les tissus responsables de la prolifération cellulaire sont complètement incapables de détecter flg22, probablement pour éviter une réponse immunitaire qui perturberait la croissance. En revanche, les tissus entourant cette région centrale sont particulièrement immunocompétents : en temps normal, ils sont peu réactifs à la présence de flg22, mais deviennent hyperactifs et induisent un fort ralentissement de la croissance un fois qu'ils expriment le récepteur FLS2. Ces résultats nous aident à comprendre comment les plantes régulent l'activation de leurs défenses immunitaires pour éviter une suractivation qui serait néfaste à son développement et à son microbiote, tout en maintenant leur protection contre les pathogènes.

1 GENERAL INTRODUCTION

1.1. THE LAYERED INNATE IMMUNE SYSTEM OF LAND PLANTS

Invisible to our naked eyes, they are everywhere. In the air, in the water or in the soil, they cover every surface, colonize every environment, even the harshest ones. It is therefore no wonder that microbes have always interacted with more complex organisms. Most microbes are simple opportunists that will leap at the chance to access free resources. However, hidden among the crowd, some pathogens evolved remarkable capacities to invade specific hosts. Fortunately, multicellular organisms developed immunity to counteract these trespassers. Although animals are commonly known to possess an immune system, it is sometimes forgotten that plants can defend themselves as well. Plants lack the adaptive immune system that allows animals to remember previous infections, but they have developed a robust and much simpler innate immune system which prevents most diseases. In contrast to the intricate immune arsenal of animals, which is constituted of many specialized cells such as macrophages, neutrophils or monocytes, to cite a few, every single plant cell can rely on itself to detect microorganisms and mount the appropriate defences (Dangl and Jones, 2001). Such defences come in three flavours and are constituted of the interconnected layers of constitutive barriers and inducible responses (Nürnberger and Brunner, 2002).

The constitutive defences consist of physical barriers and pre-formed chemicals, also called phytoanticipins (Nürnberger and Lipka, 2005; VanEtten *et al.*, 1994). Cell wall modifications can block microbial invasion (Miedes *et al.*, 2014). For instance, the leaf cuticle prevents pathogens penetration, notably fungi that need to secrete hydrolytic enzymes like cutinases, esterases and lipases to break into the epidermis (Ziv *et al.*, 2018). Secondary cell wall strengthening with lignin, an aromatic polymer, can also decrease initial pathogen colonization (Miedes *et al.*, 2014; Vance *et al.*, 1980). Consequently, overexpression of lignin biosynthesis genes leads to increased resistance to pathogens, whereas plant with reduced lignin content are more susceptible (Bhuiyan *et al.*, 2009; Miedes *et al.*, 2014; Shadle *et al.*, 2003; Shi *et al.*, 2012; Way *et al.*, 2002). In the root, suberin forms a structural barrier and was suggested to restrict the entry of pathogenic bacteria, fungi or even beneficial mycorrhizas into the stele (Geldner, 2013; Reinhardt and Rost, 1995; Vasse *et al.*, 1995). As an example of pre-formed chemicals, latex is produced in a

diverse range of plants and constitutively contains defensive peptidases (Ramos *et al.*, 2019).

By contrast, inducible defences are only triggered upon microbe detection. The Microbes-Associated Molecular Patterns (MAMP)-Triggered Immunity (MTI) constitutes a powerful first layer of defence and protects the plant against a diverse range of pathogens and opportunists. It relies on the perception of strongly conserved microbial patterns (MAMPs), or “elicitors”, by Pattern Recognition Receptors (PRRs) located at the plasma membrane. The second layer, called Effector-Triggered Immunity (ETI), targets specialized pathogens that escaped the first line of defences. It is based on the precise recognition of pathogen-specific effectors by intracellular Nucleotide-binding and Leucine-Rich repeat domain proteins (NLRs) and eventually leads to a hypersensitive cell death response at the site of infection. The MTI and ETI are shaped by the constant arms race between hosts and microbes (Dangl and Jones, 2001). Jones and Dangl (2006) proposed a “zigzag” model to explain how both layers are interconnected. Avirulent microbes, whose MAMPs are recognized by PRRs, induce MTI, which then halts colonization. In contrast, successful pathogens deploy effectors that counteract immune responses and cause an Effector-Triggered Susceptibility (ETS). Plants that recognize effectors directly or indirectly through specific NLRs then induce ETI and keep at bay the invaders. Several rounds of evolution will see the alternation of ETS and ETI dependently on the appearance of new effectors and corresponding NLRs (Dangl and Jones, 2001). The complex interplay between effectors and NLRs is nicely reviewed in Asai and Shirasu (2015); Khan *et al.* (2016) and Toruño *et al.* (2016).

It must be noted that MTI and ETI are not occurring sequentially in the course of an infection. Two recent preprints suggested that the MAMP- and effector-triggered immunities are mutually potentiated to induce strong defence against pathogens. The ETI notably enhances PTI signalling component expression to compensate for their turnover. Reversely, the ETI requires PTI to provide an effective resistance to pathogens (Ngou *et al.*, 2020; Yuan *et al.*, 2020a). Therefore, the traditional MTI-ETI dichotomy is now progressively replaced by a general concept of innate immune system, in which extracellular and intracellular “danger signals” are sensed by a common surveillance system. This includes, in addition to MAMPs and effectors, endogenous Damage-Associated

Molecular Patterns (DAMPs) released by plants after wounding by pathogens or herbivores (Gust *et al.*, 2017; Heil and Land, 2014; Saijo *et al.*, 2018). Cook *et al.* (2015) also proposed an alternative “Invasion Model”, in which Invasion Patterns (IPs) are sensed by IP receptors (IPRs), erasing the distinction between MTI and ETI. Whatever the model chosen, it remains critical to decipher the molecular and regulatory mechanisms of the innate immune system to better understand how plants and microbes interact together.

1.2. MAMPs AND DAMPs AS DANGER SIGNALS FOR INNATE IMMUNITY

The MAMP-triggered immunity relies on different types of Pattern Recognition Receptors. While a few are particularly well characterized, the repertoire of MAMPs and their cognate receptors is now exponentially extending (see an exhaustive list by Boutrot and Zipfel (2017)). PRRs are generally divided into two groups: receptor-like kinases (RLKs) and receptor-like proteins (RLPs). Both receptors are formed by an extracellular and a transmembrane domains, but in addition, RLKs harbour an intracellular kinase domain (Boutrot and Zipfel, 2017; Couto and Zipfel, 2016; Saijo *et al.*, 2018). These receptors are localised at the plasma membrane, where they form “signalling platforms” with many co-receptors and receptor-like kinases (Bücherl *et al.*, 2017). Together, they sense the presence of highly conserved epitopes of microbial molecules (Zipfel, 2008). These MAMPs are derived from essential, slowly evolving molecules, therefore preventing, in principle, pathogens to escape immunity (Jones and Dangl, 2006). MAMPs are found in all types of microorganisms, from bacteria to fungi and oomycetes, and include a diversity of molecules. PRRs are classified according to the type of their ectodomains, which usually corresponds to the nature of the ligands perceived. While Leucine-Rich Repeat (LRR) domains recognize mainly peptides and proteins, lysin (LysM) and lectin-like (LEC) motifs recognize sugars and fatty acids residues (Saijo *et al.*, 2018; Wan *et al.*, 2019). A couple of them have been extensively characterised.

1.2.1. MICROBES-ASSOCIATED MOLECULAR PATTERNS

The best studied MAMPs perceived by *Arabidopsis thaliana* are peptides derived from the bacterial flagellin and the EF-Tu elongation factor. The flagellin elicitor, a highly conserved small peptide of 22 amino acids, accordingly named flg22, is recognized by the receptor FLAGELLIN SENSING 2 (FLS2) (Chinchilla *et al.*, 2006, 2007; Felix *et al.*, 1999; Gómez-Gómez and Boller, 2000; Gómez-Gómez *et al.*, 1999; Zipfel *et al.*, 2004). Interestingly, the full flagellin protein cannot induce MTI. Indeed, the flg22 sequence is buried inside the flagellin molecule, so that flagellin should be processed by proteases and the β -galactosidase 1 (BGAL1) to release the flg22 peptide (Buscaill *et al.*, 2019; Fliegmann and Felix, 2016).

EF-Tu is one of the most abundant and slowly evolving bacterial protein (Lathe and Bork, 2001). The elf18 peptide, derived from an 18-amino acids epitope at its N-

terminus, is perceived by the LRR-RLK receptors EFR (EF-Tu RECEPTOR) (Kunze *et al.*, 2004; Zipfel *et al.*, 2006).

Several PRRs and their cognate ligands were added to the list in the last decade. Chitin is a major component of the fungal cell wall and is sensed by the LysM-RLK homodimers CERK1 (CHITIN ELICITOR RECEPTOR KINASE 1) (Miya *et al.*, 2007; Petutschnig *et al.*, 2010; Wan *et al.*, 2008) associated to LYK5 (LYSM-CONTAINING RECEPTOR-LIKE KINASE 5) (Cao *et al.*, 2014), or by LYM2 (LYSM DOMAIN GPI-ANCHORED PROTEIN 2) (Faulkner *et al.*, 2013). Bacterial cell walls can release peptidoglycan (PGN) which is perceived by the LysM-RLPs AtLYM1 and AtLYM3 (Willmann *et al.*, 2011). Recently, the LEC-RLK LORE (LIPOOLIGOSACCHARIDE-SPECIFIC REDUCED ELICITATION) was shown to bind free medium-chain 3-hydroxy fatty acid (mc-3-OH-FA) derived from the lipid A moiety of lipopolysaccharides (LPS), a major outer membrane component of gram negative bacteria (Kutschera *et al.*, 2019; Ranf *et al.*, 2015). In addition to exogenous MAMPs, PRRs can also recognize endogenous signals indicating cell-damage.

1.2.2. DAMAGE-ASSOCIATED MOLECULAR PATTERNS

DAMPs initiate an analogous mechanism to MAMP perception and are perceived by similar PRR families. They can be separated between primary and secondary endogenous danger signals. The first ones are pieces of cell wall or intracellular compounds abnormally present in the apoplast, released passively upon damage. They are considered as classical DAMPs, since they are constitutive component of plant cells that do not require to be synthesised or secreted *de novo*. A few true DAMPs were identified so far, such as oligogalacturonides (OGs), extracellular ATP (eATP), cutin monomers or cellobiose, but their corresponding receptor is often still unknown (Gust *et al.*, 2017). In *A. thaliana*, only two DAMP receptors were identified. The WAK1 (WALL-ASSOCIATED KINASE1) receptor binds OGs, which are fragments of cell-wall derived pectin (Brutus *et al.*, 2010). In addition, eATP is thought to be sensed by the LEC-RLK DORN1 (DOES NOT RESPOND TO NUCLEOTIDES 1)(Choi *et al.*, 2014).

In contrast to classical DAMPs, secondary danger signals are actively synthesised by plants and released upon wounding, sometimes through secretion. Secondary danger signals are often described as phytochemicals that modulate MTI responses (Gust *et al.*,

2017). They are usually small peptides processed by proteolytic cleavage from larger proteins. As such, systemin is an 18-amino acids peptide found in tomato, cleaved from a larger prosystemin protein after damage perception and released in the apoplast (McGurl *et al.*, 1992; Pearce *et al.*, 1991). Similarly, the peptides AtPep (1 to 3, 5 and 8) are induced by wounding and need to be processed from ELICITOR PEPTIDE PRECURSORS (PROPEPs) prior sensing by two LRR receptor kinases, PEPR1 and 2 (PEP1 RECEPTOR 1/2) (Bartels and Boller, 2015). While PEPR1 can bind the eight known AtPeps, PEPR2 interacts only with AtPep1 and AtPep2 (Krol *et al.*, 2010; Yamaguchi *et al.*, 2006). In contrast to systemin, PROPEPs do not encode N-terminal signal peptide for secretion, suggesting they are released by tissue damage, though it is still debated if secretion could occur (Huffaker *et al.*, 2006; Yamaguchi and Huffaker, 2011). Hander *et al.* (2019) recently proposed that PROPEP1 is localized at the tonoplast of undamaged cells. After laser ablation, they observed that the METACASPASE 4, activated by Ca²⁺ entry, cleaved PROPEP1 protein and released AtPep1, which will then diffuse to neighbouring cells to induce defence responses, making it a *bona fide* classical DAMPs.

From the recognition of MAMPs and DAMPs to the actual defence mechanisms, intricate signalling processes will take place, incorporating environmental and endogenous inputs to deliver a precise and controlled immune response.

1.3.MAMP-TRIGGERED IMMUNITY SIGNALLING: FLS2 AND FLG22

Upon perception of elicitors, all currently studied MAMPs and DAMPs induce surprisingly similar downstream responses, starting from a common signalling cascade involving calcium influx, ROS production, MITOGEN-ACTIVATED PROTEIN KINASE (MAPK) phosphorylation cascades and hormonal signalling, until the induction of actual defence mechanisms (Tang *et al.*, 2017; Wan *et al.*, 2019). However, the formation and regulation of the PRRs platforms, the composition of their intricate signalling networks or the localisation of immune responses can be slightly different depending on the elicitor perceived. The next paragraphs therefore focus on the mechanisms observed in response to the best studied MAMP, the flg22 peptide and its receptor FLS2.

1.3.1. PRRs FORM TIGHTLY REGULATED SIGNALLING PLATFORMS

Most LRR-containing receptor kinases (LRR-RK) interact with co-receptors from the SERK (SOMATIC EMBRYOGENESIS RECEPTOR-LIKE KINASE) protein family upon ligand perception. Additionally, they scaffold into nanodomains of receptor complexes (Bücherl *et al.*, 2017; Roux *et al.*, 2011; Wan *et al.*, 2019). As such, FLS2 associates principally to BRI1-ASSOCIATED RECEPTOR KINASE (BAK1/SERK3)(Chinchilla *et al.*, 2007). Interestingly, BAK1 also interacts with the brassinosteroid receptor BRI1 (BRASSINOSTEROID INSENSITIVE 1) to regulate growth (Li *et al.*, 2002; Nam and Li, 2002). Yet, how does BAK1 specifically activate one or the other pathway is not completely understood. Perraki *et al.* (2018) showed that some conserved phosphosites of the kinase domain are required specifically for the immune function of BAK1, but not for its developmental role. Moreover, FLS2-BAK1 and BRI1-BAK1 complexes are localized in distinct nanodomains at the plasma membrane (Bücherl *et al.*, 2017).

FLS2/BAK1 complex, in resting state, constitutively associates with several other proteins, which tightly regulate FLS2-BAK1 interactions to avoid a constant activation of immunity. BIR2 and BIR3 (BAK1-INTERACTING RECEPTOR-LIKE KINASE) prevent the interaction of FLS2 and BAK1 in absence of flg22 (Halter *et al.*, 2014; Imkampe *et al.*, 2017). The receptor-like kinases ANXUR1 and 2 also inhibit the formation of the signalling complex (Mang *et al.*, 2017). Receptor-like cytoplasmic kinase (RLCKs) in their inactive state, like BIK1 (BOTRYTIS-INDUCED KINASE1) or PBL1 (PBS1-LIKE 1), also constitutively interact

with the FLS2/BAK1 complex (Lu *et al.*, 2010; Veronese *et al.*, 2006; Zhang *et al.*, 2010). BIK1 homeostasis is closely controlled: the CALCIUM DEPENDENT PROTEIN KINASE CPK28 associates with non-activated BIK1 to promote its degradation by phosphorylating E3 ligases (Monaghan *et al.*, 2014). The protein phosphate PP2C38 also dephosphorylates BIK1 to maintain it in an inactive state (Couto *et al.*, 2016). In addition, LRR-RK FLS2-INTERACTING RECEPTOR (FIR) or the heterotrimeric G-proteins XLG2/AGB1/AGG1/2 stabilize the signalling complex (Liang *et al.*, 2016; Smakowska-Luzan *et al.*, 2018). All those mechanisms ensure a tight regulation of immunity, that is ultimately triggered upon MAMP/DAMP perception.

1.3.2. SIGNALLING AT THE PLASMA MEMBRANE UPON MAMP PERCEPTION

Flg22 acts as a molecular glue between FLS2 and BAK1 to induce MTI signalling (Hohmann *et al.*, 2017; Sun *et al.*, 2013). Upon its perception, the inhibitory proteins BIR2 and BIR3 dissociate from FLS2/BAK1 (Halter *et al.*, 2014; Imkampe *et al.*, 2017) while components of the scaffolding complex such as FERONIA (FER), IMPAIRED OOMYCETE SUSCEPTIBILITY 1 (IOS1) and LORELEI-LIKE-GPI-ANCHORED PROTEIN 1 (LLG1) promote and stabilize FLS2/BAK1 association (Li *et al.*, 2015; Shen *et al.*, 2017; Stegmann *et al.*, 2017; Yeh *et al.*, 2016). Flg22 binding induces rapid transphosphorylation of FLS2 and BAK1 (Chinchilla *et al.*, 2007; Heese *et al.*, 2007; Schulze *et al.*, 2010). Then, BAK1 phosphorylates several RLCKs, like BIK1 or PBL1. This releases them from the complex to further activate downstream signalling (Lin *et al.*, 2013). BIK1 has a preponderant role in MTI and is required for FLS2, EFR, PEPR1/2 and CERK1-induced responses (Liu *et al.*, 2013; Lu *et al.*, 2010; Veronese *et al.*, 2006; Zhang *et al.*, 2010). Non-phosphorylated BIK1 is ubiquitinated to prevent its overaccumulation (Wang *et al.*, 2018).

FLS2 is also quickly recycled after induction of MTI signalling. Indeed, flg22 perception causes the turnover of FLS2 by BAK1- and clathrin-dependent endocytosis upon 10-20 min (Boller and Felix, 2009; Keinath *et al.*, 2010; Mbengue *et al.*, 2016; Robatzek *et al.*, 2006). Endocytosed FLS2 is then targeted to degradation after ubiquitination by PUB12 and PUB13 (PLANT U-BOX12/13), allowing signal desensitization and the cell to replenish its pool of uninduced FLS2 (Lu *et al.*, 2011; Robatzek *et al.*, 2006; Smith *et al.*, 2014).

With a better understanding of the apoplastic events allowing signal perception, we can now focus on the intracellular downstream mechanisms permitting signal transduction.

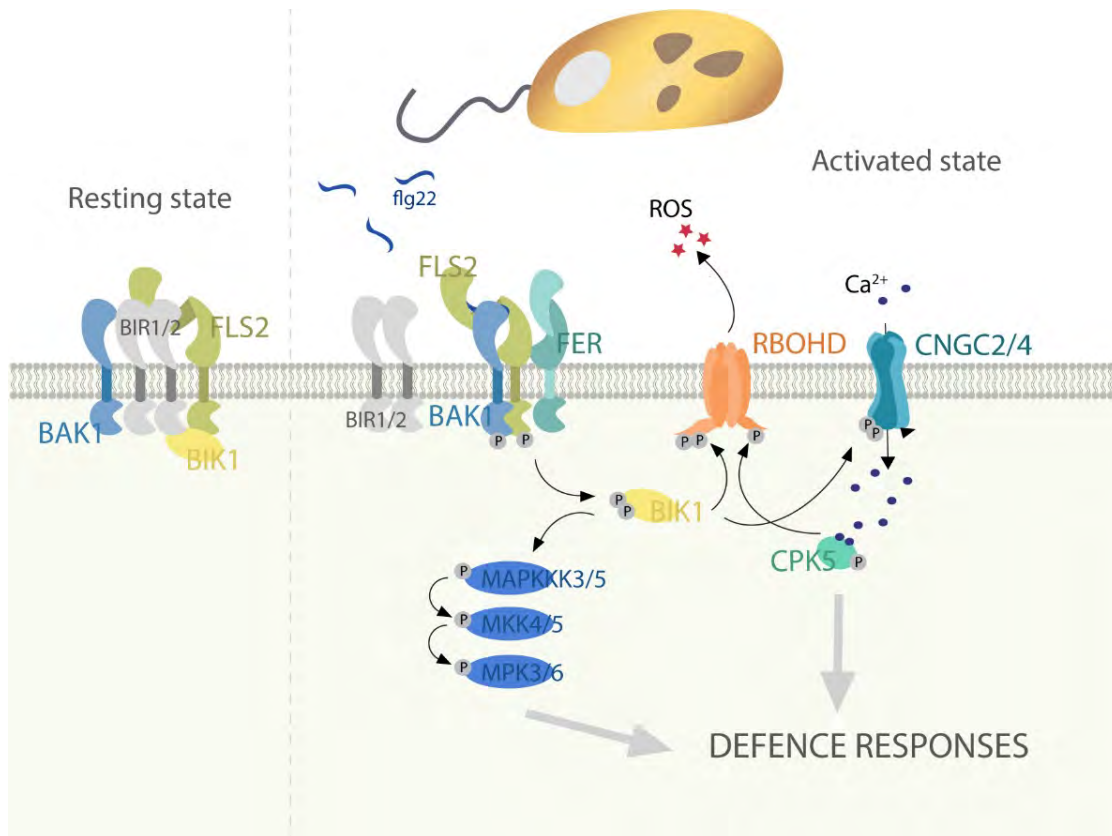


Figure 1 : Simplified view of immune signalling in response to flg22.

Upon flg22 perception, BIR1/2 dissociate from FLS2 and BAK1, which interact and cross-phosphorylate. BAK1 is phosphorylated by FLS2/BAK1 and induces both MAPK phosphorylation cascades and ROS production through RBOHD phosphorylation. BIK1 also activates the Ca²⁺ channel CNGC2/4. Entry of calcium is sensed by CPK5 that phosphorylates RBOHD. MAPK cascade and calcium signalling lead to activation of immune responses.

1.3.3. TRANSDUCTION OF IMMUNE SIGNAL – EARLY RESPONSES

Ca²⁺ SIGNALLING

Elicitors such as flg22 trigger immediate changes in ions fluxes, and notably cytosolic calcium entry (Boller and Felix, 2009; Seybold *et al.*, 2014). Indeed, BIK1 and PBL1 directly or indirectly regulate the opening of calcium channels (Ranf *et al.*, 2014). Glutamate-receptors were implicated in calcium burst upon flg22 detection (Kwaaitaal *et al.*, 2011), but this finding could not be confirmed by Thor and Peiter (2014). Activated FLS2 was shown to directly associate and inhibit the Ca²⁺ exporter AUTOINHIBITED CA²⁺-ATPASE, ISOFORM 8 and 10 (ACA8/10), which increases cytosolic calcium concentration

(Frey *et al.*, 2012). Recently, Tian *et al.* (2019) demonstrated that BIK1 directly phosphorylates the CYCLIC NUCLEOTIDE GATED CHANNEL dimers CNGC2 and 4, inducing cytosolic Ca²⁺ increase in response to pathogens.

Cytosolic calcium increase propagates by waves through the plant and is thought to induce responses in distal tissues (Choi *et al.*, 2016; Gilroy *et al.*, 2014, 2016; Stanley *et al.*, 2018). Interestingly, different MAMPs can trigger distinct calcium signatures which are assumed to dictate response specificity (Ranf *et al.*, 2011; Thor, 2019). Changes in calcium concentration are then perceived by diverse proteins: calmodulin (CaM), CaM-like proteins (CMLs), calcineurin B-like proteins (CBLs), CBL-interacting protein kinases (CIPKs) or Ca²⁺-dependent kinases (CDPKs or CPK), all of which modulate downstream immune responses, such as MAPK activation, ROS production, hormone signalling or directly gene expression (Boudsocq *et al.*, 2010; Choi *et al.*, 2016; Thor, 2019).

REACTIVE OXYGEN SPECIES

In addition to calcium signalling, MAMPs induce in the first 2 minutes upon perception the production of reactive oxygen species (ROS) (Boller and Felix, 2009). The NADPH oxidase RESPIRATORY BURST OXIDASE HOMOLOG D (RBOHD) is essential for MTI induction, but RBOHF plays also a minor role (Zhang *et al.*, 2007). Activated RBOHD produces O₂⁻ that is converted by superoxide dismutases into H₂O₂. RBOHD binds to FLS2 and BIK1 in absence of ligand and is activated and phosphorylated upon flg22 perception by the combined effect of BIK1, PBL2 and CPK5 (Dubiella *et al.*, 2013; Kadota *et al.*, 2014; Li *et al.*, 2014b). Interestingly, RBOHD is also positively regulated by several RLCK (*i.e.* PBL1, BSK1)(Shi *et al.*, 2013; Zhang *et al.*, 2010) and the MAP4K SIK1 (SERINE/THREONINE KINASE 1)(Zhang *et al.*, 2018).

ROS production is tightly linked to cytosolic calcium concentration changes, therefore both pathways are often described as a ROS-Ca²⁺ wave, propagating on long distances (Gilroy *et al.*, 2014, 2016; Miller *et al.*, 2009). Ca²⁺ is indeed required for ROS signalling through direct binding to RBOHD, or through indirect activation of RBOHD by CPK proteins (Drerup *et al.*, 2013; Dubiella *et al.*, 2013; Ranf *et al.*, 2011). Moreover, ROS production is inhibited by the Ca²⁺ channel inhibitor LaCl₃ (Ranf *et al.*, 2008). Reversely, ROS (in particular H₂O₂) was proposed to induce calcium signalling by activating Ca²⁺ channels,

which would further increase MTI responses in a feed forward loop (Choi *et al.*, 2016; Pei *et al.*, 2000; Rentel and Knight, 2004). Increase in cytosolic Ca²⁺ concentration was suggested to induce the ROS-sensitive channel TPC1 (TWO-PORE CHANNEL 1) and to propagate through plasmodesmata. However, TPC1 is not involved in the flg22-mediated calcium response (Ranf *et al.*, 2008).

ROS mainly act as secondary messengers, but they also have direct effects such as antimicrobial and cell wall crosslinking properties (Boller and Felix, 2009). Moreover, ROS are required for stomata closure and callose deposition in response to pathogens (Mersmann *et al.*, 2010; Zhang *et al.*, 2007).

ROS and Ca²⁺ are well-established as the early steps of signal transduction, but MAPK phosphorylation cascades are also involved as a parallel chain of events leading to the defence response.

MITOGEN-ACTIVATED PROTEIN KINASE CASCADE

Activated PRRs also induce MAPK phosphorylation cascades, allowing to transduce MAMP-perception into an appropriate transcriptional response. These signalling modules are constituted of MAPKKK (Mitogen-Activated Protein Kinase Kinase Kinase or MEKK), MAPKK (MAP Kinase Kinase) and MAPK (Meng and Zhang, 2013). Two distinct MAPK pathways were involved in MTI (Tang *et al.*, 2017). The first one relies on the phosphorylation of MKK4/MKK5 - MAPK3/MAPK6 (Asai *et al.*, 2002; Tang *et al.*, 2017). It was recently proposed that MAPKKK3 and MAPKKK5 are implicated in MAPK3/6 activation, although their effects are not consistent across different MAMP signalling pathways. Supporting this suggestion, BIK1 and other RLCKs associate with and phosphorylate MAPKKK3/5 (Bi *et al.*, 2018; Sun *et al.*, 2018; Yamada *et al.*, 2016). The second cascade involves MEKK1 - MKK1/MKK2 - MPK4 and was shown to downregulate some immune responses such as salicylic acid (SA) and ROS production (Pitzschke *et al.*, 2009).

Upon activation, MAPK cascades phosphorylate proteins and transcription factors, mainly WRKY DNA-BINDING PROTEINS (WRKYs), that in turn activate defence genes. MAPK cascades play a large role in the MAMP-induced transcriptional response. 36% of the flg22-upregulated genes and 68% of the downregulated genes were influenced in at least

one of the *mpk3*, *mpk4*, and *mpk6* mutants (Frei dit Frey *et al.*, 2014). MAPKs modulate defence hormones synthesis and signalling, phytoalexin biosynthesis, hypersensitive cell death response and stomatal immunity. Interestingly, MAPK cascade and ROS signalling are independent of each other, but might crosstalk in downstream signalling (Meng and Zhang, 2013), which also includes hormonal regulation.

DEFENCE HORMONES

In addition to ROS/Ca²⁺ burst and phosphorylation cascade, MTI responses affect hormonal signalling. MAMP perception induces the synthesis of ethylene (ET), and salicylic and jasmonic acid (SA and JA) signalling (Boller and Felix, 2009). Interestingly, SA and ET/JA are in many cases antagonistic. SA signalling is central to responses to biotrophic and hemibiotrophic pathogens whereas the ET and JA pathways contribute to defence against necrotrophic pathogens (Glazebrook, 2005; Pieterse *et al.*, 2012). However, the three pathways can also act synergistically since the analysis of *dde2/ein2/pad4/sid2* quadruple mutant, impaired in JA, ET, *PHYTOALEXIN-DEFICIENT 4* (PAD4), and SA signalling pathways, revealed that all three hormones act positively in *flg22/elf18*-mediated MTI and mainly control late responses (Tsuda *et al.*, 2009). These will then directly affect the microbial invaders responsible for the induction of MTI signalling.

1.4. DOWNSTREAM DEFENCE RESPONSES AS FINAL OUTPUT OF MTI

The intricate signalling networks occurring during MTI responses eventually induce a set of defence mechanisms to protect the plant against the perceived microbes. Among these responses, the production of antimicrobial compounds and the strengthening of cell walls are key features hindering the penetration of pathogens.

In contrast to phytoanticipins, constitutively synthesized by the plant, phytoalexins are low molecular mass secondary metabolites with antimicrobial activity, produced upon perception of MAMPs, DAMPs or pathogens (Ahuja *et al.*, 2012). In *A. thaliana*, flg22 triggers the production of camalexin, generally in a limited region neighbouring the pathogen-induced lesion (Denoux *et al.*, 2008; Kliebenstein *et al.*, 2005; Schuegger *et al.*, 2007). Camalexin production is directly regulated by the WRKY33 transcription factor, itself activated by the MKK4/5 - MPK3/6 pathway (Meng and Zhang, 2013; Pitzschke *et al.*, 2009). Coumarins are also synthesized by a vast range of species in response to pathogens and have antimicrobial properties against fungi, oomycetes and bacteria (Stringlis *et al.*, 2019a).

Additionally, MAMP-triggered immunity typically induces the formation of cell wall depositions containing callose, an amorphous β -(1,3)-glucan polymer that serves as a matrix for localized antimicrobial compound accumulation (Gómez-Gómez *et al.*, 1999; Luna *et al.*, 2010). Callose is also a constituent of papillae formed at the penetration site of pathogens (Voigt, 2014). Callose biosynthetic genes are induced by flg22 and require the transcription factor MYB51 (MYB DOMAIN PROTEIN 51) and CYP81F2 (CYTOCHROME P450, FAMILY 81, SUBFAMILY F, POLYPEPTIDE 2) involved in the glucosinolate pathway. Indeed, the callose synthase uses breakdown products of indole glucosinolates. Callose synthesis is also dependent of ethylene signalling both in root and shoot (Clay *et al.*, 2009; Millet *et al.*, 2010).

Lignin-impregnation of cell walls was one of the first described responses at the cellular scale to living pathogens (mostly fungi) and was correlated with hypersensitive responses leading to controlled cell-death (Baayen *et al.*, 1996; Bhuiyan *et al.*, 2009; Lawton and Lamb, 1987; Menden *et al.*, 2007; Nicholson and Hammerschmidt, 1992; Vance *et al.*, 1980). Nevertheless, some “elicitor preparations” consisting of boiled extracts of pathogens

were also reported to induce accumulation of monolignols and lignin deposition in wheat, cucumber and *Picea abies* cell culture (Campbell and Ellis, 1992; Lange *et al.*, 1995; Menden *et al.*, 2007; Siegrist *et al.*, 1994). The use of pure MAMPs and DAMPs later confirmed that lignin deposition was a direct effect of MTI responses. Smit and Dubery (1997) showed that a protein-lipopolysaccharide elicitor of *Verticillium* induced lignin deposition in cotton sprout. Chitin induces the production of lignin-like components in cell culture of *Pinus* and the upregulation of lignin biosynthesis genes in rice (Kaku *et al.*, 2006; Lesney, 1989). Robertsen (1986) identified several elicitors inducing lignin in cucumber hypocotyls, while Adams-Phillips *et al.* (2010) reported an elf18-driven lignification in *A. thaliana*. More recently, flg22 was shown to induce *MYB15*-dependent seedling lignification (Chezem *et al.*, 2017). Lignin was often linked to non-host resistance and blocks pathogens progress in leaves (Bhuiyan *et al.*, 2009; Lee *et al.*, 2019; Nicholson and Hammerschmidt, 1992; Vance *et al.*, 1980).

Suberin is a large constituent of plant preformed barriers (Bernards, 2002; Geldner, 2013; Kamula *et al.*, 1994; Thomas *et al.*, 2007). However, suberin deposition can also be induced in roots of soybean after *Phytophthora sojae* infection and influences cultivar resistance (Ranathunge *et al.*, 2008). However, I could not find evidence in the literature that suberisation would be triggered in response to a single MAMP.

Other defence mechanisms are induced by MTI in addition to phytoalexin production and cell wall strengthening. MAMPs trigger stomatal closure to avoid pathogens entry (Melotto *et al.*, 2017), increase the expression of secondary danger signals as PROPEP2/3 (Bartels *et al.*, 2013; Yamaguchi and Huffaker, 2011), increase the transcription of PRRs (Boutrot *et al.*, 2010; Tintor *et al.*, 2013) and the generation of pathogenesis-related (PR) proteins (Boller and Felix, 2009).

MAMP- and DAMP-triggered immunity is indeed a very intricate mechanism that starts from the recognition of simple “danger signal” molecules and leads to a complex array of defensive weapons. These diverse responses converge to form a protective physical and chemical barrier and allow the plant to survive despite the omnipresence of pathogens.

1.5. GROWTH AND DEFENCE: AIMING FOR THE EQUILIBRIUM

MTI allows plants to deal with various microorganisms but does not come without a cost. Indeed, plants must allocate their limited resources wisely between growth and defence. Overresponsive mutants with constitutive defences were shown to bear increased fitness costs and to display stunted growth (Heil *et al.*, 2000; Todesco *et al.*, 2010).

The most flagrant impact of MTI on the growth-defence trade-off is the inhibition of seedling growth after long-term treatment with MAMPs or DAMPs (Gómez-Gómez and Boller, 2000; Jing *et al.*, 2020; Zipfel *et al.*, 2006). Seedling growth inhibition is a hallmark of MTI induction. The exact mechanism behind this process is still unclear but can be explained broadly by resource reallocation and hormonal crosstalk.

A recurrent explanation was that the brassinosteroid (BR) and MTI pathways would compete for their common BAK1 co-receptor. Their crosstalk was rather unidirectional, as brassinosteroid application was reported to inhibit flagellin-triggered defence (Belkhadir *et al.*, 2012, 2014). However, the trade-off was then shown to be independent of BAK1 since BR treatment did not affect the physical interaction of FLS2 and BAK1 (Albrecht *et al.*, 2012). Later on, Lozano-Durán *et al.* (2013) demonstrated that induction of BZR1 (BRASSINAZOLE-RESISTANT 1) through BR signalling was required and sufficient to inhibit the MTI pathway. BZR1 activates a handful of inhibitors of immune signalling such as HBI1 (HOMOLOG OF BEE2 INTERACTING WITH IBH 1) or WRKY40 (Bai *et al.*, 2012; Fan *et al.*, 2014; Lozano-Durán *et al.*, 2013; Malinovsky *et al.*, 2014). Reversely, MTI signalling can inhibit the brassinosteroid pathway through repression of HBI1 and BIK1-mediated phosphorylation of BR1 (Fan *et al.*, 2014; Lin *et al.*, 2013). Overall, brassinosteroid and MTI signalling crosstalk to control the balance between growth and defence.

The trade-off between growth and defence could also involve the FERONIA receptor, which was shown to coordinate many biological processes, including development, growth and defence response. FER is not only important for the scaffolding of PRR signalling platforms (Stegmann *et al.*, 2017), but is required for cell elongation during the vegetative growth (Guo *et al.*, 2009). FER has a structural role, independent of its kinase activity, for the ligand-induced dimerization of FLS2 and BAK1; consequently, the *fer*

mutant displays reduced MAMP-responses. However, a flg22-activated RALF23 (RAPID ALKALINIZATION FACTOR 23) ligand binds to FER and negatively regulates PRR complex formation, likely to avoid overactivation of immune responses (Gronnier *et al.*, 2020; Stegmann *et al.*, 2017). *Fer* mutants were also reported to be specifically resistant to powdery mildew, suggesting that FER can also negatively affects the immune responses (Kessler *et al.*, 2010).

More and more findings illustrate the interactions between growth and defence pathways, usually involving interactions between hormonal signalling. For example, salicylic acid and jasmonate signalling can override the development-oriented auxin and gibberellin pathways (Huot *et al.*, 2014). Flagellin also induces the expression of the microRNA miR393, which degrades activators of the auxin signal route, implicated in stem development and root architecture (Navarro *et al.*, 2006). Developmental programs also repress immune responses. Thus, DELLA proteins, a group of gibberellin-signalling repressors, form a feedback regulatory loop with the plant immune regulator ENHANCED DISEASE SUSCEPTIBILITY 1 (EDS1) (Li *et al.*, 2019). MTI signalling is also downregulated by the root growth-promoting hormones phytosulfokine (PSKs) and PLANT PEPTIDE CONTAINING SULFATED TYROSINE1 (PSY1). Indeed, mutants for the respective receptors *pskr1* and *psy1r* exhibit enhanced MAMP responses (Amano *et al.*, 2007; Igarashi *et al.*, 2012; Matsubayashi and Sakagami, 2006).

The crosstalk between growth and defence is of crucial importance for plant development. Indeed, plants need to suppress growth when attacked by a pathogen to ensure that all resources go to their defence and their survival. On the other hand, in absence of threat, it makes sense that plants would allocate their resources towards growth. However, plants are never in such a simple interaction with a single pathogen. They are constantly in contact with bacteria, archaea, fungi and protists of all kinds, and must cope with damages caused by herbivores, insects or nematodes. Moreover, only few microorganisms are actual pathogens, and we still do not understand whether plants can really discriminate them from inoffensive microbes. In that context of a densely microbe-populated environment, a tight control of immune responses on the plant side is required to equilibrate the trade-off between growth and defence.

1.6. THE RHIZOSPHERE, A MELTING POT OF BIOTIC INTERACTIONS

The last decades of research on MAMP-triggered immunity revealed complex and evolving mechanisms regulating the detection of microbes and leading to effective defences. They allowed us to understand why some plants were susceptible to specific pathogens, and why other were resistant. They also highlighted the constant co-evolution between pathogens and plants. However, the study of MTI was often restricted to events occurring on plant leaves, and mostly overlooked the fact that roots are also affected by pathogens. Despite their importance in many physiological processes, little interest has been given to defences in the “hidden half” of the plants, probably because of the difficulty to study organs buried in the ground. Using an anthropomorphic analogy, roots are often described as an inverted gut, foraging the soil for water and nutrients. Moreover, like for animals, they recruit and host a specific and very diverse microbiota that provides services to the plant, such as nutrient acquisition or protection against pathogens. How plants deal with such a complex community, how they recruit and influence their microbiome, how they regulate their defence system to avoid pathogens to spread while keeping a healthy microbiome, are some of the emerging questions of the plant-microbe interactions field.

1.6.1. THE RHIZOSPHERE COMMUNITY OR THE 2ND GENOME OF THE PLANT

The study of soil microbiota was long hindered by the impossibility to culture most soil microorganisms. However, the emergence of new generation high-throughput sequencing technologies and corresponding computational tools allowed to shed light on one of the richest microbial community on Earth and assess its composition (Bulgarelli *et al.*, 2013; Hacquard, 2016; Pascale *et al.*, 2020). The root releases photo-assimilates and exudates that attract a subset community of the soil microbiota in its close periphery, called the rhizosphere (Berendsen *et al.*, 2012; Bulgarelli *et al.*, 2013; Durán *et al.*, 2018; Hacquard *et al.*, 2017; Massalha *et al.*, 2017a). This less complex but more specialized community still includes a rich variety of microbes such as bacteria, fungi, archaea and protists. In comparison, the leaf microbiota is predominantly composed of bacteria, though the phyllosphere bacterial composition presents a taxonomic overlap with the rhizosphere community (Bai *et al.*, 2015; Bulgarelli *et al.*, 2013).

Roots are mostly colonized by the bacterial phyla *Gamma-proteobacteria*, *Beta-proteobacteria*, *Actinobacteria* and *Bacteroidetes*, specifically enriched in the “endosphere” compartment, the community living inside or in very close association to the roots (Bai *et al.*, 2015; Bulgarelli *et al.*, 2012; Durán *et al.*, 2018; Lundberg *et al.*, 2012). This community structure can be found in all flowering plants (Bai *et al.*, 2015; Bulgarelli *et al.*, 2015; Edwards *et al.*, 2015; Schlaeppi *et al.*, 2014). Root-colonizing fungi are mostly represented by member of the *Basidiomycota* and the *Ascomycota* phyla, and, in contrast to bacteria, seem more subjected to variation depending on plant biogeography (Durán *et al.*, 2018; Hassani *et al.*, 2018). Much less studied, protists known to interact with plants are generally part of the *Oomycota* and *Cercozoa* lineages (Gao *et al.*, 2018; Hassani *et al.*, 2018; Sapp *et al.*, 2018).

Microbes living in and on the roots display a vast repertoire of behaviours. At the extreme end of the spectrum are found symbiotic organisms that require morphological changes to accommodate their development. Thus, arbuscular mycorrhizas form intracellular structures called arbuscules and extend the plant root network with their hyphae, increasing plant access to mineral nutrients. In exchange of phosphates, roots provide lipids and carbohydrates (Gutjahr and Parniske, 2013). This symbiotic association is occurring in 70-90% of land plant species and co-evolved since at least 400 Mya (Gutjahr and Parniske, 2013; Parniske, 2008). Similarly, the more recent symbiotic nodule-forming rhizobacteria provide their host with nitrogen. Both symbionts rely on a similar symbiotic pathway, underlining their shared evolutionary origins (Martin *et al.*, 2017).

At the opposite end of the microbial scope are biotrophic and necrotrophic pathogens, that prefer their host respectively alive or dead. Although less visible than foliar pathogens, they can have drastic impact on plant development and cause root rot, wilting, growth inhibition or plant death. Fungi and oomycetes are the most prevalent, such as *Fusarium oxysporum*, *Verticilium spp.*, *Rhizoctonia solani*, and *Pythium* or *Phytophthora spp.*, respectively. Only a few bacteria can infect roots: *Ralstonia solanacearum*, *Erwinia spp.* or the well-known *Agrobacterium tumefaciens* that causes crown gall formation, are the best described. Soilborne pathogens often reside in the soil under a dormant form or as saprophytes until root exudates induce their growth (Bais *et al.*, 2006; De Coninck *et al.*, 2015; Pascale *et al.*, 2020).

Most of the remaining microorganisms colonizing roots do not have such extreme lifestyles. Many are described as commensals that benefit from, but do not harm the plant. Some are even beneficial, while others are opportunistic pathogens waiting for the appropriate moment to show their dark side. All these microbes rely on exudates and dead cells released by the root as a source of nutrients, but they can also provide the plant with specific functions (Bulgarelli *et al.*, 2013; Pascale *et al.*, 2020). Therefore, they are generally considered as the second genome of the plant, to the point that the combination of the host and its microbiome is currently defined as a single functional entity called the “holobiont” (Hassani *et al.*, 2018; Rosenberg and Zilber-Rosenberg, 2016).

1.6.2. MICROBIOTA AS A PROVIDER OF SERVICES

Many functions provided by the rhizosphere microbiota eventually impact plant growth. The exact mode of action of Plant-Growth Promoting Rhizobacteria (PGPRs, mainly *Pseudomonas* but also *Azospirillum*) is still poorly understood, but one of the mechanisms they use relies on the enhancement of nutrient availability (Bulgarelli *et al.*, 2013; Goswami *et al.*, 2016; Pascale *et al.*, 2020). Indeed, rhizobacteria can either fix or denitrify nitrogen, increase phosphorus and iron solubilization by the production of organic acids or siderophores, respectively. Non-mycorrhizal plants can also rely on endophytic fungi to increase phosphate uptake, such as *Colletotrichum tofieldiae* or *Serendipita indica* (Castrillo *et al.*, 2017; Hiruma *et al.*, 2016; Pascale *et al.*, 2020; Yadav *et al.*, 2010). Some beneficial microbes can also stimulate the plant iron-deficiency response to increase iron absorption (Martínez-Medina *et al.*, 2017; Pascale *et al.*, 2020; Zamioudis *et al.*, 2015; Zhou *et al.*, 2016). Alternatively, microbes can interfere with plant hormones by producing auxins or analogues of salicylic and jasmonic acids, or by degrading ethylene, known to repress plant growth (Stringlis *et al.*, 2018a). The rhizosphere community can also impact indirectly growth by competing with pathogenic microorganisms, production of antimicrobial compounds or through Induced Systemic Resistance (ISR). ISR relies on the PGPR-mediated activation of several hormonal responses leading to the priming of defences. Such an energy-saving strategy allows a faster and stronger defence induction only upon further pathogen attack (Pieterse *et al.*, 2014).

Roots growing in this this multi-organismal context challenge constantly the growth-defence trade-off paradigm. Knowing that a large part of the commensal and beneficial microbial communities can also induce MAMP-triggered immunity, it seems essential that plants precisely regulate or target their defences in order to conserve a healthy microbiome while getting pathogens under control. Root defences must be particularly adapted to such a complex environment, and therefore cannot be expected to be identical to defences in the shoot.

1.7. IMMUNITY IN THE ROOT, A STORY OF COMPARTMENTATION

1.7.1. ROOT ANATOMY AND BARRIERS

Roots are constituted of concentric cell layers defined as distinct tissues: the epidermis, the cortex, the endodermis and the pericycle surround the vascular central cylinder, also called the stele (Fig.1). Roots lack, generally, an impermeable cuticle, which allows nutrients to reach the vasculature by diffusion and active transport (Barberon, 2017; Geldner, 2013). Newly generated cells are found in the meristematic zone located at the root tip (Schiefelbein and Benfey, 1991). They are covered by the root cap, constituted of the columella cells directly below the quiescent centre, and by the lateral root cap cells that surround the meristematic region. In addition to its role in gravitropism, the root cap protects the meristem from physical damages caused by penetration in the soil. Moreover, during the first three days after germination, the root cap cells display a thin cuticle, involved in salt stress protection. Root cap cells are perpetually growing and shed layer by layer once a new row of cells is generated (Barlow, 2002). These “root cap border cells” still secrete exudates once detached, and are thought to release extracellular DNA to trap pathogens (Driouich *et al.*, 2013; Hawes *et al.*, 2016).

Roots display a developmental gradient across their longitudinal axis, with newly generated cells being pushed away from the meristematic region the more they differentiate. Once they reach the elongation zone (EZ), cells stop to divide and start to elongate, before they enter the differentiation zone (DZ) where they develop their final features (Schiefelbein and Benfey, 1991). It is only in that region that the structural barriers of the endodermis are established. The lignified Casparian strip ensures an apoplastic diffusion barrier for nutrients (Naseer *et al.*, 2012), while suberin lamellae depositions, appearing later in development, block the uptake of water and nutrients from the apoplast to the endodermal cytoplasm (Barberon *et al.*, 2016). Similar barriers can be observed in the exodermis, the outermost cortical cell layer, located just below the epidermis. Overall, roots are complex organs with tissue-specific structural properties which interfere with microbial colonization.

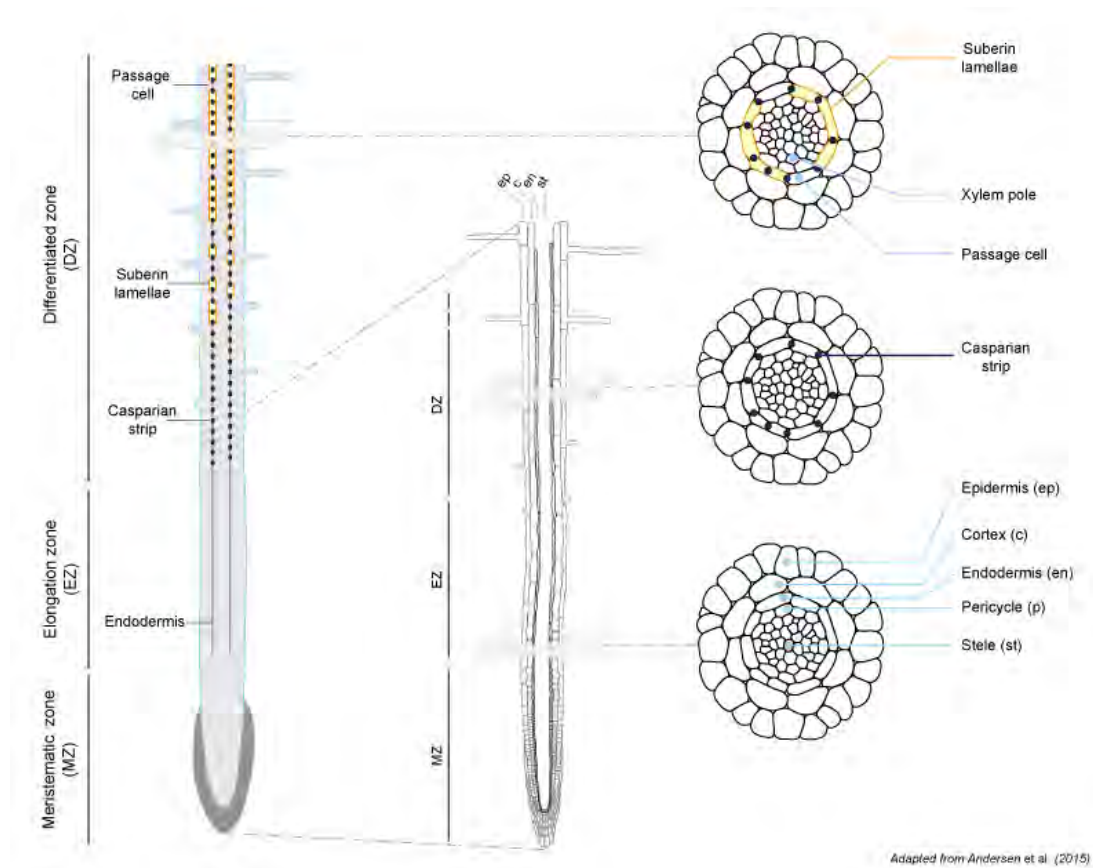


Figure 2 : Anatomical structure of the root with a close-up view of the model organism *Arabidopsis thaliana*.

Roots are divided in three parts: the meristematic zone (MZ), the elongation zone (EZ) and the differentiated zone (DZ). The EZ starts when cells begin to elongate and stops at the appearance of the first root hair cells. Once differentiated, cells establish a diffusion barrier made of two features. The Casparian strip seals the endodermal cells together and blocks the apoplastic diffusion. The endodermis (en) is later coated with suberin lamellae. Some cells, called endodermal passage cells, are situated in front of the xylem poles and remain devoid of suberin to allow nutrient exchange.

1.7.2. INTERACTION OF RHIZOSPHERE MICROBES WITH THE ROOT

Though recent progresses in metagenomics allowed to decipher the general composition of the root microbiome and its functions (Bulgarelli *et al.*, 2013), data on the spatial structure of the community are still scarce. They are mostly based on histological studies of pathogen infections, deciphering their entry points and invasion routes. The different root tissues and regions have indeed distinct properties that shape the preference of microbes for a specific niche.

Microbes that attempt to colonize the root will first meet the epidermis. In leaves, pathogens often enter through stomata or hydathodes to bypass the cuticle (Faulkner and Robatzek, 2012; Ziv *et al.*, 2018). However, the absence of cuticle on the root make it easier for the rhizosphere microbiota to directly interact with the cell walls. The rhizosphere

community is nevertheless not homogenous. DeAngelis *et al.* (2009) showed that microorganisms spread along the root following a longitudinal gradient and tend to accumulate around the root tip and root hairs. Around 8% of taxa retrieved from their analysis of wild oat (*Avena fatua*) display root-zone dependent enrichment. Some bacteria from *Bacteroides* phyla or from *Bacillus*, *Rhizobium* and *Azospirillum* genus concentrate at the root tip or in the elongation zone. This might be due to local variations in metabolites released alongside the root axis (Cardinale *et al.*, 2015; Massalha *et al.*, 2017b; Pini *et al.*, 2017; Santos *et al.*, 2017, 2011). Other bacteria strains like *Pseudomonas fluorescens* or *Azospirillum brasilense* are found in mature regions or all along the root. Root hairs also form a specific niche and their absence alter the microbiota composition (Eynck *et al.*, 2007; Robertson-Albertyn *et al.*, 2017; Santos *et al.*, 2017; Schmidt *et al.*, 2018; Zhou *et al.*, 2020). Interestingly, bacteria tend to accumulate in the ridge between epidermis cell borders (Schmidt *et al.*, 2018).

A fraction of this microbiota colonizes also the endosphere (Berg *et al.*, 2014). Most of endophytes subsist inside or in between the epidermis and cortex cells (Bulgarelli *et al.*, 2013; Schmidt *et al.*, 2018). Their progression is thought to be stopped by endodermal barriers (Geldner, 2013). Thus, the mutualist *Piriformospora indica* enters the root in the differentiated region and colonizes only the epidermis and the cortex (Jacobs *et al.*, 2011). Arbuscular mycorrhizal fungi need to cross the exodermis to form arbuscules in the cortical region. Interestingly, they do so by entering through exodermal passage cells, which are exempt of suberin lamellae (Enstone *et al.*, 2002). Interestingly, in *Petunia*, these same cells express specifically the PDR1 exporter, which releases strigolactone hormone known to attract arbuscular mycorrhizal fungi (Borghi *et al.*, 2016; Kretzschmar *et al.*, 2012; Steinkellner *et al.*, 2007).

Successful pathogens usually penetrate the root until the stele, where they use the vasculature to spread throughout the plant. Fungi tend to grow intracellularly, using appressoria to break through the cell walls, but they can also extend their hyphae in the apoplast. Thus, *Verticillium longisporum* colonizes the xylem of *Brassica napus* crossing the cell wall (Eynck *et al.*, 2007). The oomycete *Phytophthora parasitica* invades root hairs or the elongation zone (Attard *et al.*, 2010). In contrast, soilborne bacterial pathogens like *Ralstonia solanacearum* invade roots between cells and develop extracellularly, inducing cell death in the endodermis (Digonnet *et al.*, 2012; Faulkner and Robatzek, 2012).

Nevertheless, damaged sites, or zones with weaker barriers, are preferential entry points for microbes. Like many commensals, *R. solanacearum* and *F. oxysporum* target the elongation zone where endodermal barriers are not yet established, possibly allowing invaders to break into more easily (Czymmek *et al.*, 2007; Digonnet *et al.*, 2012). Several bacteria (*R. solanacearum*, *Rhizobia*) and fungi (*F. oxysporum*, *F. solani*) also accumulate and penetrate at lateral root emergence sites (Czymmek *et al.*, 2007; Digonnet *et al.*, 2012; Perrine-Walker *et al.*, 2007; Zhou *et al.*, 2020). Indeed, the formation of the primordia, going through the endodermis and outer layers, causes the Casparian strip to be temporarily degraded and the suberin deposition to be remodelled (Ursache *et al.*, 2020; Vermeer *et al.*, 2014).

The many inhabitants of the rhizosphere and endosphere have as diverse colonization mechanisms as life strategies. Whether the spatial composition of the root community is controlled by plant defence responses is so far unknown. Although root structural barriers have always been considered important to protect the root, no clear data supports a role against pathogens or other members of the microbiota. Moreover, their effect might strongly vary from one microbe to another. However, roots can also induce immune responses.

1.7.3. MAMP-TRIGGERED IMMUNITY ALSO OCCURS IN THE ROOT

In contrast to root symbiosis, little is known about the root-specific molecular processes activated in response to pathogens or commensals. Analyses using classical or confocal microscopy permitted to decipher the mode of entry and the propagation of some pathogens in great details. However, these descriptive investigations did not focus on the actual activation of defences (see review De Coninck *et al.*, 2015).

Nevertheless, the study of various patho-systems could report that hormonal pathways usually involved in shoots were also induced in the root by soil microbes (Chuberre *et al.*, 2018; De Coninck *et al.*, 2015). Despite this similarity, the activation of *Arabidopsis* genes known to be triggered by defence pathways (later called “reporter” or “marker” genes) was somewhat different between root and shoot (Badri *et al.*, 2009). These discrepancies were also observed for other *Brassica* species (Papadopoulou *et al.*, 2018; Tytgat *et al.*, 2013). The usual antagonism between the salicylic acid and the jasmonic

acid/ethylene pathway was not always conserved: indeed, *Phytophthora parasitica* surprisingly induces both SA and JA/ET pathways during its necrotrophic phase, while in leaves, necrotrophy is generally admitted to activate only the JA/ET pathway (Attard *et al.*, 2010). In addition, single cell ablation of root epidermis can induce ethylene but not JA, the classical hallmark of wounding response in leaves (Marhavý *et al.*, 2019).

It is only recently that some studies shed light on MTI signalling in roots. Like in leaves, MAMPs, DAMPs and root knot nematodes elicitors induce ROS burst, calcium influxes, phosphorylation of AtMAPK3 and 6, activation of marker genes and camalexin production (Jacobs *et al.*, 2011; Jing *et al.*, 2020; Millet *et al.*, 2010; Ranf *et al.*, 2011; Teixeira *et al.*, 2016; Wyrsh *et al.*, 2015). Flagellin-induced callose deposition was also dependent on ethylene, yet independent of salicylic acid (Millet *et al.*, 2010). Among the strongest genes induced by MAMPs and DAMPs can be found *FRK1* (*FLG22-INDUCED RECEPTOR-LIKE KINASE 1*), *PER5* (*PEROXIDASE 5*), *MYB51*, *WRKY11* or *CYP71A12* (Beck *et al.*, 2014; Jacobs *et al.*, 2011; Marhavý *et al.*, 2019; Millet *et al.*, 2010; Poncini *et al.*, 2017; Yu *et al.*, 2019a; Zhou *et al.*, 2020). Moreover, flg22 causes the release of DNA-containing extracellular traps by pea root border cells, that can immobilize *R. solanacearum* pathogens (Hawes *et al.*, 2011; Tran *et al.*, 2016). In response to flg22 and PGN, root border cells of *Arabidopsis* and flax also produce ROS, callose deposition and induction of defence genes (Plancot *et al.*, 2013).

Interestingly, each MAMP induces its specific spatial pattern of defence. The development of new transcriptional read-outs of immunity, based on GUS staining or fluorochrome tags, offers today a first glimpse at the delicate cartography of defence (Millet *et al.*, 2010; Poncini *et al.*, 2017). As such, AtPep1 induces stronger Ca²⁺ and immune transcriptional read-out responses in the root than in the shoot (Poncini *et al.*, 2017; Ranf *et al.*, 2011). Similarly, chitin generates callose depositions all along the root (Millet *et al.*, 2010). On the other hand, flagellin- and peptidoglycan-triggered gene activation and callose formation are restricted to the elongation zone and lateral root primordia. Yet, Jacobs *et al.* (2011) observed flg22-elicited callose deposition on the whole root. Flg22- and elf18-induced calcium waves are also severely reduced in the root in comparison to leaves (Ranf *et al.*, 2011). Consistently, elf18 has no effect on defence reporters or callose deposition in the root (Millet *et al.*, 2010). Altogether, these data indicate that root defence responses are either abolished (elf18) or strongly downregulated (flg22 and PGN) for bacterial elicitors.

The responses to flagellin are particularly interesting since they are locally confined to sites particularly attractive for bacteria like the root tip or the lateral root primordia (Millet *et al.*, 2010).

One might ask how defences can be reduced or enclosed to such a restricted area. Ranf *et al.* (2011) suggested the involvement of PRRs, because the predicted expression levels for *FLS2* and *EFR* were extremely low in roots compared to shoot. By contrast, *PEPR1* and *PEPR2* are strongly expressed in the whole root or in the stele, respectively (Bartels *et al.*, 2013). Accordingly, Beck *et al.* (2014) showed that *FLS2* accumulates in wounded spots and stomata on leaves and was restricted to the stele and lateral primordia in roots. However, *FLS2* expression was excluded from the elongation zone and was surprisingly not coinciding with flg22-inducible defences. To assess the role of *FLS2* expression pattern in the confinement of immune responses, Wyrsh *et al.* (2015) expressed *FLS2* in specific root tissues. They observed that MTI responses were maintained independently of the cell-type expressing *FLS2*. Moreover, the strength of the response was not proportional to the amount of *FLS2* proteins expressed. Despite the lack of resolution of their analysis, they proposed that flg22-mediated immune responses were cell-autonomous, and that flg22-responsiveness was not constant across tissues.

Overall, even if the core machinery of MAMP-triggered immunity is conserved between shoot and roots, substantial differences have been described, notably concerning the precise localisation of immune responses. Such a delicate spatial control of immune response might prove to be central to balance growth and defence.

1.8. SCOPE OF THE PHD THESIS

Despite decades of research on the interaction between plants and pathogens, very little interest was given, until recently, to the activation of MAMP-triggered immune responses in the roots. However, the rapid development of microbiome analyses is now putting into light the complex community living in the rhizosphere. Understanding how plants accommodate so many different microorganisms while keeping immune responses under control is now at the heart of the plant-pathogen field. In that context, regulation of PRRs is thought to play a key role to regulate the activation of defences and to define the structure of the root microbiota. Despite the local component of MTI, immune responses were rarely assessed with cellular resolution. The main goal of this thesis project was to precisely map MTI responses and to investigate the biological significance of spatial regulation of immunity in the roots.

Root were shown to restrict most of their bacterial MAMP-triggered immune responses in the elongation zone. However, it was not understood how plants regulate the localization of their defence. In **Chapter 2**, we investigate, in collaboration with Dr. Feng Zhou, how root damages can gate plant immune responses in otherwise unresponsive root zones. This chapter is a published article in *Cell* extended with complementary information and experiments.

Although MTI is generally considered as an intrinsic feature of all plant cells, there is now increasing evidence suggesting that not all root tissues respond equivalently. However, tissue competency and its impact on growth was never assessed with a cellular resolution. In **Chapter 3**, I combined tissue-specific expression of the FLS2 receptor with cell type-specific markers of defence to map flg22-responsiveness throughout the root. This allowed me to identify lines that are super-competent to flg22 perception with severe effects on root growth. The chapter is a manuscript posted on BioRxiv, now under review in *Current Biology*.

In **Chapter 4**, I investigated how plants with misbalanced growth-defence trade-off are impacted by their microbiome and how, in turn, they influence the structure of the rhizosphere community.

Commensal bacteria can also modulate MTI responses to avoid activation of defences. In **Chapter 5**, I used our previously identified super-competent line to screen a collection of *Pseudomonas protegens* CHA0 mutants to identify possible mechanisms of MTI suppression.

MAMP and DAMP-triggered immunity can mutually amplify their responses, using the ethylene signalling cascade as an intermediary. However, this dependency to ethylene was not yet shown in roots. The **Chapter 6** explores the link between AtPep1, flg22 and ethylene signalling.

Lignin deposition is a characteristic component of pathogen defence but was rarely used as a direct output of MTI. In **Chapter 7**, I described the similarity between flg22-inducible lignin deposition and compensatory lignin induced in response to the loss of Casparian strip integrity. This chapter presents data obtained in collaboration with Dr. Yan Ma.

Chapter 8 contains concluding remarks integrating results from all chapters and provides perspectives for future studies.

1.9. LITERATURE

- Adams-Phillips, L., Briggs, A.G., and Bent, A.F. (2010). Disruption of Poly(ADP-ribosyl)ation Mechanisms Alters Responses of *Arabidopsis* to Biotic Stress. *Plant Physiol.* *152*, 267–280.
- Ahuja, I., Kissen, R., and Bones, A.M. (2012). Phytoalexins in defense against pathogens. *Trends Plant Sci.* *17*, 73–90.
- Albrecht, C., Boutrot, F., Segonzac, C., Schwessinger, B., Gimenez-Ibanez, S., Chinchilla, D., Rathjen, J.P., de Vries, S.C., and Zipfel, C. (2012). Brassinosteroids inhibit pathogen-associated molecular pattern-triggered immune signaling independent of the receptor kinase BAK1. *Proc. Natl. Acad. Sci.* *109*, 303–308.
- Amano, Y., Tsubouchi, H., Shinohara, H., Ogawa, M., and Matsubayashi, Y. (2007). Tyrosine-sulfated glycopeptide involved in cellular proliferation and expansion in *Arabidopsis*. *Proc. Natl. Acad. Sci.* *104*, 18333–18338.
- Asai, S., and Shirasu, K. (2015). Plant cells under siege: plant immune system versus pathogen effectors. *Curr. Opin. Plant Biol.* *28*, 1–8.
- Asai, T., Tena, G., Plotnikova, J., Willmann, M.R., Chiu, W.-L., Gomez-Gomez, L., Boller, T., Ausubel, F.M., and Sheen, J. (2002). MAP kinase signalling cascade in *Arabidopsis* innate immunity. *Nature* *415*, 977–983.
- Attard, A., Gourgues, M., Callemeyn-Torre, N., and Keller, H. (2010). The immediate activation of defense responses in *Arabidopsis* roots is not sufficient to prevent *Phytophthora parasitica* infection. *New Phytol.* *187*, 449–460.
- Baayen, R.P., Ouellette, G.B., and Rioux, D. (1996). Compartmentalization of decay in carnations resistant to *Fusarium oxysporum f. sp. dianthi*. *Phytopathology* *86*, 1018–1031.
- Badri, D.V., Quintana, N., Kassis, E.G.E., Kim, H.K., Choi, Y.H., Sugiyama, A., Verpoorte, R., Martinoia, E., Manter, D.K., and Vivanco, J.M. (2009). An ABC Transporter Mutation Alters Root Exudation of Phytochemicals That Provoke an Overhaul of Natural Soil Microbiota. *Plant Physiol.* *151*, 2006–2017.
- Bai, M.-Y., Fan, M., Oh, E., and Wang, Z.-Y. (2012). A Triple Helix-Loop-Helix/Basic Helix-Loop-Helix Cascade Controls Cell Elongation Downstream of Multiple Hormonal and Environmental Signaling Pathways in *Arabidopsis*. *Plant Cell* *24*, 4917–4929.
- Bai, Y., Müller, D.B., Srinivas, G., Garrido-Oter, R., Potthoff, E., Rott, M., Dombrowski, N., Münch, P.C., Spaepen, S., Remus-Emsermann, M., *et al.* (2015). Functional overlap of the *Arabidopsis* leaf and root microbiota. *Nature* *528*, 364–369.
- Bais, H.P., Weir, T.L., Perry, L.G., Gilroy, S., and Vivanco, J.M. (2006). The Role of Root Exudates in Rhizosphere Interactions with Plants and Other Organisms. *Annu. Rev. Plant Biol.* *57*, 233–266.
- Barberon, M. (2017). The endodermis as a checkpoint for nutrients. *New Phytol.* *213*, 1604–1610.
- Barberon, M., Vermeer, J.E.M., De Bellis, D., Wang, P., Naseer, S., Andersen, T.G., Humbel, B.M., Nawrath, C., Takano, J., Salt, D.E., *et al.* (2016). Adaptation of Root Function by Nutrient-Induced Plasticity of Endodermal Differentiation. *Cell.* *164*, 447 – 459.
- Barlow, P.W. (2002). The Root Cap: Cell Dynamics, Cell Differentiation and Cap Function. *J. Plant Growth Regul.* *21*, 261–286.
- Bartels, S., and Boller, T. (2015). Quo vadis, Pep? Plant elicitor peptides at the crossroads of immunity, stress, and development. *J. Exp. Bot.* *66*, 5183–5193.

- Bartels, S., Lori, M., Mbengue, M., Verk, M. van, Klauser, D., Hander, T., Böni, R., Robatzek, S., and Boller, T. (2013). The family of Peps and their precursors in *Arabidopsis*: differential expression and localization but similar induction of pattern-triggered immune responses. *J. Exp. Bot.* *64*, 5309–5321.
- Beck, M., Wyrsh, I., Strutt, J., Wimalasekera, R., Webb, A., Boller, T., and Robatzek, S. (2014). Expression patterns of *FLAGELLIN SENSING 2* map to bacterial entry sites in plant shoots and roots. *J. Exp. Bot.* *65*, 6487–6498.
- Belkhadir, Y., Jaillais, Y., Epple, P., Balsemão-Pires, E., Dangl, J.L., and Chory, J. (2012). Brassinosteroids modulate the efficiency of plant immune responses to microbe-associated molecular patterns. *Proc. Natl. Acad. Sci.* *109*, 297–302.
- Belkhadir, Y., Yang, L., Hetzel, J., Dangl, J.L., and Chory, J. (2014). The growth–defense pivot: crisis management in plants mediated by LRR-RK surface receptors. *Trends Biochem. Sci.* *39*, 447–456.
- Berendsen, R.L., Pieterse, C.M.J., and Bakker, P.A.H.M. (2012). The rhizosphere microbiome and plant health. *Trends Plant Sci.* *17*, 478–486.
- Berg, G., Grube, M., Schloter, M., and Smalla, K. (2014). Unraveling the plant microbiome: looking back and future perspectives. *Front. Microbiol.* *5*.
- Bernards, M.A. (2002). Demystifying suberin. *Can. J. Bot.* *80*, 227–240.
- Bhuiyan, N.H., Selvaraj, G., Wei, Y., and King, J. (2009). Gene expression profiling and silencing reveal that monolignol biosynthesis plays a critical role in penetration defence in wheat against powdery mildew invasion. *J. Exp. Bot.* *60*, 509–521.
- Bi, G., Zhou, Z., Wang, W., Li, L., Rao, S., Wu, Y., Zhang, X., Menke, F.L.H., Chen, S., and Zhou, J.-M. (2018). Receptor-Like Cytoplasmic Kinases Directly Link Diverse Pattern Recognition Receptors to the Activation of Mitogen-Activated Protein Kinase Cascades in *Arabidopsis*. *Plant Cell* *30*, 1543–1561.
- Boller, T., and Felix, G. (2009). A Renaissance of Elicitors: Perception of Microbe-Associated Molecular Patterns and Danger Signals by Pattern-Recognition Receptors. *Annu. Rev. Plant Biol.* *60*, 379–406.
- Borghi, L., Liu, G.-W., Emonet, A., Kretzschmar, T., and Martinoia, E. (2016). The importance of strigolactone transport regulation for symbiotic signaling and shoot branching. *Planta* *243*, 1351–1360.
- Boudsocq, M., Willmann, M.R., McCormack, M., Lee, H., Shan, L., He, P., Bush, J., Cheng, S.-H., and Sheen, J. (2010). Differential innate immune signalling via Ca²⁺ sensor protein kinases. *Nature* *464*, 418–422.
- Boutrot, F., and Zipfel, C. (2017). Function, Discovery, and Exploitation of Plant Pattern Recognition Receptors for Broad-Spectrum Disease Resistance. *Annu. Rev. Phytopathol.* *55*, 257–286.
- Boutrot, F., Segonzac, C., Chang, K.N., Qiao, H., Ecker, J.R., Zipfel, C., and Rathjen, J.P. (2010). Direct transcriptional control of the *Arabidopsis* immune receptor FLS2 by the ethylene-dependent transcription factors EIN3 and EIL1. *Proc. Natl. Acad. Sci.* *107*, 14502–14507.
- Brutus, A., Sicilia, F., Macone, A., Cervone, F., and Lorenzo, G.D. (2010). A domain swap approach reveals a role of the plant wall-associated kinase 1 (WAK1) as a receptor of oligogalacturonides. *Proc. Natl. Acad. Sci.* *107*, 9452–9457.
- Bücherl, C.A., Jarsch, I.K., Schudoma, C., Segonzac, C., Mbengue, M., Robatzek, S., MacLean, D., Ott, T., and Zipfel, C. (2017). Plant immune and growth receptors share common signalling components but localise to distinct plasma membrane nanodomains. *ELife* *6*, e25114.

- Bulgarelli, D., Rott, M., Schlaeppi, K., Ver Loren van Themaat, E., Ahmadinejad, N., Assenza, F., Rauf, P., Huettel, B., Reinhardt, R., Schmelzer, E., *et al.* (2012). Revealing structure and assembly cues for *Arabidopsis* root-inhabiting bacterial microbiota. *Nature* *488*, 91–95.
- Bulgarelli, D., Schlaeppi, K., Spaepen, S., van Themaat, E.V.L., and Schulze-Lefert, P. (2013). Structure and Functions of the Bacterial Microbiota of Plants. *Annu. Rev. Plant Biol.* *64*, 807–838.
- Bulgarelli, D., Garrido-Oter, R., Münch, P.C., Weiman, A., Dröge, J., Pan, Y., McHardy, A.C., and Schulze-Lefert, P. (2015). Structure and Function of the Bacterial Root Microbiota in Wild and Domesticated Barley. *Cell Host Microbe* *17*, 392–403.
- Buscaill, P., Chandrasekar, B., Sanguankiattichai, N., Kourelis, J., Kaschani, F., Thomas, E.L., Morimoto, K., Kaiser, M., Preston, G.M., and Ichinose, Y. (2019). Glycosidase and glycan polymorphism control hydrolytic release of immunogenic flagellin peptides. *PLANT Sci.* *364*, eaav0748.
- Campbell, M.M., and Ellis, B.E. (1992). Fungal elicitor-mediated responses in pine cell cultures. *Planta* *186*, 409–417.
- Cao, Y., Liang, Y., Tanaka, K., Nguyen, C.T., Jedrzejczak, R.P., Joachimiak, A., and Stacey, G. (2014). The kinase LYK5 is a major chitin receptor in *Arabidopsis* and forms a chitin-induced complex with related kinase CERK1. *ELife* *3*, e03766.
- Cardinale, M., Grube, M., Erlacher, A., Quehenberger, J., and Berg, G. (2015). Bacterial networks and co-occurrence relationships in the lettuce root microbiota. *Environ. Microbiol.* *17*, 239–252.
- Castrillo, G., Teixeira, P.J.P.L., Paredes, S.H., Law, T.F., de Lorenzo, L., Feltcher, M.E., Finkel, O.M., Breakfield, N.W., Mieczkowski, P., Jones, C.D., *et al.* (2017). Root microbiota drive direct integration of phosphate stress and immunity. *Nature* *543*, 513–518.
- Chezem, W.R., Memon, A., Li, F.-S., Weng, J.-K., and Clay, N.K. (2017). SG2-type R2R3-MYB transcription factor MYB15 controls defense-induced lignification and basal immunity in *Arabidopsis*. *The Plant Cell* *29*, 1907–1926.
- Chinchilla, D., Bauer, Z., Regenass, M., Boller, T., and Felix, G. (2006). The *Arabidopsis* Receptor Kinase FLS2 Binds flg22 and Determines the Specificity of Flagellin Perception. *Plant Cell* *18*, 465–476.
- Chinchilla, D., Zipfel, C., Robatzek, S., Kemmerling, B., Nürnberger, T., Jones, J.D.G., Felix, G., and Boller, T. (2007). A flagellin-induced complex of the receptor FLS2 and BAK1 initiates plant defence. *Nature* *448*, 497–500.
- Choi, J., Tanaka, K., Cao, Y., Qi, Y., Qiu, J., Liang, Y., Lee, S.Y., and Stacey, G. (2014). Identification of a Plant Receptor for Extracellular ATP. *Science* *343*, 290–294.
- Choi, W.-G., Hilleary, R., Swanson, S.J., Kim, S.-H., and Gilroy, S. (2016). Rapid, Long-Distance Electrical and Calcium Signaling in Plants. *Annu. Rev. Plant Biol.* *67*, 287–307.
- Chuberre, C., Plancot, B., Driouich, A., Moore, J.P., Bardor, M., Gügi, B., and Vitré, M. (2018). Plant Immunity Is Compartmentalized and Specialized in Roots. *Front. Plant Sci.* *9*, 1692.
- Clay, N.K., Adio, A.M., Denoux, C., Jander, G., and Ausubel, F.M. (2009). Glucosinolate Metabolites Required for an *Arabidopsis* Innate Immune Response. *Science* *323*, 95–101.
- Couto, D., and Zipfel, C. (2016). Regulation of pattern recognition receptor signalling in plants. *Nat. Rev. Immunol.* *16*, 537.
- Couto, D., Niebergall, R., Liang, X., Bücherl, C.A., Sklenar, J., Macho, A.P., Ntoukakis, V., Derbyshire, P., Altenbach, D., Maclean, D., *et al.* (2016). The *Arabidopsis* Protein Phosphatase PP2C38 Negatively Regulates the Central Immune Kinase BIK1. *PLOS Pathog.* *12*, e1005811.
- Czymmek, K.J., Fogg, M., Powell, D.H., Sweigard, J., Park, S.-Y., and Kang, S. (2007). In vivo time-lapse documentation using confocal and multi-photon microscopy reveals the mechanisms of

- invasion into the *Arabidopsis* root vascular system by *Fusarium oxysporum*. *Fungal Genet. Biol.* *44*, 1011–1023.
- Dangl, J.L., and Jones, J.D.G. (2001). Plant pathogens and integrated defence responses to infection. *Nature* *411*, 826–833.
- De Coninck, B., Timmermans, P., Vos, C., Cammue, B.P.A., and Kazan, K. (2015). What lies beneath: belowground defense strategies in plants. *Trends Plant Sci.* *20*, 91–101.
- DeAngelis, K.M., Brodie, E.L., DeSantis, T.Z., Andersen, G.L., Lindow, S.E., and Firestone, M.K. (2009). Selective progressive response of soil microbial community to wild oat roots. *ISME J.* *3*, 168–178.
- Denoux, C., Galletti, R., Mammarella, N., Gopalan, S., Werck, D., De Lorenzo, G., Ferrari, S., Ausubel, F.M., and Dewdney, J. (2008). Activation of Defense Response Pathways by OGs and Flg22 Elicitors in *Arabidopsis* Seedlings. *Mol. Plant* *1*, 423–445.
- Digonnet, C., Martinez, Y., Denancé, N., Chasseray, M., Dabos, P., Ranocha, P., Marco, Y., Jauneau, A., and Goffner, D. (2012). Deciphering the route of *Ralstonia solanacearum* colonization in *Arabidopsis thaliana* roots during a compatible interaction: focus at the plant cell wall. *Planta* *236*, 1419–1431.
- Drerup, M.M., Schlücking, K., Hashimoto, K., Manishankar, P., Steinhorst, L., Kuchitsu, K., and Kudla, J. (2013). The Calcineurin B-Like Calcium Sensors CBL1 and CBL9 Together with Their Interacting Protein Kinase CIPK26 Regulate the *Arabidopsis* NADPH Oxidase RBOHF. *Mol. Plant* *6*, 559–569.
- Drriouch, A., Follet-Gueye, M.-L., Vitré-Gibouin, M., and Hawes, M. (2013). Root border cells and secretions as critical elements in plant host defense. *Curr. Opin. Plant Biol.* *16*, 489–495.
- Dubiella, U., Seybold, H., Durian, G., Komander, E., Lassig, R., Witte, C.-P., Schulze, W.X., and Romeis, T. (2013). Calcium-dependent protein kinase/NADPH oxidase activation circuit is required for rapid defense signal propagation. *Proc. Natl. Acad. Sci.* *110*, 8744–8749.
- Durán, P., Thiergart, T., Garrido-Oter, R., Agler, M., Kemen, E., Schulze-Lefert, P., and Hacquard, S. (2018). Microbial Interkingdom Interactions in Roots Promote *Arabidopsis* Survival. *Cell* *175*, 973-983.e14.
- Edwards, J., Johnson, C., Santos-Medellín, C., Lurie, E., Podishetty, N.K., Bhatnagar, S., Eisen, J.A., and Sundaresan, V. (2015). Structure, variation, and assembly of the root-associated microbiomes of rice. *Proc. Natl. Acad. Sci.* *112*, E911–E920.
- Enstone, D.E., Peterson, C.A., and Ma, F. (2002). Root Endodermis and Exodermis: Structure, Function, and Responses to the Environment. *J. Plant Growth Regul.* *21*, 335–351.
- Eynck, C., Koopmann, B., Grunewaldt-Stoecker, G., Karlovsky, P., and Tiedemann, A. von (2007). Differential interactions of *Verticillium longisporum* and *V. dahliae* with *Brassica napus* detected with molecular and histological techniques. *Eur. J. Plant Pathol.* *118*, 259–274.
- Fan, M., Bai, M.-Y., Kim, J.-G., Wang, T., Oh, E., Chen, L., Park, C.H., Son, S.-H., Kim, S.-K., Mudgett, M.B., et al. (2014). The bHLH Transcription Factor HBI1 Mediates the Trade-Off between Growth and Pathogen-Associated Molecular Pattern-Triggered Immunity in *Arabidopsis*. *Plant Cell* *26*, 828–841.
- Faulkner, C., and Robatzek, S. (2012). Plants and pathogens: putting infection strategies and defence mechanisms on the map. *Curr. Opin. Plant Biol.* *15*, 699–707.
- Faulkner, C., Petutschnig, E., Benitez-Alfonso, Y., Beck, M., Robatzek, S., Lipka, V., and Maule, A.J. (2013). LYM2-dependent chitin perception limits molecular flux via plasmodesmata. *Proc. Natl. Acad. Sci.* *110*, 9166–9170.

- Felix, G., Duran, J.D., Volko, S., and Boller, T. (1999). Plants have a sensitive perception system for the most conserved domain of bacterial flagellin. *Plant J.* *18*, 265–276.
- Fliegmann, J., and Felix, G. (2016). Immunity: Flagellin seen from all sides. *Nat. Plants* *2*, 1–2.
- Frei dit Frey, N., Garcia, A.V., Bigeard, J., Zaag, R., Bueso, E., Garmier, M., Pateyron, S., de Tauzia-Moreau, M.-L., Brunaud, V., Balzergue, S., *et al.* (2014). Functional analysis of *Arabidopsis* immune-related MAPKs uncovers a role for MPK3 as negative regulator of inducible defences. *Genome Biol.* *15*, R87.
- Frey, N.F. dit, Mbengue, M., Kwaaitaal, M., Nitsch, L., Altenbach, D., Häweker, H., Lozano-Duran, R., Njo, M.F., Beeckman, T., Huettel, B., *et al.* (2012). Plasma Membrane Calcium ATPases Are Important Components of Receptor-Mediated Signaling in Plant Immune Responses and Development. *Plant Physiol.* *159*, 798–809.
- Gao, Z., Karlsson, I., Geisen, S., Kowalchuk, G., and Jousset, A. (2018). Protists: Puppet Masters of the Rhizosphere Microbiome. *Trends Plant Sci.* *24*, 165 - 176.
- Geldner, N. (2013). The Endodermis. *Annu. Rev. Plant Biol.* *64*, 531–558.
- Gilroy, S., Suzuki, N., Miller, G., Choi, W.-G., Toyota, M., Devireddy, A.R., and Mittler, R. (2014). A tidal wave of signals: calcium and ROS at the forefront of rapid systemic signaling. *Trends Plant Sci.* *19*, 623–630.
- Gilroy, S., Białasek, M., Suzuki, N., Górecka, M., Devireddy, A., Karpinski, S., and Mittler, R. (2016). ROS, Calcium and Electric Signals: Key Mediators of Rapid Systemic Signaling in Plants. *Plant Physiol.* *171*, 1606.
- Glazebrook, J. (2005). Contrasting Mechanisms of Defense Against Biotrophic and Necrotrophic Pathogens. *Annu. Rev. Phytopathol.* *43*, 205–227.
- Gómez-Gómez, L., and Boller, T. (2000). FLS2: An LRR Receptor-like Kinase Involved in the Perception of the Bacterial Elicitor Flagellin in *Arabidopsis*. *Mol. Cell* *5*, 1003–1011.
- Gómez-Gómez, L., Felix, G., and Boller, T. (1999). A single locus determines sensitivity to bacterial flagellin in *Arabidopsis thaliana*. *Plant J.* *18*, 277–284.
- Goswami, D., Thakker, J.N., and Dhandhukia, P.C. (2016). Portraying mechanics of plant growth promoting rhizobacteria (PGPR): A review. *Cogent Food Agric.* *2*, 1127500.
- Guo, H., Li, L., Ye, H., Yu, X., Algreen, A., and Yin, Y. (2009). Three related receptor-like kinases are required for optimal cell elongation in *Arabidopsis thaliana*. *Proc. Natl. Acad. Sci.* *106*, 7648–7653.
- Gust, A.A., Pruitt, R., and Nürnberger, T. (2017). Sensing Danger: Key to Activating Plant Immunity. *Trends Plant Sci.* *22*, 779–791.
- Gutjahr, C., and Parniske, M. (2013). Cell and Developmental Biology of Arbuscular Mycorrhiza Symbiosis. *Annu. Rev. Cell Dev. Biol.* *29*, 593–617.
- Hacquard, S. (2016). Disentangling the factors shaping microbiota composition across the plant holobiont. *New Phytol.* *209*, 454–457.
- Hacquard, S., Spaepen, S., Garrido-Oter, R., and Schulze-Lefert, P. (2017). Interplay Between Innate Immunity and the Plant Microbiota. *Annu. Rev. Phytopathol.* *55*, 565–589.
- Halter, T., Imkampe, J., Mazzotta, S., Wierzba, M., Postel, S., Bücherl, C., Kiefer, C., Stahl, M., Chinchilla, D., Wang, X., *et al.* (2014). The Leucine-Rich Repeat Receptor Kinase BIR2 Is a Negative Regulator of BAK1 in Plant Immunity. *Curr. Biol.* *24*, 134–143.

- Hander, T., Fernández-Fernández, Á.D., Kumpf, R.P., Willems, P., Schatowitz, H., Rombaut, D., Staes, A., Nolf, J., Pottier, R., Yao, P., *et al.* (2019). Damage on plants activates Ca²⁺-dependent metacaspases for release of immunomodulatory peptides. *Science* 363, eaar7486.
- Hassani, M.A., Durán, P., and Hacquard, S. (2018). Microbial interactions within the plant holobiont. *Microbiome* 6, 58.
- Hawes, M., Allen, C., Turgeon, B.G., Curlango-Rivera, G., Minh Tran, T., Huskey, D.A., and Xiong, Z. (2016). Root Border Cells and Their Role in Plant Defense. *Annu. Rev. Phytopathol.* 54, 143–161.
- Hawes, M.C., Curlango-Rivera, G., Wen, F., White, G.J., VanEtten, H.D., and Xiong, Z. (2011). Extracellular DNA: The tip of root defenses? *Plant Sci.* 180, 741–745.
- Heese, A., Hann, D.R., Gimenez-Ibanez, S., Jones, A.M.E., He, K., Li, J., Schroeder, J.I., Peck, S.C., and Rathjen, J.P. (2007). The receptor-like kinase SERK3/BAK1 is a central regulator of innate immunity in plants. *Proc. Natl. Acad. Sci. U. S. A.* 104, 12217–12222.
- Heil, M., and Land, W.G. (2014). Danger signals – damaged-self recognition across the tree of life. *Plant Biot. Interact.* 5, 578.
- Heil, M., Hilpert, A., Kaiser, W., and Linsenmair, K.E. (2000). Reduced growth and seed set following chemical induction of pathogen defence: does systemic acquired resistance (SAR) incur allocation costs? *J. Ecol.* 88, 645–654.
- Hiruma, K., Gerlach, N., Sacristán, S., Nakano, R.T., Hacquard, S., Kracher, B., Neumann, U., Ramírez, D., Bucher, M., O’Connell, R.J., *et al.* (2016). Root Endophyte *Colletotrichum tofieldiae* Confers Plant Fitness Benefits that Are Phosphate Status Dependent. *Cell* 165, 464–474.
- Hohmann, U., Lau, K., and Hothorn, M. (2017). The Structural Basis of Ligand Perception and Signal Activation by Receptor Kinases. *Annu. Rev. Plant Biol.* 68, 109–137.
- Huffaker, A., Pearce, G., and Ryan, C.A. (2006). An endogenous peptide signal in *Arabidopsis* activates components of the innate immune response. *Proc. Natl. Acad. Sci.* 103, 10098–10103.
- Igarashi, D., Tsuda, K., and Katagiri, F. (2012). The peptide growth factor, phytosulfokine, attenuates pattern-triggered immunity. *Plant J.* 71, 194–204.
- Imkampe, J., Halter, T., Huang, S., Schulze, S., Mazzotta, S., Schmidt, N., Manstretta, R., Postel, S., Wierzbza, M., Yang, Y., *et al.* (2017). The *Arabidopsis* Leucine-Rich Repeat Receptor Kinase BIR3 Negatively Regulates BAK1 Receptor Complex Formation and Stabilizes BAK1. *Plant Cell* 29, 2285–2303.
- Jacobs, S., Zechmann, B., Molitor, A., Trujillo, M., Petutschnig, E., Lipka, V., Kogel, K.-H., and Schäfer, P. (2011). Broad-Spectrum Suppression of Innate Immunity Is Required for Colonization of *Arabidopsis* Roots by the Fungus *Piriformospora indica*. *Plant Physiol.* 156, 726–740.
- Jing, Y., Shen, N., Zheng, X., Fu, A., Zhao, F., Lan, W., and Luan, S. (2020). Danger-Associated Peptide Regulates Root Immune Responses and Root Growth by Affecting ROS Formation in *Arabidopsis*. *Int. J. Mol. Sci.* 21, 4590.
- Kadota, Y., Sklenar, J., Derbyshire, P., Stransfeld, L., Asai, S., Ntoukakis, V., Jones, J.D., Shirasu, K., Menke, F., Jones, A., *et al.* (2014). Direct Regulation of the NADPH Oxidase RBOHD by the PRR-Associated Kinase BIK1 during Plant Immunity. *Mol. Cell* 54, 43–55.
- Kaku, H., Nishizawa, Y., Ishii-Minami, N., Akimoto-Tomiya, C., Dohmae, N., Takio, K., Minami, E., and Shibuya, N. (2006). Plant cells recognize chitin fragments for defense signaling through a plasma membrane receptor. *Proc. Natl. Acad. Sci.* 103, 11086–11091.
- Kamula, S.A., Peterson, C.A., and Mayfield, C.I. (1994). Impact of the exodermis on infection of roots by *Fusarium culmorum*. *Plant Soil* 167, 121–126.

- Keinath, N.F., Kierszniowska, S., Lorek, J., Bourdais, G., Kessler, S.A., Shimosato-Asano, H., Grossniklaus, U., Schulze, W.X., Robatzek, S., and Panstruga, R. (2010). PAMP (Pathogen-associated Molecular Pattern)-induced Changes in Plasma Membrane Compartmentalization Reveal Novel Components of Plant Immunity. *J. Biol. Chem.* *285*, 39140–39149.
- Kessler, S.A., Shimosato-Asano, H., Keinath, N.F., Wuest, S.E., Ingram, G., Panstruga, R., and Grossniklaus, U. (2010). Conserved Molecular Components for Pollen Tube Reception and Fungal Invasion. *Science* *330*, 968–971.
- Khan, M., Subramaniam, R., and Desveaux, D. (2016). Of guards, decoys, baits and traps: pathogen perception in plants by type III effector sensors. *Curr. Opin. Microbiol.* *29*, 49–55.
- Kliebenstein, D.J., Rowe, H.C., and Denby, K.J. (2005). Secondary metabolites influence *Arabidopsis/Botrytis* interactions: variation in host production and pathogen sensitivity. *Plant J.* *44*, 25–36.
- Kretschmar, T., Kohlen, W., Sasse, J., Borghi, L., Schlegel, M., Bachelier, J.B., Reinhardt, D., Bours, R., Bouwmeester, H.J., and Martinoia, E. (2012). A petunia ABC protein controls strigolactone-dependent symbiotic signalling and branching. *Nature* *483*, 341–344.
- Krol, E., Mentzel, T., Chinchilla, D., Boller, T., Felix, G., Kemmerling, B., Postel, S., Arents, M., Jeworutzki, E., Al-Rasheid, K.A.S., *et al.* (2010). Perception of the *Arabidopsis* Danger Signal Peptide 1 Involves the Pattern Recognition Receptor AtPEPR1 and Its Close Homologue AtPEPR2. *J. Biol. Chem.* *285*, 13471–13479.
- Kunze, G., Zipfel, C., Robatzek, S., Niehaus, K., Boller, T., and Felix, G. (2004). The N Terminus of Bacterial Elongation Factor Tu Elicits Innate Immunity in *Arabidopsis* Plants. *Plant Cell* *16*, 3496–3507.
- Kutschera, A., Dawid, C., Gisch, N., Schmid, C., Raasch, L., Gerster, T., Schäffer, M., Smakowska-Luzan, E., Belkhadir, Y., Vlot, A.C., *et al.* (2019). Bacterial medium-chain 3-hydroxy fatty acid metabolites trigger immunity in *Arabidopsis* plants. *Science* *364*, 178–181.
- Kwaaitaal, M., Huisman, R., Maintz, J., Reinstädler, A., and Panstruga, R. (2011). Ionotropic glutamate receptor (iGluR)-like channels mediate MAMP-induced calcium influx in *Arabidopsis thaliana*. *Biochem. J.* *440*, 355–373.
- Lange, B.M., Lapierre, C., and Jr, H.S. (1995). Elicitor-Induced Spruce Stress Lignin (Structural Similarity to Early Developmental Lignins). *Plant Physiol.* *108*, 1277–1287.
- Lathe, W.C., and Bork, P. (2001). Evolution of tuf genes: ancient duplication, differential loss and gene conversion. *FEBS Lett.* *502*, 113–116.
- Lawton, M.A., and Lamb, C.J. (1987). Transcriptional activation of plant defense genes by fungal elicitor, wounding, and infection. *Mol. Cell. Biol.* *7*, 335–341.
- Lee, M.-H., Jeon, H.S., Kim, S.H., Chung, J.H., Roppolo, D., Lee, H.-J., Cho, H.J., Tobimatsu, Y., Ralph, J., and Park, O.K. (2019). Lignin-based barrier restricts pathogens to the infection site and confers resistance in plants. *EMBO J.* *38*, e101948.
- Lesney, M.S. (1989). Growth responses and lignin production in cell suspensions of *Pinus elliottii* 'elicited' by chitin, chitosan or mycelium of *Cronartium quercum f.sp. fusiforme*. *Plant Cell Tissue Organ Cult.* *19*, 23–31.
- Li, C., Yeh, F.-L., Cheung, A.Y., Duan, Q., Kita, D., Liu, M.-C., Maman, J., Luu, E.J., Wu, B.W., Gates, L., *et al.* (2015). Glycosylphosphatidylinositol-anchored proteins as chaperones and co-receptors for FERONIA receptor kinase signaling in *Arabidopsis*. *ELife* *4*, e06587.

- Li, J., Wen, J., Lease, K.A., Doke, J.T., Tax, F.E., and Walker, J.C. (2002). BAK1, an *Arabidopsis* LRR Receptor-like Protein Kinase, Interacts with BRI1 and Modulates Brassinosteroid Signaling. *Cell* *110*, 213–222.
- Li, L., Li, M., Yu, L., Zhou, Z., Liang, X., Liu, Z., Cai, G., Gao, L., Zhang, X., Wang, Y., *et al.* (2014). The FLS2-Associated Kinase BIK1 Directly Phosphorylates the NADPH Oxidase RbohD to Control Plant Immunity. *Cell Host Microbe* *15*, 329–338.
- Li, Y., Yang, Y., Hu, Y., Liu, H., He, M., Yang, Z., Kong, F., Liu, X., and Hou, X. (2019). DELLA and EDS1 Form a Feedback Regulatory Module to Fine-Tune Plant Growth–Defense Tradeoff in *Arabidopsis*. *Mol. Plant* *12*, 1485–1498.
- Liang, X., Ding, P., Lian, K., Wang, J., Ma, M., Li, L., Li, L., Li, M., Zhang, X., Chen, S., *et al.* (2016). *Arabidopsis* heterotrimeric G proteins regulate immunity by directly coupling to the FLS2 receptor. *ELife* *5*, e13568.
- Lin, W., Lu, D., Gao, X., Jiang, S., Ma, X., Wang, Z., Mengiste, T., He, P., and Shan, L. (2013). Inverse modulation of plant immune and brassinosteroid signaling pathways by the receptor-like cytoplasmic kinase BIK1. *Proc. Natl. Acad. Sci.* *110*, 12114–12119.
- Liu, Z., Wu, Y., Yang, F., Zhang, Y., Chen, S., Xie, Q., Tian, X., and Zhou, J.-M. (2013). BIK1 interacts with PEPRs to mediate ethylene-induced immunity. *Proc. Natl. Acad. Sci.* *110*, 6205–6210.
- Lozano-Durán, R., Macho, A.P., Boutrot, F., Segonzac, C., Somssich, I.E., and Zipfel, C. (2013). The transcriptional regulator BZR1 mediates trade-off between plant innate immunity and growth. *ELife* *2*, e00983.
- Lu, D., Wu, S., Gao, X., Zhang, Y., Shan, L., and He, P. (2010). A receptor-like cytoplasmic kinase, BIK1, associates with a flagellin receptor complex to initiate plant innate immunity. *Proc. Natl. Acad. Sci.* *107*, 496–501.
- Lu, D., Lin, W., Gao, X., Wu, S., Cheng, C., Avila, J., Heese, A., Devarenne, T.P., He, P., and Shan, L. (2011). Direct Ubiquitination of Pattern Recognition Receptor FLS2 Attenuates Plant Innate Immunity. *Science* *332*, 1439–1442.
- Luna, E., Pastor, V., Robert, J., Flors, V., Mauch-Mani, B., and Ton, J. (2010). Callose Deposition: A Multifaceted Plant Defense Response. *Mol. Plant. Microbe Interact.* *24*, 183–193.
- Lundberg, D.S., Lebeis, S.L., Paredes, S.H., Yourstone, S., Gehring, J., Malfatti, S., Tremblay, J., Engelbrektson, A., Kunin, V., Rio, T.G. del, *et al.* (2012). Defining the core *Arabidopsis thaliana* root microbiome. *Nature* *488*, 86–90.
- Malinovsky, F.G., Batoux, M., Schwessinger, B., Youn, J.H., Stransfeld, L., Win, J., Kim, S.-K., and Zipfel, C. (2014). Antagonistic Regulation of Growth and Immunity by the *Arabidopsis* Basic Helix-Loop-Helix Transcription Factor HOMOLOG OF BRASSINOSTEROID ENHANCED EXPRESSION2 INTERACTING WITH INCREASED LEAF INCLINATION1 BINDING bHLH1. *Plant Physiol.* *164*, 1443–1455.
- Mang, H., Feng, B., Hu, Z., Boisson-Dernier, A., Franck, C.M., Meng, X., Huang, Y., Zhou, J., Xu, G., Wang, T., *et al.* (2017). Differential Regulation of Two-Tiered Plant Immunity and Sexual Reproduction by ANXUR Receptor-Like Kinases. *Plant Cell* *29*, 3140–3156.
- Marhavý, P., Kurenda, A., Siddique, S., Déneraud Tendon, V., Zhou, F., Holbein, J., Hasan, M.S., Grundler, F.M., Farmer, E.E., and Geldner, N. (2019). Single-cell damage elicits regional, nematode-restricting ethylene responses in roots. *EMBO J.* *38*, e100972.
- Martin, F.M., Uroz, S., and Barker, D.G. (2017). Ancestral alliances: Plant mutualistic symbioses with fungi and bacteria. *Science* *356*, eaad4501.

- Martínez-Medina, A., Wees, S.C.M.V., and Pieterse, C.M.J. (2017). Airborne signals from *Trichoderma* fungi stimulate iron uptake responses in roots resulting in priming of jasmonic acid-dependent defences in shoots of *Arabidopsis thaliana* and *Solanum lycopersicum*. *Plant Cell Environ.* *40*, 2691–2705.
- Massalha, H., Korenblum, E., Tholl, D., and Aharoni, A. (2017a). Small molecules below-ground: the role of specialized metabolites in the rhizosphere. *Plant J.* *90*, 788–807.
- Massalha, H., Korenblum, E., Malitsky, S., Shapiro, O.H., and Aharoni, A. (2017b). Live imaging of root-bacteria interactions in a microfluidics setup. *Proc. Natl. Acad. Sci.* *114*, 4549.
- Matsubayashi, Y., and Sakagami, Y. (2006). Peptide Hormones in Plants. *Annu. Rev. Plant Biol.* *57*, 649–674.
- Mbengue, M., Bourdais, G., Gervasi, F., Beck, M., Zhou, J., Spallek, T., Bartels, S., Boller, T., Ueda, T., Kuhn, H., *et al.* (2016). Clathrin-dependent endocytosis is required for immunity mediated by pattern recognition receptor kinases. *Proc. Natl. Acad. Sci.* *113*, 11034–11039.
- McGurl, B., Pearce, G., Orozco-Cardenas, M., and Ryan, C.A. (1992). Structure, expression, and antisense inhibition of the systemin precursor gene. *Science* *255*, 1570–1573.
- Melotto, M., Zhang, L., Oblessuc, P.R., and He, S.Y. (2017). Stomatal Defense a Decade Later. *Plant Physiol.* *174*, 561–571.
- Menden, B., Kohlhoff, M., and Moerschbacher, B.M. (2007). Wheat cells accumulate a syringyl-rich lignin during the hypersensitive resistance response. *Phytochemistry* *68*, 513–520.
- Meng, X., and Zhang, S. (2013). MAPK Cascades in Plant Disease Resistance Signaling. *Annu. Rev. Phytopathol.* *51*, 245–266.
- Mersmann, S., Bourdais, G., Rietz, S., and Robatzek, S. (2010). Ethylene Signaling Regulates Accumulation of the FLS2 Receptor and Is Required for the Oxidative Burst Contributing to Plant Immunity. *Plant Physiol.* *154*, 391–400.
- Miedes, E., Vanholme, R., Boerjan, W., and Molina, A. (2014). The role of the secondary cell wall in plant resistance to pathogens. *Front. Plant Sci.* *5*.
- Miller, G., Schlauch, K., Tam, R., Cortes, D., Torres, M.A., Shulaev, V., Dangl, J.L., and Mittler, R. (2009). The Plant NADPH Oxidase RBOHD Mediates Rapid Systemic Signaling in Response to Diverse Stimuli. *Sci. Signal.* *2*, ra45.
- Millet, Y.A., Danna, C.H., Clay, N.K., Songnuan, W., Simon, M.D., Werck-Reichhart, D., and Ausubel, F.M. (2010). Innate Immune Responses Activated in *Arabidopsis* Roots by Microbe-Associated Molecular Patterns. *Plant Cell* *22*, 973–990.
- Miya, A., Albert, P., Shinya, T., Desaki, Y., Ichimura, K., Shirasu, K., Narusaka, Y., Kawakami, N., Kaku, H., and Shibuya, N. (2007). CERK1, a LysM receptor kinase, is essential for chitin elicitor signaling in *Arabidopsis*. *Proc. Natl. Acad. Sci.* *104*, 19613–19618.
- Monaghan, J., Matschi, S., Shorinola, O., Rovenich, H., Matei, A., Segonzac, C., Malinovsky, F.G., Rathjen, J.P., MacLean, D., Romeis, T., *et al.* (2014). The Calcium-Dependent Protein Kinase CPK28 Buffers Plant Immunity and Regulates BIK1 Turnover. *Cell Host Microbe* *16*, 605–615.
- Nam, K.H., and Li, J. (2002). BRI1/BAK1, a Receptor Kinase Pair Mediating Brassinosteroid Signaling. *Cell* *110*, 203–212.
- Naseer, S., Lee, Y., Lapierre, C., Franke, R., Nawrath, C., and Geldner, N. (2012). Casparian strip diffusion barrier in *Arabidopsis* is made of a lignin polymer without suberin. *Proc. Natl. Acad. Sci.* *109*, 10101–10106.

- Navarro, L., Dunoyer, P., Jay, F., Arnold, B., Dharmasiri, N., Estelle, M., Voinnet, O., and Jones, J.D.G. (2006). A Plant miRNA Contributes to Antibacterial Resistance by Repressing Auxin Signaling. *Science* *312*, 436–439.
- Ngou, B.P.M., Ahn, H.-K., Ding, P., and Jones, J.D. (2020). Mutual Potentiation of Plant Immunity by Cell-surface and Intracellular Receptors. *BioRxiv* 2020.04.10.034173.
- Nicholson, R.L., and Hammerschmidt, R. (1992). Phenolic Compounds and Their Role in Disease Resistance. *Annu. Rev. Phytopathol.* *30*, 369–389.
- Nürnbergger, T., and Brunner, F. (2002). Innate immunity in plants and animals: emerging parallels between the recognition of general elicitors and pathogen-associated molecular patterns. *Curr. Opin. Plant Biol.* *5*, 318–324.
- Nürnbergger, T., and Lipka, V. (2005). Non-host resistance in plants: new insights into an old phenomenon. *Mol. Plant Pathol.* *6*, 335–345.
- Papadopoulou, G.V., Maedicke, A., Grosser, K., van Dam, N.M., and Martínez-Medina, A. (2018). Defence signalling marker gene responses to hormonal elicitation differ between roots and shoots. *AoB PLANTS* *10*, ply031.
- Parniske, M. (2008). Arbuscular mycorrhiza: the mother of plant root endosymbioses. *Nat. Rev. Microbiol.* *6*, 763–775.
- Pascale, A., Proietti, S., Pantelides, I.S., and Stringlis, I.A. (2020). Modulation of the Root Microbiome by Plant Molecules: The Basis for Targeted Disease Suppression and Plant Growth Promotion. *Front. Plant Sci.* *10*, 1741.
- Pearce, G., Strydom, D., Johnson, S., and Ryan, C.A. (1991). A Polypeptide from Tomato Leaves Induces Wound-Inducible Proteinase Inhibitor Proteins. *Science* *253*, 895–897.
- Pei, Z.-M., Murata, Y., Benning, G., Thomine, S., Klüsener, B., Allen, G.J., Grill, E., and Schroeder, J.I. (2000). Calcium channels activated by hydrogen peroxide mediate abscisic acid signalling in guard cells. *Nature* *406*, 731–734.
- Perraki, A., DeFalco, T.A., Derbyshire, P., Avila, J., Séré, D., Sklenar, J., Qi, X., Stransfeld, L., Schwessinger, B., Kadota, Y., *et al.* (2018). Phosphocode-dependent functional dichotomy of a common co-receptor in plant signalling. *Nature* *561*, 248–252.
- Perrine-Walker, F.M., Prayitno, J., Rolfe, B.G., Weinman, J.J., and Hocart, C.H. (2007). Infection process and the interaction of rice roots with rhizobia. *J. Exp. Bot.* *58*, 3343–3350.
- Petutschnig, E.K., Jones, A.M.E., Serazetdinova, L., Lipka, U., and Lipka, V. (2010). The LysM-RLK CERK1 is a major chitin binding protein in *Arabidopsis thaliana* and subject to chitin-induced phosphorylation. *J. Biol. Chem.* *285*, 28902–28911.
- Pieterse, C.M.J., Van der Does, D., Zamioudis, C., Leon-Reyes, A., and Van Wees, S.C.M. (2012). Hormonal Modulation of Plant Immunity. *Annu. Rev. Cell Dev. Biol.* *28*, 489–521.
- Pieterse, C.M.J., Zamioudis, C., Berendsen, R.L., Weller, D.M., Wees, S.C.M.V., and Bakker, P.A.H.M. (2014). Induced Systemic Resistance by Beneficial Microbes. *Annu. Rev. Phytopathol.* *52*, 347–375.
- Pini, F., East, A.K., Appia-Ayme, C., Tomek, J., Karunakaran, R., Mendoza-Suárez, M., Edwards, A., Terpolilli, J.J., Roworth, J., Downie, J.A., *et al.* (2017). Bacterial Biosensors for in Vivo Spatiotemporal Mapping of Root Secretion. *Plant Physiol.* *174*, 1289–1306.
- Pitzschke, A., Schikora, A., and Hirt, H. (2009). MAPK cascade signalling networks in plant defence. *Curr. Opin. Plant Biol.* *12*, 421–426.

- Plancot, B., Santaella, C., Jaber, R., Kiefer-Meyer, M.C., Follet-Gueye, M.-L., Leprince, J., Gattin, I., Souc, C., Driouich, A., and Vické-Gibouin, M. (2013). Deciphering the Responses of Root Border-Like Cells of *Arabidopsis* and Flax to Pathogen-Derived Elicitors. *Plant Physiol.* *163*, 1584–1597.
- Poncini, L., Wyrsh, I., Tendon, V.D., Vorley, T., Boller, T., Geldner, N., Métraux, J.-P., and Lehmann, S. (2017). In roots of *Arabidopsis thaliana*, the damage-associated molecular pattern AtPep1 is a stronger elicitor of immune signalling than flg22 or the chitin heptamer. *PLOS ONE* *12*, e0185808.
- Ramos, M.V., Demarco, D., Souza, I.C. da C., and Freitas, C.D.T. de (2019). Laticifers, Latex, and Their Role in Plant Defense. *Trends Plant Sci.* *24*, 553–567.
- Ranathunge, K., Thomas, R.H., Fang, X., Peterson, C.A., Gijzen, M., and Bernards, M.A. (2008). Soybean Root Suberin and Partial Resistance to Root Rot Caused by *Phytophthora sojae*. *Phytopathology* *98*, 1179–1189.
- Ranf, S., Wünnenberg, P., Lee, J., Becker, D., Dunkel, M., Hedrich, R., Scheel, D., and Dietrich, P. (2008). Loss of the vacuolar cation channel, AtTPC1, does not impair Ca²⁺ signals induced by abiotic and biotic stresses. *Plant J.* *53*, 287–299.
- Ranf, S., Eschen-Lippold, L., Pecher, P., Lee, J., and Scheel, D. (2011). Interplay between calcium signalling and early signalling elements during defence responses to microbe- or damage-associated molecular patterns. *Plant J.* *68*, 100–113.
- Ranf, S., Eschen-Lippold, L., Fröhlich, K., Westphal, L., Scheel, D., and Lee, J. (2014). Microbe-associated molecular pattern-induced calcium signaling requires the receptor-like cytoplasmic kinases, PBL1 and BIK1. *BMC Plant Biol.* *14*, 374.
- Ranf, S., Gisch, N., Schäffer, M., Illig, T., Westphal, L., Knirel, Y.A., Sánchez-Carballo, P.M., Zähringer, U., Hückelhoven, R., Lee, J., *et al.* (2015). A lectin S-domain receptor kinase mediates lipopolysaccharide sensing in *Arabidopsis thaliana*. *Nat. Immunol.* *16*, 426–433.
- Reinhardt, D.H., and Rost, T.L. (1995). Salinity accelerates endodermal development and induces an exodermis in cotton seedling roots. *Environ. Exp. Bot.* *35*, 563–574.
- Rentel, M.C., and Knight, M.R. (2004). Oxidative Stress-Induced Calcium Signaling in *Arabidopsis*. *Plant Physiol.* *135*, 1471–1479.
- Robatzek, S., Chinchilla, D., and Boller, T. (2006). Ligand-induced endocytosis of the pattern recognition receptor FLS2 in *Arabidopsis*. *Genes Dev.* *20*, 537–542.
- Robertsen, B. (1986). Elicitors of the production of lignin-like compounds in cucumber hypocotyls. *Physiol. Mol. Plant Pathol.* *28*, 137–148.
- Robertson-Albertyn, S., Alegria Terrazas, R., Balbirnie, K., Blank, M., Janiak, A., Szarejko, I., Chmielewska, B., Karcz, J., Morris, J., Hedley, P.E., *et al.* (2017). Root Hair Mutations Displace the Barley Rhizosphere Microbiota. *Front. Plant Sci.* *8*, 1094.
- Rosenberg, E., and Zilber-Rosenberg, I. (2016). Microbes Drive Evolution of Animals and Plants: the Hologenome Concept. *MBio* *7*, e01395-15.
- Roux, M., Schwessinger, B., Albrecht, C., Chinchilla, D., Jones, A., Holton, N., Malinovsky, F.G., Tör, M., Vries, S. de, and Zipfel, C. (2011). The *Arabidopsis* Leucine-Rich Repeat Receptor-Like Kinases BAK1/SERK3 and BKK1/SERK4 Are Required for Innate Immunity to Hemibiotrophic and Biotrophic Pathogens. *Plant Cell* *23*, 2440–2455.
- Saijo, Y., Loo, E.P., and Yasuda, S. (2018). Pattern recognition receptors and signaling in plant-microbe interactions. *Plant J.* *93*, 592–613.
- Santos, A.R.S., Etto, R.M., Furmam, R.W., Freitas, D.L. de, Santos, K.F. d’Eça N., Souza, E.M. de, Pedrosa, F. de O., Ayub, R.A., Steffens, M.B.R., and Galvão, C.W. (2017). Labeled *Azospirillum brasilense*

- wild type and excretion-ammonium strains in association with barley roots. *Plant Physiol. Biochem.* *118*, 422–426.
- Sapp, M., Ploch, S., Fiore-Donno, A.M., Bonkowski, M., and Rose, L.E. (2018). Protists are an integral part of the *Arabidopsis thaliana* microbiome. *Environ. Microbiol.* *20*, 30–43.
- Schiefelbein, J.W., and Benfey, P.N. (1991). The development of plant roots: new approaches to underground problems. *Plant Cell* *3*, 1147–1154.
- Schlaeppli, K., Dombrowski, N., Oter, R.G., Ver Loren van Themaat, E., and Schulze-Lefert, P. (2014). Quantitative divergence of the bacterial root microbiota in *Arabidopsis thaliana* relatives. *Proc. Natl. Acad. Sci.* *111*, 585–592.
- Schmidt, H., Nunan, N., Höck, A., Eickhorst, T., Kaiser, C., Wobken, D., and Raynaud, X. (2018). Recognizing Patterns: Spatial Analysis of Observed Microbial Colonization on Root Surfaces. *Front. Environ. Sci.* *6*, 61.
- Schuhegger, R., Rauhut, T., and Glawischnig, E. (2007). Regulatory variability of camalexin biosynthesis. *J. Plant Physiol.* *164*, 636–644.
- Schulze, B., Mentzel, T., Jehle, A.K., Mueller, K., Beeler, S., Boller, T., Felix, G., and Chinchilla, D. (2010). Rapid Heteromerization and Phosphorylation of Ligand-activated Plant Transmembrane Receptors and Their Associated Kinase BAK1. *J. Biol. Chem.* *285*, 9444–9451.
- Seybold, H., Trempel, F., Ranf, S., Scheel, D., Romeis, T., and Lee, J. (2014). Ca²⁺ signalling in plant immune response: from pattern recognition receptors to Ca²⁺ decoding mechanisms - Seybold - 2014 - - Wiley Online Library. *New Phytol.* *204*, 782–790.
- Shadle, G.L., Wesley, S.V., Korth, K.L., Chen, F., Lamb, C., and Dixon, R.A. (2003). Phenylpropanoid compounds and disease resistance in transgenic tobacco with altered expression of l-phenylalanine ammonia-lyase. *Phytochemistry* *64*, 153–161.
- Shen, Q., Bourdais, G., Pan, H., Robatzek, S., and Tang, D. (2017). *Arabidopsis* glycosylphosphatidylinositol-anchored protein LLG1 associates with and modulates FLS2 to regulate innate immunity. *Proc. Natl. Acad. Sci.* *114*, 5749–5754.
- Shi, H., Liu, Z., Zhu, L., Zhang, C., Chen, Y., Zhou, Y., Li, F., and Li, X. (2012). Overexpression of cotton (*Gossypium hirsutum*) dirigent1 gene enhances lignification that blocks the spread of *Verticillium dahliae*. *Acta Biochim Biophys Sin* *44*, 555–564.
- Shi, H., Shen, Q., Qi, Y., Yan, H., Nie, H., Chen, Y., Zhao, T., Katagiri, F., and Tang, D. (2013). BR-SIGNALING KINASE1 Physically Associates with FLAGELLIN SENSING2 and Regulates Plant Innate Immunity in *Arabidopsis*. *Plant Cell* *25*, 1143–1157.
- Siegrist, J., Jeblick, W., and Kauss, H. (1994). Defense Responses in Infected and Elicited Cucumber (*Cucumis sativus* L.) Hypocotyl Segments Exhibiting Acquired Resistance. *Plant Physiol.* *105*, 1365–1374.
- Smakowska-Luzan, E., Mott, G.A., Parys, K., Stegmann, M., Howton, T.C., Layeghifard, M., Neuhold, J., Lehner, A., Kong, J., Grünwald, K., *et al.* (2018). An extracellular network of *Arabidopsis* leucine-rich repeat receptor kinases. *Nature* *553*, 342.
- Smit, F., and Dubery, I.A. (1997). Cell wall reinforcement in cotton hypocotyls in response to a *Verticillium dahliae* elicitor. *Phytochemistry* *44*, 811–815.
- Smith, J.M., Salamango, D.J., Leslie, M.E., Collins, C.A., and Heese, A. (2014). Sensitivity to Flg22 Is Modulated by Ligand-Induced Degradation and de Novo Synthesis of the Endogenous Flagellin-Receptor FLAGELLIN-SENSING2. *Plant Physiol.* *164*, 440–454.

- Souza, C. de A., Li, S., Lin, A.Z., Boutrot, F., Grossmann, G., Zipfel, C., and Somerville, S. (2017). Cellulose-derived oligomers act as damage-associated molecular patterns and trigger defense-like responses. *Plant Physiol.* *173*, 2383-2398.
- Stanley, C.E., Shrivastava, J., Brugman, R., Heinzlmann, E., Swaay, D. van, and Grossmann, G. (2018). Dual-flow-RootChip reveals local adaptations of roots towards environmental asymmetry at the physiological and genetic levels. *New Phytol.* *217*, 1357–1369.
- Stegmann, M., Monaghan, J., Smakowska-Luzan, E., Rovenich, H., Lehner, A., Holton, N., Belkhadir, Y., and Zipfel, C. (2017). The receptor kinase FER is a RALF-regulated scaffold controlling plant immune signaling. *Science* *355*, 287–289.
- Steinkellner, S., Lenzemo, V., Langer, I., Schweiger, P., Khaosaad, T., Toussaint, J.-P., and Vierheilig, H. (2007). Flavonoids and Strigolactones in Root Exudates as Signals in Symbiotic and Pathogenic Plant-Fungus Interactions. *Molecules* *12*, 1290–1306.
- Stringlis, I.A., Zhang, H., Pieterse, C.M.J., Bolton, M.D., and Jonge, R. de (2018). Microbial small molecules – weapons of plant subversion. *Nat. Prod. Rep.* *35*, 410–433.
- Stringlis, I.A., de Jonge, R., and Pieterse, C.M.J. (2019). The Age of Coumarins in Plant–Microbe Interactions. *Plant Cell Physiol.* *60*, 1405-1419.
- Sun, T., Nitta, Y., Zhang, Q., Wu, D., Tian, H., Lee, J.S., and Zhang, Y. (2018). Antagonistic interactions between two MAP kinase cascades in plant development and immune signaling. *EMBO Rep.* *19*, e45324.
- Sun, Y., Li, L., Macho, A.P., Han, Z., Hu, Z., Zipfel, C., Zhou, J.-M., and Chai, J. (2013). Structural Basis for flg22-Induced Activation of the *Arabidopsis* FLS2-BAK1 Immune Complex. *Science* *342*, 624–628.
- Tang, D., Wang, G., and Zhou, J.-M. (2017). Receptor Kinases in Plant-Pathogen Interactions: More Than Pattern Recognition. *Plant Cell* *29*, 618–637.
- Teixeira, M.A., Wei, L., and Kaloshian, I. (2016). Root-knot nematodes induce pattern-triggered immunity in *Arabidopsis thaliana* roots. *New Phytol.* *211*, 276–287.
- Thomas, R., Fang, X., Ranathunge, K., Anderson, T.R., Peterson, C.A., and Bernards, M.A. (2007). Soybean Root Suberin: Anatomical Distribution, Chemical Composition, and Relationship to Partial Resistance to *Phytophthora sojae*. *Plant Physiol.* *144*, 299–311.
- Thor, K. (2019). Calcium—Nutrient and Messenger. *Front. Plant Sci.* *10*, 440.
- Thor, K., and Peiter, E. (2014). Cytosolic calcium signals elicited by the pathogen-associated molecular pattern flg22 in stomatal guard cells are of an oscillatory nature. *New Phytol.* *204*, 873–881.
- Tian, W., Hou, C., Ren, Z., Wang, C., Zhao, F., Dahlbeck, D., Hu, S., Zhang, L., Niu, Q., Li, L., *et al.* (2019). A calmodulin-gated calcium channel links pathogen patterns to plant immunity. *Nature* *572*, 131–135.
- Tintor, N., Ross, A., Kanehara, K., Yamada, K., Fan, L., Kemmerling, B., Nürnberger, T., Tsuda, K., and Saijo, Y. (2013). Layered pattern receptor signaling via ethylene and endogenous elicitor peptides during *Arabidopsis* immunity to bacterial infection. *Proc. Natl. Acad. Sci.* *110*, 6211–6216.
- Todesco, M., Balasubramanian, S., Hu, T.T., Traw, M.B., Horton, M., Epple, P., Kuhns, C., Sureshkumar, S., Schwartz, C., Lanz, C., *et al.* (2010). Natural allelic variation underlying a major fitness trade-off in *Arabidopsis thaliana*. *Nature* *465*, 632–636.

- Toruño, T.Y., Stergiopoulos, I., and Coaker, G. (2016). Plant-Pathogen Effectors: Cellular Probes Interfering with Plant Defenses in Spatial and Temporal Manners. *Annu. Rev. Phytopathol.* *54*, 419–441.
- Tran, T.M., MacIntyre, A., Hawes, M., and Allen, C. (2016). Escaping Underground Nets: Extracellular DNases Degrade Plant Extracellular Traps and Contribute to Virulence of the Plant Pathogenic Bacterium *Ralstonia solanacearum*. *PLOS Pathog* *12*, e1005686.
- Tsuda, K., Sato, M., Stoddard, T., Glazebrook, J., and Katagiri, F. (2009). Network Properties of Robust Immunity in Plants. *PLoS Genet* *5*, e1000772.
- Tytgat, T.O.G., Verhoeven, K.J.F., Jansen, J.J., Raaijmakers, C.E., Bakx-Schotman, T., McIntyre, L.M., Putten, W.H. van der, Biere, A., and Dam, N.M. van (2013). Plants Know Where It Hurts: Root and Shoot Jasmonic Acid Induction Elicit Differential Responses in Brassica oleracea. *PLOS ONE* *8*, e65502.
- Ursache, R., Vieira-Teixeira, C.D.J., Tendon, V.D., Gully, K., Bellis, D.D., Schmid-Siegert, E., Andersen, T.G., Shekhar, V., Calderon, S., Pradervand, S., *et al.* (2020). GDSL-domain containing proteins mediate suberin biosynthesis and degradation, enabling developmental plasticity of the endodermis during lateral root emergence. *BioRxiv* 2020.06.25.171389.
- Vance, C.P., Kirk, T.K., and Sherwood, R.T. (1980). Lignification as a Mechanism of Disease Resistance. *Annu. Rev. Phytopathol.* *18*, 259–288.
- VanEtten, H.D., Mansfield, J.W., Bailey, J.A., and Farmer, E.E. (1994). Two Classes of Plant Antibiotics: Phytoalexins versus “Phytoanticipins.” *Plant Cell* *6*, 1191–1192.
- Vasse, J., Frey, P., and Trigalet, A. (1995). Microscopic studies of intercellular infection and protoxylem invasion of tomato roots by *Pseudomonas solanacearum*. *MPMI-Mol. Plant Microbe Interact.* *8*, 241–251.
- Vermeer, J.E.M., Wangenheim, D. von, Barberon, M., Lee, Y., Stelzer, E.H.K., Maizel, A., and Geldner, N. (2014). A Spatial Accommodation by Neighboring Cells Is Required for Organ Initiation in *Arabidopsis*. *Science* *343*, 178–183.
- Veronese, P., Nakagami, H., Bluhm, B., AbuQamar, S., Chen, X., Salmeron, J., Dietrich, R.A., Hirt, H., and Mengiste, T. (2006). The Membrane-Anchored BOTRYTIS-INDUCED KINASE1 Plays Distinct Roles in *Arabidopsis* Resistance to Necrotrophic and Biotrophic Pathogens. *Plant Cell* *18*, 257–273.
- Voigt, C.A. (2014). Callose-mediated resistance to pathogenic intruders in plant defense-related papillae. *Front. Plant Sci.* *5*, 168.
- Wan, J., Zhang, X.-C., Neece, D., Ramonell, K.M., Clough, S., Kim, S., Stacey, M.G., and Stacey, G. (2008). A LysM Receptor-Like Kinase Plays a Critical Role in Chitin Signaling and Fungal Resistance in *Arabidopsis*. *Plant Cell* *20*, 471–481.
- Wan, W.-L., Fröhlich, K., Pruitt, R.N., Nürnberger, T., and Zhang, L. (2019). Plant cell surface immune receptor complex signaling. *Curr. Opin. Plant Biol.* *50*, 18–28.
- Wang, J., Grubb, L.E., Wang, J., Liang, X., Li, L., Gao, C., Ma, M., Feng, F., Li, M., Li, L., *et al.* (2018). A Regulatory Module Controlling Homeostasis of a Plant Immune Kinase. *Mol. Cell* *69*, 493-504.e6.
- Way, H.M., Kazan, K., Mitter, N., Goulter, K.C., Birch, R.G., and Manners, J.M. (2002). Constitutive expression of a phenylalanine ammonia-lyase gene from *Stylosanthes humilis* in transgenic tobacco leads to enhanced disease resistance but impaired plant growth. *Physiol. Mol. Plant Pathol.* *60*, 275–282.
- Willmann, R., Lajunen, H.M., Erbs, G., Newman, M.-A., Kolb, D., Tsuda, K., Katagiri, F., Fliegmann, J., Bono, J.-J., Cullimore, J.V., *et al.* (2011). *Arabidopsis* lysin-motif proteins LYM1 LYM3 CERK1

- mediate bacterial peptidoglycan sensing and immunity to bacterial infection. *Proc. Natl. Acad. Sci.* *108*, 19824–19829.
- Wyrsh, I., Domínguez-Ferreras, A., Geldner, N., and Boller, T. (2015). Tissue-specific FLAGELLIN-SENSING 2 (FLS2) expression in roots restores immune responses in *Arabidopsis fls2* mutants. *New Phytol.* *206*, 774–784.
- Yadav, V., Kumar, M., Deep, D.K., Kumar, H., Sharma, R., Tripathi, T., Tuteja, N., Saxena, A.K., and Johri, A.K. (2010). A Phosphate Transporter from the Root Endophytic Fungus *Piriformospora indica* Plays a Role in Phosphate Transport to the Host Plant. *J. Biol. Chem.* *285*, 26532–26544.
- Yamada, K., Yamaguchi, K., Shirakawa, T., Nakagami, H., Mine, A., Ishikawa, K., Fujiwara, M., Narusaka, M., Narusaka, Y., Ichimura, K., *et al.* (2016). The *Arabidopsis* CERK1-associated kinase PBL27 connects chitin perception to MAPK activation. *EMBO J.* *35*, 2468–2483.
- Yamaguchi, Y., and Huffaker, A. (2011). Endogenous peptide elicitors in higher plants. *Curr. Opin. Plant Biol.* *14*, 351–357.
- Yamaguchi, Y., Pearce, G., and Ryan, C.A. (2006). The cell surface leucine-rich repeat receptor for AtPep1, an endogenous peptide elicitor in *Arabidopsis*, is functional in transgenic tobacco cells. *Proc. Natl. Acad. Sci.* *103*, 10104–10109.
- Yeh, Y.-H., Panzeri, D., Kadota, Y., Huang, Y.-C., Huang, P.-Y., Tao, C.-N., Roux, M., Chien, H.-C., Chin, T.-C., Chu, P.-W., *et al.* (2016). The *Arabidopsis* Malectin-Like/LRR-RLK IOS1 is Critical for BAK1-Dependent and BAK1-Independent Pattern-Triggered Immunity. *Plant Cell* *28*, 1701–1721.
- Yu, K., Liu, Y., Tichelaar, R., Savant, N., Lagendijk, E., Kuijk, S.J.L. van, Stringlis, I.A., Dijken, A.J.H. van, Pieterse, C.M.J., Bakker, P.A.H.M., *et al.* (2019). Rhizosphere-Associated *Pseudomonas* Suppress Local Root Immune Responses by Gluconic Acid-Mediated Lowering of Environmental pH. *Curr. Biol.* *29*, 3913-3920.e4.
- Yuan, M., Jiang, Z., Bi, G., Nomura, K., Liu, M., He, S.Y., Zhou, J.-M., and Xin, X.-F. (2020). Pattern-recognition receptors are required for NLR-mediated plant immunity. *BioRxiv* 2020.04.10.031294
- Zamioudis, C., Korteland, J., Pelt, J.A.V., Hamersveld, M. van, Dombrowski, N., Bai, Y., Hanson, J., Verk, M.C.V., Ling, H.-Q., Schulze-Lefert, P., *et al.* (2015). Rhizobacterial volatiles and photosynthesis-related signals coordinate MYB72 expression in *Arabidopsis* roots during onset of induced systemic resistance and iron-deficiency responses. *Plant J.* *84*, 309–322.
- Zhang, J., Shao, F., Li, Y., Cui, H., Chen, L., Li, H., Zou, Y., Long, C., Lan, L., Chai, J., *et al.* (2007). A *Pseudomonas syringae* Effector Inactivates MAPKs to Suppress PAMP-Induced Immunity in Plants. *Cell Host Microbe* *1*, 175–185.
- Zhang, J., Li, W., Xiang, T., Liu, Z., Laluk, K., Ding, X., Zou, Y., Gao, M., Zhang, X., Chen, S., *et al.* (2010). Receptor-like Cytoplasmic Kinases Integrate Signaling from Multiple Plant Immune Receptors and Are Targeted by a *Pseudomonas syringae* Effector. *Cell Host Microbe* *7*, 290–301.
- Zhang, M., Chiang, Y.-H., Toruño, T.Y., Lee, D., Ma, M., Liang, X., Lal, N.K., Lemos, M., Lu, Y.-J., Ma, S., *et al.* (2018). The MAP4 Kinase SIK1 Ensures Robust Extracellular ROS Burst and Antibacterial Immunity in Plants. *Cell Host Microbe* *24*, 379-391.e5.
- Zhou, C., Guo, J., Zhu, L., Xiao, X., Xie, Y., Zhu, J., Ma, Z., and Wang, J. (2016). *Paenibacillus polymyxa* BFKC01 enhances plant iron absorption via improved root systems and activated iron acquisition mechanisms. *Plant Physiol. Biochem.* *105*, 162–173.
- Zhou, F., Emonet, A., Déneraud Tendon, V., Marhavy, P., Wu, D., Lahaye, T., and Geldner, N. (2020). Co-incidence of Damage and Microbial Patterns Controls Localized Immune Responses in Roots. *Cell* *180*, 440-453.e18.

- Zipfel, C. (2008). Pattern-recognition receptors in plant innate immunity. *Curr. Opin. Immunol.* *20*, 10–16.
- Zipfel, C., Robatzek, S., Navarro, L., Oakeley, E.J., Jones, J.D.G., Felix, G., and Boller, T. (2004). Bacterial disease resistance in *Arabidopsis* through flagellin perception. *Nature* *428*, 764–767.
- Zipfel, C., Kunze, G., Chinchilla, D., Caniard, A., Jones, J.D.G., Boller, T., and Felix, G. (2006). Perception of the Bacterial PAMP EF-Tu by the Receptor EFR Restricts *Agrobacterium*-Mediated Transformation. *Cell* *125*, 749–760.
- Ziv, C., Zhao, Z., Gao, Y.G., and Xia, Y. (2018). Multifunctional Roles of Plant Cuticle During Plant-Pathogen Interactions. *Front. Plant Sci.* *9*, 1088.

2 CO-INCIDENCE OF DAMAGE AND MICROBIAL PATTERNS CONTROLS LOCALIZED IMMUNE RESPONSES IN ROOTS

2.1. RATIONAL OF THE STUDY

As we uncover the rich diversity of the soil microbiome, we start to understand that the interactions occurring in the rhizosphere are extremely complex. How plants can deal with such a variety of partners is one of the key questions largely remaining unanswered. It is fascinating to realize that plants can at the same time defend against pathogens but still accommodate a rich microbiota. Latest advances in the study of root innate immunity showed that plants confine their defence responses in the elongating zone of the root and keep their differentiated zone silent (Millet *et al.*, 2010; Poncini *et al.*, 2017). This is thought to avoid the overactivation of their innate immune system. However, the exact mechanism and the biological relevance of this regulation is so far unknown.

An understanding of the interaction occurring in the rhizosphere will indeed requires a change of scale in our methodology, so that we can no longer average immune responses at the whole organ level. New tools such as fluorescent cellular markers of defence or single-cell ablation techniques are now available to bring back the spatial dimension of immunity. They already proved useful to characterize the non-systemic, regional responses to single-cell damage (Hander *et al.*, 2019; Marhavý *et al.*, 2019) and to map defences on the root with a true cellular resolution (Poncini *et al.*, 2017). Moreover, these studies revealed that damage responses are remarkably important in roots (Marhavý *et al.*, 2019; Poncini *et al.*, 2017).

The following article provides a first explanation for the confinement of defences at the elongation zone. It describes how plants use damages to elegantly gate the induction of responses in mature part of the root, protecting tissues against deleterious bacteria but limiting immune responses to harmless microbes.

2.2. CONTRIBUTIONS

In this chapter, the main results were obtained by Feng Zhou, who carried out all published experiments and participate in the writing of the manuscript with Niko Geldner.

As second author, I provided the first description of *UBQ10::FLS2-GFP fls2* coupled to *PER5::NLS-3mVenus* (described in details in Chapter 3). I also crossed *ein2-1* and *etr1-1* mutants with reporters of MTI (*PER5/MYB51/WRKY11*) and *FLS2* expression or protein fusion. I additionally generated the *FLS2::NLS-tdTomato* construct for co-localisation of *FLS2* and MAMP reporters and *FLS2_{long}::FLS2-3myc-mVenus-3'UTR* in *fls2* background for complementation experiments. I also replicated experiments in parallel to F. Zhou, or carried out exploratory work to assess the implication of ethylene in damage-induced *FLS2* expression, to test *flg22* and *Atpep1* diffusion in the root and to characterize lateral-root dependent MAMP-responsiveness (see Appendices). Finally, I participated in discussion and proof-read the manuscript.

Valérie Dénervaud Tendon generated transcriptional read-out of immunity: *PER5/MYB51/WRKY11::NLS-mVenus*.

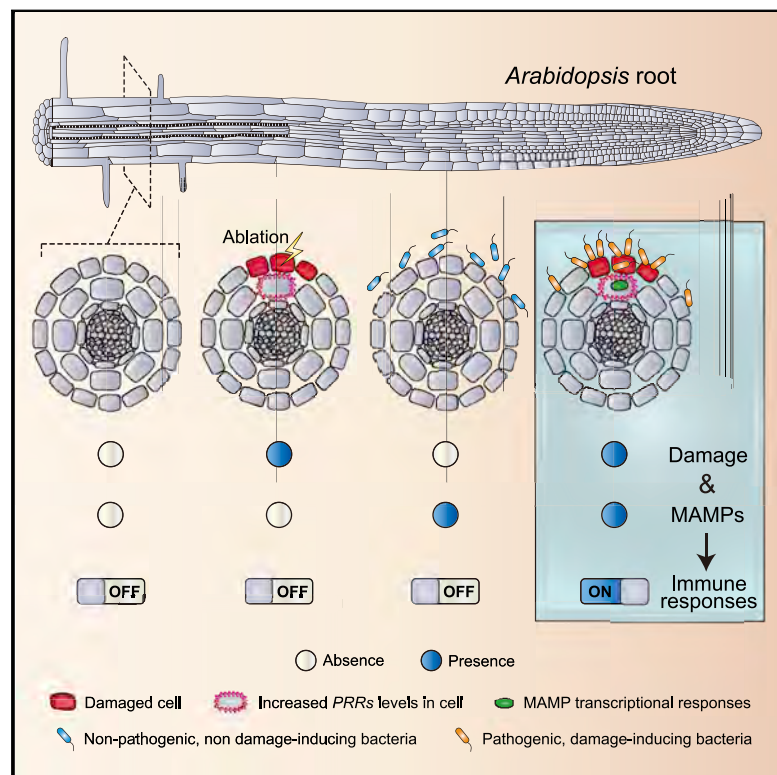
Dousheng Wu was involved in experimental work with *Ralstonia solanacearum*.

Peter Marhavy and Thomas Lahaye revised the manuscript and were involved in discussion of project.

2.3. ORIGINAL ARTICLE

Co-occurrence of Damage and Microbial Patterns Controls Localized Immune Responses in Roots

Graphical Abstract



Authors

Feng Zhou, Aurélie Emonet, Valérie Déneraud Tendon, Peter Marhavy, Dousheng Wu, Thomas Lahaye, Niko Geldner

Correspondence

feng.zhou@unil.ch (F.Z.), niko.geldner@unil.ch (N.G.)

In Brief

Roots require both microbial molecular patterns and plant tissue damage in order to mount localized antibacterial immune responses, revealing an effective way to respond appropriately to pathogens while sparing commensals.

Highlights

- *Arabidopsis* roots request cell damage to mount a strong, localized immune response
- Damaged cells upregulate pattern-recognition receptor expression in their neighbors
- Endodermal barriers compartmentalize immune responses in differentiated cell-types
- Damage-gating can minimize immune responses against non-pathogenic root colonizers



Co-occurrence of Damage and Microbial Patterns Controls Localized Immune Responses in Roots

Feng Zhou,^{1,*} Aurélia Emonet,¹ Valérie Déneraud Tendon,¹ Peter Marhavy,^{1,3} Dousheng Wu,² Thomas Lahaye,² and Niko Geldner^{1,4,*}

¹Department of Plant Molecular Biology, Biophore, UNIL-Sorge, University of Lausanne, 1015 Lausanne, Switzerland

²ZMBP-General Genetics, University of Tübingen, Auf der Morgenstelle 32, 72076 Tübingen, Germany

³Present address: Umea Plant Science Centre (UPSC), Department of Forest Genetics and Plant Physiology, Swedish University of Agricultural Sciences (SLU), 90183 Umea, Sweden

⁴Lead Contact

*Correspondence: feng.zhou@unil.ch (F.Z.), niko.geldner@unil.ch (N.G.)

<https://doi.org/10.1016/j.cell.2020.01.013>

SUMMARY

Recognition of microbe-associated molecular patterns (MAMPs) is crucial for the plant's immune response. How this sophisticated perception system can be usefully deployed in roots, continuously exposed to microbes, remains a mystery. By analyzing MAMP receptor expression and response at cellular resolution in *Arabidopsis*, we observed that differentiated outer cell layers show low expression of pattern-recognition receptors (PRRs) and lack MAMP responsiveness. Yet, these cells can be gated to become responsive by neighbor cell damage. Laser ablation of small cell clusters strongly upregulates PRR expression in their vicinity, and elevated receptor expression is sufficient to induce responsiveness in non-responsive cells. Finally, localized damage also leads to immune responses to otherwise non-immunogenic, beneficial bacteria. Damage-gating is overridden by receptor overexpression, which antagonizes colonization. Our findings that cellular damage can “switch on” local immune responses helps to conceptualize how MAMP perception can be used despite the presence of microbial patterns in the soil.

INTRODUCTION

A number of defined molecular patterns and corresponding receptors have been identified and shown to elicit a conserved set of molecular responses (Macho and Zipfel, 2014). However, identical microbial patterns from symbiotic or commensal microbes should be equally perceived (Pel and Pieterse, 2013). This is especially apparent in the microbe-rich soil environment of roots, whose outer cell layers do not possess protective barriers comparable to leaves. Recent breakthroughs in root microbiome research have heightened the interest in understanding how constitutive activation of PRRs by non-pathogenic microbes is avoided, while

maintaining their effectiveness in defense (Castrillo et al., 2017; Finkel et al., 2017; Garrido-Oter et al., 2018; Yu et al., 2019). The molecular outlines of microbe-associated molecular pattern (MAMP) perception were characterized in systems allowing for quantitative, time-resolved measurements of early responses (Felix et al., 1999). In *Arabidopsis* (Chinchilla et al., 2006; Gómez-Gómez et al., 1999), leaf-disk reactive oxygen species (ROS) assays, phosphorylated mitogen-activated protein kinase (MAPK) blots, quantitative PCR (qPCR), or genome-wide transcription profiling became popular tools (Zipfel et al., 2004, 2006). Although such assays establish the molecular components of PRR signal transduction, they do not allow for a meaningful degree of spatial resolution, because they average cellular responses across entire organs. Actual, initial pathogen/microbe contacts, however, are localized to a few cells and cell types and this highly relevant spatial dimension of responses has remained largely unresolved. When studied, significant differences between single-cell and whole seedling responses were observed (Thor and Peiter, 2014). Roots mount an autonomous MAMP response (Poncini et al., 2017; Wyrsh et al., 2015) and β -glucuronidase (GUS) reporters, or callose deposition, revealed a restricted response to high concentrations of the bacterial MAMP, flg22, mainly in the root cap and root transition/elongation zone (Jacobs et al., 2011; Millet et al., 2010). GUS reporter assays are destructive, however, and remain below single-cell or tissue resolution. Moreover, the causes of this spatially restricted MAMP response have remained obscure, as well as its potential biological relevance.

In order to address these questions, we combined new and recently published fluorescent marker lines, based on a triple mVENUS fused to a nuclear localization signal (NLS-3xmVENUS) (Poncini et al., 2017; Vermeer et al., 2014). This allows for analysis of MAMP responses *in vivo* and at true cellular resolution. These highly sensitive markers were selected for good expression and stable responses, across transgenic lines and in successive generations. The promoters selected were based on well-established and widely used MAMP responsive genes. *PER5* (*PEROXIDASE 5*) was chosen from public databases as a strong and early MAMP-induced gene that is highly induced in roots (Hruz et al., 2008; Wyrsh et al., 2015); *WRKY11* (*WRKY DNA-BINDING PROTEIN 11*) is a



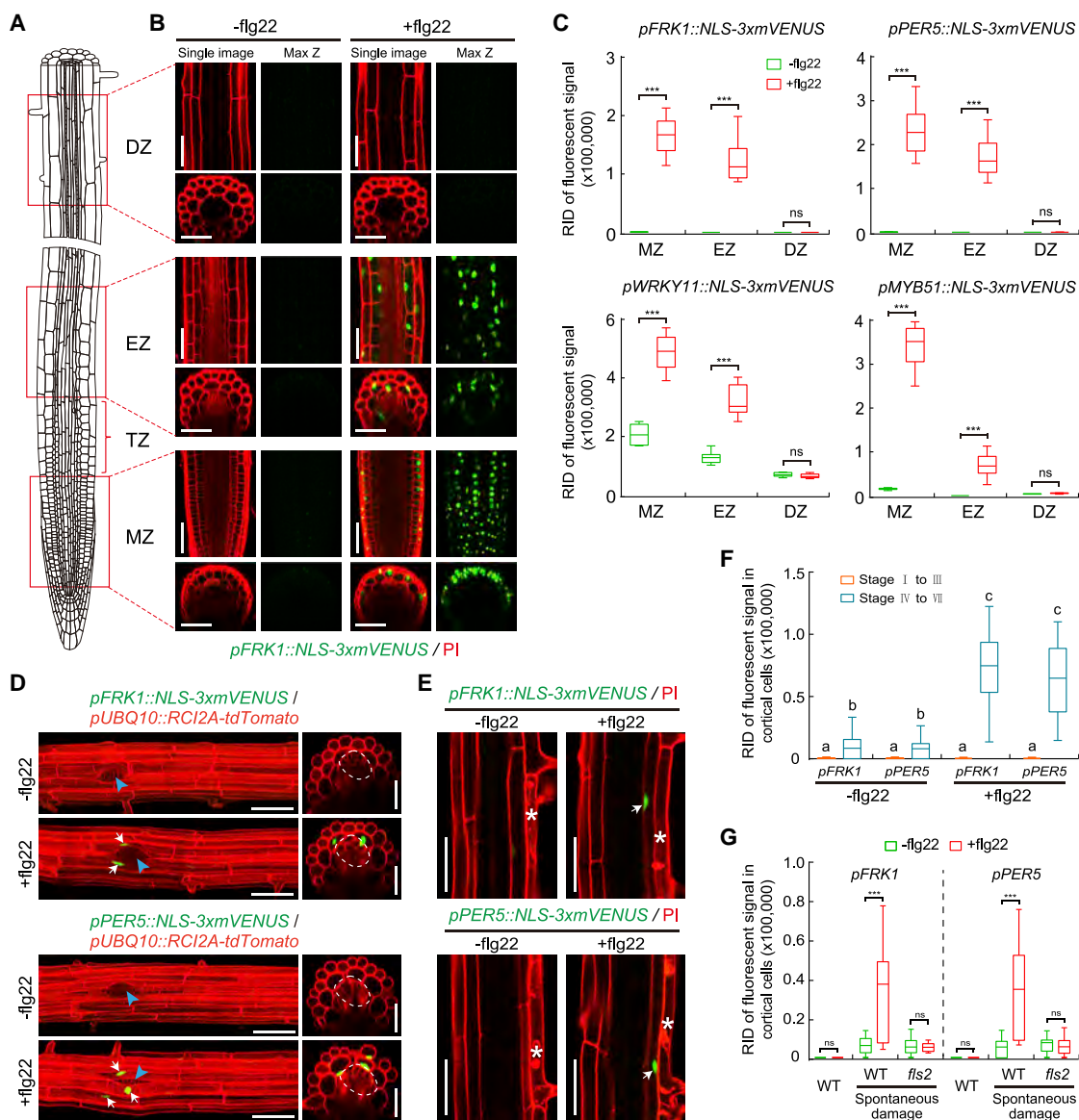


Figure 1. Flg22-Induced MAMP Responses Are Spatially Confined in Arabidopsis Roots

(A) Schematic of a 6-day-old *Arabidopsis* root showing the different developmental zones. Three different zones were imaged: meristematic zone (MZ), elongation zone (EZ), and differentiation zone (DZ). TZ indicates the transition zone.

(B) The expression pattern of one representative MAMP promoter marker lines (*pFRK1*) in response to 1 μ M flg22 treatment for 6 h. Images correspond to the zones indicated in (A). Images in the differentiated zone were always taken at a distance of 25 endodermal cells after onset of cell elongation. In each treatment, single confocal section (single image, left) and maximal projections of z stacks (max z, right) are presented; median longitudinal and transverse (xz) section views are shown on the top and bottom, respectively. Nuclear-localized mVENUS signals (green) are co-visualized with propidium iodide (PI, red). Scale bar, 50 μ m.

(C) Quantitative analysis of mVENUS signal intensities of the four MAMP markers in the absence (–) or presence (+) of flg22. RID, raw intensity density. RID of total fluorescent signals in a single image is the sum of the RID of each nuclear signal in the imaged area. RID of fluorescent signal of per nucleus = the size of the mVENUS signal area of a nucleus (number of pixels) \times the average fluorescent intensity of the pixels for the nucleus. Boxplot centers show median (n = 12 roots). Asterisks (***) indicate statistically significant differences between means by ANOVA and Tukey's test analysis. ns, not significant.

(D) MAMP responsiveness during lateral root primordium (LRP) formation. Images of stage IV lateral root in 8-day-old seedlings of double marker lines, highlighting plasma membrane of all root cells through *pUBQ10::RC12A-tdTomato* expression (red) in addition to the MAMP responses (green). Maximum projections of longitudinal (left panel) and transverse sections (right panel) are shown. In transverse sections, a single red-channel image was overlaid with the green-channel maximum projection in order to obtain a clear plasma membrane outline. Arrows indicate cell nuclei with MAMP marker responses. The shape of emerged LRP is indicated by dotted circle in the orthogonal view, and site of emergence is indicated by a blue arrowhead in longitudinal maximum projections. Scale bar, 50 μ m.

(E) Spontaneous, non-induced cell death (asterisks) causes flg22 responsiveness (arrows) in neighboring cortical cell layer. Damaged epidermal cells are highlighted by PI staining. Scale bar, 50 μ m.

(legend continued on next page)

representative of the WRKY transcription factor family, shown to mediate MAMP signaling and to be early-response genes themselves (Asai et al., 2002; Navarro et al., 2004). *MYB51* (*MYB DOMAIN PROTEIN 51*) was shown to be transcriptionally regulated by MAMPs and to control production of major *Arabidopsis* defense metabolites (Clay et al., 2009; Gigolashvili et al., 2007). We also generated *FRK1* (*FLG22-INDUCED RECEPTOR-LIKE KINASE 1*), a receptor-like protein of unknown function shown to be a strong and early MAMP-induced transcript (Asai et al., 2002; Boudsocq et al., 2010).

RESULTS

flg22-Induced MAMP Responses Are Spatially Restricted in *Arabidopsis* Roots

Among the four MAMP markers generated, we found that *PER5* and *FRK1*, especially, displayed very low background before, and good induction upon, stimulation (Figures 1A–1C and S1A) (Poncini et al., 2017). For precise assignment of signals to specific cells and cell types, we generated double marker lines with a constitutively expressed, plasma membrane-targeted red fluorescent protein (Figure 1D). Alternatively, counterstaining with the red fluorescent cell wall stain propidium iodide (PI) was done.

Using these markers, we confirmed that MAMP-responses are confined to the root cap, transition/elongation zone, with an absent, or orders-of-magnitudes weaker, response in differentiated root parts, even at high doses of flg22 (1 μ M) (Figures 1A–1C and S1A) (Millet et al., 2010). flg22, a peptide fragment of bacterial flagellin and a well-established elicitor in plants, was used as a prototypical MAMP (Felix et al., 1999). Lack of responses in differentiated roots is not due to a problem with peptide penetration, because the active, fluorescently labeled flg22 (TAMRA-flg22) fully penetrated the root until the endodermal diffusion barrier (Figures S1B and S1C). Thus, the absence of responses in the endodermis, cortex, and epidermis are not due to a block in MAMP penetration, while absence in the differentiated stele might be due to the endodermal diffusion barrier. The spatially restricted responses we observe are not observed only for flg22, because other MAMPs, such as nlp20 or a medium-chain 3-hydroxy fatty acid (3-OH-C10:0) (Böhm et al., 2014; Kutschera et al., 2019), display very similar response patterns (Figure S1D). elf18, another well-characterized bacterial MAMP (Kunze et al., 2004), showed very little response in roots overall, while the fungal chitin was the only MAMP that elicited some direct response in the differentiated zone.

Our high-resolution mapping of MAMP/flg22 responses revealed intriguing, spatially confined exceptions to the attenuated MAMP responses in differentiated roots. The first exception are emerging lateral roots, where adjacent cortical cells—that have become pushed, separated, possibly damaged, by the emerging primordium—consistently showed a strong response to MAMP treatment (Figures 1D, 1F, S1E, and S1F). The second exception

we observed was a flg22 responsiveness in cells whose immediate neighbor had undergone sporadic cell death (Figures 1E, 1G, and S1G). Thus, differentiated roots have the capacity to respond to MAMPs and this responsiveness can be induced in a highly localized manner.

Laser-Induced Cell Ablation Causes Localized MAMP Responsiveness in Roots

The intriguing spatial association of MAMP responsiveness and neighbor-cell-death prompted us to induce reproducible and precise cellular damage and observe its effect on flg22 responsiveness. By ablating small clusters of distinct root cell types with a pulsed infrared laser, we observed a strong enhancement of flg22 responsiveness in immediately neighboring cell layers only (Figures 2A, 2B, S2A, and S2B). Importantly, ablation on its own led to no, or very little, induction of MAMP marker genes (Figures 2A, 2B, S2A, and S2B), showing that cellular damage per se is insufficient to induce a robust MAMP response. Already single-cell ablations induced flg22 responsiveness, but the effects became gradually more pronounced when more cells were ablated (Figures S2C and S2D), prompting us to use ablation of three or four cells as our standard. Time-lapse analysis showed that the earliest observable responses occurred at 4 h after flg22 treatment (Figure S3), leading us to use 6 h for most treatments. Introgression of our marker lines into an *fls2* mutant demonstrated a full dependency of the responses on a functional FLS2 receptor (Figures S2E and S2F). Interestingly, we observed directionality to damage induction, with inward-lying tissue layers generally responding the strongest. Cells of the stele responded strongly to flg22 upon epidermis, cortex, and endodermis ablation, while ablation of an epidermal cell did not cause flg22-responsiveness in epidermal neighbors (Figures 2A, 2B, S2A, and S2B). To explain the lack of responses in epidermal neighbors, one could postulate that mechanical stimulation is required for induction. Sudden pressure differences would only occur in cortex, but not in epidermal cells upon ablation, because epidermal cells do not experience counter-pressure from overlying cells. Another possibility might be that a collapse of plasmodesmatal integrity is perceived, and there are differences in quality and degree of plasmodesmatal connections between cortical and epidermal neighbors.

In the differentiated zone, absence of MAMP responsiveness without damage—even at high levels of flg22 (1 μ M)—makes observation of the enhancement of MAMP responsiveness upon damage very obvious, leading to an essentially switch-like, qualitative change. Many commensal and root-pathogenic bacteria, however, preferentially colonize the root transition/elongation zone, which displays a direct response to high-doses of flg22, not requiring damage. Yet, when we used 100 nM of flg22, we saw only weak induction of MAMP responses in this zone (Figures 2C and 2D). In this situation of suboptimal stimulation, epidermal cell damage strongly enhanced response to flg22 in cortical cells, similar to the differentiation zone. Thus, although most easily observed in differentiated roots, damage-induced

(F and G) Quantification of *FRK1* and *PER5* response to different developmental stages of lateral root emergence (F) and to non-induced (spontaneous) cell death in different backgrounds (G) with or without flg22 application. Boxplot centers show median ($n = 10$ roots). Different letters in (F) ($p < 0.05$) and asterisks in (G) ($p < 0.001$) indicate statistically significant differences between means by ANOVA and Tukey's test analysis. ns, not significant. See also Figure S1.

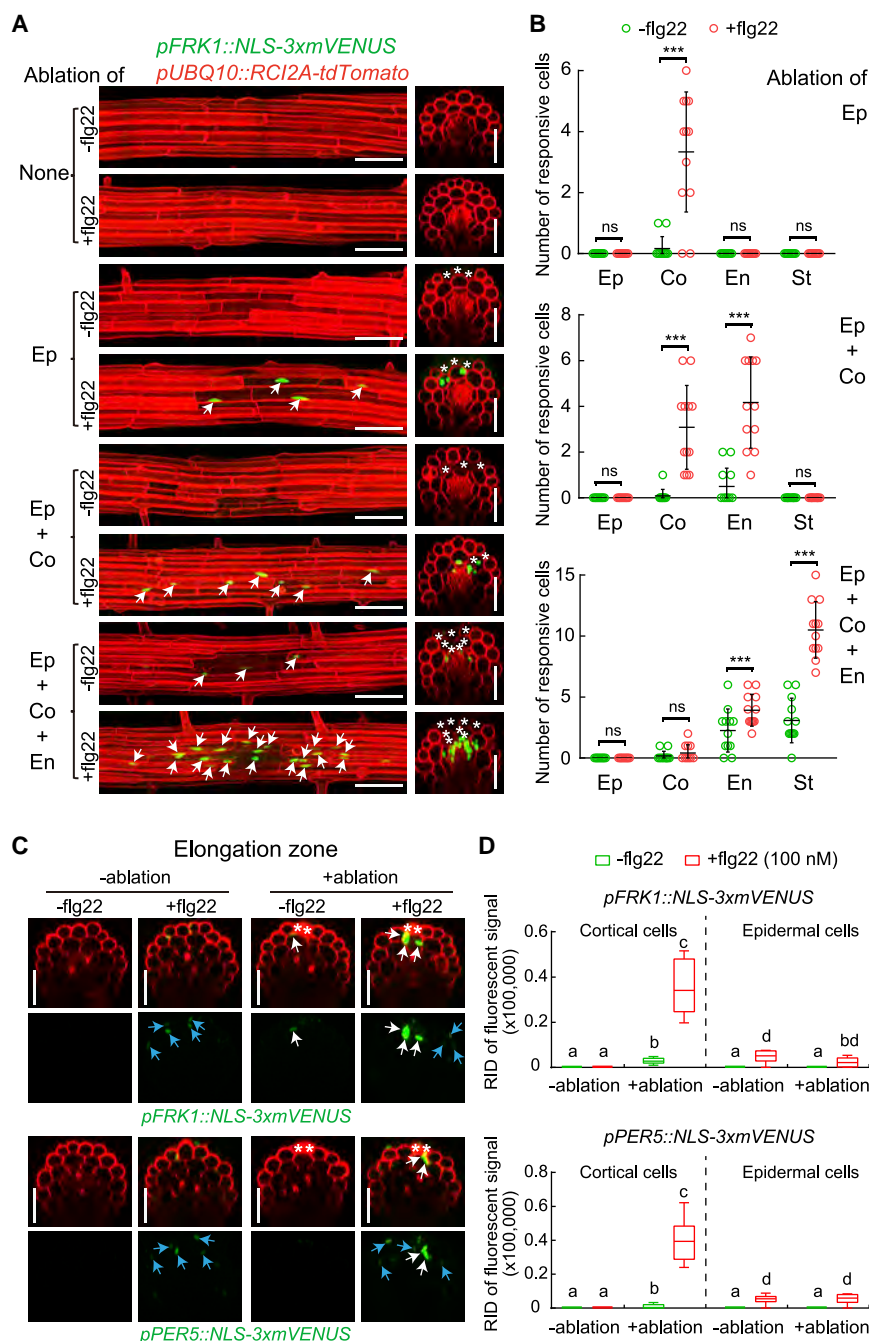


Figure 2. Restricted Cell Damage Causes Localized MAMP Responsiveness in Roots

(A) In differentiated roots, laser ablation of different cell types induces localized *FRK1* response only in the presence of flg22 (+flg22, 1 μ M, 6 h), but not on its own (-flg22). Nuclear-localized signals of *FRK1* reporter (green), co-visualized with the plasma membrane marker (see Figure 1D) (red). Images were taken at 25 endodermal cells after onset of cell elongation. Maximal projections of longitudinal and transverse sections are shown in left and right panels, respectively. White asterisks indicate laser-ablated cells. Arrows indicate *FRK1* responsive nuclei. RID, see legend Figure 1C. Scale bar, 50 μ m.

(B) Quantification of experiments shown in (A). Column scatterplot of the number of *FRK1* responsive cells in different cell types after laser ablation in the absence (green) or presence (red) of flg22. Each circle represents an individual laser ablation of one root ($n = 12$ roots). Graph depicts mean values and SD (error bars). Asterisks ($p < 0.001$) indicate statistically significant differences between means by ANOVA and Tukey's test analysis. ns, not significant. Ep, epidermis; Co, cortex; En, endodermis; St, stele.

(C) Damage of epidermal cells induces strong and localized *FRK1* and *PER5* response only in the presence of "suboptimal" (low) levels of flg22 (+flg22, 100 nM, 6 h), but not on its own (-flg22). Nuclear-localized signals of *FRK1* and *PER5* reporter (green) visualized alone (bottom panels, -PI) or co-visualized with PI staining (upper panels, +PI). White asterisks indicate laser-ablated cells. Arrows in white and blue indicate MAMP responsive nuclei by laser ablation and direct low level flg22 (100 nM) treatment in cortical and epidermal cells, respectively. Laser ablation and confocal images were taken at two or three cells just after onset of cell elongation. Scale bar, 50 μ m.

(D) RID quantification of experiments shown in (C). Boxplot centers show median ($n = 12$ roots). RID, raw intensity density. Different letters indicate statistically significant differences ($p < 0.001$) between means by ANOVA and Tukey's test analysis.

See also Figures S2, S3, and S5.

enhancement of MAMP responsiveness might be a widespread, possibly general, phenomenon in roots.

Presence of DAMPs Alone Are Not Sufficient to Induce MAMP Responses

How cellular damage is perceived by neighboring cells is not well understood, but one important element is thought to be the release of damage-associated molecular patterns (DAMPs), which can be abundant, but largely cytosolic molecules such as adenosine triphosphate (ATP), or small peptides, such as

such as oligogalacturonides (OGs) and cellobiose are additionally acting as DAMPs (Boller and Felix, 2009; Lotze et al., 2007; Souza et al., 2017). Interestingly, even when applied systemically at high concentrations, either individually or as a cocktail, DAMPs alone were not able to induce the strong and consistent flg22 responsiveness that we observe upon actual cellular damage (Figures 3A and 3B). AtPEP1 treatment alone caused some slight induction of *FRK1*—but not *PER5* responsiveness—in the stele, but could not induce any MAMP responsiveness in differentiated outer cell layers. This suggests that perception

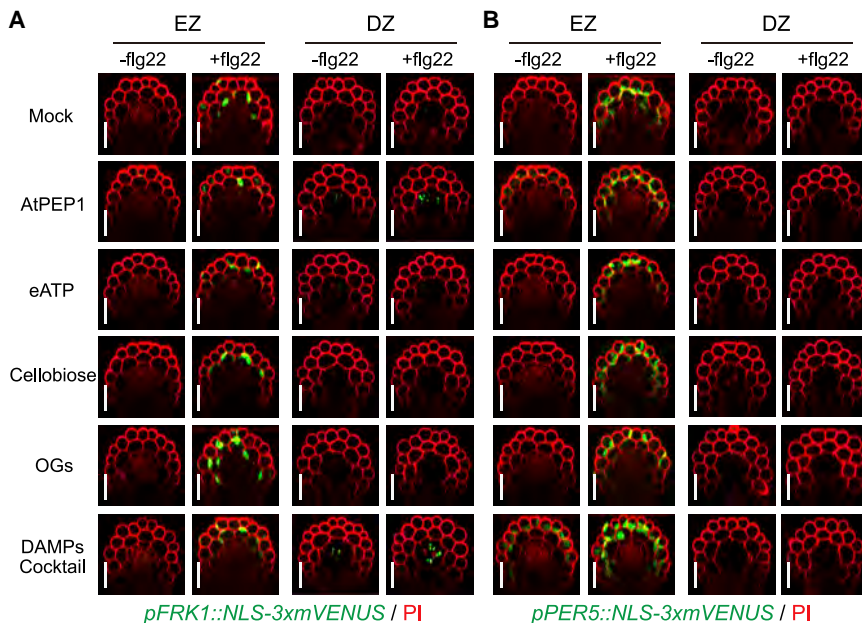


Figure 3. Presence of DAMPs Alone Are Not Sufficient to Induce MAMP Responses

(A and B) Representative pictures of the expression pattern of *FRK1* (A) and *PER5* (B) markers in elongation zone (EZ) and differentiation zone (DZ) treated with a combination of flg22 and four types of DAMPs. Six-day-old roots were treated with each DAMP alone or combined with flg22 for 6 h. DAMPs cocktail is a mixture of all four tested DAMPs. The chemicals were used for treatment at the following concentrations: 1 μ M flg22; 1 μ M AtPEP1; 100 μ M eATP; 100 μ M cellobiose; 50 μ g/mL OGs. Nuclear-localized mVENUS signals (green) co-visualized with PI counterstaining (red). Maximal projections of mVENUS signals and image overlaid in transverse sections done as described previously. Note that AtPEP1 leads a relatively weak *FRK1* response only in some differentiated stelal cells, which is not the case for *PER5* marker, rather than in cortical or endodermal cells that we observed upon actual cellular damage and that DAMPs cocktail, but not single DAMP, is able to activate a weak *PER5* responsiveness in the elongation zone. Scale bar, 50 μ m.

of neighbor cell damage is more complex than a simple presence of DAMPs, relying on additional cues, possibly ion and osmolyte release or mechanical stress, caused by cellular disintegration.

MAMP Receptor Expression Is Induced by Cell Ablation and Is Sufficient to Induce Responsiveness

We found that expressing the MAMP receptor *FLS2* under a constitutive *UBIQUITIN 10* promoter (*pUBQ10*) was sufficient to install responsiveness to flg22 in differentiated outer root cell layers (Figure 4A). This indicates that *FLS2* itself is the only component restricting the ability of differentiated root cells to respond to flg22, implying that all other necessary downstream components (such as BRI1-associated kinase [BAK1], Botrytis-induced kinase [BIK1], MAPKs, WRKYs, etc.) are present. This fits with earlier observations of MAMP receptor mis-expression in other organs or species (Lacombe et al., 2010; Wyrsh et al., 2015). Consequently, we wanted to also monitor *FLS2* expression at single-cell resolution after damage. The currently used *FLS2* promoter complements *fls2* (Zipfel et al., 2004) and roughly matches the spatial patterns of MAMP responses (our work and [Beck et al., 2014]). However, the promoter is of small size (less than 1,000 bp), shows important line-to-line variability and in some cases does not match with MAMP responses (Beck et al., 2014). We therefore additionally generated a longer promoter line (*pFLS2_{long}*) (Figure S4A), which showed less variability and an average pattern that is largely consistent with the described flg22-induced MAMP responses (Figure S4D), i.e., responses adjacent to emerging lateral roots or enhancement of responses to ethylene (Figures S4E and S4F). *FLS2* expression from this longer promoter fragment also complemented the absence of flg22 responses in *fls2* background (Figures S4B and S4C).

In contrast to the MAMP response markers, we found that *FLS2* is transcriptionally activated upon wounding alone, both in differentiation and elongation zone of the root (Figures 4B–

4D, 4F, and 4G), readily explaining how cells can become responsive upon wounding. Indeed, the timing and spatial extent of *FLS2* upregulation matched the observed pattern of MAMP responsiveness (compare Figures 4B–4D and 4F with Figures 2A–2D and S3, respectively). We confirmed that, although less easily quantifiable, a local upregulation of *FLS2* protein could also be observed using *pFLS2::FLS2-GFP* reporter line (Figure 4E). To fully correlate local *FLS2* activation upon damage with MAMP responsiveness, we generated double marker lines of *pFLS2::NLS-tdTomato* and mVENUS MAMP reporters and found that the near-totality of neighboring MAMP responsive cells were also positive for *FLS2* expression when treated with flg22 upon ablation (Figures 4H, 4I, S4G, and S4H). Previously, *pFLS2::GUS* reporter lines showed signal in regions around large-scale wound sites, but relevance for MAMP signaling was not established at the time (Beck et al., 2014). Our co-visualization of receptor expression and MAMP responses now additionally reveals that transcriptional MAMP responses can be strictly cell autonomous, allowing for a very fine-grained activation of immunity. This degree of spatial specificity is surprising, considering that flg22 stimulation was shown to induce ROS production, depolarization, and even propagating calcium waves, all of which have the potential to induce non-cell autonomous responses (Jeworutzki et al., 2010; Keinath et al., 2015).

Induction of MAMP Responsiveness by Damage Does Not Require Ethylene Signaling

FLS2 expression is also known to strongly depend on ethylene (Boutrot et al., 2010; Mersmann et al., 2010) and recent work from our group demonstrated that single cell ablation causes regional induction of ethylene production (Marhavý et al., 2019). Although the spatial patterns of ethylene production reporters upon ablation (extending over many cellular distances, mainly in the stele, no induction of immediate neighbors) did not match the observed *FLS2* induction pattern (Marhavý

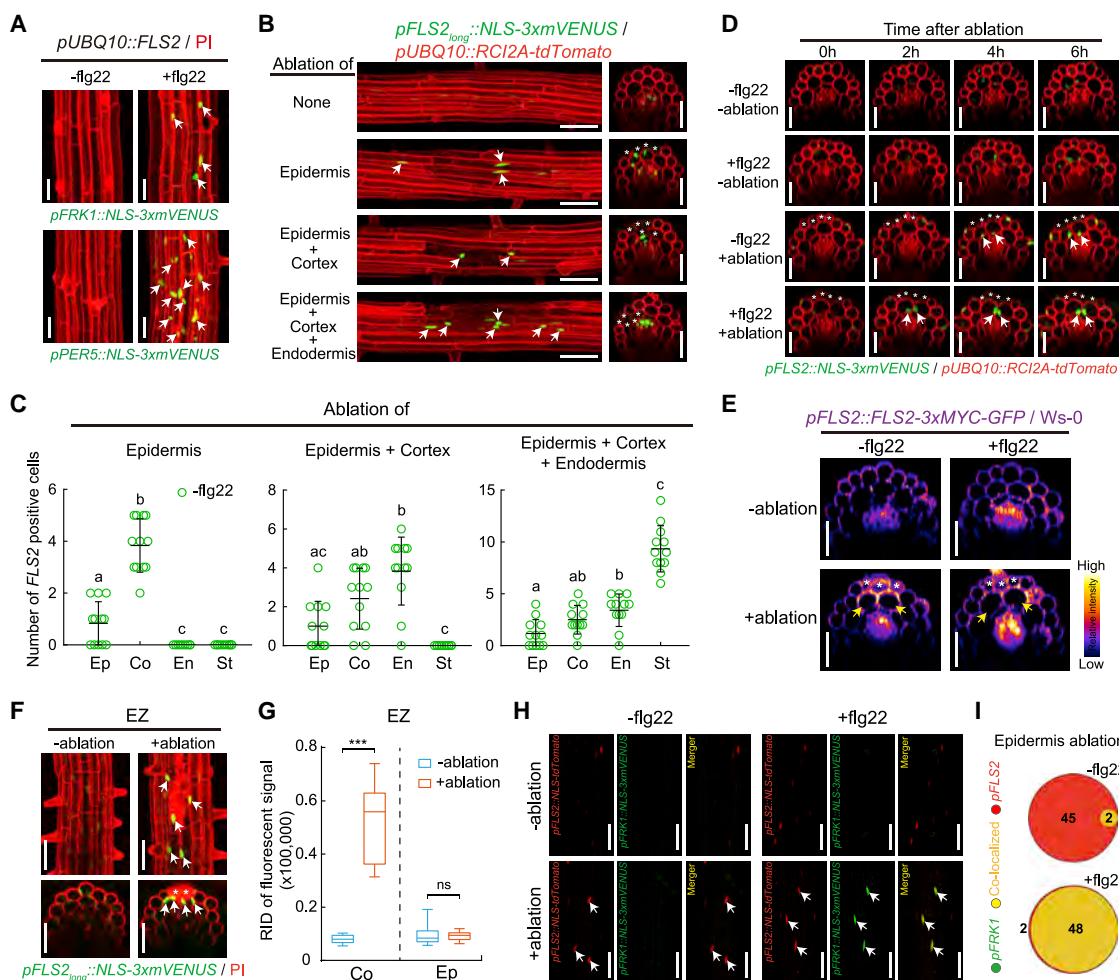


Figure 4. Localized FLS2 Expression Induced by Neighbor Cell Death

(A) Expression of *FRK1* and *PER5* marker (green) with or without flg22 treatment (1 μ M, 6 h) in differentiated zone (DZ) of a *pUBQ10::FLS2* transgenic background. Marker line was counterstained with PI (red). Arrows indicate MAMP responsive nuclei. Scale bar, 50 μ m.

(B) Laser ablation of different cell types (without flg22 treatment) induces localized *FLS2* expression in 6-day-old differentiated roots. Nuclear-localized mVENUS signals of *FLS2* promoter marker (green) co-visualized with plasma membrane marker (red). Images overlaid was done as described before and pictures were taken at 25 endodermal cells after onset of cell elongation. Asterisks highlight laser-ablated cells and arrows indicate *FLS2*-positive nuclei. Scale bar, 50 μ m.

(C) Quantification of the number of *FLS2*-positive cells in different cell types shown in (B). Column scatterplot of the number of *FRK1* responsive cells after laser ablation in the absence (green) or presence (red) of flg22. Each circle represents an individual laser ablation of one root (n = 12 roots). Graph depicts mean values and SD (error bars). Asterisks ($p < 0.001$) indicate statistically significant differences between means by ANOVA and Tukey's test analysis. ns, not significant. Ep, epidermis; Co, cortex; En, endodermis; St, stele.

(D) Real-time monitored *FLS2* induction after laser ablation of differentiated epidermal cells with or without flg22 application in orthogonal view. Asterisks and arrows highlight laser-ablated cells and *FLS2*-positive nuclei, respectively. Scale bar, 50 μ m.

(E) Maximal projections of orthogonal view of accumulation of *FLS2*-fused protein (*FLS2*-GFP) by ablation of epidermal cells. Yellow arrows highlight upregulated *FLS2*-GFP fluorescence (fire LUT of ImageJ software) in neighboring cortical cells. White asterisks indicate damaged cell by laser ablation. Scale bar, 50 μ m.

(F and G) Cell damage activates localized *FLS2* expression level in the undifferentiated zone. In (F), nuclear-localized signals of *FLS2* (green) co-visualized with the PI staining (red), and white arrows highlighted positive nuclei neighboring damaged epidermal cells. Boxplot centers in (G) show median (n = 12 roots). RID, raw intensity density, see legend Figure 1C. Asterisks letters indicate statistically significant differences (***) between means by ANOVA and Tukey's test analysis. ns, not significant. EZ, elongation zone; Ep, epidermis; Co, cortex. Scale bar, 50 μ m.

(H) *FLS2* expression was co-visualized with *FRK1* expression in cortical cells after laser ablation of adjacent epidermal cells. *FLS2* promoter-driven nuclear tdTomato signal (red) and nuclear MAMP reporter signal (green) are co-localizing (yellow) in the presence of flg22 application for 6 h. Arrows indicate MAMP responsive or/and *FLS2*-positive nuclei. Scale bar, 50 μ m.

(I) Venn diagrams showing the number of co-localized cells in cortex (yellow) of *FLS2*-positive (red) and MAMP-responsive cells (green) caused by laser-ablation of epidermal cells. The total cell number for each marker was added from 10 independent ablation events. The size of each circle reflects relative cell numbers. See also Figures S4 and S5.

et al., 2019), we nonetheless tested whether *FLS2* upregulation after damage depended on ethylene.

By combining *FLS2* reporter and MAMP markers in strong ethylene-insensitive mutants, *ein2-1* and *etr1-1*, we could observe a very strong dependency of MAMP responses on ethylene signaling in the elongation zone (Figures S5A and S5B), consistent with a previous study (Millet et al., 2010). However, both sporadic and laser-induced cell damage were still able to induce MAMP responsiveness, independently of ethylene signaling (Figures S5A and S5B). This also applies to lateral root emergence, where cortical cells showed upregulation of *FLS2* expression independently of ethylene signaling (Figure S5C). Treating wild-type MAMP marker lines with ethylene biosynthesis inhibitor corroborated these results (Figure S5D). Consequently, induction of *FLS2* expression itself upon damage was also found to be fully independent on ethylene signaling, although the basal expression levels in the untreated controls were strongly reduced (Figures S5E and S5F). These findings now provide a rationale for earlier observations noting that impaired flg22 signaling in ethylene mutants is not observed in assays involving dissected (wounded) tissues (Mersmann et al., 2010). Importantly, we establish an abiotic stress input into immune signaling that appears to work fully independently of the important stress hormone ethylene.

Casparian Strips Compartmentalize flg22 Responses in Differentiated Roots

In light of the comparatively high expression of *FLS2* in the stele of differentiated roots, we tested whether a mutant defective in Casparian strips, the extracellular diffusion barrier in roots (Geldner, 2013), would display flg22 responsiveness, because of penetration of flg22 into the stele. Indeed, fluorescently labeled flg22 is blocked by the Casparian strip and penetrates into the stele in the barrier mutant (*schengen3-3* [*sgn3-3*]) (Figure S1F). Yet, to our surprise, no flg22 response was observed in the stele of a *sgn3* mutant with endogenous *FLS2* expression (Figure 5A). However, when a constitutively expressing *pUBQ10::FLS2* line was used, a strong flg22 response could be observed in the stele of the endodermal barrier mutant, but not of wild-type (Figures 5B and 5C). This result illustrates the ability of the Casparian strip to compartmentalize perception of immune peptides within the root. Interestingly, however, the wild-type, steady-state levels of *FLS2* expression that we observe in the stele are apparently insufficient to cause MAMP-responsiveness, while enhanced receptor expression from the *UBQ10* promoter is sufficient to install responsiveness. This suggests a thresholded relationship between *FLS2* expression and flg22-dependent transcriptional output.

Suberin Lamellae Interfere with flg22 Perception in the Endodermis

While the Casparian strip functions to block extracellular diffusion of substances (e.g., microbial patterns) into the stele, a second cell wall modification—endodermal suberin lamellae—eventually surrounds the entire endodermis and is thought to inhibit uptake of molecules into the endodermis, because the hydrophobic suberin layer does not allow molecules from the cell wall to reach the endodermal plasma membrane (Figures 5C and 5D) (Barberon et al., 2016). We therefore wanted to see

whether suberization interferes with the ability of endodermal cells to perceive flg22. Indeed, we found that early differentiated endodermis (25 cells after onset of elongation, *non-suberized*) still respond to flg22 in a *pUBQ10::FLS2* line, while they are unresponsive in older endodermal cells (55 cells after onset of elongation, *suberized*) (Figures 5C and 5E). We confirmed absence and presence of suberin at 25 and 55 cells, respectively, using a previously established suberization marker, *pGPAT5::mCITRINE-SYP122* (Barberon et al., 2016; Naseer et al., 2012) (Figure S6A). By inducing precocious and enhanced suberization by two different mechanisms, using either the *enhanced suberin 1* (*esb1*) mutant or treatment with abscisic acid (ABA) (Barberon et al., 2016; Hosmani et al., 2013; Wang et al., 2019), flg22 responsiveness was suppressed in early endodermis (25 cells) (Figures 5C and 5E), demonstrating that protective suberization of a cell is incompatible with continued perception of microbial patterns (Figure 5D). This suppression of endodermal responses by suberization could not only be observed in the constitutive *FLS2*-expressing line, but also with endogenously expressed *FLS2*, after ablation of epidermis and cortex. In this case again, we found that endodermal flg22 responses, observed in early differentiated cells, were abrogated in *esb1* (Figures 5F, S6B, and S6C) or upon ABA treatment (Figures S6D and S6E). We ascertained that ABA does not cause a general suppression of MAMP responses, because responses in the root elongation zone are maintained upon ABA treatment (Figure S6F).

Cell Damage Activates Expression of Multiple Pattern-Recognition Receptors

We then broadened our observations based on *FLS2* to other MAMP receptors by establishing transcriptional reporter lines for three additional *PRRs*, the *EF-TU RECEPTOR (EFR)* (Zipfel et al., 2006), the *CHITIN ELICITOR RECEPTOR KINASE 1 (CEK1)* (Miya et al., 2007), as well as the *nlp20* receptor *RECEPTOR-LIKE PROTEIN 23 (RLP23)* (Albert et al., 2015). In all three cases, a very similar, localized upregulation of receptor expression upon laser-induced cell damage was observed (Figures 6A and 6B), suggesting that cell damage leads to a rather generalized upregulation of response capacity to MAMPs.

We then used an independent MAMP, 3-OH-C10:0, the newly described ligand for the *LIPOLIGOSACCHARIDE-SPECIFIC REDUCED ELICITATION (LORE)* receptor kinase (Ranf et al., 2015). Similar to the other *PRRs*, *LORE* expression is strongly induced upon damage in the early differentiated cells (Figures 6C and 6E). 3-OH-C10:0 elicits direct MAMP responses in the elongation zone, but not in the differentiation zone, similar to flg22 (Figure 6D). More importantly, upon damage, a strong enhancement of responses to 3-OH-C10:0 was observed in the early differentiation zone (Figures 6D and 6F), showing that the observed damage-gating of MAMP responses is not restricted to flg22-*FLS2* module, but is also observed for a non-peptidic, conserved bacterial pattern, perceived by a non-LRR type receptor.

Local Gating of Immune Responses by Damage in Root-Bacteria Interactions

Finally, we tested whether our observations are relevant in the context of actual, bacterial root colonization. For this, we first used the model commensal/beneficial *Pseudomonas protegens*

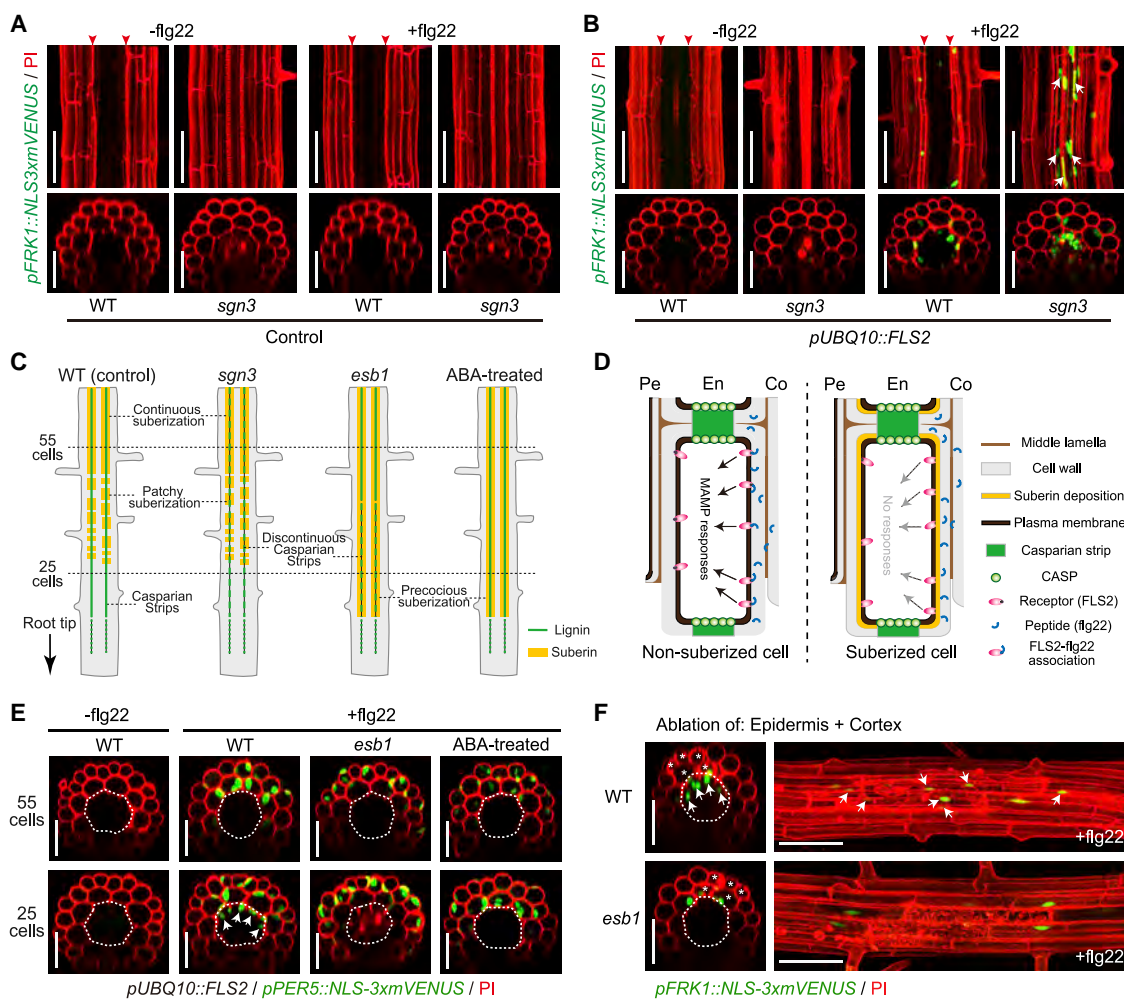


Figure 5. Endodermal Barriers Compartmentalize MAMP Responses in Differentiated Roots

(A and B) Expression pattern of *FRK1* marker in the absence or presence of flg22 in the differentiated zone of WT and endodermal barrier-defective *sgn3-3* roots in Col-0 (A) and *pUBQ10::FLS2* lines (B). Arrowheads indicate site of PI penetration block by the Casparian strips. Note the penetration of PI signals (red) into the stele in *sgn3-3* mutants, revealing their barrier defects. Arrows in (B) indicate MAMP-responsive (*FRK1*-positive) nuclei (green) in the stele of *sgn3-3*. Maximal projections of confocal image stacks were taken at 25 endodermal cells after the onset of cell elongation. Nuclear-localized mVENUS signals (green) counterstained with PI. Scale bar, 50 μ m.

(C) Schematic view of the two endodermal barriers—Casparian strips and suberin lamella—in different backgrounds (WT, *sgn3-3*, and *esb1-1* mutants) and ABA treatment. Lignin and suberin deposition in the endodermis are represented by green and yellow lines, respectively.

(D) Schematic depicting the putative role of suberin lamellae in restricting receptor-peptide recognition on the cell surface. Primary stage and secondary stage of endodermal differentiation are presented by non-suberized (left) and suberized (right) endodermal cells, respectively. In non-suberized cells, peptides can access to the endodermal plasma membrane through apoplastic movement. The resulting plasma membrane-localized receptor-peptide (*FLS2*-flg22) association is capable of activating downstream MAMP responses inside the cell. By contrast, in suberized cells, direct MAMP signal perception on the cell surface is blocked by the presence of suberin lamellae between plasma membranes and primary cell walls of endodermal cells, interrupting the downstream responses.

(E) Representative images depicting expression of *PER5* reporter combined with *FLS2* constitutive expression line (*pUBQ10::FLS2*) in different backgrounds (WT and *esb1-1* mutant) or pre-treatment with ABA (1 μ M, 18 h). Dotted circles and arrows indicate the boundary between endodermal and cortical layers, and endodermal *PER5* responsive nuclei, respectively. Scale bar, 50 μ m.

(F) Co-ablation of epidermal and cortical cells triggers responsiveness to flg22 in differentiated endodermal cells of WT, but not in the precociously suberizing *esb1-1* mutant. White asterisks indicate damaged cells by laser ablation. Maximal projections of confocal image stacks. Image overlays done as described for Figure 1D. Dotted circles and arrows indicate the boundary between endodermal and cortical layer, and endodermal *FRK1* responsive nuclei, respectively. Scale bar, 50 μ m. See also Figure S6.

strain CHA0 (CHA0) (Haas and Défago, 2005; Haas and Keel, 2003). Indeed, despite strong colonization of seedling roots on plates and floating hydroponic roots, no significant MAMP response could be observed in undamaged, differentiated roots

(Figures 7A and S7A–S7C). However, when cell ablation was combined with colonization, the cells neighboring the damage site were showing a MAMP response to the presence of the bacteria (Figures 7B and 7C). As with flg22 treatments, MAMP

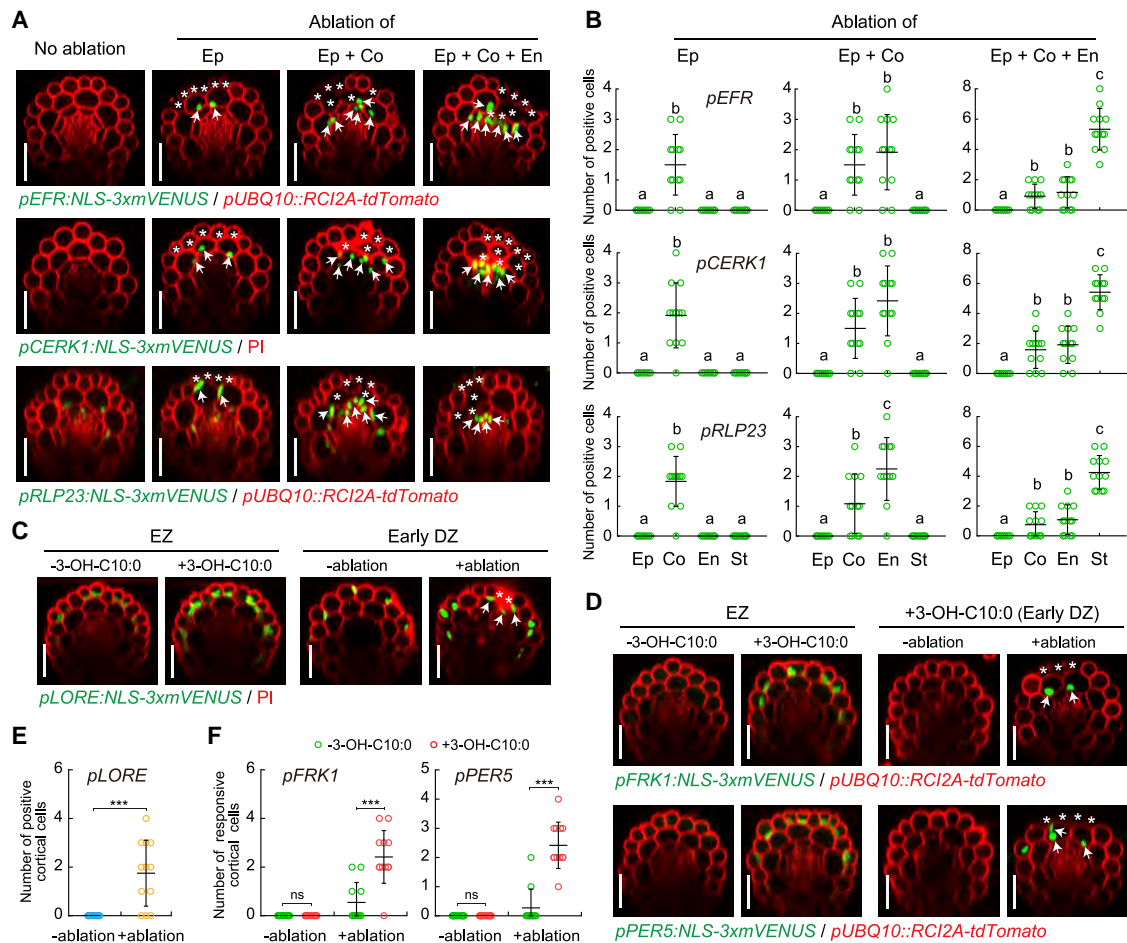


Figure 6. Cell Damage Activates Expression of Multiple Pattern-Recognition Receptors

(A and B) Representative images (A) and quantitative analysis by column scatterplots (B) of promoter activation of three additional *PRRs* after laser ablation of different cell types in differentiated roots. Nuclear-localized mVENUS signals for each *PRR* reporter (green) co-visualized with plasma membrane marker, *pUBQ10::RCIA2A-tdTomato* or PI counterstaining (red). Maximum projections of Z stack of mVENUS signals were combined with single red-channel images. White asterisks indicate laser-ablated cells. Arrows indicate *PRR* promoter-positive nuclei. Each circle in (B) represents individual laser ablation event of one root ($n = 12$ roots). Graph depicts mean values and SD (error bars). Different letters indicate significant differences between means by ANOVA and Tukey's test ($p < 0.001$). Ep, epidermis; Co, cortex; En, endodermis; St, stele. Scale bar, 50 μm .

(C) The expression pattern of another *PRR* reporter, *LORE* in response to 1 μM 3-OH-C10:0 treatment in the elongation zone (EZ) and cell ablation in the early differentiation zone (DZ), respectively. Maximum projections of z stack of mVENUS signals were combined with single red-channel images. Scale bar, 50 μm . (D) The expression pattern of MAMP reporters in response to 3-OH-C10:0 treatment in the elongation zone or combined with ablation in the early differentiation zone. White asterisks and arrows in (C) and (D) indicate laser-ablated cells and reporters positive/responsive nuclei in cortical cells, respectively. Scale bar, 50 μm .

(E and F) Quantitative analysis by column scatterplot of *LORE* reporter (E) and MAMP responsiveness (F) in the absence (–) or presence (+) of laser ablation in 3-hydroxydecanoic acid treated (+3-OH-C10:0) or untreated (–3-OH-C10:0) roots. Each circle represents individual laser ablation event of one root ($n = 12$ roots). Graph depicts mean values and SD (error bars). Asterisks indicate significant differences between means by ANOVA and Tukey's test ($p < 0.001$).

responses to the bacteria were also observed around lateral root emergence sites and upon spontaneous damage (Figure 7A). Next, we tested a root pathogenic bacterium, *Ralstonia solanacearum* GMI1000 (GMI1000) (Genin and Boucher, 2004). Interestingly, GMI1000 colonization initially does not cause cell damage, nor a strong MAMP response (Figure 7D). However, progression of infection eventually leads to cell death of some epidermal cells, which is then associated with a localized upregulation of MAMP responses in neighboring cells (Figures 7D and S7A–S7C). Our bacterial colonization experiments demon-

strate that cellular damage and lateral root emergence does not only unlock MAMP responsiveness to high doses of pure MAMPs such as flg22, or 3-OH-C10:0, but is also effective in unlocking responses to the more complex and probably much less concentrated cocktail of MAMPs associated with actual bacterial colonization. Interestingly, flg22 derived from GMI1000 flagellin was found not to activate the *Arabidopsis* FLS2 receptor (Pfund et al., 2004; Wei et al., 2018). This indicates that the damage-associated MAMP responses we observe upon GMI1000 infection must be caused by MAMPs other than flg22.

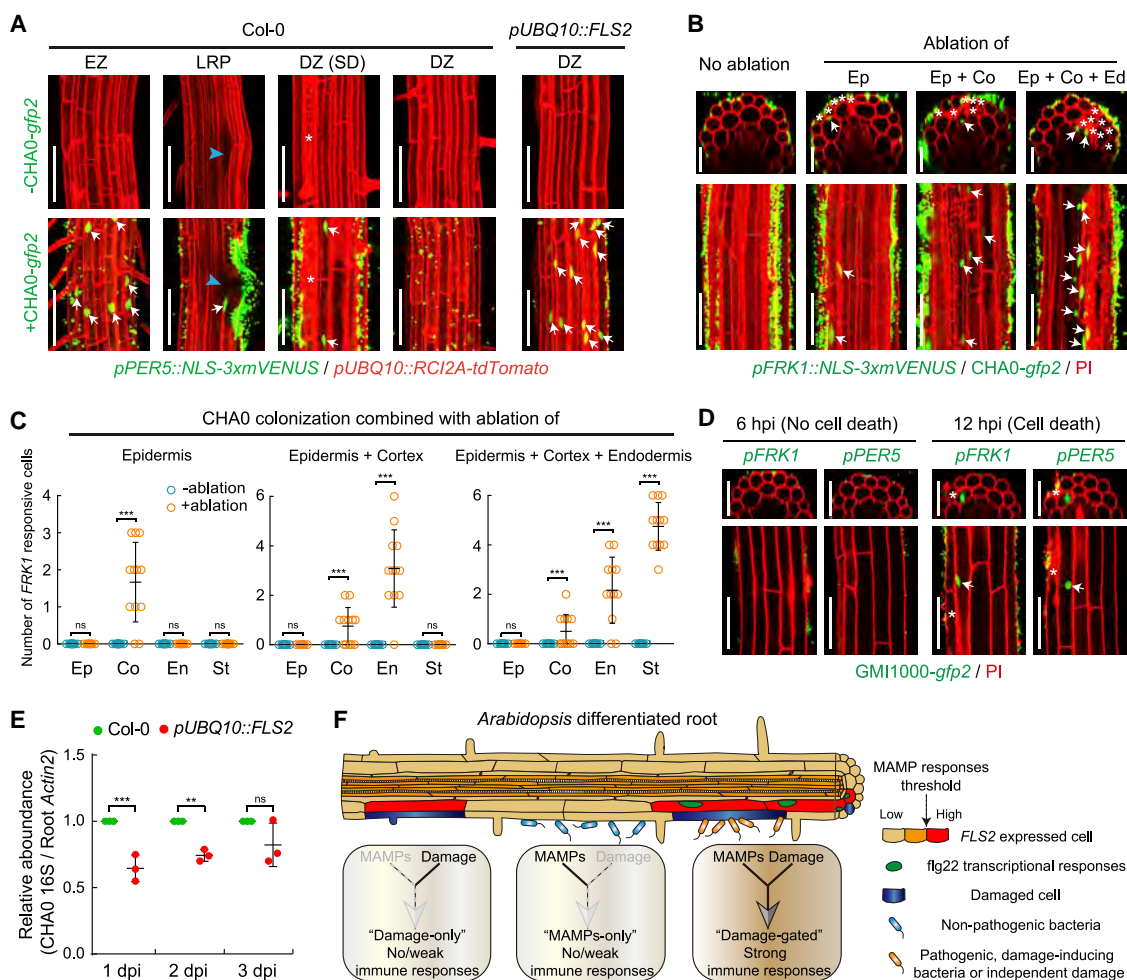


Figure 7. Local Gating of Immune Responses by Damage in Root-Bacteria Interaction

(A) Comparison of *PER5* responsiveness in different developmental zones of control (Col-0) and *FLS2*-overexpressing line (*pUBQ10::FLS2*) in the absence (–*CHA0-gfp2*) or presence (+*CHA0-gfp2*) of bacterial colonization for 9h. MZ, meristematic zone; EZ, elongation zone; DZ, differentiation zone; LRP, lateral root primordium. A blue arrowhead indicates the site of lateral root emergence. White asterisks and arrows indicate non-induced damaged cells and *PER5* responsive nuclei, respectively. Scale bar, 50 μ m.

(B) Laser-induced cell damages can cause MAMP responsiveness (as *FRK1* marker-positive cells) in differentiated roots in response to non-pathogenic *CHA0* microbe colonization. Laser ablation was performed on indicated cell layer(s) followed by 9 h colonization by *CHA0-gfp2* strain ($OD_{600} = 0.1$). Laser-ablated cells are indicated by white asterisks. Arrows indicate localized *FRK1* responses (green), easily distinguished by size and shape from green fluorescent bacteria. Counterstained with PI (red). Image overlays done as described before. Scale bar, 50 μ m.

(C) Quantification of experiments shown in (A). Column scatterplots of the number of *FRK1* responsive cells in different cell types without (blue, –ablation) or with (orange, +ablation) laser damage of different cell layer(s). Each circle represents an individual laser ablation event of one root ($n = 12$ roots). Graph depicts mean values and SD (error bars). Asterisks indicate significant differences between means (** $p < 0.01$ and *** $p < 0.001$) by ANOVA and Tukey's test analysis. ns, not significant. Ep, epidermis; Co, cortex; En, endodermis; St, stele.

(D) Local MAMP responses could also be observed in cells adjacent to damaged cells, observed 12 h post infection (hpi) with the root pathogenic bacteria *GMI1000-gfp2*. By contrast, upon infection with *GMI1000* for short time course (6 hpi), no cell death, and no MAMP response were observed in differentiated cortical cells. Damaged cells associated with *GMI1000* infection are indicated by white asterisks. Arrows indicate localized MAMP responses (green), counterstained with PI (red). Scale bar, 50 μ m.

(E) Quantitative measurement of relative *CHA0* abundance in Col-0 and *pUBQ10::FLS2* roots at indicated colonization time point. Roots colonized with *CHA0-gfp2* strain or mock solvent were collected and their DNA used for real-time PCR using a 16S primer pair described in the STAR Methods. Ct values were normalized to Ct values obtained by a primer set (*AtACTIN2*) amplifying plant-derived DNA. Values are shown with means \pm SD (3 biological replicates, see Figure S7E). Asterisks (** $p < 0.01$ and *** $p < 0.001$) indicate statistically significant differences based on ANOVA and Tukey's test analysis. ns, not significant.

(F) Schematic model of one of *PRRs*, *FLS2* expression pattern in *Arabidopsis* roots and damage-gated local MAMP responses during root-bacteria interaction. Plant roots request both presence of MAMPs and damage before mounting strong immune responses. This model can help to explain how these important *PRRs* can be usefully employed by plant roots, despite the continuous presence of high amounts of commensal or beneficial microbes while maintaining resistance to pathogenic, damage-inducing bacteria.

In addition, the similar, local upregulation of MAMP responsiveness seen upon GMI1000-induced damage further suggests that the phenomenon we describe here is not specific to laser-ablation induced cell damage (already indicated by our observations that MAMP responsiveness also occurs adjacent to sites of spontaneous cell death).

Intriguingly, our constitutively expressing *pUBQ10::FLS2* line, showed direct MAMP responses to CHA0, in the absence of damage (Figure 7A). Such a constitutive, non-damage-gated defense activation should interfere with root colonization of a commensal bacterium such as CHA0 and might be quantifiable, in contrast to a local interference with microbial colonization upon laser-induced damage, which would be impossible for us to quantify. We indeed found a slight, but consistently lower degree of root colonization in plate assays in *pUBQ10::FLS2* lines, both by qPCR-based quantification and colony forming units (CFU) counting (Figures 7E and S7D–S7G). Thus, a restricted, damage-gated MAMP responsiveness of roots contributes to allow for root colonization by innocuous or beneficial bacterial species.

DISCUSSION

Plant roots generate an attractive environment for a subset of soil-borne microbes. These microbes, in turn, affect roots by manipulating plant hormones, signaling, nutrient acquisition, or growth of other microbes, using large sets of genes associated with their root-colonizing life-style (Levy et al., 2017). One important function that promotes colonization is thought to be the ability of some bacteria to suppress MAMP responses, thus avoiding production of anti-microbial compounds and inhibition of root growth. Suppression of MAMP perception by non-pathogenic colonizers has been reported, but is just starting to be understood in mechanistic terms (Garrido-Oter et al., 2018; Pel and Pieterse, 2013; Yu et al., 2019). Type III secretion system (T3SS) effectors are known to suppress MAMP perception (Chisholm et al., 2006), yet appear to be associated with a pathogenic (or symbiotic) life-style, with commensal/beneficial bacteria either not possessing a T3SS or containing only few recognizable T3SS proteins whose functions remain enigmatic (Loper et al., 2012; Stringlis et al., 2019). Our findings now provide an additional level of explanation of how non-pathogenic microbes can successfully colonize roots—by simply avoiding damage and the strong enhancement of immune responses that comes with it (Figure 7F). From the plant-side, such a damage-gating of immune responses is economical, as it avoids constitutive activation of defenses and localizes them to sites where aggressive microbial colonizers might induce cellular damage or where damage due to other causes has generated potential pathogen entry points. For innocuous, root-colonizing bacteria, such a system would alleviate the need to repress plant immunity, as long as colonization proceeds without damage. It will be intriguing to see whether the suppression of MAMP responses by non-pathogenic bacteria still allows for damage-induced enhancement of MAMP responsiveness, in contrast to suppression by type III effectors, which can directly interfere with signaling components downstream of MAMP receptors and can thus be expected to suppress MAMP perception in absence or presence of damage.

An initial pathogenic infection in soil is bound to be localized, involving one or a few cells. Manipulations and molecular readouts at single-cell resolution are therefore of crucial importance for a mechanistic understanding of root-microbe interactions. Recently, we reported that single-cell damage causes surface depolarization, actively propagating calcium signals, ROS, and ethylene production in a surprisingly large region around the single-cell wound (Marhavý et al., 2019). Here, we demonstrate that ablation of clusters of a few cells causes an ethylene-independent, much more restricted, upregulation of MAMP responsiveness, difficult, or impossible to observe by standard molecular readouts or standard methods of wounding. Recently, damage of root cap tissue in meristems was shown to lead to jasmonate receptor-dependent regeneration responses (Zhou et al., 2019). Although we have focused on the differentiated and transition/elongation zone of the root—in which we do not observe regeneration responses—it would be intriguing to investigate whether and how the damage-gating of immune responses described here can be integrated with tissue regeneration. A recent report proposes that loss of cellular integrity causes calcium increases, activating AtPEP1 processing and release into the apoplast, where it could report damage to neighboring cells (Hander et al., 2019). Yet, the damage-induced gain of MAMP responsiveness that we observe here is not reconstituted by co-treatment with AtPEP1 or other DAMPs. We therefore propose that local, non-propagating signals are additionally required for a damage response, such as mechanical stresses on neighboring cell walls or plasmodesmatal collapse, induced by loss of turgor and cellular disintegration in the neighbor. Our data suggest that DAMP release might be a necessary element of damage perception, but is, on its own, insufficient to reconstitute actual cellular damage. In the future, it will be fascinating to use single-cell damage to investigate the immediate molecular events and mechanism that translate loss of cellular integrity into immune responsiveness of adjacent cells.

STAR★METHODS

Detailed methods are provided in the online version of this paper and include the following:

- KEY RESOURCES TABLE
- LEAD CONTACT AND MATERIALS AVAILABILITY
- EXPERIMENTAL MODEL AND SUBJECT DETAILS
 - Plant material
 - Plant growth conditions
 - Bacterial strains and growth conditions
- METHOD DETAILS
 - Generation of transgenic lines
 - Elicitor, hormone and inhibitor treatments
 - Confocal settings and image processing
 - Laser ablation setup
 - Bacterial transformation and infection assay
 - Quantification of CHA0 colonization
- QUANTIFICATION AND STATISTICAL ANALYSIS
- DATA AND CODE AVAILABILITY
- ADDITIONAL RESOURCES

SUPPLEMENTAL INFORMATION

Supplemental Information can be found online at <https://doi.org/10.1016/j.cell.2020.01.013>.

ACKNOWLEDGMENTS

We specially thank Thomas Boller and Jean-Pierre Métraux for many initial discussions on this project. We also would like to thank Jordan Vacheron, Christoph Keel, Youssef Belkadir, and all members from the Geldner lab for sharing material and for helpful discussions and input on the project. This work was supported by funds to N.G. from an ERC Consolidator Grant (GA-N: 616228-ENDOFUN) and two consecutive SNSF grants (CRSII3_136278 and 31003A_156261). F.Z. was supported by an EMBO Long-Term Fellowship (ALTF 1139-2014). P.M. was supported by a Federation of European Biochemical Societies (FEBS) Long-Term Fellowship.

AUTHOR CONTRIBUTIONS

F.Z. and N.G. conceived, designed, and coordinated the project. F.Z., A.E., V.D.T., and D.W. performed all experimental work. F.Z. and N.G. wrote the manuscript. F.Z., A.E., P.M., T.L., and N.G. revised the manuscript and were involved in the discussion of the work.

DECLARATION OF INTERESTS

The authors declare no competing interests.

Received: August 22, 2019

Revised: November 13, 2019

Accepted: January 8, 2020

Published: February 6, 2020

REFERENCES

- Albert, I., Böhm, H., Albert, M., Feiler, C.E., Imkampe, J., Wallmeroth, N., Brancato, C., Raaymakers, T.M., Oome, S., Zhang, H., et al. (2015). An RLP23-SOBIR1-BAK1 complex mediates NLP-triggered immunity. *Nat. Plants* **1**, 15140.
- Alonso, J.M., Hirayama, T., Roman, G., Nourizadeh, S., and Ecker, J.R. (1999). EIN2, a bifunctional transducer of ethylene and stress responses in *Arabidopsis*. *Science* **284**, 2148–2152.
- Asai, T., Tena, G., Plotnikova, J., Willmann, M.R., Chiu, W.-L., Gomez-Gomez, L., Boller, T., Ausubel, F.M., and Sheen, J. (2002). MAP kinase signalling cascade in *Arabidopsis* innate immunity. *Nature* **415**, 977–983.
- Bao, Y., Lies, D.P., Fu, H., and Roberts, G.P. (1991). An improved Tn7-based system for the single-copy insertion of cloned genes into chromosomes of gram-negative bacteria. *Gene* **109**, 167–168.
- Barberon, M., Vermeer, J.E.M., De Bellis, D., Wang, P., Naseer, S., Andersen, T.G., Humbel, B.M., Nawrath, C., Takano, J., Salt, D.E., and Geldner, N. (2016). Adaptation of Root Function by Nutrient-Induced Plasticity of Endodermal Differentiation. *Cell* **164**, 447–459.
- Beck, M., Wyrsh, I., Strutt, J., Wimalasekera, R., Webb, A., Boller, T., and Robatzek, S. (2014). Expression patterns of flagellin sensing 2 map to bacterial entry sites in plant shoots and roots. *J. Exp. Bot.* **65**, 6487–6498.
- Böhm, H., Albert, I., Oome, S., Raaymakers, T.M., Van den Ackerveken, G., and Nürnberger, T. (2014). A conserved peptide pattern from a widespread microbial virulence factor triggers pattern-induced immunity in *Arabidopsis*. *PLoS Pathog.* **10**, e1004491.
- Boller, T., and Felix, G. (2009). A renaissance of elicitors: perception of microbe-associated molecular patterns and danger signals by pattern-recognition receptors. *Annu. Rev. Plant Biol.* **60**, 379–406.
- Boudsocq, M., Willmann, M.R., McCormack, M., Lee, H., Shan, L., He, P., Bush, J., Cheng, S.-H., and Sheen, J. (2010). Differential innate immune signaling via Ca²⁺ sensor protein kinases. *Nature* **464**, 418–422.
- Boutrot, F., Segonzac, C., Chang, K.N., Qiao, H., Ecker, J.R., Zipfel, C., and Rathjen, J.P. (2010). Direct transcriptional control of the *Arabidopsis* immune receptor FLS2 by the ethylene-dependent transcription factors EIN3 and EIL1. *Proc. Natl. Acad. Sci. USA* **107**, 14502–14507.
- Castrillo, G., Teixeira, P.J.P.L., Paredes, S.H., Law, T.F., de Lorenzo, L., Feltcher, M.E., Finkel, O.M., Breakfield, N.W., Mieczkowski, P., Jones, C.D., et al. (2017). Root microbiota drive direct integration of phosphate stress and immunity. *Nature* **543**, 513–518.
- Chang, C., Kwok, S.F., Bleecker, A.B., and Meyerowitz, E.M. (1993). *Arabidopsis* ethylene-response gene ETR1: similarity of product to two-component regulators. *Science* **262**, 539–544.
- Chinchilla, D., Bauer, Z., Regenass, M., Boller, T., and Felix, G. (2006). The *Arabidopsis* receptor kinase FLS2 binds flg22 and determines the specificity of flagellin perception. *Plant Cell* **18**, 465–476.
- Chisholm, S.T., Coaker, G., Day, B., and Staskawicz, B.J. (2006). Host-microbe interactions: shaping the evolution of the plant immune response. *Cell* **124**, 803–814.
- Clay, N.K., Adio, A.M., Denoux, C., Jander, G., and Ausubel, F.M. (2009). Glucosinolate metabolites required for an *Arabidopsis* innate immune response. *Science* **323**, 95–101.
- Clough, S.J., and Bent, A.F. (1998). Floral dip: a simplified method for *Agrobacterium*-mediated transformation of *Arabidopsis thaliana*. *Plant J.* **16**, 735–743.
- Digonnet, C., Martinez, Y., Denancé, N., Chasseray, M., Dabos, P., Ranocha, P., Marco, Y., Jauneau, A., and Goffner, D. (2012). Deciphering the route of *Ralstonia solanacearum* colonization in *Arabidopsis thaliana* roots during a compatible interaction: focus at the plant cell wall. *Planta* **236**, 1419–1431.
- Felix, G., Duran, J.D., Volko, S., and Boller, T. (1999). Plants have a sensitive perception system for the most conserved domain of bacterial flagellin. *Plant J.* **18**, 265–276.
- Finkel, O.M., Castrillo, G., Herrera Paredes, S., Salas González, I., and Dangl, J.L. (2017). Understanding and exploiting plant beneficial microbes. *Curr. Opin. Plant Biol.* **38**, 155–163.
- Garrido-Oter, R., Nakano, R.T., Dombrowski, N., Ma, K.-W., McHardy, A.C., and Schulze-Lefert, P.; AgBiome Team (2018). Modular Traits of the Rhizobiales Root Microbiota and Their Evolutionary Relationship with Symbiotic Rhizobia. *Cell Host Microbe* **24**, 155–167.
- Geldner, N. (2013). The endodermis. *Annu. Rev. Plant Biol.* **64**, 531–558.
- Genin, S., and Boucher, C. (2004). Lessons learned from the genome analysis of *ralstonia solanacearum*. *Annu. Rev. Phytopathol.* **42**, 107–134.
- Gigolashvili, T., Berger, B., Mock, H.-P., Müller, C., Weisshaar, B., and Flügge, U.-I. (2007). The transcription factor HIG1/MYB51 regulates indolic glucosinolate biosynthesis in *Arabidopsis thaliana*. *Plant J.* **50**, 886–901.
- Gómez-Gómez, L., and Boller, T. (2000). FLS2: an LRR receptor-like kinase involved in the perception of the bacterial elicitor flagellin in *Arabidopsis*. *Mol. Cell* **5**, 1003–1011.
- Gómez-Gómez, L., Felix, G., and Boller, T. (1999). A single locus determines sensitivity to bacterial flagellin in *Arabidopsis thaliana*. *Plant J.* **18**, 277–284.
- Granada, G.A., and Sequeira, L. (1983). Survival of *Pseudomonas solanacearum* in soil, rhizosphere, and plant roots. *Can. J. Microbiol.* **29**, 433–440.
- Haas, D., and Défago, G. (2005). Biological control of soil-borne pathogens by fluorescent pseudomonads. *Nat. Rev. Microbiol.* **3**, 307–319.
- Haas, D., and Keel, C. (2003). Regulation of antibiotic production in root-colonizing *Pseudomonas* spp. and relevance for biological control of plant disease. *Annu. Rev. Phytopathol.* **41**, 117–153.
- Hander, T., Fernández-Fernández, Á.D., Kumpf, R.P., Willems, P., Schatowitz, H., Rombaut, D., Staes, A., Nolf, J., Pottier, R., Yao, P., et al. (2019). Damage on plants activates Ca²⁺-dependent metacaspases for release of immunomodulatory peptides. *Science* **363**, eaar7486.
- Hosmani, P.S., Kamiya, T., Danku, J., Naseer, S., Geldner, N., Guerinet, M.L., and Salt, D.E. (2013). Dirigent domain-containing protein is part of the

- machinery required for formation of the lignin-based Casparian strip in the root. *Proc. Natl. Acad. Sci. USA* **110**, 14498–14503.
- Hruz, T., Laule, O., Szabo, G., Wessendorp, F., Bleuler, S., Oertle, L., Widmayer, P., Gruissem, W., and Zimmermann, P. (2008). Genevestigator v3: a reference expression database for the meta-analysis of transcriptomes. *Adv. Bioinforma.* **2008**, 420747.
- Jacobs, S., Zechmann, B., Molitor, A., Trujillo, M., Petutschnig, E., Lipka, V., Kogel, K.-H., and Schäfer, P. (2011). Broad-spectrum suppression of innate immunity is required for colonization of *Arabidopsis* roots by the fungus *Piriformospora indica*. *Plant Physiol.* **156**, 726–740.
- Jeworutzki, E., Roelfsema, M.R.G., Anschütz, U., Krol, E., Elzenga, J.T.M., Felix, G., Boller, T., Hedrich, R., and Becker, D. (2010). Early signaling through the *Arabidopsis* pattern recognition receptors FLS2 and EFR involves Ca-associated opening of plasma membrane anion channels. *Plant J.* **62**, 367–378.
- Jousset, A., Schuldes, J., Keel, C., Maurhofer, M., Daniel, R., Scheu, S., and Thuermer, A. (2014). Full-Genome Sequence of the Plant Growth-Promoting Bacterium *Pseudomonas protegens* CHA0. *Genome Announc.* **2**, e00322-14.
- Keinath, N.F., Waadt, R., Brugman, R., Schroeder, J.I., Grossmann, G., Schumacher, K., and Krebs, M. (2015). Live Cell Imaging with R-GECO1 Sheds Light on flg22- and Chitin-Induced Transient [Ca²⁺]_{cyt} Patterns in *Arabidopsis*. *Mol. Plant* **8**, 1188–1200.
- Koch, B., Jensen, L.E., and Nybroe, O. (2001). A panel of Tn7-based vectors for insertion of the *gfp* marker gene or for delivery of cloned DNA into Gram-negative bacteria at a neutral chromosomal site. *J. Microbiol. Methods* **45**, 187–195.
- Kunze, G., Zipfel, C., Robatzek, S., Niehaus, K., Boller, T., and Felix, G. (2004). The N terminus of bacterial elongation factor Tu elicits innate immunity in *Arabidopsis* plants. *Plant Cell* **16**, 3496–3507.
- Kutschera, A., Dawid, C., Gisch, N., Schmid, C., Raasch, L., Gerster, T., Schäffer, M., Smakowska-Luzan, E., Belkhadir, Y., Vlot, A.C., et al. (2019). Bacterial medium-chain 3-hydroxy fatty acid metabolites trigger immunity in *Arabidopsis* plants. *Science* **364**, 178–181.
- Lacombe, S., Rougon-Cardoso, A., Sherwood, E., Peeters, N., Dahlbeck, D., van Esse, H.P., Smoker, M., Rallapalli, G., Thomma, B.P.H.J., Staskawicz, B., et al. (2010). Interfamily transfer of a plant pattern-recognition receptor confers broad-spectrum bacterial resistance. *Nat. Biotechnol.* **28**, 365–369.
- Lampropoulos, A., Sutkovic, Z., Wenzl, C., Maegle, I., Lohmann, J.U., and Forner, J. (2013). GreenGate—a novel, versatile, and efficient cloning system for plant transgenesis. *PLoS ONE* **8**, e83043.
- Levy, A., Salas Gonzalez, I., Mittelviehhaus, M., Clingenpeel, S., Herrera Paredes, S., Miao, J., Wang, K., Devescovi, G., Stillman, K., Monteiro, F., et al. (2017). Genomic features of bacterial adaptation to plants. *Nat. Genet.* **50**, 138–150.
- Loper, J.E., Hassan, K.A., Mavrodi, D.V., Davis, E.W., 2nd, Lim, C.K., Shaffer, B.T., Elbourne, L.D.H., Stockwell, V.O., Hartney, S.L., Breakwell, K., et al. (2012). Comparative genomics of plant-associated *Pseudomonas* spp.: insights into diversity and inheritance of traits involved in multitrophic interactions. *PLoS Genet.* **8**, e1002784.
- Lotze, M.T., Zeh, H.J., Rubartelli, A., Sparvero, L.J., Amoscato, A.A., Washburn, N.R., Devera, M.E., Liang, X., Tör, M., and Billiar, T. (2007). The grateful dead: damage-associated molecular pattern molecules and reduction/oxidation regulate immunity. *Immunol. Rev.* **220**, 60–81.
- Macho, A.P., and Zipfel, C. (2014). Plant PRRs and the activation of innate immune signaling. *Mol. Cell* **54**, 263–272.
- Marhavý, P., Kurenda, A., Siddique, S., Dénervaud Tendon, V., Zhou, F., Holbein, J., Hasan, M.S., Grundler, F.M., Farmer, E.E., and Geldner, N. (2019). Single-cell damage elicits regional, nematode-restricting ethylene responses in roots. *EMBO J.* **38**, e100972.
- Mersmann, S., Bourdais, G., Rietz, S., and Robatzek, S. (2010). Ethylene signaling regulates accumulation of the FLS2 receptor and is required for the oxidative burst contributing to plant immunity. *Plant Physiol.* **154**, 391–400.
- Millet, Y.A., Danna, C.H., Clay, N.K., Songnuan, W., Simon, M.D., Werck-Reichhart, D., and Ausubel, F.M. (2010). Innate immune responses activated in *Arabidopsis* roots by microbe-associated molecular patterns. *Plant Cell* **22**, 973–990.
- Miya, A., Albert, P., Shinya, T., Desaki, Y., Ichimura, K., Shirasu, K., Narusaka, Y., Kawakami, N., Kaku, H., and Shibuya, N. (2007). CERK1, a LysM receptor kinase, is essential for chitin elicitor signaling in *Arabidopsis*. *Proc. Natl. Acad. Sci. USA* **104**, 19613–19618.
- Naseer, S., Lee, Y., Lapierre, C., Franke, R., Nawrath, C., and Geldner, N. (2012). Casparian strip diffusion barrier in *Arabidopsis* is made of a lignin polymer without suberin. *Proc. Natl. Acad. Sci. USA* **109**, 10101–10106.
- Navarro, L., Zipfel, C., Rowland, O., Keller, I., Robatzek, S., Boller, T., and Jones, J.D.G. (2004). The transcriptional innate immune response to flg22. Interplay and overlap with Avr gene-dependent defense responses and bacterial pathogenesis. *Plant Physiol.* **135**, 1113–1128.
- Péchy-Tarr, M., Borel, N., Kupferschmid, P., Turner, V., Binggeli, O., Radovanovic, D., Maurhofer, M., and Keel, C. (2013). Control and host-dependent activation of insect toxin expression in a root-associated biocontrol pseudomonad. *Environ. Microbiol.* **15**, 736–750.
- Pel, M.J.C., and Pieterse, C.M.J. (2013). Microbial recognition and evasion of host immunity. *J. Exp. Bot.* **64**, 1237–1248.
- Pfister, A., Barberon, M., Alassimone, J., Kalmbach, L., Lee, Y., Vermeer, J.E., Yamazaki, M., Li, G., Maurel, C., Takano, J., et al. (2014). A receptor-like kinase mutant with absent endodermal diffusion barrier displays selective nutrient homeostasis defects. *eLife* **3**, e03115.
- Pfand, C., Tans-Kersten, J., Dunning, F.M., Alonso, J.M., Ecker, J.R., Allen, C., and Bent, A.F. (2004). Flagellin is not a major defense elicitor in *Ralstonia solanacearum* cells or extracts applied to *Arabidopsis thaliana*. *Mol. Plant Microbe Interact.* **17**, 696–706.
- Poncini, L., Wyrsh, I., Dénervaud Tendon, V., Vorley, T., Boller, T., Geldner, N., Métraux, J.-P., and Lehmann, S. (2017). In roots of *Arabidopsis thaliana*, the damage-associated molecular pattern AtPep1 is a stronger elicitor of immune signalling than flg22 or the chitin heptamer. *PLoS ONE* **12**, e0185808.
- Ranf, S., Gisch, N., Schäffer, M., Illig, T., Westphal, L., Knirel, Y.A., Sánchez-Carballo, P.M., Zähringer, U., Hückelhoven, R., Lee, J., and Scheel, D. (2015). A lectin S-domain receptor kinase mediates lipopolysaccharide sensing in *Arabidopsis thaliana*. *Nat. Immunol.* **16**, 426–433.
- Robatzek, S., Chinchilla, D., and Boller, T. (2006). Ligand-induced endocytosis of the pattern recognition receptor FLS2 in *Arabidopsis*. *Genes Dev.* **20**, 537–542.
- Roux, S.J., and Steinebrunner, I. (2007). Extracellular ATP: an unexpected role as a signaler in plants. *Trends Plant Sci.* **12**, 522–527.
- Saad, M., de Zelicourt, A., Rolli, E., Synek, L., and Hirt, H. (2018). Quantification of Root Colonizing Bacteria. *Bio Protoc.* **8** <https://doi.org/10.21769/BioProtoc.2927>.
- Schneider, C.A., Rasband, W.S., and Eliceiri, K.W. (2012). NIH Image to ImageJ: 25 years of image analysis. *Nat. Methods* **9**, 671–675.
- Shimada, T.L., Shimada, T., and Hara-Nishimura, I. (2010). A rapid and non-destructive screenable marker, FAST, for identifying transformed seeds of *Arabidopsis thaliana*. *Plant J.* **61**, 519–528.
- Smith, A.W., and Iglewski, B.H. (1989). Transformation of *Pseudomonas aeruginosa* by electroporation. *Nucleic Acids Res.* **17**, 10509.
- Souza, C.A., Li, S., Lin, A.Z., Boutrot, F., Grossmann, G., Zipfel, C., and Somerville, S.C. (2017). Cellulose-Derived Oligomers Act as Damage-Associated Molecular Patterns and Trigger Defense-Like Responses. *Plant Physiol.* **173**, 2383–2398.
- Stringlis, I.A., Zamioudis, C., Berendsen, R.L., Bakker, P.A.H.M., and Pieterse, C.M.J. (2019). Type III Secretion System of Beneficial Rhizobacteria *Pseudomonas simiae* WCS417 and *Pseudomonas defensor* WCS374. *Front. Microbiol.* **10**, 1631.
- Thor, K., and Peiter, E. (2014). Cytosolic calcium signals elicited by the pathogen-associated molecular pattern flg22 in stomatal guard cells are of an oscillatory nature. *New Phytol.* **204**, 873–881.

- Toyota, M., Spencer, D., Sawai-Toyota, S., Jiaqi, W., Zhang, T., Koo, A.J., Howe, G.A., and Gilroy, S. (2018). Glutamate triggers long-distance, calcium-based plant defense signaling. *Science* 361, 1112–1115.
- Vermeer, J.E.M., von Wangenheim, D., Barberon, M., Lee, Y., Stelzer, E.H.K., Maizel, A., and Geldner, N. (2014). A spatial accommodation by neighboring cells is required for organ initiation in *Arabidopsis*. *Science* 343, 178–183.
- Voisard, C., Keel, C., and Dèfago, G. (1989). Cyanide production by *Pseudomonas fluorescens* helps suppress black root rot of tobacco under gnotobiotic conditions. *EMBO J.* 8, 351–358.
- Wang, P., Calvo-Polanco, M., Reyt, G., Barberon, M., Champeyroux, C., Santoni, V., Maurel, C., Franke, R.B., Ljung, K., Novak, O., et al. (2019). Surveillance of cell wall diffusion barrier integrity modulates water and solute transport in plants. *Sci. Rep.* 9, 4227.
- Wei, Y., Caceres-Moreno, C., Jimenez-Gongora, T., Wang, K., Sang, Y., Lozano-Duran, R., and Macho, A.P. (2018). The *Ralstonia solanacearum* csp22 peptide, but not flagellin-derived peptides, is perceived by plants from the Solanaceae family. *Plant Biotechnol. J.* 16, 1349–1362.
- Wyrsh, I., Domínguez-Ferreras, A., Geldner, N., and Boller, T. (2015). Tissue-specific FLAGELLIN-SENSING 2 (FLS2) expression in roots restores immune responses in *Arabidopsis* fls2 mutants. *New Phytol.* 206, 774–784.
- Yamaguchi, Y., Pearce, G., and Ryan, C.A. (2006). The cell surface leucine-rich repeat receptor for AtPep1, an endogenous peptide elicitor in *Arabidopsis*, is functional in transgenic tobacco cells. *Proc. Natl. Acad. Sci. USA* 103, 10104–10109.
- Yu, K., Liu, Y., Tichelaar, R., Savant, N., Lagendijk, E., van Kuijk, S.J.L., Stringlis, I.A., van Dijken, A.J.H., Pieterse, C.M.J., Bakker, P.A.H.M., et al. (2019). Rhizosphere-Associated *Pseudomonas* Suppress Local Root Immune Responses by Gluconic Acid-Mediated Lowering of Environmental pH. *Curr. Biol.* 29, 3913–3920.
- Zhang, X., Henriques, R., Lin, S.-S., Niu, Q.-W., and Chua, N.-H. (2006). *Agrobacterium*-mediated transformation of *Arabidopsis thaliana* using the floral dip method. *Nat. Protoc.* 1, 641–646.
- Zhou, W., Lozano-Torres, J.L., Blilou, I., Zhang, X., Zhai, Q., Smart, G., Li, C., and Scheres, B. (2019). A Jasmonate Signaling Network Activates Root Stem Cells and Promotes Regeneration. *Cell* 177, 942–956.
- Zipfel, C., Robatzek, S., Navarro, L., Oakeley, E.J., Jones, J.D.G., Felix, G., and Boller, T. (2004). Bacterial disease resistance in *Arabidopsis* through flagellin perception. *Nature* 428, 764–767.
- Zipfel, C., Kunze, G., Chinchilla, D., Caniard, A., Jones, J.D.G., Boller, T., and Felix, G. (2006). Perception of the bacterial PAMP EF-Tu by the receptor EFR restricts *Agrobacterium*-mediated transformation. *Cell* 125, 749–760.

STAR★METHODS

KEY RESOURCES TABLE

REAGENT or RESOURCE	SOURCE	IDENTIFIER
Bacterial and Virus Strains		
<i>Pseudomonas protegens</i> CHA0	Voisard et al., 1989	NCBI:txid1124983
<i>Pseudomonas protegens</i> CHA0- <i>gfp2</i>	Péchy-Tarr et al., 2013	N/A
<i>Ralstonia solanacearum</i> GMI1000	Granada and Sequeira, 1983	NCBI:txid267608
<i>Ralstonia solanacearum</i> GMI1000- <i>gfp2</i>	This paper	N/A
Chemicals, Peptides, and Recombinant Proteins		
flg22 _{CHA0}	Peptide Specialty Laboratories GmbH	N/A
AtPEP1	Peptide Specialty Laboratories GmbH	N/A
nlp20	Peptide Specialty Laboratories GmbH	N/A
elf18	Peptide Specialty Laboratories GmbH	N/A
TAMRA-flg22 _{Pa}	Peptron	N/A
TAMRA-AtPEP1	Peptron	N/A
Propidium iodide (PI)	Sigma-Aldrich	Cat#P4170
Extracellular ATP (eATP)	Sigma-Aldrich	Cat#A2383
D-(+)-Cellobiose	Sigma-Aldrich	Cat#C7252
(±)-3-Hydroxydecanoic acid (3-OH-C10:0)	Sigma-Aldrich	Cat#H3648
Chitin from shrimp shells	Sigma-Aldrich	Cat#C9752
Galacturonan oligosaccharide mixture DP10-DP15 (OGs)	Elicityl	GAT114
(±)-Abscisic acid (ABA)	Sigma-Aldrich	Cat#A1049
Aminoethoxyvinylglycine (AVG)	Sigma-Aldrich	Cat#A6685
1-Aminocyclopropane-1-carboxylic acid (ACC)	Sigma-Aldrich	Cat#A3903
Critical Commercial Assays		
MESA BLUE qPCR MasterMix Plus for SYBR Assay	Eurogentec	RT-SY2X-03+WOUB
Experimental Models: Organisms/Strains		
<i>Arabidopsis thaliana</i> : WT Col-0	NASC	NCBI:txid3702
<i>Arabidopsis</i> : <i>fls2</i>	Zipfel et al., 2004	SALK_062054C
<i>Arabidopsis</i> : <i>sgn3-3</i>	Pfister et al., 2014	SALK_043282
<i>Arabidopsis</i> : <i>esb1-1</i>	Hosmani et al., 2013	NASC ID: N2106042
<i>Arabidopsis</i> : <i>ein2-1</i>	Alonso et al., 1999	NASC ID: N65994
<i>Arabidopsis</i> : <i>etr1-1</i>	Chang et al., 1993	NASC ID: N237
<i>Arabidopsis</i> : <i>pGPAT5::mCITRINE-SYP122</i>	Barberon et al., 2016	Transgenic Col-0
<i>Arabidopsis</i> : <i>pPER5::NLS-3xmVENUS</i>	Poncini et al., 2017	Transgenic Col-0
<i>Arabidopsis</i> : <i>pPER5::NLS-3xmVENUS, pUBQ10::RCI2A-tdTomato</i>	This paper	Transgenic Col-0
<i>Arabidopsis</i> : <i>pWRKY11::NLS-3xmVENUS</i>	Poncini et al., 2017	Transgenic Col-0
<i>Arabidopsis</i> : <i>pWRKY11::NLS-3xmVENUS, pUBQ10::RCI2A-tdTomato</i>	This paper	Transgenic Col-0
<i>Arabidopsis</i> : <i>pMYB51::NLS-3xmVENUS</i>	Poncini et al., 2017	Transgenic Col-0
<i>Arabidopsis</i> : <i>pMYB51::NLS-3xmVENUS, pUBQ10::RCI2A-tdTomato</i>	This paper	Transgenic Col-0
<i>Arabidopsis</i> : <i>pFRK1::NLS-3xmVENUS</i>	This paper	Transgenic Col-0
<i>Arabidopsis</i> : <i>pFRK1::NLS-3xmVENUS, pUBQ10::RCI2A-tdTomato</i>	This paper	Transgenic Col-0
<i>Arabidopsis</i> : <i>pFLS2::NLS-3xmVENUS</i>	This paper	Transgenic Col-0
<i>Arabidopsis</i> : <i>pFLS2::NLS-3xmVENUS, pUBQ10::RCI2A-tdTomato</i>	This paper	Transgenic Col-0
<i>Arabidopsis</i> : <i>pFLS2_{long}::NLS-3xmVENUS, pUBQ10::RCI2A-tdTomato</i>	This paper	Transgenic Col-0
<i>Arabidopsis</i> : <i>pEFR::NLS-3xmVENUS, pUBQ10::RCI2A-tdTomato</i>	This paper	Transgenic Col-0

(Continued on next page)

Continued

REAGENT or RESOURCE	SOURCE	IDENTIFIER
<i>Arabidopsis</i> : pCERK1::NLS-3xmVENUS, pUBQ10::RCI2A-tdTomato	This paper	Transgenic Col-0
<i>Arabidopsis</i> : pRLP23::NLS-3xmVENUS, pUBQ10::RCI2A-tdTomato	This paper	Transgenic Col-0
<i>Arabidopsis</i> : pLORE::NLS-3xmVENUS	This paper	Transgenic Col-0
<i>Arabidopsis</i> : pFLS2::FLS2-3xMYC-GFP	Robatzek et al., 2006	Transgenic Ws-0
<i>Arabidopsis</i> : pFLS2 _{long} ::FLS2-3xMYC-mVENUS	This paper	<i>fls2</i> mutant
<i>Arabidopsis</i> : pPER5::NLS-3xmVENUS, pFLS2 _{long} ::FLS2-3xMYC-mVENUS	This paper	<i>fls2</i> mutant
<i>Arabidopsis</i> : pUBQ10::FLS2	This paper	Transgenic Col-0
<i>Arabidopsis</i> : pFRK1::NLS-3xmVENUS, pUBQ10::FLS2	This paper	Transgenic Col-0
<i>Arabidopsis</i> : pPER5::NLS-3xmVENUS, pUBQ10::FLS2	This paper	Transgenic Col-0
<i>Arabidopsis</i> : pFRK1::NLS-3xmVENUS, pFLS2::NLS-tdTomato	This paper	Transgenic Col-0
<i>Arabidopsis</i> : pPER5::NLS-3xmVENUS, pFLS2::NLS-tdTomato	This paper	Transgenic Col-0
Oligonucleotides		
Primers for cloning reporter lines, see Table S1	This paper	N/A
Primer: CHA0 16S gene Forward: TGAAGAAGGTCTTCGGAT TGTAAGC	This paper	N/A
Primer: CHA0 16S gene Reverse: GCTACACAGGAAATCCACCACCCT	This paper	N/A
Primer: <i>Arabidopsis</i> housekeeping gene <i>AtACTIN2</i> Forward: CTGGATCGGTGGTTCCATTC	This paper	N/A
Primer: <i>Arabidopsis</i> housekeeping gene <i>AtACTIN2</i> Reverse: CCTGGACCTGCCTCATCATAC	This paper	N/A
Recombinant DNA		
pFRK1::NLS-3xmVENUS	This study	N/A
pPER5::NLS-3xmVENUS	This study	N/A
pWRKY11::NLS-3xmVENUS	This study	N/A
pMYB51::NLS-3xmVENUS	This study	N/A
pFLS2::NLS-3xmVENUS	This study	N/A
pFLS2 _{long} ::NLS-3xmVENUS	This study	N/A
pEFR::NLS-3xmVENUS	This study	N/A
pCERK1::NLS-3xmVENUS	This study	N/A
pRLP23::NLS-3xmVENUS	This study	N/A
pLORE::NLS-3xmVENUS	This study	N/A
pFLS2::NLS-tdTomato	This study	N/A
pUBQ10::RCI2A-tdTomato	This study	N/A
pUBQ10::FLS2	This study	N/A
pFLS2 _{long} ::FLS2-3xMYC-mVENUS	This study	N/A
Software and Algorithms		
Fiji (ImageJ)	Schneider et al., 2012	https://imagej.nih.gov/ij/
Zeiss Zen 2011	https://www.zeiss.com/corporate/int/home.html	N/A
GraphPad Prism 7.0	https://www.graphpad.com	N/A

LEAD CONTACT AND MATERIALS AVAILABILITY

Further information and requests for resources and reagents should be directed to and will be fulfilled by the Lead Contact, Niko Geldner (niko.geldner@unil.ch). Plasmids and transgenic plant seeds generated in this study will be made available on request, but we may require a payment and/or a completed Materials Transfer Agreement if there is potential for commercial application.

EXPERIMENTAL MODEL AND SUBJECT DETAILS

Plant material

Arabidopsis thaliana ecotype Columbia (Col-0) was used as wild-type control for all experiments. The *fls2* (SALK_062054C), and *sgn3-3* and *esb1-1* mutants were previously described (Zipfel et al., 2004; Pfister et al., 2014; Hosmani et al., 2013). The *ein2-1* and *etr1-1* mutants were provided by the Nottingham *Arabidopsis* Stock Centre (NASC) and was originally reported in Alonso et al. (1999) and Chang et al. (1993). MAMP response reporter lines *pPER5::NLS-3xmVENUS*, *pWRKY11::NLS-3xmVENUS* and *pMYB51::NLS-3xmVENUS* were described previously (Poncini et al., 2017). Suberization marker *pGPAT5::mCITRINE-SYP122* was generated and reported previously (Barberon et al., 2016). *pFLS2::FLS2-3xMYC-GFP* line was obtained from Prof. Thomas Boller's group (Robatzek et al., 2006).

Plant growth conditions

For all experiments, plant seeds were surface-sterilized in 70% EtOH for 10 min, then washed twice in 99% ethanol and dried in sterile conditions. Seeds were stratified at 4°C in the dark on 0.8% half Murashige and Skoog (MS) agar plates without addition of sucrose. Plant roots were grown vertically for 6 d at 22°C under continuous days.

Bacterial strains and growth conditions

The GFP-tagged *Pseudomonas protegens* strain, CHA0-*gfp2* (CHA0::attTn7-*gfp2*; Gm^r) and the GFP-labeled *Ralstonia solanacearum* strain, GMI1000-*gfp2* (GMI1000::attTn7-*gfp2*; Gm^r) were provided by Prof. Christoph Keel (Péchy-Tarr et al., 2013) and generated by electroporation transformation method (See in METHOD DETAILS), respectively. Bacterial strains were incubated overnight in liquid LB medium (1% tryptone, 0.5% yeast extract and 1% NaCl, for CHA0-*gfp2*) or BG medium (1% peptone, 0.1% Casamino acid, 0.1% yeast extract and 0.5% glucose, for GMI1000-*gfp2*) supplemented with 30 µl/ml gentamycin at 28°C. Bacterial cells were collected by centrifugation, and resuspended in sterile MiliQ water for further root inoculation assays.

METHOD DETAILS

Generation of transgenic lines

For generating expression constructs, the In-Fusion Advantage PCR Cloning Kit (Clontech), Gateway Cloning Technology (Invitrogen) and GreenGate Cloning System (Lampropoulos et al., 2013) were used. See Table S1 for primer details. All plasmids were transformed by heat shock into *Agrobacterium tumefaciens* GV3101 strain with or without pSoup plasmid and then transformed into the corresponding plant lines by floral dipping method (Clough and Bent, 1998; Zhang et al., 2006). Several independent transgenic lines were analyzed, and the strongest line of each construct was selected for further studies.

For labeling of the plasma membrane, *pUBQ10::RCI2A-tdTomato* construct was generated using a triple Gateway reaction recombining the following plasmids: pDONR P4-P1R-*pUBQ10*, pDONR 221-*RCI2A* (containing the coding sequence of the small plasma membrane localized protein RARE-COLD-INDUCIBLE 2A (AtRCI2A)), pDONR P2R-P3-*tdTomato* and pK7m34GW (destination vector containing the kanamycin resistance gene for *in planta* selection). The resulting plasmid was transformed into Col-0 plants. Transcriptional reporters were created using the following promoters: *pFRK1* (Asai et al., 2002), *pFLS2* (Zipfel et al., 2004), *pFLS2_{long}*, *pEFR* (Zipfel et al., 2006), *pCERK1* (Miya et al., 2007), *pRLP23* (Albert et al., 2015), *pLORE* (Ranf et al., 2015). Fragments were PCR-amplified and cloned into HindIII site of *pGreenHygromycin-NLS-3xmVENUS* (Vermeer et al., 2014). The resulting constructs were introduced into Col-0 or *pUBQ10::RCI2A-tdTomato* background.

To overexpress *FLS2* gene in MAMP marker lines, the *pUBQ10::FLS2* plasmid was constructed using double Gateway cloning. The full-length genomic *FLS2* DNA, including the *FLS2* coding region, 227 bp of upstream sequence, and 953 bp downstream sequence was cloned into the entry clone pDONR 221. This vector was then combined to the entry clone pDONR P4-P1R-*pUBQ10* and the destination vector pK7m24GW to create the final expression clone *pUBQ10::FLS2*. The resulting construct was transformed into stable MAMP marker lines, which were then introduced into the *sgn3-3* mutant background by genetic crossing. For generating *FLS2* complementation line, the *pFLS2_{long}::FLS2-3xMYC-mVENUS* plasmid was constructed by double Gateway cloning. Full-length genomic *FLS2* fragment fused with triple MYC tag followed by a mVENUS sequence was cloned into pDONR 221. This vector was then combined with an entry clone pDONR P4-P1R-*pFLS2_{long}* and the destination vector pFR7m24GW (destination vector containing the *FastRed* cassette for transgenic seed selection) (Shimada et al., 2010) to create the final expression clone, which was transformed into *fls2* mutant background.

To combine *FLS2* and MAMP-reporters in the same background, *pFLS2::NLS-tdTomato* plasmid was constructed using GreenGate Cloning System. *pFLS2* short promoter was PCR-amplified and cloned into pGGA (plasmid Green Gate A) entry vector to generate pGGA-*pFLS2*, which was then recombined using Greengate reaction with the following plasmids: pGGB-SV40-NLS, pGGC-*tdTomato*, pGGD-*dummy*, pGGE-*UBQ10terminator*, pGGF-*FastRed* and pGGZ-*empty* destination vector. The final construct possesses the *FastRed* cassette for transgenic plant selection. The obtained construct was transformed into a stable MAMP marker background.

Elicitor, hormone and inhibitor treatments

flg22_{CHA0} oligopeptide from *Pseudomonas protegens* CHA0 (TRLSSGLKINSKDDAAGLQIA) (Jousset et al., 2014), nlp20 oligopeptide from *Phytophthora parasitica* (PpNLP) (AIMYSWYFPKDSPTGLGHR) (Böhm et al., 2014), elf18 oligopeptide from *E. coli* strain GI826 (Ac-SKEKFERTKPHVNVGTIG) (Kunze et al., 2004) and *Arabidopsis thaliana* Plant Elicitor Peptide 1, AtPEP1 (ATKVKAKQRG KEKVSSGRPGQHN) (Yamaguchi et al., 2006) were chemically synthesized by Peptide Specialty Laboratories GmbH (<https://www.peptid.de/>). The peptides were dissolved in deionized water to obtain 1 mM stock solution and further dilutions were done with half MS medium. Fluorescently-labeled peptides TAMRA-flg22_{Pa} and TAMRA-AtPEP1 were synthesized by Peptron (<http://www.peptron.com/>) and dissolved in water to a final concentration of 1 μ M for all assays. Extracellular ATP (eATP), D-(+)-cellobiose (cellobiose), (\pm)-3-Hydroxydecanoic acid (3-OH-C10:0) and chitin were obtained from Sigma-Aldrich. Galacturonan oligosaccharide mixture DP10-DP15 (OGs) was purchased from Elicityl (<https://www.elicityl-oligotech.com/>). These chemicals were dissolved in water to the stock concentrations of 100 mM for eATP, 1 mM for 3-OH-C10:0 and cellobiose, 2 mg/ml for chitin and 5 mg/ml for OGs. For hormone treatments, (\pm)-Abscisic acid (ABA) was stored as a 50 mM stock solution in methanol and 1-Aminocyclopropane-1-carboxylic acid (ACC) as a 20 mM stock solution in water. For ethylene biosynthesis inhibitor treatment, Aminoethoxyvinylglycine (AVG) was dissolved in water as a 10 mM stock solution.

For microscopic analysis of *pFLS2* reporter and MAMP marker lines under various treatments, six-day-old seedlings were carefully transferred into liquid half MS medium containing the mentioned chemical molecules using 12-well culture plates (CytoOne™). The seedlings were observed under confocal microscopy after 6h treatment, unless otherwise specified, in standard growth condition. A pool of 10-12 homozygous seedlings from the T3 generation was analyzed for each assay. At least three independent replicates were performed.

Confocal settings and image processing

Confocal laser scanning microscopy was performed on a Zeiss LSM880 inverted confocal scanning microscope. Pictures were taken with a 40 \times water immersion objectives. For more detailed analyses in large area of interest, imaging was performed thanks to Z-scan with tile-scan (overlap 10%). For green and red fluorophores, the following excitation and detection windows were used: mVENUS/GFP 488 nm, 500-530 nm; mCITRINE 496 nm, 530 nm; PI 520 nm, 590 nm; tdTomato 550 nm, 580 nm; TAMRA 560 nm, 570-610 nm. Sequential scanning was used to avoid interference between fluorescence channels. Confocal images after treatments and/or ablations were taken following the “four identical criteria,” that is, using the same position in the roots, the same laser detection intensity, the same laser scanning area, and the same interval and number of slices for Z stack projection.

Laser ablation setup

The sample preparation and manipulation for laser ablation was done as described before (Marhavý et al., 2019). Briefly, six-day-old seedlings were carefully transferred from half MS medium plate into a Chambered Coverglass (Nunc Lab-Tek, 2-well format, Thermo Scientific). In each well 4-5 roots lied alongside the cover glass, and then the entire root parts were covered with a block of solid half MS medium (approximately equal to 1 mL in liquid volume). Finally, chambers were covered with lid and mounted onto the confocal microscopy for time-lapse imaging and cell-type-specific laser ablation. Cell ablation experiments were performed on a Zeiss LSM880 Confocal/Multiphoton (Mai-Tai Spectra-Physics Multiphoton laser). Parameters for ablation were set as below: 40 \times water immersion objective, scaling dimensions (xyz), laser 800 nm -2% , beam splitter MBS_InVis: MBS 760+, pixel dwell: 0.8 μ s. A region of interest (ROI) was drawn through the cell prior to ablation.

To combine laser ablation-caused cell damage with flg22 treatment in Chambered Coverglass system, we first ablated specific root cells and then immediately added 500 μ L of 3 μ M flg22 solution into the chamber to obtain a final concentration of 1 μ M flg22. After 6h treatment, the liquid solution was removed carefully to avoid roots movement, and then confocal images were taken directly for reporter lines expressing the plasma membrane marker. For the lines devoid of plasma membrane marker, plasma membrane outline and damaged cells can be labeled clearly by adding 50 μ L of PI solution (5x) onto the agar block of half MS medium for 10 min before observation.

Bacterial transformation and infection assay

To obtain the GFP-labeled *Ralstonia solanacearum* GMI1000 strain, GMI1000-*gfp2* (GMI1000::attTn7-*gfp2*; Gm^r), we introduced a GFP fluorescent tag into the bacterial genome by electroporation transformation method as described before (Smith and Iglewski, 1989). Briefly, GMI1000 was grown in BG broth (1% Bacto peptone, 0.1% casamino acids, 0.1% yeast extract, 0.5% glucose) with vigorous shaking at 28°C until early log phase (OD₆₀₀ = 0.4-0.6). 1.5 mL of pre-culture cells were harvested by centrifugation at 13,000 g for 2 min at 4°C, pellet was resuspended with the same volume MOPS-Glycerol (MOPS 1 mM with 15% Glycerol, keep on ice), re-centrifuged, washed in 1/3 volume of wash medium (MOPS-Glycerol) and finally re-suspended in 1/15 volume (75 μ L) of MOPS-Glycerol. The cell suspension was chilled on ice for 30 min prior to electroporation. 5 μ L of delivery vector, pBK-miniTn7-*gfp2* (Koch et al., 2001) and 5 μ L of a helper plasmid DNA pUXBF13 (Bao et al., 1991), were gently mixed with cell suspension and then transferred to pre-chilled 0.2 cm cuvettes (Bio-Rad). Electroporation was performed using the following settings: capacitance, 25 μ F; voltage, 2.4 kV; resistance, 200 Ω ; pulse length, < 5 msec. 1 mL of SOC medium was then immediately added and the mix incubated with shaking for 1 h at 28°C. Finally, the mixture was plated on BG solid medium supplemented with 30 μ L/ml gentamycin and incubated at 28°C until colonies have grown.

For bacterial infection on the roots, two different infection assays were used for both bacteria: drop dipping infection on solid MS plate and floating hydroponic inoculation. For drop dipping infection, we followed the method as described previously (Digonnet et al., 2012) with some modifications. In short, six-day-old seedlings were selected for uniform growth and transferred to half MS agar plates carefully. After incubation overnight in LB (for CHA0) or BG (for GMI1000) medium, bacteria were collected, washed and resuspended in distilled water. 10 μ L of bacterial suspension at an optical density of $OD_{600} = 0.1$ (10^8 cfu/ml) was applied to the seedling by depositing small droplets along the whole root. Infected plates were then grown vertically for one to three days before microscopic observation according to the experiments. For floating hydroponic infection, four seeds were evenly spread on a small patch of sterile mesh (2 cm x 2 cm), which was then deposited onto a half MS agar plate for germination. After 3 days, when roots grew across the holes of mesh, we transferred the seedlings-supporting mesh onto a 12-well cell culture plates, containing 7 mL of hydroponic solution by well (the seedlings-supporting mesh floating on the solution). Grown for another 4 days, the bacterial suspension was then added in the hydroponic solution of each well to a final OD_{600} of 0.1. Roots were infected by bacteria for 6 h to 12 h before observation under confocal microscope.

For combining CHA0 infection with laser ablation, we used the Chambered Coverglass system similarly to flg22 treatment. Briefly, after ablation, 500 μ L of bacterial suspension at an optical density of $OD_{600} = 0.1$ was gently added into the chamber to avoid roots movement. After 6 h infection, the bacterial solution was removed carefully, and confocal images were taken on Zeiss LSM 880.

Quantification of CHA0 colonization

For qPCR analysis of bacterial colonization, the experiment was performed as described previously (Garrido-Oter et al., 2018) with minor modification. In brief, four-day-old seedlings were carefully transferred to solid half MS plate containing CHA0 at final density of $OD_{600} = 0.002$. After inoculation at the indicated time point, three roots for each sample were collected from plates and briefly washed once in sterile water for 5 s to remove non-attached bacterial cells. After removal of excess water with a filter paper (Whatman, UK), roots were frozen in liquid nitrogen and stored at -80°C until further processing. DNA was extracted using the DNeasy Plant Mini Kit (QIAGEN, Germany) according to the manufacturer's instructions. qPCR was performed in a 20 μ L reaction mixture containing 10 μ L MESA BLUE qPCR 2X MasterMix Plus for SYBR[®] Assay (Eurogentec, Belgium), 30 ng DNA template, 0.5 μ M forward primer and 0.5 μ M reverse primer. PCR was performed by a QuantStudio 3 Real-Time PCR System (Thermo Fisher Scientific, USA) using the following cycles: 95°C for 2 min, followed by 40 cycles of 95°C for 10 s, 58°C for 30 s, and 72°C for 30 s. Data from three biological replicates were analyzed following the delta-Ct method, which was used to estimate the relative abundance of bacteria to the abundance of plant DNA. Primers sequence used for qPCR are: 499_500 for CHA0 16S gene and plant housekeeping gene *AtACTIN2* for normalization.

For calculate the number of CHA0 colonization, the experiment was conducted by CFU counting (Saad et al., 2018). Briefly, four-day-old seedlings were transferred to new half MS agar plates containing CHA0 ($OD_{600} = 0.002$). Parts of their roots grown for indicated colonization time point were cut, gently washed by dipping in distilled water, and then ground in Eppendorf tubes using TissueLyser II (QIAGEN, Germany) with stainless steel beads. Each sample was resuspended in 500 μ L of extraction buffer (10 mM MgCl_2 , 0.01% Silwet L-77) to homogenize the plant material. Samples were diluted 4,000-fold, and then spread on LB agar plates supplemented with 30 μ l/ml gentamycin. The CFU were counted after 36h incubation at 28°C until colonies are clearly visible. Calculated number of CFU was normalized per centimeter of root length (total root length was determined based on images of root systems before their harvest). The experiment was conducted in three biological replicates, each with three technical replicates per condition; each sample consisted of three roots.

QUANTIFICATION AND STATISTICAL ANALYSIS

For quantifying the nuclear-localized fluorescence intensity of MAMP markers and *FLS2* reporter, confocal images were analyzed with the Fiji package (<http://fiji.sc/Fiji>). Contrast and brightness were adjusted in the same manner for all images. In short, first, we set a defined threshold value for the same experiment between control and treatments. For example, all signals below a gray value threshold of 30 were excluded from quantification to avoid autofluorescence signal and weak non-MAMP responsive signal. Note that this threshold value is not fixed between different reporters and can be adjusted according to their fluorescent intensity. Second, after setting the detectable size of pixel to avoid noise signal, the size of the total area with signal (number of pixels) can be determined, which, multiplied by the average intensity of the pixels for each area, give the total fluorescence intensity for each nucleus, called "RawIntDen" - raw intensity density (RID). Finally, the overall score of an image is the sum of the RID values of all particles (nuclei).

Counting of the numbers of MAMP-responsive and/or *PRR*-positive cells in different root cell types was obtained as follows: a threshold value was set for removing noise signals. In some cases, for reporter lines or specific cell layers showing weak MAMP-responsive and/or *PRR*-positive fluorescence, we elevated the threshold value to separate the basal level of fluorescence and the weak non-MAMP responsive signals from the strongly induced MAMP-responsive signals. All signals below a given gray value threshold were excluded from the cell nuclei counting. The score average was obtained from 10-12 images of replicate roots.

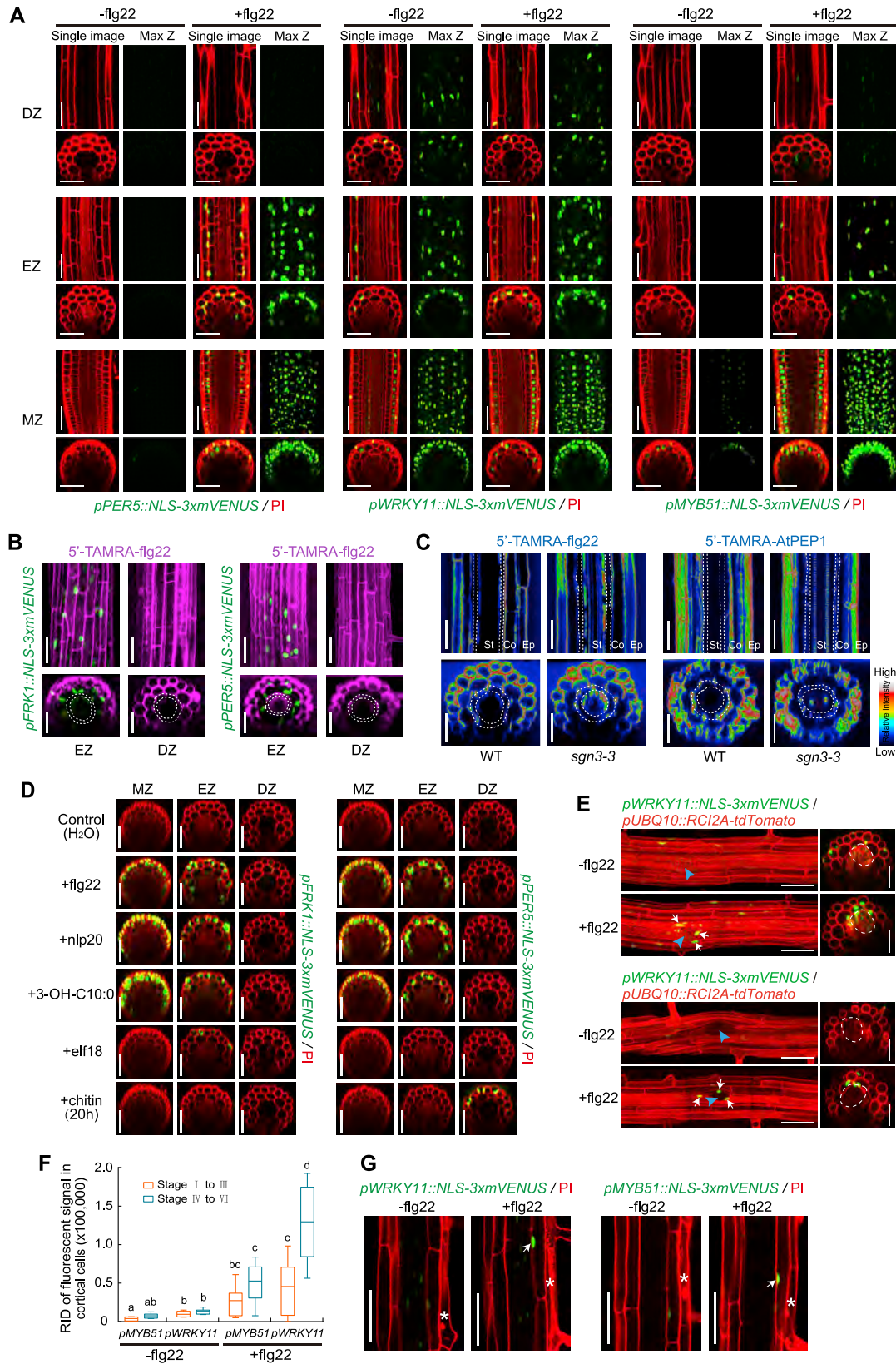
All statistical analyses were done with the Graphpad Prism 7.0 software (<https://www.graphpad.com/>). One-way ANOVA was performed, and Tukey's test was subsequently used as a multiple comparison procedure. Details about the statistical approaches used can be found in the figure legends. The data are presented as mean \pm SD, and "n" represents number of plant roots.

DATA AND CODE AVAILABILITY

This study did not generate any unique datasets or code.

ADDITIONAL RESOURCES

This study did not generate any additional resources.



(legend on next page)

Figure S1. Localized MAMP Responsiveness in *Arabidopsis* Differentiated Roots, Related to Figure 1

(A) The expression pattern of three additional MAMP markers, *PER5*, *WRKY11* and *MYB51* in response to 1 μ M flg22 treatment. Images taken are corresponding to the same position as in Figure 1A. Images in differentiated zone were always taken at a distance of 25 endodermal cells after onset of cell elongation. In each treatment, single confocal section (Single image, left panels) and maximal projections of Z stacks (Max Z, right panels) are presented; median longitudinal and transverse (xz) section views are shown in upper and bottom panels, respectively. Nuclear-localized mVENUS signals (green) are co-visualized with propidium iodide (PI, red). MZ, meristematic zone; EZ, elongation zone; DZ, differentiation zone. Scale bar, 50 μ m.

(B and C) Fluorescently-labeled peptide 5'-TAMRA-flg22 penetrates into roots through the apoplast. 5'-TAMRA-flg22 is functional and can activate distinct MAMP responses in the elongation zone (EZ) and differentiation zone (DZ) of the roots (B). Six-day-old roots were treated with 1 μ M 5'-TAMRA-flg22 for 6h. Nuclear-localized mVENUS signals (green) co-visualized with TAMRA fluorescence (magenta). Representative images of the comparison of 5'-TAMRA-flg22 and 5'-TAMRA-AtPEP1 movement between WT and *sgn3-3* mutant background (C). Transverse and longitudinal view of the endodermal cell layer is indicated between dotted lines or circles. Note penetration of TAMRA fluorescence (royal LUT in ImageJ software) into the stele of *sgn3-3* mutant after 1 h peptide application. Maximum projections of longitudinal and transverse section views are shown in upper and bottom panel, respectively. Ep, epidermis; Co, cortex; St, stele. Scale bar, 50 μ m.

(D) Comparison of the response pattern of *FRK1* and *PER5* markers upon stimulation with different MAMPs. The chemicals were used at the following concentrations: 1 μ M flg22, nlp20, 3-OH-C10:0, elf18 and 100 μ g/ml chitin. All images were taken after 6 h treatment unless otherwise specified. Nuclear-localized mVENUS signals (green) are co-visualized with propidium iodide (PI, red). MZ, meristematic zone; EZ, elongation zone; DZ, differentiation zone. Scale bar, 50 μ m.

(E) flg22 responsiveness during lateral root primordium (LRP) formation. Images of stage IV of lateral root development of 8-day-old seedlings of double marker lines, highlighting plasma membrane of all root cells through *pUBQ10::RC12A-tdTomato* expression (red) in addition to the MAMP responses (green, indicated by white arrows). The shape of emerged LRP is indicated by dotted circle in the orthogonal view, site of emergence is indicated by a blue arrowhead in longitudinal maximum projections. Image overlays done as described for Figure 1D. Scale bar, 50 μ m.

(F) Quantification of *MYB51* and *WRKY11* markers in response to different developmental stages of lateral root emergence with or without flg22 application. Boxplot centers show median (n = 10 roots). Different letters indicate statistically significant differences ($p < 0.05$, ANOVA and Tukey's test). RID, see legend Figure 1C.

(G) Spontaneous, non-induced cell death (asterisks) causes flg22 responsiveness (arrows) in neighboring cortical cell layer. Damaged differentiated epidermal cells are highlighted by PI staining.

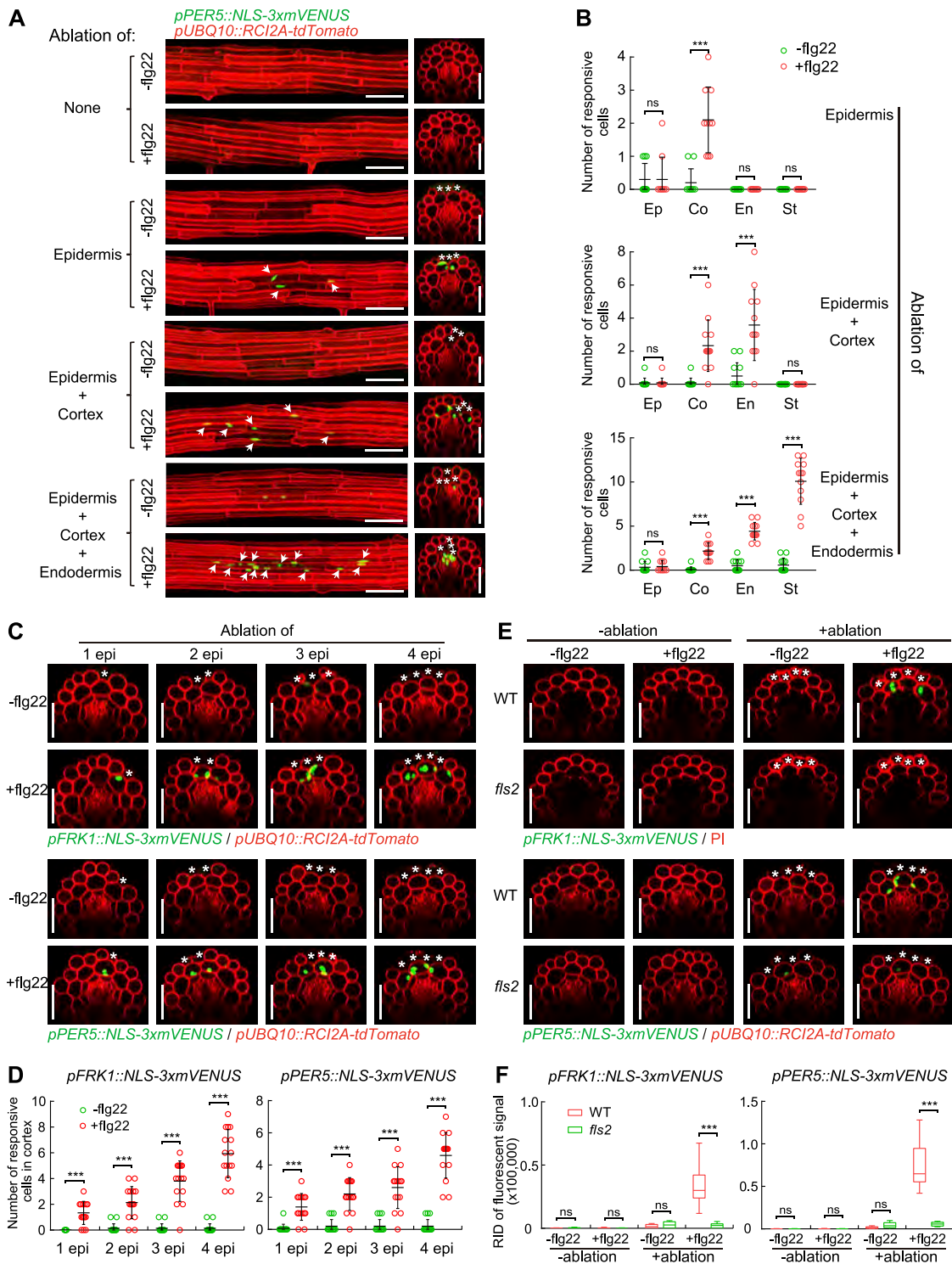


Figure S2. Laser Ablation-induced MAMP Responsiveness Rely on Cell Damage Extent and Functional FLS2, Related to Figure 2

(A and B) Representative images (A) and quantitative analysis by column scatterplot (B) of *PER5* responsiveness after laser ablation of different cell types in differentiated roots. Laser ablation and all images were at 25 endodermal cells after the onset of cell elongation. Nuclear-localized mVENUS signals for each *PRR* reporter (green) co-visualized with plasma membrane marker, *pUBQ10::RCI2A-tdTomato* (red). Maximum projections of Z stack of mVENUS signals were combined with single red-channel images (see Figure 2A). White asterisks indicate laser-ablated cells. Arrows indicate *PER5* responsive nuclei. Scale bar, 50 μ m. Each circle in (B) represents individual laser ablation event of one root (n = 12 roots). Graph depicts mean values and SD (error bars). Asterisks indicate significant differences between means by ANOVA and Tukey's test ($p < 0.001$). ns, not significant. Ep, epidermis; Co, cortex; En, endodermis; St, stele. Scale bar, 50 μ m.

(legend continued on next page)

(C and D) Representative images (C) and quantification by column scatterplot (D) of MAMP responsiveness after laser ablation of different epidermal cell numbers with or without flg22 for 6 h in differentiated roots. Nuclear-localized mVENUS signals of *FRK1* and *PER5* reporters (green) co-visualized with the plasma membrane marker, *pUBQ10::RC12A::tdTomato* (red). White asterisk indicates damaged cell by laser ablation. Scale bar, 50 μm . Each circle in (D) represents individual laser ablation event ($n = 12$). Data represent mean values and SD (error bars). 1 epi, one epidermal cell; 2 epi, two epidermal cells; etc. (E and F) Orthogonal views (E) and RID quantification (F) of *FRK1* and *PER5* responsiveness in WT and *fis2* mutant background after combining without (-ablation) or with (+ablation) damage of epidermal cells in the absence or presence of flg22 for 6 h. Scale bar, 50 μm . Boxplot centers in (F) show median. Asterisks indicate significant differences between means ($p < 0.001$) by ANOVA and Tukey's test analysis ($n = 10$ independent ablation events). ns, not significant. RID, see legend [Figure 1C](#).

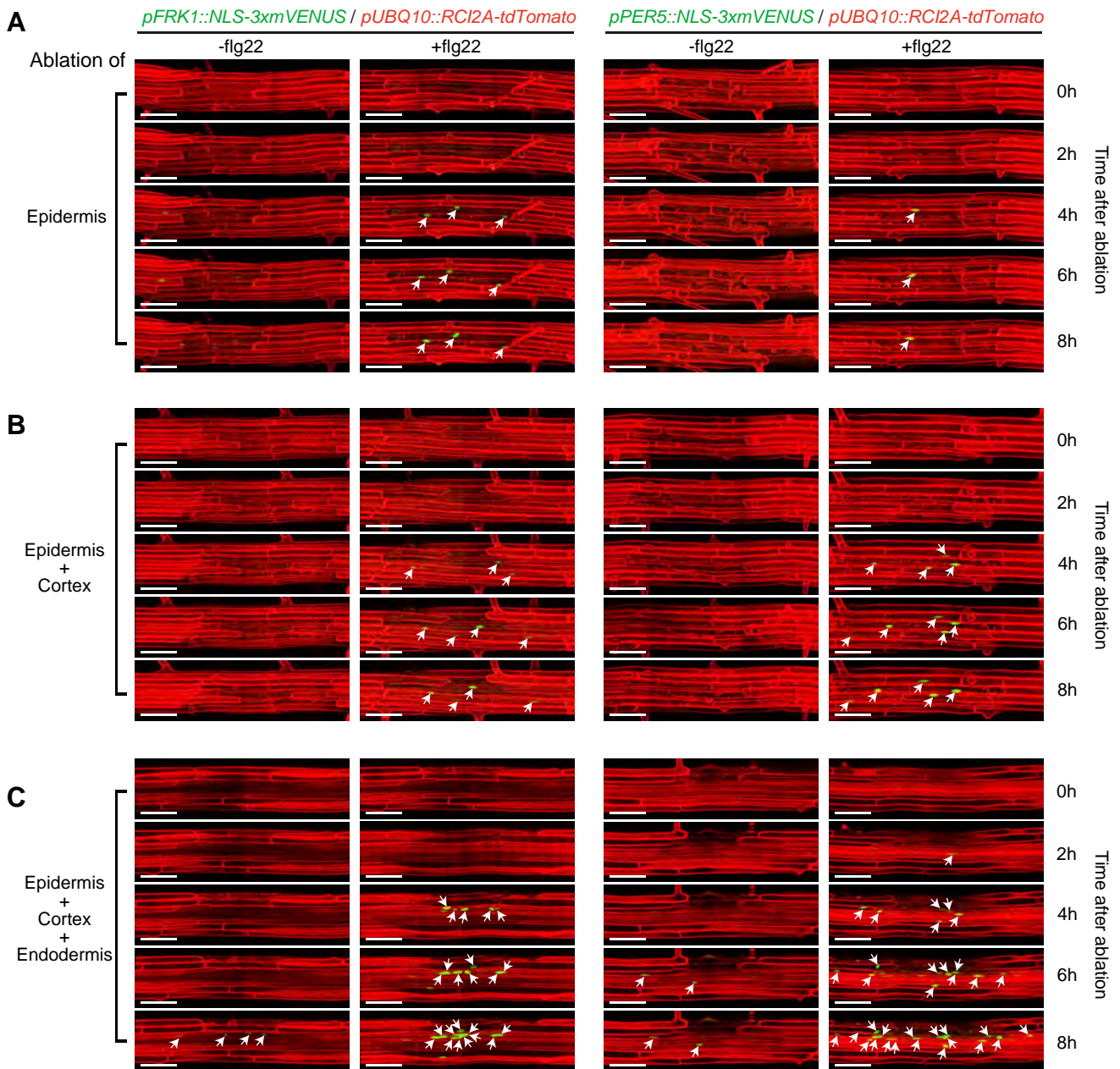


Figure S3. Time-Lapse Images of Ablation-Triggered Fig22 Responses, Related to Figure 2

(A-C) Real-time monitored MAMP responsiveness after laser ablation of different cell types in differentiated root cells. The combination of ablated cell types shown as following: (A) epidermal cells; (B) epidermal and cortical cells; (C) epidermal, cortical and endodermal cells. Nuclear-localized mVENUS signals of *FRK1* and *PER5* reporters (green) co-visualized with the plasma membrane marker, *pUBQ10::RCI2A:tdTomato* (red). Laser ablation and all images were at 25 endodermal cells after the onset of cell elongation. Maximal projections of Z stack of mVENUS signals and plasma membrane outline was merged together for longitudinal section view. White asterisk indicates damaged cell by laser ablation. Arrows indicate MAMP responsive nuclei. Scale bar, 50 μm .

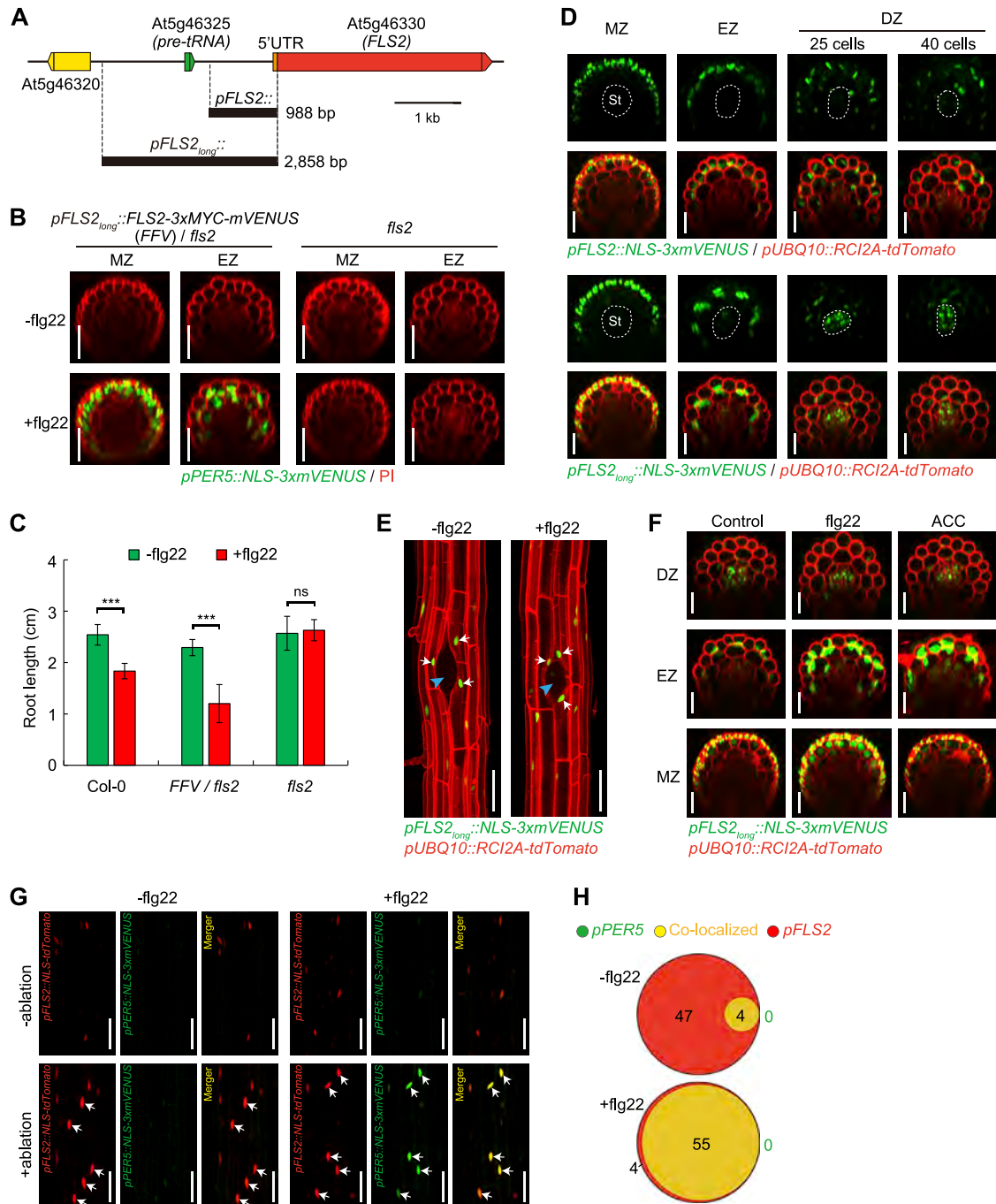


Figure S4. FLS2 Expression Patterns in Arabidopsis Roots, Related to Figure 4

(A) Schematic map of two *FLS2* promoters with different length and neighboring genome region. The shorter promoter, *pFLS2* was cloned from original study (Gómez-Gómez and Boller, 2000). The longer one, *pFLS2_{long}* promoter, covers the sequence of *pFLS2*, then extending to the upstream region of another neighboring gene *At5g46325*, a putative *pre-tRNA* gene. Color box: gene locus; black line: intergenic sequence.

(B and C) The longer promoter *pFLS2_{long}*, driving an *FLS2*-mVENUS construct, was shown to rescue MAMP responses in *fls2* mutant background. Complementation analysis of *PER5* maker induction (B) and root growth inhibition (C) in response to flg22 treatment. Asterisks in (C) indicate statistically significant differences ($p < 0.001$) between means by ANOVA and Tukey's test analysis. ns, not significant. MZ, meristematic zone; EZ, elongation zone. Scale bar, 25 μ m. (D) Comparison of the expression patterns between the two promoters in different zones of the root. Nuclear-localized *FLS2* mVENUS signals only (green, upper panel) or co-visualized with plasma membrane marker (red, bottom panel). For differentiation zone (DZ), longitudinal sections of images were taken at 25 or 40 endodermal cell numbers after the onset of cell elongation, respectively. Dotted circles indicate the stele (St). Scale bar, 25 μ m.

(legend continued on next page)

(E) Localized *FLS2* induction during lateral root primordium (LRP) formation without (-) or with (+) flg22. Maximal projections of longitudinal sections were showing the stage IV of lateral root development of eight-day-old seedlings. Site of emergence is indicated by a blue arrowhead. Arrows indicate *FLS2*-induced nuclei. Scale bar, 50 μ m.

(F) Activity of *pFLS2_{long}* promoter under flg22 (1 μ M) or ACC (10 μ M) induction condition for 6 h in different zones of the root. Scale bar, 25 μ m.

(G) *FLS2* expression were co-visualized with *PER5* expression in cortical cells after laser ablation of adjacent epidermal cells. *FLS2* promoter-driven nuclear tdTomato signal (red) and nuclear MAMP reporter signals (green) are co-localizing (yellow) in the presence of flg22 application for 6 h. Arrows indicate MAMP responsive or/and *FLS2*-positive nuclei. Scale bar, 50 μ m.

(H) Venn diagrams showing the number of co-localized cells in cortex (yellow) of *FLS2*-positive (red) and *PER5*-responsive cells (green) caused by laser-ablation of epidermal cells. The total cell number for each marker was accumulated from 10 independent ablation events. The relative size of each circle reflects counted cell numbers.

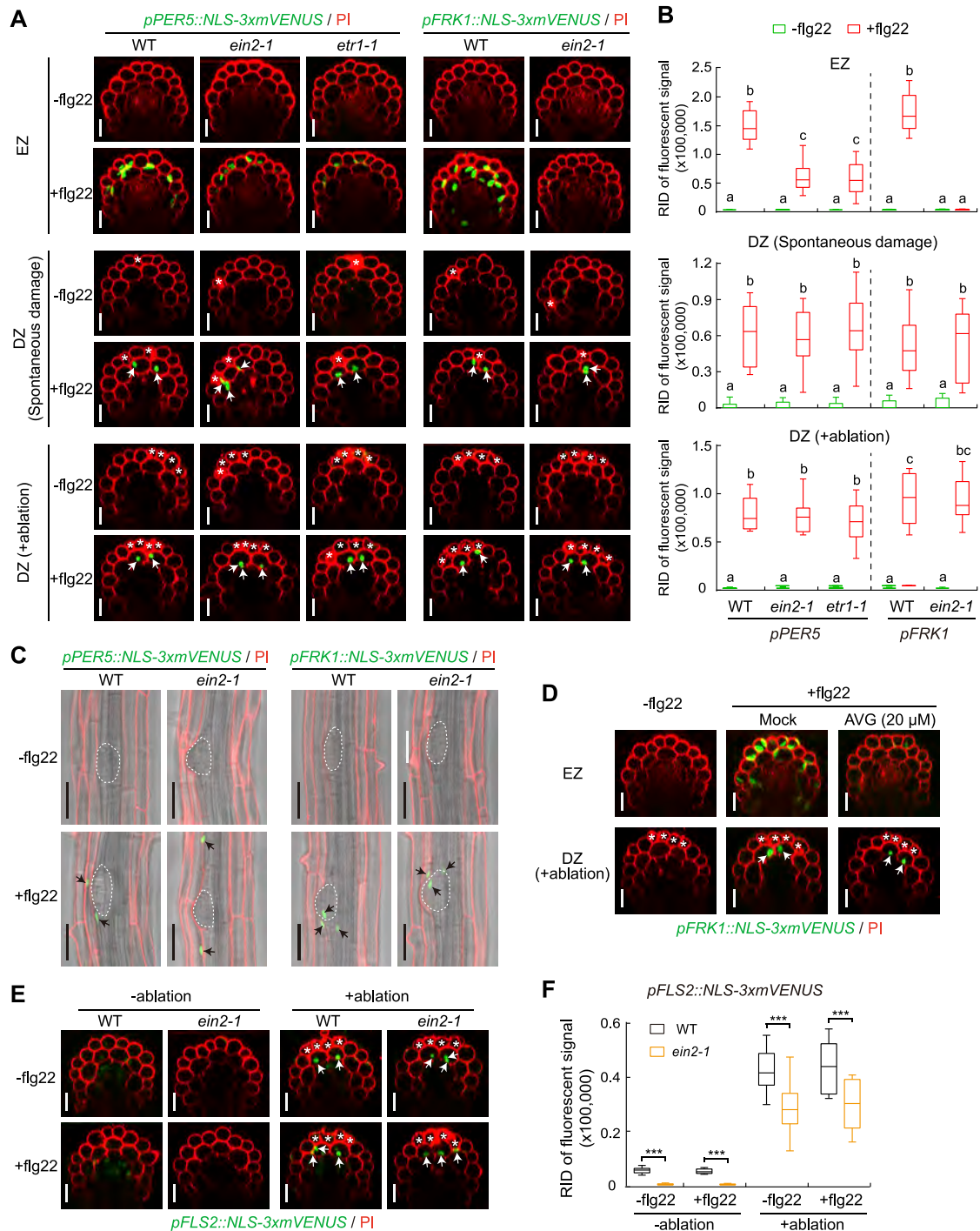


Figure S5. Unlocking of Flg22 Responsiveness by Cell Damage Is Independent of Ethylene Signaling, Related to Figures 2 and 4

(A and B) Representative images (A) and quantitative analysis by boxplot chart (B) of *PER5* and *FRK1* responsiveness without (-) or with (+) flg22 treatment in WT and ethylene insensitive mutants, *ein2-1* and *etr1-1*, elongating roots (upper panel), spontaneously damaged roots (middle panel) and laser-ablated differentiated roots (bottom panel). Note MAMP responsiveness in elongation zone is partially or completely dependent on ethylene signaling as MAMP fluorescent signals, compared to WT, are highly decreased (*PER5*) or fully abolished (*FRK1*) in ethylene insensitive mutants after flg22 application for 6 h. Nuclear-localized mVENUS signals (green) co-visualized with PI counterstaining (red). White asterisks indicate damaged cells. In (B), boxplot centers show median (n = 12 roots). Different letters ($p < 0.001$) indicate statistically significant differences between means by ANOVA and Tukey's test analysis. RID, raw intensity density. Scale bar, 50 μ m. (C) Longitudinal view of maximum projection of MAMP responsiveness in the absence (-) or presence (+) of flg22 in WT and *ein2-1* mutant LRP formation site. Emerged LRP shape is highlighted by dotted circle in the bright-field background (gray). Black arrows indicate responsive nuclei. Scale bar, 50 μ m.

(legend continued on next page)

(D) Maximum projection of *FRK1* reporter in elongated cells (upper panel) or laser-ablated differentiated cells (bottom panel) pre-treated with ethylene biosynthesis inhibitor, 2-aminoethoxyvinyl glycine (AVG) for 2 h. Scale bar, 50 μm .

(E and F) Confocal images (E) and RID quantitative analysis (F) of *FLS2* induction without (-ablation) or with (+ablation) laser-damaged epidermal cells in comparison between WT and *ein2-1* differentiated roots. Laser ablations were performed at 25 endodermal cells after onset of cell elongation. White asterisks indicate damaged cells. Boxplot centers in (F) show median (n = 12 roots). Asterisks ($p < 0.001$) indicate statistically significant differences between means by ANOVA and Tukey's test analysis. RID, see legend [Figure 1C](#). Scale bar, 50 μm .

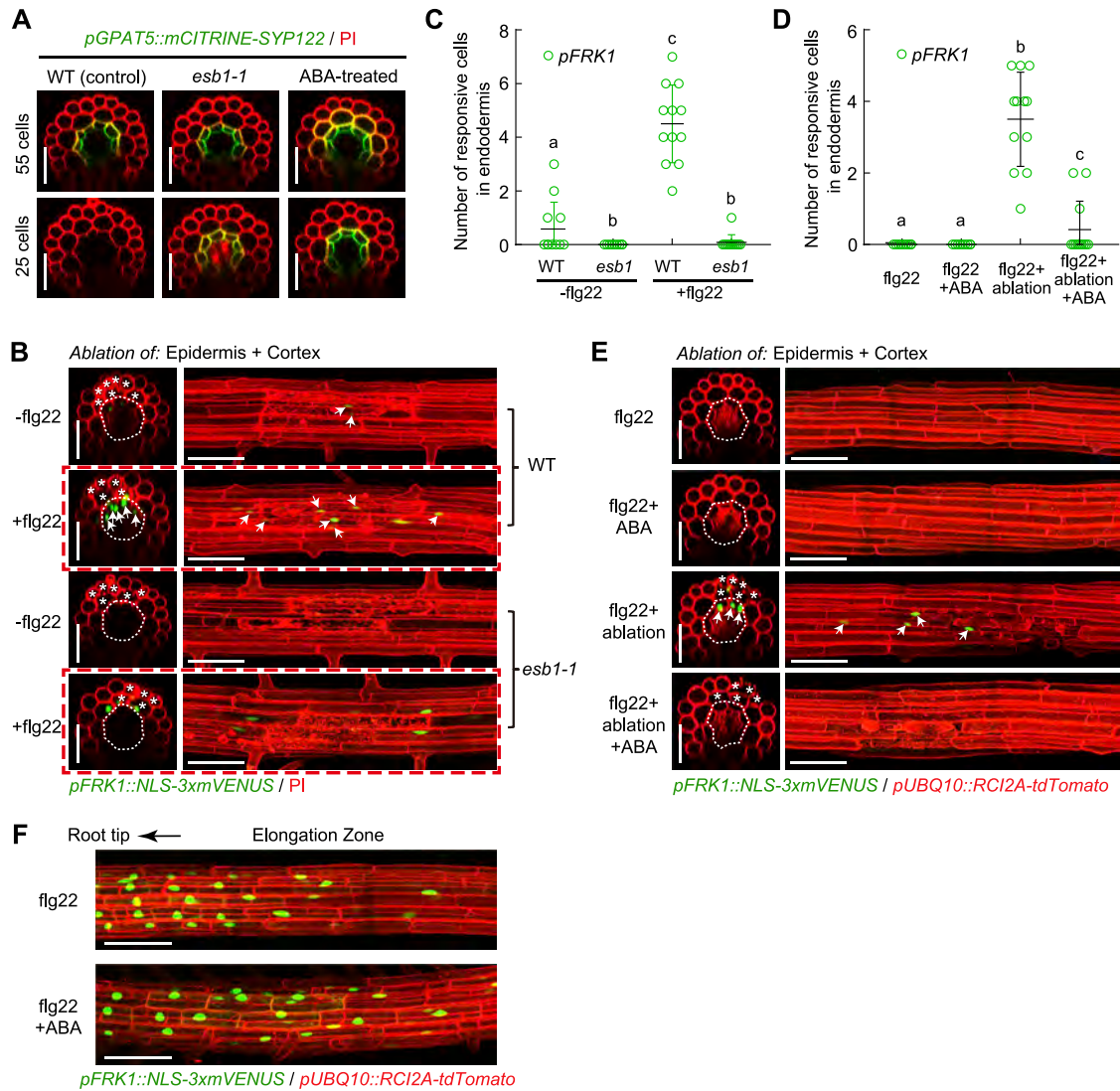


Figure S6. Suberin Lamellae Interfere with flg22 Perception in the Endodermis, Related to Figure 5

(A) Suberin plasma membrane marker *pGPAT5::mCITRINE-SYP122* expression (green) along the root developmental stages in different backgrounds (WT and *esb1-1* mutant) or treated with 1 μ M ABA (WT background) prior to observation. The *GPAT5* reporter line counterstained with PI (red). Images were taken at 25 or 55 endodermal cell numbers after the onset of cell elongation, respectively.

(B and C) Representative images (B) and quantitative analysis by column scatterplot (C) of co-ablation of epidermal and cortical cells triggers responsiveness to flg22 in differentiated endodermal cells of WT, but not in the precociously-suberizing *esb1-1* mutant (B). Nuclear-localized mVENUS signals (green) co-visualized with PI staining or plasma membrane marker (red). Maximum projections of transverse (left panel) and longitudinal sections (right panel) are shown. Arrows represent endodermal *FRK1*-responsive cell nuclei. White asterisks indicate damaged cells by laser ablation, taken at 25 endodermal cells after the onset of cell elongation. Note images in red dotted box were used for Figure 5D. Each circle in (C) represents individual laser ablation event of one root (n = 12 roots). Values are means \pm SD. Individual letters indicate statistically significant differences ($p < 0.001$, ANOVA and Tukey's test).

(D and E) Quantification (D) and images (E) of co-ablation of epidermal and cortical cells triggers responsiveness to flg22 in differentiated endodermal cells of non-treated control, but not in ABA pre-treated roots (E). Each circle in (D) represents individual laser ablation event of one root (n = 12 roots). Values are means \pm SD. Individual letters indicate statistically significant differences ($p < 0.001$, ANOVA and Tukey's test).

(F) ABA treatment did not affect MAMP responses in elongating root cells. Six-day-old roots were pre-treated with 1 μ M ABA prior to flg22 application for 6h. Pictures are maximum projections of confocal Z stacks. ABA pre-treatment in (D-F) was performed for 18 h. Scale bar, 50 μ m.

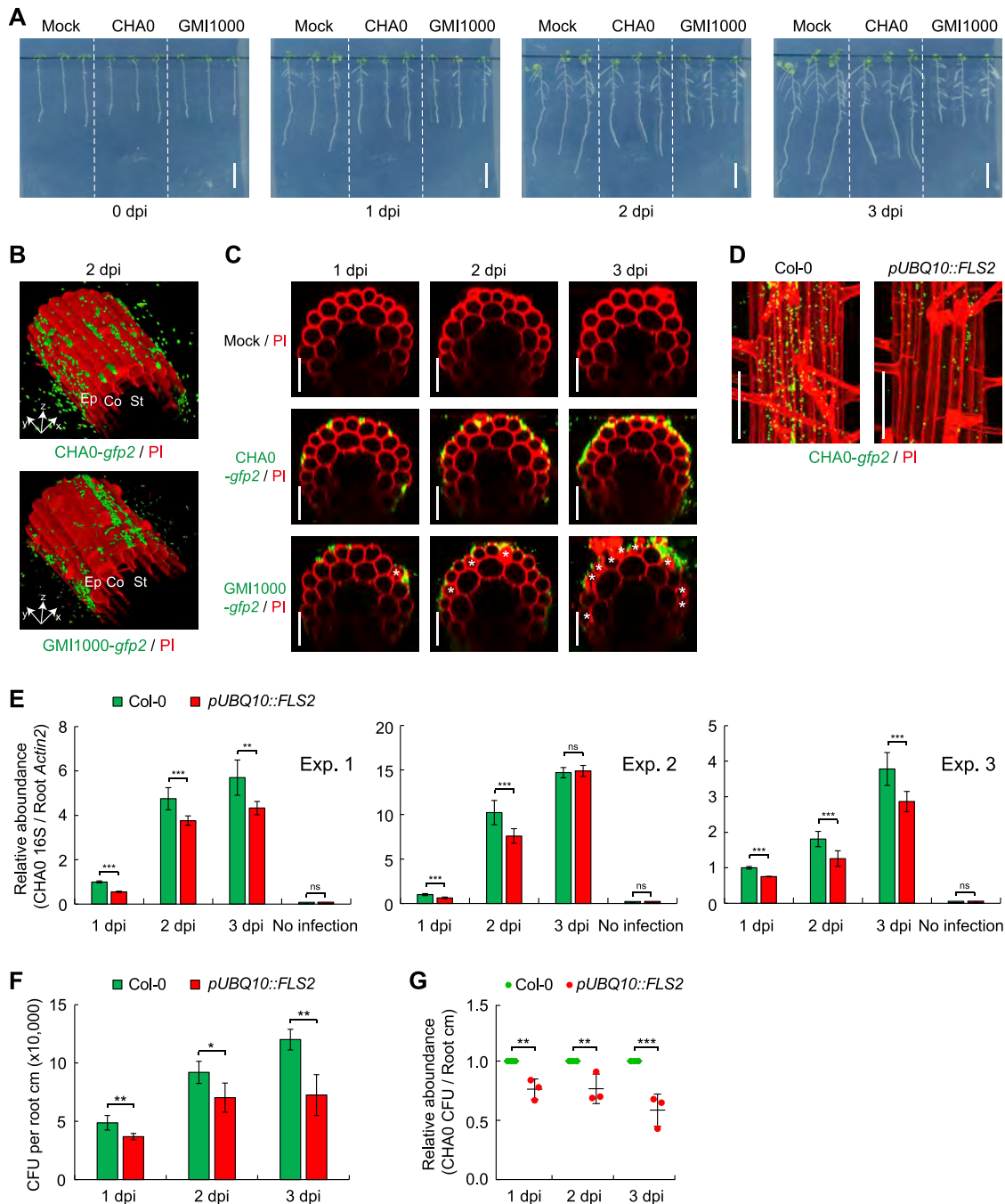


Figure S7. Bacterial Colonization of *Arabidopsis* Roots in an *In Vitro* System, Related to Figure 7

(A) Photographs of Col-0 roots infection with non-pathogenic (CHA0) or pathogenic (GMI1000) root bacteria on solid half MS medium plate. Six-day-old roots were inoculated with water (mock, left), CHA0 (middle) or GMI1000 (right) for the indicated time. Note pronounced root growth arrest in the presence of the pathogenic bacterium GMI1000. dpi, days post inoculation. Scale bar, 2 cm.

(B) Bacterial colonization on the surface of differentiated epidermal cells in the view of the 3D-stacks. Pictures are maximum projections of confocal Z stacks taken around the 25th endodermal cell after onset of elongation. Ep, epidermis; Co, cortex; St, stele.

(C) Orthogonal view of confocal images showing colonization and the extent of damage on epidermal cells after inoculation with CHA0 (middle panel) or GMI1000 (bottom panel) for the indicated time, compared to the mock (upper panel). White asterisks indicate damaged cells. Scale bar, 50 μ m.

(D) Representative images showing CHA0-*gfp2* colonization on differentiated roots of Col-0 and *pUBQ10::FLS2* root at 2 dpi. Pictures are maximum projections of confocal Z stacks. GFP-labeled bacteria (green) were co-visualized with PI staining (red). Scale bar, 50 μ m.

(E) Three biological replicates of quantitative measurement of CHA0 abundance in Col-0 and *pUBQ10::FLS2* roots at indicated inoculation time point. Roots inoculated with CHA0-*gfp2* strain or mock solvent were collected and their DNA was used for real-time PCR using CHA0 16S primer pair (499_500).

(legend continued on next page)

Ct values were normalized to Ct values obtained by a primer pair (*AtACTIN2*) amplifying plant-derived DNA. Values are shown with means \pm SD (n = 3 roots).

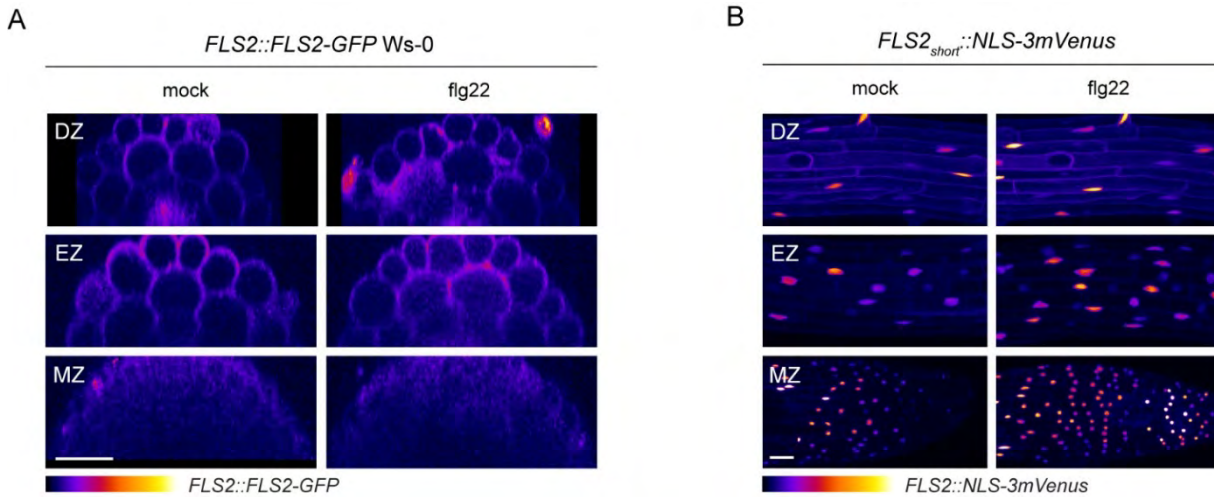
(F and G) CFU counting of CHA0 colonization in Col-0 and *pUBQ10::FLS2* roots. Four-day-old seedlings were transferred onto half MS plates containing CHA0 ($OD_{600} = 0.002$). Three roots were collected for each sample at indicated colonization time point. CFU of CHA0 abundance was normalized to per root centimeter (cm) (F) and the ratio of bacterial abundance was relatively compared to Col-0 (G). Values are shown with means \pm SD (3 biological replicates). Asterisks (* $p < 0.05$, ** $p < 0.01$ and *** $p < 0.001$) indicate statistically significant differences based on ANOVA and Tukey's test analysis.

2.4. APPENDICES

In parallel of our study on the coincidence of damage and MAMPs for localized immune responses, I carried out some complementary experiments to assess the implication of ethylene for *FLS2* increased expression observed after damage. In addition, I tested the effect of DAMPs on *FLS2* expression. Since the gating of MTI in the unresponsive differentiated zone was also observed around lateral roots, I did some preliminary works to characterise in details the induction of immunity in these regions. Although these data are sometimes still preliminary and were not published in Zhou *et al.* (2020), I felt that they are worth mentioning and complete our previous results.

2.4.1. FLG22 PEPTIDE INCREASES SLIGHTLY *FLS2* EXPRESSION

Our work provided evidence that damage alone was able to induce *FLS2* expression, which was then responsible for gating of immunity in the differentiated root (Zhou *et al.*, 2020, Fig.4). However, we wanted to assess whether flg22 also induces *FLS2* expression and reinforced the gating effect. Data supporting the flg22-driven induction of *FLS2* expression in the elongation zone can be found in Fig.4E and Fig.S4F (Zhou *et al.*, 2020). I present here extended results. The tagged *FLS2* protein was also visualized in the meristematic and elongation zone (App.1A). Its expression was slightly increased after treatment with flg22, but only in the elongation zone, confirming the expression analysis. In addition, I also tested the impact of flg22 on the *FLS2* transcriptional reporter using the traditional *pFLS2_{short}* promoter (Zipfel *et al.*, 2004). Flg22 could induce its activity (App.1B), as for the *pFLS2_{long}* promoter, later generated (Zhou *et al.*, 2020).



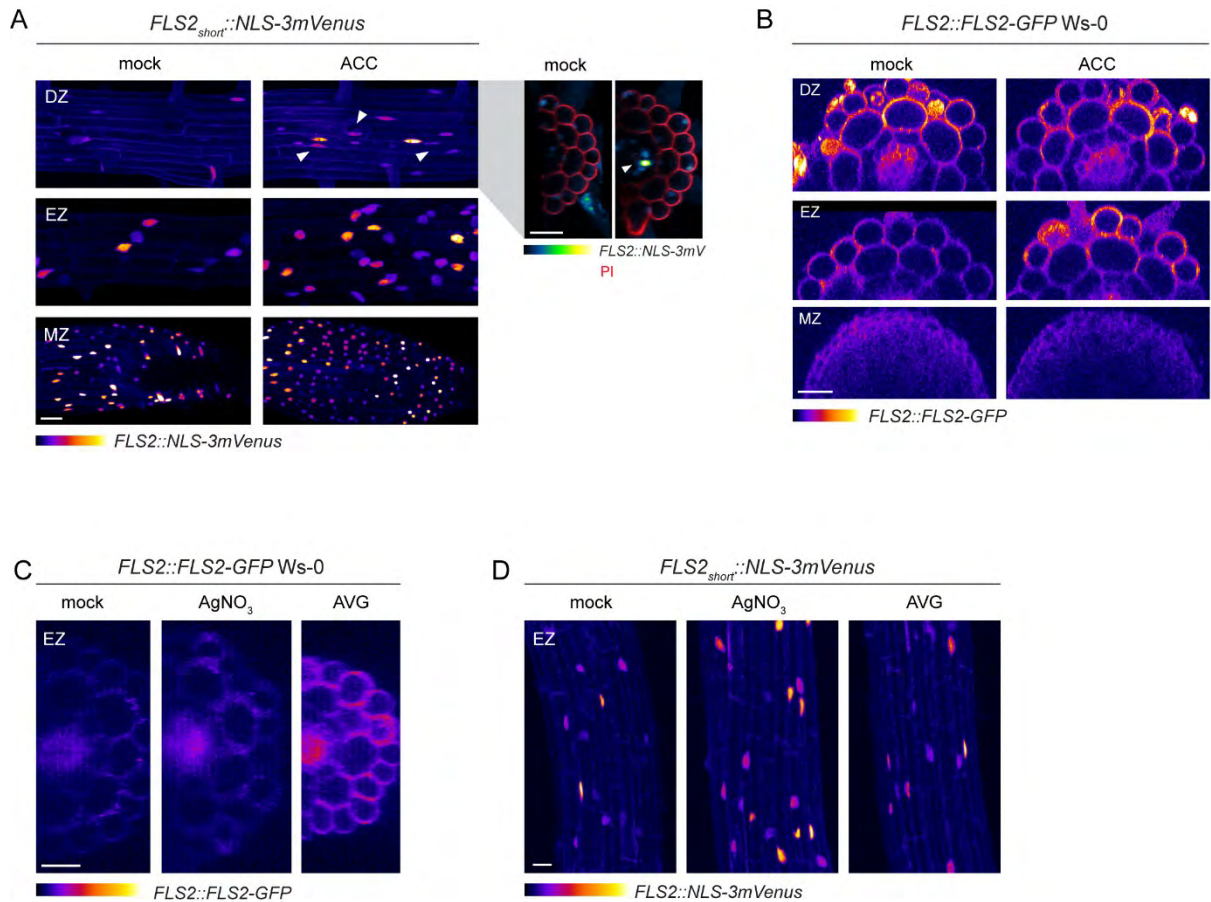
Appendix 1 : flg22 induces *FLS2* expression

(A) Orthogonal view of accumulation of FLS2-fused protein (FLS2-GFP, Fire LUT) in response to 1 μ M flg22 or mock after 7h treatment in liquid $\frac{1}{2}$ MS medium. Scale bar, 25 μ m.

(B) Flg22 treatment weakly activates the short *FLS2* promoter in the meristematic zone (MZ) and the elongation zone (EZ). Maximum projection of *FLS2_{short}::NLS-3mVenus* in response to 1 μ M flg22 or mock, 24h treatment using the “combined” method. Scale bar, 25 μ m.

2.4.2. ETHYLENE TRANSCRIPTIONALLY ACTIVATES *FLS2*

Using ethylene mutants *ein2-1* and *etr1-1*, we previously showed that ethylene signalling was not required for damage-induced gating of immune responses. Amongst the evidence provided, we controlled that ethylene treatment induces *FLS2* expression using the *FLS2_{long}::NLS-3mVenus* reporter (Zhou *et al.*, 2020)(Fig.S5, S4F). In addition, I show here the effect of ACC treatment on *FLS2_{short}::NLS-3mVenus* and *FLS2::FLS2-GFP* lines. Despite the variability in its pattern, p*FLS2_{short}* promoter was activated by ACC in the elongation zone, similarly to p*FLS2_{long}* promoter. However, it was also induced in the stele of the differentiated zone, probably due to difference in experimental conditions (App.2A). By contrast, I could not consistently detect an increase of FLS2 protein accumulation in any zone (App.2B). A high turnover rate might mask FLS2-GFP accumulation, despite the elevated transcription observed in the *FLS2_{short}:: and FLS2_{long}::NLS-3mVenus* lines. Reversely, I tested the impact of the ethylene inhibitors AVG and AgNO₃ on *FLS2::FLS2-GFP* and *FLS2_{short}::NLS-3mVenus* (App.2C, 2D), but *FLS2* responses were variable, with either no difference between mock and treatment or increased *FLS2* expression.



Appendix 2: Ethylene modulates *FLS2* expression

(A) ACC triggers the induction of *FLS2_{short}::NLS-3mVenus* reporter (Fire LUT) in the elongation zone and in the stele of the differentiated zone (white arrowheads). Seedlings were treated for 24 h on plate containing 1 μ M ACC. Maximum projection of z-stacks imaging meristematic (MZ), elongation (EZ) and differentiated (DZ) zones. For the DZ, maximal projection of transverse sections views of *FLS2* expression pattern co-visualised with cell wall (PI staining, red). Scale bar, 25 μ m.

(B) Orthogonal view of accumulation of *FLS2*-fused protein (*FLS2*-GFP, Fire LUT) in response to 1 μ M ACC or mock after 5.5h treatment in liquid $\frac{1}{2}$ MS medium. Scale bar, 25 μ m.

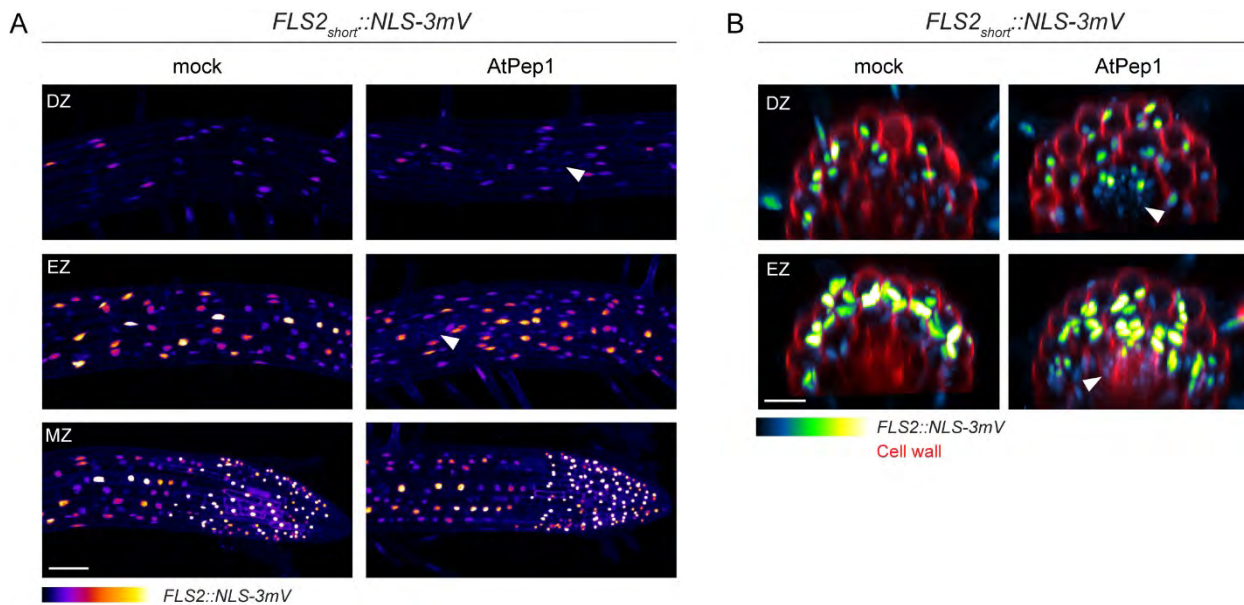
(C) Orthogonal view of accumulation of *FLS2*-fused protein (*FLS2*-GFP, Fire LUT) in the EZ in response to 5 μ M AgNO_3 , 5 μ M AVG or mock after 24h treatment on plate. Scale bar, 25 μ m.

(D) *FLS2_{short}::NLS-3mVenus* marker (Fire LUT) response in the EZ to 2 μ M AgNO_3 , 2 μ M AVG or mock after 24h treatment on plate. Scale bar, 25 μ m.

2.4.3. ATPEP1 SLIGHTLY INCREASES *FLS2* EXPRESSION IN THE STELE

Since damages gate the response to flg22 in the differentiated zone, we postulated that ablation could be mimicked by DAMPs treatment (Zhou *et al.*, 2020). In parallel to combined treatment of flg22 and DAMPs, I also tested whether *FLS2* could be directly induced by AtPep1. I could detect a slight increase of *FLS2* expression in the stele, mostly in the elongation and the early differentiated zone (20c after onset of elongation) (App.3). Interestingly, combined treatment with AtPep1 and flg22 also increased *FRK1* expression

in the stele of the differentiated zone compared to single treatment with AtPep1 (Zhou *et al.*, Fig.3A). The fact that AtPep1 treatment could modulate *FLS2* expression in the stele and enhances flg22-responses is surprising considering the non-responsiveness of this tissue described in Chapter 3.



Appendix 3: AtPep1 induces *FLS2* expression in the differentiated stele

(A) Maximum projection of z-stacks taken in MZ, EZ or DZ of *FLS2_{short}::NLS-3mVenus* (Fire LUT) seedlings treated for 24 h with 1 μ M AtPep1 (combined method). Scale bar, 50 μ m.

(B) Orthogonal view of pictures in (A). Note the increase of *FLS2* signal (GreenFireBlue LUT) in the stele (white arrowheads). Cell walls are highlighted with PI staining (red). Scale bar, 25 μ m.

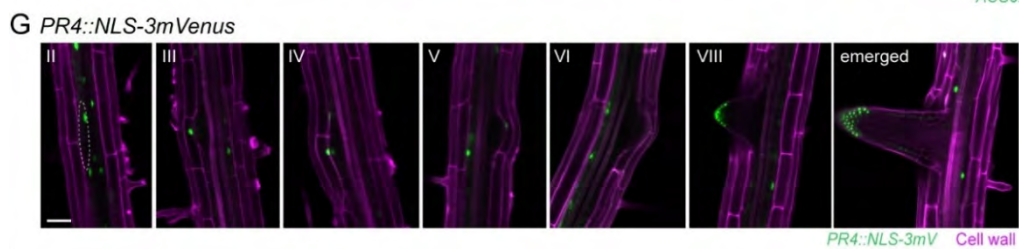
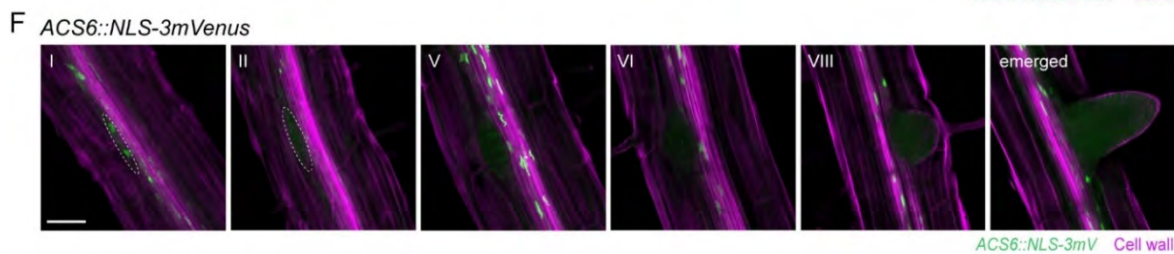
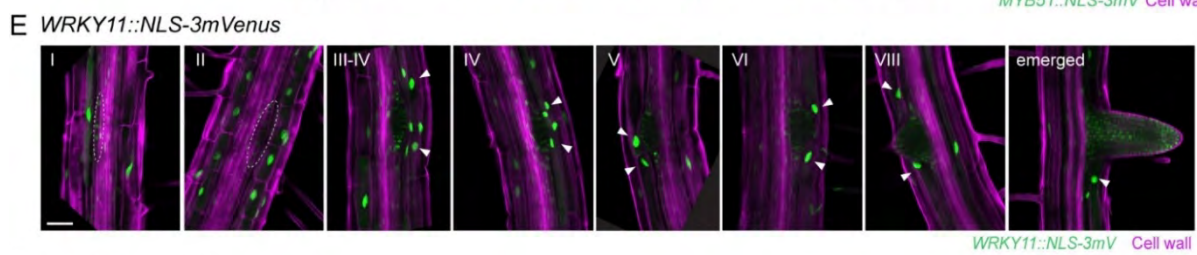
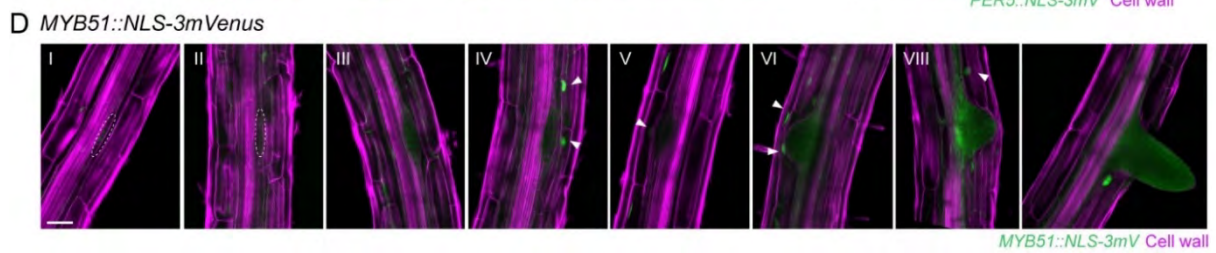
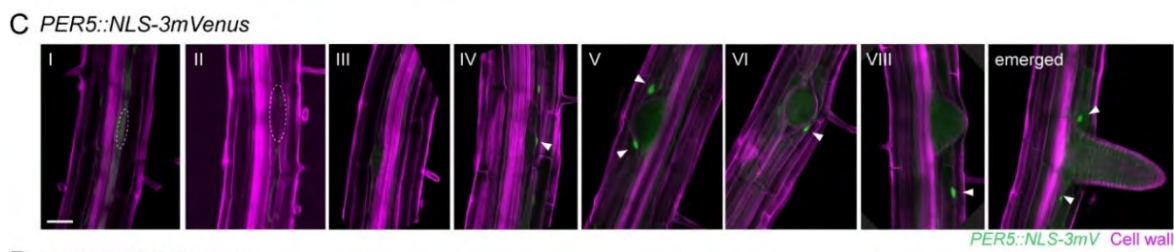
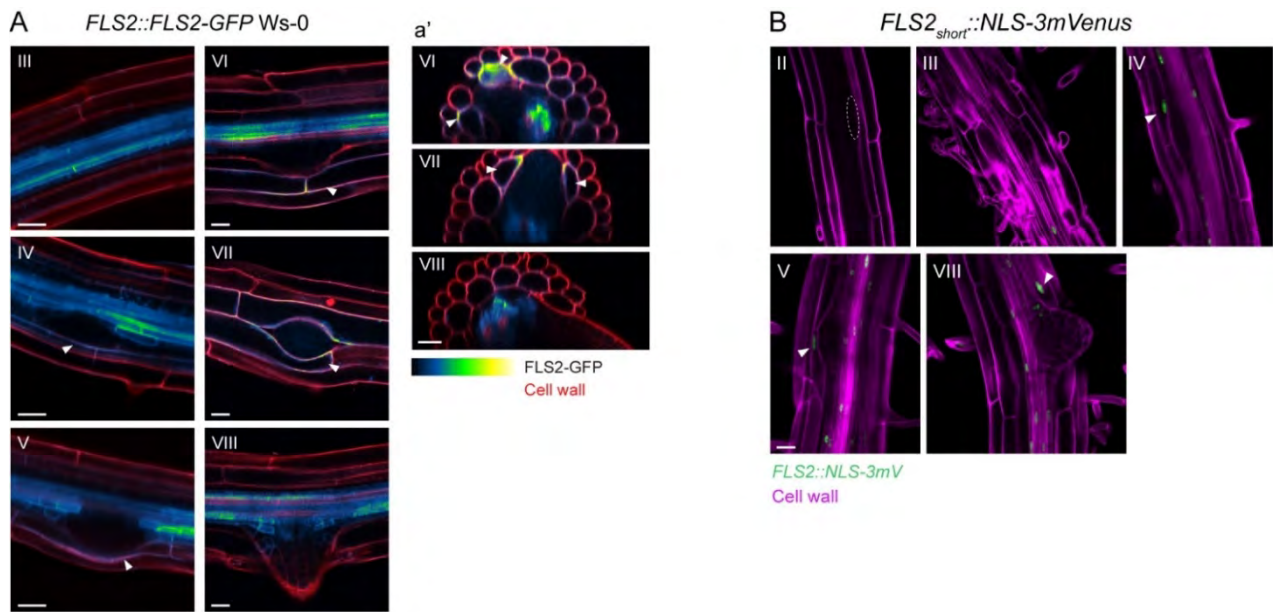
MZ, meristematic zone; EZ, elongation zone; DZ, differentiated zone.

2.4.4. *FLS2* EXPRESSION IN CORTICAL CELLS AROUND LATERAL ROOTS CORRELATES WITH RESPONSIVENESS TO FLG22

The differentiation zone is usually “insensitive” to flg22, except after damage or around lateral root primordia. We previously showed that *FLS2* is induced in cortical cells surrounding the primordia (Zhou *et al.*, 2020, Fig.S4E). In addition, I realized a descriptive analysis of *FLS2* expression across the different stages of lateral root development and found that *FLS2* promoter and *FLS2*-GFP recombinant protein were expressed from stage IV until stage VIII (App.4A, B).

I also assessed the timing of *PER5*, *WRKY11* and *MYB51* appearance around lateral roots after flg22 treatment. All of them were expressed in cortical cells adjacent to the lateral roots and appear after the stage IV of primordia development, which was consistent with the expression of *FLS2* (App.4C, D, E). Nevertheless, increase of *FLS2* or MTI markers expression was not observed for all primordia of stage IV or later. Since ethylene regulates *FLS2* expression (Boutrot *et al.*, 2010; Mersmann *et al.*, 2010), I also described *PR4* (*PATHOGENESIS-RELATED 4/HEVEIN-LIKE*) and *ACS6* (*ACC SYNTHASE 6*) ethylene markers (Poncini *et al.*, 2017). *PR4* expression was increased in cortical cells surrounding the primordia. However, *PR4* signal was also constitutively expressed in cortex in later regions (App.4G). In contrast, *ACS6* was expressed in young primordia then disappears after stage III. However, *ACS6* was not found in any cortical cells (App.4F).

To clearly correlate *FLS2* expression with immune transcriptional read-outs induction, I used the double reporter lines expressing *FLS2::NLS-tdTomato* with MTI reporters and assessed whether both markers were co-localized in the same cells. From stage I to III, most cells neither induce *FLS2* nor any of the markers (App.5A'-E'). At later stages, *FLS2* is induced in more than 80% of the primordia. Treatment with flg22 triggers co-expression of *PER5*, *MYB51* and *WRKY11*, but not *ACS6* nor *PR4* (App.5). It must be noted that cells that express *FLS2* did not always induce immune read-outs in response to flg22. Reversely, in a few cases, induction of MAMP markers occurred without increased expression of *FLS2*. Taken together, increased MAMP sensitivity around lateral roots is imperfectly correlated to *FLS2* expression and is independent of ethylene responses. Although other *ACS* genes expressed in the root could be involved (Tsuchisaka and Theologis, 2004), we showed that damage-induced increased defence expression in the differentiated zone was independent of ethylene (Zhou *et al.*, 2020), suggesting that the same mechanism could apply to lateral root emergence sites.



Appendix 4 : FLS2 and immune transcriptional read-outs are expressed around the emergence site of lateral roots.

(A) FLS2-GFP protein fusion (GreenFireBlue LUT) is expressed in cortical cells surrounding primordia from stage IV of lateral root development. Cell walls are highlighted with PI (red). (a') Orthogonal view of pictures of stage VI to VIII. Roman numbers, stage of the primordia; white arrowheads, cortex cells expressing FLS2. Scale bar, 25 μ m.

(B) *FLS2* promoter (green) is active in cortical cells surrounding primordia from stage IV onwards. Cell wall is highlighted by Calcofluor White staining (magenta). Roman number, stage of the primordia; white arrowheads, cortex cells expressing *FLS2*; dashed circle, primordia. Scale bar, 25 μ m.

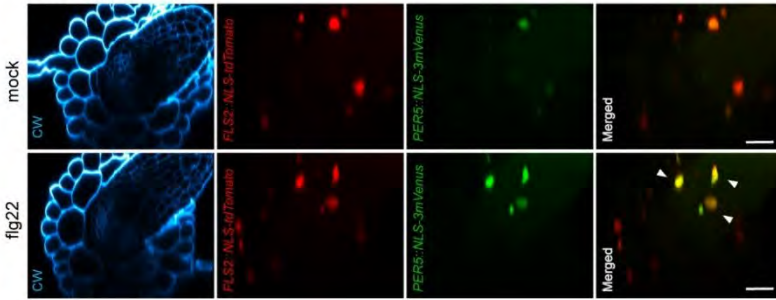
(C-E) *PER5::NLS-3mVenus* (C), *MYB51::NLS-3mVenus* (D) and *WRKY11::NLS-3mVenus* (E) (green) are induced in cortex cells surrounding primordia from stage IV onwards

(F) *ACS6::NLS-3mVenus* is expressed in the stele and does not correlate with LR emergence.

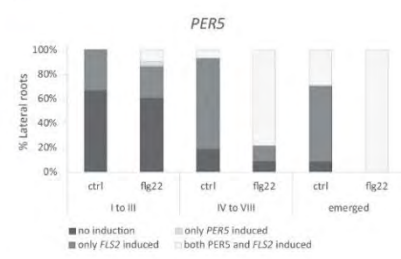
(G) *PR4::NLS-3mVenus* is sometimes induced in cortex cells around LR after flg22 treatment.

(C-G) Seedlings were treated with 1 μ M flg22 for 24h. Cell wall is highlighted by Calcofluor White staining (magenta). Roman number, stage of the primordia; white arrowheads, cortical cells expressing immune transcriptional read-outs; dashed circle, primordia. Scale bar, 50 μ m.

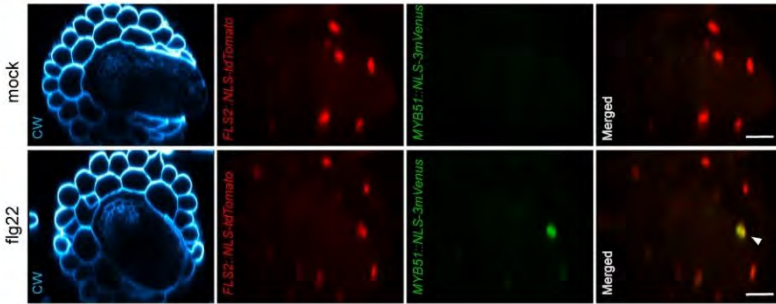
A *FLS2* and *PER5*



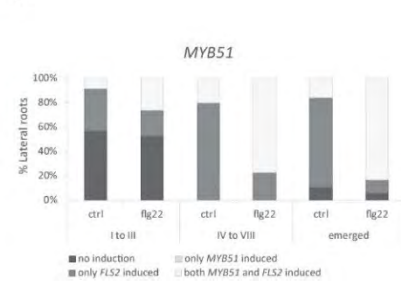
A'



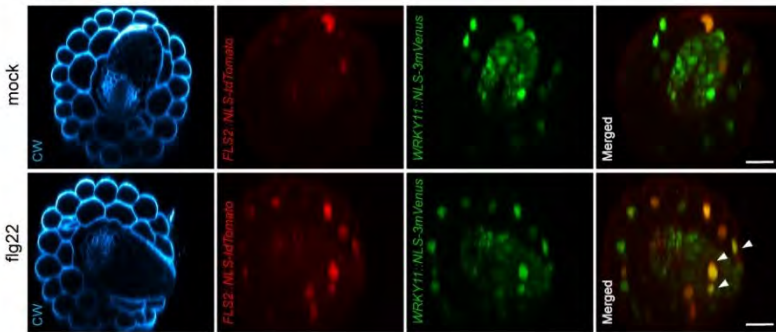
B *FLS2* and *MYB51*



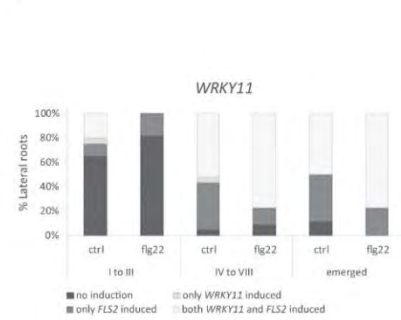
B'



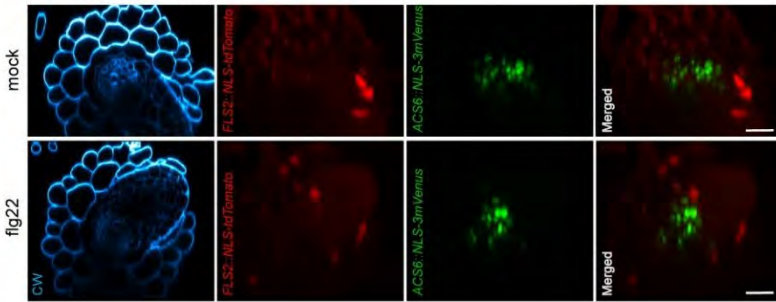
C *FLS2* and *WRKY11*



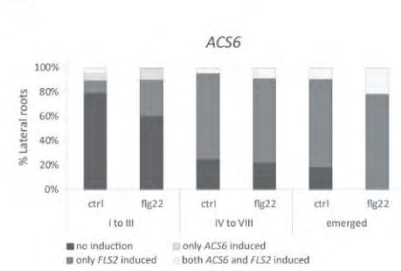
C'



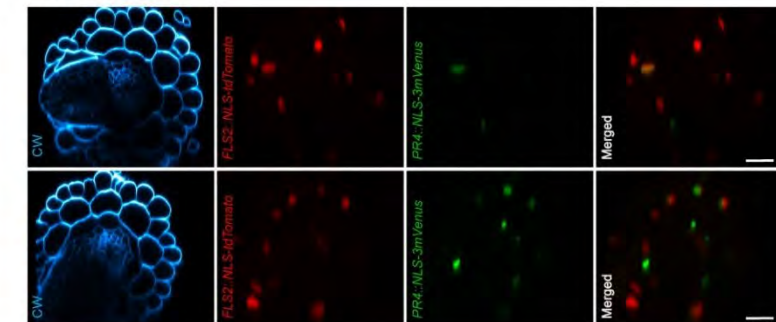
D *FLS2* and *ACS6*



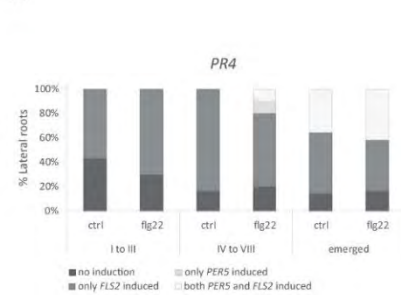
D'



E *FLS2* and *PR4*



E'



Appendix 5 : *FLS2* is co-expressed with immune read-outs but not with ethylene reporters

(A-C) *FLS2* expression was co-visualized with *PER5* (A), *MYB51* (B) and *WRKY11* (C) expression in cells surrounding emerged lateral root. *FLS2* promoter-driven nuclear tdTomato signal (red) and nuclear immune read-out signal (green) are co-localizing (yellow) in the presence of 1 μ M flg22 application for 6 h. Scale bar, 25 μ m.

(D-E) *FLS2* expression was co-visualized with *ACS6* (D) and *PR4* (E) expression in cells surrounding primordia. *FLS2* promoter-driven nuclear tdTomato signal (red) and nuclear immune read-out signal (green) are not co-localizing. Seedlings were treated for 6h with 1 μ M flg22. Scale bar, 25 μ m.

(A'-E') Quantification of percentage of lateral roots showing no induction of *FLS2* or immune markers expression, only induction of *FLS2*, only induction of immune markers or co-expression of *FLS2* and immune markers. Percentages were calculated for three different developmental stages (I to III, IV to VIII or emerged lateral roots) and for *PER5* (A'), *MYB51* (B'), *WRKY11* (C'), *ACS6* (D') and *PR4* (E') transcriptional read-outs. Analysis was performed after application of 1 μ M flg22 or mock for 6 h in liquid ½ MS.

2.5. SUPPLEMENTARY MATERIAL AND METHODS

2.5.1. PLANT MATERIAL AND GROWTH CONDITIONS

We used *A. thaliana* ecotype Columbia for most experiments. *FLS2::FLS2-3myc-GFP* line in ecotype Wassilewskija Ws-0 was offered by Prof. Tomas Boller's group (Robatzek *et al.*, 2006). *FLS2_{short}::NLS-3xmVenus* was described in (Zhou *et al.*, 2020). MTI and ethylene signalling reporter, as well as their combination with *FLS2::NLS-tdTomato* construct, were characterized previously (Marhavý *et al.*, 2019; Poncini *et al.*, 2017; Zhou *et al.*, 2020).

For all experiments, plant seeds were surface sterilized with chlorine gas for 2,5 hours. Seeds were stratified for minimum 2 days at 4°C in the dark and seedlings were grown vertically on half-strength Murashige and Skoog (MS) 0.8% agar plates at 22°C in continuous light for 5 days.

2.5.2. ELICITOR AND INHIBITOR TREATMENT

Commercial flg22 peptide (QRLSTGSRINSAKDDAAGLQIA) was obtained from EZBioLab, while AtPEP1 (ATKVKAKQRGKEKVSSGRPGQHN) were synthesized by Peptide Specialty Laboratories GmbH. 1 - aminocyclopropane-1-carboxylic acid (ACC) was dissolved in water as a 20 mM stock solution. 2 - aminoethoxyvinyl glycine (AVG) and AgNO₃ (Sigma-Aldrich) were conserved as a 10 mM stock solution in water.

Elicitor and chemical treatments were performed according to one of the following protocols. Seedlings were carefully transferred into 6-well culture plates containing liquid ½ MS medium supplemented with elicitor to the mentioned concentration ("liquid treatment"). Alternatively, seedlings grown on small ½ MS petri dishes were submersed with 1.5 ml of elicitor solution directly onto the plate, then incubated horizontally before analysis ("combined method"). For ACC or ethylene inhibitor treatments, seedlings were transferred on ½ MS plates supplemented with the defined concentration of chemicals.

2.5.3. FIXATION AND STAINING

For live imaging, plasma membrane outline was labelled by mounting seedlings in 15 µM (10mg/ml) PI solution. Lateral root imaging was done after fixation using the Clearsee procedure as described previously (Emonet *et al.*, 2020; Ursache *et al.*, 2018).

2.5.4. MICROSCOPY

Pictures were taken on a Zeiss LSM880, LSM700 or a Leica SP8 inverted confocal scanning microscope, using a 63x oil immersion objective (LSM880), 63x water immersion objective (SP8), 40x water immersion objective (SP8, LSM880 and LSM700). For *FLS2* and immune transcriptional read-outs visualisation, the excitation and detection windows were set as follows: GFP/PI (488nm; 500-530nm and 600-650nm); mVenus (514nm; 520-550nm), calcofluor (405nm, 425-475nm), tdTomato (554 nm, 580-620 nm).

2.5.5. QUANTIFICATION

Quantification of *FLS2* and immune read-outs co-localization was done as follows. Pictures were taken for each primordium found along the roots, then were grouped according to the developmental stage of the primordia: from stage I to III, from IV to VIII or “emerged” (Péret *et al.*, 2009). Pictures were then classified depending on the induction of the two markers into one of the following groups: no induction of *FLS2* nor defence marker, induction of *FLS2* but no induction of defence marker, induction of defence marker but no induction of *FLS2*, combined induction of *FLS2* and defence marker. Induction was considered positive when at least one nucleus of the cortical cells surrounding the lateral root was obviously brighter than the neighbouring nuclei. Combined induction was only considered if at least one nucleus expressed strongly both *FLS2* and the defence marker. Two replicates were combined.

2.6. LITERATURE

- Boutrot, F., Segonzac, C., Chang, K.N., Qiao, H., Ecker, J.R., Zipfel, C., and Rathjen, J.P. (2010). Direct transcriptional control of the *Arabidopsis* immune receptor FLS2 by the ethylene-dependent transcription factors EIN3 and EIL1. *Proc. Natl. Acad. Sci.* *107*, 14502–14507.
- Emonet, A., Zhou, F., Vacheron, J., Heiman, C.M., Tendon, V.D., Ma, K.-W., Schulze-Lefert, P., Keel, C., and Geldner, N. (2020). Spatially Restricted Immune Responses Allow for Root Meristematic Activity During Bacterial Colonisation. *BioRxiv* 2020.08.03.233817.
- Hander, T., Fernández-Fernández, Á.D., Kumpf, R.P., Willems, P., Schatowitz, H., Rombaut, D., Staes, A., Nolf, J., Pottier, R., Yao, P., *et al.* (2019). Damage on plants activates Ca²⁺-dependent metacaspases for release of immunomodulatory peptides. *Science* *363*, eaar7486.
- Marhavý, P., Kurenda, A., Siddique, S., Dénervaud Tendon, V., Zhou, F., Holbein, J., Hasan, M.S., Grundler, F.M., Farmer, E.E., and Geldner, N. (2019). Single-cell damage elicits regional, nematode-restricting ethylene responses in roots. *EMBO J.* *38*, e100972.
- Mersmann, S., Bourdais, G., Rietz, S., and Robatzek, S. (2010). Ethylene Signaling Regulates Accumulation of the FLS2 Receptor and Is Required for the Oxidative Burst Contributing to Plant Immunity. *Plant Physiol.* *154*, 391–400.
- Millet, Y.A., Danna, C.H., Clay, N.K., Songnuan, W., Simon, M.D., Werck-Reichhart, D., and Ausubel, F.M. (2010). Innate Immune Responses Activated in *Arabidopsis* Roots by Microbe-Associated Molecular Patterns. *Plant Cell* *22*, 973–990.
- Péret, B., De Rybel, B., Casimiro, I., Benková, E., Swarup, R., Laplaze, L., Beeckman, T., and Bennett, M.J. (2009). *Arabidopsis* lateral root development: an emerging story. *Trends Plant Sci.* *14*, 399–408.
- Poncini, L., Wyrsh, I., Tendon, V.D., Vorley, T., Boller, T., Geldner, N., Métraux, J.-P., and Lehmann, S. (2017). In roots of *Arabidopsis thaliana*, the damage-associated molecular pattern AtPep1 is a stronger elicitor of immune signalling than flg22 or the chitin heptamer. *PLOS ONE* *12*, e0185808.
- Robatzek, S., Chinchilla, D., and Boller, T. (2006). Ligand-induced endocytosis of the pattern recognition receptor FLS2 in *Arabidopsis*. *Genes Dev.* *20*, 537–542.
- Tsuchisaka, A., and Theologis, A. (2004). Unique and Overlapping Expression Patterns among the *Arabidopsis* 1-Amino-Cyclopropane-1-Carboxylate Synthase Gene Family Members. *Plant Physiol.* *136*, 2982–3000.
- Ursache, R., Andersen, T.G., Marhavý, P., and Geldner, N. (2018). A protocol for combining fluorescent proteins with histological stains for diverse cell wall components. *Plant J.* *93*, 399–412.
- Zhou, F., Emonet, A., Dénervaud Tendon, V., Marhavý, P., Wu, D., Lahaye, T., and Geldner, N. (2020). Co-occurrence of Damage and Microbial Patterns Controls Localized Immune Responses in Roots. *Cell* *180*, 440–453.e18.
- Zipfel, C., Robatzek, S., Navarro, L., Oakeley, E.J., Jones, J.D.G., Felix, G., and Boller, T. (2004). Bacterial disease resistance in *Arabidopsis* through flagellin perception. *Nature* *428*, 764–767.

3 SPATIALLY RESTRICTED IMMUNE RESPONSES
ALLOW FOR ROOT MERISTEMATIC ACTIVITY
DURING BACTERIAL COLONISATION

3.1. RATIONAL OF THE STUDY

How do plants determine which tissues should be protected and which tissues can accommodate the presence of commensal bacteria without deploying their full arsenal? In the previous chapter, we showed that MTI responses are restricted to the elongation zone, but can be gated by damages in differentiated regions (Zhou *et al.*, 2020). However, it is not understood clearly why, in the first place, are the elongating cells the most responsive. As described previously, a common conception is that the elongation zone is a vulnerable point, lacking any physical barriers, but highly colonized by bacteria (Faulkner and Robatzek, 2012). Roots would therefore need to protect that sensitive region with inducible defences. Nevertheless, the molecular mechanism behind this increased responsiveness remains obscure.

It becomes more and more evident that the regulation of PRRs plays a role in the spatial confinement of defences. Indeed, *FLS2* is expressed at bacterial entry points of the root (Beck *et al.*, 2014) and immune responses gating in the differentiated zone is mediated by the upregulation of *FLS2* (Zhou *et al.*, 2020). However, *FLS2* expression pattern does not coincide entirely with the pattern of defence, calling into question the strict involvement of PRRs in shaping plant immunity. Whether all cells can mount an immune response provided they express the appropriate PRRs is indeed unknown. Wyrsh *et al.* (2015) showed that ectopic *FLS2* expression, independently of its location, could rescue *fls2* mutant. However, their study crucially lacks resolution to infer whether MTI responses are strictly cell-autonomous. Moreover, little is known on the different tissue-specificity of MTI markers.

Finally, we do not understand whether the restriction of flg22-responses at specific location has a biological relevance. We might wonder what the impact on plant development would be if defences were no longer restricted to the elongation zone. Interestingly, the immune response pattern of plants ectopically expressing *FLS2* was never assessed, as well as its effect on the response to commensal bacteria.

The following manuscript, posted on BioRxiv (DOI: <https://doi.org/10.1101/2020.08.03.233817>) and currently under review in *Current Biology*, highlights the preponderant role of *FLS2* expression in shaping flg22-response pattern in the root. By expressing *FLS2* in different tissues and regions of the roots, we characterised, with cellular

resolution, both cell-type specific and non-specific responses and discriminate cell autonomous from non-cell autonomous signals elicited by flg22 perception. Our analysis also revealed that the central region of the meristem is refractory to immune induction, even after overexpression of *FLS2* in these tissues. In contrast, the epidermal meristem has a strong competency for flg22-mediated responses, but this immune activation is incompatible with meristematic activity, leading to meristem collapse and strong root growth inhibition. We showed that such super-competent line also triggers strong defences in response to commensal bacteria that were innocuous in wild-type plants, revealing the importance of correctly localized immune responses to sustain normal growth.

3.2. CONTRIBUTIONS

In this chapter, I did most experiments presented in the manuscript and the appendixes. Mutant $\Delta fleQ$ and $\Delta fliC$ for *Pseudomonas protegens* strain CHA0 were generated in Prof. Christoph Keel's lab by P. Kupferschmied, Jordan Vacheron and Clara Gremaud. Jordan Vacheron carried out the motility assay.

Paul Schulze-Lefert hosted me in his lab and gave me access to the At-SPHERE culture collection.

Niko Geldner and I co-wrote the manuscript, which was reviewed by Feng Zhou, Christoph Keel, Jordan Vacheron and Ka-Wai Ma.

3.3. MANUSCRIPT

Manuscript posted on BioRxiv (<https://doi.org/10.1101/2020.08.03.233817>), under review in Current Biology.

Spatially Restricted Immune Responses Allow for Root Meristematic Activity During Bacterial Colonisation

Authors

Aurélia Emonet¹, Feng Zhou^{1,4}, Jordan Vacheron², Clara Margot Heiman², Valérie Dénervaud Tendon¹, Ka-Wai Ma³, Paul Schulze-Lefert³, Christoph Keel², Niko Geldner^{1,5,*}

Affiliations

¹Department of Plant Molecular Biology, Biophore, UNIL-Sorge, University of Lausanne, 1015 Lausanne, Switzerland

²Department of Fundamental Microbiology, Biophore, UNIL-Sorge, University of Lausanne, 1015 Lausanne, Switzerland

³Max Planck Institute for Plant Breeding Research, 50829 Cologne, Germany

⁴Present address: National Key Laboratory of Plant Molecular Genetics, CAS Center for Excellence in Molecular Plant Sciences, Chinese Academy of Sciences, Shanghai 200032, China

⁵Lead Contact

*Correspondence: niko.geldner@unil.ch (N.G.)

Summary (150 words)

Plants circumscribe microbe-associated molecular pattern (MAMP)-triggered immune responses to weak points of the roots. This spatially restricted immunity was suggested to avoid constitutive responses to rhizosphere microbiota. To demonstrate its relevance, we combined cell-type specific expression of the plant flagellin receptor (FLS2) with fluorescent defence markers and mapped immune competency at cellular resolution. Our analysis distinguishes cell-autonomous and non-cell autonomous responses and reveals lignification to be tissue-independent, contrasting cell-type specific suberisation. Importantly, our analysis divides the non-responsive meristem into a central zone refractory to FLS2 expression, and a cortex that becomes highly sensitised by FLS2 expression, causing meristem collapse upon MAMP exposure. Meristematic epidermal expression generates super-competent lines that detect native bacterial flagellin and bypass the absence of response to commensals, providing a powerful tool for studying root immunity. Our precise manipulations and read-outs demonstrate incompatibility of meristematic activity and defence and the importance of cell-resolved studies of plant immunity.

Introduction

Plant roots host a vast range of microorganisms in their rhizosphere. Amongst those, some can act as pathogens, negatively impacting plant growth and reproduction. However, the plant's sophisticated innate immune system keeps the vast majority of pathogens at bay. This MAMP-triggered immunity (MTI) rests on the recognition of highly conserved microbial molecules, recognised by plasma membrane-localised pattern-recognition receptors (PRRs) (Zipfel, 2008). One of the most investigated MAMPs is a 22 amino acid fragment of the bacterial flagellin protein (flg22). It is detected by the FLAGELLIN SENSING 2 (FLS2) receptor (Felix *et al.*, 1999; Gómez-Gómez and Boller, 2000; Gómez-Gómez *et al.*, 1999; Zipfel *et al.*, 2004) and induces a signalling cascade including ROS production, calcium signalling, MAPKs (MITOGEN-ACTIVATED PROTEIN KINASE) phosphorylation and gene transcription, eventually leading to defence responses, such as callose and lignin deposition or phytoalexin production (Lee *et al.*, 2019; Li *et al.*, 2016).

Yet, plant PRRs equally perceive MAMPs from commensal or beneficial microbes, which are part of the normal plant rhizosphere. Whereas MTI is associated with growth inhibition (Chinchilla *et al.*, 2007; Gómez-Gómez and Boller, 2000), a plethora of publications have established a growth promoting action of the soil microbiome (Berendsen *et al.*, 2012). It therefore becomes particularly interesting to understand how roots accommodate a rhizosphere community, while avoiding a constant activation of PRRs and the growth-defence trade-off that comes with it. Many researchers have argued that the growth inhibition can be overcome by the ability of commensal microorganisms to suppress plant immunity (Yu *et al.*, 2019b). In addition, it was recently shown that the root has an inherently dampened MTI until it encounters damage, which locally boosts immune responsiveness (Zhou *et al.*, 2020).

Indeed, root immune responses are generally lower than in the shoot, often because of an absence or low abundance of PRRs (Beck *et al.*, 2014; Faulkner and Robatzek, 2012). Interestingly, plants restrict their defence to regions considered vulnerable. These coincide with regions where protective endodermal barriers are absent or broken, such as in the elongation zone and at the lateral root emergence sites. It is also where bacteria are found to preferentially

accumulate (Beck *et al.*, 2014; Bulgarelli *et al.*, 2013; De Coninck *et al.*, 2015; Faulkner and Robatzek, 2012; Millet *et al.*, 2010; Poncini *et al.*, 2017; Zhou *et al.*, 2020).

Here, we set out to address the relevance of spatially limited responses. Wyrsh *et al.* (2015) ectopically expressed *FLS2* under tissue-specific promoters and their data suggested that all root tissues were competent to mount an immune response provided that *FLS2* is expressed, although the nature of the tissue had a large influence on the strength of the innate immunity responses. Yet, the immune read-outs used in this work were at whole-plant or organ-level resolution and did not allow the authors to ascertain from which cell-type responses were originating, or whether responses were cell-autonomous, regional or systemic. Specifically, MAMP-induced ROS production, as well as cytosolic calcium increases, are known to act in a paracrine, even systemic fashion (Dubiella *et al.*, 2013; Gilroy *et al.*, 2014, 2016; Marhavý *et al.*, 2019). Calcium waves were reported to initiate in the root elongation zone and to spread across tissues after flg22 treatment (Keinath *et al.*, 2015; Stanley *et al.*, 2018), opening the possibility that MAMP responses are induced in cell layers far away from the site of perception.

To address this issue, we combined new fluorescent markers lines with cell-type-specific *FLS2* receptor lines. These marker lines use a triple mVenus fluorochrome coupled to a nuclear localisation signal (*prom::NLS-3xmVenus*). Combining concatemerisation with nuclear concentration generates high sensitivity and allows for a clear cellular assignment, not achievable with cytosolic, ER or PM-localised markers. These lines now enable us to observe damage and defence responses with cellular resolution, adding a crucial layer of complexity to our analyses (Marhavý *et al.*, 2019; Poncini *et al.*, 2017; Vermeer *et al.*, 2014; Zhou *et al.*, 2020). We also added fluorescence-based markers that have been used for assessing cytosolic calcium changes triggered by flg22 at single cell resolution (Thor and Peiter, 2014).

This has allowed us to manipulate and quantitatively map defence responses at cellular resolution in the root. Our approach revealed the presence of regions refractory to *FLS2* presence, as well as others which are super-competent. We show that inappropriate *FLS2* expression has drastic impact on root development, affecting growth, cell wall composition and cell viability. To assess the impact of *FLS2* misexpression in response to natural microbiota, we use our super-competent lines in the presence of commensal bacteria, normally not detected

by wild-type plants. We demonstrate stimulation of FLS2 directly by native, bacteria-derived flagellin and reveal the importance of spatial restriction of immune responses in order to adequately balance growth and defence.

Results

Tissue-specific expression of *FLS2*

In order to analyse the ability of the different root tissues to respond to flg22, we used lines expressing *FLS2* under cell-type-specific promoters in an *fls2* mutant background (Wyrsh *et al.*, 2015). We selected lines expressing *FLS2-GFP* driven by three different tissue-specific promoters: *WEREWOLF* for epidermis (*WER::FLS2*), *CASPARIAN STRIP DOMAIN PROTEIN 1* for endodermis (*CASP1::FLS2*), and *SHORT-ROOT* for inner cell layers (*SHR::FLS2*). As controls, we monitored *FLS2-GFP* driven by the constitutive promoter *UBIQUITIN 10* (*UBQ10::FLS2*) and by the native *FLS2* promoter (*FLS2::FLS2*). As described previously, endogenous *FLS2* expression was observed principally in the differentiated stele (Beck *et al.*, 2014) (Fig.1A) but also weakly in all tissues from the elongation to the differentiated zone, as well as in root cap cells (Zhou *et al.*, 2020) (Fig.1B). *WER::FLS2*, by contrast, was strongly expressed in the epidermis of the meristematic zone (Fig.1), as predicted (Lee and Schiefelbein, 1999), with some weak signal in the older cortex (elongation zone) (Fig.S1A). In agreement with its established expression (Benfey *et al.*, 1993; Helariutta *et al.*, 2000), we detected *SHR::FLS2* in the stele close to the meristem (Fig.1), but also faintly in the neighbouring endodermis, suggesting that either *FLS2* proteins or mRNAs move through plasmodesmata (Fig.S1D). *CASP1::FLS2* had the predicted exclusive expression in differentiated endodermis (Fig.1, S1B) and *UB10::FLS2* was detected in all tissues throughout the root, from meristem to differentiation zone (Fig.1, S1C).

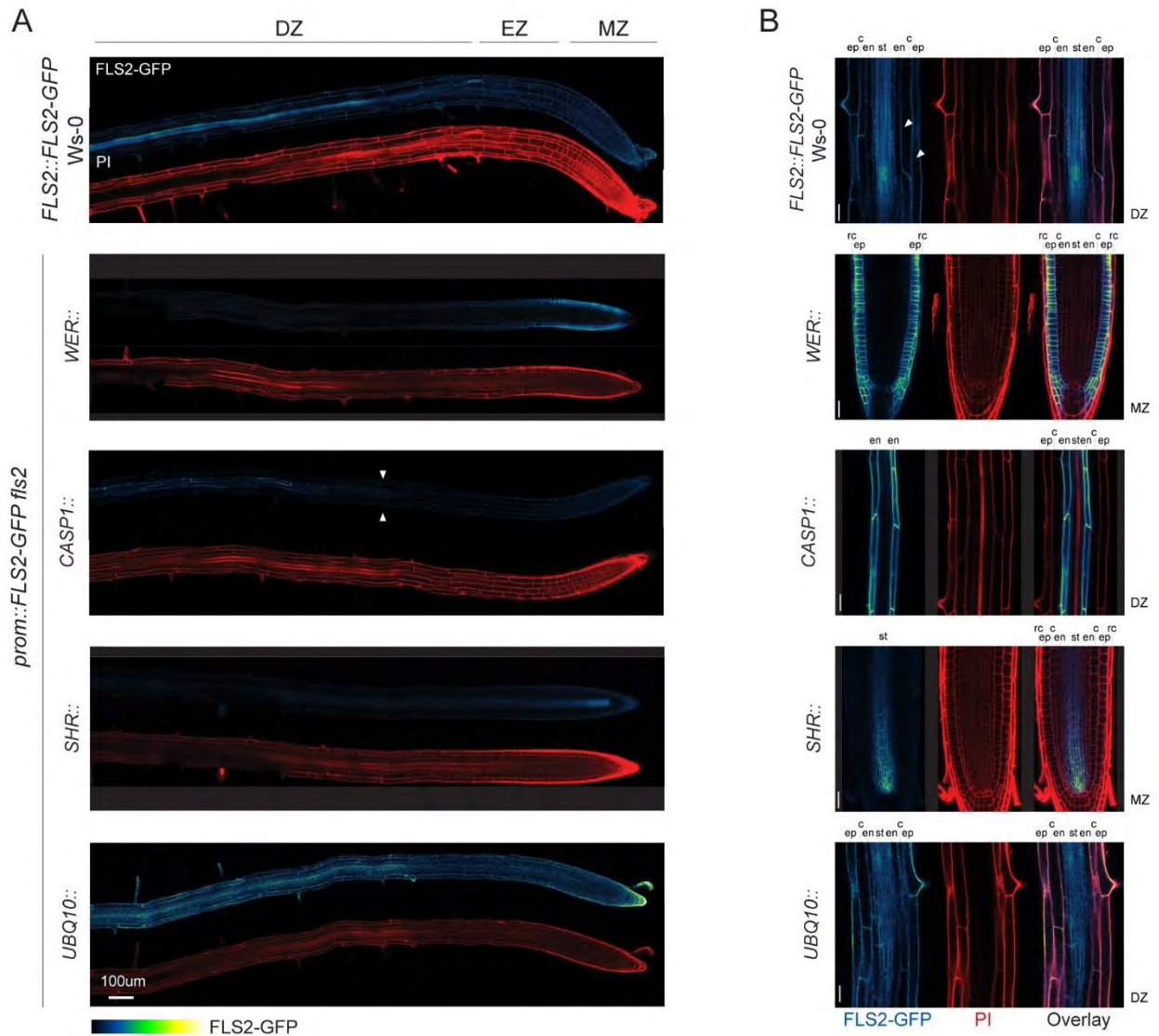


Figure 1: Tissue-specific promoters drive FLS2 receptor expression ectopically

(A) Tile scan of *fls2* roots complemented with GFP-tagged FLS2 receptor under epidermal (WER::), endodermal (CASP1::), central cylinder (SHR::) and ubiquitous (UBQ10::) promoters. For comparison, endogenous FLS2 expression is shown in FLS2::FLS2-GFP Ws-0 lines. Root shape is highlighted with PI staining cell wall (PI, red). Scale bar, 100µm. Developmental regions of the roots are labelled: differentiated zone (DZ), elongation zone (EZ), meristematic zone (MZ). **(B)** Close up view of FLS2-GFP expression at selected regions of the complemented lines. FLS2 driven by its endogenous promoter is expressed in all tissues in the differentiated zone (DZ). Note that in contrast to previous report, low FLS2 expression is observed in epidermis and cortex (white arrow). In the meristem (MZ), WER promoter expresses FLS2 specifically in epidermis (ep) and root cap (rc), SHR promoter in the stele (st) and endodermis (en). In the differentiated zone (DZ), FLS2 is expressed in all tissues under UBQ10 promoter, but is restricted to endodermis with CASP1 promoter. FLS2-GFP (BlueGreen) is co-visualized with PI-stained cell wall (red). Separated and overlaid channels (right column) are presented. Scale bar, 25µm. ep, epidermis; c, cortex; en, endodermis; st, stele; rc, root cap cells.

Ectopic FLS2 expression alters MTI response patterns

We crossed our selection of FLS2 lines with two typical MTI transcriptional markers, *PEROXIDASE 5 (PER5)* and *MYB DOMAIN PROTEIN 51 (MYB51)*, and generated homozygous lines at all three loci (marker, *prom::FLS2* and *fls2*). As control, we used the two markers in wild-type Col-0 background. Markers were chosen for their strong response to flg22 and their divergent response patterns (Poncini *et al.*, 2017; Wyrsh *et al.*, 2015; Zhou *et al.*, 2020). In addition, we developed a pipeline using tissue-specific quantitative analysis, for measuring and comparing MTI responses in an unbiased fashion (Fig. S2). For this, we additionally introduced ubiquitous nuclear markers (*UBQ10::NLS-mTurquoise* or *UBQ10::NLS-tdTomato*) in all our genotypes, which allows to call all nuclei as separate, individual 3D Regions-of-Interests (ROIs), even those with weak or absent MTI-response. After mock or flg22 treatment and fixation, cell-wall-stained roots were imaged at three different zones of the root: Meristem (MZ), Elongation (EZ) and Differentiation (DZ). Each nucleus was automatically detected as a 3D object and the obtained nuclei object maps were then combined to the cell wall marker channels to manually curate and assign each nucleus to a tissue. Once the selected nuclei were assigned, mean intensity for each cell type per zone per treatment per genotype were calculated and colour coded for the generation of a quantitative MTI-response atlas for each *prom::FLS2* line (Fig.S2, values in Fig.S4).

Our cell-specific quantification and microscopic analysis confirmed that *PER5* is not expressed in absence of flg22 treatment (Fig.2A, 2BC), but that *MYB51* presents a basal, flg22-independent expression in the epidermis and root cap cells of the undifferentiated tissues (MZ and EZ) and in the stele and the cortex of the DZ (Fig.S3A, S3C). In wild-type plants, both MAMP markers are strongly induced in the EZ, recapitulating previous observations (Fig.2A and S3A) (Millet *et al.*, 2010; Poncini *et al.*, 2017; Zhou *et al.*, 2020). Specifically, *PER5* is triggered almost exclusively in the elongating epidermis and root cap cells (Fig.2B, 2C, 2D). *MYB51* induction is restricted to these same tissues close to the meristem, but induction expands to cortex and pericycle cells in the later root (Fig.S3C, S3D).

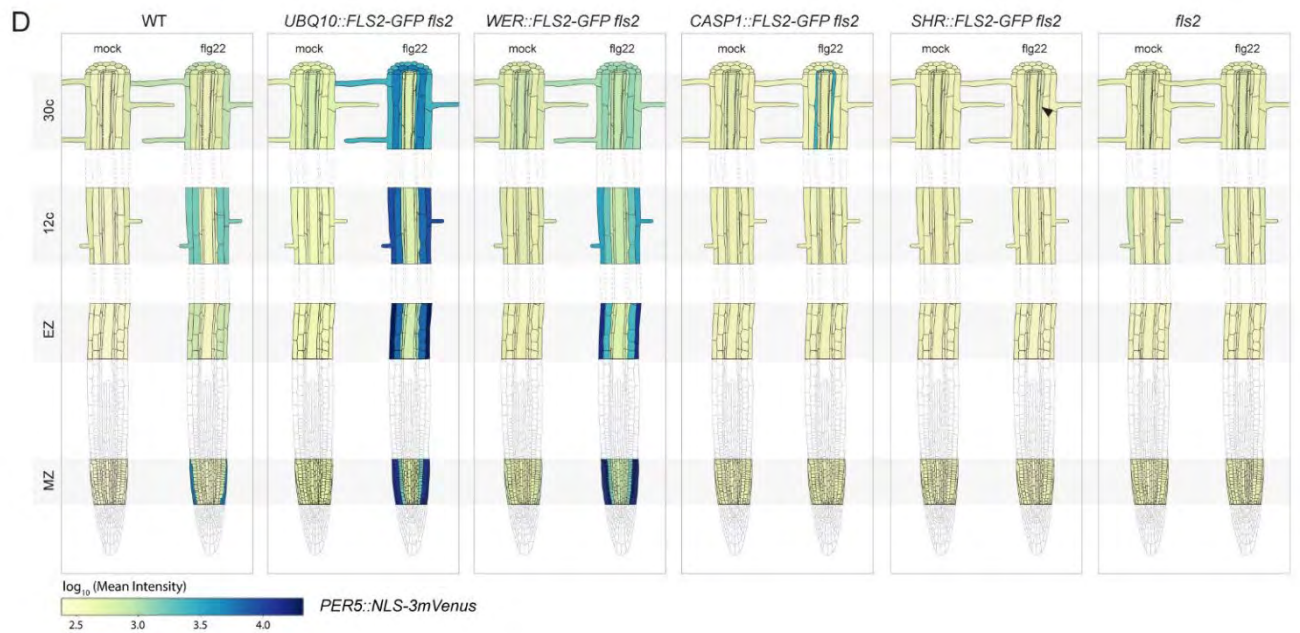
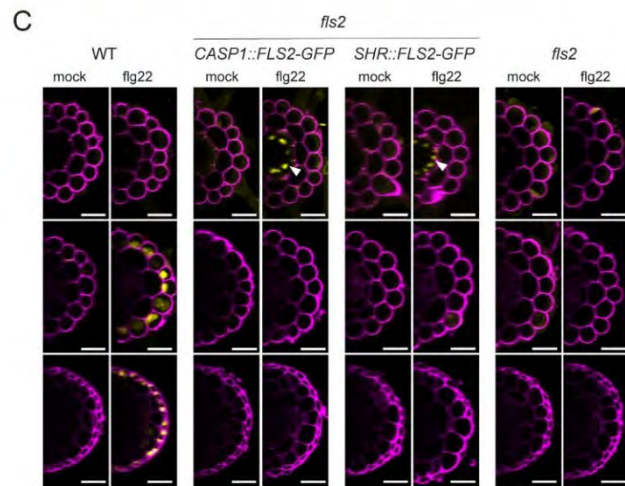
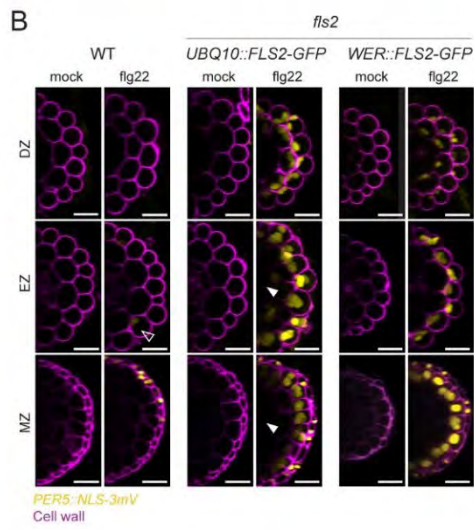
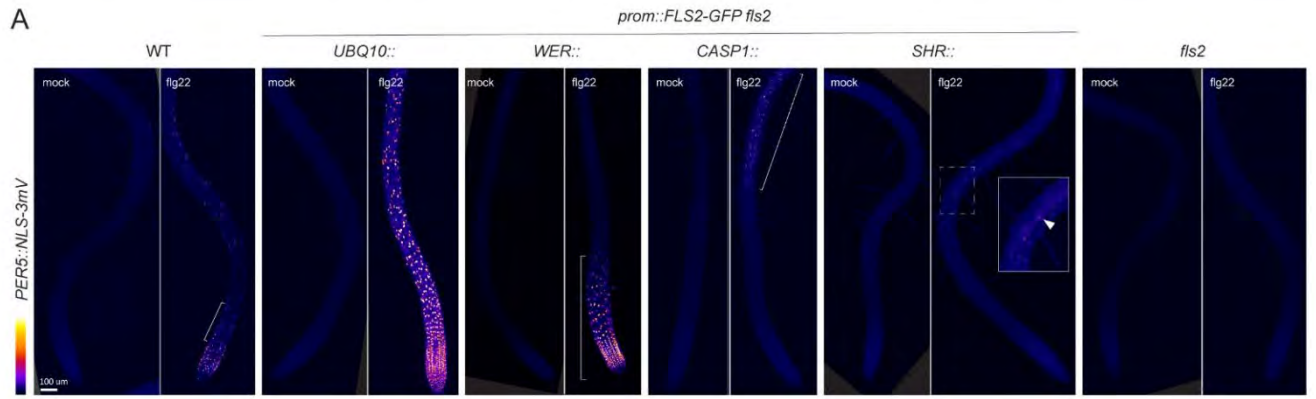


Figure 2: *PER5* marker gene is induced cell-autonomously by flg22 treatment

(A) Overview of *PER5::NLS-3mVenus* marker response to flg22 in different *FLS2* recombinant lines. Tile scan images of 1 μ M flg22 treated plants versus mock. Pictures were taken with similar settings. Settings were always identical between mock and corresponding flg22 treatment. Region of responsiveness is modified by the different expression patterns of *FLS2*. Brackets indicate responsive regions. For *SHR*, close-up view was generated with increased brightness to highlight stellar signal (white arrow). Scale bar, 100 μ m. **(B)** Maximal projection of transverse sections views of *PER5* expression pattern in *UBQ10::* and *WER::FLS2-GFP fls2* compared to WT shown for meristematic zone (MZ), elongation zone (EZ) and differentiated zone (DZ, 30 cells after start of elongation). Seedlings were treated for 24h with 1 μ M flg22. Note the refractory region in the central cylinder in *UBQ10::FLS2* (white arrows). Nuclear localized mVenus signal (yellow) was co-displayed with propidium iodide cell wall marker (PI, purple). Images were taken with similar settings, but corresponding mock and flg22 treatment pictures for each zone separately always have identical parameters. Note that epidermal signal in flg22-treated wild-type seedlings is faint (EZ, black arrow), due to settings chosen to avoid saturation of signal in the transgenic lines. Compare to Fig.2C, WT. Scale bar, 25 μ m. **(C)** Maximal projection of transverse section views of *PER5::NLS-3mVenus* expression pattern in *CASP1::* and *SHR::FLS2-GFP fls2* as well as WT and *fls2* control. White arrows point at ectopic response in the endodermis. Images were acquired as in Fig.2B., with similar settings between genotypes, but with identical parameter for corresponding mock and flg22 treatment. Pictures were acquired with increased gain compared to Fig.2B due to lower average signal intensity. Scale bar, 25 μ m. **(D)** Quantitative map of *PER5::NLS-3mVenus* responses inferred from tissue specific quantification after 24h treatment with 1 μ M flg22. Nuclear signals were quantified in ROI delimited with *UBQ10::NLS-mTurquoises2* for all tissue-specific promoter lines, while wild-type (WT) signal was quantified with *UBQ10::NLS-tdTomato* marker. Mean intensity is therefore comparable between *prom::FLS2-GFP fls2* lines, but not to wild-type.

For both markers, changing expression of *FLS2* had an obvious impact on the pattern of responses. Rather than remaining restricted to the elongation zone, *PER5* and *MYB51* induction largely follows the ectopic *FLS2* expression pattern. The defence markers extend to the whole root in *UBQ10::FLS2*, while they are restricted to the DZ or the MZ in *CASP1::FLS2* and *WER::FLS2*, respectively (Fig.2A and S3A). As expected, the *fls2* mutant does not respond to flg22 in any tissue.

PER5 responds only in the differentiated endodermis in the *CASP1::FLS2* recombinant line, which matches with the very specific expression pattern of *CASP1* promoter. For *WER::FLS2* line, the *PER5* response also follows *FLS2* expression. We could quantify a strong response in root cap cells and the meristematic epidermis, extending until the early DZ, as well as in cortex cells, where we could also detect *FLS2* protein (Fig.2B, 2C, 2D, S1A). In contrast to *PER5*, we detected *MYB51* response to flg22 not only in cells expressing *FLS2*, but also some degree of induction in neighbouring cells (Fig. S3B, S3C, S3D). Intensity ratio between flg22 and mock treated plants were calculated and represented graphically in Fig.S5. Non-cell-autonomous responses were obvious for *MYB51* in the DZ of *CASP1::FLS2*. Although *FLS2* is specifically expressed in the

endodermis, we could barely detect any *MYB51* responses in this tissue, while the neighbouring stele and cortex cells strongly up-regulated *MYB51* (Fig.S3C, S3D, S5). Similarly, flg22 treatment led to *MYB51* expression not only in the epidermis and cortex, but also in central tissues in *WER::FLS2*. Thus, we concluded that *MYB51* induction by MAMPs is controlled by non-cell autonomous mechanisms, in contrast with the strict cell-autonomy of *PER5* and *FRK1* (this work and Zhou *et al.*, 2020).

FLS2 expression is insufficient to cause flg22-responses in the vascular meristem

Intriguingly, some tissues were also completely refractory to flg22-triggered responses. Despite a clear presence of FLS2 in the vascular meristem (Fig.1B), flg22 treatment did not trigger *PER5* or *MYB51* in *SHR* and *UBQ10::FLS2* lines (Fig.2, S3), except for some weak *MYB51* induction in meristematic pericycle cells in *UBQ10::FLS2* (Fig.S3D, S5). We conclude that flg22-induction of *MYB51* in the pericycle is due to a non-cell autonomous signal from outer cell layers. Thus, central meristematic tissues differ from outer tissue layers in their competence to respond to flg22 in the presence of receptor.

Ca²⁺ waves are non-cell autonomous responses

Cytosolic Ca²⁺ increases are among the earliest responses upon MAMP perception, preceding transcriptional changes (Jeworutzki *et al.*, 2010; Seybold *et al.*, 2014). In roots, Ca²⁺ influx after flg22 perception was shown to spread across tissues (Keinath *et al.*, 2015). However, since many cells express some degree of *FLS2* in wild-type, it is impossible to dissect to what extent such waves represent a non-cell autonomous propagation of the Ca²⁺ signalling, or are due to flg22 diffusion and direct stimulation of the different tissue layers and regions. We therefore introduced the intensity-based Ca²⁺ reporter *R-GECO1* in our transgenic lines (Keinath *et al.*, 2015). We observed in *WER::FLS2* that, like in WT (Movie 1 and 6), calcium signals initiate in the epidermis and spread to inner tissues (Fig.3AB, Movies 2 and 7). Since the receptor was not expressed in central tissues, this clearly demonstrates the non-cell autonomous nature of FLS2-stimulated calcium signalling. This spreading of Ca²⁺ could be observed in all recombinant lines tested, with the intriguing feature that wave direction could be manipulated – *i.e.* in both

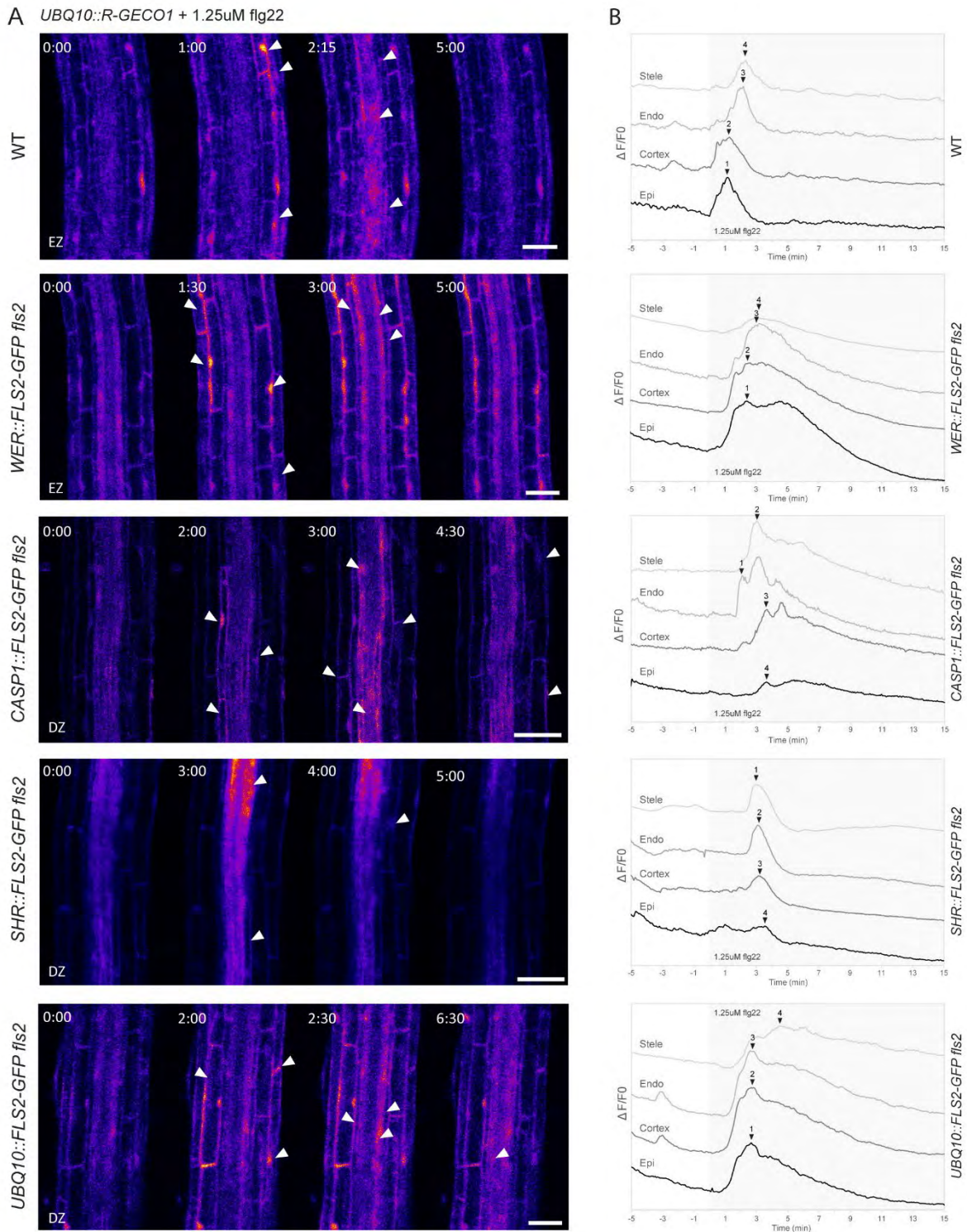


Figure 3: Ca²⁺ waves are non-cell autonomous responses

(A) Ca²⁺-dependent signal in the *prom::FLS2-GFP fls2* lines in response to 1.25 μ M flg22. Time series of *UBQ10::R-GECO1* fluorescence: pictures are longitudinal middle sections of roots at the elongation zone (EZ) or differentiated zone (DZ). Time 0:00 corresponds to the start of flg22 treatment. White arrows point at tissues showing a strong increase in Ca²⁺ content. Scale bar, 25 μ m. (B) Normalized R-GECO1 fluorescence intensity ($\Delta F/F0$) measured in tissue-specific ROIs. Values present the dynamics of Ca²⁺ cytosolic concentration in response to flg22 in the root shown in (A) for each tissue type. Black arrows point at the maximum intensity of the trace. Grey background corresponds to flg22 treatment.

CASP1::FLS2 and *SHR::FLS2* lines, the wave started first in the endodermis then spread to outer and inner tissues (Fig.3CD, Movie 8 and 9). Moreover, in these two lines, the wave starts in the differentiated zone rather than in the elongation zone (Movies 3 and 4). When *FLS2* was expressed in all tissues under *UBQ10* promoter, all tissues respond almost simultaneously (Fig.3E, Movie 5 and 10). Taken together, while transcriptional read-outs are largely cell-autonomous, with some degree of tissue-specificity, cytosolic calcium increases represent a non-cell autonomous signalling branch. This implies that even cells that are neither exposed to MAMPs, nor possessing perception capacity, are nonetheless rapidly receiving some sort of stress signal in the form of a calcium wave.

Epidermal meristematic expression of *FLS2* leads to flg22 hypersensitivity and meristem collapse

As demonstrated above, *FLS2* ectopic expression can profoundly alter the pattern of immune responses in the root. To test whether this change affects root development, we assessed root length of seedlings transferred on flg22-containing medium. As expected, treated wild-type plants showed only a mild reduction in root length. By contrast, the root length of the constitutive, overexpressing *UBQ10::FLS2* line was strongly reduced with additionally stunted shoot development (Fig.4A and 4B). More surprisingly, a strong root length inhibition was also observed in the *WER::FLS2* line, although this line expresses *FLS2* only in young epidermal and root cap cells. *SHR::FLS2* and *CASP1::FLS2*, by contrast, showed root growth similar to wild-type.

In order to precisely identify the tissue responsible for root growth inhibition, we generated two additional *prom::FLS2* lines using the *RCH1* (*RECOGNITION OF C.HIGGINSIANUM*) and *PRP3* (*PROLINE-RICH PROTEIN 3*) promoters (Marquès-Bueno *et al.*, 2015). *RCH1* is expressed in the whole meristem, while *PRP3* is expressed strongly in differentiating root hair cells (Fig.S1E). While *PER5* induction followed the expression of *FLS2* in both lines (Fig. S1GH), only *RCH1::FLS2* presents an increased root growth inhibition (Fig.S1F), whereas *PRP3::FLS2* responds as wild-type (Fig.S1I). Therefore, we conclude that it is the expression of *FLS2* in meristematic epidermal cell layers that causes hypersensitive root growth inhibition in response to flg22. Indeed, when comparing the pattern of *PER5* expression between wild-type and *WER::FLS2* at high resolution, it is evident that only the meristematic epidermal cells show strong *PER5* induction in *WER::FLS2*,

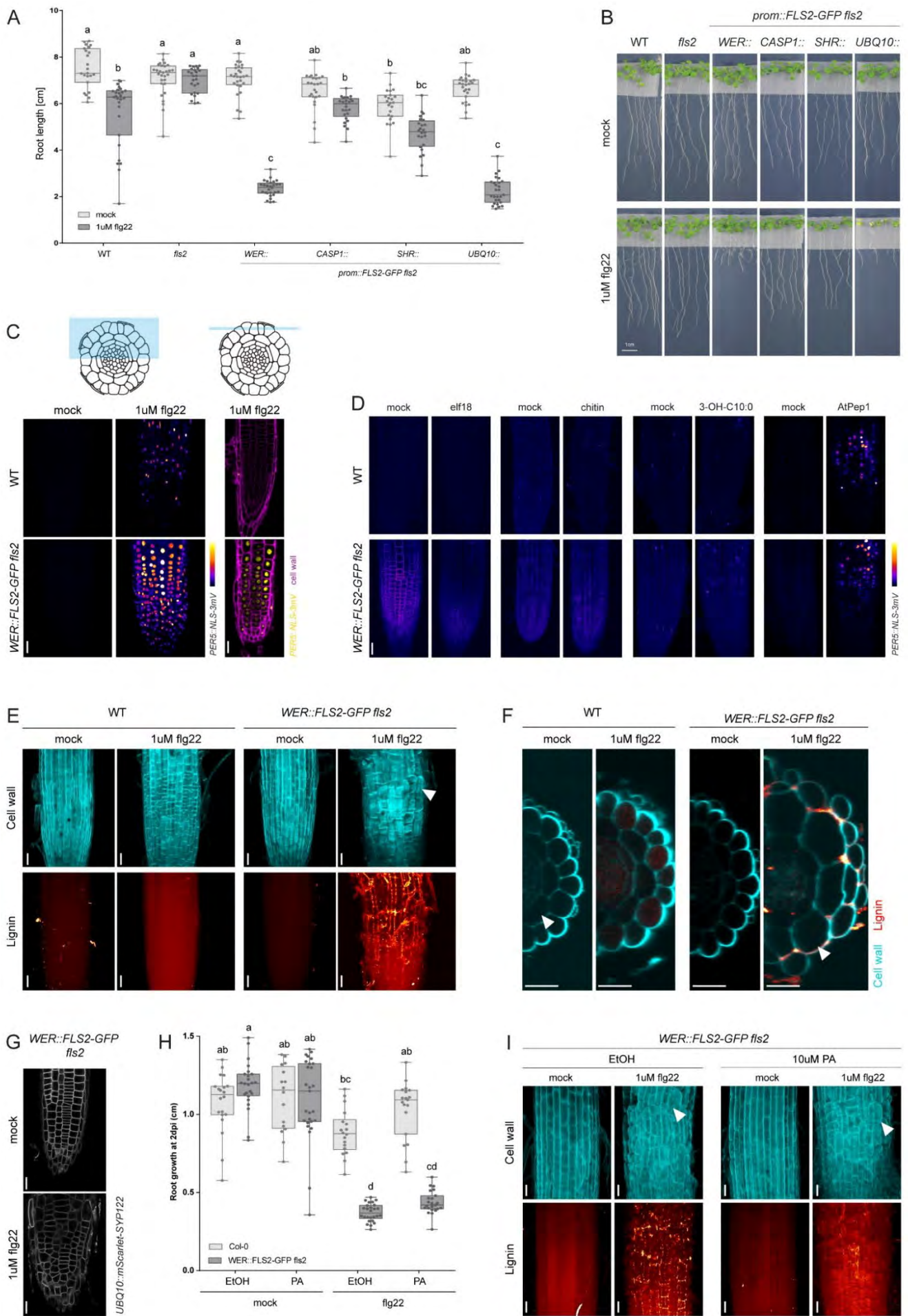


Figure 4: Epidermal meristematic expression of *FLS2* leads to flg22 hypersensitivity and meristem collapse

(A) Flg22 treatment increases root growth inhibition in *WER::FLS2* hypersensitive line. Root length quantification of *prom::FLS2-GFP fls2* lines transferred on 1 μ M flg22 for 6dpi. Boxplot centre represents the median (n=23 to 28 roots). Different letters indicate statistically significant difference between means by Kruskal-Wallis test and Dunn's multiple comparison. (B) Representative pictures of seedlings transferred for 6 days on 1 μ M flg22. Scale bar, 1cm. (C) Flg22 induces strongly *PER5::NLS-3mVenus* in the epidermis of *WER::FLS2-GFP fls2* hypersensitive line. On the right, maximum projection of z-stacks taken in root tips of plants treated for 24h with 1 μ M flg22 or mock. Schematic represents the depth of the z-stack. Pictures were taken with identical settings. Scale bar, 25 μ m. (D) *WER::FLS2-GFP fls2* hypersensitivity is specific to flg22. *WER::FLS2-GFP fls2* and wild-type plants were treated for 24h with either 1 μ M elf18, 2 μ g/ml chitin, 1 μ M 3-OH-C10:0 or 1 μ M AtPep1. Maximum projection of z-stacks taken in root tips. *PER5* induction is highlighted with mVenus (Fire LUT). Parameters were identical for mock and treatment. Scale bar, 25 μ m. (E) Treatment of *WER::FLS2-GFP fls2* for 2 days with 1 μ M flg22 induces meristem swelling and lignin deposition. Upper panel shows median projection of calcofluor white stained cell wall in the transition zone of the root tip (blue). Note bulky cells of the epidermis (white arrowhead). Lower panel presents maximum projection of lignin deposition stained with basic fuchsin (red). Lignin accumulates between cells only in *WER::FLS2-GFP fls2* after flg22 treatment. Scale bar, 25 μ m. (F) Cross-section of pictures in (E). Cell wall stained with calcofluor white (blue) is co-visualized with lignin stained with basic fuchsin (red). Flg22 treatment induces massive swelling of cortex cells (white arrowheads) only in *WER::FLS2-GFP fls2*. Lignin is principally deposited between epidermal and cortex cells. Epidermal cells are pushed apart by the swelling cortex and are sometimes missing. Scale bar, 25 μ m. (G) Epidermal view of plasma membrane visualized by the construct *UBQ10::mScarlet-SYP122* in *WER::FLS2-GFP fls2*. Cell division is disorganized after 1 μ M flg22 treatment. Scale bar, 25 μ m. (H) Inhibition of monolignol synthesis does not rescue meristem flg22-driven increased root growth inhibition of *WER::FLS2-GFP fls2*. Root growth measured after overnight pre-treatment with 10 μ M PA inhibitor followed by 36h 1 μ M flg22 combined to 10 μ M PA treatment. Boxplot centre represents the median (16 \leq n \leq 27). Different letters indicate statistically significant difference (p<0.05) between means by Kruskal-Wallis test and Dunn's multiple comparison. (I) Flg22 induces meristem swelling despite inhibition of monolignol by PA treatment. Pictures taken from samples quantified in (H). Upper panel shows median projection of calcofluor white stained cell wall in the transition zone of root tip (blue). Lower panel presents maximum projection of lignin deposition stained with basic fuchsin (red). White arrowheads points at examples of bulky cells. Scale bar, 25 μ m.

whereas root cap cells show flg22 responsiveness in both lines. This suggests that MTI in epidermal cells is the cause of super-competent response (Fig. 4C). Importantly, neither the MAMPs elf18, chitin or the LPS fragment 3-OH-C10:0, nor Atpep1 showed enhanced *PER5* in *WER::FLS2* (Fig.4D). This demonstrates that ectopic *FLS2* expression does not cause a global upregulation of responsiveness to MAMPs, but specifically affect flg22 signalling.

Interestingly, treatment of *WER::FLS2* super-competent line with flg22 induces profound morphological changes in the root, not observed in wild-type. After two days of treatment, cells reaching the transition zone start to swell and division patterns become disorganized, giving rise to bulky meristem shapes (Fig.4E, upper panel, 4G). Virtual cross-sections revealed that cortex

cells expand tremendously, dislocating epidermal cells (Fig.4F). Thus, precise spatial regulation of *FLS2* expression levels is necessary to avoid severe growth inhibition caused by flg22-induced disorganized cell expansion in the meristem.

FLS2 ectopic expression leads to cell-autonomous, flg22-triggered lignin deposition

MTI is known to modify cell wall composition, such as callose deposition or lignification (Chezem *et al.*, 2017; Lee *et al.*, 2019; Millet *et al.*, 2010). Indeed, lignin or suberin depositions are long-known damage and immune responses (Bernards, 2002; Hijwegen, 1963; Kamula *et al.*, 1994; Messner and Boll, 1993; Ranathunge *et al.*, 2008; Thomas *et al.*, 2007), but have not been widely adopted in modern studies on MTI (Lange *et al.*, 1995; Mandal and Mitra, 2007), see (Chezem *et al.*, 2017; Lee *et al.*, 2019) for exceptions.

Interestingly, we found that flg22 treatment induced strong lignification from transition to differentiated zone in *WER::FLS2* (Fig. 4E and S6A). Lignin was deposited between epidermis and cortex cells, mainly at the corners (Fig. 4F). In younger regions, lignin was also found between epidermis and root cap cells. All other recombinant lines also showed lignin deposition following their respective *FLS2* expression pattern, except in the stele, matching the absence of *PER5* response in these tissues (Fig.S6B). Interestingly, no lignin deposition could be observed in flg22-treated wild-type roots (Fig.4E, S6), fitting with previous reports (Chezem *et al.* (2017)). It is intriguing to speculate that *PER5*, ROS-production and other flg22-responsive genes, categorised as "oxidative stress" response genes (Tognolli *et al.*, 2002), are actually part of a lignification response that stays below a productive threshold in wild-type, but pivots into a full lignification upon flg22-stimulation of *FLS2* overexpression lines.

The stronger root growth inhibition observed in the super-competent *WER::FLS2* line could be due to the impact of lignin deposition in the transition zone. To test if cell wall reinforcement by lignin prevents cell division and elongation, we inhibited lignin formation with the monolignol synthesis inhibitor piperonylic acid (PA), expecting to restore root growth (Fig. 4I). Nevertheless, even in the absence of lignin, *WER::FLS2* still showed root meristem collapse and stronger RGI than wild-type (Fig. 4H).

Suberin lamellae deposition after flg22 treatment is an endodermis-specific response

Ectopic lignin deposition occurs in the endodermis as a compensatory mechanism for deficient Casparian strip formation, and is often followed by suberin lamellae deposition (Doblas *et al.*, 2017). We wanted to assess whether the overactivation of MTI could trigger the deposition of suberin in cells expressing *FLS2*. In wild-type untreated plants, suberin is usually present in the endodermis only, starting in the late differentiation zone by patches (“patchy zone”), then progressing to a fully suberized zone (Andersen *et al.*, 2015, 2018).

In wild-type, suberin was not induced by flg22 (Fig.5AB). In contrast, lines expressing *FLS2* in the endodermis, such as *CASP1::*, *SHR::* and *UBQ10::FLS2*, showed increased endodermal suberization, leading to a complete disappearance of the patchy zone (Fig. 5B). Earlier suberisation is not simply due to earlier differentiation of endodermal cells due to growth arrest, since *WER::FLS2* still conserved a normal proportion of patchy and suberized zone despite its shorter root length. Reversely, *CASP1::* and *SHR::FLS2* root growth was not affected by flg22, but suberin formed nevertheless much earlier. Therefore, flg22 can induce suberization only when expressed in the endodermis. This endodermis-specific suberisation is a nice demonstration of a flg22 response that only occurs in a specific cellular context.

Super-competent *WER::FLS2* line can detect native bacterial flagellin

The strong impact of flg22 on *WER::FLS2* root growth and cell wall modification prompted us to evaluate whether commensal bacteria would have a similar effects. Indeed, plants that mount ectopic defences in sensitive tissues might suffer from the presence of usually harmless bacteria and tip the balance between growth and defence. The model commensal/beneficial *Pseudomonas protegens* CHA0 does not induce MTI responses in wild-type plants, except at high concentration or if the root is wounded (Zhou *et al.*, 2020). However, when inoculated on *WER::FLS2* line, a very evident *PER5* induction could be observed, although no synthetic flg22 peptide was added (Fig.6A). This experiment is therefore a first clear example, where a flg22 response is caused by actual, living bacteria. This flagellin must be released and processed into *FLS2*-binding smaller peptides (Buscaill *et al.*, 2019).

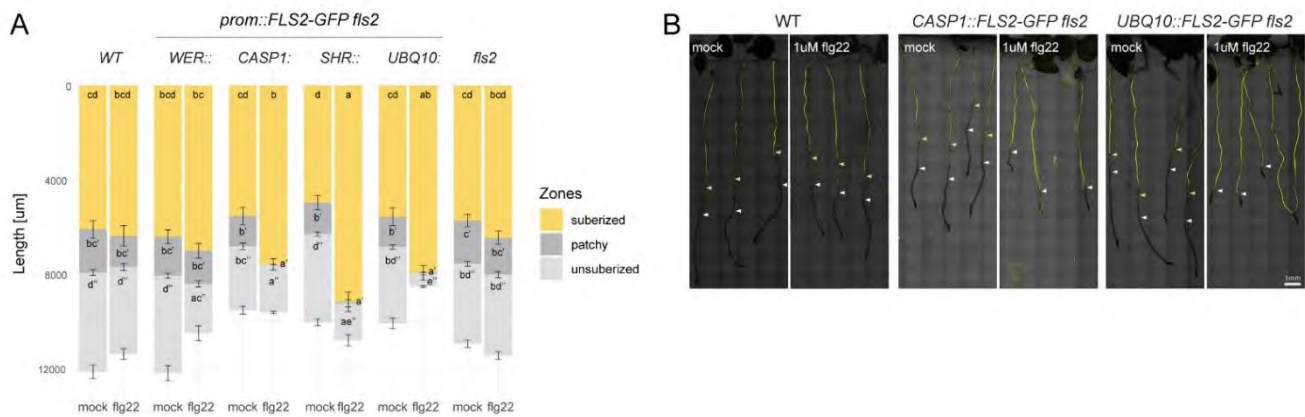


Figure 5: Suberin deposition is triggered by flg22 when endodermal cells expressed FLS2

(A) Quantification of suberized zone length in seedlings treated for 1 day with 1 μM flg22 (18 \leq n \leq 27). Data of two replicates were pooled. Roots regions were classified as suberized, patchy and unsuberized zones. Error bars represent standard error (SE). Different letters indicate statistically significant differences amongst lines for the specified zone ($p < 0.05$). Multiple comparison was performed using ANOVA and Tukey's tests for the suberized zone, whereas Kruskal-Wallis and Dunn's tests were used multiple comparison of patchy and non-suberized zones. **(B)** Whole root views of suberin lamellae deposition in *CASP1::* and *UBQ10::FLS2-GFP fls2* lines compared to wild-type after 1 μM flg22 treatment vs mock. Suberin was stained with fluorol yellow. White arrowheads start of patchy zone; yellow arrowheads, start of fully suberized zones. Scale bar, 1mm.

To confirm that the induction of *PER5* was caused by native, bacterial flg22, we infected seedlings with a CHA0 mutant defective for *fleQ*, required for the induction of flagellum development (Arora *et al.*, 1997; Kupferschmied, 2015), as well as *fliC*, coding for the flagellin protein (Yamaguchi *et al.*, 1984). In contrast to the wild-type strain, $\Delta f leQ$ and $\Delta f liC$ mutants could not trigger any response in *WER::FLS2*, demonstrating that defences are induced by the direct FLS2-mediated detection of bacteria-derived flagellin molecules (Fig.6A). We then assessed the impact of CHA0 bacteria on root growth. Surprisingly, despite its induction of *PER5*, CHA0 did not significantly enhance root growth inhibition in *WER::FLS2* compared to wild-type (Fig.6B). One explanation would be that some commensal bacteria are able to attenuate the excessive MAMP-triggered immune responses in *WER::FLS2*, thus avoiding root growth inhibition and deleterious defence responses (Garrido-Oter *et al.*, 2018; Pel and Pieterse, 2013). Indeed, Ma *et al.* (2020) were unable to observe any growth phenotype of *WER::FLS2* plants grown in non-sterile soil. Interestingly, they reported that 41% of root commensals can suppress MAMP-triggered root growth inhibition in mono-associations.

Bacterial community members have diverse impact on *WER::FLS2*

In order to obtain a more comprehensive picture of how *WER::FLS2* affects responses to bacteria, we screened a set of 34 bacterial isolates from the At-SPHERE culture collection of Cologne (Bai *et al.*, 2015) for both induction of *PER5* marker and enhanced root growth inhibition in *WER::FLS2* compared to wild-type lines. We selected isolates to represent bacteria from all phyla, with a bias towards bacteria predicted to possess a flg22 peptide sequence recognised by the FLS2 receptor (Fig.6C, Table S1) (Garrido-Oter *et al.*, 2018). Amongst the 17 strains predicted to be recognized by FLS2 based on their sequence, only 10 triggered an enhanced *PER5* marker induction in *WER::FLS2*. Moreover, five additional strains, without a predicted recognizable flg22 sequence, had the same effect. This underlines the problematic of predicting flg22 activity from sequence and the potential of the *WER::FLS2* line to rapidly test experimentally, whether a native bacterial flg22 can be detected by the plant.

Although half of bacterial isolates could induce *PER5* marker specifically in the *WER::FLS2* line, only 5 of them affected *WER::FLS2* root growth more strongly than WT, though often with great variation (Fig.6C, Table S1). However, *Pseudomonas* isolate R569 caused strongly enhanced *PER5* induction (Fig.6D) and root growth inhibition compared to WT (Fig.6E). This effect was very robust and was repeatedly observed both in Lausanne and Cologne laboratory growth conditions (Fig.S7C). We demonstrated that commercial, synthesized flg22 from *Pseudomonas aeruginosa* as well as from isolate R569 (flg22_{R569}) similarly induced *PER5* marker expression and inhibited root growth. These effects were abrogated in the *fls2* mutant background (Fig.S7B). We conclude that the commensal R569 isolate induces MTI responses in the *WER::FLS2* line through its native flg22 peptide, which then causes an unbalancing of growth and defence not observed when the bacterium grows on wild-type roots.

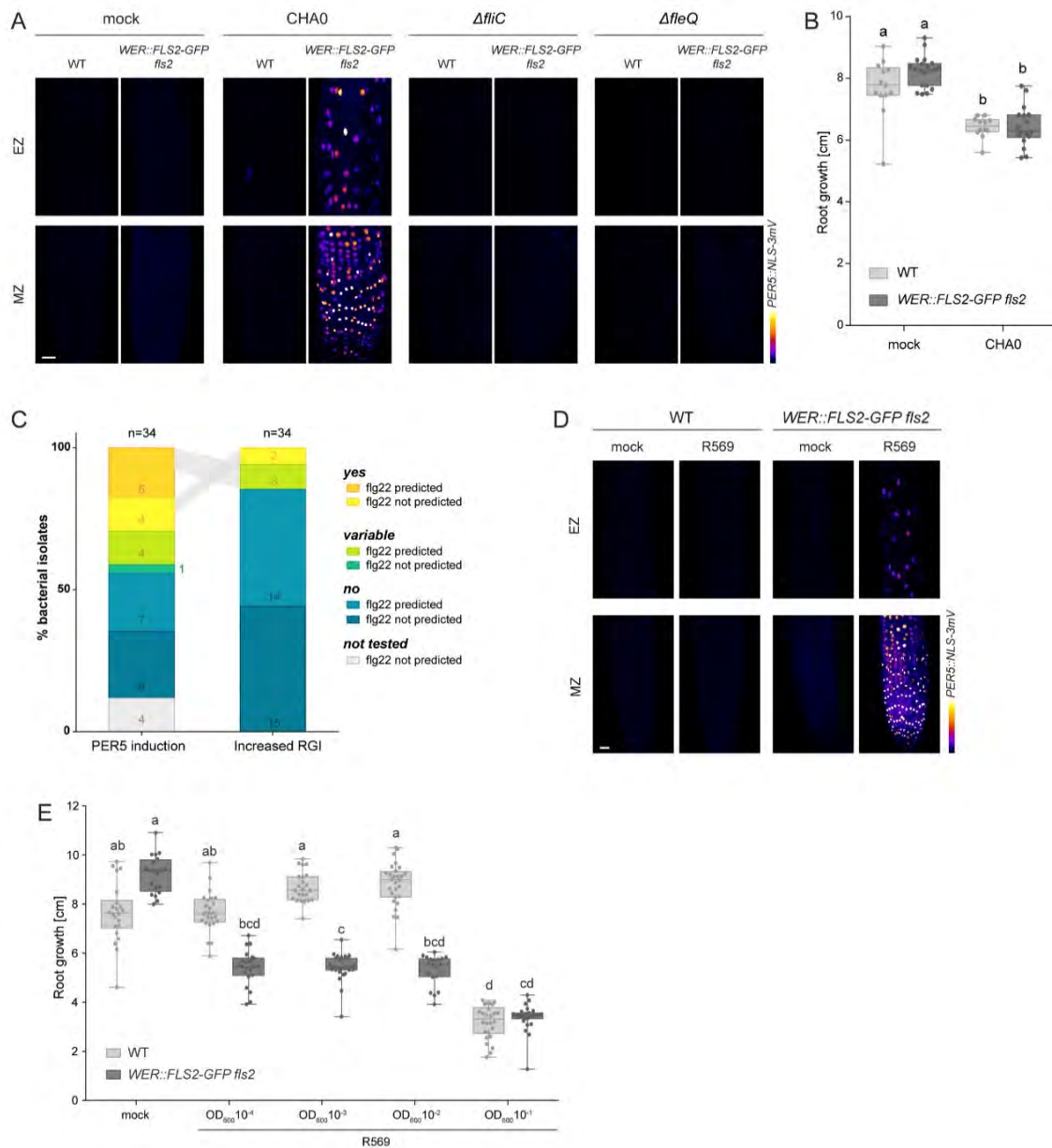


Figure 6: WER::FLS2 line detects endogenous bacterial flg22

(A) CHA0 bacteria trigger a strong induction of *PER5::NLS-3mVenus* marker (Fire LUT) on *WER::FLS2-GFP fls2*. Mutants $\Delta fliC$ and $\Delta fleQ$ defective for flagellum lose their ability to induce detectable MTI. $\Delta fliC$ mutant was confirmed by motility assay (see Fig.S7D). Maximum projection of z-stacks imaging meristematic (MZ) and elongation (EZ) zones treated with drop inoculation of bacterial solution of a concentration of $OD_{600} = 0.01$ or mock, respectively. Images were acquired at 1dpi. Acquisition done with identical settings. Scale bar, 25 μ m. **(B)** CHA0 do not induce consistently increased root growth inhibition in *WER::FLS2-GFP fls2*. Root growth was quantified at 6 dpi on plate inoculated with bacteria at $OD_{600} = 10^{-3}$. Different letters indicate statistically significant differences ($p < 0.05$). Multiple comparison was performed using ANOVA and Tukey's test. **(C)** Proportion of natural isolates from At-SPHERE culture collection triggering stronger *PER5::NLS-3mVenus* induction and increased root growth inhibition (RGI) on *WER::FLS2-GFP fls2* compared to wild-type seedlings (yes), or not (no). Bacteria classified in "variable" presented contradictory results between replicates. Bacteria flg22 sequence was predicted to be recognized by FLS2 (flg22 predicted) or not (flg22 not predicted). Numbers of bacterial isolates in each category are indicated in colour. Grey surfaces indicate identical bacteria strains. **(D)** *Pseudomonas* isolate R569 from At-SPHERE culture

collection triggers strong *PER5::NLS-3mVenus* (Fire LUT) induction on *WER::FLS2-GFP fls2*. Seedlings were imaged after one-day treatment with $OD_{600} = 0.01$. Maximum projection of z-stacks at meristematic zone (MZ) and elongation zone (EZ). Scale bar, 25 μ m. **(E)** Isolate R569 induces a robust increased root growth inhibition on *WER::FLS2-GFP fls2* compared to wild-type plants. High concentration of bacteria ($OD_{600} = 0.1$) is deleterious to both genotypes. Root growth was quantified at 6 dpi on plate inoculated with bacteria at $OD_{600} = 10^{-1}$ to 10^{-4} . Different letters indicate statistically significant differences ($p < 0.05$). Multiple comparison was performed using Kruskal-Wallis and Dunn's test.

Discussion

It is not understood why only a restricted subset of root tissues can directly respond to MAMPs in the absence of other stimuli (Millet *et al.*, 2010; Poncini *et al.*, 2017; Zhou *et al.*, 2020). The combination of tissue-specific receptor expression and cellular resolution read-outs presented here provides insights into the consequences of altering the spatial patterns of MTI in roots. Our work reveals three important features of MAMP responses.

First, different MTI responses are highly tissue-specific and varying in cell-autonomy. Suberin, for example, is only induced in the endodermis. While *PER5* induction is strictly cell autonomous, *MYB51* and calcium signals are found in cell lacking *FLS2* receptor. It will be important to describe larger numbers of response genes for a comprehensive view of MTI. Cell-type specific transcriptomic analysis can complete our understanding of tissue-specific immune pathways (Rich-Griffin *et al.*, 2020). Our *prom::FLS2* lines coupled to transcriptional read-outs can now help to distinguish cell-autonomous responses from indirect activation by MTI.

Secondly, we found that the vascular meristem is refractory to flg22 even when expressing *FLS2* receptor. The seemingly contradictory finding in Wyrsh *et al.* (2015) can be explained by the whole-organ read-outs used, as well as use of *LBD16::FLS2*, thought to be stele-specific, but that we found to also slightly express in other tissues (Fig.S1J). Lack of downstream signalling components or increased activity of negative regulators could both be responsible for the stele's inability to respond to flg22. The vascular meristem might be particularly vulnerable to an activation of defence as it contains early-differentiating phloem providing nutrition and hormones to the growing meristem.

Finally, we observed root regions that can be rendered super-competent by *FLS2* expression. We speculate that epidermal meristematic cells are not responsive in wild-type (Millet *et al.*,

2010; Zhou *et al.*, 2020), because only the outer root cap cells can mount MAMP responses that are not detrimental to meristem function. This might be linked to the particular fate of root cap cells that enter apoptosis once they reach the transition zone (Fendrych *et al.*, 2014; Kumpf and Nowack, 2015) and excrete mucilage and secondary metabolites influencing root microbiota (Bulgarelli *et al.*, 2013; Kumpf and Nowack, 2015). By contrast, epidermal cells might only maintain a competency to respond, if root cap damages by pathogens or other stresses induce *FLS2* expression. Indeed, we clearly showed that constitutive expression of *FLS2* in the meristematic epidermis leads to drastic changes in the root structure upon flg22 treatment in ways that could be detrimental to growth.

Though lignification upon actual bacterial infection is well documented (Lee *et al.*, 2019; Nicholson and Hammerschmidt, 1992; Vance *et al.*, 1980), treatment with single MAMP was rarely seen to stimulate root lignin deposition (Adams-Phillips *et al.*, 2010; Chezem *et al.*, 2017; Robertsen, 1986; Smit and Dubery, 1997). Here we show that strong *FLS2* expression reveals the capacity of MTI responses to modify cell walls, probably overriding endogenous negative feedbacks that prevent this from happening in wild-type. This provides an opportunity to study MTI-induced lignification in a simplified and reproducible setting. Interestingly, ectopic corner lignification together with defence genes induction are also observed in response to CIF2 peptide treatment in the endodermis (Alassimone *et al.*, 2016; Doblaz *et al.*, 2017; Fujita *et al.*, 2020, 2020; Pfister *et al.*, 2014), suggesting the developmental SCHENGEN pathway shares similarities with MTI responses. Nevertheless, lignification is only partly explaining the severe root growth inhibition we observe. Other factors produced in response to flg22 might also interfere with meristem function, such as basic coumarins (Stringlis *et al.*, 2019a), which inhibit cellulose, resulting in meristem swelling similar to the one observed on *WER::FLS2* (Hara *et al.*, 1973).

Our work also reveals that overexpression of a single PRR in a competent, but otherwise non-responsive cell-type, bypasses the absence of visual immune responses to commensal bacteria (Garrido-Oter *et al.*, 2018; Millet *et al.*, 2010; Yu *et al.*, 2019a; Zhou *et al.*, 2020). Though bacteria can also inhibit MTI (Couto and Zipfel, 2016; Yu *et al.*, 2019b), MAMPs produced by rhizosphere bacteria might often be too low in concentration to activate MTI responses in the first place.

Therefore, roots might appear largely unresponsive to bacterial presence without additional stresses (Zhou *et al.*, 2020). The obvious root growth phenotype triggered by MTI in *WER::FLS2* lines proves to be a powerful tool to investigate the effect of commensals on root immune responses. Our super-competent lines have allowed for the first time to directly observe stimulation of FLS2 by a native flagellin peptide from an avirulent bacterium. Generally, the cocktail of elicitors that bacteria are thought to release prevent assignment of a MAMP response to an individual MAMP (Tang *et al.*, 2017). The *WER::FLS2* line now generates a cell type that responds only to a single MAMP and can test predictions about flg22 peptide detectability, release and processing. Extending our approach, the ectopic overexpression of potential PRR receptors in the epidermal meristem cells could be used to functionally pair novel receptors and ligands.

It has become evident that immune responses cannot be understood without taking into consideration the specificities of different cell type and developmental stages. Our data establishes the necessity for the plant to spatially restrict its immune response. This spatial allocation of defence capacities might in turn influence the microbial colonization pattern of the rhizosphere. The new tools presented will pave the way for a better understanding of bacterial community structures in roots.

Acknowledgement

We thank the Central Imaging Facility (CIF) of the University of Lausanne for expert technical support. We particularly thank Thomas Boller (Basel), Jean-Pierre Métraux (Fribourg), Silke Lehman (Fribourg) and Ines Wyrsh (Basel) for initiating this project with us. We thank Youssef Belkhadir (Vienna), Thorsten Nürnberger (Tübingen), Corné Pieterse (Utrecht), Cyril Zipfel (Zürich) and Peter Kupferschmid (Bern) as well as all members from the Geldner lab for sharing material and/or helpful discussions and input. Finally, we are grateful to Artan Graf and Yasmine Genolet for their patience and assiduity for the manual curation of cell-type specific quantification. This work was supported by funds to N.G. from an ERC Consolidator Grant (GA-N: 616228–ENDOFUN) and two consecutive SNSF grants (CRSII3_136278 and 31003A_156261). F.Z. was supported by an EMBO Long-Term Fellowship (ALTF 1139–2014).

Author contributions

A.E. and N.G. conceived, designed, and coordinated the project. A.E., F.Z., J.V., C.M.H., V.D.T. performed all experimental work. A.E. and N.G. wrote the manuscript. A.E., F.Z., J.V., K.M., P.S.L., C.K. and N.G. revised the manuscript and were involved in the discussion of the work.

Declaration of interests

The authors declare no competing interests.

Material and methods

Plant material

Arabidopsis thaliana ecotype Columbia Col-0 was used for most experiments. The T-DNA line *FLS2* was obtained from NASC (SALK_062054C) and originally described in (Zipfel *et al.*, 2004). The recombinant *WER::FLS2-3myc-GFP*, *CASP1::FLS2-3myc-GFP*, *SHR::FLS2-3myc-GFP*, *UBQ10::FLS2-3myc-GFP*, *LBD16::FLS2-3myc-GFP* in *fls2* (SAIL691_C04) background, as well as *FLS2::FLS2-3myc-GFP* in Wassilewskija Ws-0 background were provided by Prof. Thomas Boller's group (Robatzek *et al.*, 2006; Wyrsh *et al.*, 2015). The defence marker lines *PER5::NLS-3mVenus* and *MYB51::NLS-3mVenus* are described in (Poncini *et al.*, 2017). Calcium signalling analysis was carried out thanks to the line *UBQ10::R-GECO1* kindly shared by Prof. Melanie Krebs's group (Keinath *et al.*, 2015).

PER5::NLS-3mVenus and *MYB51::NLS-3mVenus* lines were crossed to the four recombinant lines *WER::*, *CASP1::*, *SHR::* and *UBQ10::FLS2-3myc-GFP fls2* lines as well as to the *fls2* mutant. In addition, *UBQ10::R-GECO1* was first crossed to *fls2* mutant, then the resulting homozygous line was crossed again to the four recombinant lines (*WER::/CASP1::/SHR::/UBQ10::FLS2-3myc-GFP fls2*), so that F1 could be directly used for experiments. For quantification of tissue-specific nuclear signal, the constructs *UBQ10::NLS-mTurquoise* or *UBQ10::NLS-tdTomato* were transformed by floral dipping method in all *PER5::/MYB51::NLS-3mVenus* marked *prom::FLS2-3myc-GFP fls2*, *fls2* and wild-type lines (Clough and Bent, 1998). In addition, *RCH1::FLS2-GFP*, *PRP3::FLS2-GFP* and *GRP::FLS2-GFP* were transformed in *fls2* (SALK_062054C).

Plant growth conditions

For all experiments, seeds were surface-sterilized by gaseous chlorine for 2.5 hours or immersed in a solution of 70% EtOH 0.01% Triton-X-100 for 5 min, washed once in 96% EtOH and dried under sterile conditions. Seeds were stratified in the obscurity for 2 days, then germinated on 1% agar plates containing half-strength Murashige and Skoog ($\frac{1}{2}$ MS) medium and 500mg/l MES (Duchefa). Seedlings were grown vertically for 5 days before analysis (otherwise differently specified) in continuous light at 23°C.

For experiments done in Cologne, seeds were sown on 1% Bacto-Agar supplemented with $\frac{1}{2}$ MS with 250mg/l of MES. Seedlings were grown in a light cabinet with short day conditions (10h light-14h dark, 21°/19°C, 65% relative humidity).

Bacterial strains and growth conditions

Pseudomonas protegens strain CHA0 used in this study is a tobacco root isolate with plant-beneficial activities (Stutz *et al.*, 1986). CHA0 mutants $\Delta fliC$ and $\Delta fleQ$ carrying in-frame deletions in the *fliC* and *fleQ* genes, respectively, were generated using the suicide vector pEMG and the I-SceI system (Kupferschmied, 2015; Martínez-García and Lorenzo, 2011) adapted to *P. protegens* (Kupferschmied *et al.*, 2014) with plasmids and primers listed in Supplemental Table S2. The *Pseudomonas* R569 and other natural commensal bacterial isolates were obtained from the At-SPHERE culture collection (Bai *et al.*, 2015). CHA0 strains and commensal isolates were routinely cultured at 28°C in, respectively, lysogeny broth (LB) medium (1% tryptone, 0.5% yeast extract and 1% NaCl) or half-strength tryptic soy broth (TSB) (Sigma-Aldrich).

Plant plasmid construction

Generation of expression constructs was performed with both In-Fusion Advantage PCR Cloning Kit (Clontech) and Gateway Cloning Technology (Invitrogen).

For nuclei labelling with blue fluorochrome, used for quantification, *UBQ10::NLS-mTurquoise2* was generated by triple Gateway recombination reaction using the entry clones pDONR P4-*pUBQ10*-P1R (Zhou *et al.*, 2020), pDONR P1-*NLS-mTurquoise2*-P2 and pDONR P2R-*2R3e-nosT*-P3 (Siligato *et al.*, 2016) with the destination vector pK7m34GW,0 containing a kanamycin resistance gene for plant selection. For the red version of nuclei labelling, the plasmid

UBQ10::NLS-tdTomato was used for its FastRed in plantae selection system. Briefly, pDONR P4-*pUBQ10-P1R* (Zhou *et al.*, 2020) and pDONR P1-*NLS-tdTomato-P2* were combined with the destination vector pFR7m24GW by double Gateway reaction. pDONR P1-*NLS-tdTomato-P2* was previously generated using in-Fusion cloning to integrate the NLS sequence to pDONR P1-*tdTomato-P2*.

RCH1::FLS2-GFP, *PRP3::FLS2-GFP* and *GRP::FLS2-GFP* were generated combining the respective entry clones pDONR L4-*pRCH1-R1* and L4-*pPRP3-R1* (SWELL lines)(Marquès-Bueno *et al.*, 2015), or pDONR L4-*pGRP-R1* (Andersen *et al.*, 2018), with pDon207 containing the L1-*FLS2-3xmyc-GFP-L2* sequence (Wyrsh *et al.*, 2015), in the destination clone pH7m24GW,3.

Elicitors and inhibitors treatments

Commercial flg22_{Pa} peptide from *Pseudomonas aeruginosa* (QRLSTGSRINSAKDDAAGLQIA) was ordered from EZBioLab. Elf18 oligopeptide from *Escherichia coli* strain GI826 (Ac-SKEKFERTKPHVNVGTIG), *A. thaliana* Plant Elicitor Peptide 1, AtPEP1 (ATKVKAKQRGKEKVSSGRPGQHN) and flg22_{R569} peptide (NRLSTGKKINSAKDDAAGMQIA) from the isolate *Pseudomonas* R569 were synthesized by Peptide Specialty Laboratories GmbH. (±)-3-Hydroxydecanoic acid (3-OH-C10:0) and chitin were obtained from Sigma-Aldrich. All elicitors were dissolved in deionized MilliQ sterile water at the respective stock concentration of 1mM for flg22_{Pa}, flg22_{R569}, elf18, AtPep1 and 3-OH-C10:0; and 2mg/ml for chitin. For the inhibition of monolignol synthesis, piperonylic acid (PA, Sigma-Aldrich) was dissolved in absolute EtOH at a concentration of 20mM for stock solution.

For elicitor treatments, chemicals were diluted in liquid half strength MS medium (½ MS) to the indicated concentration. Seedlings were grown vertically for 4 days on small ½ MS petri dishes (5.5cm diameter), then 1.5ml of elicitor solution was gently poured over the seedlings to avoid damages induced by transfer. Care was taken that all roots were properly submersed. Seedlings were incubated horizontally for 24h before live imaging analysis of 5-day-old plants or fixation.

For root growth analysis, 5day-old seedlings were carefully transferred on new ½ MS agar plates containing 1µM flg22_{Pa} or flg22_{R569} and grown vertically for 6 days in standard growth conditions.

For combined treatment with PA and flg22, Col-0 and *WER::FLS2* seedlings were grown for 4 days on ½ MS plates, then were transferred on agar plates supplemented with 10µM PA or ethanol as control. To overcome PA degradation by light but still conserve proper root growth in control conditions, plates were inserted in black boxes open to the top, allowing roots to grow in the obscurity but leaves to reach the light. Roots were hidden from top light using black sterile plastic caches. After overnight pre-treatment, seedlings were again transferred on plates containing 10µM PA/EtOH with/without 1µM flg22/mock, using the same black boxes. Their root tip location was recorded. 48h after the first transfer, root growth was measured and seedlings were fixed as described.

Microscopy settings and image processing

Imaging was performed on either a Zeiss LSM880, LSM700 or a Leica SP8 inverted confocal scanning microscope. Pictures were taken with a 63x oil immersion objective (Zeiss LSM880), 63x water immersion objective (Leica SP8), 40x water immersion objective (Leica SP8), as well as 20x or 10x dry immersion objectives for tile-scan with 10% overlap (Zeiss LSM880 or LSM700).

The excitation and detection windows were set as following: for visualisation of FLS2 and defence markers, on Leica SP8, GFP/PI (488nm, 500-530nm and 600-670nm); GFP/mVenus/PI (488nm, 490-508nm; 514nm, 517-560nm and 600-670nm, sequential scan), on Zeiss LSM880, GFP/PI(488nm, 500-530nm and 600-650nm respectively), mVenus (514nm, 520-550nm). For lignin analysis: on Zeiss LSM880, calcofluor (405nm, 425-475nm), basic fuchsin (561nm, 600-650nm). For cell-specific quantification: on Zeiss LSM880, DirectRed 23/mVenus/mTurquoise2 (561nm, 580-700nm; 514nm, 520-590nm; 458nm, 460-500nm; sequential scan) and Calcofluor/mVenus/tdTomato (405nm, 415-450nm; 514nm, 520-545nm; 561nm; 570-640nm, sequential scan). For calcium analysis: Zeiss LSM880, R-GECO1 (561nm, 580-640nm). For suberin staining: on Zeiss LSM700, fluorol yellow (488nm, 500-600nm).

Images were processed using the Fiji software. For cross-section maximum projection of MAMP-induced signal (Fig.2B, 2C, S3B, S3C), z-stack pictures were resliced then realigned thanks to the Descriptor-based series registration (2d/3d + t) plugin. A maximum projection of the MAMP marker channel was then merged to a representative single stack of the PI-stained cell wall channel.

Fixation and staining

Fixation and cell-wall staining were performed according to adapted Clearsee protocol (Kurihara *et al.*, 2015; Ursache *et al.*, 2018). Briefly, 5-day-old seedlings were fixed for 1h at room temperature under vacuum in 4% paraformaldehyde PBS solution, using 6-well plates, then washed twice for 1min with PBS. Once fixed, seedlings were cleared in Clearsee solution for at least 24h under mild shaking. To visualize cell wall for quantification, clearing solution was exchanged with either 0.1% Calcofluor White or 0.1% Direct Red 23 in Clearsee solution. After at least respectively 30min and 2h of staining, the staining solution was removed and samples rinsed once in fresh Clearsee solution, then washed for 30min in a renewed Clearsee solution with gentle shaking before mounting.

For combined cell wall and lignin staining, fixed and cleared samples were incubated overnight in a Clearsee solution supplemented with 0.2% Basic Fuchsin and 0.1% Calcofluor White. Once the dye solution removed, samples were rinsed once, washed firstly 30min then at least 1.5h before observation.

Cell-specific quantification

To realize the complete atlas of defence marker responses, the different *prom::FLS2* lines analysed were first transformed with *UBQ10::nls-mTurquoise2* to delimit nuclei. Alternatively, wild-type *PER5::* and *MYB51::NLS-3Venus* lines were transformed with *UBQ10::nls-tdTomato*, which comprise a FastRed rather than a Kanamycin selection. This allowed to quantify directly the T1 and skip one generation. After *flg22* treatment, seedlings were fixed in Clearsee and their cell wall stained with DirectRed23, or Calcofluor White respectively. Z-stack were imaged on half section of the roots at 4 different positions, *i.e.* meristematic zone (MZ), elongation zone (EZ), 12 cells and 30 cells after the onset of elongation for 3 to 6 roots by treatment (mock and *flg22*) and by genotype. Three channels were acquired sequentially for the nuclei (*mTurquoise2* or *tdTomato*), the cell wall (DirectRed23 or Calcofluor White) and the defence markers *PER5* and *MYB51* (mVenus), using the same settings on all pictures for mVenus channel. However, wild-type *UBQ10::NLS-tdTomato* and *prom::FLS2 UBQ10::NLS-mTurquoise2* were imaged with distinct settings due to difference of intensity of the nuclei-labelling constructs. Pictures were processed on Fiji software with a custom batch macro automatizing the following pipeline

(Schneider *et al.*, 2012). Images were first resliced from the top, then the three channels were separated. A Gaussian blur was applied on the nuclear and cell wall marker channels, while the PTI marker channel was left untouched to not affect the signal to measure. In a second step, the cell wall channel was subtracted to the nuclear channel to reduce the unspecific background noise of the *UBQ10::nls-mTurquoise2* marker. The “cleaned” nuclear marker channel was transform to 8 bits to facilitate further processing.

We then used the 3D suite to generate a 3-dimensional Region Of Interest (ROI) for each nucleus (Ollion *et al.*, 2013). We first applied the plugin 3D iterative thresholding on the 8bits-cleaned-nuclear marker channel (Gul-Mohammed *et al.*, 2014). In this process, all possible thresholds are tested, which will detect objects for all thresholds. Subsequently, the algorithm will define the best object segmentation for each of the object, which means that different objects can be segmented with different threshold. This is particularly useful to detect objects with variable intensity in an uneven background, to which a single intensity threshold would either miss many objects or include background noise. We used the following settings: min vol pix = 250, max vol pix = 10000, min threshold = 0, min contrast (exp) = 5, criteria method = COMPACTNESS, threshold method = STEP, Segment results = All, value method = 10.0, Starts at mean = on. The plugin gives as output the 3D threshold delimiting all the future ROIs, *i.e.* the nuclei to quantify. It must be noted that depending on the pictures, some nuclei can be missed, or false positive can be added, but all pictures were then manually curated in a later step. The output came as 2-channels-images, whose last channel is completely black and can be removed by the splitting channel function.

We then use the 3D object counter plugin to define all ROIs, based on the 3D threshold obtained previously, and to redirect the analysis on the defence marker channel (Bolte and Cordelières, 2006). Options were set using the 3D OC Options as following: all parameters were selected, *i.e.* “Volume”, “Nb of Obj. voxels”, “Nb of Surf. voxels”, “Integrated Density”, “Mean Gray Value”, “Std Dev Gray Value”, “Median Gray Value”, “Minimum Gray Value”, “Maximum Gray Value”, “Centroid”, “Mean distance to surface”, “Std Dev distance to surface”, “Median distance to surface”, “Centre of mass”, and “Bounding box”. In addition, we ticked both parameters “Close original images while processing” and “Show masked image. The maps’ parameters were set as

follows: dots size = 5, font size = 12, “Show numbers” and “White numbers” were ticked. Importantly, the “Results Table Parameters” should be set on: “Store results within a table named after the image”, which allows to keep track of the files in batch mode. Finally, the measures were “Redirected to” the defence marker channel. After setting all the parameters, the analyse “3D Object Counter” was run. Threshold was set to 1 and minimum size filter to 10. The following maps and result tables were asked to be shown: objects, centroids, statistics, summary.

The process gives in output four different files. The “Centroid map” shows the centre of each ROI by a dot, numbered accordingly. The “Object map” is the representation of all ROIs, each of them being numbered. Our macro merges this map to both the cell wall marker channel and the nuclei channel for later identification of nuclei. The 3D Object counter also provides a .csv file called “Statistics” with all parameters measured for each nucleus. The last file provided is the “Masked image”, which represent the defence marker channel masked by the threshold.

To terminate the quantification, each data set was manually curated to assign a tissue (epidermis, cortex, endodermis, stele or root cap) to each nucleus. A maximum of around 20 nuclei by tissue type and by picture were identified. “Mean Gray Values” was extracted and use for analysis. Mean nuclear intensity for each genotype, treatment, root region and tissue were calculated and colour coded using the `heatmaply()` function in R (`heatmaply` library). Atlas maps were drawn according to these coloured values. Fold changes for *MYB51* induction were calculated and colour-coded using the same procedure.

Ca²⁺ imaging on roots and quantification

For calcium responses analysis, *UBQ10::R-GECO1* samples were mounted as follows. Seedlings, once at a time, were glued to a large (60mm) coverslip previously sprayed with medical adhesive (Adapt Medical Adhesive Spray, Hollister). A silicon isolator (Grace Bio-Labs Press-to-seal silicon isolator, No PSA, 20mm diameter, Sigma) was then quickly placed around the seedling and 600µl of sterile germination medium (0.75mM CaCl₂, 1mM KCl, 0.25mM Ca(NO₃)₂•4H₂O, 1mM MgSO₄•7H₂O, 0.2mM KH₂PO₄, 50µM NaFe(III)EDTA, 50µM H₃BO₃, 5µM MnCl₂•4H₂O, 10µM ZnSO₄•7H₂O, 0.5µM CuSO₄•5H₂O, 0.1µM Na₂MoO₃, pH adjusted to 5.6 with NaOH) was dropped on the root. The drop was spread with a pipet tip to cover the whole surface delimited by the

silicon isolator and the seedling let to rest for at least 20min. For full root imaging, tile scans combined to time laps were performed under Zeiss LSM880 confocal laser scanning microscope with 20x objective as described above. As few tiles as possible were selected to limit time acquisition, no averaging was done, and pinhole was entirely open. Images were taken continuously, with an average time interval of 5 to 7 seconds. Acquisition of baseline signal was performed for 5min, then 7.5 μ l of 100 μ M flg22 diluted in water was added to the germination medium solution. Acquisition was continued for at least 20min. For tissue-specific imaging and quantification, small z-stack (~ 8 slices) with 5 μ m intervals were taken on half a root in the elongation zone for wild-type and *WER::FLS2* samples, or in the differentiated zone for *CASP1::SHR::UBQ10::FLS2*.

R-GECO1 signal was quantified for each tissue on the z-stack acquisition. ROIs delimiting a tissue type were drawn manually on the most appropriate stack (*i.e.* that presents a clear surface view if possible), using maximum projection of 2 stacks when necessary.

Fractional fluorescence changes $\Delta F/F$ were calculated for each ROI from background corrected intensity values as $(F-F_0)/F_0$, where F_0 is equal to the average fluorescent intensity of the baseline of the measure, on 4 min from $t=0$.

Suberin staining

To highlight suberin lamellae, seedlings were fixed and stained with the methanol-based fluorol yellow staining protocol as described in (Fujita *et al.*, 2020). Samples were imaged using the Zeiss LSM700 as described above.

Bacterial root inoculation assays

PTI assays were performed by drop inoculation on agar plates. Briefly, 2 μ l of bacterial suspension (cells centrifuged and resuspended in fresh LB or 50% TSB for CHA0 and R569, respectively) of $OD_{600} = 0.01$ was added to the tip of 5-day-old seedlings. Once the drop dried, seedlings were grown vertically in standard conditions for 1 to 3 days. For the fast screening of bacterial isolates, roots were observed under a Leica DM 5500B epifluorescence microscope (GFP lamp). Representative pictures of roots were imaged using confocal scanning microscopy (Leica SP8) after a short wash in deionized H₂O.

Root growth inhibition assays were completed on agar plates inoculated with bacteria at mentioned concentrations. Briefly, bacterial cultures were grown as previously described in 50% TSB, then centrifuged and resuspended in fresh medium. OD_{600} was measured and adjusted to 100x the desired concentration. 500 μ l of concentrated bacterial inoculum was then added to 50ml of semi solid $\frac{1}{2}$ MS medium afore cooled down to around 30°C. Inoculated media were gently mixed by inverting several times, then poured in square petri dishes. Five-day-old *WER::FLS2* and wild-type Col-0 seedlings previously grown on mesh (15mm x 100mm, on top of the plate), were transferred with sterile forceps on the inoculated plates. Seedlings were selected for similar root size, the ones being obviously too long or too short removed from the mesh with sterile toothpicks. After transfer, root tip locations were marked for keeping track of growth, then plants were grown in standard conditions for 6 days. One day post-inoculation, root tip positions were again recorded, and all seedlings that completely stopped to grow were dismissed from the analysis. This ensured that only seedlings that recovered properly from the transfers were considered. Plates were scanned at 6 dpi and root growth measured using Fiji plugins "Simple Neurite Tracer" (Frangi *et al.*, 1998).

Swimming assay

Overnight culture of CHA0 and DfliC adjusted to $OD_{600} = 0.1$. Ten microliters of this bacterial suspension were spotted at the centre of a NA plate. Bacterial motility was observed after 24 hours of incubation at 25 °C.

Statistical analysis

Statistical analyses were done using R3.6.0 or Graphpad Prism 7.0 software (<https://www.graphpad.com/>). For multiple comparison, ANOVA followed by Tukey's Honestly Significant difference (HSD) test were applied when linear model assumptions were met. On the contrary, Kruskal-Wallis test followed by Dunn's multiple comparison test were performed. For analysis of suberization along the roots, comparisons were performed for each zone separately, and different letters indicates significant differences for a given zone (a, b, c or a', b', c' or a'', b'', c'').

References

- Adams-Phillips, L., Briggs, A.G., and Bent, A.F. (2010). Disruption of poly(ADP-ribosyl)ation mechanisms alters responses of *Arabidopsis* to biotic stress. *Plant Physiol.* *152*, 267–280.
- Alassimone, J., Fujita, S., Doblas, V.G., Dop, M. van, Barberon, M., Kalmbach, L., Vermeer, J.E.M., Rojas-Murcia, N., Santuari, L., Hardtke, C.S., *et al.* (2016). Polarly localized kinase SGN1 is required for Casparian strip integrity and positioning. *Nat. Plants* *2*, 1–10.
- Andersen, T.G., Barberon, M., and Geldner, N. (2015). Suberization — the second life of an endodermal cell. *Curr. Opin. Plant Biol.* *28*, 9–15.
- Andersen, T.G., Naseer, S., Ursache, R., Wybouw, B., Smet, W., De Rybel, B., Vermeer, J.E.M., and Geldner, N. (2018). Diffusible repression of cytokinin signalling produces endodermal symmetry and passage cells. *Nature* *555*, 529–533.
- Arora, S.K., Ritchings, B.W., Almira, E.C., Lory, S., and Ramphal, R. (1997). A transcriptional activator, FleQ, regulates mucin adhesion and flagellar gene expression in *Pseudomonas aeruginosa* in a cascade manner. *J. Bacteriol.* *179*, 5574–5581.
- Bai, Y., Müller, D.B., Srinivas, G., Garrido-Oter, R., Potthoff, E., Rott, M., Dombrowski, N., Münch, P.C., Spaepen, S., Remus-Emsermann, M., *et al.* (2015). Functional overlap of the *Arabidopsis* leaf and root microbiota. *Nature* *528*, 364–369.
- Beck, M., Wyrsh, I., Strutt, J., Wimalasekera, R., Webb, A., Boller, T., and Robatzek, S. (2014). Expression patterns of FLAGELLIN SENSING 2 map to bacterial entry sites in plant shoots and roots. *J. Exp. Bot.* *65*, 6487–6498.
- Benfey, P.N., Linstead, P.J., Roberts, K., Schiefelbein, J.W., Hauser, M.T., and Aeschbacher, R.A. (1993). Root development in *Arabidopsis*: four mutants with dramatically altered root morphogenesis. *Development* *119*, 57–70.
- Berendsen, R.L., Pieterse, C.M.J., and Bakker, P.A.H.M. (2012). The rhizosphere microbiome and plant health. *Trends Plant Sci.* *17*, 478–486.
- Bernards, M.A. (2002). Demystifying suberin. *Can. J. Bot.* *80*, 227–240.
- Bolte, S., and Cordelières, F.P. (2006). A guided tour into subcellular colocalization analysis in light microscopy. *J. Microsc.* *224*, 213–232.
- Bulgarelli, D., Schlaeppi, K., Spaepen, S., van Themaat, E.V.L., and Schulze-Lefert, P. (2013). Structure and Functions of the Bacterial Microbiota of Plants. *Annu. Rev. Plant Biol.* *64*, 807–838.
- Buscaill, P., Chandrasekar, B., Sanguankiatichai, N., Kourelis, J., Kaschani, F., Thomas, E.L., Morimoto, K., Kaiser, M., Preston, G.M., and Ichinose, Y. (2019). Glycosidase and glycan polymorphism control hydrolytic release of immunogenic flagellin peptides. *PLANT Sci.* *364*, eaav0748.
- Chezem, W.R., Memon, A., Li, F.-S., Weng, J.-K., and Clay, N.K. (2017). SG2-type R2R3-MYB transcription factor MYB15 controls defense-induced lignification and basal immunity in *Arabidopsis*. *The Plant Cell* *29*, 1907–1926.
- Chinchilla, D., Zipfel, C., Robatzek, S., Kemmerling, B., Nürnberger, T., Jones, J.D.G., Felix, G., and Boller, T. (2007). A flagellin-induced complex of the receptor FLS2 and BAK1 initiates plant defence. *Nature* *448*, 497–500.
- Clough, S.J., and Bent, A.F. (1998). Floral dip: a simplified method for *Agrobacterium*-mediated transformation of *Arabidopsis thaliana*. *Plant J.* *16*, 735–743.

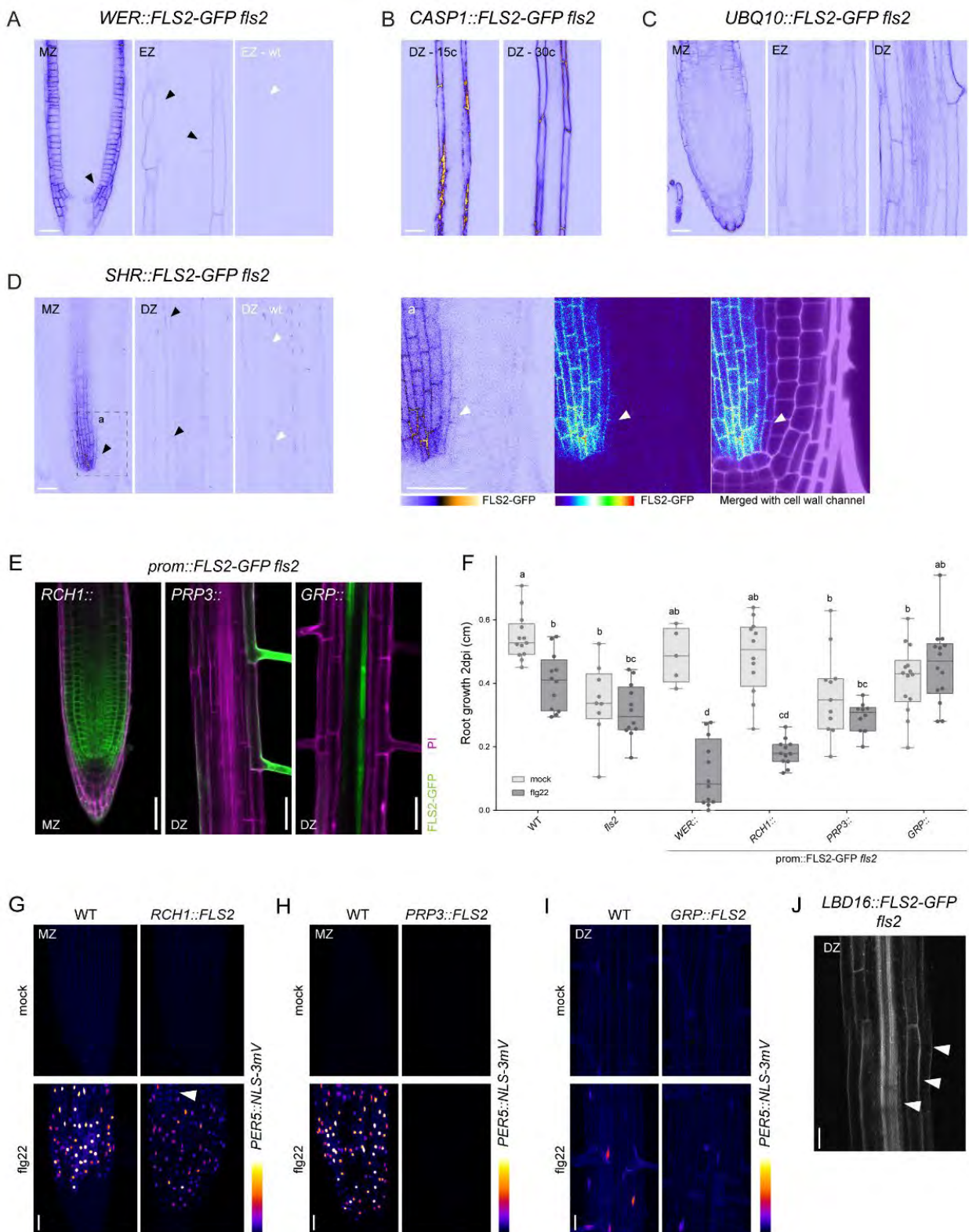
- Couto, D., and Zipfel, C. (2016). Regulation of pattern recognition receptor signalling in plants. *Nat. Rev. Immunol.* *16*, 537.
- De Coninck, B., Timmermans, P., Vos, C., Cammue, B.P.A., and Kazan, K. (2015). What lies beneath: belowground defense strategies in plants. *Trends Plant Sci.* *20*, 91–101.
- Doblas, V.G., Smakowska-Luzan, E., Fujita, S., Alassimone, J., Barberon, M., Madalinski, M., Belkhadir, Y., and Geldner, N. (2017). Root diffusion barrier control by a vasculature-derived peptide binding to the SGN3 receptor. *Science* *355*, 280–284.
- Dubiella, U., Seybold, H., Durian, G., Komander, E., Lassig, R., Witte, C.-P., Schulze, W.X., and Romeis, T. (2013). Calcium-dependent protein kinase/NADPH oxidase activation circuit is required for rapid defense signal propagation. *Proc. Natl. Acad. Sci.* *110*, 8744–8749.
- Faulkner, C., and Robatzek, S. (2012). Plants and pathogens: putting infection strategies and defence mechanisms on the map. *Curr. Opin. Plant Biol.* *15*, 699–707.
- Felix, G., Duran, J.D., Volko, S., and Boller, T. (1999). Plants have a sensitive perception system for the most conserved domain of bacterial flagellin. *Plant J.* *18*, 265–276.
- Fendrych, M., Van Hautegeem, T., Van Durme, M., Olvera-Carrillo, Y., Huysmans, M., Karimi, M., Lippens, S., Guérin, C.J., Krebs, M., Schumacher, K., *et al.* (2014). Programmed cell death controlled by ANAC033/SOMBRERO determines root cap organ size in *Arabidopsis*. *Curr. Biol.* *24*, 931–940.
- Frangi, A.F., Niessen, W.J., Vincken, K.L., and Viergever, M.A. (1998). Multiscale vessel enhancement filtering. In *Medical Image Computing and Computer-Assisted Intervention — MICCAI'98*, W.M. Wells, A. Colchester, and S. Delp, eds. (Berlin, Heidelberg: Springer), pp. 130–137.
- Fujita, S., De Bellis, D., Edel, K.H., Köster, P., Andersen, T.G., Schmid-Siegert, E., Déneraud Tendon, V., Pfister, A., Marhavý, P., Ursache, R., *et al.* (2020). SCHENGEN receptor module drives localized ROS production and lignification in plant roots. *EMBO J.* *9*, e103894.
- Garrido-Oter, R., Nakano, R.T., Dombrowski, N., Ma, K.-W., McHardy, A.C., and Schulze-Lefert, P. (2018). Modular traits of the rhizobiales root microbiota and their evolutionary relationship with symbiotic rhizobia. *Cell Host Microbe* *24*, 155-167.e5.
- Gilroy, S., Suzuki, N., Miller, G., Choi, W.-G., Toyota, M., Devireddy, A.R., and Mittler, R. (2014). A tidal wave of signals: calcium and ROS at the forefront of rapid systemic signaling. *Trends Plant Sci.* *19*, 623–630.
- Gilroy, S., Białasek, M., Suzuki, N., Górecka, M., Devireddy, A., Karpinski, S., and Mittler, R. (2016). ROS, calcium and electric signals: key mediators of rapid systemic signaling in plants. *Plant Physiol.* pp.00434.2016.
- Gómez-Gómez, L., and Boller, T. (2000). FLS2: An LRR receptor-like kinase involved in the perception of the bacterial elicitor flagellin in *Arabidopsis*. *Mol. Cell* *5*, 1003–1011.
- Gómez-Gómez, L., Felix, G., and Boller, T. (1999). A single locus determines sensitivity to bacterial flagellin in *Arabidopsis thaliana*. *Plant J.* *18*, 277–284.
- Gul-Mohammed, J., Arganda-Carreras, I., Andrey, P., Galy, V., and Boudier, T. (2014). A generic classification-based method for segmentation of nuclei in 3D images of early embryos. *BMC Bioinformatics* *15*, 9.
- Hara, M., Umetsu, N., Miyamoto, C., and Tamari, K. (1973). Inhibition of the biosynthesis of plant cell wall materials, especially cellulose biosynthesis, by coumarin. *Plant Cell Physiol.* *14*, 11–28.

- Helariutta, Y., Fukaki, H., Wysłowska-Diller, J., Nakajima, K., Jung, J., Sena, G., Hauser, M.-T., and Benfey, P.N. (2000). The SHORT-ROOT gene controls radial patterning of the *Arabidopsis* root through radial signaling. *Cell* *101*, 555–567.
- Hijwegen, T. (1963). Lignification, a possible mechanism of active resistance against pathogens. *Neth. J. Plant Pathol.* *69*, 314–317.
- Jeworutzki, E., Roelfsema, M.R.G., Anschütz, U., Krol, E., Elzenga, J.T.M., Felix, G., Boller, T., Hedrich, R., and Becker, D. (2010). Early signaling through the *Arabidopsis* pattern recognition receptors FLS2 and EFR involves Ca²⁺-associated opening of plasma membrane anion channels. *Plant J.* *62*, 367–378.
- Kamula, S.A., Peterson, C.A., and Mayfield, C.I. (1994). Impact of the exodermis on infection of roots by *Fusarium culmorum*. *Plant Soil* *167*, 121–126.
- Keinath, N.F., Waadt, R., Brugman, R., Schroeder, J.I., Grossmann, G., Schumacher, K., and Krebs, M. (2015). Live cell imaging with R-GECO1 sheds light on flg22- and chitin-induced transient [Ca²⁺]_{cyt} patterns in *Arabidopsis*. *Mol. Plant* *8*, 1188–1200.
- Kumpf, R.P., and Nowack, M.K. (2015). The root cap: a short story of life and death. *J. Exp. Bot.* *66*, 5651–5662.
- Kupferschmied, P. (2015). Molecular basis and regulation of insect pathogenicity in plant-beneficial pseudomonads. Université de Lausanne, Faculté de biologie et médecine.
- Kupferschmied, P., Péchy-Tarr, M., Imperiali, N., Maurhofer, M., and Keel, C. (2014). Domain shuffling in a sensor protein contributed to the evolution of insect pathogenicity in plant-beneficial *Pseudomonas protegens*. *PLOS Pathog.* *10*, e1003964.
- Kurihara, D., Mizuta, Y., Sato, Y., and Higashiyama, T. (2015). ClearSee: a rapid optical clearing reagent for whole-plant fluorescence imaging. *Development* *142*, 4168–4179.
- Lange, B.M., Lapiere, C., and Jr, H.S. (1995). Elicitor-induced spruce stress lignin (structural similarity to early developmental lignins). *Plant Physiol.* *108*, 1277–1287.
- Lee, M.M., and Schiefelbein, J. (1999). WEREWOLF, a MYB-related protein in *Arabidopsis*, is a position-dependent regulator of epidermal cell patterning. *Cell* *99*, 473–483.
- Lee, M.-H., Jeon, H.S., Kim, S.H., Chung, J.H., Roppolo, D., Lee, H.-J., Cho, H.J., Tobimatsu, Y., Ralph, J., and Park, O.K. (2019). Lignin-based barrier restricts pathogens to the infection site and confers resistance in plants. *EMBO J.* *38*, e101948.
- Li, B., Meng, X., Shan, L., and He, P. (2016). Transcriptional Regulation of Pattern-Triggered Immunity in Plants. *Cell Host Microbe* *19*, 641–650.
- Ma K., Niu Y., Jia Y., Ordon J., Copeland C., Emonet A., Geldner N., Guan R., Stolze S. C., Nakagami H., Garrido Oter R., Schulze-Lefert P. (2020). Coordination of microbe-host homeostasis via a crosstalk with plant innate immunity. PREPRINT (Version 1) available at Research Square. DOI:10.21203/rs.3.rs-69445/v1
- Mandal, S., and Mitra, A. (2007). Reinforcement of cell wall in roots of *Lycopersicon esculentum* through induction of phenolic compounds and lignin by elicitors. *Physiol. Mol. Plant Pathol.* *71*, 201–209.
- Marhavý, P., Kurenda, A., Siddique, S., Dénervaud Tendon, V., Zhou, F., Holbein, J., Hasan, M.S., Grundler, F.M., Farmer, E.E., and Geldner, N. (2019). Single-cell damage elicits regional, nematode-restricting ethylene responses in roots. *EMBO J.* *38*, e100972.
- Marquès-Bueno, M.M., Morao, A.K., Cayrel, A., Platré, M.P., Barberon, M., Caillieux, E., Colot, V., Jaillais, Y., Roudier, F., and Vert, G. (2015). A versatile Multisite Gateway-compatible promoter and transgenic line collection for cell type-specific functional genomics in *Arabidopsis*. *Plant J.* n/a-n/a.

- Martínez-García, E., and Lorenzo, V. de (2011). Engineering multiple genomic deletions in Gram-negative bacteria: analysis of the multi-resistant antibiotic profile of *Pseudomonas putida* KT2440. *Environ. Microbiol.* *13*, 2702–2716.
- Messner, B., and Boll, M. (1993). Elicitor-mediated induction of enzymes of lignin biosynthesis and formation of lignin-like material in a cell suspension culture of spruce (*Picea abies*). *Plant Cell Tissue Organ Cult.* *34*, 261–269.
- Millet, Y.A., Danna, C.H., Clay, N.K., Songnuan, W., Simon, M.D., Werck-Reichhart, D., and Ausubel, F.M. (2010). Innate Immune Responses Activated in *Arabidopsis* Roots by Microbe-Associated Molecular Patterns. *Plant Cell* *22*, 973–990.
- Nicholson, R.L., and Hammerschmidt, R. (1992). Phenolic Compounds and Their Role in Disease Resistance. *Annu. Rev. Phytopathol.* *30*, 369–389.
- Ollion, J., Cochennec, J., Loll, F., Escudé, C., and Boudier, T. (2013). TANGO: a generic tool for high-throughput 3D image analysis for studying nuclear organization. *Bioinformatics* *29*, 1840–1841.
- Pel, M.J.C., and Pieterse, C.M.J. (2013). Microbial recognition and evasion of host immunity. *J. Exp. Bot.* *64*, 1237–1248.
- Pfister, A., Barberon, M., Alassimone, J., Kalmbach, L., Lee, Y., Vermeer, J.E., Yamazaki, M., Li, G., Maurel, C., Takano, J., *et al.* (2014). A receptor-like kinase mutant with absent endodermal diffusion barrier displays selective nutrient homeostasis defects. *ELife* *3*, e03115.
- Poncini, L., Wyrsh, I., Tendon, V.D., Vorley, T., Boller, T., Geldner, N., Métraux, J.-P., and Lehmann, S. (2017). In roots of *Arabidopsis thaliana*, the damage-associated molecular pattern AtPep1 is a stronger elicitor of immune signalling than flg22 or the chitin heptamer. *PLOS ONE* *12*, e0185808.
- Ranathunge, K., Thomas, R.H., Fang, X., Peterson, C.A., Gijzen, M., and Bernards, M.A. (2008). Soybean Root Suberin and Partial Resistance to Root Rot Caused by *Phytophthora sojae*. *Phytopathology* *98*, 1179–1189.
- Rich-Griffin, C., Eichmann, R., Reitz, M.U., Hermann, S., Woolley-Allen, K., Brown, P.E., Wiwatdirekkul, K., Esteban, E., Pasha, A., Kogel, K.-H., *et al.* (2020). Regulation of Cell Type-Specific Immunity Networks in *Arabidopsis* Roots. *Plant Cell*.
- Robatzek, S., Chinchilla, D., and Boller, T. (2006). Ligand-induced endocytosis of the pattern recognition receptor FLS2 in *Arabidopsis*. *Genes Dev.* *20*, 537–542.
- Robertsen, B. (1986). Elicitors of the production of lignin-like compounds in cucumber hypocotyls. *Physiol. Mol. Plant Pathol.* *28*, 137–148.
- Schneider, C.A., Rasband, W.S., and Eliceiri, K.W. (2012). NIH Image to ImageJ: 25 years of image analysis. *Nat. Methods* *9*, 671–675.
- Seybold, H., Trempel, F., Ranf, S., Scheel, D., Romeis, T., and Lee, J. (2014). Ca²⁺ signalling in plant immune response: from pattern recognition receptors to Ca²⁺ decoding mechanisms - Seybold - 2014 - - Wiley Online Library. *New Phytol.*
- Siligato, R., Wang, X., Yadav, S.R., Lehesranta, S., Ma, G., Ursache, R., Sevilem, I., Zhang, J., Gorte, M., Prasad, K., *et al.* (2016). MultiSite Gateway-Compatible Cell Type-Specific Gene-Inducible System for Plants. *Plant Physiol.* *170*, 627–641.
- Smit, F., and Dubery, I.A. (1997). Cell wall reinforcement in cotton hypocotyls in response to a *Verticillium dahliae* elicitor. *Phytochemistry* *44*, 811–815.

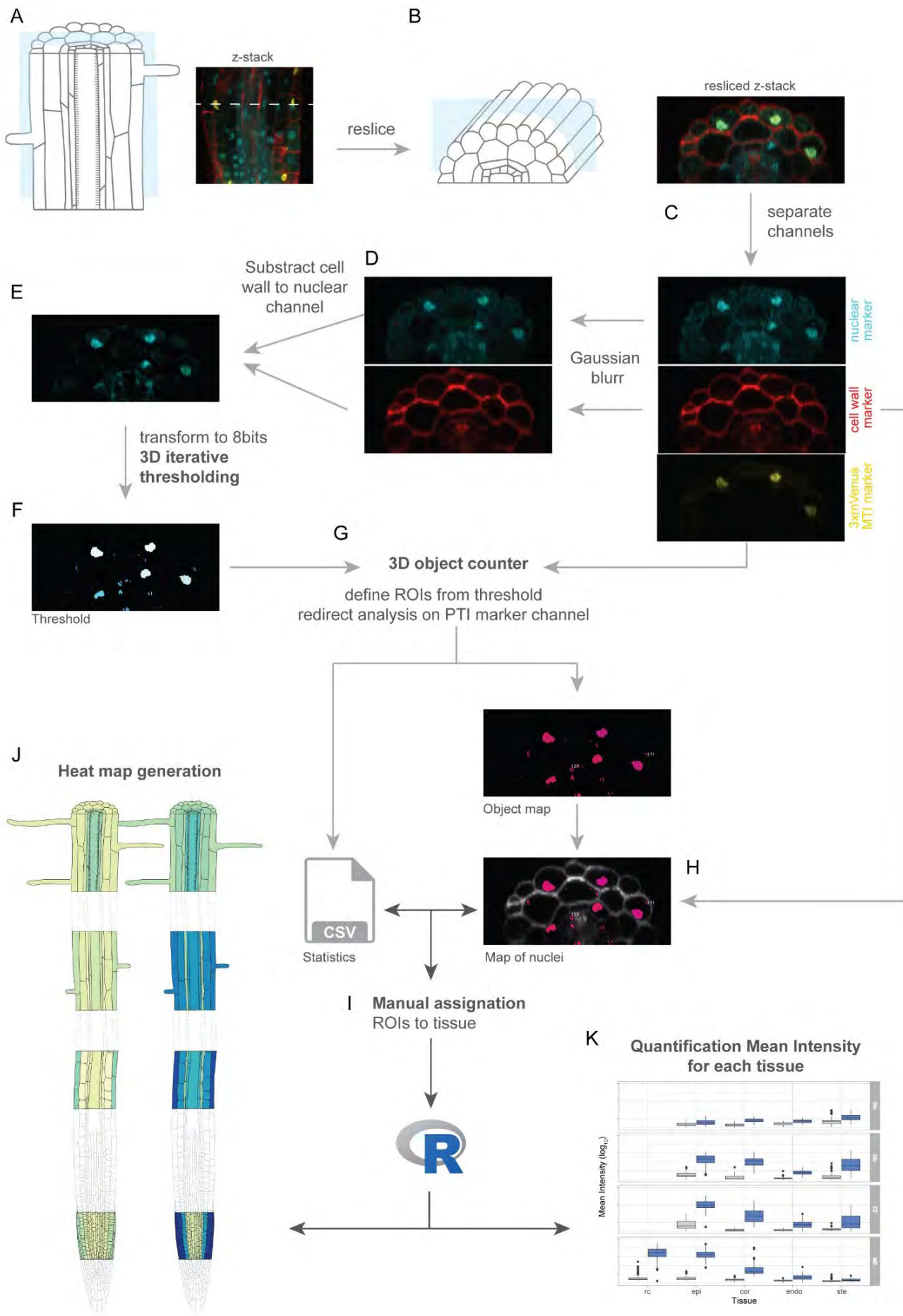
- Stanley, C.E., Shrivastava, J., Brugman, R., Heinzemann, E., Swaay, D. van, and Grossmann, G. (2018). Dual-flow-RootChip reveals local adaptations of roots towards environmental asymmetry at the physiological and genetic levels. *New Phytol.* *217*, 1357–1369.
- Stringlis, I.A., de Jonge, R., and Pieterse, C.M.J. (2019). The Age of Coumarins in Plant–Microbe Interactions. *Plant Cell Physiol.*
- Stutz, E.W., Défago, G., and Kern, H. (1986). Naturally occurring fluorescent pseudomonads involved in suppression of black root rot of tobacco. *Phytopathology* *76*, 181–185.
- Tang, D., Wang, G., and Zhou, J.-M. (2017). Receptor Kinases in Plant-Pathogen Interactions: More Than Pattern Recognition. *Plant Cell* *29*, 618–637.
- Thomas, R., Fang, X., Ranathunge, K., Anderson, T.R., Peterson, C.A., and Bernardis, M.A. (2007). Soybean Root Suberin: Anatomical Distribution, Chemical Composition, and Relationship to Partial Resistance to *Phytophthora sojae*. *Plant Physiol.* *144*, 299–311.
- Thor, K., and Peiter, E. (2014). Cytosolic calcium signals elicited by the pathogen-associated molecular pattern flg22 in stomatal guard cells are of an oscillatory nature. *New Phytol.* *204*, 873–881.
- Tognolli, M., Penel, C., Greppin, H., and Simon, P. (2002). Analysis and expression of the class III peroxidase large gene family in *Arabidopsis thaliana*. *Gene* *288*, 129–138.
- Ursache, R., Andersen, T.G., Marhavý, P., and Geldner, N. (2018). A protocol for combining fluorescent proteins with histological stains for diverse cell wall components. *Plant J.* *93*, 399–412.
- Vance, C.P., Kirk, T.K., and Sherwood, R.T. (1980). Lignification as a Mechanism of Disease Resistance. *Annu. Rev. Phytopathol.* *18*, 259–288.
- Vermeer, J.E.M., Wangenheim, D. von, Barberon, M., Lee, Y., Stelzer, E.H.K., Maizel, A., and Geldner, N. (2014). A Spatial Accommodation by Neighboring Cells Is Required for Organ Initiation in *Arabidopsis*. *Science* *343*, 178–183.
- Wyrsh, I., Domínguez-Ferrerías, A., Geldner, N., and Boller, T. (2015). Tissue-specific FLAGELLIN-SENSING 2 (FLS2) expression in roots restores immune responses in *Arabidopsis fls2* mutants. *New Phytol.* *206*, 774–784.
- Yamaguchi, S., Fujita, H., Sugata, K., Taira, T., and Iino, T. (1984). Genetic Analysis of H2, the Structural Gene for Phase-2 Flagellin in *Salmonella*. *Microbiology*, *130*, 255–265.
- Yu, K., Pieterse, C.M.J., Bakker, P.A.H.M., and Berendsen, R.L. (2019a). Beneficial microbes going underground of root immunity. *Plant Cell Environ.* *42*, 2860–2870.
- Yu, K., Liu, Y., Tichelaar, R., Savant, N., Legendijk, E., Kuijk, S.J.L. van, Stringlis, I.A., Dijken, A.J.H. van, Pieterse, C.M.J., Bakker, P.A.H.M., et al. (2019). Rhizosphere-Associated Pseudomonas Suppress Local Root Immune Responses by Gluconic Acid-Mediated Lowering of Environmental pH. *Curr. Biol.* *29*, 3913-3920.e4.
- Zhou, F., Emonet, A., Dénervaud Tendon, V., Marhavý, P., Wu, D., Lahaye, T., and Geldner, N. (2020). Coincidence of Damage and Microbial Patterns Controls Localized Immune Responses in Roots. *Cell* *180*, 440-453.e18.
- Zipfel, C. (2008). Pattern-recognition receptors in plant innate immunity. *Curr. Opin. Immunol.* *20*, 10–16.
- Zipfel, C., Robatzek, S., Navarro, L., Oakeley, E.J., Jones, J.D.G., Felix, G., and Boller, T. (2004). Bacterial disease resistance in *Arabidopsis* through flagellin perception. *Nature* *428*, 764–767.

Supplemental Information



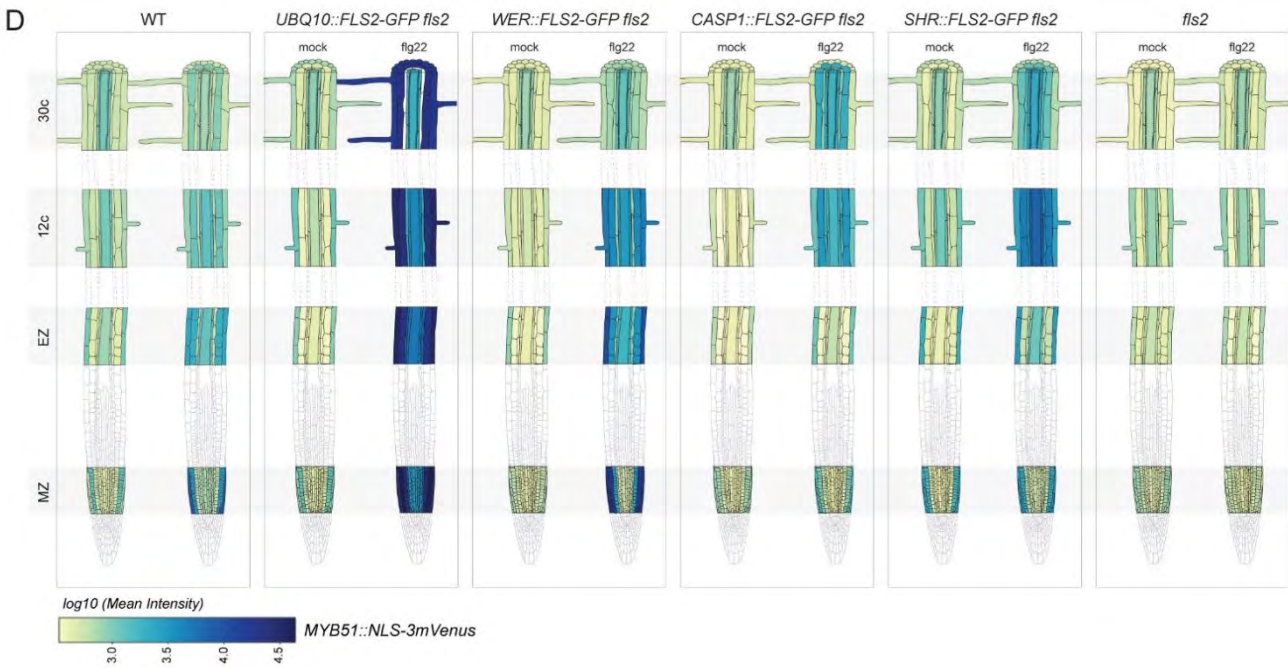
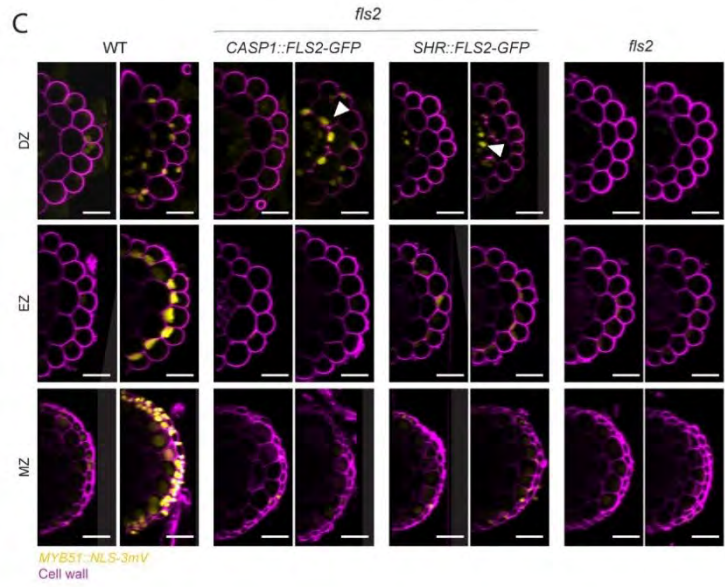
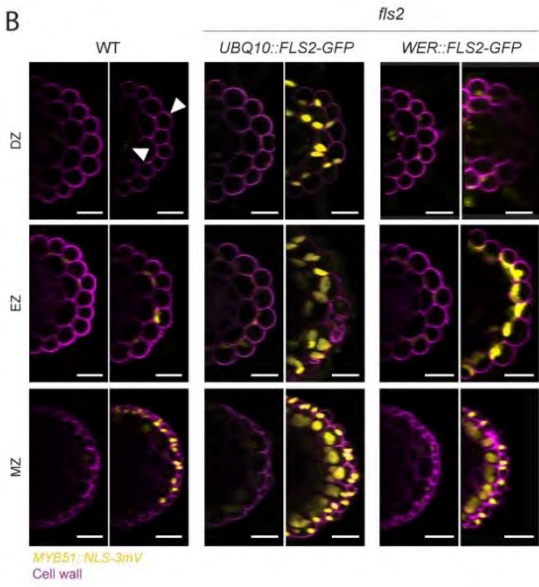
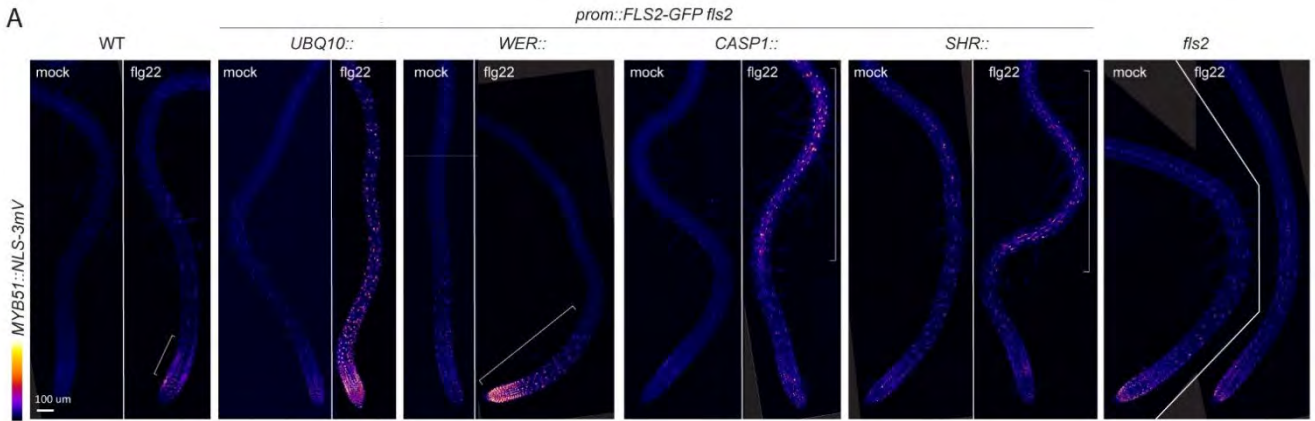
Supplemental Figure S1: Expression pattern of *prom::FLS2* complementing *fls2*.

(A) *WER::FLS2-GFP* expression. *WER* promoter expressed principally *FLS2* in epidermal cells, but some weak signal can be observed in cortex (black arrowheads). Picture of wild-type plants taken with identical setting (EZ-wt) is showed for comparison (cortical cell, white arrowhead). (B) *CASP1::FLS2-GFP* is expressed exclusively in endodermal cell line in early and later differentiated zones (15 cells respectively 30 cells after onset of elongation). (C) *UBQ10::FLS2-GFP* is expressed in all tissue types in every region of the root. (D) *SHR::FLS2-GFP* is expressed strongly in the stele of the meristem then decreases in intensity in later regions. Some weak signal can be detected in endodermal cells (black arrowheads). Picture of wild-type plants taken with identical setting (DZ-wt) is shown for comparison (endodermal cells, white arrowheads). Close-up view of dashed squared box is found in (a). *FLS2-GFP* (visualized by ICA and Thermal LUTs) is merged with cell wall stained by PI (white). White arrowheads point at endodermal cells expressing weakly *FLS2*. (E) *RCH1* promoter expresses *FLS2* in the meristem, *PRP3::* in the root hair cells and *GRP::* in the pericycle cells. *FLS2-GFP* (green) is co-visualized with PI-stained cell wall (magenta). (F) Flg22 treatment increases root growth inhibition in *WER::* and *RCH1::FLS2-GFP fls2* hypersensitive line only. Root length quantification of *prom::FLS2-GFP fls2* lines treated with 1 μ M flg22 for 2 days. Boxplot centre represents the median (5 \leq n \leq 14). Different letters indicate statistically significant difference between means by 2-ways ANOVA and Tukey's multiple comparison. (G) Maximal projection *PER5::NLS-3mVenus* marker (Fire LUT) in *RCH1::FLS2-GFP fls2* compared to WT shown for MZ. Seedlings were treated for 24h with 1 μ M flg22. Images were taken with identical settings. White arrow, epidermal signal. (H) Maximal projection *PER5::NLS-3mVenus* marker (Fire LUT) in *PRP3::FLS2-GFP fls2* compared to WT shown for MZ. Seedlings were treated for 24h with 1 μ M flg22. Images were taken with identical settings. (I) Maximal projection *PER5::NLS-3mVenus* marker (Fire LUT) in *GRP::FLS2-GFP fls2* compared to WT shown for the DZ. Seedlings were treated for 24h with 1 μ M flg22. Images were taken with identical settings. (J) *LBD16* promoter expresses *FLS2-GFP* in all tissues in the differentiated zone (DZ). Note that in contrast to previous report, *FLS2* is present in epidermis, cortex and endodermis (white arrows) in addition to the stele. Meristematic zone (MZ), elongation zone (EZ), differentiation zone (DZ). Scale bar, 25 μ M.



Supplemental Figure S2: Quantification procedure

(A) Z-stack images with 3 channels (red: cell wall, blue: *UBQ10::NLS-mTurquoise/tdTomato*, yellow: *PER5/MYB51::NLS-3mVenus*) were taken from 4 different regions of the root (meristematic zone, elongation zone, 12 cells and 30 cells after onset of elongation), for 3-6 seedlings by treatment by genotype. **(B)** Each Z-stacks are resliced to get cross-section view. The three channels are separated **(C)** and a Gaussian blur filter is applied on the cell wall and the MTI marker channel **(D)**. Blurred cell wall channel is then subtracted from blurred nuclear marker channel to remove non-nuclear background **(E)**. The obtained cleaned nuclear channel is then converted to 8-bit and a 3D iterative thresholding is performed to delimit ROI for each nuclei **(F)**. The 3D object counter plugin is then used to measure the mean signal intensity of each nuclei delimited by the obtained ROIs in the MTI marker channel. The plugin gives as output a .csv file with the measured values, a masked image of the PTI marker channel and an object map, delimiting the identified nuclei **(G)**. The object map is then coupled to the original cell wall marker to define the tissue origin of each nuclei **(H)**. Each map was then reviewed manually to assign 20 nuclei for each cell type and to complete .csv files **(I)**. Average of the mean signal intensity of each nuclear tissue-specific signal were calculated, transformed into \log_{10} and colour coded using the `heatmaply()` function in R **(J)**. Boxplots were generated to represent signal variability **(K)**.

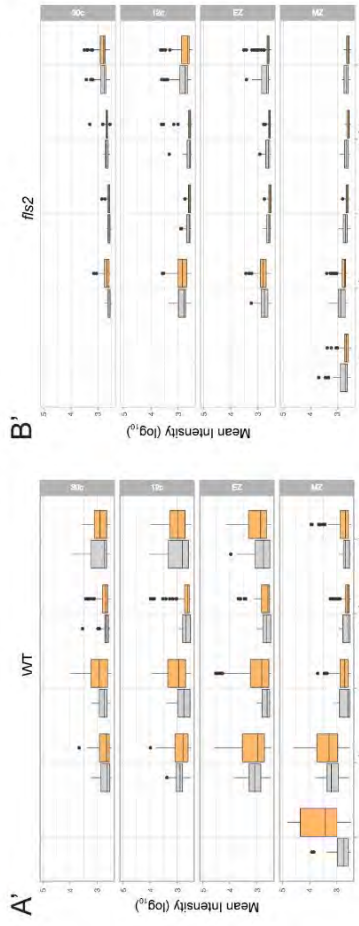


Supplemental Figure S3: MYB51 marker is induced non cell-autonomously by flg22 treatment

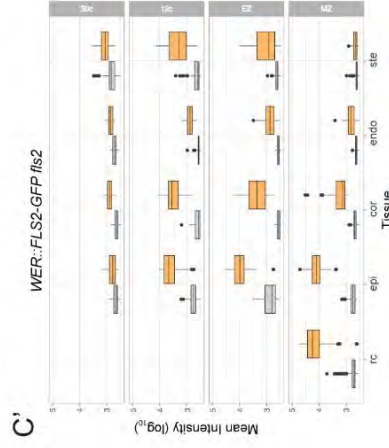
(A) Overview of *MYB51::NLS-3mVenus* response to 1 μ M flg22 after 1 day in different *prom::FLS2-GFP fls2* lines. *MYB51* zone of responsiveness follows *FLS2* expression pattern. Tile scan images were taken with similar settings. Settings are always identical between mock and corresponding flg22 treatment. Brackets indicate zone of responsiveness. Scale bar, 100 μ M. **(B)** Maximal projection of transverse sections views of *MYB51* expression pattern in *UBQ10::* and *WER::FLS2-GFP fls2* compared to WT shown for meristematic zone (MZ), elongation zone (EZ) and differentiated zone (DZ, 30 cells after start of elongation). Seedlings were treated for 24h with 1 μ M flg22. Nuclear localized mVenus signal (yellow) was co-displayed with propidium iodide cell wall marker (PI, purple). Images were taken with similar settings, while corresponding mock and flg22 treatment pictures for each zone separately have identical parameters. Pictures were acquired with low gain compare to Fig.S2C due to strong average intensity of *UBQ10::* and *WER::FLS2-GFP fls2* responses, explaining the faint signal in WT (white arrowheads). Scale bar, 25 μ m. **(C)** Maximal projection of transverse sections views of *MYB51::NLS-3mVenus* expression in *CASP1::* and *SHR::FLS2* as well as WT and *fls2*. *MYB51* expression pattern stay conserved (epidermis-cortex-stele), but intensity is increased in neighbourhood of cells expressing *FLS2*, such as in cortex in *CASP1::FLS2-GFP fls2* or stele in *SHR::FLS2-GFP fls2* (white arrowheads). Images were acquired as Fig.S2B., with similar settings between genotypes, while corresponding mock and flg22 treatment pictures have identical parameters. Due to lower average signal intensity, pictures were acquired with increased gain compare to Fig.2B. Scale bar, 25 μ M. **(D)** Quantitative map of *MYB51::NLS-3mVenus* responses inferred from tissue-specific quantification after 24h treatment with 1 μ M flg22. Nuclear signals were quantified in ROI delimited with *UBQ10::NLS-mTurquoise2* for all tissue-specific promoter lines, while wild-type (WT) signal was quantified with *UBQ10::NLS-tdTomato* marker. Mean intensity is comparable between *prom::FLS2-GFP fls2* lines but not to wild-type. Note the constitutive signal present in untreated seedlings.

MYB51::NLS-3mV
prom::FLS2-GFP fls2

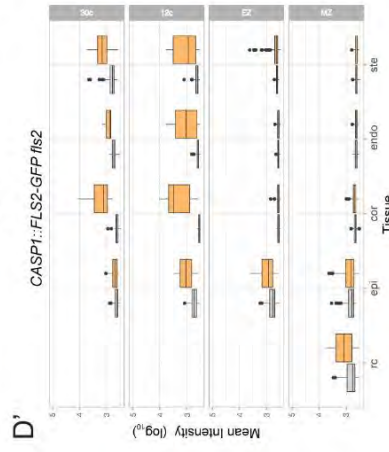
Treatment
mock
flg22



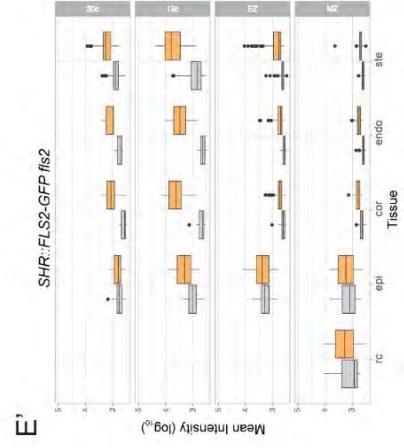
WER::FLS2-GFP fls2



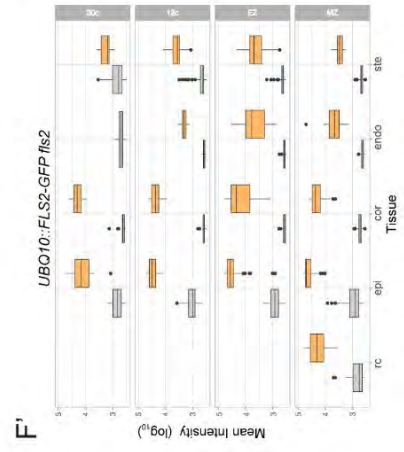
CASP1::FLS2-GFP fls2



SHR::FLS2-GFP fls2

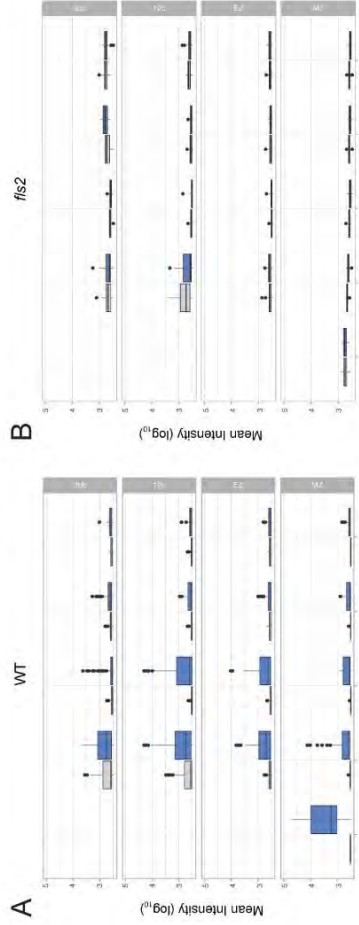


UBO10::FLS2-GFP fls2

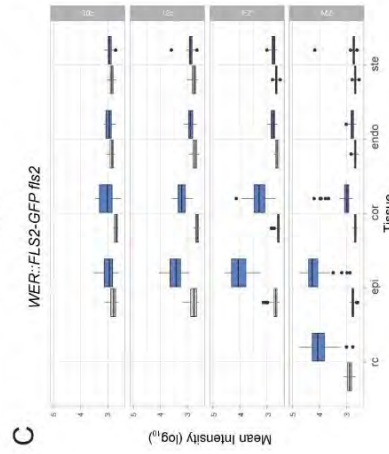


PERS::NLS-3mV
prom::FLS2-GFP fls2

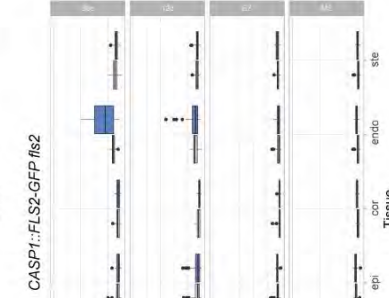
Treatment
mock
flg22



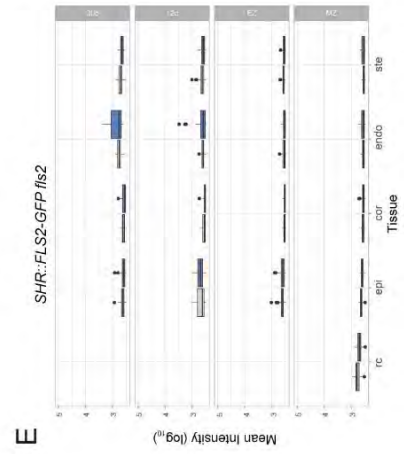
WER::FLS2-GFP fls2



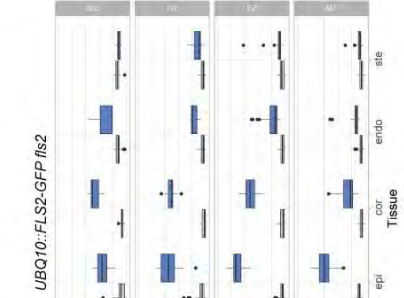
CASP1::FLS2-GFP fls2



SHR::FLS2-GFP fls2

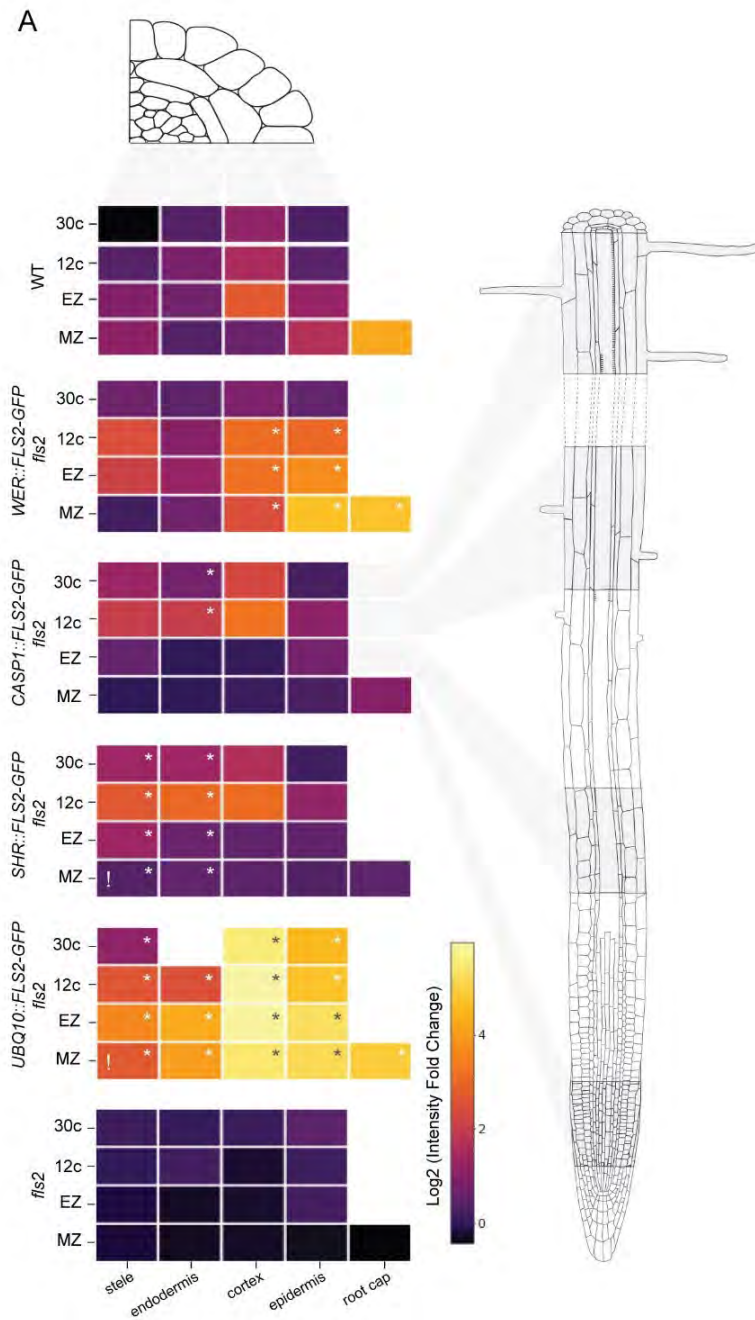


UBO10::FLS2-GFP fls2



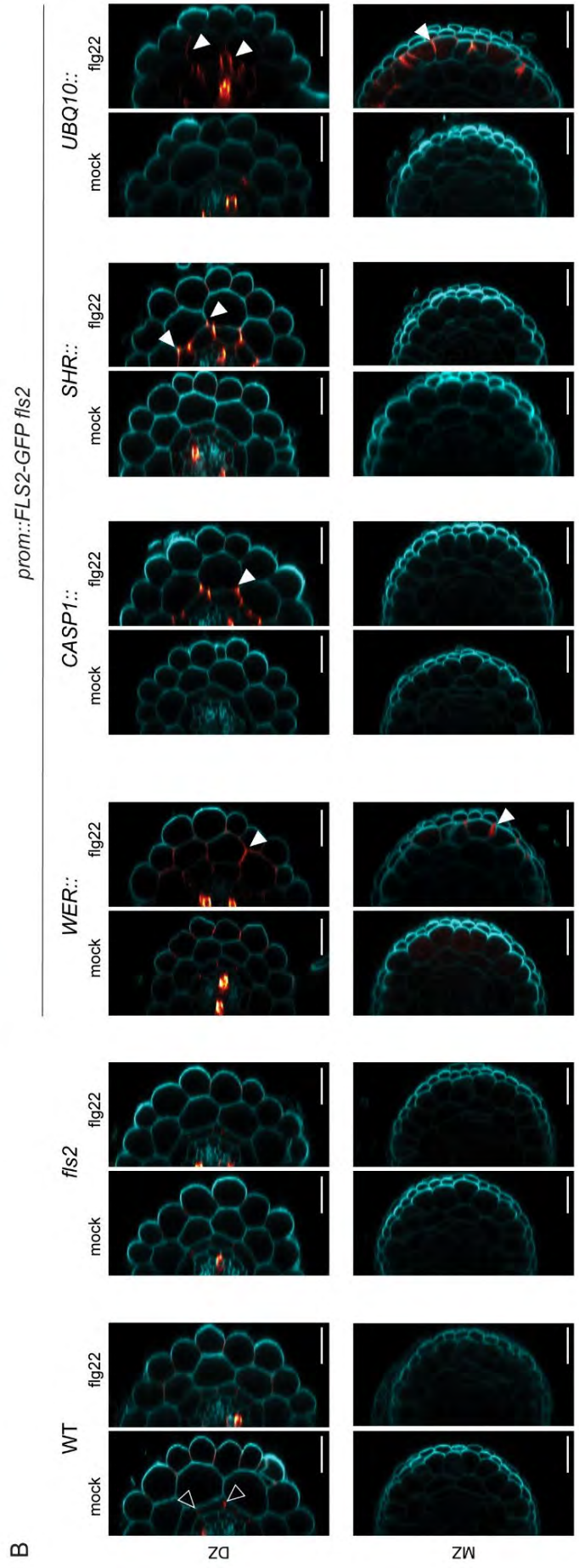
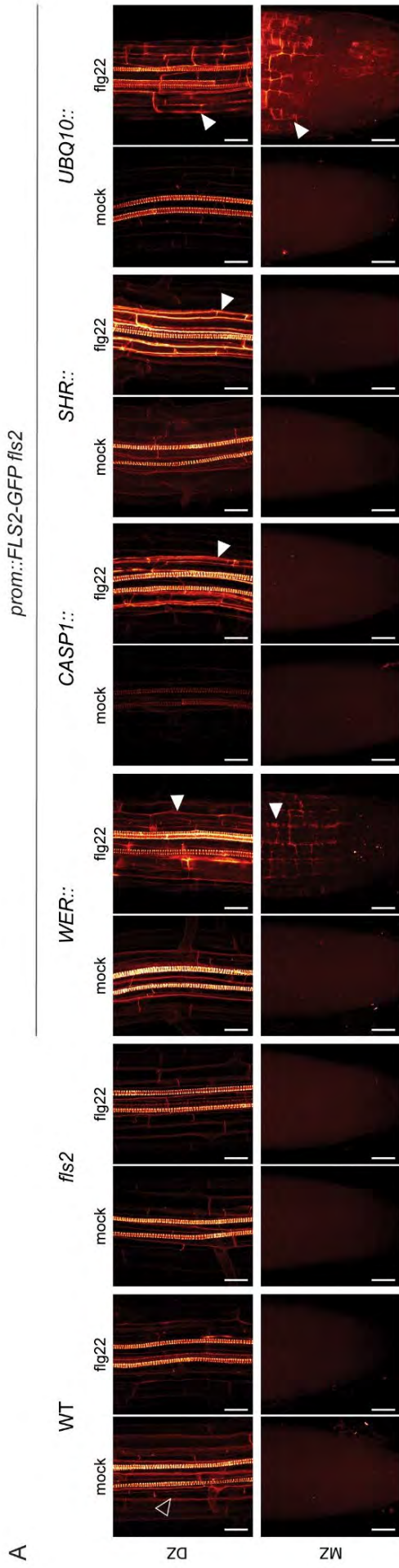
Supplemental Figure S4: *PER5* and *MYB51* tissue-specific quantification values

Boxplots for mean intensity of *PER5::NLS-3mVenus* (A-F) and *MYB51::NLS-3mVenus* (A'-F') marker calculated from tissue-specific nuclear signals for (A) wild-type plants, (B) *fls2* mutant, (C) *WER::FLS2-GFP fls2*, (D) *CASP1::FLS2-GFP fls2*, (E) *SHR::FLS2-GFP fls2* and (F) *UBQ10::FLS2-GFP fls2*. Boxplot centre represents the median. MZ, meristematic zone; EZ, elongation zone; 15c, 15 cells after onset of elongation; 30c, 30 cells after onset of elongation; rc, root cap; epi, epidermis; cor, cortex; endo, endodermis; ste, stele.



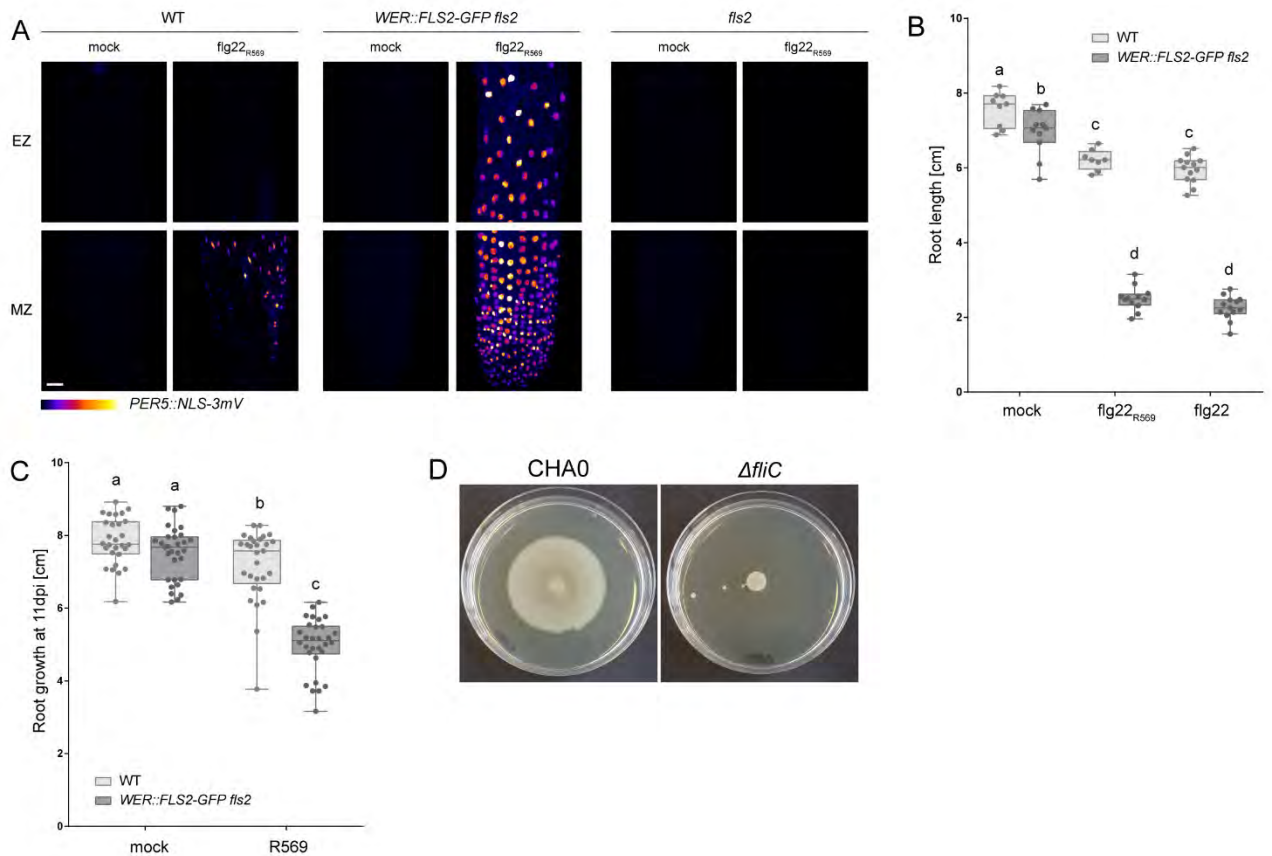
Supplemental Figure S5: Tissue-specific quantification of MYB51 fold change

Log₂ transformed fold change of intensity of *MYB51::NLS-3mVenus* in WT, *fls2* and the different *prom::FLS2-GFP fls2* lines. Pattern of induction of *MYB51* changed between the different lines but increased signal is not restricted to tissue expressing *FLS2* (stars). Note that *MYB51* can be induced in the stellar meristem in *UBQ10::FLS2* but not in *SHR::FLS2* (!). MZ, meristematic zone; EZ, elongation zone; 15c, 15 cells after onset of elongation; 30c, 30 cells after onset of elongation; rc, root cap; epi, epidermis; cor, cortex; endo, endodermis; ste, stele.



Supplemental Figure S6: Lignin deposition is a cell-autonomous process

(A) Maximum projection showing lignin deposition stained by basic fuchsin in the meristematic zone (MZ) and the differentiated zone (DZ) of the different *prom::FLS2-GFP fls2* lines after 1 day treatment with 1 μ M flg22. While neither wild-type nor *fls2* roots show lignin deposition outside of the xylem and the endodermal Casparian strip barrier, *WER::* and *UBQ10::FLS2-GFP fls2* lines deposit lignin in both MZ and DZ. In contrast, *CASP1::* and *SHR::FLS2-GFP fls2* lignified heavily the DZ only. Black arrowheads, Casparian strip. White arrowheads, ectopic lignin deposition. Scale bar, 25 μ M. **(B)** Cross section of z-stack presented in (A). Cell wall stained with calcofluor (blue) is co-visualized with lignin stained with basic fuchsin (red). *WER::FLS2-GFP* expression drives lignin deposition between cortex and epidermal cells in DZ, and between epidermal cells and root cap in MZ. This pattern is also observed in *UBQ10::FLS2*, but extends to cortex and endodermis in DZ. Both *CAPS1::* and *SHR::* deposit lignin ectopically between cortex and endodermal cells after flg22 treatment. White arrowheads, ectopic lignin. Black arrowheads, Casparian strip. Scale bar, 20 μ M.



Supplemental Figure S7: Flg22 from bacterial isolate *Pseudomonas* R569 is recognized by WER::FLS2

(A) flg22_{R569} triggers a strong induction of PER5::NLS-3mVenus marker (Fire LUT) on WER::FLS2-GFP *fls2* compared to wild-type plant, but the detection is abolished in the *fls2* mutant. Maximum projection of z-stacks imaging meristematic (MZ) and elongation (EZ) zones treated for 1 day with 1uM flg22_{R569}. Acquisition done with identical settings. Scale bar, 25μm. **(B)** flg22_{R569} inhibits root growth weakly on wild-type (WT) and strongly on WER::FLS2-GFP *fls2* in the same extent than commercial flg22 for *P. aeruginosa*. Seedlings were transferred for 7 days on plates containing 1uM flg22, flg22_{R569} or mock. Boxplot centre represents the median. Different letters indicate statistically significant difference ($p < 0.05$) between means by 2-ways ANOVA and Tukey's multiple comparison tests. **(C)** Bacterial isolate R569 induces stronger root growth inhibition on wild-type seedlings (WT) than on WER::FLS2-GFP *fls2*. Replicate carried out in Cologne with different growth conditions (see material and methods). Five-days old seedlings were transferred for 11 days on plate containing bacteria at a concentration of OD₆₀₀ = 0.01. Boxplot centre represents the median. Different letters indicate statistically significant difference ($p < 0.05$) between means by ANOVA and Tukey's multiple comparison tests. **(D)** Motility assay for CHA0 and its Δ*fliC* mutant.

Supplemental Tables

Number						fig22	MTI	RGI
At- SPHERE	Phylum	Class	Order	Family	Genus	predicted ³	WER>WT	WER>WT
Root 1464	<i>Actinobacteria</i>	<i>Actinobacteria</i>	<i>Actinomycetales</i>	<i>Microbacteriaceae</i>		no	no	no
Root 227	<i>Actinobacteria</i>	<i>Actinobacteria</i>	<i>Actinomycetales</i>	<i>Microbacteriaceae</i>		no	no/yes	no
Root 935	<i>Bacteroidetes</i>	<i>Flavobacteriia</i>	<i>Flavobacteriales</i>	<i>Flavobacteriaceae</i>	<i>Flavobacterium</i>	no	no	no
Root 444D2	<i>Firmicutes</i>	<i>Bacilli</i>	<i>Bacillales</i>	<i>Paenibacillaceae</i>	<i>Paenibacillus</i>	no	yes	no
Root 342	<i>Proteobacteria</i>	<i>Alphaproteobacteria</i>	<i>Caulobacterales</i>	<i>Caulobacteraceae</i>	<i>Caulobacter</i>	no	- ^a	no
Root 700	<i>Proteobacteria</i>	<i>Alphaproteobacteria</i>	<i>Caulobacterales</i>	<i>Caulobacteraceae</i>		no	-	no
Root 105	<i>Proteobacteria</i>	<i>Alphaproteobacteria</i>	<i>Rhizobiales</i>	<i>Hyphomicrobiaceae</i>		no	-	no
Root 1471	<i>Proteobacteria</i>	<i>Alphaproteobacteria</i>	<i>Rhizobiales</i>	<i>Phyllobacteriaceae</i>		no	- ^a	no
Root 482	<i>Proteobacteria</i>	<i>Alphaproteobacteria</i>	<i>Rhizobiales</i>	<i>Rhizobiaceae</i>	<i>Rhizobium</i>	no	no	no
Root 954	<i>Proteobacteria</i>	<i>Alphaproteobacteria</i>	<i>Rhizobiales</i>	<i>Rhizobiaceae</i>	<i>Rhizobium</i>	no	no	no
Root 142	<i>Proteobacteria</i>	<i>Alphaproteobacteria</i>	<i>Rhizobiales</i>	<i>Rhizobiaceae</i>	<i>Sinorhizobium</i>	no	no	no
Root 50	<i>Proteobacteria</i>	<i>Alphaproteobacteria</i>	<i>Sphingomonadales</i>	<i>Sphingomonadaceae</i>	<i>Sphingomonas</i>	yes	no	no
Root 1294	<i>Proteobacteria</i>	<i>Alphaproteobacteria</i>	<i>Sphingomonadales</i>	<i>Sphingomonadaceae</i>	<i>Sphingomonas</i>	yes	no	no
Root 710	<i>Proteobacteria</i>	<i>Alphaproteobacteria</i>	<i>Sphingomonadales</i>	<i>Sphingomonadaceae</i>	<i>Sphingomonas</i>	yes	no	no
Root 241	<i>Proteobacteria</i>	<i>Alphaproteobacteria</i>	<i>Sphingomonadales</i>	<i>Sphingomonadaceae</i>	<i>Sphingomonas</i>	yes	no/yes ^b	no
Root 1497	<i>Proteobacteria</i>	<i>Alphaproteobacteria</i>	<i>Sphingomonadales</i>	<i>Sphingomonadaceae</i>	<i>Sphingopyxis</i>	yes	no	no
Root 214	<i>Proteobacteria</i>	<i>Alphaproteobacteria</i>	<i>Sphingomonadales</i>	<i>Sphingomonadaceae</i>	<i>Sphingopyxis</i>	yes	yes	no/yes

Root 154	<i>Proteobacteria</i>	<i>Alphaproteobacteria</i>	<i>Sphingomonadales</i>	<i>Sphingomonadaceae</i>		yes	yes	no/yes
Root 83	<i>Proteobacteria</i>	<i>Betaproteobacteria</i>	<i>Burkholderiales</i>	<i>Alcaligenaceae</i>	<i>Achromobacter</i>	yes	no	no
Root 170	<i>Proteobacteria</i>	<i>Betaproteobacteria</i>	<i>Burkholderiales</i>	<i>Alcaligenaceae</i>	<i>Achromobacter</i>	yes	yes	no/yes
Root 565	<i>Proteobacteria</i>	<i>Betaproteobacteria</i>	<i>Burkholderiales</i>	<i>Alcaligenaceae</i>	<i>Achromobacter</i>	yes	yes ^b	no
Root 473	<i>Proteobacteria</i>	<i>Betaproteobacteria</i>	<i>Burkholderiales</i>	<i>Comamonadaceae</i>	<i>Variovorax</i>	yes	no	no
Root 568	<i>Proteobacteria</i>	<i>Betaproteobacteria</i>	<i>Burkholderiales</i>	<i>Comamonadaceae</i>		no	no	no
Root 1221	<i>Proteobacteria</i>	<i>Betaproteobacteria</i>	<i>Burkholderiales</i>	<i>Comamonadaceae</i>		yes	no/yes	no
Root 29	<i>Proteobacteria</i>	<i>Betaproteobacteria</i>	<i>Burkholderiales</i>	<i>Comamonadaceae</i>		yes	no	no
Root 16D2	<i>Proteobacteria</i>	<i>Betaproteobacteria</i>	<i>Burkholderiales</i>	<i>Comamonadaceae</i>		yes	no/yes	no
Root 209	<i>Proteobacteria</i>	<i>Betaproteobacteria</i>	<i>Burkholderiales</i>	<i>Comamonadaceae</i>		yes	yes	no
Root 401	<i>Proteobacteria</i>	<i>Gammaproteobacteria</i>	<i>Pseudomonadales</i>	<i>Pseudomonadaceae</i>	<i>Pseudomonas</i>	no	no	no
Root 562	<i>Proteobacteria</i>	<i>Gammaproteobacteria</i>	<i>Pseudomonadales</i>	<i>Pseudomonadaceae</i>	<i>Pseudomonas</i>	no	yes	no
Root 9	<i>Proteobacteria</i>	<i>Gammaproteobacteria</i>	<i>Pseudomonadales</i>	<i>Pseudomonadaceae</i>	<i>Pseudomonas</i>	no	yes	yes
Root 569	<i>Proteobacteria</i>	<i>Gammaproteobacteria</i>	<i>Pseudomonadales</i>	<i>Pseudomonadaceae</i>	<i>Pseudomonas</i>	no	yes	yes
Root 68	<i>Proteobacteria</i>	<i>Gammaproteobacteria</i>	<i>Pseudomonadales</i>	<i>Pseudomonadaceae</i>	<i>Pseudomonas</i>	yes	yes	no
Root 71	<i>Proteobacteria</i>	<i>Gammaproteobacteria</i>	<i>Pseudomonadales</i>	<i>Pseudomonadaceae</i>	<i>Pseudomonas</i>	yes	yes	no
Root 179	<i>Proteobacteria</i>	<i>Gammaproteobacteria</i>	<i>Xanthomonadales</i>	<i>Xanthomonadaceae</i>	<i>Rhodanobacter</i>	no	no ^b	no

^a not tested: bacteria did not grow in drop inoculation experiment

^b induction of *PER5* in differentiated zone for both WT and *WER::FLS2-GFP fls2*

^c Garrido-Oter *et al.* (2018)

Supplemental Table S2: Primers and plasmids used for bacterial mutagenesis.

Name	Sequence / plasmid characteristics^a	Reference
Primers		
fleQ-1	CGGGATCCATTGAAGAAACCCGTGAGGC	Peter Kupferschmied (2015)
fleQ-2	CCCAAGCTTTAAAATCACCGCCAGGTCGCG	Peter Kupferschmied (2015)
fleQ-3	CCCAAGCTTTGACGCCGTTTTTCAAGTCTTTG	Peter Kupferschmied (2015)
fleQ-4	GGAATTCATTTTCATGGCCATCGTCTTCGCG	Peter Kupferschmied (2015)
fliC-1	ATAACAGGGTAATCTGAATTatgaatcagctagagcctgt	this study
fliC-2	ccagctattacatgacgaattcctcgttg	this study
fliC-3	attcgtcatgtaatagctggctaagctttggc	this study
fliC-4	CCGGGTACCGAGCTCGAATTtcagccttggcact	this study
fliC_check_F	gacttcgcagatccgtgg	this study
fliC_check_R	aactgcggtcgaagcttg	this study
Plasmids		
pEMG	Expression vector; <i>oriR6K</i> , <i>lacZα</i> with two flanking I-SceI sites; Km ^R , Ap ^R	Martínez-García, E., and Lorenzo, V. de (2011)
pSW-2	<i>oriRK2</i> , <i>xyIS</i> , <i>P_m::I-sceI</i> ; Gm ^R	Martínez-García, E., and Lorenzo, V. de (2011)
pME8323	pEMG:: <i>ΔfleQ</i> ; suicide plasmid for the in-frame deletion of <i>fliC</i> (PPRCHA0_1656)	Peter Kupferschmied (2015)
pME11121	pEMG:: <i>ΔfliC</i> ; suicide plasmid for the in-frame deletion of <i>fliC</i> (PPRCHA0_1651)	this study

^a: Gm^r, gentamicin resistance; Km^r, kanamycin resistance.

Supplemental Videos Titles

Movie 1: Treatment of *UBQ10::R-GECO1* in WT background with 1.25uM flg22 – overview

Movie 2: Treatment of *UBQ10::R-GECO1 WER::FLS2-GFP fls2* with 1.25uM flg22 – overview

Movie 3: Treatment of *UBQ10::R-GECO1 CASP1::FLS2-GFP fls2* with 1.25uM flg22 – overview

Movie 4: Treatment of *UBQ10::R-GECO1 SHR::FLS2-GFP fls2* with 1.25uM flg22 – overview

Movie 5: Treatment of *UBQ10::R-GECO1 UBQ10::FLS2-GFP fls2* with 1.25uM flg22 – overview

Movie 6: Treatment of *UBQ10::R-GECO1* in WT background with 1.25uM flg22 – zoom in elongation zone

Movie 7: Treatment of *UBQ10::R-GECO1 WER::FLS2-GFP fls2* with 1.25uM flg22 – zoom in elongation zone

Movie 8: Treatment of *UBQ10::R-GECO1 CASP1::FLS2-GFP fls2* with 1.25uM flg22 – zoom in differentiated zone

Movie 9: Treatment of *UBQ10::R-GECO1 SHR::FLS2-GFP fls2* with 1.25uM flg22 – zoom in differentiated zone

Movie 10: Treatment of *UBQ10::R-GECO1 UBQ10::FLS2-GFP fls2* with 1.25uM flg22 – zoom in differentiated zone

3.4. APPENDICES

Although the above manuscript described the spatial regulation of *flg22*-driven immunity using only three recombinant lines, we first started with a much broader set of promoters, that we refined as the project progressed. For length restriction, this work will not be published, but will be presented in the following section in addition to complementary experiments that did not fit in the final manuscript.

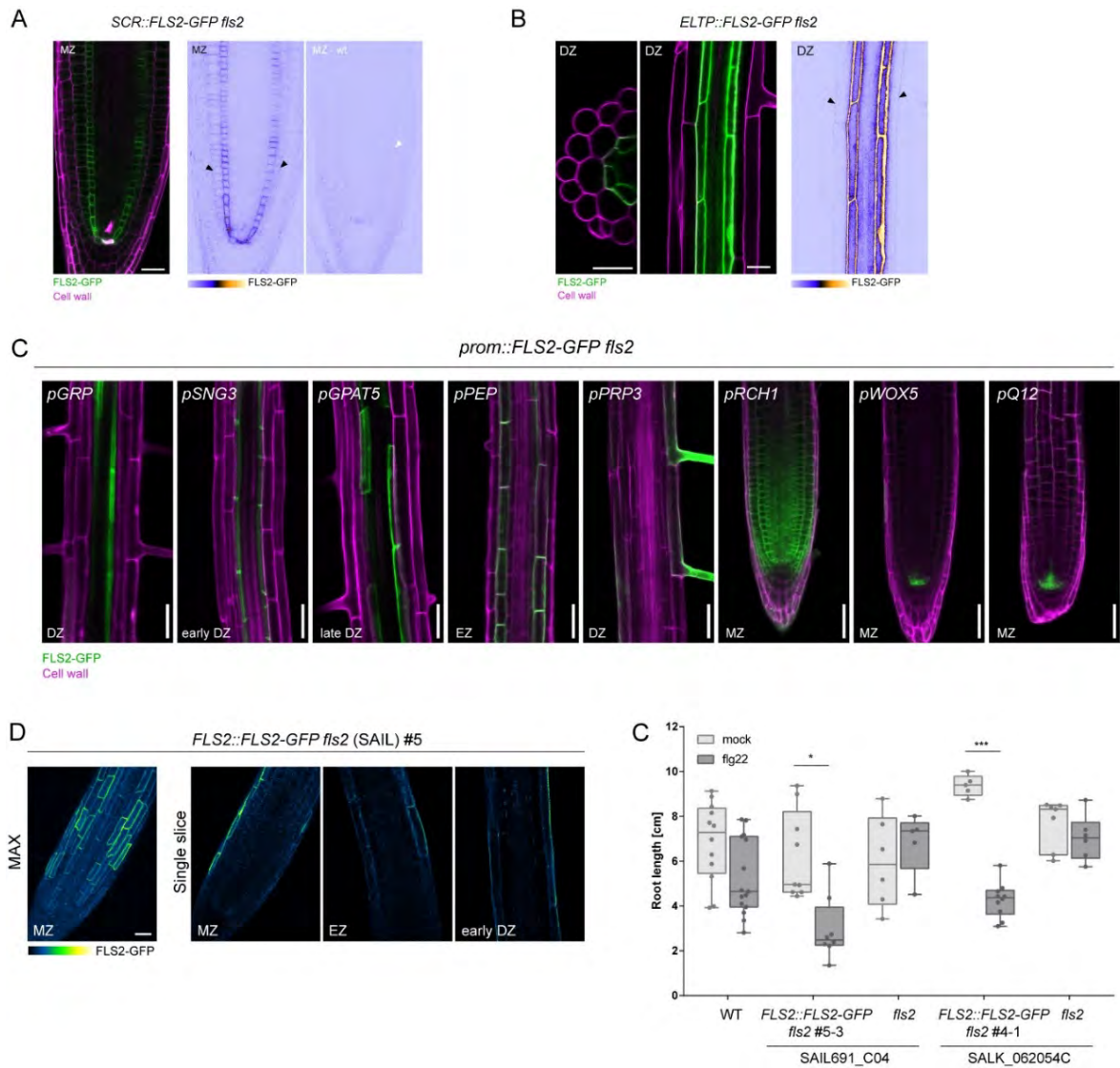
3.4.1. GENERATION OF NEW TISSUE-SPECIFIC *PROM::FLS2-GFP* LINES

As the project started, we wanted to use cell-type specific promoters to drive *FLS2* in different tissues. Not all recombinant lines published by Wyrsh *et al.* (2015) fit this criterion. Thus, *LBD16* (*LATERAL ORGAN BOUNDARIES-DOMAIN 16*) and *PGP4* (*P-GLYCOPROTEIN 4*) promoters, which should express *FLS2* in the stele and the epidermis, respectively, displayed weak unspecific *FLS2* expression in all root tissues and were discarded (Emonet *et al.*, 2020). The *SCR* (*SCARECROW*) promoter drove *FLS2* expression principally in the meristematic endodermis, as expected (Fukaki *et al.*, 1998), but also faintly in the cortex (App.6A). Similarly, the *ELTP* (*ENDODERMAL LIPID TRANSFER PROTEIN*) promoter expressed *FLS2* in the endodermis and in the cortex to a lesser extent (App.6B) (Barberon *et al.*, 2016).

To extend our *prom::FLS2* lines collection, I selected tissue-specific promoters from previously available collections (Marquès-Bueno *et al.*, 2015) (App.6C). *GLYCIN-RICH PROTEIN (GRP)* promoter was chosen to express *FLS2* in the xylem pole pericycle cells (Andersen *et al.*, 2018). Our list of endodermal promoters was completed with *GLYCEROL-3-PHOSPHATE SN-2-ACYLTRANSFERASE 5 (GPAT5)* and *SCHENGEN 3 (SGN3)*, which are active in suberized and early endodermis, respectively (Beisson *et al.*, 2007; Pfister *et al.*, 2014). *PEP* promoter was chosen to express *FLS2* in the cortex (Mustroph *et al.*, 2009). In addition, I picked *PIN-FORMED 2 (PIN2)* and *PROLIN-RICH PROTEIN 3 (PRP3)* as specific epidermal promoter. Finally, *FLS2* was also expressed under the meristematic promoters *Q12*, *WUSCHEL RELATED HOMEODOMAIN 5 (WOX5)* and *RCH1* (Lee *et al.*, 2006; Marquès-Bueno *et al.*, 2015; Narusaka *et al.*, 2004; Sarkar *et al.*, 2007). Most of them expressed *FLS2* as planned (App.6C). *WOX5* and *Q12* promoters expressed *FLS2* in the quiescent centre, *RCH1* had a broad expression pattern in the complete meristem. *PIN2* expressed *FLS2* in the cortex

and the epidermis, but its signal was less regular than other promoters so was not displayed here.

To compare the expression pattern of defences between the different recombinant lines and the normal expression of *FLS2*, we used wild-type plant background as controls. However, a more appropriate control would have been to express *FLS2-GFP* under its own promoter. The *FLS2::FLS2-GFP* line published was complementing the *Ws-0* background, a *fls2* mutant. Therefore, I also cloned the *FLS2* promoter (short version) with *FLS2-GFP* in *fls2* Col-0 background. In contrast to *FLS2::FLS2-GFP* *Ws-0* line, *FLS2_{short}::FLS2-GFP* was lowly expressed in T2, mostly in the root cap cell and in the elongating and early differentiating epidermis (App.6D). Some very faint signal could be observed in the stele. Unfortunately, most signal disappeared in T3, probably due to silencing. However, even with low expression, *FLS2_{short}::FLS2-GFP* could complement both *fls2* SAIL691_C04 and SALK_062054C mutants (App.6E).



Appendix 6 : Creation of new tissue-specific *prom::FLS2-GFP fls2* lines.

Expression patterns of *SCR::FLS2-GFP fls2* (A) and *ELTP::FLS2-GFP fls2* (B) lines (FLS2-GFP, green). Cell walls are highlighted with PI staining (magenta). Pictures on the right are visualized by ICA LUT to increase contrast (A, B).

(A) *SCR* promoter expressed principally FLS2 protein in endodermal cells, but some faint signal can be observed in cortex (black arrowheads). Picture of wild-type plants taken with identical setting (MZ-wt) is showed for comparison (cortical cell, white arrowheads). Scale bar, 25 μ m.

(B) *ELTP* promoter expressed FLS2 in endodermal cells, but some weak signal can be observed in cortex (black arrowheads). Scale bar, 25 μ m.

(C) Expression pattern of newly generated *prom::FLS2-GFP fls2* lines (FLS2-GFP, green). Cell walls are highlighted with PI staining (magenta). Scale bar, 50 μ m.

(D) Maximum projection and single slice pictures of *FLS2::FLS2-GFP fls2* T2 line (FLS2-GFP, GreenFireBlue LUT). Scale bar, 25 μ m.

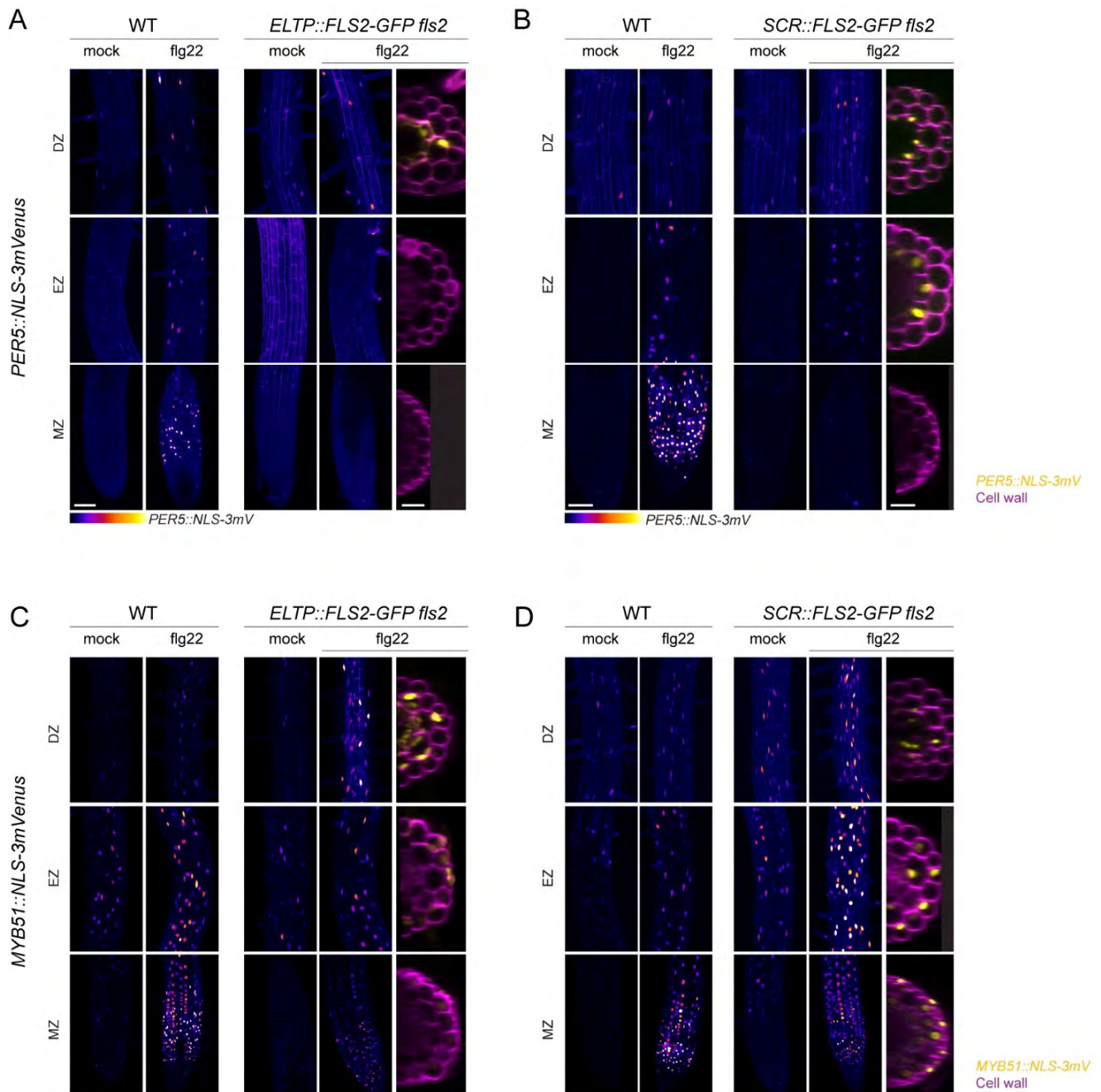
(E) *FLS2::FLS2-GFP* can complement *fls2* SAIL and SALK lines. Root length quantification of T3 lines transferred on 1 μ M flg22 for 6 dpi. Boxplot centre represents the median (5<n<=15). Different letters indicate statistically significant difference between means by Kruskal-Wallis test and Dunn's multiple comparison.

MZ, meristematic zone; EZ, elongation zone; DZ, differentiated zone.

3.4.2. INFLUENCE OF *FLS2* EXPRESSION ON MTI MARKERS

I crossed a subset of our new *prom::FLS2* lines to *PER5::NL-3xmVenus* and *MYB51::NLS-3mVenus* transcriptional read-outs in *fls2* background, so that the T1 could be readily analysed. At first, I also crossed all original *prom::FLS2* lines to *PR4::NLS-3mVenus*, which is slightly induced by *flg22* (Poncini *et al.*, 2017, Ch.6.Fig.2B). However, the effect was not robust, so I did not pursue the analysis. The complete analysis of defence patterns of *ELTP::* and *SCR::FLS2* lines is displayed in Appendix 7, and the one of newly made *RCH1/PRP3/GRP/PEP::FLS2* lines in Appendixes 8, 9 and in our manuscript (Emonet *et al.*, 2020). Due to some failed crosses, not all combinations are presented here. Since lines received from Thomas Boller's group were in *fls2* SAIL background, whereas the new lines are in *fls2* SALK background, I also crossed both *fls2* mutants with the immune markers as controls. Both lines did not respond to *flg22* (Emonet *et al.*, 2020; data not shown for *fls2* SALK).

Briefly, all recombinant lines confirmed the conclusion discussed earlier, *i.e.* *PER5* induction is strictly cell-autonomous whereas *MYB51* can be induced in a non-systemic, regional fashion (App.7, 8, 9). The restriction of *PER5* induction in trichoblasts in *PRP3::FLS2* (App.8D) further supports the cell-autonomy of *PER5*. Briefly, *ELTP::FLS2*, *PEP::FLS2* and *PRP3::FLS2* shifts the expression of *PER5* and *MYB51* in the differentiated zone (App.7AC, 8BD, 9ACD). Expressing *FLS2* under the *SCR* promoter drives *PER5* and *MYB51* responses in the elongating and differentiated zones, despite *SCR* expression being stronger in the meristematic endodermis, confirming the refractory ability of the central meristem. However, *MYB51* can be slightly induced by *flg22* in the root cap cells and the early elongating epidermal cells, most probably due to non-cell-autonomous signalling coming from the elongation zone (App.7D). The total absence of *PER5* and *MYB51* response in *GRP::FLS2* lines suggests that pericycle cells at the xylem pole might also be refractory to *FLS2*-driven responses. Consequently, the induction of *MYB51* signal observed in the stele of *SHR::FLS2*, *SCR::FLS2* and *PEP::FLS2* (Emonet *et al.*, 2020, Fig.S3; App.7D, 9D) might come from the perception of *flg22* either in central tissues of the stele, in the endodermis or the cortex.

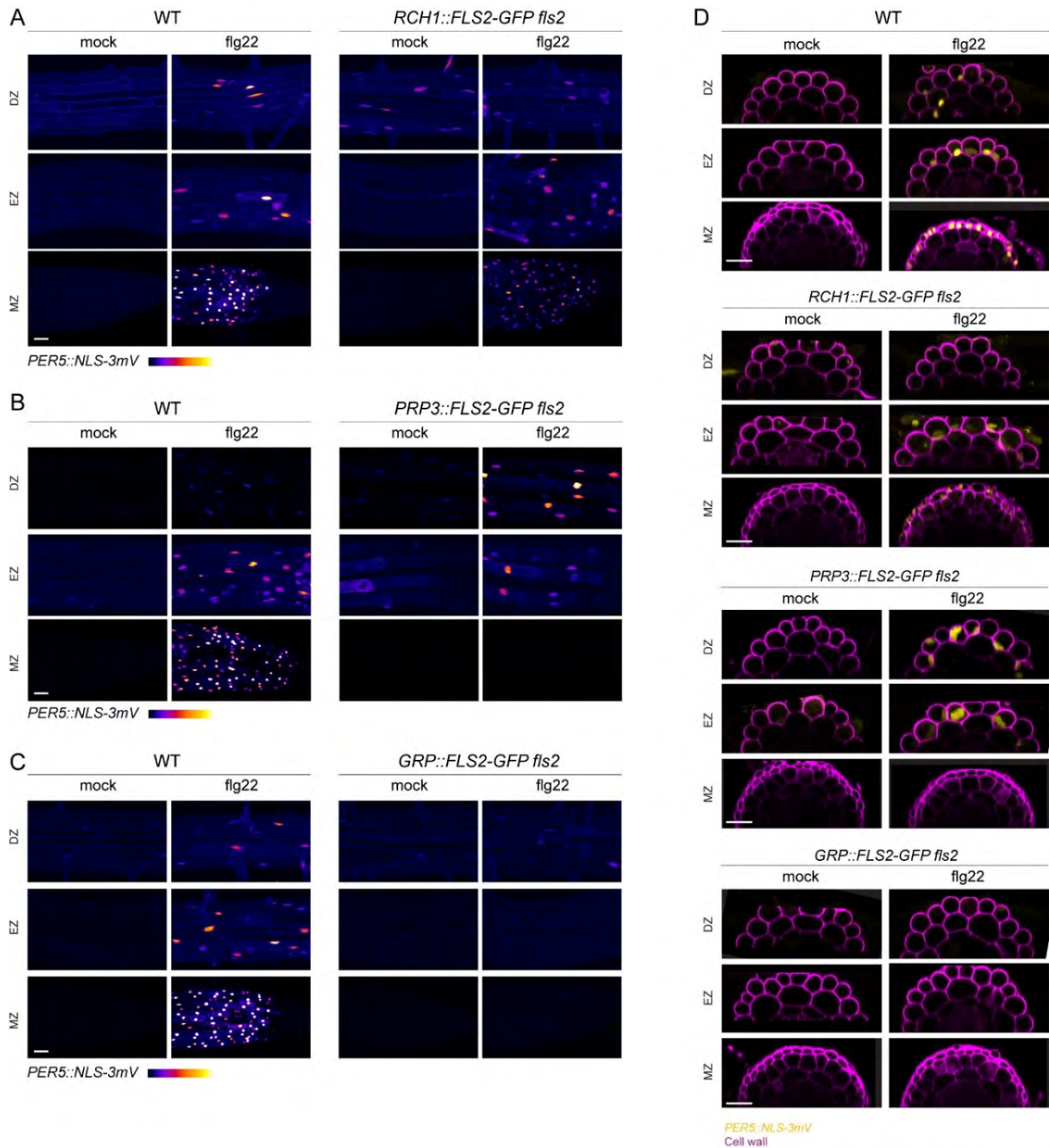


Appendix 7 : *FLS2* expression under *ELTP* and *SCR* promoters affects the pattern of immune responses

Flg22-triggered *PER5::NLS-3mVenus* induction is restricted to the differentiated endodermis and cortex cells in *ELTP::FLS2-GFP fls2* (A) and in elongating cortex cells and differentiated endodermal and cortical cells in *SCR::FLS2-GFP fls2* (B). In response to flg22, *MYB51::NLS-3mVenus* is strongly induced in the differentiated zone, particularly in cortical cells in *ELTP::FLS2-GFP fls2* (C); and in the elongation and the differentiated zone, in epidermis (EZ), cortex (EZ-DZ) and pericycle cells (DZ) in *SCR::FLS2-GFP fls2*.

Maximum projections of z-stack pictures of immune transcriptional read-outs (Fire LUT) of 1 μM flg22-treated plants versus mock. Pictures were taken with identical settings between mock and corresponding flg22 treatment, but different settings across root zones to reveal weak inductions.

Maximal projections of transverse sections views of *PER5* or *MYB51* expression patterns are shown on the right panel. Nuclear localized mVenus (yellow) signal was co-displayed with propidium iodide cell wall marker (PI, purple). MZ, meristematic zone; EZ, elongation zone; DZ, differentiated zone (30 cells after start of elongation). Scale bar, 50 μm for maximum projections, 25 μm for cross sections.

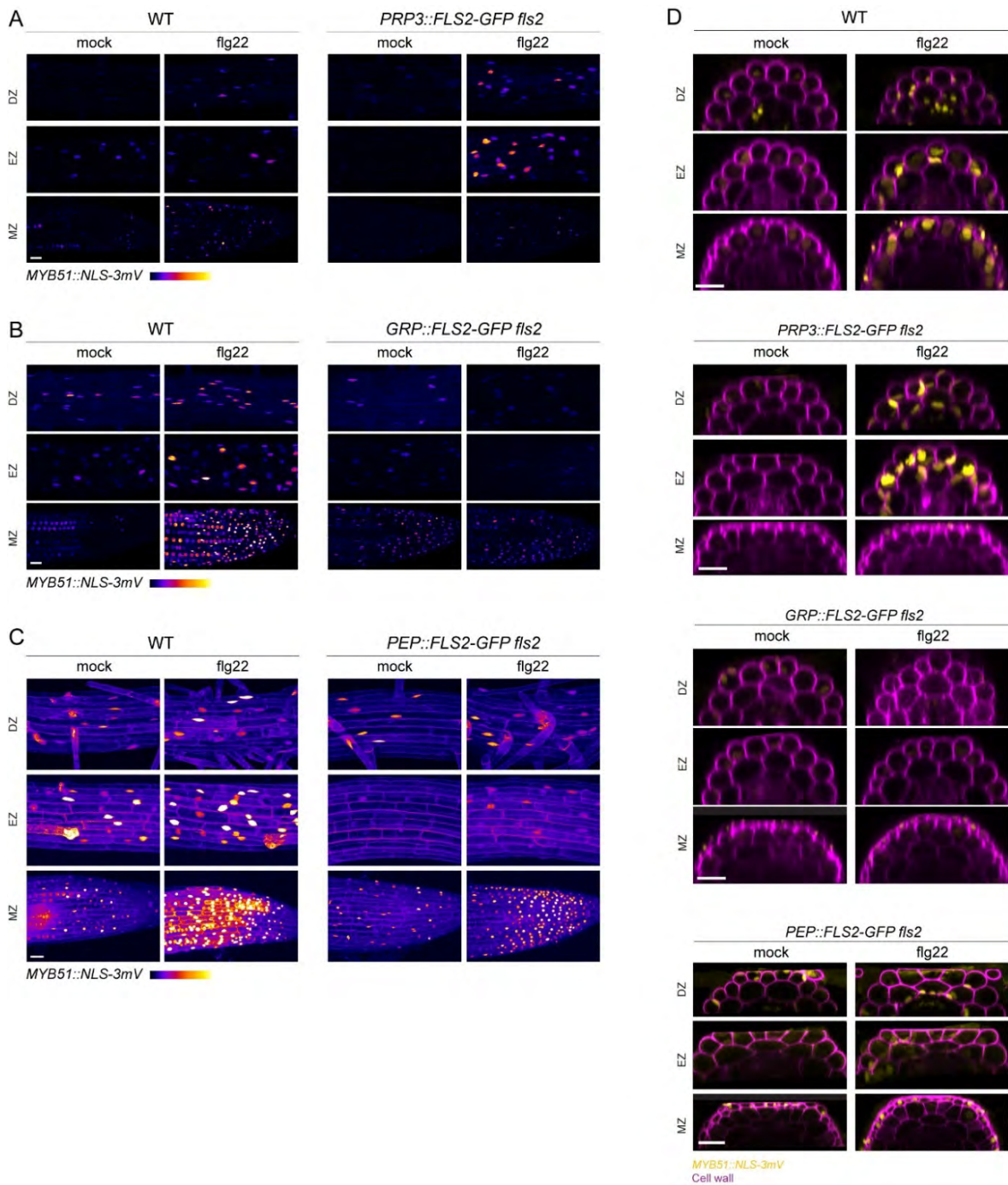


Appendix 8 : Effect of ectopic *FLS2* expression on *PER5* transcriptional read-out

(A-C) *PER5::NLS-3mVenus* response to flg22 in the meristem-specific *RCH1::FLS2-GFP fls2* (A), the differentiated epidermis-specific *PRP3::FLS2-GFP fls2* (B) and the xylem-pole pericycle-specific *GRP::FLS2-GFP fls2* (C) lines compared to WT. Note the induction of *PER5* in the meristematic and elongating epidermis with *RCH1* promoter, the expression shift to the differentiated region with *PRP3* promoter and the absence of response with *GRP* promoter. Maximum projection of z-stack pictures of mVenus signal (Fire LUT) in response to 1 μ M flg22 versus mock for 24h. Pictures were taken with identical settings between mock and corresponding flg22 treatment, but different settings across root zones to reveal weak induction.

(D) Maximal projections of transverse sections views of *PER5::NLS-3mVenus* are shown for *RCH1::PRP3::GRP::FLS2-GFP fls2* samples compared to WT, treated with 1 μ M flg22 or mock. Note that the induction of *PER5* signal is exclusively restricted to cell expressing *FLS2*. Transverse sections of pictures shown in (A-C). Signal intensity is only comparable between mock and flg22 treatment for a specific position. Nuclear localized mVenus (yellow) signal was co-displayed with propidium iodide cell wall marker (PI, purple).

MZ, meristematic zone; EZ, elongation zone; DZ, differentiated zone (30 cells after start of elongation). Scale bar, 25 μ m.



Appendix 9 : Effect of ectopic *FLS2* expression on *MYB51* transcriptional read-out

(A-C) *MYB51::NLS-3mVenus* response to flg22 in the differentiated epidermis-specific *PRP3::FLS2-GFP fls2* (A), the xylem pole pericycle-specific *GRP::FLS2-GFP fls2* (B) and the cortex-specific *PEP::FLS2-GFP fls2* (C) lines compared to WT. Note *PER5* induction shift to the differentiated region with *PRP3*, the absence of response with *GRP* and the weak induction in DZ with *PEP* promoters. Maximum projections of z-stack pictures of mVenus signal (Fire LUT) in response to 1 μ M flg22 versus mock for 24h. Pictures were taken with identical settings between mock and corresponding flg22 treatment, but different settings across root zones to reveal weak induction.

(D) Maximal projections of transverse sections views of *MYB51::NLS-3mVenus* are shown for *PRP3::/GRP::/PEP::FLS2-GFP fls2* samples compared to WT, treated with 1 μ M flg22. Note that the induction of *MYB51* signal is not restricted to cell expressing *FLS2*. Transverse sections of pictures shown in (A-C). Signal intensity is only comparable between mock and flg22 treatment for a specific position. Nuclear localized mVenus (yellow) signal was co-displayed with propidium iodide cell wall marker (PI, purple). MZ, meristematic zone; EZ, elongation zone; DZ, differentiated zone (30 cells after start of elongation). Scale bar, 25 μ m.

3.4.3. CELL-SPECIFIC QUANTIFICATION DEVELOPMENT – TRIAL WITH DAPI STAINING

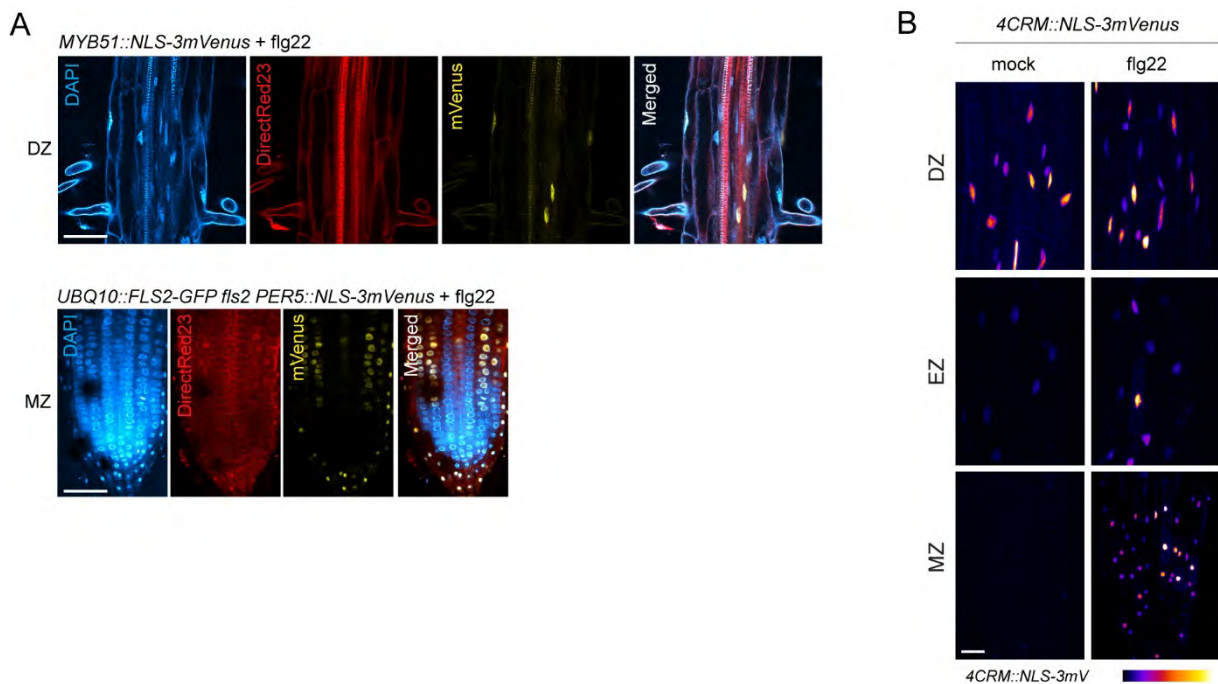
The development of the cell-specific quantification came from the realization that usual protocols, which rely on a single threshold based on the image to quantify, bias the results and identify only nuclei that show some fluorescence. For *PER5* marker, which lacks constitutive signal, it would be impossible to delimit nuclei on the control treatment. Therefore, we needed a generic marker of nuclei to attribute a Region Of Interest (ROI) to each single nucleus.

To quickly delineate all nuclei, we first use a DAPI staining protocol optimised for Clearsee fixation based on driselase digestion and methanol fixation (Material and methods) (App.10A). However, driselase often completely digested the root tip of our samples. Only meristems that were highly lignified could survive to the treatment. Therefore, we opted for the transformation with transgenic nuclear markers.

3.4.4. GENERATION OF SYNTHETIC UNIVERSAL REPORTER OF DEFENCE

Defence markers having distinct tissue-specificities make it difficult to assess whether a specific cell is inducing MTI responses using a single transcriptional read-out. Therefore, I wanted to generate a synthetic reporter of defence, which could be induced in all tissues without preferences. To do so, I cloned the synthetic 4CRM promoter identified by Lehmeier *et al.* (2016) upstream of the fluorescent nuclear reporter *NLS-3mVenus*. The 4CRM sequence is a four-time repetition of the 35bp tripartite cis-regulatory module (CRM) identified in the *DJ1E* promoter. It responds specifically to pathogens and salicylic acid. To avoid repetitive sequences and silencing, I cloned a new variant of the promoter, named *4CRM_{mod}*, where sequences between the regulatory modules are modified (Table S2).

However, the *4CRM_{mod}::NLS-3mVenus* line showed patchy and variable cytosolic signal in T1, so I did not characterise it further. *4CRM::NLS-3mVenus* displayed constitutive signal in the differentiated epidermis, cortex and central cells of the stele and in the elongating epidermis (App.10B). Flg22 treatment activates preferentially the expression of *4CRM* in the root cap cells and slightly in epidermal cells of the elongation zone, as for *PER5* reporter. Although this new reporter responds to flg22, it does not provide any advantages compared to other reporters because of its constitutive signal. Therefore, we did not use it for further analysis.



Appendix 10 : Combination of DAPI staining with Clearsee protocol and synthetic defence promoter generation

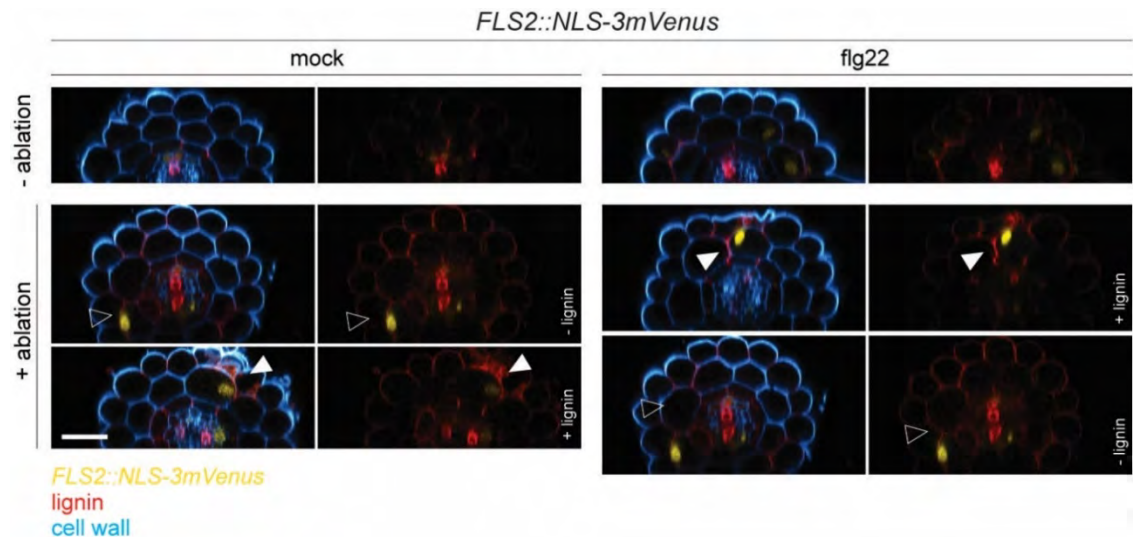
(A-B) Examples of combined DAPI and DirectRed23 staining using adapted Clearsee protocol. *MYB51::NLS-3mVenus* (A) and root tip of *UBQ10::FLS2-GFP fls2 PER5::NLS-3mVenus* line (B) treated for 24 h with 1 μ M flg22. Note that only highly lignified root tips survive the driselase treatment. Co-visualisation of nuclei stained by DAPI in all tissues (blue), cell wall stained by DirectRed23 (red) and mVenus immune reporter signal (yellow). Scale bar, 50 μ m.

(C) *4CRM::NLS-3mVenus* response (Fire LUT) to 1 μ M flg22 or mock for 22 h. *4CRM* promoter is induced by flg22 in the meristematic (MZ) and elongation zones (EZ). Note the strong constitutive signal in the differentiated zone (DZ). Scale bar, 25 μ m.

3.4.5. LIGNIN DEPOSITION AFTER CO-INCIDENCE OF DAMAGE AND FLG22 PERCEPTION

We previously showed local deposition of lignin following *FLS2* expression in plants expressing *FLS2* ectopically (Emonet *et al.*, 2020). Since damage can induce local accumulation of *FLS2* (Zhou *et al.*, 2020), I also tested whether ablation leads to lignin deposition after flg22 treatment. Ablation was done on *FLS2_{short}::NLS-3mVenus* lines to keep track of the ablated regions once seedlings fixed and stained. When combined with flg22 incubation for 24h, I could observe a faint lignin deposition around the wounded region (App.11). However, fuchsin coloration could be sometimes observed around damaged sites without flg22 treatment and, reversely, some damaged sites lacked clear lignin deposition in presence of flg22. Lignin deposition might be too low to induce consistent staining. Increasing the damage size or the incubation time might therefore heighten lignin deposition. It is compelling that Basic Fuchsin staining was also observed without

application of flg22. This suggests that damage might be sufficient to induce lignification by itself, or that Basic Fuchsin can also stain damaged cell wall. Interestingly, Ride (1975) already reported lignin deposition in response to wounding induced by *Botrytis* fungal infection, but not after wounding alone.



Appendix 11 : Lignin deposition after co-occurrence of damage and flg22 perception

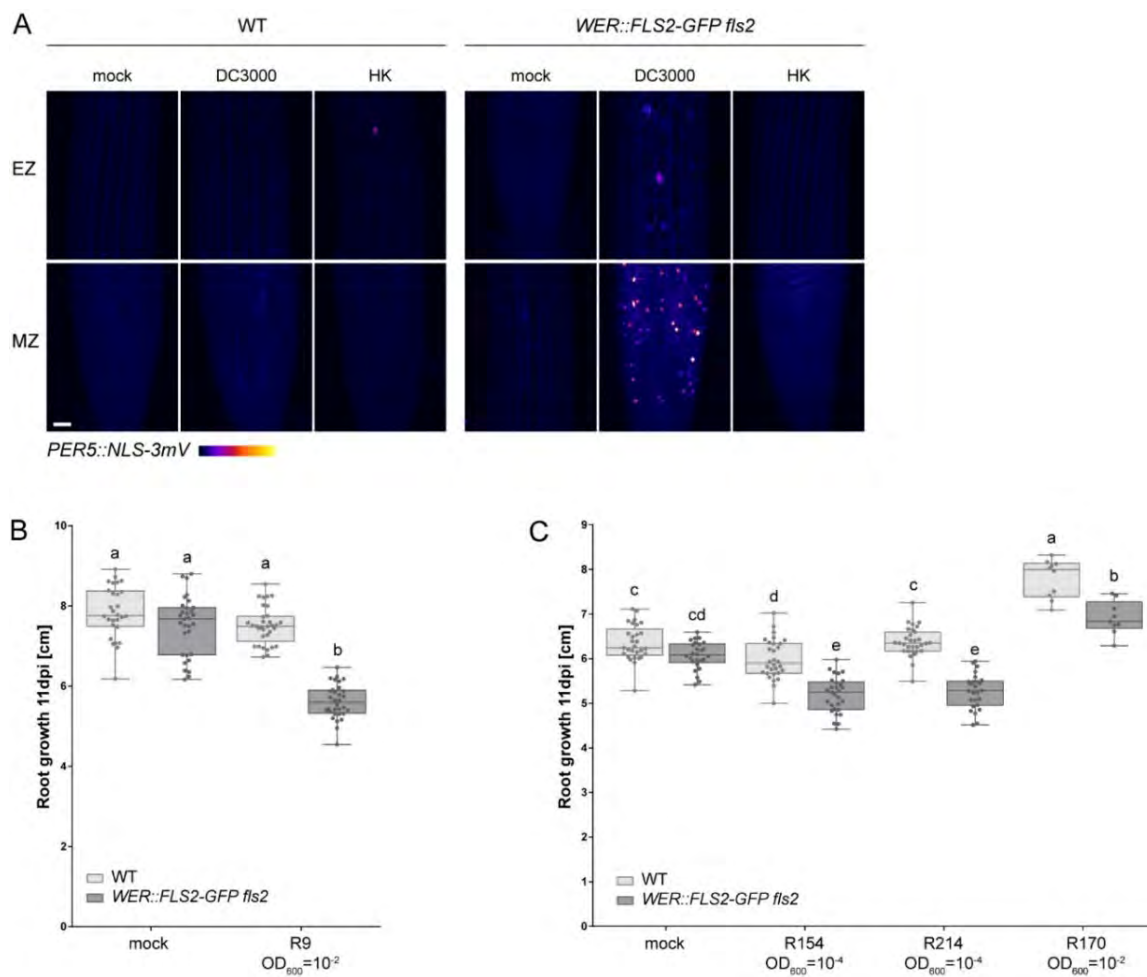
Laser ablation of epidermal cells in *FLS2_{short}::NLS-3mVenus* line induces inconsistently localized lignin deposition in 5-day-old differentiated roots. Nuclear-localized mVenus signals of *FLS2* promoter marker (yellow) co-visualized with cell wall stained by Calcofluor White (blue) and Basic Fuchsin-stained lignin (red). Ablated and control samples were treated with 1 μ M flg22 overnight. *FLS2* marker signal indicates proximity with laser-ablated cells. White arrowheads designate lignin-positive cell, black arrowheads specify lignin-negative cells. Scale bar, 25 μ m.

3.4.6. *WER::FLS2* RESPONDS STRONGLY TO THE PATHOGEN *PSEUDOMONAS SYRINGAE* STRAIN DC3000

In addition to the commensal bacteria *P. protegens* strain CHA0, I also tested root responses to the pathogen *P. syringae* strain DC3000. DC3000 inoculation induces *PER5* expression only in *WER::FLS2* whereas wild-type plants do not respond (App.12A). Surprisingly, heat-killed bacteria did not trigger *PER5* expression. The most plausible explanation is that bacterial concentration was too low ($OD_{600} = 0.01$). Alternatively, boiling could have denatured proteins required for flagellin processing or living bacteria might be required for flg22-driven MTI induction. Two very recent studies highlight that effector-triggered immunity increases the effect of MAMP-triggered immunity (Ngou *et al.*, 2020; Yuan *et al.*, 2020b). It would therefore be interesting to test whether *P. syringae* mutants lacking effectors have increased or impaired responses to flg22 on the *WER::FLS2* line.

3.4.7. SCREEN OF COMMENSAL BACTERIAL CULTURE COLLECTION FOR DIFFERENTIAL ROOT GROWTH INHIBITION

Amongst the commensal bacteria screened, we identified four supplementary strains that, similarly to the *Pseudomonas* R569, induces *PER5* expression and increases root growth inhibition. The *Pseudomonas* R9 was closely related to R569 and showed robust results in Lausanne and Cologne's growth conditions (App.12B), whereas the *Spingomonadaceae* R214 and R154, as well as the *Achromobacter* R170 increased relative RGI only in Cologne's conditions (App.12C).



Appendix 12 : *WER::FLS2* responds strongly to commensal and pathogenic bacteria

(A) *WER::FLS2* responds strongly to the pathogen *P. syringae* strain DC3000. Maximum projection of z-stack pictures of *PER5::NLS-3mVenus* signal (Fire LUT) in response to inoculation for 24 h with 2 μ l of fresh or heat-killed (HK) *P. syringae* culture at OD₆₀₀ = 0.01. MZ, meristematic zone; EZ, elongation zone. Scale bar, 25 μ m.

(B) R9 isolate induces a robust increased root growth inhibition on *WER::FLS2-GFP fls2* compared to wild-type plants.

(C) R154, R214 and R170 isolates increase root growth inhibition on *WER::FLS2-GFP fls2* only in Cologne's conditions compared to wild-type plants. (B,C) Root growth was quantified at 11 dpi on plates inoculated with bacteria at OD₆₀₀ = 10⁻² or 10⁻⁴. Experiment was performed in Cologne's growth conditions. Boxplot centre represents the median. Different letters indicate statistically significant differences (p<0.05). Multiple comparison was performed using ANOVA and Tukey's HSD test.

3.5. SUPPLEMENTARY MATERIAL AND METHODS

If not specified, plant material, bacterial strains and methods were identical to the ones used in Emonet *et al.* (2020).

3.5.1. PLANT MATERIAL AND GROWTH CONDITIONS

The lines *ELTP::FLS2-3myc-GFP*, *SCR::FLS2-3myc-GFP* and *WER::FLS2-3myc-GFP* in *fls2* (SAIL691_C04) background were offered by Prof. Thomas Boller's group. New FLS2 expressing constructs *EXP7* / *GL2* / *GRP* / *GPAT5* / *PEP* / *PRP3* / *Q12* / *RCH1* / *SGN3* / *WOX5::FLS2-3myc-GFP* were transformed in *fls2* (SALK_062054C) background, and *FLS2_{short}::FLS2-GFP* in *fls2* (SAIL691_C04) background. Similarly, the *4CRM::NLS-3mVenus* and *4CRM_{mod}::NLS-3mVenus* lines were generated through transformation with *Agrobacterium* by floral dipping method (Clough and Bent, 1998). The marker lines *PER5::NLS-3mVenus* and *MYB51::NLS-3mVenus* (Poncini *et al.*, 2017) were crossed to *prom::FL2-GFP* lines.

3.5.2. BACTERIAL STRAIN AND GROWTH CONDITIONS

The DC3000 *P. syringae* was kindly provided by Prof. Christoph Keel's group. At-SPHERE strains were genotyped using primers listed in Table S1 (Bai *et al.*, 2015).

3.5.3. PLASMID CONSTRUCTION

Generation of expression constructs was performed with classical cloning or Gateway Cloning Technology (Invitrogen). New *prom::FLS2-3myc-GFP* constructs were generated combining the destination vector pH7m24GW,3 with pDon207 containing L1-FLS2-3xmyc-GFP-L2 (Wyrsh *et al.*, 2015) and the respective entry clones using LR reaction: pDONR L4-*pGL2*-R1, L4-*pQ12*-R1, L4-*pRCH1*-R1, L4-*pPEP*-R1, L4-*pPIN2*-R1, L4-*pPRP3*-R1, L4-*pWOX5*-R1 (SWELL lines)(Marquès-Bueno *et al.*, 2015), or pDONR L4-*pFLS2_{short}*-L1 (Zhou *et al.*, 2020), L4-*pGPAT5*-L1 (Naseer *et al.*, 2012), L4-*pGRP*-R1 (Andersen *et al.*, 2018), L4-*pSGN3*-L1 (5583bp before ATG) (Pfister *et al.*, 2014).

For the generation of the universal synthetic markers of defence, sequences for 4CRM and 4CRM_{mod} were ordered from Invitrogen (Table S2). The 4CRM sequence, flanked by HindIII and EcoRI restriction sites, was then digested with the corresponding enzymes

and ligated to the expression construct *prom::NLS-3mVenus* (pJV121) previously digested at the promoter site and containing the Basta resistance cassette. The 4CRM_{mod} sequence was surrounded by KpnI HindIII and EcoRI XmaI (Table S2) restriction sites. After digestion with KpnI and XmaI restriction enzymes, the 4CRM_{mod} promoter was ligated to the entry clone pUC L4-KpnI-XmaI-R1. The final expression clone was obtained with LR reaction combining pUC L4-KpnI-4CRM_{mod}-XmaI-R1 and pEN L1-*NLS-3xmVenus*-L2 to the destination vector pFR7m24GW containing the FastRed selection cassette.

3.5.4. PLANT GENOTYPING

Primers used for *fls2* genotyping are listed in Table S1. For *fls2* SAIL691_C04, we used the following combination: oAE22-oAE21 (WT) and oAE22-oLAB12 (mutant); for *fls2* SALK_062054C, oAE5-oAE17 (WT) and oAE5-oAE3 (mutants). For *fls2* SAIL691_C04 lines complemented with *FLS2::FLS2-GFP*, primers oAE22 must be replaced by oAE74 or oAE75 to avoid to amplify the construct.

3.5.5. ADAPTED DAPI STAINING

DAPI staining was performed as follows. Samples were first fixed 1 hour in 4% PFA 0.05% Tween in PBS, then washed three times 10 min in 0.05% Tween in 1xPBS (PBST) with light shaking. The solution was then replaced by 100% methanol for 10 min, then the samples were twice rehydrated in PBST for 10 min. Next, seedlings were digested in 2.5% driselase solution for 1 hour at 37°C, then rinsed twice in PBST, followed by clearing for 2 days in Clearsee solution. After staining for 30 min in 0.1% DirectRed23, samples were rinsed and washed twice (30 min each) in Clearsee solution. Seedlings were then mounted in a mix of 200 µl of 1:100 DAPI solution (10mg/ml stock solution) combined to 700 µl Citifluor, then kept overnight in the dark at 4°C.

3.5.6. LASER ABLATION SETUP

Laser ablation was done as previously described (Marhavý *et al.*, 2019; Zhou *et al.*, 2020). Once cells ablated, 500 µl of 3 µM flg22 solution was immediately added into the agar (final concentration: 1 µM). After 24 h treatment, *FLS2::NLS-3mVenus* was visualized to ensure proper ablation, then seedlings were fixed stained as described previously.

3.6. LITERATURE

- Andersen, T.G., Naseer, S., Ursache, R., Wybouw, B., Smet, W., De Rybel, B., Vermeer, J.E.M., and Geldner, N. (2018). Diffusible repression of cytokinin signalling produces endodermal symmetry and passage cells. *Nature* 555, 529–533.
- Barberon, M., Vermeer, J.E.M., De Bellis, D., Wang, P., Naseer, S., Andersen, T.G., Humbel, B.M., Nawrath, C., Takano, J., Salt, D.E., *et al.* (2016). Adaptation of Root Function by Nutrient-Induced Plasticity of Endodermal Differentiation. *Cell*. 164, 447 – 459.
- Beck, M., Wyrsh, I., Strutt, J., Wimalasekera, R., Webb, A., Boller, T., and Robatzek, S. (2014). Expression patterns of FLAGELLIN SENSING 2 map to bacterial entry sites in plant shoots and roots. *J. Exp. Bot.* 65, 6487–6498.
- Beisson, F., Li, Y., Bonaventure, G., Pollard, M., and Ohlrogge, J.B. (2007). The Acyltransferase GPAT5 Is Required for the Synthesis of Suberin in Seed Coat and Root of *Arabidopsis*. *Plant Cell* 19, 351–368.
- Clough, S.J., and Bent, A.F. (1998). Floral dip: a simplified method for *Agrobacterium*-mediated transformation of *Arabidopsis thaliana*. *Plant J.* 16, 735–743.
- Emonet, A., Zhou, F., Vacheron, J., Heiman, C.M., Tendon, V.D., Ma, K.-W., Schulze-Lefert, P., Keel, C., and Geldner, N. (2020). Spatially Restricted Immune Responses Allow for Root Meristematic Activity During Bacterial Colonisation. *BioRxiv* 2020.08.03.233817.
- Faulkner, C., and Robatzek, S. (2012). Plants and pathogens: putting infection strategies and defence mechanisms on the map. *Curr. Opin. Plant Biol.* 15, 699–707.
- Fukaki, H., Wysocka-Diller, J., Kato, T., Fujisawa, H., Benfey, P.N., and Tasaka, M. (1998). Genetic evidence that the endodermis is essential for shoot gravitropism in *Arabidopsis thaliana*. *Plant J.* 14, 425–430.
- Lee, J.-Y., Colinas, J., Wang, J.Y., Mace, D., Ohler, U., and Benfey, P.N. (2006). Transcriptional and posttranscriptional regulation of transcription factor expression in *Arabidopsis* roots. *Proc. Natl. Acad. Sci.* 103, 6055–6060.
- Lehmeyer, M., Kanofsky, K., Hanko, E.K.R., Ahrendt, S., Wehrs, M., Machens, F., and Hehl, R. (2016). Functional dissection of a strong and specific microbe-associated molecular pattern-responsive synthetic promoter. *Plant Biotechnol. J.* 14, 61–71.
- Marhavý, P., Kurenda, A., Siddique, S., Dénervaud Tendon, V., Zhou, F., Holbein, J., Hasan, M.S., Grundler, F.M., Farmer, E.E., and Geldner, N. (2019). Single-cell damage elicits regional, nematode-restricting ethylene responses in roots. *EMBO J.* 38, e100972.
- Marquès-Bueno, M.M., Morao, A.K., Cayrel, A., Platre, M.P., Barberon, M., Caillieux, E., Colot, V., Jaillais, Y., Roudier, F., and Vert, G. (2015). A versatile Multisite Gateway-compatible promoter and transgenic line collection for cell type-specific functional genomics in *Arabidopsis*. *Plant J.* 85, 320–333.
- Mustroph, A., Zanetti, M.E., Jang, C.J.H., Holtan, H.E., Repetti, P.P., Galbraith, D.W., Girke, T., and Bailey-Serres, J. (2009). Profiling transcriptomes of discrete cell populations resolves altered cellular priorities during hypoxia in *Arabidopsis*. *Proc. Natl. Acad. Sci.* 106, 18843–18848.
- Narusaka, Y., Narusaka, M., Park, P., Kubo, Y., Hirayama, T., Seki, M., Shiraishi, T., Ishida, J., Nakashima, M., Enju, A., *et al.* (2004). RCH1, a Locus in *Arabidopsis* That Confers Resistance to the Hemibiotrophic Fungal Pathogen *Colletotrichum higginsianum*. *Mol. Plant-Microbe Interactions* 17, 749–762.

- Naseer, S., Lee, Y., Lapierre, C., Franke, R., Nawrath, C., and Geldner, N. (2012). Casparian strip diffusion barrier in *Arabidopsis* is made of a lignin polymer without suberin. *Proc. Natl. Acad. Sci.* *109*, 10101–10106.
- Ngou, B.P.M., Ahn, H.-K., Ding, P., and Jones, J.D. (2020). Mutual Potentiation of Plant Immunity by Cell-surface and Intracellular Receptors. *BioRxiv* 2020.04.10.034173.
- Pfister, A., Barberon, M., Alassimone, J., Kalmbach, L., Lee, Y., Vermeer, J.E., Yamazaki, M., Li, G., Maurel, C., Takano, J., *et al.* (2014). A receptor-like kinase mutant with absent endodermal diffusion barrier displays selective nutrient homeostasis defects. *ELife* *3*, e03115.
- Poncini, L., Wyrsh, I., Tendon, V.D., Vorley, T., Boller, T., Geldner, N., Métraux, J.-P., and Lehmann, S. (2017). In roots of *Arabidopsis thaliana*, the damage-associated molecular pattern AtPep1 is a stronger elicitor of immune signalling than flg22 or the chitin heptamer. *PLOS ONE* *12*, e0185808.
- Ride, J.P. (1975). Lignification in wounded wheat leaves in response to fungi and its possible rôle in resistance. *Physiol. Plant Pathol.* *5*, 125–134.
- Sarkar, A.K., Luijten, M., Miyashima, S., Lenhard, M., Hashimoto, T., Nakajima, K., Scheres, B., Heidstra, R., and Laux, T. (2007). Conserved factors regulate signalling in *Arabidopsis thaliana* shoot and root stem cell organizers. *Nature* *446*, 811–814.
- Wyrsh, I., Domínguez-Ferreras, A., Geldner, N., and Boller, T. (2015). Tissue-specific FLAGELLIN-SENSING 2 (FLS2) expression in roots restores immune responses in *Arabidopsis fls2* mutants. *New Phytol.* *206*, 774–784.
- Yuan, M., Jiang, Z., Bi, G., Nomura, K., Liu, M., He, S.Y., Zhou, J.-M., and Xin, X.-F. (2020). Pattern-recognition receptors are required for NLR-mediated plant immunity. *BioRxiv* 2020.04.10.031294
- Zhou, F., Emonet, A., Dénervaud Tendon, V., Marhavy, P., Wu, D., Lahaye, T., and Geldner, N. (2020). Co-occurrence of Damage and Microbial Patterns Controls Localized Immune Responses in Roots. *Cell* *180*, 440-453.e18.

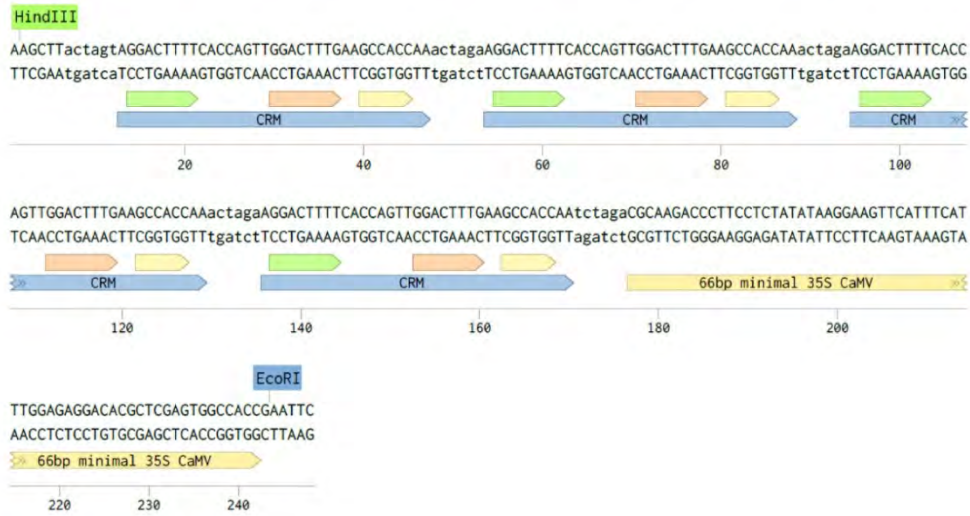
3.7. SUPPLEMENTAL TABLES

Supplemental Table 1: Primers for *fls2* genotyping and 4CRM cloning

Code	Sequence (5'-3')	Description	Type
oAE017	GTCTTGGCCTTTTCACATCC	T-DNA genotyping <i>fls2</i> SALK_062054C LP	F
oAE005	AAGCGACTTAAGGCTTGACAG	T-DNA genotyping <i>fls2</i> SALK_062054C RP	R
oAE003	ACTTAATCGCCTTGACGAC	T-DNA genotyping <i>fls2</i> SALK_062054C LB	F
oAE021	ACATGTCCGGTACTATCGCAG	T-DNA genotyping <i>fls2</i> SAIL_691C4 LP	F
oAE022	TCCATCAAGACAGCTAATGAGC	T-DNA genotyping <i>fls2</i> SAIL_691C4 RP	R
oLAB012	GCCTTTTCAGAAATGGATAAATAG CCTTGCTTCC	LB1 for SAIL lines	F
oAE074	ATGGGTCAAGATGAGGTTGTCC	<i>fls2</i> SAIL genotyping for complemented lines LP	F
oAE075	GCTTCGGTTTGGGCAATCTC	<i>fls2</i> SAIL genotyping for complemented lines	F
oAE102	AACMGGATTAGATACCKG	amplification 16S for bacteria identification	F
oAE103	ACGTCATCCCCACCTTCC	amplification 16S for bacteria identification	R

Supplemental Table 2: Synthetic promoter *4CRM* and *4CRM_{mod}* sequences

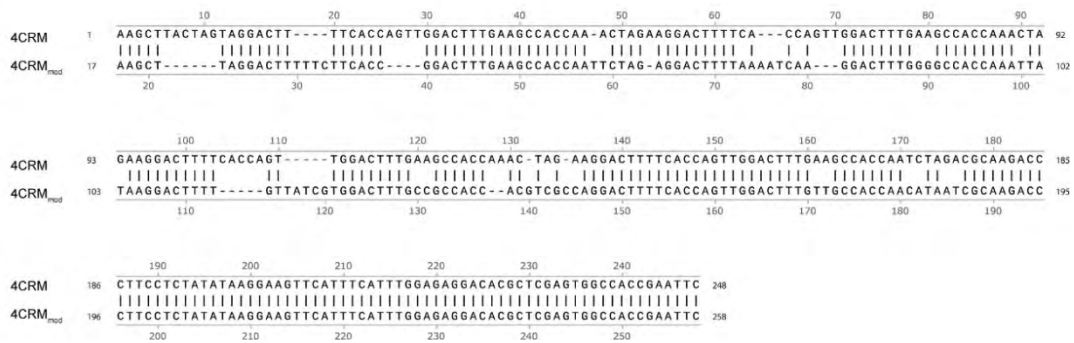
A *4CRM* promoter



B Modified *4CRM* promoter



C



(A) Sequence for *4CRM* promoter

(B) Sequence for *4CRM_{mod}* promoter

(C) Comparison of *4CRM* and *p4CRM_{mod}* sequences

4 INTERACTIONS BETWEEN THE RHIZOSPHERE AND *WER::FLS2* IMMUNE SUPER-COMPETENT LINE

4.1. CONTRIBUTIONS

Gnotobiotic experiments (FlowPot and calcine clay systems) presented in this chapter were done in collaboration with the group of Prof. Paul Schulze Lefert during a short-term internship in the *Max Planck Institute for Plant Breeding Research*. Bacterial community design was carried out together with Ruben Garrido-Oter. FlowPot and calcined clay systems were assembled, and roots collected with the help of Ka-Wai Ma. Bioinformatic analyses was done by Rui Guan. I performed all other experiments.

4.2. INTRODUCTION

4.2.1. BACTERIAL MICROBIOME: KEEPING FRIENDS CLOSE

Bacteria represent a large part of the dense root microbial community. For comparison, the rhizosphere contains 10^6 to 10^9 bacteria by gram of soil, whereas the phyllosphere (*i.e.* microbial community on the leaf surface) bacterial content reaches only 10^6 to 10^7 cells by cm^2 (Bulgarelli *et al.*, 2013; Lindow and Brandl, 2003). In contrast to other phyla, the bacterial community composition has been intensively studied during the past decades, revealing a very conserved structure across plant species. The development of metagenomic technics, culture collections and the reconstitution of synthetic communities in controlled laboratory conditions also improved our understanding of the function of specific taxa (Bai *et al.*, 2015; Busby *et al.*, 2017).

The bacterial community is particularly appropriate to understand how plants balance growth and defence, because it is mostly composed of commensal and beneficial strains. Indeed, very few root-associated bacterial pathogens (*Erwinia*, *Rhizomonas* and *Ralstonia* spp. mostly) are reported in comparison with fungi (Koike *et al.*, 2003). Moreover, bacteria are required to keep in check opportunistic pathogens. Indeed, fungi or oomycetes, isolated from healthy asymptomatic plants, have a strong detrimental impact on plant growth if bacteria are absent from the community (Durán *et al.*, 2018). Interestingly, it is precisely PRRs recognizing bacteria-derived MAMPs, such as flg22 and elf18, that are absent or lowly expressed in the roots, suggesting that plants limit their immune responses to bacteria (Millet *et al.*, 2010). More than for any other phyla, roots must keep their immune responses under control to retain bacteria in close proximity.

4.2.2. PLANTS ACTIVELY RECRUIT THEIR BACTERIAL MICROBIOME

The soil contains an extremely rich community of bacteria, with estimates going from 10000 to 50000 different species by gram of soil (Dance, 2008; Roesch *et al.*, 2007). However, this variety drops down in the rhizosphere, indicating that only a fraction of the soil bacteria can effectively colonize roots (Bulgarelli *et al.*, 2012; Lundberg *et al.*, 2012). Root exudates, constituted of mucilage, sugars, amino acids, organic and inorganic ions, and many secondary metabolites, play a major role in the recruitment of the root microbiota. Indeed, accessible organic nutrients are limited in the soil, and organotrophic bacteria are

inevitably attracted by the accumulation of rhizodeposits (Bulgarelli *et al.*, 2013). Moreover, root border-like cells are characterized by high secretory activity and provide an additional source of carbon once dead (Bulgarelli *et al.*, 2013; Kumpf and Nowack, 2015). Interestingly, 40% of the rhizosphere bacteria of *A. thaliana* can be recruited on wooden splinters, suggesting that a large part of the microbiome is actually constituted of lignocellulosic matrix-associated saprophytic microbes, non-specific to *Arabidopsis* (Bulgarelli *et al.*, 2012).

Although the taxonomic structure of the rhizosphere at the phyla level is robust and determined by root compartments, subtle differences in root assemblage are principally defined by, in order, soil types, plant species/genotypes and plant age (Durán *et al.*, 2018; Hacquard, 2016; Hacquard *et al.*, 2017; Lundberg *et al.*, 2012; Thiergart *et al.*, 2020). Interestingly, root microbiome is different between seedlings and mature plants, *Actinobacteria* and *Bacteroidetes* decreasing and increasing, respectively, over time (Chaparro *et al.*, 2014). Accordingly, root exudates also change depending on plant age. Young plants produce principally sugars and sugar alcohols, whereas older plants excrete amino acids and phenolics compounds (Chaparro *et al.*, 2013).

4.2.3. PLANT GENOTYPES INFLUENCE THE MICROBIOME COMPOSITION

Mutants and transgenic lines with altered exudates production also recruit different rhizosphere communities. *Arabidopsis* lines overexpressing the sorghum *CYP79A1* gene produce higher amount of aliphatic glucosinolates and their microbiome differs in the relative abundance of *Alphaproteobacteria* and *Acidobacteria* (Bressan *et al.*, 2009). Similarly, the *abcg30* mutant recruits more PGPRs than wild-type plants due to increased phenolics and reduced sugars excretion (Badri *et al.*, 2009). Coumarins have well-known antimicrobial properties and were recently shown to alter the rhizosphere composition (Stringlis *et al.*, 2019a). Indeed, the scopoletine biosynthesis mutant *f6'h1* (*feruloyl-coa 6-hydroxylase1*) was less colonized by bacteria able to hydrolyse coumarins (Stringlis *et al.*, 2018b) but hosted more coumarin-sensitive *Pseudomonas* strains (Voges *et al.*, 2019).

Plant nutritional status also affects the bacterial community. Thus, mutants defective in the phosphate starvation response have an atypical bacterial microbiota structure (Castrillo *et al.*, 2017). Plants subjected to iron deficiency have increased

scopolectine exudation, leading to changes in the microbiome composition (Stringlis *et al.*, 2018b).

Mutants with disrupted hormonal pathways also present an altered microbiome. The immune-compromised quadruple mutant *dde1 ein2 pad4 sid2*, lacking all three phytohormonal signalling pathways (SA, JA and ET), hosts a bacterial assemblage with lower alpha-diversity compared to wild-type plants. Salicylic acid was shown to have the strongest impact (Lebeis *et al.*, 2015). Moreover, the rhizosphere structure in the JA-signalling *myc2* mutant was also shown to be significantly different from wild-type plants (Carvalhais *et al.*, 2013, 2015).

4.2.4. MTI AS SELECTIVE PRESSURE FOR THE RECRUITMENT OF AN ADAPTED MICROBIOME

It was recently proposed that MAMP-triggered immunity could be used by the plant to select for non-immunogenic microbial interactors. In this way, non-adapted microbes would be detected and induce a strong immune response, preventing their establishment in the rhizosphere, while adapted ones would escape recognition or suppress defences, and successfully colonize the roots.

This concept is supported by the fact that only a subfraction of the microbiota harbours recognizable MAMP epitopes. Indeed, 6.25% of *Arabidopsis* bacterial isolates possess the predicted detectable flg22 sequence and 2.55% the elf18 sequence (Garrido-Oter *et al.*, 2018; Hacquard *et al.*, 2017). By contrast, the CSP elicitor binding to CORE receptor, absent of the *Arabidopsis* genome, is expressed by most *Arabidopsis* root bacteria (Hacquard *et al.*, 2017; Wang *et al.*, 2016). MAMPs have sometimes diverged from their canonical sequences and escaped recognition by their cognate receptors (Felix *et al.*, 1999; Gómez-Gómez *et al.*, 1999; Hind *et al.*, 2016; Pfund *et al.*, 2004; Sun *et al.*, 2006) (see Chapter 5). Interestingly, McCann *et al.* (2012) used this property to discover new elicitors by computational analysis, searching the microbiome for variable regions within very conserved bacterial genes. Species-specific microbiome could also be shaped by MTI responses, since many PRRs are specific to a given plant family. Thus, the EFR and LORE receptors are only found in *Brassicaceae*, while FLS3 is specific to *Solanaceae* (Hind *et al.*, 2016; Ranf *et al.*, 2015; Zipfel *et al.*, 2006).

Likewise, plants could be preferentially colonized by bacteria able to suppress MTI (see Chapter 5) (Yu *et al.*, 2019b). Thus, on 28 commensal strains tested, Yu *et al.* (2019a) not only found that the majority (23 strains) did not induce immune transcriptional read-outs, but they also observed that 42% of their samples could suppress flg22 responses. Similarly, 41% of the tested At-RSPHERE bacterial culture collection could inhibit flg22-mediated root growth inhibition in mono-association (Garrido-Oter *et al.*, 2018; Ma *et al.*, 2020). Small synthetic communities (SynComs), composed of five of these suppressive strains, also suppress part of the immune transcriptional responses induced by flg22. Moreover, the mutants *P. capeferrum* strain WCS358, which lost their suppressive ability, were shown to colonize less well the rhizosphere (Yu *et al.*, 2019a).

Induction or suppression of MTI responses also appears to affect the rhizosphere composition. For example, flg22 treatment slightly changes the bacteria relative abundances in a simple, non-suppressive synthetic rhizosphere community. In addition, plants grown with a suppressive SynCom were more susceptible to opportunistic pathogens, which reach a higher relative abundance in the community (Ma *et al.*, 2020).

We only start to understand how MTI influences the recruitment and the composition of the rhizosphere microbiota. In the previous two chapters, we showed that defence activation was spatially controlled by plant roots and that ectopic immune responses can impact meristem activity (Emonet *et al.*, 2020; Zhou *et al.*, 2020). However, we do not know if super-competent lines, as *WER::FLS2*, are also affected in non-sterile soil, which contains a complex consortium of microorganisms including MTI suppressive and non-eliciting bacteria. It is indeed not understood whether spatially restricted defences are necessary for maintaining plant growth in natural conditions. Moreover, ectopic PRR expression effect on bacterial community structure was not investigated so far. Therefore, using natural soil as well as different gnotobiotic systems (*i.e.* environment where all microorganisms are known and controlled), I assessed the effect of natural and synthetic bacterial communities on the growth of plants expressing *FLS2* ectopically. In addition, I analysed the microbiome composition of *WER::FLS2* using 16S rRNA gene amplicon surveys.

4.3. RESULTS

4.3.1. ECTOPIC EXPRESSION OF *FLS2* DOES NOT AFFECT GROWTH ON NATURAL SOILS

To observe the biological impact of *FLS2* misexpression in natural conditions, I grew several *prom::FLS2* lines on non-sterile, peat-based soil for four weeks. In contrast to seedlings inoculated on plates with single bacteria, all recombinant lines grew similarly, and none presented a significant difference in shoot or root weight (Fig.1A and 1B). When *WER::FLS2* and wild-type plants were grown on natural CAS soil in Cologne (Fig.S1A), *WER::FLS2* plants had surprisingly higher biomass than wild-type, but this effect was also sometimes observed on plates due to difference in seed quality.

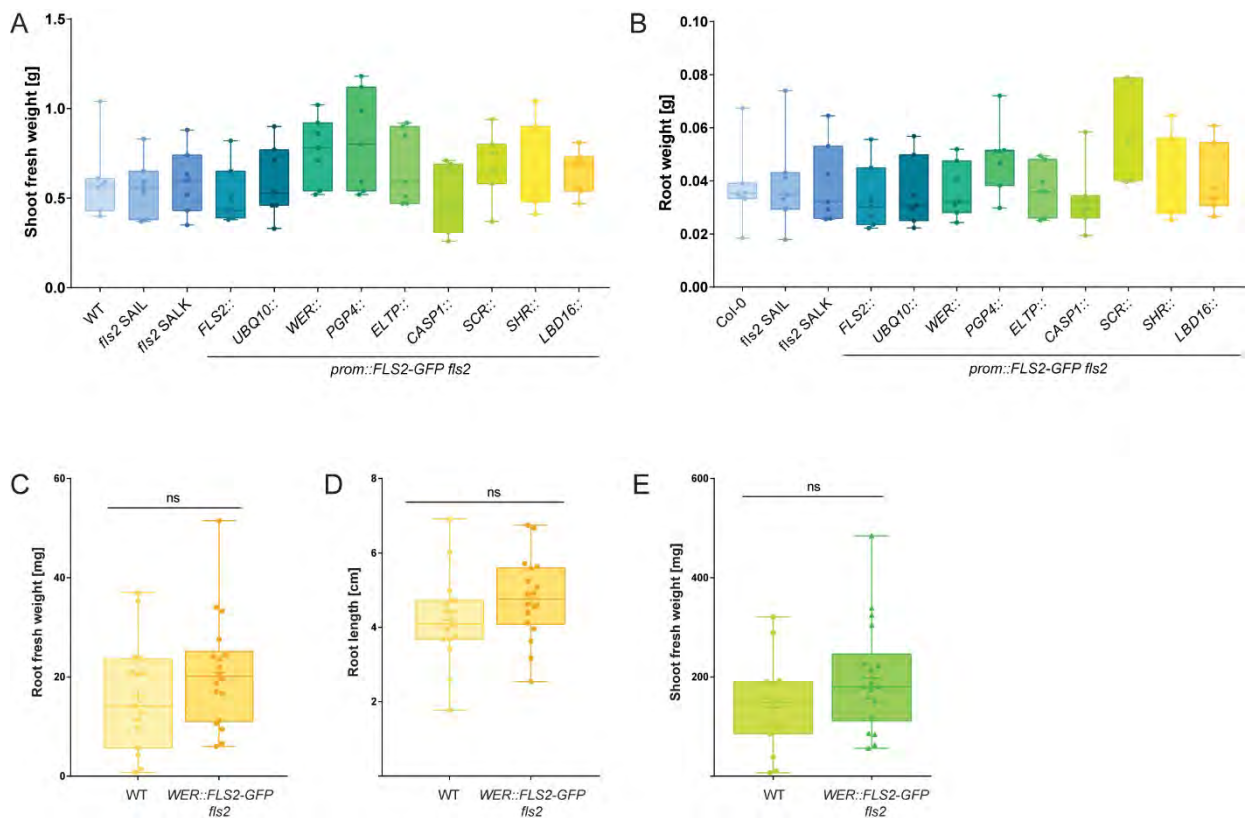


Figure 1: Ectopic expression of *FLS2* does not affect growth on non-sterile soil

(A) Shoot fresh weights and (B) root weights are not significantly different between wild-type plants and *prom::FLS2-GFP fls2* lines grown on non-sterile peat-based soil. Fresh weights were measured at 4 weeks. Multiple comparison was performed using Kruskal-Wallis and Dunn's test. No statistically significant difference was found between all samples (p -value < 0.05).

(C-E) WT and *WER::FLS2-GFP fls2* plants have similar root fresh weight (C), root length (D) and shoot fresh weight (E) when grown on non-sterile coarse sand. Binary comparisons were performed using Student t-tests. Ns, non-significant.

Roots of plants grown on natural soil are difficult to wash without breaking them. It is therefore possible that small differences in root length or weight are overlooked. Moreover, shoot weight is not the ideal proxy to assess flg22-mediated growth inhibition since flg22 does not alter *WER::FLS2* shoot growth on plate (Emonet *et al.*, 2020). To find a substrate enabling easy root harvesting, I grew wild-type plants and *WER::FLS2* lines in parallel on several soil types: fine compost soil, fine and coarse sands and clay pellet substrate (Serami), used separately or in combination (Fig.S1C). Roots were easily washed in sand substrates or Serami, but not in fine soil. Moreover, *Arabidopsis* grew badly on that medium. The mix of substrates did not provide any advantage compared to pure one.

Then, I measured root fresh weight for fine sand, coarse sand and Serami (Fig.S1B). There was no significant difference between wild-type and *WER::FLS2* for the three substrates, confirming previous results (Emonet *et al.*, 2020). Despite variability in growth and required nutrient supplementation, the ease with which roots can be isolated from sand makes it a promising candidate to replace peat-based soil. As plants growing in coarse sand looked healthier than in fine sand, I analysed in more details their root development. Root fresh weight (Fig.1C), root length (Fig.1D) or shoot fresh weight (Fig.1E) were similar between wild-type and *WER::FLS2*. Taken together, despite its increased sensitivity to flg22 on plates, *WER::FLS2* grows as wildtype on any non-sterile substrate, suggesting that the rhizosphere community must be adapted to escape or suppress immune response. Alternatively, differences in development might be too small to be detected on mature plants.

4.3.2. SINGLE BACTERIA INOCULATION IN GNOTOBIOTIC SYSTEM DOES NOT INCREASE ROOT GROWTH INHIBITION OF *WER::FLS2*

The *Pseudomonas* strain R569 was previously shown to induce a strong root growth inhibition on *WER::FLS2* (Emonet *et al.*, 2020). I reasoned that, in contrast to a complex natural microbiota, the inoculation of soil substrate with this single strain should affect *WER::FLS2* more strongly than wild type. Accordingly, this phenotype should be rescued with an assemblage of bacteria. In collaboration with the group of Prof. P. Schulze-Lefert, I used two different methods for the controlled inoculation of a single bacterial strain and a synthetic community on sterile substrate: the FlowPot (Kremer *et al.*, 2018) and the

calcined-clay systems. The FlowPot system has the advantage to rely on sterilized natural soil, allowing better plant growth and inoculation with fungi. However, roots are more difficult to harvest. In contrast, plants grown in calcined clay can be easily collected, but the system is more artificial.

Using these two methods, wild-type plants, *WER::FLS2* line and *fls2* mutants (only for FlowPot) were inoculated with a mock, the single bacterial isolate R569 or a complex synthetic community (SynCom) of 97 distinguishable strains of the At-SPHERE culture collection. Inoculation with the SynCom tends to increase shoot and root biomass in the FlowPot system (Fig.2A and 2B), as previously reported (Durán *et al.*, 2018). However, no significant difference between the three genotypes was observed for the three treatments, for both systems (Fig.2A, 2B, 2D, 2E, S2B). Therefore, *WER::FLS2* development is not affected in presence of the R569 isolate on soil, despite the strong effect observed on seedlings grown on plates. Nevertheless, shoot biomass of all genotypes were non-significantly reduced after R569 treatment on calcined clay (Fig.2D). This difference becomes significant when shoot biomasses are combined by magenta box (Fig. S2C). Similarly, R569 causes stronger leaf necrosis than mock or SynCom treatment in FlowPots (Fig.2C). Although *WER::FLS2* was more affected than wild-type in the first replicate, this results could not be reproduced in a second replicate done in Lausanne. Taken together, growth is increased when plants are inoculated with a complex SynCom, while inoculation with the isolate R569 tends to be deleterious for all genotypes, in opposition with our results on plates (Emonet *et al.*, 2020).

One of the main differences between plants grown on soil or on plates is their developmental stage. To test whether the increased competency of *WER::FLS2* seedlings was dependent on age, I grew 1-week-old seedlings on calcined clay in 6-well plates and inoculate them with mock, R569 and flg22 as positive control. However, seedlings had variable germination rates. After six days of treatment, root lengths were not significantly different between mock, R569 and flg22 treatment (Fig.S2D). In view of the strong effect of flg22 on plates, these results were surprizing. Flg22 might be adsorbed by the clay so that only few peptides reached the root.

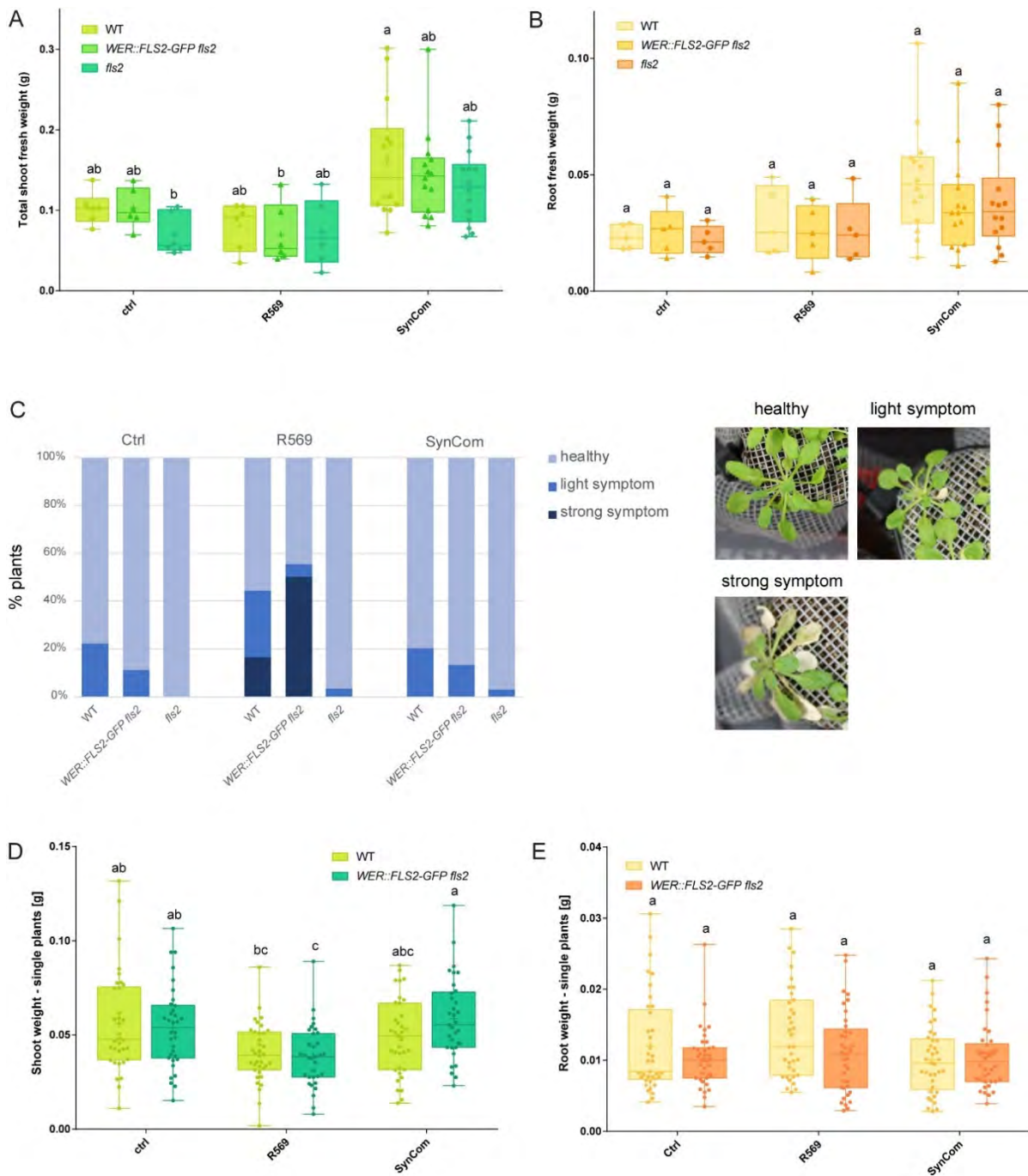


Figure 2: Bacterial inoculation in gnotobiotic system does not increase root growth inhibition on *WER::FLS2*

(A-B) Inoculation of WT, *WER::FLS2-GFP fls2* and *fls2* lines with the single strain R569 or a complex 97-members SynCom in FlowPot axenic system. SynCom inoculation tends to increase shoot (A) and root (B) biomass in all genotypes. Root and shoot weights were combined by FlowPot. No significant difference was observed across genotypes. Samples were harvested five weeks after inoculation.

(C) Inoculation with a single strain of R569 bacteria induces necrotic symptoms on WT and *WER::FLS2-GFP fls2*. Same experiment as in (A) and (B). Examples of healthy plants, light and strong symptoms are represented.

(D-E) Inoculation of WT and *WER::FLS2-GFP fls2* line with the single strain R569 or a complex 97-members SynCom in calcined clay axenic system. Inoculation with the single strain R569 tends to decrease shoot biomass (D) but does not affect root weight (E). Samples were harvested seven weeks after inoculation. Root and shoots weights were measured individually.

(A, B, D, E) Multiple comparisons were performed using Kruskal-Wallis and Dunn's test. Different letters indicate statistically significant differences ($p < 0.05$).

4.3.3. MICROBIOME COMPOSITION IS NOT SIGNIFICANTLY AFFECTED BY *WER::FLS2*

Since R569 and SynCom inoculations did not affect *WER::FLS2* growth, I analysed whether *WER::FLS2* could, in turn, modify the rhizosphere community composition to avoid strong MTI responses. The SynCom used in the previous experiments was designed to represent the natural microbiome of *A. thaliana* plants. Moreover, the 97 selected strains represent different Operational Taxonomic Units (OTU) with distinct 16S RNA sequences (Table S1), whose relative abundance could be assessed by 16S sequencing. Bacterial DNA was collected from three compartments: input culture, matrix (*i.e.* soil not touching the root) and root. Three biological replicates were inoculated in parallel with separately grown SynComs. Examining between samples variation, bacterial communities cluster according to compartments (Fig.3A), as previously observed (Bulgarelli *et al.*, 2012; Lundberg *et al.*, 2012). The input community was highly different from the matrix and root communities, but the three biological replicates were grouped together, indicating that replicates were comparable (Fig.3B). However, the bacterial communities were similar between genotypes (Fig.3C). Therefore, ectopic *FLS2* expression is not sufficient to alter the root bacterial community.

Principal-component analyses (PCoA) can overlook little differences in community composition. Thus, I compared the relative abundance of single OTUs previously shown to increase root growth inhibition of *WER::FLS2* (Chapter 2). Interestingly, R569 abundance tends to decrease slightly, but not significantly, in the root compartment of *WER::FLS2* compared to wild-type and *fls2* mutant (Fig.3D). By contrast, R569 relative abundance in matrix is similar between the three genotypes. R569 colonization might be impaired in *WER::FLS2* due to strong *flg22*-driven immune responses or because of competition with more adapted bacteria. However, the relative abundance of isolates *Pseudomonas* R9, *Achromobacter* R170 and *Sphingomonadaceae* R154 did not significantly change between genotypes (Fig.3E, 3F, 3G).

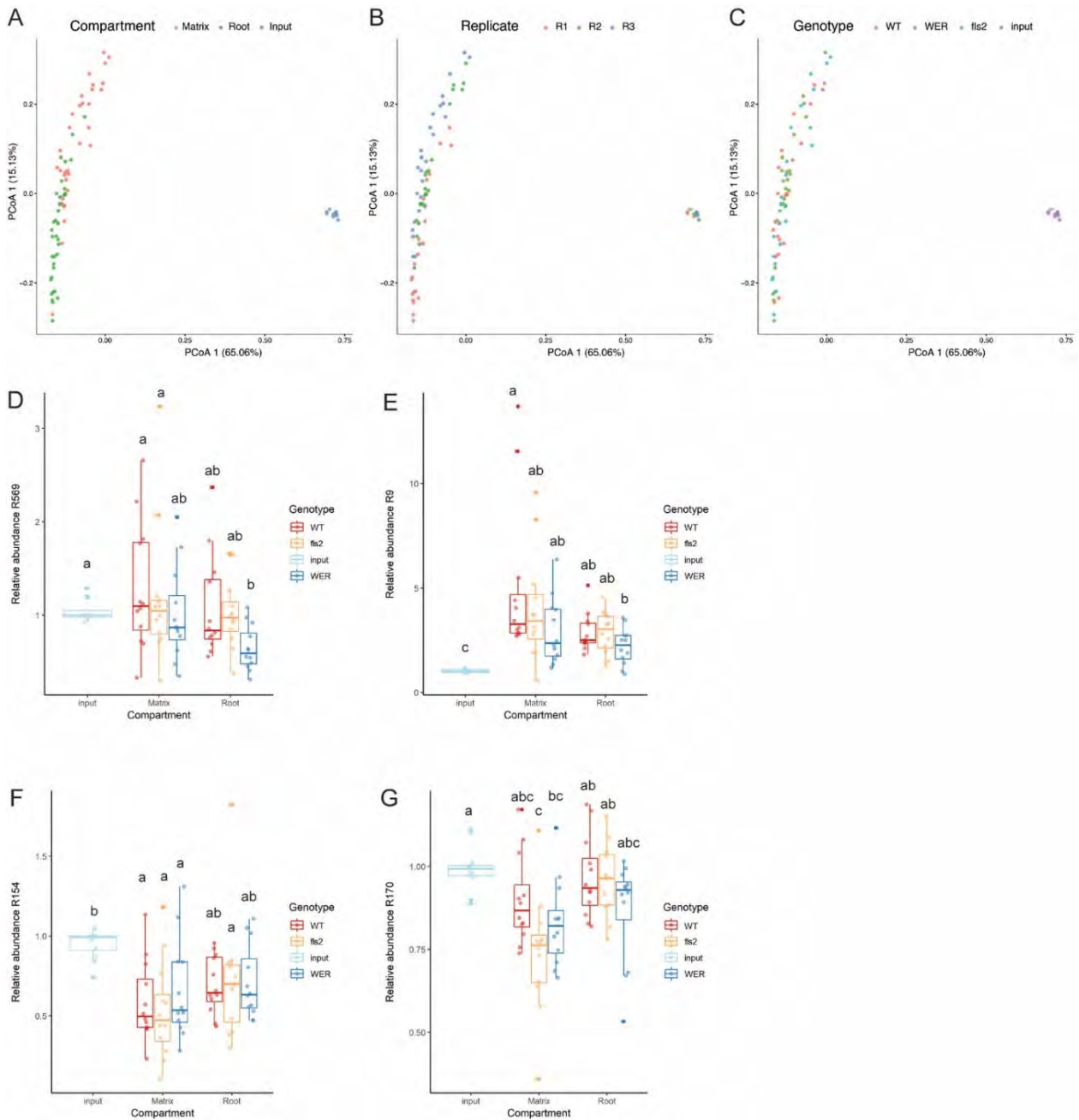


Figure 3: *WER::FLS2* does not affect the microbiome composition significantly

(A-C) Analysis of the community structure of plants inoculated with a complex SynCom in a FlowPot system. Community structure was determined using principal-component analysis. The first two dimensions of the PCoA are plotted based on Bray-Curtis distances. Samples are colour-coded according to compartments (A), replicates (B) and genotypes (C). (D-G) Relative abundances of strains R569 (D), R9 (E), R154 (F) and R170 (G) in the synthetic community inoculated on WT (*Col-0*), *fls2* mutant or *WER::FLS2-GFP fls2* (*WER*). Input represents samples of start inoculum solution. Multiple comparison analyses were performed using Kruskal-Wallis and Dunn's test. Different letters indicate statistically significant differences ($p < 0.05$).

4.4. DISCUSSION

4.4.1. RHIZOSPHERE BACTERIA SUPPRESS MTI RESPONSES IN *WER::FLS2*

Ectopic expression of *FLS2* was not only shown to alter the spatial pattern of immune responses, but could also drastically impact root growth in response to flg22 or commensal bacteria if driven in the meristematic epidermis. However, none of the tested *prom::FLS2* lines, including *WER::FLS2*, showed any growth phenotype on any non-sterile substrates tested, suggesting that the natural bacterial community can either prevent or suppress MTI responses induction.

We had originally planned to assess the suppressive ability of the root community by inoculating *WER::FLS2* plants with the *Pseudomonas* strain R569, which had a strong effect on plates, and a synthetic community representing the microbiome constitution. Unfortunately, the fact that inoculations in mono-association with R569 could not induce root growth inhibition (RGI) in all gnotobiotic systems prevents us to conclude that the rhizosphere community can effectively suppress MTI responses.

However, Ma *et al.* (2020) used *WER::FLS2* to identify bacteria that reduce flg22-mediated RGI. Many of their suppressive candidates were part of our 97-member SynCom and may have suppressed *WER::FLS2* line's strong response, potentially explaining why *WER::FLS2* growth was similar to wildtype in FlowPot and calcined clay systems. Flg22-response suppression was also observed independently in the *Sphingomonadales* R1497, also included in our SynCom (Garrido-Oter *et al.*, 2018). Interestingly, the inhibitory effect of suppressive strains was reported to be dominant, so that a combination of both suppressive and non-suppressive bacteria can inhibit flg22-responses (Ma *et al.*, 2020). Consequently, the absence of *WER::FLS2* response to a complex bacterial community might be due to suppression by the plant microbiota.

Many mechanisms could be responsible for MTI response suppression, and will be discussed in Chapter 5. However, this shows that the very strong competency of *WER::FLS2* can be easily overridden by the combined effects of the root microbiota, indicating that bacteria play a large role in the avoidance of MTI over-activation.

4.4.2. IMPACT OF THE CULTURE SYSTEM

Although strong root growth inhibition could be observed after inoculation of *Pseudomonas* R569 on agar plates, the same phenotype could not be recapitulated in any gnotobiotic system. These contradicting results highlight the importance of growth conditions and experimental methods to study plant immune responses. Why R569 bacteria cannot increase root growth inhibition on *WER::FLS2* was nevertheless puzzling.

Difference in root development could be too subtle to be detected. Indeed, R569 inoculation on plate reduces the growth of the primary root but also seem to increase the number of lateral roots. However, root biomass is also affected by R569 on plates and should be an accurate proxy for root growth inhibition (data not shown). The difference might also be compensated over the plant development, the root being desensitised after prolonged exposure to bacteria, as observed for flg22 (Smith *et al.*, 2014). Although I tried to analyse younger seedlings grown on calcined clay (Fig.S2D), the initial growth variability prevents to draw any conclusion. The experiment should be repeated on a more reliable substrate to rule out the influence of plant age.

Alternatively, depending on conditions, *Pseudomonas* R569 might partially suppress, or avoid, flg22-triggered immune responses. By contrast to our observation, Ma *et al.* (2020) characterized R569 as a “suppressive strain”. They reported that R569 reduces flg22 and Atpep1-driven growth inhibition. Therefore, it would be judicious to use a strictly non-suppressive strain, like *Pseudomonas* R9, which was also shown to induce strong root growth inhibition on *WER::FLS2* (Emonet *et al.*, 2020).

Finally, the substrate might prevent the proper perception of flg22. Indeed, even flg22 treatment on calcined clay did not affect wild type nor *WER::FLS2* growth. Many parameters could impair flg22 recognition: MAMPs could stay stuck against soil particles and be too lowly abundant to reach the root. Bacteria might also form biofilms where they no longer produce any flagellin proteins (Castiblanco and Sundin, 2016).

Taken together, it appears that the natural substrate used for synthetic community reconstruction must be carefully chosen. Ideally, it should allow an easy root phenotyping and could be suitable for microscopic analysis of MTI reporters. Such system should meet the following criteria: 1) permit a robust and reproducible growth 2) allow the retrieval of

perfectly clean roots with minimum damages, ensuring unbiased weight and length measurement, and microscopic image acquisition, 3) be easily sterilized, 4) be easily colonized by bacteria, 5) reproduce root growth inhibition in response to flg22 and 6) reproduce bacterial-triggered root growth inhibition. A summary of the different tested substrates is found in Table 1.

Table 1: Summary of the characteristics of the different tested substrates

Criteria	Robust growth (1)	Clean Roots (2)	Sterile (3)	Inoculation (SynCom) (4)	RGI after flg22 (WER) (5)	RGI after single bacteria (WER) (6)	Natural substrate	Standard Growth Conditions	References
0.5MS + MES	ok	ok	ok	ok ^a	ok	ok	no	ok	Chapter 3; 5
0.5MS	ok	ok	ok	ok ^a	ok	ok	no	ok	Chapter 5
Calcined clay - 6WellPlate	no	ok	ok	ok	no	no	no	wet ^d	Chapter 4
Calcined clay - MagentaBox	ok	ok	ok	ok		no	no	wet ^d	Chapter 4
FlowPot	ok	no	ok	ok		no	ok	wet ^d	Chapter 4
Peat-based soil	ok	no	ok	ok		no	ok	ok	Chapter 4
Serami	ok	ok	ok ^c				no	ok	Chapter 4
Fine soil	no	no	ok ^c				ok	ok	Chapter 4
Fine sand	no	ok	ok ^c				ok	ok	Chapter 4
Coarse sand	no	ok	ok ^c				ok	ok	Chapter 4
Mix fine + coarse sand	ok ^b	ok	ok ^c				ok	ok	Chapter 4

^a maximum 5 strains

^b not optimal

^c not yet tested but should be possible

^d growth conditions very humid

So far, none of the tested substrates ticked all the boxes, but sand might be promising after some optimisation. This natural substrate would also permit to establish an adapted sand-specific microbial culture collection. Miebach *et al.* (2020) proposed also a zeolite-clay system for bacterial inoculation, although zeolite might be difficult to wash from the roots. Alternatively, hydroponic culture is frequently used for microbial inoculation, notably for root exudates analysis (Korenblum *et al.*, 2020), but conditions might be very different from plants grown on soil. Recently, hydrogel-based transparent soil, a porous medium more similar to soil than hydroponic systems, was proposed for root phenotyping

(Ma *et al.*, 2019). Transparent soil allows root imaging directly in the substrate and could be used as an intermediary step between agar plate culture and sterile soil system.

4.4.3. THE RHIZOSPHERE COMMUNITY STRUCTURE IS HARDLY IMPACTED BY PRRs LOCALISATION

According to the idea that MTI recruits an adapted microbiota (Hacquard *et al.*, 2017), we speculated that expressing *FLS2* ectopically might alter the composition of the microbiome. However, our 16S analysis revealed no significant difference between wild-type plants, *fls2* mutants and *WER::FLS2* lines. The R569 isolate, however, tends to have a lower relative abundance in the rhizosphere of *WER::FLS2* compared to wildtype. Though non-significant, it corroborates the impaired colonization of *CHA0* bacteria observed on the *UBQ10::FLS2* line, which also displays a super-competency to *flg22* (Zhou *et al.*, 2020). Unfortunately, the relative abundance of three other bacteria, which we characterised previously as capable to induce both immune read-outs and relative root growth inhibition (Emonet *et al.*, 2020, Ch.3. Ap.12BC), was not altered in *WER::FLS2*. It must be noted that, compared to R569, these isolates had already variable effects on plates, some of them inducing *WER::FLS2* root growth inhibition only in Cologne's conditions but not in Lausanne. This result highlights the robustness of our 97-member SynCom composition, probably caused by the large number of selected bacteria. Indeed, the more diverse the bacterial community, the more resilient it is to perturbation and pathogen invasion (van Elsas *et al.*, 2012; Hacquard *et al.*, 2017; Kennedy *et al.*, 2002). A smaller SynCom might have rendered the effect of mis-localized MTI responses more visible.

Such weak effect on the microbiome composition might be explained by several hypotheses. The first suggestion stems from the fact that our SynCom contains suppressive bacteria that will inhibit MTI responses. Consequently, WT and *WER::FLS2* lines, if equally affected, will both fail to mount part of their immune responses and will recruit similar community. Ma *et al.* (2020) indeed observed that, whereas *flg22*-treatment can shift the relative abundances of 5-member non-suppressive SynComs, suppressive SynCom community structures were unaffected.

Alternatively, changing the expression pattern of a single PRR might not be sufficient to affect the bacterial community. Indeed, *FLS2* is constitutively expressed in wild-

type roots, so that altering its expression pattern might not drastically impact the global root assemblage (Beck *et al.*, 2014; Faulkner and Robatzek, 2012; Robatzek *et al.*, 2006; Zhou *et al.*, 2020). It would be interesting to overexpress several PRRs in the super-competent meristematic epidermis to clearly unbalance immune responses, especially with PRRs not endogenously expressed in roots. Expressing EFR, normally restricted to the shoot (Faulkner and Robatzek, 2012; Millet *et al.*, 2010), in the root meristem might have more chances to alter the microbiota composition. Interestingly, interfamily transfers of PRRs were shown to confers resistance to pathogens (EFR in *Solanaceae* or *Medicago*, CORE in *A. thaliana* or LORE in tobacco) (Lacombe *et al.*, 2010; Pfeilmeier *et al.*, 2019; Ranf *et al.*, 2015; Wang *et al.*, 2016), suggesting that non-endogenous PRRs may also inhibit the growth of non-adapted commensals.

Finally, the lack of resolution of OTUs sequencing analyses may overlook local changes in community composition. Indeed, microbial community is not homogeneous (Cardinale *et al.*, 2015) and *FLS2* ectopic expression might have altered its composition only on restricted regions of the root. Nevertheless, the spatial resolution of metagenomic analyses can be improved when roots are sampled according to developmental regions (tip, root hair region or mature parts for example) (Bulgarelli *et al.*, 2013; DeAngelis *et al.*, 2009). It would be extremely interesting to assess the repartition of bacteria along the root in response to *FLS2* expression in different tissues. This would require a growth system allowing easy retrieval of clean roots. However, separation of the roots from the soil may alter the repartitions of bacteria, so that *in situ* confocal imaging might be convenient to avoid artefacts. Microfluidic systems prove to be useful to observe the accumulation of *Bacillus subtilis* at the root tip (Massalha *et al.*, 2017b). The rhizosphere community composition could also be visualized in hydrogel-based transparent soil (Ma *et al.*, 2019). Moreover, many bacteria and fungi can be visualized by fluorescent tags to follow their colonization routes (Czymmek *et al.*, 2007; Eynck *et al.*, 2007; Götz *et al.*, 2006; Hartmann *et al.*, 2019; Massalha *et al.*, 2017b; Miebach *et al.*, 2020; Oburger and Schmidt, 2016; Rothballer *et al.*, 2005). Simultaneous imaging of several strains would be crucial to decipher the repartition of bacteria in a community context. However, fluorochrome optical properties might limit the number of bacteria assessed at the same time and this technique requires the bacteria to be transformable. Alternatively, bacterial strains could be

monitored with Fluorescent In Situ Hybridization (FISH), labelling bacteria based on distinct DNA probes. FISH was used to characterize the spatial structure of the lettuce microbiome (Cardinale *et al.*, 2015). Interestingly, the authors also used the shape of bacteria to differentiate between strains of the same family.

Assessing the biological impact of spatial confinement of defences revealed to be more challenging than expected. Finding a system reproducing the results obtained in agar will be crucial to investigate the impact of ectopic PRRs on the growth-defence trade-off. Moreover, it would be difficult to assess the fine scale interactions occurring at the root surface by usual metagenomic analysis. Combination of gnotobiotic conditions, reduced synthetic community inoculation and high-resolution imaging will allow to decipher the spatial structure of rhizosphere community and assess the role of localized immune responses.

4.5. MATERIAL AND METHODS

4.5.1. PLANT MATERIAL AND GROWTH CONDITIONS

All experiments were performed with *A. thaliana* Columbia Col-0 ecotype. *Prom::FLS2-GFP fls2* (SAIL691_C04) were previously described (Emonet *et al.*, 2020; Wyrsh *et al.*, 2015). For natural soil analyses, plants were grown for four weeks on non-sterile peat substrate (GO PP7, Jiffy, Netherland), Serami (100% untreated clay, Serami GmbH, Germany), coarse (1-1.7 mm) and fine (0.3-0.9 mm) quartz sand (Carlos Bernasconi SA, Bern, Switerland), fine sieved soil (Substrate 167, Ricoter, Aarberg, Switzerland), or a mix of selected soils to the ratio 1:1, in Percival chambers under short day conditions (10h/14h light/dark). In Cologne, plants were grown on Cologne Agricultural Soil (CAS) in greenhouse. FlowPot and calcined clay systems were grown in light cabinet under short day conditions (10h/14h light/dark, 21°/19°C, 65% relative humidity).

4.5.2. SHOOT AND ROOT BIOMASS ANALYSIS

Shoots were collected with scissors, briefly dried with absorbing paper to remove water on leaves, then weighted. Roots were gently washed in a water bath to remove as much soil as possible without breaking them, dried with paper and weighted.

4.5.3. BACTERIAL SYNTHETIC COMMUNITY PREPARATION

Commensal bacterial strains were obtained from the At-SPHERE culture collection (Bai *et al.*, 2015). The synthetic communities were designed to encompass OTUs with specific 16S RNA sequences. A list of the 97 strains selected is found in Table S1.

For FlowPots inoculation, bacteria were cultured separately, directly from glycerol stock, in 96-deep well plates filled with 800 µL/well of half strength Tryptic Soy Broth (50% TSB) medium for seven days at 26° and 150 rpm. Bacteria were then again sub-cultured for five days in 1 ml fresh media at ratio 2:5 (400 µl bacteria culture + 600 µl fresh media). Three biological replicates of the SynCom were prepared. After incubation, deep well plates were centrifuged for 10 min at 4000 rpm, supernatants were discarded with the pipet and pellets were resuspended in 200 µl of 10 mM sterile MgCl₂ (for FlowPot) or CaCl₂ (for calcined clay system), then all 200 µl bacterial cultures were pooled together in a single 50 ml falcon tube. Optical density at 600 nm was measured and the concentration of the start

culture adjusted to $OD_{600} = 0.5$. For single inoculation with *Pseudomonas* R569, bacteria were first grown on 50% solid TSB then cultured in 10x 4 ml liquid 50% TSB until they reached saturation (5 days).

The same process was applied for calcined clay inoculation with SynCom. However, for timing reason, bacteria were sub-cultured twice, once for 9 days and once for 3 days, then pooled together as described previously.

4.5.4. FLOW-POT SYSTEM

FlowPot axenic growth system was set up following the modified protocol from Kremer *et al.* (2018). Briefly, 4,5 L of soil was obtained by mixing sieved peat to vermiculite in a ratio of 2:1, then wet with MilliQ water and autoclaved (25 min, liquid program). Soil was then leaved in the oven for 24 h, then moisten again with MilliQ water, autoclaved for 25 min and leaved in the oven for 24 h, then let rest on the bench at room temperature. FlowPot were mounted as follows, with sterile material. FlowPots, made of sterile 50 ml syringes with screw-end (Jensen Global, cat. no. JG50CC-LL), cut in half, were filled firstly with a single layer of sterile Soda-glass beads (2.5-3 g/FlowPot) (Sigma-Aldrich, cat. no. Z265926), then sterile soil until the top. The FlowPot was then closed with previously sterilized fibre glass mesh (8x8cm, product number 4.926.992, Windhager) and a cable binder. Five to six FlowPots were then fitted in a sterile Microbox (Combiness, USA, model TPD1600 with XXL with filter) whose bottom was covered by a tip holder placed upside down. The open box was then placed in a Sunbag (2boxes/bag) (Sigma-Aldrich, cat. no. B7026) closed with autoclaving tape. Boxes were then autoclaved for 45 min, then closed bags were let at room temperature for three days. On a clean bench, pots were then flushed with 50ml of previously autoclaved MilliQ water, using a syringe connected by a sterile tygon tube. FlowPots were then put back in their boxes, closed with the lid. Boxes were let stand overnight at room temperature on a clean bench. The next days, FlowPots were again flushed with 50 ml sterile $\frac{1}{2}$ MS solution supplemented with 200 μ l of bacterial start culture or mock. Around 20 sterile and pre-vernalized Col-0, *fls2* or *WER::FLS2-GFP fls2* seeds were sown by pot and the boxes closed. Samples for each genotype and treatment were separated in different boxes. In total, 72 FlowPots were inoculated with either mock, R569 bacteria alone, or one of the three biological replicates of the SynCom. A 2 ml-sample of start

inoculum (before dilution) was collected, centrifuged, its supernatant discarded then freeze at - 80°C. Plants were grown for five weeks in a light cabinet. After a week, extra seedlings were removed under sterile conditions to let only three seedlings by FlowPot. For phenotyping analyses, shoots were cut and weighted, then roots were carefully cleaned in sterile water with forceps and, after excess of water removed, weighted. Roots were then collected in Lysing Matrix E tubes and deep-frozen in liquid nitrogen for microbiome analysis (root samples). Additionally, residual soil that was not in contact with the roots were collected for each FlowPot (matrix samples).

4.5.5. CALCINED CLAY

Calcined clay with 5% vermiculite (80 g /magenta box) was washed several times with tap water (until the washing water turned clear), autoclaved (210°C, 20min) then dried for 2,5 weeks until completely dehydrated. Calcined clay was then mixed with 2/3 of volume of sterile soil (see FlowPot protocol) and used to fill pre-sterilized magenta boxes to one third of their volume before autoclaving. Magenta boxes were then dried for 1 day in an oven (80°C), then inoculated with 70 ml of sterile ½ MS supplemented with 1ml of bacterial start culture. Sterile and vernalized seeds were added at each corner of the box, then grow for seven weeks. After one weeks, extra seedlings were trimmed under sterile conditions to let only four seedlings by Magenta box. For analysis, shoots and roots were collected. Roots were washed in sterile water and samples weighted.

4.5.6. SIX-WELL PLATE CALCINED CLAY SYSTEM

For small scale inoculations in 6-well plates, each well was filled with 5 ml of sterile calcined clay. Then, 2.5 ml of ½ MS solution was pipetted in each well and the plates were shaken slightly sideway to distribute the solution (using a sterile cover whose inside was covered by an aluminium foil), before one seed by well was sown. After closing the lid with some micropore tape, seeds were vernalized for two days in the fridge, then grown for six days before seedling inoculation with R569 bacteria or flg22 treatment. For bacterial inoculation, R569 strain was grown overnight in 50% TSB, then the culture pelleted and washed with MgCl₂. Bacterial culture was then diluted in ½ MS to OD₆₀₀ = 0.05 (start culture). Finally, 200 µl of start culture was inoculated in each well. For flg22 treatment, 200

μl of 125 μM solution was added at the base of each seedlings. Plants were grown for six more days before harvesting and root length analysed.

4.5.7. DNA EXTRACTION AND LIBRARY PREPARATION

Microbial community profiling was performed as described previously with some modifications (Durán *et al.*, 2018). Briefly, total DNA was extracted using the FastDNA Spin Kit for Soil (MP Biomedicals, Solon, USA). Sample were homogenized in Lysis Matrix E tubes using Precellys 24 Tissue (Lyser Bertin Technologies, Montigny-le-Bretonneux, France) and DNA eluted in 80 μl nuclease-free water. DNA concentration was quantified using Quant-iT PicoGreen dsDNA Assay kit (Invitrogen), diluted to 3,5 $\text{ng}/\mu\text{l}$ and used for 2-steps PCR amplification. V5-V7 sequence of bacterial 16S rRNA was first amplified in triplicate (primers 799F - 1192R), then the amplicons digested by Antarctic phosphatase and Exonuclease I (New England BioLabs GmbH, Frankfurt, Germany) to remove primer sequences, single-stranded DNA and to degenerate enzymes. In a second PCR, 3 μl of PCR products were then barcoded with reverse primers including barcodes and Illumina adaptors (Table S2). Then, gel purification was carried out to remove plant-specific bands and primer dimers using QIAquick Gel extraction kit (Qiagen). After DNA fluorescent quantification with Picogreen, 100 ng of each PCR products were pooled together. The library was then purified twice with Agencourt AMPure XP (Beckman COULTER). DNA concentration was finally measured with Quantus Fluorometer and adjusted to 18 $\text{ng}/\mu\text{l}$. Paired-end Illumina sequencing was performed in-house with MiSeq sequencer and custom sequencing primers.

4.5.8. 16S rRNA GENE PROCESSING AND BETA-DIVERSITY ANALYSIS

Paired 16S rRNA amplicon sequencing reads were joined (join_paired_ends QIIME, default), then demultiplexed and quality filtered (split_libraries_fastq, QIIME, with max. barcode errors 1 and phred score of 30). Finally, demultiplexed sequences were concatenated. Reference-based OTU clustering was then performed using the UPARSE-REF algorithm and chimera removed. OTU table was then normalized using the cumulative-sum scaling (CSS) method (Paulson *et al.*, 2013) and fold changes compared to input calculated. Bray-Curtis distances between samples were used for principal coordinate analysis (PCoA, cmdscale function in R).

4.5.9. STATISTIC ANALYSES

Statistical analyses were carried out using R 3.6.0 or Graphpad Prism 7.0 softwares (<https://www.graphpad.com/>). Binary comparisons were performed with Student T-test. For multiple comparisons, ANOVA followed by Tukey's HSD tests were applied when linear model assumptions were met. On the contrary, a Kruskal-Wallis test followed by Dunn's multiple comparison test was performed.

4.6. LITERATURE

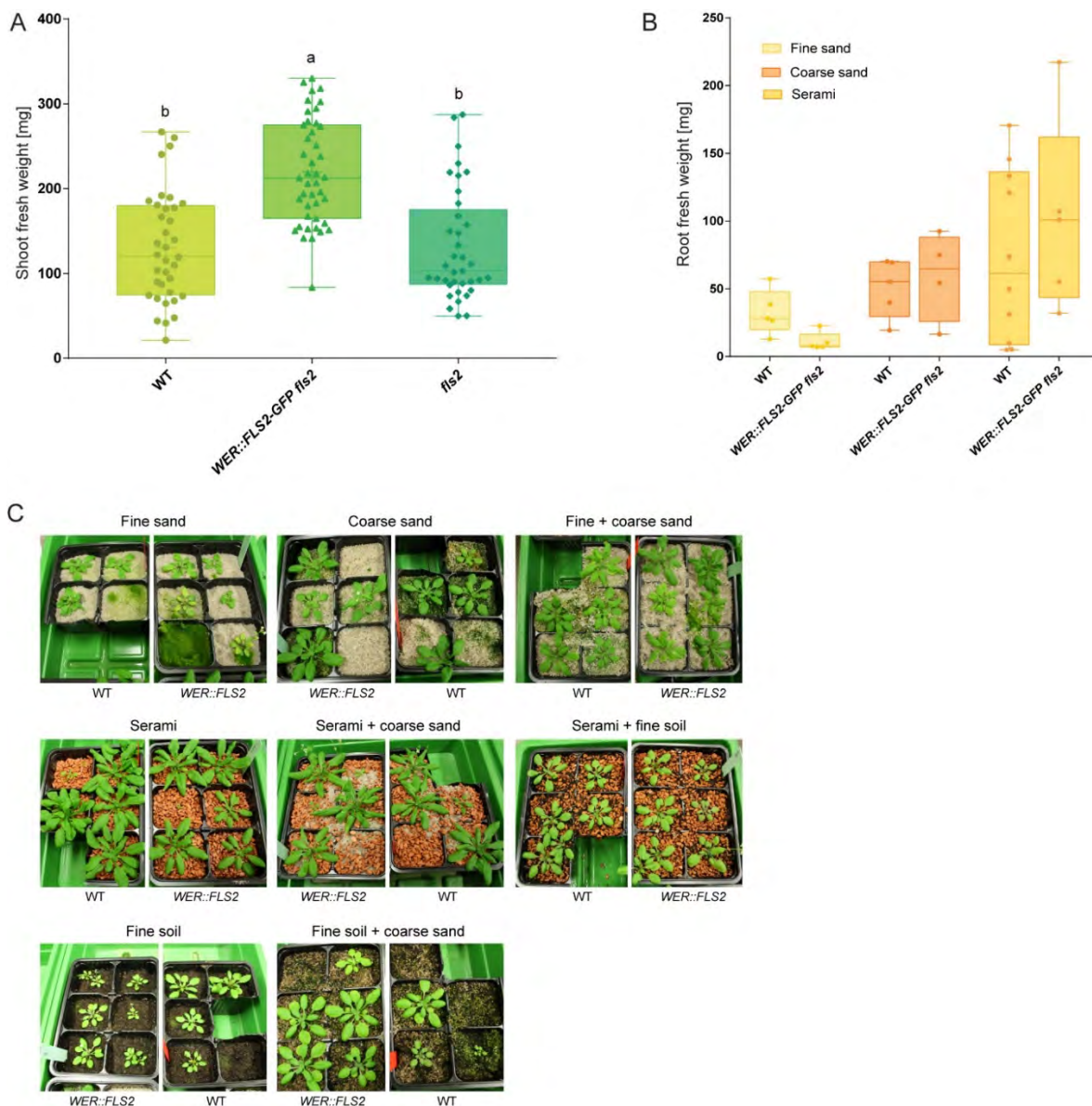
- Badri, D.V., Quintana, N., Kassis, E.G.E., Kim, H.K., Choi, Y.H., Sugiyama, A., Verpoorte, R., Martinoia, E., Manter, D.K., and Vivanco, J.M. (2009). An ABC Transporter Mutation Alters Root Exudation of Phytochemicals That Provoke an Overhaul of Natural Soil Microbiota. *Plant Physiol.* *151*, 2006–2017.
- Bai, Y., Müller, D.B., Srinivas, G., Garrido-Oter, R., Potthoff, E., Rott, M., Dombrowski, N., Münch, P.C., Spaepen, S., Remus-Emsermann, M., *et al.* (2015). Functional overlap of the *Arabidopsis* leaf and root microbiota. *Nature* *528*, 364–369.
- Beck, M., Wyrsh, I., Strutt, J., Wimalasekera, R., Webb, A., Boller, T., and Robatzek, S. (2014). Expression patterns of FLAGELLIN SENSING 2 map to bacterial entry sites in plant shoots and roots. *J. Exp. Bot.* *65*, 6487–6498.
- Bressan, M., Roncato, M.-A., Bellvert, F., Comte, G., Haichar, F. el Z., Achouak, W., and Berge, O. (2009). Exogenous glucosinolate produced by *Arabidopsis thaliana* has an impact on microbes in the rhizosphere and plant roots. *ISME J.* *3*, 1243–1257.
- Bulgarelli, D., Rott, M., Schlaeppi, K., Ver Loren van Themaat, E., Ahmadinejad, N., Assenza, F., Rauf, P., Huettel, B., Reinhardt, R., Schmelzer, E., *et al.* (2012). Revealing structure and assembly cues for *Arabidopsis* root-inhabiting bacterial microbiota. *Nature* *488*, 91–95.
- Bulgarelli, D., Schlaeppi, K., Spaepen, S., van Themaat, E.V.L., and Schulze-Lefert, P. (2013). Structure and Functions of the Bacterial Microbiota of Plants. *Annu. Rev. Plant Biol.* *64*, 807–838.
- Busby, P.E., Soman, C., Wagner, M.R., Friesen, M.L., Kremer, J., Bennett, A., Morsy, M., Eisen, J.A., Leach, J.E., and Dangl, J.L. (2017). Research priorities for harnessing plant microbiomes in sustainable agriculture. *PLOS Biol.* *15*, e2001793.
- Cardinale, M., Grube, M., Erlacher, A., Quehenberger, J., and Berg, G. (2015). Bacterial networks and co-occurrence relationships in the lettuce root microbiota. *Environ. Microbiol.* *17*, 239–252.
- Carvalhais, L.C., Dennis, P.G., Badri, D.V., Tyson, G.W., Vivanco, J.M., and Schenk, P.M. (2013). Activation of the Jasmonic Acid Plant Defence Pathway Alters the Composition of Rhizosphere Bacterial Communities. *PLOS ONE* *8*, e56457.
- Carvalhais, L.C., Dennis, P.G., Badri, D.V., Kidd, B.N., Vivanco, J.M., and Schenk, P.M. (2015). Linking Jasmonic Acid Signaling, Root Exudates, and Rhizosphere Microbiomes. *Mol. Plant-Microbe Interactions* *28*, 1049–1058.
- Castiblanco, L.F., and Sundin, G.W. (2016). New insights on molecular regulation of biofilm formation in plant-associated bacteria. *J. Integr. Plant Biol.* *58*, 362–372.
- Castrillo, G., Teixeira, P.J.P.L., Paredes, S.H., Law, T.F., de Lorenzo, L., Feltcher, M.E., Finkel, O.M., Breakfield, N.W., Mieczkowski, P., Jones, C.D., *et al.* (2017). Root microbiota drive direct integration of phosphate stress and immunity. *Nature* *543*, 513–518.
- Chaparro, J.M., Badri, D.V., Bakker, M.G., Sugiyama, A., Manter, D.K., and Vivanco, J.M. (2013). Root Exudation of Phytochemicals in *Arabidopsis* Follows Specific Patterns That Are Developmentally Programmed and Correlate with Soil Microbial Functions. *PLOS ONE* *8*, e55731.
- Chaparro, J.M., Badri, D.V., and Vivanco, J.M. (2014). Rhizosphere microbiome assemblage is affected by plant development. *ISME J.* *8*, 790–803.
- Czymmek, K.J., Fogg, M., Powell, D.H., Sweigard, J., Park, S.-Y., and Kang, S. (2007). In vivo time-lapse documentation using confocal and multi-photon microscopy reveals the mechanisms of invasion into the *Arabidopsis* root vascular system by *Fusarium oxysporum*. *Fungal Genet. Biol.* *44*, 1011–1023.

- Dance, A. (2008). Soil ecology: What lies beneath. *Nat. News* 455, 724–725.
- DeAngelis, K.M., Brodie, E.L., DeSantis, T.Z., Andersen, G.L., Lindow, S.E., and Firestone, M.K. (2009). Selective progressive response of soil microbial community to wild oat roots. *ISME J.* 3, 168–178.
- Durán, P., Thiery, T., Garrido-Oter, R., Agler, M., Kemen, E., Schulze-Lefert, P., and Hacquard, S. (2018). Microbial Interkingdom Interactions in Roots Promote *Arabidopsis* Survival. *Cell* 175, 973–983.e14.
- van Elsas, J.D., Chiurazzi, M., Mallon, C.A., Elhottová, D., Křišťůfek, V., and Salles, J.F. (2012). Microbial diversity determines the invasion of soil by a bacterial pathogen. *Proc. Natl. Acad. Sci. U. S. A.* 109, 1159–1164.
- Emonet, A., Zhou, F., Vacheron, J., Heiman, C.M., Tendon, V.D., Ma, K.-W., Schulze-Lefert, P., Keel, C., and Geldner, N. (2020). Spatially Restricted Immune Responses Allow for Root Meristematic Activity During Bacterial Colonisation. *BioRxiv* 2020.08.03.233817.
- Eynck, C., Koopmann, B., Grunewaldt-Stoecker, G., Karlovsky, P., and Tiedemann, A. von (2007). Differential interactions of *Verticillium longisporum* and *V. dahliae* with *Brassica napus* detected with molecular and histological techniques. *Eur. J. Plant Pathol.* 118, 259–274.
- Faulkner, C., and Robatzek, S. (2012). Plants and pathogens: putting infection strategies and defence mechanisms on the map. *Curr. Opin. Plant Biol.* 15, 699–707.
- Felix, G., Duran, J.D., Volko, S., and Boller, T. (1999). Plants have a sensitive perception system for the most conserved domain of bacterial flagellin. *Plant J.* 18, 265–276.
- Garrido-Oter, R., Nakano, R.T., Dombrowski, N., Ma, K.-W., McHardy, A.C., and Schulze-Lefert, P. (2018). Modular Traits of the Rhizobiales Root Microbiota and Their Evolutionary Relationship with Symbiotic Rhizobia. *Cell Host Microbe* 24, 155–167.e5.
- Gómez-Gómez, L., Felix, G., and Boller, T. (1999). A single locus determines sensitivity to bacterial flagellin in *Arabidopsis thaliana*. *Plant J.* 18, 277–284.
- Götz, M., Gomes, N.C.M., Dratwinski, A., Costa, R., Berg, G., Peixoto, R., Mendonça-Hagler, L., and Smalla, K. (2006). Survival of gfp-tagged antagonistic bacteria in the rhizosphere of tomato plants and their effects on the indigenous bacterial community. *FEMS Microbiol. Ecol.* 56, 207–218.
- Hacquard, S., Spaepen, S., Garrido-Oter, R., and Schulze-Lefert, P. (2017). Interplay Between Innate Immunity and the Plant Microbiota. *Annu. Rev. Phytopathol.* 55, 565–589.
- Hartmann, A., Fischer, D., Kinzel, L., Chowdhury, S.P., Hofmann, A., Baldani, J.I., and Rothballer, M. (2019). Assessment of the structural and functional diversities of plant microbiota: Achievements and challenges – A review. *J. Adv. Res.* 19, 3–13.
- Hind, S.R., Strickler, S.R., Boyle, P.C., Dunham, D.M., Bao, Z., O’Doherty, I.M., Baccile, J.A., Hoki, J.S., Viox, E.G., Clarke, C.R., *et al.* (2016). Tomato receptor FLAGELLIN-SENSING 3 binds flgII-28 and activates the plant immune system. *Nat. Plants* 2, 1–8.
- Kennedy, T.A., Naeem, S., Howe, K.M., Knops, J.M.H., Tilman, D., and Reich, P. (2002). Biodiversity as a barrier to ecological invasion. *Nature* 417, 636–638.
- Koike, S.T., Subbarao, K.V., Davis, R.M., and Turini, T.A. (2003). Vegetable Diseases Caused by Soilborne Pathogens. *ANR Publ.* 8099.
- Korenblum, E., Dong, Y., Szymanski, J., Panda, S., Jozwiak, A., Massalha, H., Meir, S., Rogachev, I., and Aharoni, A. (2020). Rhizosphere microbiome mediates systemic root metabolite exudation by root-to-root signaling. *Proc. Natl. Acad. Sci.* 117, 3874–3883.

- Kremer, J.M., Paasch, B.C., Rhodes, D., Thireault, C., Froehlich, J.E., Schulze-Lefert, P., Tiedje, J.M., and He, S.Y. (2018). FlowPot axenic plant growth system for microbiota research. *BioRxiv* 254953.
- Kumpf, R.P., and Nowack, M.K. (2015). The root cap: a short story of life and death. *J. Exp. Bot.* *66*, 5651–5662.
- Lacombe, S., Rougon-Cardoso, A., Sherwood, E., Peeters, N., Dahlbeck, D., van Esse, H.P., Smoker, M., Rallapalli, G., Thomma, B.P.H.J., Staskawicz, B., *et al.* (2010). Interfamily transfer of a plant pattern-recognition receptor confers broad-spectrum bacterial resistance. *Nat. Biotechnol.* *28*, 365–369.
- Lebeis, S.L., Paredes, S.H., Lundberg, D.S., Breakfield, N., Gehring, J., McDonald, M., Malfatti, S., Glavina Del Rio, T., Jones, C.D., Tringe, S.G., *et al.* (2015). Salicylic acid modulates colonization of the root microbiome by specific bacterial taxa. *Science* *349*, 860–864.
- Lindow, S.E., and Brandl, M.T. (2003). Microbiology of the Phyllosphere. *Appl. Environ. Microbiol.* *69*, 1875–1883.
- Lundberg, D.S., Lebeis, S.L., Paredes, S.H., Yourstone, S., Gehring, J., Malfatti, S., Tremblay, J., Engelbrektson, A., Kunin, V., Rio, T.G. del, *et al.* (2012). Defining the core *Arabidopsis thaliana* root microbiome. *Nature* *488*, 86–90.
- Ma, L., Shi, Y., Siemianowski, O., Yuan, B., Egner, T.K., Mirnezami, S.V., Lind, K.R., Ganapathysubramanian, B., Venditti, V., and Cademartiri, L. (2019). Hydrogel-based transparent soils for root phenotyping in vivo. *Proc. Natl. Acad. Sci.* *116*, 11063–11068.
- Ma K., Niu Y., Jia Y., Ordon J., Copeland C., Emonet A., Geldner N., Guan R., Stolze S. C., Nakagami H., Garrido Oter R., Schulze-Lefert P. (10 September 2020). Coordination of microbe-host homeostasis via a crosstalk with plant innate immunity. PREPRINT (Version 1) available at Research Square. DOI:10.21203/rs.3.rs-69445/v1
- Massalha, H., Korenblum, E., Malitsky, S., Shapiro, O.H., and Aharoni, A. (2017). Live imaging of root-bacteria interactions in a microfluidics setup. *Proc. Natl. Acad. Sci.* *114*, 4549.
- McCann, H.C., Nahal, H., Thakur, S., and Guttman, D.S. (2012). Identification of innate immunity elicitors using molecular signatures of natural selection. *Proc. Natl. Acad. Sci.* *109*, 4215–4220.
- Miebach, M., Schlechter, R.O., Clemens, J., Jameson, P.E., and Remus-Emsermann, M.N.P. (2020). Litterbox - A gnotobiotic zeolite-clay system to investigate *Arabidopsis*-microbe interactions. *BioRxiv* 2020.01.28.922625.
- Millet, Y.A., Danna, C.H., Clay, N.K., Songnuan, W., Simon, M.D., Werck-Reichhart, D., and Ausubel, F.M. (2010). Innate Immune Responses Activated in *Arabidopsis* Roots by Microbe-Associated Molecular Patterns. *Plant Cell* *22*, 973–990.
- Oburger, E., and Schmidt, H. (2016). New Methods To Unravel Rhizosphere Processes. *Trends Plant Sci.* *21*, 243–255.
- Pfeilmeier, S., George, J., Morel, A., Roy, S., Smoker, M., Stransfeld, L., Downie, J.A., Peeters, N., Malone, J.G., and Zipfel, C. (2019). Expression of the *Arabidopsis thaliana* immune receptor EFR in *Medicago truncatula* reduces infection by a root pathogenic bacterium, but not nitrogen-fixing rhizobial symbiosis. *Plant Biotechnol. J.* *17*, 569–579.
- Pfund, C., Tans-Kersten, J., Dunning, F.M., Alonso, J.M., Ecker, J.R., Allen, C., and Bent, A.F. (2004). Flagellin Is Not a Major Defense Elicitor in *Ralstonia solanacearum* Cells or Extracts Applied to *Arabidopsis thaliana*. *Mol. Plant. Microbe Interact.* *17*, 696–706.
- Ranf, S., Gisch, N., Schäffer, M., Illig, T., Westphal, L., Knirel, Y.A., Sánchez-Carballo, P.M., Zähringer, U., Hückelhoven, R., Lee, J., *et al.* (2015). A lectin S-domain receptor kinase mediates lipopolysaccharide sensing in *Arabidopsis thaliana*. *Nat. Immunol.* *16*, 426–433.

- Robatzek, S., Chinchilla, D., and Boller, T. (2006). Ligand-induced endocytosis of the pattern recognition receptor FLS2 in *Arabidopsis*. *Genes Dev.* *20*, 537–542.
- Roesch, L.F.W., Fulthorpe, R.R., Riva, A., Casella, G., Hadwin, A.K.M., Kent, A.D., Daroub, S.H., Camargo, F.A.O., Farmerie, W.G., and Triplett, E.W. (2007). Pyrosequencing enumerates and contrasts soil microbial diversity. *ISME J.* *1*, 283–290.
- Rothballer, M., Schmid, M., Fekete, A., and Hartmann, A. (2005). Comparative in situ analysis of ipdC-gfpmut3 promoter fusions of *Azospirillum brasilense* strains Sp7 and Sp245. *Environ. Microbiol.* *7*, 1839–1846.
- Smith, J.M., Salamango, D.J., Leslie, M.E., Collins, C.A., and Heese, A. (2014). Sensitivity to Flg22 Is Modulated by Ligand-Induced Degradation and de Novo Synthesis of the Endogenous Flagellin-Receptor FLAGELLIN-SENSING2. *Plant Physiol.* *164*, 440–454.
- Stringlis, I.A., Yu, K., Feussner, K., de Jonge, R., Van Bentum, S., Van Verk, M.C., Berendsen, R.L., Bakker, P.A.H.M., Feussner, I., and Pieterse, C.M.J. (2018). MYB72-dependent coumarin exudation shapes root microbiome assembly to promote plant health. *Proc. Natl. Acad. Sci.* *115*, E5213–E5222.
- Stringlis, I.A., de Jonge, R., and Pieterse, C.M.J. (2019). The Age of Coumarins in Plant–Microbe Interactions. *Plant Cell Physiol.* *60*, 1405–1419.
- Sun, W., Dunning, F.M., Pfund, C., Weingarten, R., and Bent, A.F. (2006). Within-Species Flagellin Polymorphism in *Xanthomonas campestris pv campestris* and Its Impact on Elicitation of *Arabidopsis* FLAGELLIN SENSING2–Dependent Defenses. *Plant Cell* *18*, 764–779.
- Voges, M.J.E.E., Bai, Y., Schulze-Lefert, P., and Sattely, E.S. (2019). Plant-derived coumarins shape the composition of an *Arabidopsis* synthetic root microbiome. *Proc. Natl. Acad. Sci.* *116*, 12558–12565.
- Wang, L., Albert, M., Einig, E., Fürst, U., Krust, D., and Felix, G. (2016). The pattern-recognition receptor CORE of *Solanaceae* detects bacterial cold-shock protein. *Nat. Plants* *2*, 1–9.
- Wyrsh, I., Domínguez-Ferrerías, A., Geldner, N., and Boller, T. (2015). Tissue-specific FLAGELLIN-SENSING 2 (FLS2) expression in roots restores immune responses in *Arabidopsis fls2* mutants. *New Phytol.* *206*, 774–784.
- Yu, K., Pieterse, C.M.J., Bakker, P.A.H.M., and Berendsen, R.L. (2019a). Beneficial microbes going underground of root immunity. *Plant Cell Environ.* *42*, 2860–2870.
- Yu, K., Liu, Y., Tichelaar, R., Savant, N., Legendijk, E., Kuijk, S.J.L. van, Stringlis, I.A., Dijken, A.J.H. van, Pieterse, C.M.J., Bakker, P.A.H.M., *et al.* (2019b). Rhizosphere-Associated *Pseudomonas* Suppress Local Root Immune Responses by Gluconic Acid-Mediated Lowering of Environmental pH. *Curr. Biol.* *29*, 3913–3920.e4.
- Zhou, F., Emonet, A., Déneraud Tendon, V., Marhavy, P., Wu, D., Lahaye, T., and Geldner, N. (2020). Co-occurrence of Damage and Microbial Patterns Controls Localized Immune Responses in Roots. *Cell* *180*, 440–453.e18.
- Zipfel, C., Kunze, G., Chinchilla, D., Caniard, A., Jones, J.D.G., Boller, T., and Felix, G. (2006). Perception of the Bacterial PAMP EF-Tu by the Receptor EFR Restricts *Agrobacterium*-Mediated Transformation. *Cell* *125*, 749–760.

4.7. SUPPLEMENTAL FIGURES AND TABLES

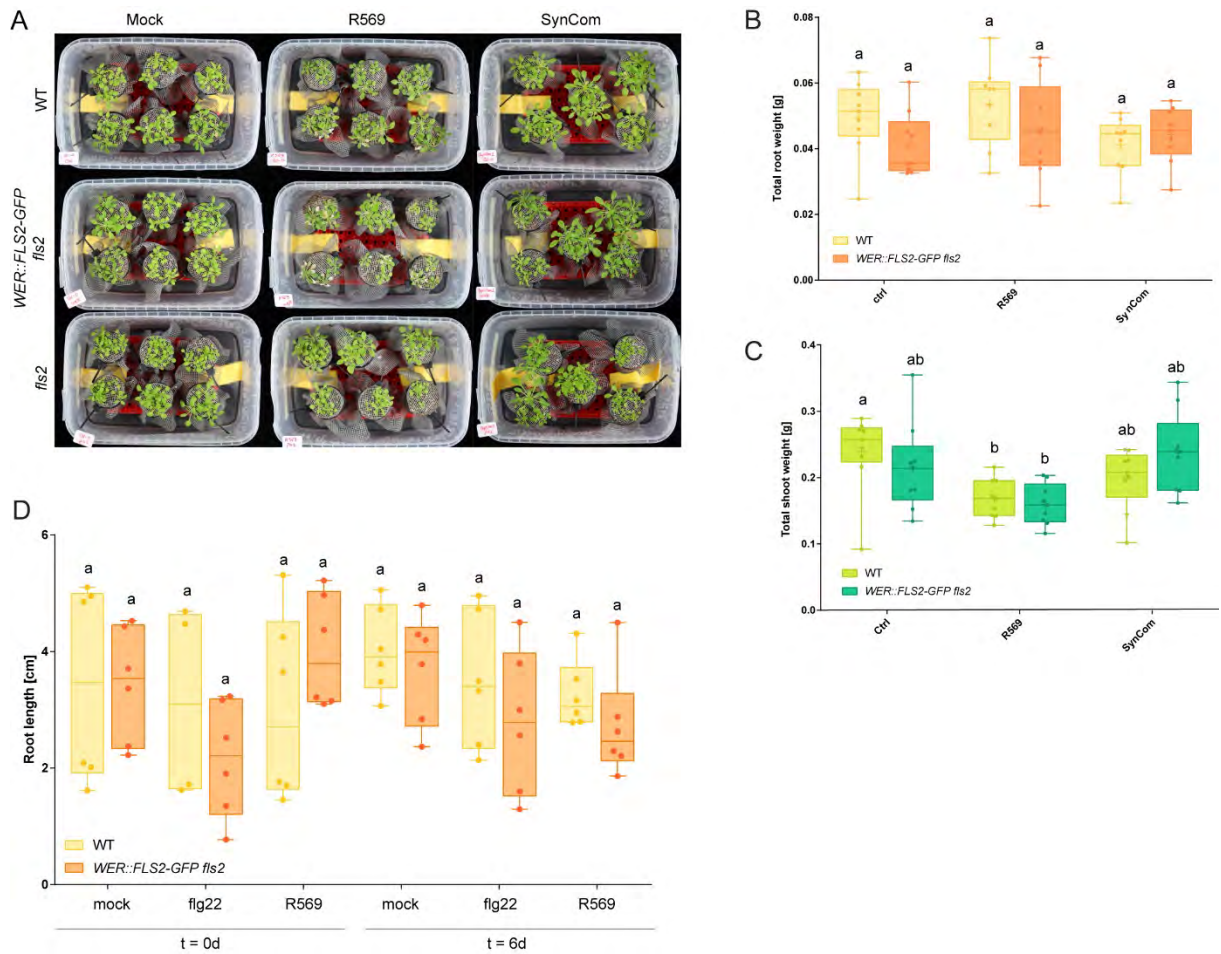


Supplemental Figure 1: Ectopic expression of *FLS2* does not affect growth on various non-sterile substrates

(A) *WER::FLS2-GFP fls2* has more biomass than WT and *fls2* plants when grown on non-sterile natural CAS soil (Cologne). Fresh weight was measured at six weeks. Different letters indicate statistically significant differences ($p < 0.05$). Multiple comparison was performed using Kruskal-Wallis and Dunn's test.

(B) Root fresh weight is not significantly different between WT plants and *WER::FLS2-GFP fls2* lines grown on non-sterile Serami, coarse sand and fine sand substrates. Root weight was measured at four weeks. Different letters indicate statistically significant differences ($p < 0.05$). Multiple comparison was performed using Kruskal-Wallis and Dunn's test.

(C) Representative pictures of plants grown on different substrates. Note the variability among replicates.



Supplemental Figure 2: Bacterial inoculation in gnotobiotic systems does not cause stronger root growth inhibition of *WER::FLS2*

(A) Representative pictures of FlowPots five weeks after inoculation. Note that plants inoculated with the complex SynCom are bigger than WT, and that plants inoculated with R569 have more lesions.

(B-C) Inoculation of WT and *WER::FLS2-GFP fls2* lines with the single strain R569 or a complex 97-members SynCom in calcined clay axenic system. Root and shoots weights were combined by Magenta box. Inoculation with the single strain R569 decreases shoot biomass (C) but does not affect root weight (B). Samples were harvested seven weeks after inoculation. Multiple comparison was performed using ANOVA followed by Tukey's HSD test for (B) and Kruskal-Wallis followed by Dunn's test for (C). Different letters indicate statistically significant differences ($p < 0.05$).

(D) WT and *WER::FLS2-GFP fls2* one-week-old seedlings were treated with $10 \mu\text{M}$ flg22 or inoculated with R569 (final $\text{OD}_{600} = 4 \times 10^{-4}$) on sterile calcined clay in 6-well plates. None of the treatment induced a significant difference between WT and *WER::FLS2-GFP fls2*. Note the high variability even before inoculation. Multiple comparison was performed using Kruskal-Wallis and Dunn's test. Different letters indicate statistically significant differences ($p < 0.05$).

Supplemental Table S1: Composition and taxonomy of the 97-member complex SynCom

Isolate ID	OTU	Kingdom	Phylum	Class	Order	Family	Genus
Root137	OTU_139	<i>Bacteria</i>	<i>Actinobacteria</i>	<i>Actinobacteria</i>	<i>Actinomycetales</i>	<i>Cellulomonadaceae</i>	<i>Cellulomonas</i>
Root101	OTU_168	<i>Bacteria</i>	<i>Actinobacteria</i>	<i>Actinobacteria</i>	<i>Actinomycetales</i>	<i>Intrasporangiaceae</i>	<i>Janibacter</i>
Root181	OTU_153	<i>Bacteria</i>	<i>Actinobacteria</i>	<i>Actinobacteria</i>	<i>Actinomycetales</i>	<i>Intrasporangiaceae</i>	
Root456	OTU_232	<i>Bacteria</i>	<i>Actinobacteria</i>	<i>Actinobacteria</i>	<i>Actinomycetales</i>	<i>Intrasporangiaceae</i>	
Root1464	OTU_238	<i>Bacteria</i>	<i>Actinobacteria</i>	<i>Actinobacteria</i>	<i>Actinomycetales</i>	<i>Microbacteriaceae</i>	<i>Agromyces</i>
Root4	OTU_66	<i>Bacteria</i>	<i>Actinobacteria</i>	<i>Actinobacteria</i>	<i>Actinomycetales</i>	<i>Microbacteriaceae</i>	<i>Agromyces</i>
Root81	OTU_112	<i>Bacteria</i>	<i>Actinobacteria</i>	<i>Actinobacteria</i>	<i>Actinomycetales</i>	<i>Microbacteriaceae</i>	<i>Agromyces</i>
Root166	OTU_248	<i>Bacteria</i>	<i>Actinobacteria</i>	<i>Actinobacteria</i>	<i>Actinomycetales</i>	<i>Microbacteriaceae</i>	<i>Microbacterium</i>
Root322	OTU_87	<i>Bacteria</i>	<i>Actinobacteria</i>	<i>Actinobacteria</i>	<i>Actinomycetales</i>	<i>Microbacteriaceae</i>	<i>Microbacterium</i>
Root53	OTU_219	<i>Bacteria</i>	<i>Actinobacteria</i>	<i>Actinobacteria</i>	<i>Actinomycetales</i>	<i>Microbacteriaceae</i>	<i>Microbacterium</i>
Root61	OTU_116	<i>Bacteria</i>	<i>Actinobacteria</i>	<i>Actinobacteria</i>	<i>Actinomycetales</i>	<i>Microbacteriaceae</i>	<i>Microbacterium</i>
Root112D2	OTU_37	<i>Bacteria</i>	<i>Actinobacteria</i>	<i>Actinobacteria</i>	<i>Actinomycetales</i>	<i>Microbacteriaceae</i>	
Root1293	OTU_82	<i>Bacteria</i>	<i>Actinobacteria</i>	<i>Actinobacteria</i>	<i>Actinomycetales</i>	<i>Microbacteriaceae</i>	
Root227	OTU_202	<i>Bacteria</i>	<i>Actinobacteria</i>	<i>Actinobacteria</i>	<i>Actinomycetales</i>	<i>Microbacteriaceae</i>	
Root332	OTU_131	<i>Bacteria</i>	<i>Actinobacteria</i>	<i>Actinobacteria</i>	<i>Actinomycetales</i>	<i>Microbacteriaceae</i>	
Root135	OTU_137	<i>Bacteria</i>	<i>Actinobacteria</i>	<i>Actinobacteria</i>	<i>Actinomycetales</i>	<i>Mycobacteriaceae</i>	<i>Mycobacterium</i>
Root265	OTU_59	<i>Bacteria</i>	<i>Actinobacteria</i>	<i>Actinobacteria</i>	<i>Actinomycetales</i>	<i>Mycobacteriaceae</i>	<i>Mycobacterium</i>
Root236	OTU_159	<i>Bacteria</i>	<i>Actinobacteria</i>	<i>Actinobacteria</i>	<i>Actinomycetales</i>	<i>Nocardioideae</i>	<i>Aeromicrobium</i>
Root495	OTU_74	<i>Bacteria</i>	<i>Actinobacteria</i>	<i>Actinobacteria</i>	<i>Actinomycetales</i>	<i>Nocardioideae</i>	<i>Aeromicrobium</i>
Root122	OTU_43	<i>Bacteria</i>	<i>Actinobacteria</i>	<i>Actinobacteria</i>	<i>Actinomycetales</i>	<i>Nocardioideae</i>	<i>Nocardioides</i>
Root1257	OTU_264	<i>Bacteria</i>	<i>Actinobacteria</i>	<i>Actinobacteria</i>	<i>Actinomycetales</i>	<i>Nocardioideae</i>	<i>Nocardioides</i>
Root140	OTU_157	<i>Bacteria</i>	<i>Actinobacteria</i>	<i>Actinobacteria</i>	<i>Actinomycetales</i>	<i>Nocardioideae</i>	<i>Nocardioides</i>
Root190	OTU_233	<i>Bacteria</i>	<i>Actinobacteria</i>	<i>Actinobacteria</i>	<i>Actinomycetales</i>	<i>Nocardioideae</i>	<i>Nocardioides</i>
Root79	OTU_129	<i>Bacteria</i>	<i>Actinobacteria</i>	<i>Actinobacteria</i>	<i>Actinomycetales</i>	<i>Nocardioideae</i>	<i>Nocardioides</i>

Root472D3	OTU_62	<i>Bacteria</i>	<i>Actinobacteria</i>	<i>Actinobacteria</i>	<i>Actinomycetales</i>	<i>Nocardioideae</i>	
Root614	OTU_122	<i>Bacteria</i>	<i>Actinobacteria</i>	<i>Actinobacteria</i>	<i>Actinomycetales</i>	<i>Nocardioideae</i>	
Root918	OTU_53	<i>Bacteria</i>	<i>Actinobacteria</i>	<i>Actinobacteria</i>	<i>Actinomycetales</i>	<i>Promicromonosporaceae</i>	
Root1295	OTU_86	<i>Bacteria</i>	<i>Actinobacteria</i>	<i>Actinobacteria</i>	<i>Actinomycetales</i>	<i>Streptomyetaceae</i>	<i>Streptomyces</i>
Root1310	OTU_189	<i>Bacteria</i>	<i>Actinobacteria</i>	<i>Actinobacteria</i>	<i>Actinomycetales</i>	<i>Streptomyetaceae</i>	<i>Streptomyces</i>
Root264	OTU_58	<i>Bacteria</i>	<i>Actinobacteria</i>	<i>Actinobacteria</i>	<i>Actinomycetales</i>	<i>Streptomyetaceae</i>	<i>Streptomyces</i>
Root431	OTU_101	<i>Bacteria</i>	<i>Actinobacteria</i>	<i>Actinobacteria</i>	<i>Actinomycetales</i>	<i>Streptomyetaceae</i>	<i>Streptomyces</i>
Root107	OTU_173	<i>Bacteria</i>	<i>Actinobacteria</i>	<i>Actinobacteria</i>	<i>Actinomycetales</i>	<i>Streptomyetaceae</i>	
Root420	OTU_201	<i>Bacteria</i>	<i>Bacteroidetes</i>	<i>Flavobacteriia</i>	<i>Flavobacteriales</i>	<i>Flavobacteriaceae</i>	<i>Flavobacterium</i>
Root901	OTU_21	<i>Bacteria</i>	<i>Bacteroidetes</i>	<i>Flavobacteriia</i>	<i>Flavobacteriales</i>	<i>Flavobacteriaceae</i>	<i>Flavobacterium</i>
Root935	OTU_41	<i>Bacteria</i>	<i>Bacteroidetes</i>	<i>Flavobacteriia</i>	<i>Flavobacteriales</i>	<i>Flavobacteriaceae</i>	<i>Flavobacterium</i>
Root11	OTU_120	<i>Bacteria</i>	<i>Firmicutes</i>	<i>Bacilli</i>	<i>Bacillales</i>	<i>Bacillaceae</i>	<i>Bacillus</i>
Root920	OTU_222	<i>Bacteria</i>	<i>Firmicutes</i>	<i>Bacilli</i>	<i>Bacillales</i>	<i>Bacillaceae</i>	<i>Bacillus</i>
Root147	OTU_254	<i>Bacteria</i>	<i>Firmicutes</i>	<i>Bacilli</i>	<i>Bacillales</i>	<i>Bacillaceae</i>	
Root444D2	OTU_121	<i>Bacteria</i>	<i>Firmicutes</i>	<i>Bacilli</i>	<i>Bacillales</i>	<i>Paenibacillaceae</i>	<i>Paenibacillus</i>
Root52	OTU_218	<i>Bacteria</i>	<i>Firmicutes</i>	<i>Bacilli</i>	<i>Bacillales</i>	<i>Paenibacillaceae</i>	<i>Paenibacillus</i>
Root1279	OTU_64	<i>Bacteria</i>	<i>Proteobacteria</i>	<i>Alphaproteobacteria</i>	<i>Caulobacterales</i>	<i>Caulobacteraceae</i>	<i>Brevundimonas</i>
Root1472	OTU_170	<i>Bacteria</i>	<i>Proteobacteria</i>	<i>Alphaproteobacteria</i>	<i>Caulobacterales</i>	<i>Caulobacteraceae</i>	<i>Caulobacter</i>
Root342	OTU_197	<i>Bacteria</i>	<i>Proteobacteria</i>	<i>Alphaproteobacteria</i>	<i>Caulobacterales</i>	<i>Caulobacteraceae</i>	<i>Caulobacter</i>
Root1277	OTU_60	<i>Bacteria</i>	<i>Proteobacteria</i>	<i>Alphaproteobacteria</i>	<i>Caulobacterales</i>	<i>Caulobacteraceae</i>	
Root700	OTU_161	<i>Bacteria</i>	<i>Proteobacteria</i>	<i>Alphaproteobacteria</i>	<i>Caulobacterales</i>	<i>Caulobacteraceae</i>	
Root123D2	OTU_235	<i>Bacteria</i>	<i>Proteobacteria</i>	<i>Alphaproteobacteria</i>	<i>Rhizobiales</i>	<i>Bradyrhizobiaceae</i>	<i>Afipia</i>
Root105	OTU_171	<i>Bacteria</i>	<i>Proteobacteria</i>	<i>Alphaproteobacteria</i>	<i>Rhizobiales</i>	<i>Hyphomicrobiaceae</i>	
Root685	OTU_93	<i>Bacteria</i>	<i>Proteobacteria</i>	<i>Alphaproteobacteria</i>	<i>Rhizobiales</i>	<i>Hyphomicrobiaceae</i>	
Root483D1	OTU_15	<i>Bacteria</i>	<i>Proteobacteria</i>	<i>Alphaproteobacteria</i>	<i>Rhizobiales</i>	<i>Methylobacteriaceae</i>	<i>Methylobacterium</i>
Root670	OTU_103	<i>Bacteria</i>	<i>Proteobacteria</i>	<i>Alphaproteobacteria</i>	<i>Rhizobiales</i>	<i>Methylobacteriaceae</i>	
Root102	OTU_127	<i>Bacteria</i>	<i>Proteobacteria</i>	<i>Alphaproteobacteria</i>	<i>Rhizobiales</i>	<i>Phyllobacteriaceae</i>	<i>Mesorhizobium</i>

Root157	OTU_223	<i>Bacteria</i>	<i>Proteobacteria</i>	<i>Alphaproteobacteria</i>	<i>Rhizobiales</i>	<i>Phyllobacteriaceae</i>	<i>Mesorhizobium</i>
Root172	OTU_13	<i>Bacteria</i>	<i>Proteobacteria</i>	<i>Alphaproteobacteria</i>	<i>Rhizobiales</i>	<i>Phyllobacteriaceae</i>	<i>Mesorhizobium</i>
Root552	OTU_165	<i>Bacteria</i>	<i>Proteobacteria</i>	<i>Alphaproteobacteria</i>	<i>Rhizobiales</i>	<i>Phyllobacteriaceae</i>	<i>Mesorhizobium</i>
Root554	OTU_9	<i>Bacteria</i>	<i>Proteobacteria</i>	<i>Alphaproteobacteria</i>	<i>Rhizobiales</i>	<i>Phyllobacteriaceae</i>	<i>Mesorhizobium</i>
Root100	OTU_229	<i>Bacteria</i>	<i>Proteobacteria</i>	<i>Alphaproteobacteria</i>	<i>Rhizobiales</i>	<i>Phyllobacteriaceae</i>	
Root491	OTU_77	<i>Bacteria</i>	<i>Proteobacteria</i>	<i>Alphaproteobacteria</i>	<i>Rhizobiales</i>	<i>Rhizobiaceae</i>	<i>Agrobacterium</i>
Root564	OTU_50	<i>Bacteria</i>	<i>Proteobacteria</i>	<i>Alphaproteobacteria</i>	<i>Rhizobiales</i>	<i>Rhizobiaceae</i>	<i>Agrobacterium</i>
Root1203	OTU_52	<i>Bacteria</i>	<i>Proteobacteria</i>	<i>Alphaproteobacteria</i>	<i>Rhizobiales</i>	<i>Rhizobiaceae</i>	<i>Rhizobium</i>
Root1204	OTU_91	<i>Bacteria</i>	<i>Proteobacteria</i>	<i>Alphaproteobacteria</i>	<i>Rhizobiales</i>	<i>Rhizobiaceae</i>	<i>Rhizobium</i>
Root1212	OTU_115	<i>Bacteria</i>	<i>Proteobacteria</i>	<i>Alphaproteobacteria</i>	<i>Rhizobiales</i>	<i>Rhizobiaceae</i>	<i>Rhizobium</i>
Root149	OTU_247	<i>Bacteria</i>	<i>Proteobacteria</i>	<i>Alphaproteobacteria</i>	<i>Rhizobiales</i>	<i>Rhizobiaceae</i>	<i>Rhizobium</i>
Root708	OTU_39	<i>Bacteria</i>	<i>Proteobacteria</i>	<i>Alphaproteobacteria</i>	<i>Rhizobiales</i>	<i>Rhizobiaceae</i>	<i>Rhizobium</i>
Root231	OTU_267	<i>Bacteria</i>	<i>Proteobacteria</i>	<i>Alphaproteobacteria</i>	<i>Rhizobiales</i>	<i>Rhizobiaceae</i>	<i>Sinorhizobium</i>
Root278	OTU_32	<i>Bacteria</i>	<i>Proteobacteria</i>	<i>Alphaproteobacteria</i>	<i>Rhizobiales</i>	<i>Rhizobiaceae</i>	<i>Sinorhizobium</i>
Root274	OTU_231	<i>Bacteria</i>	<i>Proteobacteria</i>	<i>Alphaproteobacteria</i>	<i>Rhizobiales</i>	<i>Rhizobiaceae</i>	
Root672	OTU_102	<i>Bacteria</i>	<i>Proteobacteria</i>	<i>Alphaproteobacteria</i>	<i>Sphingomonadales</i>	<i>Sphingomonadaceae</i>	<i>Novosphingobium</i>
Root241	OTU_130	<i>Bacteria</i>	<i>Proteobacteria</i>	<i>Alphaproteobacteria</i>	<i>Sphingomonadales</i>	<i>Sphingomonadaceae</i>	<i>Sphingomonas</i>
Root50	OTU_230	<i>Bacteria</i>	<i>Proteobacteria</i>	<i>Alphaproteobacteria</i>	<i>Sphingomonadales</i>	<i>Sphingomonadaceae</i>	<i>Sphingomonas</i>
Root710	OTU_200	<i>Bacteria</i>	<i>Proteobacteria</i>	<i>Alphaproteobacteria</i>	<i>Sphingomonadales</i>	<i>Sphingomonadaceae</i>	<i>Sphingomonas</i>
Root1497	OTU_221	<i>Bacteria</i>	<i>Proteobacteria</i>	<i>Alphaproteobacteria</i>	<i>Sphingomonadales</i>	<i>Sphingomonadaceae</i>	<i>Sphingopyxis</i>
Root154	OTU_142	<i>Bacteria</i>	<i>Proteobacteria</i>	<i>Alphaproteobacteria</i>	<i>Sphingomonadales</i>	<i>Sphingomonadaceae</i>	
Root170	OTU_245	<i>Bacteria</i>	<i>Proteobacteria</i>	<i>Betaproteobacteria</i>	<i>Burkholderiales</i>	<i>Alcaligenaceae</i>	<i>Achromobacter</i>
Root565	OTU_97	<i>Bacteria</i>	<i>Proteobacteria</i>	<i>Betaproteobacteria</i>	<i>Burkholderiales</i>	<i>Alcaligenaceae</i>	<i>Achromobacter</i>
Root83	OTU_110	<i>Bacteria</i>	<i>Proteobacteria</i>	<i>Betaproteobacteria</i>	<i>Burkholderiales</i>	<i>Alcaligenaceae</i>	<i>Achromobacter</i>
Root219	OTU_203	<i>Bacteria</i>	<i>Proteobacteria</i>	<i>Betaproteobacteria</i>	<i>Burkholderiales</i>	<i>Comamonadaceae</i>	<i>Acidovorax</i>
Root267	OTU_61	<i>Bacteria</i>	<i>Proteobacteria</i>	<i>Betaproteobacteria</i>	<i>Burkholderiales</i>	<i>Comamonadaceae</i>	<i>Acidovorax</i>
Root70	OTU_147	<i>Bacteria</i>	<i>Proteobacteria</i>	<i>Betaproteobacteria</i>	<i>Burkholderiales</i>	<i>Comamonadaceae</i>	<i>Acidovorax</i>

Root411	OTU_96	<i>Bacteria</i>	<i>Proteobacteria</i>	<i>Betaproteobacteria</i>	<i>Burkholderiales</i>	<i>Comamonadaceae</i>	<i>Variovorax</i>
Root1217	OTU_117	<i>Bacteria</i>	<i>Proteobacteria</i>	<i>Betaproteobacteria</i>	<i>Burkholderiales</i>	<i>Comamonadaceae</i>	
Root1272	OTU_63	<i>Bacteria</i>	<i>Proteobacteria</i>	<i>Betaproteobacteria</i>	<i>Burkholderiales</i>	<i>Comamonadaceae</i>	
Root209	OTU_126	<i>Bacteria</i>	<i>Proteobacteria</i>	<i>Betaproteobacteria</i>	<i>Burkholderiales</i>	<i>Comamonadaceae</i>	
Root404	OTU_150	<i>Bacteria</i>	<i>Proteobacteria</i>	<i>Betaproteobacteria</i>	<i>Burkholderiales</i>	<i>Comamonadaceae</i>	
Root405	OTU_123	<i>Bacteria</i>	<i>Proteobacteria</i>	<i>Betaproteobacteria</i>	<i>Burkholderiales</i>	<i>Comamonadaceae</i>	
Root189	OTU_199	<i>Bacteria</i>	<i>Proteobacteria</i>	<i>Betaproteobacteria</i>	<i>Burkholderiales</i>	<i>Oxalobacteraceae</i>	<i>Herbaspirillum</i>
Root418	OTU_100	<i>Bacteria</i>	<i>Proteobacteria</i>	<i>Betaproteobacteria</i>	<i>Burkholderiales</i>	<i>Oxalobacteraceae</i>	<i>Janthinobacterium</i>
Root1280	OTU_45	<i>Bacteria</i>	<i>Proteobacteria</i>	<i>Gammaproteobacteria</i>	<i>Pseudomonadales</i>	<i>Moraxellaceae</i>	<i>Acinetobacter</i>
Root562	OTU_57	<i>Bacteria</i>	<i>Proteobacteria</i>	<i>Gammaproteobacteria</i>	<i>Pseudomonadales</i>	<i>Pseudomonadaceae</i>	<i>Pseudomonas</i>
Root569	OTU_33	<i>Bacteria</i>	<i>Proteobacteria</i>	<i>Gammaproteobacteria</i>	<i>Pseudomonadales</i>	<i>Pseudomonadaceae</i>	<i>Pseudomonas</i>
Root68	OTU_178	<i>Bacteria</i>	<i>Proteobacteria</i>	<i>Gammaproteobacteria</i>	<i>Pseudomonadales</i>	<i>Pseudomonadaceae</i>	<i>Pseudomonas</i>
Root9	OTU_95	<i>Bacteria</i>	<i>Proteobacteria</i>	<i>Gammaproteobacteria</i>	<i>Pseudomonadales</i>	<i>Pseudomonadaceae</i>	<i>Pseudomonas</i>
Root65	OTU_269	<i>Bacteria</i>	<i>Proteobacteria</i>	<i>Gammaproteobacteria</i>	<i>Xanthomonadales</i>	<i>Xanthomonadaceae</i>	<i>Pseudoxanthomonas</i>
Root179	OTU_18	<i>Bacteria</i>	<i>Proteobacteria</i>	<i>Gammaproteobacteria</i>	<i>Xanthomonadales</i>	<i>Xanthomonadaceae</i>	<i>Rhodanobacter</i>
Root480	OTU_107	<i>Bacteria</i>	<i>Proteobacteria</i>	<i>Gammaproteobacteria</i>	<i>Xanthomonadales</i>	<i>Xanthomonadaceae</i>	
Root604	OTU_69	<i>Bacteria</i>	<i>Proteobacteria</i>	<i>Gammaproteobacteria</i>	<i>Xanthomonadales</i>	<i>Xanthomonadaceae</i>	
Root690	OTU_35	<i>Bacteria</i>	<i>Proteobacteria</i>	<i>Gammaproteobacteria</i>	<i>Xanthomonadales</i>	<i>Xanthomonadaceae</i>	
Root76	OTU_174	<i>Bacteria</i>	<i>Proteobacteria</i>	<i>Gammaproteobacteria</i>	<i>Xanthomonadales</i>	<i>Xanthomonadaceae</i>	

Supplemental Table S2: List of barcodes used for MiSeq Sequencing

Sample ID	Barcode Sequence	LinkerPrimerSequence	ReversePrimer
fp.13	TCCCTGTCTCC	AGATCGGAAGAGCACACGTCTGAACTCCAGTCA	AGATCGGAAGAGCGTCGTGTAGGGAAAGAGTGT
fp.14	ACGAGACTGATT	AGATCGGAAGAGCACACGTCTGAACTCCAGTCA	AGATCGGAAGAGCGTCGTGTAGGGAAAGAGTGT
fp.15	ACCGGTATGTAC	AGATCGGAAGAGCACACGTCTGAACTCCAGTCA	AGATCGGAAGAGCGTCGTGTAGGGAAAGAGTGT
fp.16	TGCATACACTGG	AGATCGGAAGAGCACACGTCTGAACTCCAGTCA	AGATCGGAAGAGCGTCGTGTAGGGAAAGAGTGT
fp.17	TGGTCAACGATA	AGATCGGAAGAGCACACGTCTGAACTCCAGTCA	AGATCGGAAGAGCGTCGTGTAGGGAAAGAGTGT
fp.18	ATCGCACAGTAA	AGATCGGAAGAGCACACGTCTGAACTCCAGTCA	AGATCGGAAGAGCGTCGTGTAGGGAAAGAGTGT
fp.19	GTCGTGTAGCCT	AGATCGGAAGAGCACACGTCTGAACTCCAGTCA	AGATCGGAAGAGCGTCGTGTAGGGAAAGAGTGT
fp.20	TACAGCGCATA	AGATCGGAAGAGCACACGTCTGAACTCCAGTCA	AGATCGGAAGAGCGTCGTGTAGGGAAAGAGTGT
fp.21	ATCCTTTGGTTC	AGATCGGAAGAGCACACGTCTGAACTCCAGTCA	AGATCGGAAGAGCGTCGTGTAGGGAAAGAGTGT
fp.22	AGTCGAACGAGG	AGATCGGAAGAGCACACGTCTGAACTCCAGTCA	AGATCGGAAGAGCGTCGTGTAGGGAAAGAGTGT
fp.23	ACCAGTGA	AGATCGGAAGAGCACACGTCTGAACTCCAGTCA	AGATCGGAAGAGCGTCGTGTAGGGAAAGAGTGT
fp.24	CCAATACGCCTG	AGATCGGAAGAGCACACGTCTGAACTCCAGTCA	AGATCGGAAGAGCGTCGTGTAGGGAAAGAGTGT
fp.25	GCAACACCATCC	AGATCGGAAGAGCACACGTCTGAACTCCAGTCA	AGATCGGAAGAGCGTCGTGTAGGGAAAGAGTGT
fp.26	AGTCGTGCACAT	AGATCGGAAGAGCACACGTCTGAACTCCAGTCA	AGATCGGAAGAGCGTCGTGTAGGGAAAGAGTGT
fp.27	AGTTACGAGCTA	AGATCGGAAGAGCACACGTCTGAACTCCAGTCA	AGATCGGAAGAGCGTCGTGTAGGGAAAGAGTGT
fp.28	TTGCGTTAGCAG	AGATCGGAAGAGCACACGTCTGAACTCCAGTCA	AGATCGGAAGAGCGTCGTGTAGGGAAAGAGTGT
fp.29	TACGAGCCCTAA	AGATCGGAAGAGCACACGTCTGAACTCCAGTCA	AGATCGGAAGAGCGTCGTGTAGGGAAAGAGTGT
fp.30	TGTCGCAATAG	AGATCGGAAGAGCACACGTCTGAACTCCAGTCA	AGATCGGAAGAGCGTCGTGTAGGGAAAGAGTGT
fp.31	ACAATAGACACC	AGATCGGAAGAGCACACGTCTGAACTCCAGTCA	AGATCGGAAGAGCGTCGTGTAGGGAAAGAGTGT
fp.32	TCTCTACCACTC	AGATCGGAAGAGCACACGTCTGAACTCCAGTCA	AGATCGGAAGAGCGTCGTGTAGGGAAAGAGTGT
fp.33	CGATCGAACACT	AGATCGGAAGAGCACACGTCTGAACTCCAGTCA	AGATCGGAAGAGCGTCGTGTAGGGAAAGAGTGT
fp.34	ATTGCAAGCAAC	AGATCGGAAGAGCACACGTCTGAACTCCAGTCA	AGATCGGAAGAGCGTCGTGTAGGGAAAGAGTGT
fp.35	AGCGTCCACATC	AGATCGGAAGAGCACACGTCTGAACTCCAGTCA	AGATCGGAAGAGCGTCGTGTAGGGAAAGAGTGT
fp.36	TCGACCAAACAC	AGATCGGAAGAGCACACGTCTGAACTCCAGTCA	AGATCGGAAGAGCGTCGTGTAGGGAAAGAGTGT
fp.37	TGTGTTACTCCT	AGATCGGAAGAGCACACGTCTGAACTCCAGTCA	AGATCGGAAGAGCGTCGTGTAGGGAAAGAGTGT
fp.38	TGCACAGTCGCT	AGATCGGAAGAGCACACGTCTGAACTCCAGTCA	AGATCGGAAGAGCGTCGTGTAGGGAAAGAGTGT
fp.39	TTCTAGAGTGCG	AGATCGGAAGAGCACACGTCTGAACTCCAGTCA	AGATCGGAAGAGCGTCGTGTAGGGAAAGAGTGT
fp.40	ACACCTGCGATC	AGATCGGAAGAGCACACGTCTGAACTCCAGTCA	AGATCGGAAGAGCGTCGTGTAGGGAAAGAGTGT
fp.41	ATTCCTCTCCAC	AGATCGGAAGAGCACACGTCTGAACTCCAGTCA	AGATCGGAAGAGCGTCGTGTAGGGAAAGAGTGT
fp.42	CATCGACGAGTT	AGATCGGAAGAGCACACGTCTGAACTCCAGTCA	AGATCGGAAGAGCGTCGTGTAGGGAAAGAGTGT
fp.43	CACCACAGAATC	AGATCGGAAGAGCACACGTCTGAACTCCAGTCA	AGATCGGAAGAGCGTCGTGTAGGGAAAGAGTGT
fp.44	GGTCTTAGCACC	AGATCGGAAGAGCACACGTCTGAACTCCAGTCA	AGATCGGAAGAGCGTCGTGTAGGGAAAGAGTGT
fp.45	TATCGCGCGATA	AGATCGGAAGAGCACACGTCTGAACTCCAGTCA	AGATCGGAAGAGCGTCGTGTAGGGAAAGAGTGT
fp.46	CTCTACGAACAG	AGATCGGAAGAGCACACGTCTGAACTCCAGTCA	AGATCGGAAGAGCGTCGTGTAGGGAAAGAGTGT
fp.47	CTCCTCCCTTAC	AGATCGGAAGAGCACACGTCTGAACTCCAGTCA	AGATCGGAAGAGCGTCGTGTAGGGAAAGAGTGT
fp.48	CGTGTATGTGG	AGATCGGAAGAGCACACGTCTGAACTCCAGTCA	AGATCGGAAGAGCGTCGTGTAGGGAAAGAGTGT
fp.49	ATTAGCAGCGTA	AGATCGGAAGAGCACACGTCTGAACTCCAGTCA	AGATCGGAAGAGCGTCGTGTAGGGAAAGAGTGT
fp.50	CAAGTTTCCGCG	AGATCGGAAGAGCACACGTCTGAACTCCAGTCA	AGATCGGAAGAGCGTCGTGTAGGGAAAGAGTGT
fp.51	CCTTGTTACCT	AGATCGGAAGAGCACACGTCTGAACTCCAGTCA	AGATCGGAAGAGCGTCGTGTAGGGAAAGAGTGT
fp.52	AACCAGCAGATT	AGATCGGAAGAGCACACGTCTGAACTCCAGTCA	AGATCGGAAGAGCGTCGTGTAGGGAAAGAGTGT
fp.53	CTAGAGCTCCA	AGATCGGAAGAGCACACGTCTGAACTCCAGTCA	AGATCGGAAGAGCGTCGTGTAGGGAAAGAGTGT
fp.54	CACGCAGTCTAC	AGATCGGAAGAGCACACGTCTGAACTCCAGTCA	AGATCGGAAGAGCGTCGTGTAGGGAAAGAGTGT
fp.55	ACAAACATGGTC	AGATCGGAAGAGCACACGTCTGAACTCCAGTCA	AGATCGGAAGAGCGTCGTGTAGGGAAAGAGTGT
fp.56	TCGAAACATGCA	AGATCGGAAGAGCACACGTCTGAACTCCAGTCA	AGATCGGAAGAGCGTCGTGTAGGGAAAGAGTGT

fp.57	TTCCCACCCATT	AGATCGGAAGAGCACACGTCTGAACTCCAGTCA	AGATCGGAAGAGCGTCGTGTAGGGAAAGAGTGT
fp.58	AGCAGAACATCT	AGATCGGAAGAGCACACGTCTGAACTCCAGTCA	AGATCGGAAGAGCGTCGTGTAGGGAAAGAGTGT
fp.59	GAAACATCCCAC	AGATCGGAAGAGCACACGTCTGAACTCCAGTCA	AGATCGGAAGAGCGTCGTGTAGGGAAAGAGTGT
fp.60	CTGTCAGTGACC	AGATCGGAAGAGCACACGTCTGAACTCCAGTCA	AGATCGGAAGAGCGTCGTGTAGGGAAAGAGTGT
fp.61	CGGATCTAGTGT	AGATCGGAAGAGCACACGTCTGAACTCCAGTCA	AGATCGGAAGAGCGTCGTGTAGGGAAAGAGTGT
fp.62	TTCTCCATCACA	AGATCGGAAGAGCACACGTCTGAACTCCAGTCA	AGATCGGAAGAGCGTCGTGTAGGGAAAGAGTGT
fp.63	ATTAGGACGAC	AGATCGGAAGAGCACACGTCTGAACTCCAGTCA	AGATCGGAAGAGCGTCGTGTAGGGAAAGAGTGT
fp.64	GGTTTAACACGC	AGATCGGAAGAGCACACGTCTGAACTCCAGTCA	AGATCGGAAGAGCGTCGTGTAGGGAAAGAGTGT
fp.65	AGACAGTAGGAG	AGATCGGAAGAGCACACGTCTGAACTCCAGTCA	AGATCGGAAGAGCGTCGTGTAGGGAAAGAGTGT
fp.66	GCAGATTTCCAG	AGATCGGAAGAGCACACGTCTGAACTCCAGTCA	AGATCGGAAGAGCGTCGTGTAGGGAAAGAGTGT
fp.67	AGATGATCAGTC	AGATCGGAAGAGCACACGTCTGAACTCCAGTCA	AGATCGGAAGAGCGTCGTGTAGGGAAAGAGTGT
fp.68	TATCACCGGCAC	AGATCGGAAGAGCACACGTCTGAACTCCAGTCA	AGATCGGAAGAGCGTCGTGTAGGGAAAGAGTGT
fp.69	CCAGATATAGCA	AGATCGGAAGAGCACACGTCTGAACTCCAGTCA	AGATCGGAAGAGCGTCGTGTAGGGAAAGAGTGT
fp.70	GGTCTCTACAG	AGATCGGAAGAGCACACGTCTGAACTCCAGTCA	AGATCGGAAGAGCGTCGTGTAGGGAAAGAGTGT
fp.71	ACAGCTCAAACA	AGATCGGAAGAGCACACGTCTGAACTCCAGTCA	AGATCGGAAGAGCGTCGTGTAGGGAAAGAGTGT
fp.72	ATAGCGAACTCA	AGATCGGAAGAGCACACGTCTGAACTCCAGTCA	AGATCGGAAGAGCGTCGTGTAGGGAAAGAGTGT
fp.73	AACCGCATAAGT	AGATCGGAAGAGCACACGTCTGAACTCCAGTCA	AGATCGGAAGAGCGTCGTGTAGGGAAAGAGTGT
fp.74	CTTGAGAAATCG	AGATCGGAAGAGCACACGTCTGAACTCCAGTCA	AGATCGGAAGAGCGTCGTGTAGGGAAAGAGTGT
fp.75	CAGTCGTTAAGA	AGATCGGAAGAGCACACGTCTGAACTCCAGTCA	AGATCGGAAGAGCGTCGTGTAGGGAAAGAGTGT
fp.76	CTTCCAACTCAT	AGATCGGAAGAGCACACGTCTGAACTCCAGTCA	AGATCGGAAGAGCGTCGTGTAGGGAAAGAGTGT
fp.77	AATAGCATGTCTG	AGATCGGAAGAGCACACGTCTGAACTCCAGTCA	AGATCGGAAGAGCGTCGTGTAGGGAAAGAGTGT
fp.78	AAGTCACACACA	AGATCGGAAGAGCACACGTCTGAACTCCAGTCA	AGATCGGAAGAGCGTCGTGTAGGGAAAGAGTGT
fp.79	CACACAAAGTCA	AGATCGGAAGAGCACACGTCTGAACTCCAGTCA	AGATCGGAAGAGCGTCGTGTAGGGAAAGAGTGT
fp.80	GTTCTCCATTA	AGATCGGAAGAGCACACGTCTGAACTCCAGTCA	AGATCGGAAGAGCGTCGTGTAGGGAAAGAGTGT
fp.81	CATCAAGCATAG	AGATCGGAAGAGCACACGTCTGAACTCCAGTCA	AGATCGGAAGAGCGTCGTGTAGGGAAAGAGTGT
fp.82	CAAGCCCTAGTA	AGATCGGAAGAGCACACGTCTGAACTCCAGTCA	AGATCGGAAGAGCGTCGTGTAGGGAAAGAGTGT
fp.83	CCTCTGAGAGCT	AGATCGGAAGAGCACACGTCTGAACTCCAGTCA	AGATCGGAAGAGCGTCGTGTAGGGAAAGAGTGT
fp.84	ACAAGAACCTTG	AGATCGGAAGAGCACACGTCTGAACTCCAGTCA	AGATCGGAAGAGCGTCGTGTAGGGAAAGAGTGT
fp.85	TCATTCCACTCA	AGATCGGAAGAGCACACGTCTGAACTCCAGTCA	AGATCGGAAGAGCGTCGTGTAGGGAAAGAGTGT
fp.86	ACCATCCAACGA	AGATCGGAAGAGCACACGTCTGAACTCCAGTCA	AGATCGGAAGAGCGTCGTGTAGGGAAAGAGTGT
fp.87	ATGCCGGTAATA	AGATCGGAAGAGCACACGTCTGAACTCCAGTCA	AGATCGGAAGAGCGTCGTGTAGGGAAAGAGTGT
fp.88	TCAACCCGTGAA	AGATCGGAAGAGCACACGTCTGAACTCCAGTCA	AGATCGGAAGAGCGTCGTGTAGGGAAAGAGTGT
fp.89	TCTGTAGAGCCA	AGATCGGAAGAGCACACGTCTGAACTCCAGTCA	AGATCGGAAGAGCGTCGTGTAGGGAAAGAGTGT
fp.90	TCGGATCTGTGA	AGATCGGAAGAGCACACGTCTGAACTCCAGTCA	AGATCGGAAGAGCGTCGTGTAGGGAAAGAGTGT
fp.91	ACTACCTCTTCA	AGATCGGAAGAGCACACGTCTGAACTCCAGTCA	AGATCGGAAGAGCGTCGTGTAGGGAAAGAGTGT
fp.92	CTATCCAAGTGG	AGATCGGAAGAGCACACGTCTGAACTCCAGTCA	AGATCGGAAGAGCGTCGTGTAGGGAAAGAGTGT
fp.93	AGCCAGTCATAC	AGATCGGAAGAGCACACGTCTGAACTCCAGTCA	AGATCGGAAGAGCGTCGTGTAGGGAAAGAGTGT
fp.94	GAGTTAGCATCA	AGATCGGAAGAGCACACGTCTGAACTCCAGTCA	AGATCGGAAGAGCGTCGTGTAGGGAAAGAGTGT
fp.95	TAAGACTACTGG	AGATCGGAAGAGCACACGTCTGAACTCCAGTCA	AGATCGGAAGAGCGTCGTGTAGGGAAAGAGTGT
fp.96	GTCTCTCCCTT	AGATCGGAAGAGCACACGTCTGAACTCCAGTCA	AGATCGGAAGAGCGTCGTGTAGGGAAAGAGTGT

5 MODULATION OF MTI BY COMMENSALS

5.1. INTRODUCTION

5.1.1. MECHANISMS OF MTI AVOIDANCE AND SUPPRESSION BY THE MICROBIOME

To survive along the root, rhizosphere microorganisms had to adapt to their host and develop several strategies to escape plant immune responses. Indeed, a large part of the commensals isolated from plant roots does not induce immune transcriptional read-outs (Emonet *et al.*, 2020; Yu *et al.*, 2019a; see Chapter 4).

AVOIDING MAMP-DRIVEN INDUCTION OF IMMUNE RESPONSES

A first effective bacterial strategy is to remain *incognito* and to evade the recognition by PRRs (Yu *et al.*, 2019b). As previously discussed, bacteria present only a selection of MAMPs amongst the full palette of recognizable elicitors described until now. For instance, only a small percentage of *Arabidopsis* rhizosphere bacteria produces flagellin peptides that are effectively recognized by FLS2 (Garrido-Oter *et al.*, 2018; Hacquard *et al.*, 2017). The selective pressure induced by MTI responses led also to variation in MAMP sequences. Many studies reported flg22 variants, both in pathogens such as *R. solanacearum* or adapted commensals like *Sinorhizobium meliloti*, which completely fails to induce immune response in *Arabidopsis* (Felix *et al.*, 1999; Gómez-Gómez *et al.*, 1999; Hind *et al.*, 2016; Lopez-Gomez *et al.*, 2012; Pfund *et al.*, 2004; Sun *et al.*, 2006; Trdá *et al.*, 2014; Yu *et al.*, 2019b).

In addition to sequence variation, bacteria can protect their flagellin monomers by glycosylation to avoid recognition by FLS2. In turn, plants secrete glucosidases to degrade this sugar shield and access the flg22 peptide (Buscaill *et al.*, 2019). Similarly, some fungi secrete Ecp6 or Avr4 effectors that bind to chitin and eventually strengthen the fungal cell walls (van den Burg *et al.*, 2006; Jonge *et al.*, 2010). *Piriformospora indica* produces the β -glucan-binding lectin FBG1. It was proposed that FBG1/ β -glucan complexes compete with free β -glucan fragments to bind the β -glucan receptors with higher affinity and block the induction of downstream responses (Wawra *et al.*, 2016). MAMPs can also be directly degraded by bacteria, notably by AprA extracellular alkaline proteases (Bardoel *et al.*, 2011). Ma *et al.* (2020) also report that two strains of the At-SPHERE collection can degrade flg22 peptides by an unknown mechanism.

Interestingly, bacteria stop to produce flagellin proteins when switching to biofilm mode, which could be a mean to evade immune recognition (Castiblanco and Sundin, 2016; Engl *et al.*, 2014). Biofilms, which consist of aggregate of non-motile bacteria, are produced when bacteria reach the surface of the root (Ramey *et al.*, 2004) and are required for host attachment and virulence, for example by xylem-colonizing pathogens (Castiblanco and Sundin, 2016; Mishra *et al.*, 2012).

ACTIVE SUPPRESSION OF MTI RESPONSES

A second strategy used by bacteria is to directly suppress MAMP-triggered immune responses. The ability to inhibit immune responses was long described for pathogens and contributes to their virulence. However, there is increasing evidence that root commensal and beneficial microbes also modulate MTI. Millet *et al.* (2010) showed that the PGPR *Pseudomonas simiae* strain WCS417R and the pathogen *P. syringae* strain DC3000 inhibit flg22-responses. Similarly, the beneficial bacteria *Bacillus subtilis* FB17 suppresses callose deposition and *CYP71A12*, *MYB51* and *WRKY11* expression (Lakshmanan *et al.*, 2012). Partial transcriptomic downregulation of flg22-responsive genes was also observed after inoculation with *P. simiae* WCS417R (Stringlis *et al.*, 2018c), the *Rhizobium* isolate R129E (Garrido-Oter *et al.*, 2018) and a synthetic bacterial community suppressing flg22-triggered root growth inhibition (RGI) (Ma *et al.*, 2020). Interestingly, *PER5*, *FRK1* and *RBOHD* were part of the flg22-transcriptional responses down-regulated by the RGI-suppressive community. By contrast, a cluster of defence genes, containing *MYB51* and *CYP71A12*, is induced by both RGI-suppressive and non-suppressive bacterial community, suggesting that bacteria might specifically target a subset of the immune responses. This partial suppression could explain why some bacteria induce *PER5* immune transcriptional read-out, but do not cause stronger root growth inhibition on *WER::FLS2* (Emonet *et al.*, 2020).

MTI suppression is very often achieved by the injection of effectors, targeting component of the immune signalling pathway, and requires the expression of the type III secretion system (T3SS). Countless mechanisms have been described for pathogen infections and are reviewed by Asai and Shirasu (2015), Couto and Zipfel (2016) and Toruño *et al.* (2016). Effectors directly targeting MTI signalling are also found in beneficial

microbes such as *Pseudomonas* (*P. simiae* WCS417, *P. defensor* WCS374, other *P. fluorescens* strains, etc.) and *Rhizobia* (Loper *et al.*, 2012; Stringlis *et al.*, 2019b; Yu *et al.*, 2019b). Thus, the rhizobial effector NopM suppresses ROS burst, while NopL blocks the signal transduction of the MAPK cascade (Bartsev *et al.*, 2004; Xin *et al.*, 2012).

However, many commensal bacteria lack a functional T3SS and therefore rely on other mechanisms to suppress MTI (Levy *et al.*, 2018; Teixeira *et al.*, 2019). Rhizosphere bacteria can, for example, modulate plant hormonal pathways. Thus, *B. subtilis* FB17 and *Piriformospora indica* suppress flg22-responses dependent on jasmonic acid (JA) signalling (Jacobs *et al.*, 2013; Lakshmanan *et al.*, 2012). Similarly, *P. syringae* inhibition of flg22 responses was independent of T3SS, but required the production of the phytotoxin coronatine, which mimics JA-Ile, the active form of jasmonic acid (Millet *et al.*, 2010).

Bacterial surface components can also modulate plant-bacteria interactions. Lipopolysaccharides (LPS) are anchored in the outer leaflet of the outer membrane of most gram-negative bacteria. LPS are different between species and are composed of a relatively conserved lipid A domain and a core oligosaccharide domain, decorated with variable O-antigens (Kutschera and Ranf, 2019). LPS are potent virulence factors in animals and part of the lipid A moiety, composed of 3-OH-FAs, is recognized as MAMPs by the LORE receptor (Kutschera *et al.*, 2019; Ranf *et al.*, 2015). O-antigens are very variable and adapt to changing environmental conditions. In animal, LPS structure alteration was shown to avoid immune recognition, but this process was so far not reported in plants (Ranf, 2016). However, LPS suppress the oxidative burst in symbiosis between *Rhizobium* and legumes by an unknown mechanism, which was speculated to rely on specific recognition of LPS by receptors (Albus *et al.*, 2001; Gibson *et al.*, 2008; Scheidle *et al.*, 2005; Tellström *et al.*, 2007).

Interestingly, biofilm components *per se* can be used to suppress MTI. Biofilms are mainly composed of exopolysaccharides (EPS). Aslam *et al.* (2008) showed that EPS produced by *M. meliloti* block flg22 responses through chelation of calcium ions.

Finally, it was recently proposed that the PGPRs *Pseudomonas simiae* WCS417R and *Pseudomonas capeferrum* WCS358 produce gluconic acid, which acidifies their growth medium and inhibits flg22-triggered immune responses. Indeed, two WCS358 mutants,

ApqqF and *ΔcyoB*, impaired in gluconic acid production, failed to suppress flg22-induced responses (Yu *et al.*, 2019a).

5.1.2. *PSEUDOMONAS PROTEGENS* STRAIN CHA0 AS MODEL FOR COMMENSAL COLONIZATION

The *P. protegens* strain CHA0 is among the best characterized root beneficial bacteria with plant-protecting activity. It was shown to suppress soil-borne diseases (Haas 2003), mainly by production of the antifungal compounds 2,4-diacetylphloroglucinol (DAPG) and pyoluteorin (PLT) (Keel *et al.*, 1990, 1992; Maurhofer *et al.*, 1992, 1992). CHA0 also improves plant growth by gluconate-mediated solubilization of phosphate in limiting conditions (de Werra *et al.*, 2009). In addition, CHA0 infects larvae of the plant pest insects *Galleria mellonella* (Flury *et al.*, 2017), colonizes the gut of *Pieris brassicae* and competes with their microbiota using their type VI secretion system (Vacheron *et al.*, 2019). CHA0 bacteria can colonize *A. thaliana*, where they live as commensals at the surface of the root. They usually fail to induce immune transcriptional read-outs except in the elongation zone and around damaged root tissues if inoculated at high concentration (Emonet *et al.*, 2020; Zhou *et al.*, 2020).

We have previously shown that CHA0 native flagellin is detected by the *WER::FLS2* super-competent line, induces strong *PER5* responses but does not affect root growth, suggesting that CHA0 can inhibit at least a subset of flg22-induced responses by an unknown mechanism (Emonet *et al.*, 2020). Most studies investigating the suppression of MTI rely on the combination of bacterial inoculation with flg22 treatment (Yu *et al.*, 2019a; Ma *et al.*, 2020). However, this approach overlooks MTI avoidance mechanisms and relies on very strong concentration of artificially applied MAMPs. Here, we use the *WER::FLS2* super-competent line in mono-association with bacteria to bypass such limitation. The *WER::FLS2* line has also the advantage, that any effect observed specifically in this line, reveals a FLS2-dependent response, rather than the effect driven by multiple MAMPs. We took advantage of the large collection of CHA0 mutants available to screen for components involved in the suppression of root growth inhibition (RGI response) or *PER5* transcriptional responses, induced specifically by native flagellin.

5.2. RESULTS

5.2.1. SELECTION OF CHA0 CANDIDATE MUTANTS IMPAIRED IN FLS2-RESPONSES SUPPRESSION

In collaboration with the group of Prof. Christophe Keel, we selected a set of sixteen CHA0 mutants possibly affecting MTI responses (Table S1). We focused on mutations in components potentially involved in direct suppression of immune responses, but we also included candidates that could affect more generally the virulence and the colonization capacity of CHA0.

Many factors are important CHA0 colonization capacities, from toxin and enzyme secretion to bacterial cell envelop components. We first selected mutants with defects in secondary metabolism or global regulators that could affect virulence. The mutant *ΔphlABCD* is impaired in biosynthesis of DAPG, a major toxic compound produced by CHA0 on roots. It was shown to reduce root growth and to induce defences (Flury *et al.*, 2017). Similarly, the *ofaABC* genes control the biosynthesis of cyclic lipopeptide orfamides. These metabolites affect cell membranes and have a broad-spectrum toxicity on microorganisms or insects (Flury *et al.*, 2017), but their impact on plants was never tested. We also included a mutant defective for the global regulator *gacA*, involved in the general production of secondary metabolites (Laville *et al.*, 1992).

In addition to mutant for secondary metabolites, we included bacteria deficient for the formation of the cell envelop. LPS modification and virulence in response to Mg²⁺ is controlled by the two-component system sensors *phoQ/phoP* (Kupferschmied, 2015). In addition to both single mutants *ΔphoQ* and *ΔphoP*, we also analysed the mutants *Δwzx*, *Δobc3* and *ΔwbpL*, lacking either short OSA type O-antigens (dominant LPS surface structure), long Fcl-type O-antigens, or both, respectively. Indeed, the gene *wbpL* encodes a glycosyltransferase initiating the “capping” of LPS (Kupferschmied *et al.*, 2016).

Colonization can also be affected by bacteria motility and their ability to form biofilms. The *fleQ* gene controls both flagella biogenesis and exopolysaccharides synthesis and contributes to the switch between the two modes of growth (Arora *et al.*, 1997; Hickman and Harwood, 2008). The *ΔfleQ* mutant is indeed aflagellate and was included in our analysis (Jain and Kazmierczak, 2014). In addition, we selected the septuple mutant

ΔpgaABCD ΔpslA ΔalgD ΔpelD defective for the synthesis of all known exopolysaccharides (C.Terrettaz, *unpublished*). To specifically target flagellin synthesis, we finally pick an insertion mutant *fliC::pEMG* that produces non-functional flagellin (Kupferschmied, 2015).

To test if pH-mediated suppression of MTI responses (Yu *et al.*, 2019a) was also involved in the suppression of relative root growth inhibition by CHA0, we included in our selection four mutants impaired in gluconate synthesis. *Δgcd* is defective for the glucose dehydrogenase enzyme required for the oxidation of glucose into gluconic acid. Since this reaction requires as cofactor the pyrroloquinoline quinone, we also analysed the insertion mutant *pqqF:Tn5* (Schnider *et al.*, 1995; de Werra *et al.*, 2009). The *Δgcd* mutant has pleiotropic effects including increase of the DAPG synthesis and pyoverdine siderophores. To rule out their effect, we included the double mutants *Δgcd ΔphlACBD* and *Δgcd pvd::Tn* (Bangera and Thomashow, 1999).

Finally, we took advantage of the screen to include more miscellaneous mutations that might have a role in plant colonization. Type VI secretion system is used by CHA0 to compete with other bacteria when infecting insect gut. Mutants for T6SS are less virulent on insects (Vacheron *et al.*, 2019). T6SS were identified in phytopathogens but also in commensals. It was shown to be involved in interbacterial competition or for the external secretion of compounds such as siderophores, but no direct injection of effectors in plant cells could be so far demonstrated (Bernal *et al.*, 2018). To test whether T6SS modulates MTI, we analysed the mutant *ΔT6SS*, defective in the core apparatus of the T6SS, and the mutant *ΔvgrG1b-mod*, affecting a gene module encoding a spike, an effector and an immunity protein required for T6SS function (Vacheron *et al.*, 2019). We finally tested the mutant *ΔrebB1-3*, encoding putative puncturing pistons called R-bodies. Although its function is still unknown, *rebB1-3* is highly expressed when CHA0 is inoculated on plant roots, but had no impact on virulence to insect (Flury *et al.*, 2016).

5.2.2. *P. PROTEGENS* CHA0 DOES NOT INHIBIT *PER5* INDUCTION

We first assayed all bacteria with a quick screen for *PER5* induction in *WER::FLS2* compared to wild type plants, using a stereomicroscope and confocal imaging for confirmation. Both lines were drop-inoculated with CHA0 mutants and observed at 24h, 48h and 72h. Binocular observations were qualitative and unprecise, but confirmed that wild-type plants did not respond in the meristematic zone (with the exception of some discrete cells) to CHA0 nor any mutants (Fig1A). As expected, *Pseudomonas* R569, as positive control, induced consistently *PER5* over 3 days in *WER::FLS2* (Fig.1AB). CHA0 wild-type strain triggered a detectable and specific *PER5* induction in *WER::FLS2* lines until 3 dpi and most mutants retained this ability (Fig.1AB). This indicates that the absence of root growth inhibition previously observed in CHA0 was not linked to late *PER5* suppression (Emonet *et al.*, 2020).

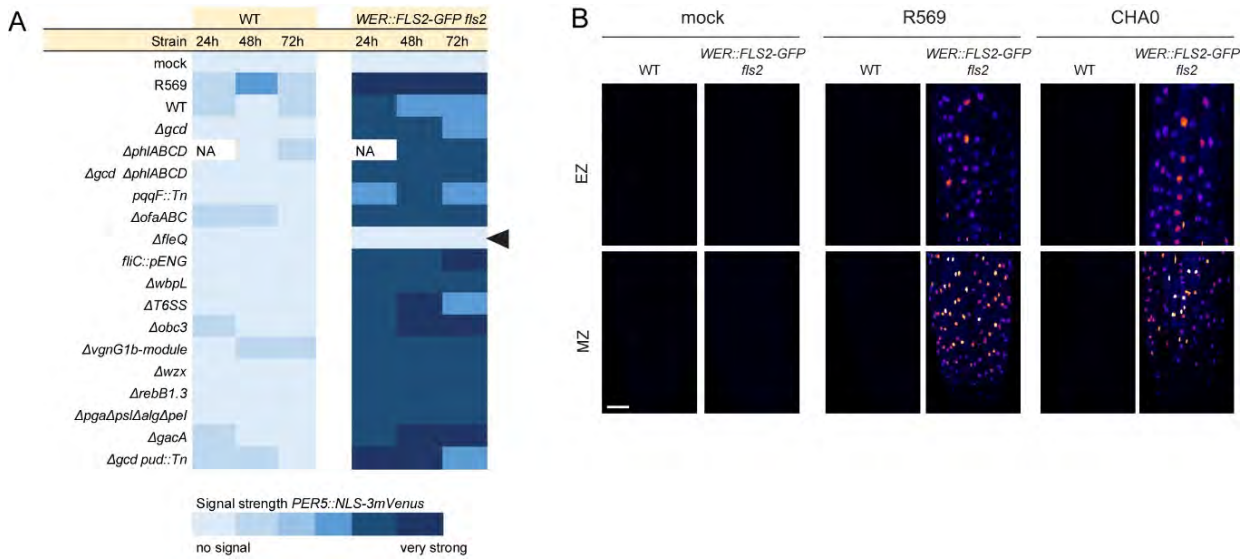


Figure 1: Mutants screen for defects in *PER5* transcriptional read-out induction

(A) Summary graph of *PER5::NLS-3mVenus* responses to the mutant strains of CHA0, assessed in the meristematic zone by binocular. Coloured values are subjective. Only $\Delta fleQ$ mutants fails to induce *PER5* on *WER::FLS2-GFP fls2* (black arrowhead).

(B) *PER5::NLS-3mVenus* marker (Fire LUT) is induced by CHA0 and R569 on *WER::FLS2-GFP fls2* at 3 dpi. Maximum projection of z-stacks pictures of seedlings treated with drop-inoculation of bacterial solution ($OD_{600} = 0.01$) or mock, respectively. Images were acquired in the meristematic (MZ) and elongation (EZ) zones. Acquisition was done with identical settings. Scale bar, 25 μm .

Only the aflagellate mutant $\Delta fleQ$ failed to induce *PER5* (Fig.1A) (Ch.3; Emonet *et al.*, 2020). However, the insertion mutant *fliC::pEMG*, mutated in the gene coding for flagellin, could still activate *PER5* expression (Fig.1A). It could be that, although the *fliC* protein was non-functional due to the transposon insertion, this mutant still contained the *flg22* epitope. We later confirmed that the complete deletion mutant $\Delta fliC$ avoids MTI induction (Emonet *et al.*, 2020).

5.2.3. CHA0 MUTANTS IMPAIRED IN pH REGULATION TEND TO LOSE FLS2-SPECIFIC RGI SUPPRESSION

Different MTI outcomes can be independent, such as ROS burst and MAPK cascade. Moreover, commensal bacteria were several times shown to inhibit only a sector of *flg22*-triggered responses (Garrido-Oter *et al.*, 2018; Stringlis *et al.*, 2018c; Ma *et al.*, 2020). Therefore, we assessed their effect on root growth compared to *Pseudomonas* CHA0 and R569 (Fig.S1).

R569 treatment inhibits wild-type root growth, but drives a stronger inhibition on *WER::FLS2* (Fig.2A, S1A, S1C). The difference between wild-type and *WER::FLS2* root growth inhibition (RGI) is defined as the “relative RGI” and represents the direct effect of the native flagellin of these bacteria. By contrast, CHA0 generally inhibits root growth of wild-type and *WER::FLS2* to the same extent (relative RGI = 0) (Fig.S1A 1st part, S1C 2nd part), indicating that it can suppress part of FLS2 signalling. However, it should be noted that, depending on replicates, CHA0 can sometimes induce a small relative RGI (Fig. 2A, S1C 1st part), but weaker than for R569 treatment.

Highly concentrated bacterial treatments ($OD_{600} = 1$ to 0.1 for wild-type strains) usually completely stop root growth and prevents wild-type and *WER::FLS2* comparison. Therefore, different bacterial concentrations were tested until root growth was only slightly affected in both plant genotypes. A start inoculum of $OD_{600} = 10^{-2}$ (Fig.S1A, S1B) or 10^{-4} (Fig.S1C, S1D) was appropriate for most mutants. However, mutants for Δwzx , $\Delta gcd pvd::Tn$ and $\Delta rebB1.3$ strongly inhibit root growth for both genotypes even when inoculated with a start concentration of $OD_{600} = 10^{-4}$ (Fig. S1C). Therefore, short O-antigen (Δwzx), pH regulation coupled to siderophore synthesis ($\Delta gcd \Delta pvd::Tn$) and R-bodies ($\Delta rebB1.3$) might be required to generally avoid/suppress MTI responses.

We then looked for mutants that induce a stronger root growth inhibition on *WER::FLS2* than on wild-type (increased relative RGI). To better visualize the relative RGI, the differential root growth for each bacterial/mock treatment was calculated, *i.e.* the difference between the root growth of *WER::FLS2* and the mean root growth of wild-type plants (differential growth = WER - mean (WT)) (Fig.2B, S1B, S1D). It is then possible to visually compare the differential growths between mock and bacterial inoculation to assess the relative RGI. Since the differential growth of mock treatment should be close to zero, the differential growth gives an estimate of the relative RGI. A summary of all replicates is found in Table 1. It must be noted that most results had a strong variability.

Table 1: Summary of root growth inhibition screen

Name	Mutant	Group	OD ₆₀₀ = 10 ^x	Increased RGI
CHA0178	$\Delta pqqF::Tn$	pH	-2 * -2 -4 -4 -4	3/5
CHA1196	Δgcd	pH	-2 * -2 -4 -4 -4	3/5
CHA1242	$\Delta gcd \Delta phiABCD$	pH	-2 * -2 -4 -4 -4	2.5/5
CHA5101	$\Delta ofaABC$	2nd. metabolites	-2 -2 -4	2/3
CHA5234	$\Delta pgaABCD \Delta psIA \Delta algD \Delta pelD$	EPS	-2 -3 -4 -4	2/3
CHA5161	$\Delta wbpL$	LPS/OPS	-2 -2	2/2
CHA5133	$\Delta phoQ$	regulation/TCS sensor	-2 * -3 -4 -4	0.5/2
CHA5221	$\Delta rebB1.3$	R bodies	-3 -4	0.5/1
CHA5105	$\Delta fleQ$	regulation/flagella	-2 * -2 -3 -4 * -4	1/5
CHA1241	$\Delta phiABCD$	2nd. metabolites	-2 -2	0/2
CHA5128	$\Delta fliC::pENG$	flagella	-2 -2	0/2
CHA5182	$\Delta obc3$	LPS/OPS	-2 * -2 * -3 -4	0/2
CHA5175	$\Delta T6SS$	T6SS	-2 -3 -4	0/2
sAE119	$\Delta phoP$	regulation/TCS sensor	-2 -3 -4	0/2
CHA5255	$\Delta gacA$	regulation/TCS sensor	-2	0/1
CHA5273	$\Delta gcd \Delta pvd::Tn$	pH	-2 * -3 -4	-
CHA5206	Δwzx	LPS/OPS	-2 * -3 * -4	-
CHA5086	$\Delta vgrG1b$ module+	T6SS	-2	-

relative RGI CHA0 < mutant (green)

relative RGI CHA0 = mutant (yellow)

relative RGI CHA0 > mutant (red)

failed colonization (light grey)

strong inhibition for both WT and *WER::FLS2* (dark grey)

only half the seedlings show the effect (square)

star (*) indicates significant difference (p < 0.05)

Each column represents a biological replicate. Numbers indicate the concentration of bacteria used (e.g. -2 represents OD₆₀₀ = 10⁻²). Colours correspond to difference of relative RGI between CHA0 and mutants: yellow, relative RGI_{CHA0} = relative RGI_{mutant}; green, relative RGI_{CHA0} < relative RGI_{mutant}; red, relative RGI_{CHA0} > relative RGI_{mutant}; light grey, RGI induced by the mutant is too strong to compare WT and *WER::FLS2-GFP fls2* lines. Mutants causing stronger relative RGI failed to suppress FLS2-dependent RGI response (green) and represent the best candidates. Mutants showing very strong inhibition of root growth on both genotypes (light grey) might be defective for genes generally inhibiting immune responses and were not included in the count of "Increased RGI" responses. Square, only half of the seedlings of the replicate shows the effect; star, significant difference calculated between differential growths of CHA0 and mutants (p < 0.05). Multiple comparison performed with Kruskal-Wallis and Dunn's test.

Although most differences in differential growth were not significant, a slight trend was visible for mutants impaired in pH regulation (three mutants out of four, *i.e.* *pqqF::Tn*, *Δgcd* and *Δgcd ΔphiABCD*) (Fig.2AB, S1AB, Table 1). This supports data from Yu *et al.* (2020), indicating that low pH suppresses flg22-responses. As control, *ΔfleQ* mutant, lacking flagellin, is not recognized by FLS2 and do not cause a relative RGI (WT root growth smaller than

WER::FLS2 root growth, as in mock) (Fig.2AB). Moreover, $\Delta ofaABC$ (Fig.S2B) and $\Delta pgaABCD$ $\Delta plsA$ $\Delta algD$ $\Delta pelD$ mutants (Fig.S1D) have also a tendency to increase the relative RGI. Cyclic lipopeptide orfamides and exopolysaccharides might therefore be involved in *flg22*-response suppression by *CHA0*. The $\Delta wbpL$ mutant, impaired in O-antigen capping of LPS, also increases the relative RGI (Fig.S1B). Taken together, the impact of the different mutations was rather weak, but mutants impaired in pH regulation were the most promising candidates.

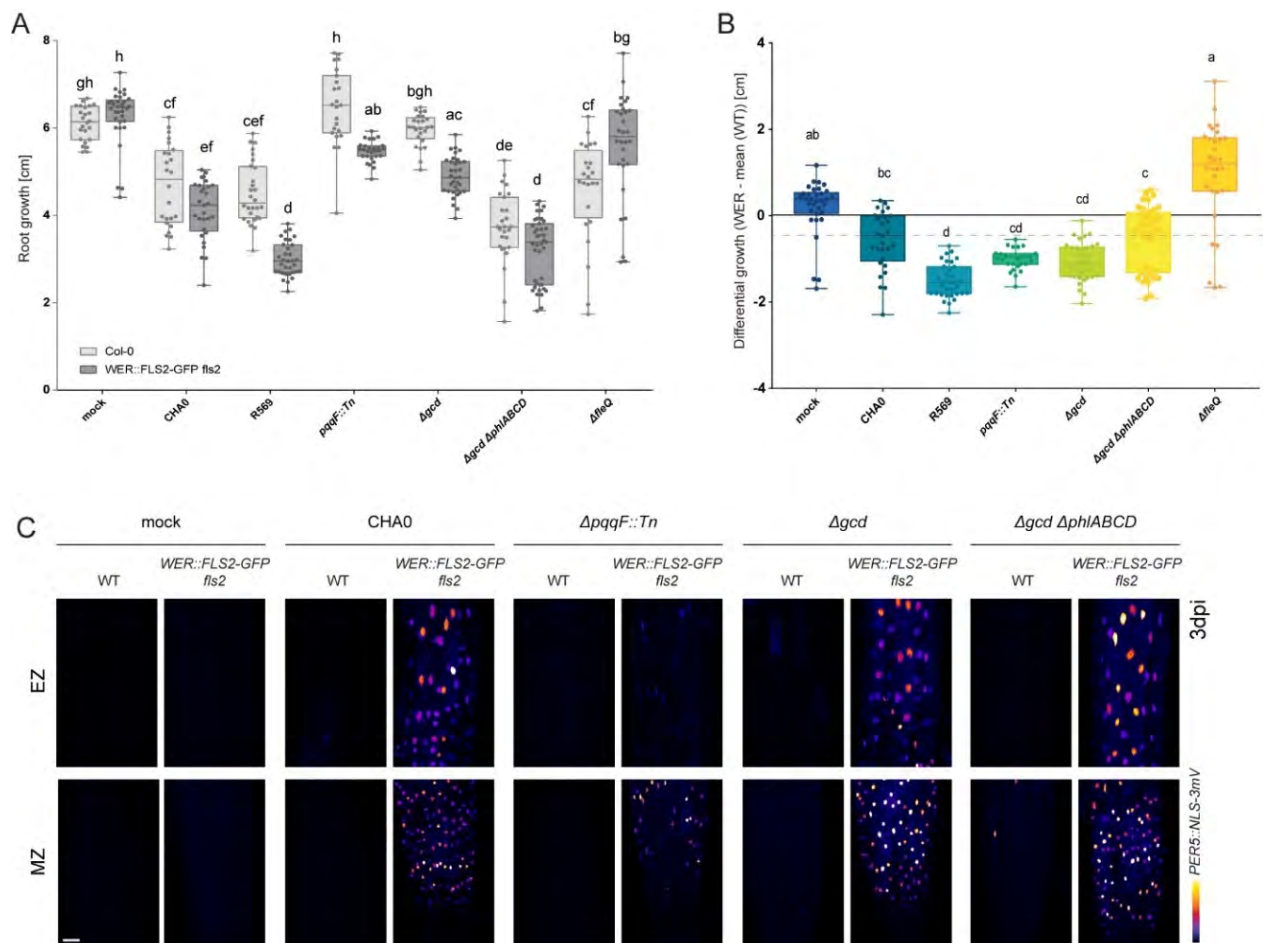


Figure 2: *CHA0* mutants defective in gluconate synthesis induce stronger RGI and modulate *PER5* expression on *WER::FLS2-GFP fls2*.

(A) Gluconate-synthesis defective mutants *pqqF::Tn5*, Δgcd and $\Delta gcd \Delta phiABCD$ tend to induce stronger root growth inhibition in *WER::FLS2-GFP fls2* compared to WT plants. $\Delta fleQ$ mutant reduce the relative RGI compared to *CHA0*. Root growth was measured at 6 dpi on plates inoculated with bacteria at $OD_{600} = 10^{-4}$.

(B) Differential growth calculated from data in (A) as follows: $WER_{values} - \text{mean}(WT_{values})$. Dotted line, *CHA0* reference value. Mutants impaired in pH regulation have decreased differential growth compared to *CHA0*. Different letters indicate statistically significant differences ($p < 0.05$). Multiple comparison was performed using Kruskal-Wallis and Dunn's test (A and B).

(C) Induction of *PER5::NLS-3mVenus* (Fire LUT) on *WER::FLS2-GFP fls2* is increased in meristem with mutants Δgcd and $\Delta gcd \Delta phiABCD$. *pqqF::Tn5* reduces the induction of *PER5*. Maximum projection of z-stacks imaging in meristematic (MZ) and elongation (EZ) zones treated with drop inoculation of bacterial solution ($OD_{600} = 0.01$) or mock, respectively. Images were acquired at 3 dpi. See Fig.S2 for results at 1 dpi. Acquisition done with identical settings. Scale bar, 25 μm .

Mutants impaired in pH regulation were not obviously different from CHA0 for *PER5* transcriptional read-out induction when analysed at the binocular (Fig.1A). Therefore, we used confocal imaging to detect slight changes (Fig.2C, S2A). CHA0 and pH mutants induced *PER5* similarly at 1 dpi. (Fig.S2A). However, after 3 dpi, *PER5* signal expression was slightly increased in *WER::FLS2* after inoculation with *Δgcd* and *Δgcd ΔphlACBD* mutants, compared to CHA0 wild-type strain (Fig.2C). Surprisingly, *pqqF:Tn5* inoculation lead to reduced *PER5* induction compared to CHA0. A preliminary quantification of the global fluorescence tends to support these observations, particularly at 2 dpi (only five seedlings/treatment quantified) (Fig.S2B).

5.2.4. *PSEUDOMONAS SIMIAE* WCS417R AND *PSEUDOMONAS CAPEFERRUM* WCS358 PARTIALLY INHIBIT *PER5* INDUCTION

Since the difference observed with CHA0 mutants defective in pH regulation was very weak, the experiments were repeated with bacterial strains reported to strongly inhibit MTI responses. We used *P. simiae* strain WCS417 and *P. capeferrum* strain WCS358, which suppress *flg22* responses by acidification, and the two associated WCS358 *ΔcyoB* and *ΔpqqF* mutants impaired in gluconic acid synthesis (Yu *et al.*, 2019a).

Surprisingly, WCS417 and WCS358 induced *PER5* expression in the *WER::FLS2* line at both 1 and 3 dpi (Fig.3A), indicating they do not completely inhibit immune responses mediated by FLS2, like previously described for CHA0. At 1dpi, both *ΔcyoB* and *ΔpqqF* mutants display the same phenotype than the wild-type strain WCS358. However, after 3 days, *ΔcyoB* inoculation caused a stronger *PER5* induction than WCS358, supporting the fact that bacteria defective in pH regulation failed to suppress MTI responses. By contrast, *ΔpqqF* abolished *PER5* induction. Interestingly, this phenocopies perfectly the CHA0 *pqqF:Tn5* mutant, suggesting that pyrroloquinoline quinone is required for the induction of the *PER5* gene.

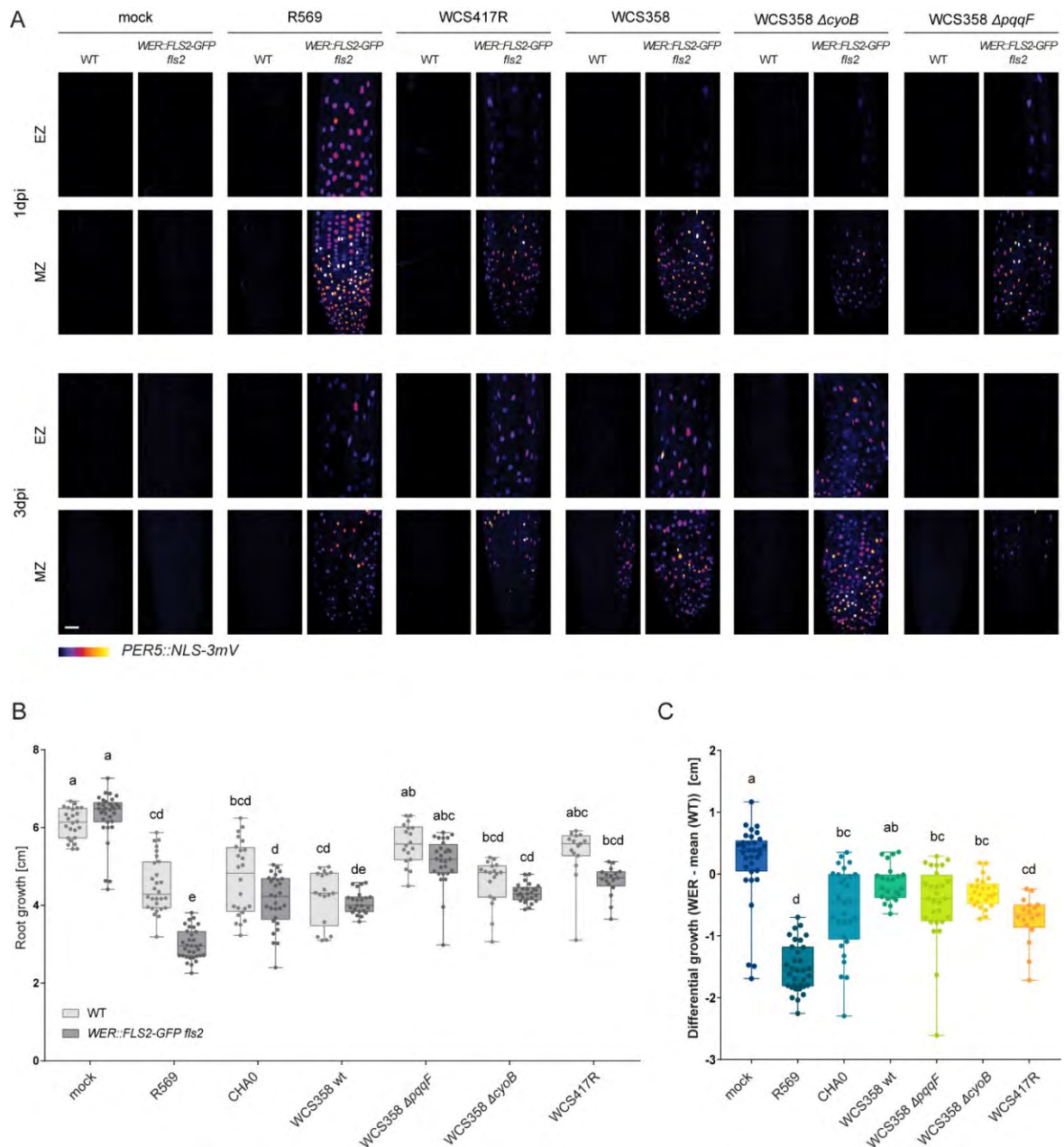


Figure 3: WCS417R and WCS358 cause attenuated *PER5* induction and a reduced relative root growth inhibition compared to R569

(A) WCS417R and WCS358 induce *PER5::NLS-3mVenus* marker (Fire LUT) only in *WER::FLS2-GFP fls2*, but to a lesser extent than R569 at 1 and 3 dpi. Mutants of WCS358 $\Delta cyoB$ and $\Delta pqqF$ trigger increased, respectively, decreased *PER5* responses compared to wild-type strain WCS358. Maximum projection of z-stacks imaging of meristematic (MZ) and elongation (EZ) zones treated with drop-inoculation of mock or bacterial solution ($OD_{600} = 0.01$). Images were acquired at 1 and 3 dpi. Acquisition done with identical settings. Scale bar, 25 μm .

(B) WCS417R and WCS358, as well as the mutants $\Delta cyoB$ and $\Delta pqqF$, induce a relative RGI similar to CHA0 but weaker than R569 effect. Root growth was measured at 6 dpi on plates inoculated with bacteria ($OD_{600} = 10^{-4}$).

(C) Differential growth calculated from data in (B). Seedlings inoculated with WCS417R, WCS358 and associated mutants have similar differential growth than after CHA0 treatment. Different letters indicate statistically significant differences ($p < 0.05$). Multiple comparison was performed using Kruskal-Wallis and Dunn's test (B, C).

5.2.5. *P. SIMIAE* WCS417R AND *P. CAPEFERRUM* WCS358 PARTIALLY SUPPRESS RELATIVE RGI INDEPENDENTLY OF GLUCONATE SYNTHESIS

We also assessed the effect of *P. simiae* strain WCS417 and *P. capeferrum* strain WCS358 on root growth of wild-type and WER::FLS2 lines. When inoculated in agar plates for 6 days, WCS417R, WCS358 and the two mutants $\Delta cyoB$ and $\Delta pqqF$ induced a small relative root growth inhibition similar to the effect of CHA0 strain, and much weaker than the positive control with R569 (Fig.3B, 3C). In that sense, none of the two genes mutated seem to be required, in these conditions, for the inhibition of FLS2-specific RGI, which seemingly contradicts results reported by Yu *et al.* (2019a). Though WCS417R and WCS358 were shown to inhibit flg22-mediated *CYP71A12* activation, their effect on seedling growth inhibition was not tested. Therefore, it is possible that these bacteria only modulate a specific subset of MTI responses including *CYP71A12*, *MYB51* and *PER5*.

5.3. DISCUSSION

5.3.1. VARIABILITY OF RESULTS – NOTE OF CAUTION

Flg22-sensitivity of the super-competent *WER::FLS2* line is an effective tool to easily screen bacterial strains for immune transcriptional read-out activation and root growth inhibition. Screening a collection of CHA0 mutants, we looked for genes involved in native flagellin-response suppression. However, root growth inhibition in response to bacteria was extremely variable, even when using the same concentration (OD_{600}) of bacteria, making the results difficult to interpret. Large differences between technical replicates within the same experiment were often observed. This results in very different outcomes when comparing the relative root growth inhibition induced by mutants and wild-type bacteria (see Table 1). Moreover, this makes it difficult to choose the most appropriate bacterial starting concentration.

CHA0 had also variable effects on *WER::FLS2* root growth inhibition. Indeed, depending on replicates, the differential growth induced by CHA0 was either null (inhibition in *WER::FLS2* equal to WT, no RGI) or negative (inhibition in *WER::FLS2* > WT, small RGI), making the comparison of mutant phenotypes difficult. These differences eventually caused a strong variability between replicates (Table 1).

Overall, it must be kept in mind that most data presented here illustrate tendencies rather than robust results and must be interpreted with caution. It would be worth adapting experimental conditions to minimize variability. Moreover, mutation in CHA0 might affect the bacterial intrinsic growth ability. It should be crucial to test the growth rate of each mutant separately to ensure that the observed effect really reflects bacterial suppression ability. It would be also interesting to monitor bacterial growth directly on root to assess the impact of wild-type and *WER::FLS2* immune responses on the different mutants.

5.3.2. LIPOPOLYSACCHARIDE AND EXOPOLYSACCHARIDE SYNTHESIS MUTANTS

Despite the strong variability encountered across experiments, we could observe some weak phenotypes for two out of three mutants in LPS capping. While the $\Delta wbpL$ mutant, impaired in all types of O-antigen, only reduces the relative RGI between WT and *WER::FLS2*, the mutant Δwzx , defective for short O-antigen, induces an extreme root growth

inhibition on both wild-type and *WER::FLS2* plants. By contrast, the mutant $\Delta obc3$, defective only in long O-antigen, causes the same effect than wild-type CHA0 strains.

O-antigen LPS defective mutants are often described as less viable pathogens that are more sensitive to ROS (Berry *et al.*, 2009; Clifford *et al.*, 2013; Kutschera and Ranf, 2019; Li *et al.*, 2014a; Petrocelli *et al.*, 2012). They are also more easily prone to cell lysis, which should cause increased MAMP release and consequently boosts ROS burst. Indeed, the *Xylella fastidiosa* mutant *wzy*, impaired in O-antigen polymerisation, induces stronger immune responses and ROS production in grapevine (Rapicavoli *et al.*, 2018). The same mechanism could explain the severe growth inhibition observed in the CHA0 Δwzx mutant lacking short O-antigens. A second possibility could be that short O-antigens hide several MAMPs at the bacterial surface, like in animals (Ranf, 2016). Consequently, the Δwzx mutant would be recognized by both wild-type and *WER::FLS2* plants, which will cause strong RGI.

However, these hypotheses do not explain why CHA0 without any O-antigen capping ($\Delta wbpL$) triggers only a mild increase in relative root growth inhibition, specific to native flagellin perception. O-capping might be important for general features of bacterial development that could compensate the strong impact of short O-antigen absence. Indeed, defect in O-capping in *Pseudomonas aeruginosa* was shown to affect biofilm formation (Lau *et al.*, 2009). Altered biofilms could compromise the effect of mutation in short-O antigens, for example preventing efficient bacterial colonization.

Since the mutant for all known exopolysaccharides $\Delta pgaABCD \Delta pslA \Delta algD \Delta pelD$ also induced a relative RGI slightly stronger than wild-type CHA0 strains, biofilms might be important to avoid or inhibit flg22-triggered immunity. Pathogens impaired in exopolysaccharides production were shown to be less virulent and to induce stronger immune responses (Araud-Razou *et al.*, 1998; Denny, 1995; Kemp *et al.*, 2004; Yu *et al.*, 1999). For example, *R. solanacearum* mutants with defective production of the N-acetyl-galactosamine-rich major EPS polymer could infect tomato roots but could not invade their xylem. It was suggested that EPS polymers prevent the agglutination and the direct attachment of bacteria onto the cell wall, thus avoiding the induction of defences (Araud-Razou *et al.*, 1998).

5.3.3. GLUCONATE SYNTHESIS AFFECTS *PER5* INDUCTION

Yu *et al.* (2019) recently showed that flg22-responses suppression by commensals was dependent on acidification. Using *Pseudomonas* CHA0, we could observe that mutants defective in gluconate synthesis (Δgcd and $\Delta gcd \Delta phiABCD$) increased slightly *PER5* induction. Accordingly, the WCS358 mutant $\Delta cyoB$ also increased the activation of the *PER5* transcriptional read-out, suggesting that production of gluconic acid might indeed be required to reduce native flagellin-responses.

However, for both CHA0 and WCS358 strains, the corresponding mutants *pqqF::Tn5* and $\Delta pqqF$ strongly reduced *PER5* induction, which contrasts with the increase of *CYP71A12* and *MYB51* defence markers observed by Yu *et al.* (2019). Pyrroloquinoline quinone (PQQ) was shown to be important for bacterial growth (Shen *et al.*, 2012; Velterop *et al.*, 1995). Reduced induction of *PER5* could be simply due to fewer bacteria present around the root. However, Yu *et al.* (2019) found that both $\Delta cyoB$ and $\Delta pqqF$ were growing even better than wild type bacteria on root exudates. However, they observed that the mutation of *pqqF* impaired WCS358 rhizosphere colonization. The effect was much less pronounced for $\Delta cyoB$ mutants. This could suggest that $\Delta pqqF$ mutants are more sensitive to plant defences. Interestingly, PQQ was shown to protect bacterial cells against oxidative damages. Bacteria producing PQQ had also a higher tolerance to hydrogen peroxides

(Misra *et al.*, 2012). Consequently, plants might kill more easily the $\Delta pqqF$ mutants and hinder plant colonization. This might explain the weak activation of immune read-outs compared to other mutants, less sensitive to the plant arsenal. Alternatively, the $\Delta pqqF$ mutant overproduces the antibiotic pyoluteorin (Schnider *et al.*, 1995). This might have an undescribed effect on plant roots.

This nevertheless does not explain why WCS358 $\Delta pqqF$ can strongly induce *CYP71A12* and *MYB51* (Yu *et al.*, 2019a). We have previously mentioned that different transcriptional read-outs have distinct patterns of induction (Poncini *et al.*, 2017; Zhou *et al.*, 2020). Therefore, *PER5* might respond differently to WCS358 $\Delta pqqF$ than *CYP71A12* and *MYB51*. Indeed, *WCS417R* and *WCS358* also failed to suppress *WRKY11* (Yu *et al.*, 2019a).

5.3.4. IS ACIDIFICATION RESPONSIBLE FOR SUPPRESSION OF ROOT GROWTH INHIBITION?

Mutants impaired in gluconate synthesis had variable effects on root growth. Three out of the four “pH mutants” slightly increased the relative RGI compared to CHA0, included *ΔpqqF*, which contrasts with its effect on *PER5* induction. Moreover, *Δgcd pvd::Tn* also strongly reduced root growth of both wild type and *WER::FLS2*. The *pvd::Tn* mutation prevents the synthesis of the pyoverdine siderophore, suggesting an important role for pyoverdine in the suppression of plant immune responses. By contrast to *PER5* induction, WCS358 *ΔcyoB* and *ΔpqqF* strains induced the same relative RGI than wildtype strains.

Why so many discrepancies? Firstly, it should be remembered that the *PER5* transcriptional read-out assays, the RGI assays as well as the experiments performed by Yu *et al.* (2019a) were done in different experimental conditions: drop-inoculation on roots, bacterial inoculation inside agar plate or liquid culture with flg22 treatment, respectively. Moreover, the three methods highlight responses at different time points. Drop-inoculation ensures that bacteria form a thick colony at the root surface. Patches of bacteria were indeed easily visible at the microscope. It might therefore be easier for bacteria to modify locally the rhizosphere environment. By contrast, bacteria growing inside the agar might have increased difficulties to acidify their medium. Interestingly, Yu *et al.* (2019a) grew seedlings in liquid culture supplemented with 5g/l of sucrose, a dimer of fructose and glucose. This last sugar is the substrate of the bacterial glucose dehydrogenase enzyme (*gcd* gene) that produces gluconic acid to acidify the growth medium. Therefore, the ability of *Pseudomonas* to inhibit flg22-responses might be dependent of sucrose availability, questioning its biological relevance *in plantae*.

The variability observed might also come from the comparison of three different strains of bacteria. *P. protegens* CHA0 might have a stronger ability to produce gluconate compared to WCS358. This could be easily verified by an *in vitro* assay. Finally, it has to be noted that Yu *et al.* (2019a) only analysed the induction of transcriptional read-outs, but never assessed the inhibitory effect of acidification directly on root growth. Therefore, gluconate-mediated inhibition of flg22-responses might only affect *MYB51*, *CAP71A12* and *PER5* expression. Overall, inhibition of immune responses only mildly relies on pH alteration and probably depends on the amount of glucose present in the environment.

Low pH was previously shown to induce calcium influx and to desensitise the plant to flg22 responses (Westphal *et al.*, 2019). Indeed, acidification induces transcriptional changes overlapping with MTI responses, such as increased expression of *WRKYs* and calcium-dependent genes (Lager *et al.*, 2010). Therefore, pH-mediated inhibition of immune responses might only operate when plants are pre-inoculated with bacteria decreasing the pH, then treated with flg22. This could explain why the effect of CHA0 and WCS “pH mutants” was small on RGI assay since successive treatment with flg22 was not used.

In summary, despite a strong variability dependent on experimental conditions, we could highlight some genes potentially implicated in the suppression of native flagellin-responses (*PER5* induction and RGI), involved in gluconate synthesis, biofilm formation or LPS capping. Therefore, the super-competent line *WER::FLS2* made possible the analysis of the direct suppression of flg22-triggered immunity without relying on co-treatment with flg22, and proved to be a useful tool to assess the regulation of MTI.

5.4. MATERIAL AND METHODS

If not specified, plant material, bacterial strains, methods and statistical analyses were identical to the ones used in Emonet *et al.* (2020).

5.4.1. BACTERIAL STRAINS AND GROWTH CONDITIONS

Pseudomonas protegens CHA0 and its mutants were offered by Prof. Christoph Keel. An exhaustive list and references are found in Table S1. *Pseudomonas* R569 was obtained from At-SPHERE culture collection (Cologne) (Bai *et al.*, 2015). *P. simiae* WCS417 and *P. capeferrum* WCS358, as well as the corresponding mutants $\Delta cyoB$ and $\Delta pqqF$, were kindly provided by Prof. Corné Pieterse (Yu *et al.*, 2019a). For selection, WCS bacteria were inoculated on ½ TSB plates supplemented with 150 mg/ml of rifampicin acid and incubated at 28°C for minimum 24h. For experiments, bacteria were routinely cultured without antibiotics at 28°C on half-strength tryptic soy broth (TSB).

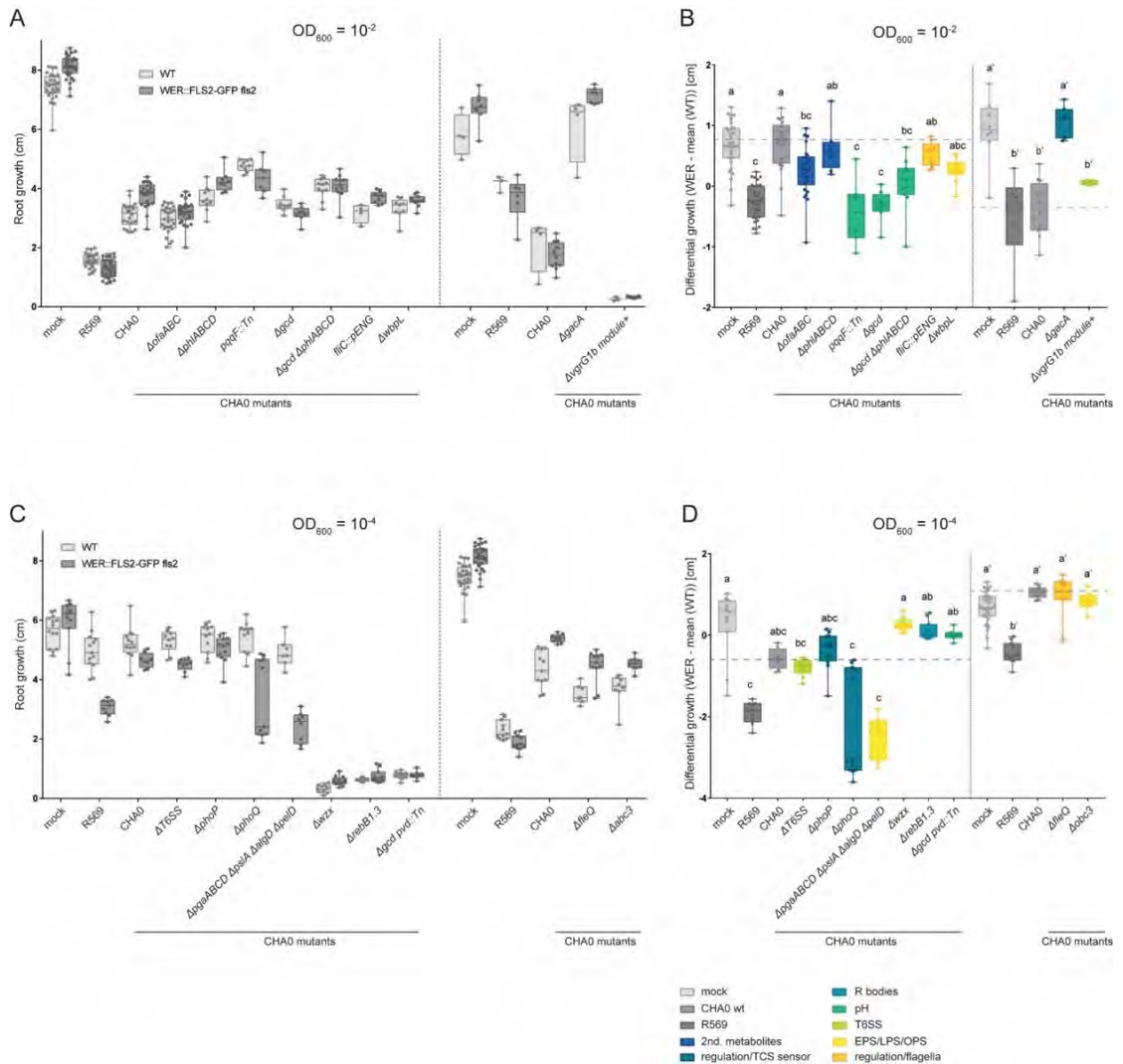
5.4.2. BACTERIAL ROOT INOCULATION ASSAYS

Infection assays were performed as described previously, with the drop inoculation method for microscopy analyses or in agar plate for root growth assays (Emonet *et al.*, 2020). For RGI assays, plates were scanned at 6 dpi and root growth measured using Fiji plugins Simple Neurite Tracer (Frangi *et al.*, 1998).

5.4.3. QUANTIFICATION OF *PER5* SIGNALLING

Images were processed using the Fiji software. Quantification of *PER5* induction was done on five roots by genotype and by treatment. Raw Intensity Density was measured on the complete picture and the mean calculated.

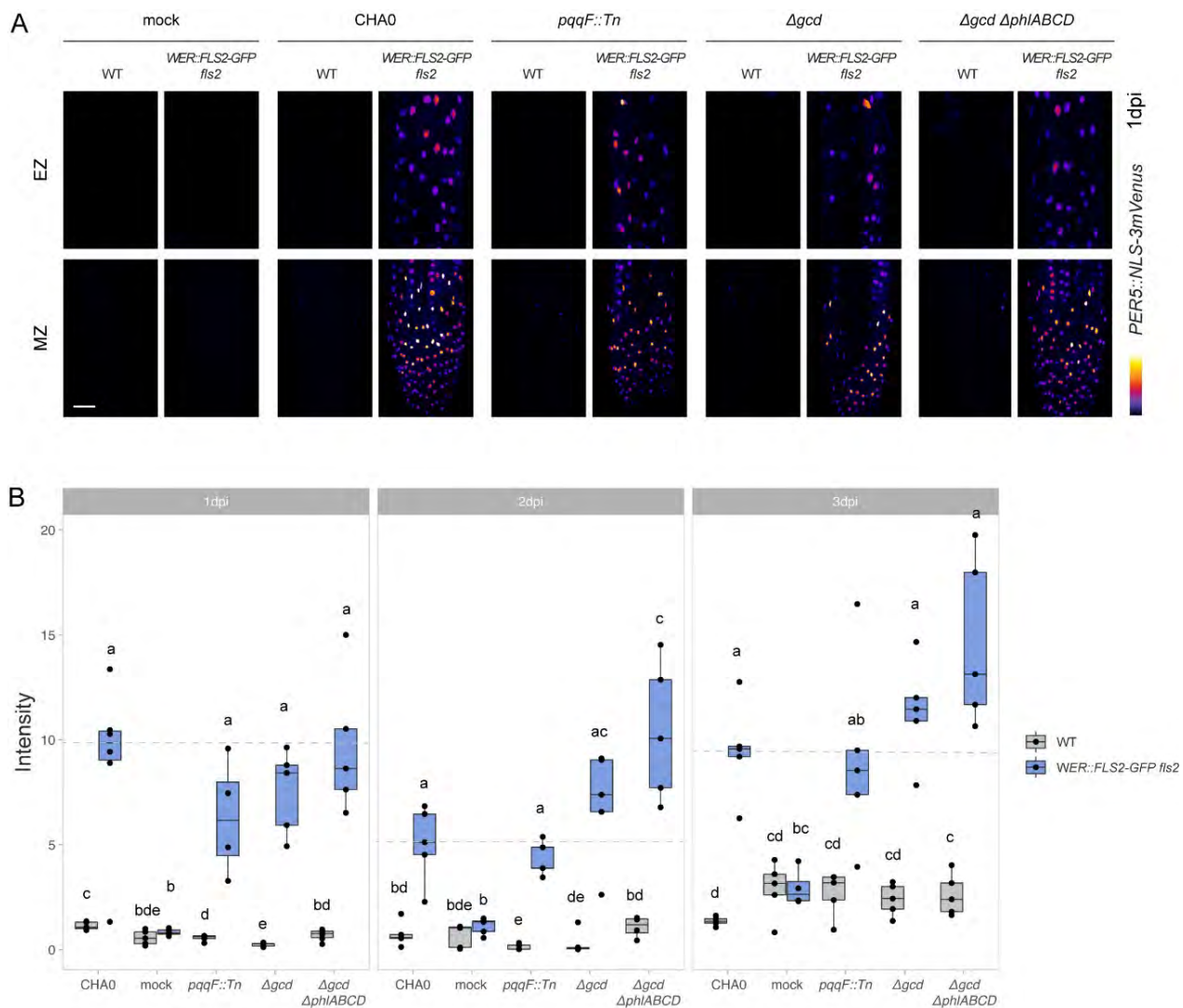
5.5. SUPPLEMENTAL FIGURES AND TABLES



Supplemental Figure 1: Mutant screen for increased RGI highlights candidate genes involved in LPS capping and exopolysaccharide synthesis

(A and C) CHA0 mutants influence root growth of WT and *WER::FLS2-GFP fls2*. Growth was measured at 6 dpi on plate inoculated with bacteria at $OD_{600} = 10^{-2}$ (A) and 10^{-4} (C). Note the strong growth inhibition on both genotypes caused by Δwzx , $\Delta\text{gcd pvd}::\text{Tn}$ and $\Delta\text{rebB1.3}$. Vertical line separates two different experiments.

(B and D) Differential growth calculated from data in (A) and (C), respectively. Note the reduction of differential growth for pH-related mutants Δgcd , $\Delta\text{gcd } \Delta\text{phiABC}$, $\text{pqqF}::\text{Tn5}$ (B); EPS/LPS mutants, ΔwbpL (B) and $\Delta\text{pgaABCD } \Delta\text{psIA } \Delta\text{algD } \Delta\text{pelD}$ (D) and secondary metabolism mutant ΔofaABC (B). Dotted line, CHA0 reference value. Different letters indicate statistically significant differences ($p < 0.05$). Multiple comparisons were performed using Kruskal-Wallis and Dunn's tests (B 1st part, D) or ANOVA and Tukey's HSD tests (B 2nd part).



Supplemental Figure 2: Mutants screen for defects in *PER5* transcriptional read-out induction

(A) Mutants *pqqF::Tn5*, *Δgcd* and *Δgcd ΔphiACBD* induce *PER5::NLS-3mVenus* (Fire LUT) similarly on *WER::FLS2-GFP fls2* and WT at 1 dpi. Same experiment than Fig.2C. Maximum projections of z-stacks pictures of seedlings treated with drop-inoculation of bacterial solution ($OD_{600} = 0.01$) or mock, respectively. Images were acquired at 1 dpi in the meristematic (MZ) and elongation (EZ) zones. Acquisition was done with identical settings. Scale bar, 25 μ m.

(B) Preliminary quantification of *PER5::NLS-3mVenus* signal from the experiment in (A). Fluorescence of five seedlings/treatment was measured. Multiple comparisons were performed using Kruskal-Wallis and Pairwise Wilcoxon Rank Sum Tests. Different letters indicate significant differences ($p < 0.05$).

Table S1: List of CHA0 mutants and references

Name	Mutant	Group	Mutant phenotype	Remark	Reference
CHA1241	<i>ΔphlABCD</i>	2nd. metabolites	Defective for 2,4-diacetylphloroglucinol (DAPG) biosynthesis	Major toxic compound produced on roots; affects root growth, induces plant defences	Flury <i>et al.</i> (2017)
CHA5101	<i>ΔofaABC</i>	2nd. metabolites	Defective for the biosynthesis of cyclic lipopeptide orfamide	Affects cell membranes, broad-spectrum toxic effects on microorganisms, insects, unknown for plants	Flury <i>et al.</i> (2017)
CHA5234	<i>ΔpgaABCD ΔpslA ΔalgD ΔpelD</i>	EPS	Defective for all four known EPS: Psl, alginate, Pel and PNAG	Exopolysaccharides, possible involvement in biofilm formation and host colonization	C. Terrettaz, unpublished
CHA5128	<i>fliC::pENG</i>	flagella	Defective for flagellin FliC (with Flg22 epitope), flagella negative	Motility, MAMP, immune defence inducer	Kupferschmied (2015)
CHA5161	<i>ΔwbpL</i>	LPS/OPS	Defective for the initiating glycosyltransferase WbpL	No short (OSA-type) and no long (Fcl-type) O-antigens = no capping	Kupferschmied <i>et al.</i> (2016)
CHA5182	<i>Δobc3</i>	LPS/OPS	Defective for entire cluster specifying long LPS O-polysaccharide	No long LPS O-antigen: similar to <i>Rhizobium</i> O-antigen, unknown role in plant interaction, phage receptor	Kupferschmied <i>et al.</i> (2016)
CHA5206	<i>Δwzx</i>	LPS/OPS	Defective for flippase Wzx	No short OSA type O-antigen	Kupferschmied <i>et al.</i> (2016)
CHA0178	<i>pqqF::Tn</i>	pH	Defective for pyrroloquinoline quinone, cofactor of Gcd	Results in reduced medium acidification	Schnider <i>et al.</i> (1995)
CHA1196	<i>Δgcd</i>	pH	Defective for glucose dehydrogenase (glucose to gluconate)	Results in reduced medium acidification; secondary effects on DAPG and Pvd	de Werra <i>et al.</i> (2009)
CHA1242	<i>Δgcd ΔphlABCD</i>	pH	Defective for glucose dehydrogenase and DAPG	Reduced medium acidification and lack of major broad-spectrum toxic compound	M. Péchyne Tarr, unpublished
CHA5273	<i>Δgcd pvd::Tn</i>	pH	Defective for glucose dehydrogenase and pyoverdine (Pvd)	Reduced medium acidification and lack of major siderophore (iron chelator)	M. Péchyne Tarr, unpublished
CHA5221	<i>ΔrebB1.3</i>	R bodies	Defective for R-bodies, putative membrane puncturing pistons	Function unknown, no role in insects, highly expressed on plant roots	Flury <i>et al.</i> (2016); P. Vesga unpublished
CHA5105	<i>ΔfleQ</i>	regulation/ flagella	Defective for flagella and EPS regulator FleQ	Regulator of flagella biogenesis and EPS synthesis, c-di-GMP-dependent	M. Péchyne Tarr, unpublished
CHA5133	<i>ΔphoQ</i>	regulation/ TCS sensor	Defective for TCS sensor PhoQ	Sensor of TCS controlling LPS modification systems and virulence in response to Mg ²⁺	Kupferschmied (2015)
CHA5255	<i>ΔgacA</i>	regulation/ TCS sensor	Defective for global regulator GacA (response regulator of TCS)	Defective for multiple traits, including production of secondary metabolites	new by C. Terrettaz; Laville <i>et al.</i> (1992)
sAE119	<i>ΔphoP</i>	regulation/ TCS sensor	Defective for TCS sensor PhoP	Sensor of TCS controlling LPS modification systems and virulence in response to Mg ²⁺	Kupferschmied (2015)
CHA5086	<i>ΔvgrG1b module+</i>	T6SS	Defective for the T6SS VgrG1b spike, effectors, adaptors, +	Reduced virulence, function unknown	Vacheron <i>et al.</i> (2019)
CHA5175	<i>ΔT6SS</i>	T6SS	Defective for the type VI secretion core apparatus	Reduced virulence, cellular injection of toxic effectors	Vacheron <i>et al.</i> (2019)

Supplemental Table S2: Primers for *Pseudomonas capeferrum* WCS358 genotyping

Code	Sequence (5'-3')	Description	Type
oAE144	CGGTTTACAAGCATAACTAGTGCGGC	Genotyping WCS358 bacteria	F
oAE145	CTCGTTTCACGCTGAATATGGCTC	Genotyping WCS358 bacteria	R
oAE146	CGATCCTGATCATCATCGCGCTG	Genotyping WCS358 $\Delta cyoB$ bacteria	F
oAE147	GGTTCATGCCTTCGTA CTGTGCGAC	Genotyping WCS358 $\Delta cyoB$ bacteria	R
oAE148	TCAAAGCCGAACCGCTGTATGC	Genotyping WCS358 $\Delta pqqF$ bacteria	F
oAE149	CAGGTCATTAGCCTGTCGGATTG	Genotyping WCS358 $\Delta pqqF$ bacteria	R

5.6. LITERATURE

- Albus, U., Baier, R., Holst, O., Pühler, A., and Niehaus, K. (2001). Suppression of an elicitor-induced oxidative burst reaction in *Medicago sativa* cell cultures by *Sinorhizobium meliloti* lipopolysaccharides. *New Phytol.* *151*, 597–606.
- Araud-Razou, I., Vasse, J., Montrozier, H., Etchebar, C., and Trigalet, A. (1998). Detection and Visualization of the Major Acidic Exopolysaccharide of *Ralstonia solanacearum* and its Role in Tomato Root Infection and Vascular Colonization. *Eur. J. Plant Pathol.* *104*, 795–809.
- Arora, S.K., Ritchings, B.W., Almira, E.C., Lory, S., and Ramphal, R. (1997). A transcriptional activator, FleQ, regulates mucin adhesion and flagellar gene expression in *Pseudomonas aeruginosa* in a cascade manner. *J. Bacteriol.* *179*, 5574–5581.
- Asai, S., and Shirasu, K. (2015). Plant cells under siege: plant immune system versus pathogen effectors. *Curr. Opin. Plant Biol.* *28*, 1–8.
- Aslam, S.N., Newman, M.-A., Erbs, G., Morrissey, K.L., Chinchilla, D., Boller, T., Jensen, T.T., De Castro, C., Ierano, T., Molinaro, A., *et al.* (2008). Bacterial Polysaccharides Suppress Induced Innate Immunity by Calcium Chelation. *Curr. Biol.* *18*, 1078–1083.
- Bangera, M.G., and Thomashow, L.S. (1999). Identification and Characterization of a Gene Cluster for Synthesis of the Polyketide Antibiotic 2,4-Diacetylphloroglucinol from *Pseudomonas fluorescens* Q2-87. *J. Bacteriol.* *181*, 3155–3163.
- Bardoel, B.W., Ent, S. van der, Pel, M.J.C., Tommassen, J., Pieterse, C.M.J., Kessel, K.P.M. van, and Strijp, J.A.G. van (2011). *Pseudomonas* Evades Immune Recognition of Flagellin in Both Mammals and Plants. *PLoS Pathog.* *7*, e1002206.
- Bartsev, A.V., Deakin, W.J., Boukli, N.M., McAlvin, C.B., Stacey, G., Malnoë, P., Broughton, W.J., and Staehelin, C. (2004). NopL, an Effector Protein of *Rhizobium sp.* NGR234, Thwarts Activation of Plant Defense Reactions. *Plant Physiol.* *134*, 871–879.
- Bernal, P., Llamas, M.A., and Filloux, A. (2018). Type VI secretion systems in plant-associated bacteria. *Environ. Microbiol.* *20*, 1–15.
- Berry, M.C., McGhee, G.C., Zhao, Y., and Sundin, G.W. (2009). Effect of a *waaL* mutation on lipopolysaccharide composition, oxidative stress survival, and virulence in *Erwinia amylovora*. *FEMS Microbiol. Lett.* *291*, 80–87.
- van den Burg, H.A., Harrison, S.J., Joosten, M.H.A.J., Vervoort, J., and de Wit, P.J.G.M. (2006). *Cladosporium fulvum* Avr4 Protects Fungal Cell Walls Against Hydrolysis by Plant Chitinases Accumulating During Infection. *Mol. Plant-Microbe Interactions* *19*, 1420–1430.
- Buscaill, P., Chandrasekar, B., Sanguankiatichai, N., Kourelis, J., Kaschani, F., Thomas, E.L., Morimoto, K., Kaiser, M., Preston, G.M., and Ichinose, Y. (2019). Glycosidase and glycan polymorphism control hydrolytic release of immunogenic flagellin peptides. *PLANT Sci.* *364*, eaav0748.
- Castiblanco, L.F., and Sundin, G.W. (2016). New insights on molecular regulation of biofilm formation in plant-associated bacteria. *J. Integr. Plant Biol.* *58*, 362–372.
- Clifford, J.C., Rapicavoli, J.N., and Roper, M.C. (2013). A Rhamnose-Rich O-Antigen Mediates Adhesion, Virulence, and Host Colonization for the Xylem-Limited Phytopathogen *Xylella fastidiosa*. *Mol. Plant-Microbe Interactions* *26*, 676–685.
- Couto, D., and Zipfel, C. (2016). Regulation of pattern recognition receptor signalling in plants. *Nat. Rev. Immunol.* *16*, 537.

- Denny, T.P. (1995). Involvement of Bacterial Polysaccharides in Plant Pathogenesis. *Annu. Rev. Phytopathol.* 33, 173–197.
- Emonet, A., Zhou, F., Vacheron, J., Heiman, C.M., Tendon, V.D., Ma, K.-W., Schulze-Lefert, P., Keel, C., and Geldner, N. (2020). Spatially Restricted Immune Responses Allow for Root Meristematic Activity During Bacterial Colonisation. *BioRxiv* 2020.08.03.233817.
- Engl, C., Waite, C.J., McKenna, J.F., Bennett, M.H., Hamann, T., and Buck, M. (2014). Chp8, a Diguanylate Cyclase from *Pseudomonas syringae* pv. *Tomato* DC3000, Suppresses the Pathogen-Associated Molecular Pattern Flagellin, Increases Extracellular Polysaccharides, and Promotes Plant Immune Evasion. *MBio* 5, e01168-14.
- Felix, G., Duran, J.D., Volko, S., and Boller, T. (1999). Plants have a sensitive perception system for the most conserved domain of bacterial flagellin. *Plant J.* 18, 265–276.
- Flury, P., Aellen, N., Ruffner, B., Péchy-Tarr, M., Fataar, S., Metla, Z., Dominguez-Ferrerias, A., Bloemberg, G., Frey, J., Goesmann, A., *et al.* (2016). Insect pathogenicity in plant-beneficial pseudomonads: phylogenetic distribution and comparative genomics. *ISME J.* 10, 2527–2542.
- Flury, P., Vesga, P., Péchy-Tarr, M., Aellen, N., Dennert, F., Hofer, N., Kupferschmied, K.P., Kupferschmied, P., Metla, Z., Ma, Z., *et al.* (2017). Antimicrobial and Insecticidal: Cyclic Lipopeptides and Hydrogen Cyanide Produced by Plant-Beneficial *Pseudomonas* Strains CHA0, CMR12a, and PCL1391 Contribute to Insect Killing. *Front. Microbiol.* 8, 100.
- Frangi, A.F., Niessen, W.J., Vincken, K.L., and Viergever, M.A. (1998). Multiscale vessel enhancement filtering. In *Medical Image Computing and Computer-Assisted Intervention — MICCAI'98*, W.M. Wells, A. Colchester, and S. Delp, eds. (Berlin, Heidelberg: Springer), pp. 130–137.
- Garrido-Oter, R., Nakano, R.T., Dombrowski, N., Ma, K.-W., McHardy, A.C., and Schulze-Lefert, P. (2018). Modular Traits of the Rhizobiales Root Microbiota and Their Evolutionary Relationship with Symbiotic Rhizobia. *Cell Host Microbe* 24, 155-167.e5.
- Gibson, K.E., Kobayashi, H., and Walker, G.C. (2008). Molecular Determinants of a Symbiotic Chronic Infection. *Annu. Rev. Genet.* 42, 413–441.
- Gómez-Gómez, L., Felix, G., and Boller, T. (1999). A single locus determines sensitivity to bacterial flagellin in *Arabidopsis thaliana*. *Plant J.* 18, 277–284.
- Hacquard, S., Spaepen, S., Garrido-Oter, R., and Schulze-Lefert, P. (2017). Interplay Between Innate Immunity and the Plant Microbiota. *Annu. Rev. Phytopathol.* 55, 565–589.
- Hickman, J.W., and Harwood, C.S. (2008). Identification of FleQ from *Pseudomonas aeruginosa* as a c-di-GMP-responsive transcription factor. *Mol. Microbiol.* 69, 376–389.
- Hind, S.R., Strickler, S.R., Boyle, P.C., Dunham, D.M., Bao, Z., O'Doherty, I.M., Baccile, J.A., Hoki, J.S., Viox, E.G., Clarke, C.R., *et al.* (2016). Tomato receptor FLAGELLIN-SENSING 3 binds flgII-28 and activates the plant immune system. *Nat. Plants* 2, 1–8.
- Jacobs, S., Kogel, K.-H., and Schäfer, P. (2013). Root-Based Innate Immunity and Its Suppression by the Mutualistic Fungus *Piriformospora indica*. In *Piriformospora Indica*, A. Varma, G. Kost, and R. Oelmüller, eds. (Springer Berlin Heidelberg), pp. 223–237.
- Jain, R., and Kazmierczak, B.I. (2014). A Conservative Amino Acid Mutation in the Master Regulator *FleQ* Renders *Pseudomonas aeruginosa* Aflagellate. *PLoS ONE* 9, e97439.
- Jonge, R. de, Esse, H.P. van, Kombrink, A., Shinya, T., Desaki, Y., Bours, R., Krol, S. van der, Shibuya, N., Joosten, M.H.A.J., and Thomma, B.P.H.J. (2010). Conserved Fungal LysM Effector Ecp6 Prevents Chitin-Triggered Immunity in Plants. *Science* 329, 953–955.

- Keel, C., OBERHANSLI, T., WIRTHNER, P., Voisard, C., Haas, D., and Défago, G. (1990). Pseudomonads as antagonists of plant pathogens in the rhizosphere: role of the antibiotic 2, 4-diacetylphloroglucinol in the suppression of black root rot of tobacco. *Symbiosis* 9, 327-341.
- Keel, C., Schnider, U., Maurhofer, M., Voisard, C., Laville, J., Burger, U., Wirthner, P.J., Haas, D., and Défago, G. (1992). Suppression of root diseases by *Pseudomonas fluorescens* CHA0: importance of the bacterial secondary metabolite 2, 4-diacetylphloroglucinol. *Mol. Plant. Microbe Interact.* 5, 4-13.
- Kemp, B.P., Horne, J., Bryant, A., and Cooper, R.M. (2004). *Xanthomonas axonopodis* pv. *manihotis gumD* gene is essential for EPS production and pathogenicity and enhances epiphytic survival on cassava (*Manihot esculenta*). *Physiol. Mol. Plant Pathol.* 64, 209-218.
- Kupferschmied, P. (2015). Molecular basis and regulation of insect pathogenicity in plant-beneficial pseudomonads. Université de Lausanne, Faculté de biologie et médecine.
- Kupferschmied, P., Chai, T., Flury, P., Blom, J., Smits, T.H.M., Maurhofer, M., and Keel, C. (2016). Specific surface glycan decorations enable antimicrobial peptide resistance in plant-beneficial pseudomonads with insect-pathogenic properties. *Environ. Microbiol.* 18, 4265-4281.
- Kutschera, A., and Ranf, S. (2019). The multifaceted functions of lipopolysaccharide in plant-bacteria interactions. *Biochimie* 159, 93-98.
- Kutschera, A., Dawid, C., Gisch, N., Schmid, C., Raasch, L., Gerster, T., Schäffer, M., Smakowska-Luzan, E., Belkhadir, Y., Vlot, A.C., *et al.* (2019). Bacterial medium-chain 3-hydroxy fatty acid metabolites trigger immunity in *Arabidopsis* plants. *Science* 364, 178-181.
- Lager, I., Andréasson, O., Dunbar, T.L., Andreasson, E., Escobar, M.A., and Rasmusson, A.G. (2010). Changes in external pH rapidly alter plant gene expression and modulate auxin and elicitor responses. *Plant Cell Environ.* 33, 1513-1528.
- Lakshmanan, V., Kitto, S.L., Caplan, J.L., Hsueh, Y.-H., Kearns, D.B., Wu, Y.-S., and Bais, H.P. (2012). Microbe-Associated Molecular Patterns-Triggered Root Responses Mediate Beneficial Rhizobacterial Recruitment in *Arabidopsis*. *Plant Physiol.* 160, 1642-1661.
- Lau, P.C.Y., Lindhout, T., Beveridge, T.J., Dutcher, J.R., and Lam, J.S. (2009). Differential Lipopolysaccharide Core Capping Leads to Quantitative and Correlated Modifications of Mechanical and Structural Properties in *Pseudomonas aeruginosa* Biofilms. *J. Bacteriol.* 191, 6618-6631.
- Laville, J., Voisard, C., Keel, C., Maurhofer, M., Défago, G., and Haas, D. (1992). Global control in *Pseudomonas fluorescens* mediating antibiotic synthesis and suppression of black root rot of tobacco. *Proc. Natl. Acad. Sci.* 89, 1562-1566.
- Levy, A., Salas Gonzalez, I., Mittelviefhaus, M., Clingenpeel, S., Herrera Paredes, S., Miao, J., Wang, K., Devescovi, G., Stillman, K., Monteiro, F., *et al.* (2018). Genomic features of bacterial adaptation to plants. *Nat. Genet.* 50, 138-150.
- Li, C.-H., Wang, K.-C., Hong, Y.-H., Chu, T.-H., Chu, Y.-J., Chou, I.-C., Lu, D.-K., Chen, C.-Y., Yang, W.-C., Lin, Y.-M., *et al.* (2014). Roles of Different Forms of Lipopolysaccharides in *Ralstonia solanacearum* Pathogenesis. *Mol. Plant-Microbe Interactions* 27, 471-478.
- Loper, J.E., Hassan, K.A., Mavrodi, D.V., Ii, E.W.D., Lim, C.K., Shaffer, B.T., Elbourne, L.D.H., Stockwell, V.O., Hartney, S.L., Breakwell, K., *et al.* (2012). Comparative Genomics of Plant-Associated *Pseudomonas* spp.: Insights into Diversity and Inheritance of Traits Involved in Multitrophic Interactions. *PLOS Genet.* 8, e1002784.
- Lopez-Gomez, M., Sandal, N., Stougaard, J., and Boller, T. (2012). Interplay of flg22-induced defence responses and nodulation in *Lotus japonicus*. *J. Exp. Bot.* 63, 393-401.

- Ma K., Niu Y., Jia Y., Ordon J., Copeland C., Emonet A., Geldner N., Guan R., Stolze S. C., Nakagami H., Garrido Oter R., Schulze-Lefert P. (10 September 2020). Coordination of microbe-host homeostasis via a crosstalk with plant innate immunity. PREPRINT (Version 1) available at Research Square. DOI:10.21203/rs.3.rs-69445/v1
- Maurhofer, M., Keel, C., Schnider, U., Voisard, C., Haas, D., and Defago, G. (1992). Influence of enhanced antibiotic production in *Pseudomonas fluorescens* strain CHA0 on its disease suppressive capacity. *Phytopathol. USA* 82, 190-195.
- Millet, Y.A., Danna, C.H., Clay, N.K., Songnuan, W., Simon, M.D., Werck-Reichhart, D., and Ausubel, F.M. (2010). Innate Immune Responses Activated in *Arabidopsis* Roots by Microbe-Associated Molecular Patterns. *Plant Cell* 22, 973–990.
- Mishra, M., Byrd, M.S., Sergeant, S., Azad, A.K., Parsek, M.R., McPhail, L., Schlesinger, L.S., and Wozniak, D.J. (2012). *Pseudomonas aeruginosa* Psl polysaccharide reduces neutrophil phagocytosis and the oxidative response by limiting complement-mediated opsonization. *Cell. Microbiol.* 14, 95–106.
- Misra, H.S., Rajpurohit, Y.S., and Khairnar, N.P. (2012). Pyrroloquinoline-quinone and its versatile roles in biological processes. *J. Biosci.* 37, 313–325.
- Petrocelli, S., Tondo, M.L., Daurelio, L.D., and Orellano, E.G. (2012). Modifications of *Xanthomonas axonopodis* pv. *citri* Lipopolysaccharide Affect the Basal Response and the Virulence Process during Citrus Canker. *PLOS ONE* 7, e40051.
- Pfund, C., Tans-Kersten, J., Dunning, F.M., Alonso, J.M., Ecker, J.R., Allen, C., and Bent, A.F. (2004). Flagellin Is Not a Major Defense Elicitor in *Ralstonia solanacearum* Cells or Extracts Applied to *Arabidopsis thaliana*. *Mol. Plant. Microbe Interact.* 17, 696–706.
- Poncini, L., Wyrsh, I., Tendon, V.D., Vorley, T., Boller, T., Geldner, N., Métraux, J.-P., and Lehmann, S. (2017). In roots of *Arabidopsis thaliana*, the damage-associated molecular pattern AtPep1 is a stronger elicitor of immune signalling than flg22 or the chitin heptamer. *PLOS ONE* 12, e0185808.
- Ramey, B.E., Koutsoudis, M., Bodman, S.B. von, and Fuqua, C. (2004). Biofilm formation in plant-microbe associations. *Curr. Opin. Microbiol.* 7, 602–609.
- Ranf, S. (2016). Immune Sensing of Lipopolysaccharide in Plants and Animals: Same but Different. *PLOS Pathog.* 12, e1005596.
- Ranf, S., Gisch, N., Schäffer, M., Illig, T., Westphal, L., Knirel, Y.A., Sánchez-Carballo, P.M., Zähringer, U., Hüchelhoven, R., Lee, J., *et al.* (2015). A lectin S-domain receptor kinase mediates lipopolysaccharide sensing in *Arabidopsis thaliana*. *Nat. Immunol.* 16, 426–433.
- Rapicavoli, J.N., Blanco-Ulate, B., Muszyński, A., Figueroa-Balderas, R., Morales-Cruz, A., Azadi, P., Dobruchowska, J.M., Castro, C., Cantu, D., and Roper, M.C. (2018). Lipopolysaccharide O-antigen delays plant innate immune recognition of *Xylella fastidiosa*. *Nat. Commun.* 9, 390.
- Scheidle, H., Groß, A., and Niehaus, K. (2005). The Lipid A substructure of the *Sinorhizobium meliloti* lipopolysaccharides is sufficient to suppress the oxidative burst in host plants. *New Phytol.* 165, 559–566.
- Schnider, U., Keel, C., Voisard, C., Défago, G., and Haas, D. (1995). Tn5-directed cloning of *pqq* genes from *Pseudomonas fluorescens* CHA0: mutational inactivation of the genes results in overproduction of the antibiotic pyoluteorin. *Appl. Environ. Microbiol.* 61, 3856–3864.
- Shen, Y.-Q., Bonnot, F., Imsand, E.M., RoseFigura, J.M., Sjölander, K., and Klinman, J.P. (2012). Distribution and Properties of the Genes Encoding the Biosynthesis of the Bacterial Cofactor, Pyrroloquinoline Quinone. *Biochemistry* 51, 2265–2275.

- Stringlis, I.A., Proietti, S., Hickman, R., Verk, M.C.V., Zamioudis, C., and Pieterse, C.M.J. (2018). Root transcriptional dynamics induced by beneficial rhizobacteria and microbial immune elicitors reveal signatures of adaptation to mutualists. *Plant J.* *93*, 166–180.
- Stringlis, I.A., Zamioudis, C., Berendsen, R.L., Bakker, P.A.H.M., and Pieterse, C.M.J. (2019). Type III Secretion System of Beneficial Rhizobacteria *Pseudomonas simiae* WCS417 and *Pseudomonas defensor* WCS374. *Front. Microbiol.* *10*, 1631.
- Sun, W., Dunning, F.M., Pfund, C., Weingarten, R., and Bent, A.F. (2006). Within-Species Flagellin Polymorphism in *Xanthomonas campestris* pv *campestris* and Its Impact on Elicitation of *Arabidopsis* FLAGELLIN SENSING2-Dependent Defenses. *Plant Cell* *18*, 764–779.
- Teixeira, P.J.P., Colaianni, N.R., Fitzpatrick, C.R., and Dangl, J.L. (2019). Beyond pathogens: microbiota interactions with the plant immune system. *Curr. Opin. Microbiol.* *49*, 7–17.
- Tellström, V., Usadel, B., Thimm, O., Stitt, M., Küster, H., and Niehaus, K. (2007). The Lipopolysaccharide of *Sinorhizobium meliloti* Suppresses Defense-Associated Gene Expression in Cell Cultures of the Host Plant *Medicago truncatula*. *Plant Physiol.* *143*, 825–837.
- Toruño, T.Y., Stergiopoulos, I., and Coaker, G. (2016). Plant-Pathogen Effectors: Cellular Probes Interfering with Plant Defenses in Spatial and Temporal Manners. *Annu. Rev. Phytopathol.* *54*, 419–441.
- Trdá, L., Fernandez, O., Boutrot, F., Héloir, M.-C., Kelloniemi, J., Daire, X., Adrian, M., Clément, C., Zipfel, C., Dorey, S., *et al.* (2014). The grapevine flagellin receptor VvFLS2 differentially recognizes flagellin-derived epitopes from the endophytic growth-promoting bacterium *Burkholderia phytofirmans* and plant pathogenic bacteria. *New Phytol.* *201*, 1371–1384.
- Vacheron, J., Péchy-Tarr, M., Brochet, S., Heiman, C.M., Stojiljkovic, M., Maurhofer, M., and Keel, C. (2019). T6SS contributes to gut microbiome invasion and killing of an herbivorous pest insect by plant-beneficial *Pseudomonas protegens*. *ISME J.* *13*, 1318–1329.
- Velterop, J.S., Sellink, E., Meulenber, J.J., David, S., Bulder, I., and Postma, P.W. (1995). Synthesis of pyrroloquinoline quinone in vivo and in vitro and detection of an intermediate in the biosynthetic pathway. *J. Bacteriol.* *177*, 5088–5098.
- Wawra, S., Fesel, P., Widmer, H., Timm, M., Seibel, J., Leson, L., Kessler, L., Nostadt, R., Hilbert, M., Langen, G., *et al.* (2016). The fungal-specific β -glucan-binding lectin FGB1 alters cell-wall composition and suppresses glucan-triggered immunity in plants. *Nat. Commun.* *7*, 13188.
- de Werra, P., Péchy-Tarr, M., Keel, C., and Maurhofer, M. (2009). Role of Gluconic Acid Production in the Regulation of Biocontrol Traits of *Pseudomonas fluorescens* CHA0. *Appl. Environ. Microbiol.* *75*, 4162–4174.
- Westphal, L., Strehmel, N., Eschen-Lippold, L., Bauer, N., Westermann, B., Rosahl, S., Scheel, D., and Lee, J. (2019). pH effects on plant calcium fluxes: lessons from acidification-mediated calcium elevation induced by the γ -glutamyl-leucine dipeptide identified from *Phytophthora infestans*. *Sci. Rep.* *9*, 1–14.
- Wyrsh, I., Domínguez-Ferreras, A., Geldner, N., and Boller, T. (2015). Tissue-specific FLAGELLIN-SENSING 2 (FLS2) expression in roots restores immune responses in *Arabidopsis fls2* mutants. *New Phytol.* *206*, 774–784.
- Xin, D.-W., Liao, S., Xie, Z.-P., Hann, D.R., Steinle, L., Boller, T., and Staehelin, C. (2012). Functional Analysis of NopM, a Novel E3 Ubiquitin Ligase (NEL) Domain Effector of *Rhizobium* sp. Strain NGR234. *PLOS Pathog.* *8*, e1002707.

- Yu, J., Peñaloza-Vázquez, A., Chakrabarty, A.M., and Bender, C.L. (1999). Involvement of the exopolysaccharide alginate in the virulence and epiphytic fitness of *Pseudomonas syringae* pv. *syringae*. *Mol. Microbiol.* *33*, 712–720.
- Yu, K., Liu, Y., Tichelaar, R., Savant, N., Lagendijk, E., Kuijk, S.J.L. van, Stringlis, I.A., Dijken, A.J.H. van, Pieterse, C.M.J., Bakker, P.A.H.M., *et al.* (2019). Rhizosphere-Associated *Pseudomonas* Suppress Local Root Immune Responses by Gluconic Acid-Mediated Lowering of Environmental pH. *Curr. Biol.* *29*, 3913-3920.e4.
- Yu, K., Pieterse, C.M.J., Bakker, P.A.H.M., and Berendsen, R.L. (2019b). Beneficial microbes going underground of root immunity. *Plant Cell Environ.* *42*, 2860–2870.
- Zhou, F., Emonet, A., Dénervaud Tendon, V., Marhavy, P., Wu, D., Lahaye, T., and Geldner, N. (2020). Co-incidence of Damage and Microbial Patterns Controls Localized Immune Responses in Roots. *Cell* *180*, 440-453.e18.

6 INTERPLAY BETWEEN FLG22, ATPEP1 AND ETHYLENE-MEDIATED IMMUNE RESPONSES

6.1. INTRODUCTION

Immunity induced by biotrophic pathogens used to be considered as a mechanism distinct from damage responses: the first one depends on salicylic acid signalling while the second requires the antagonist jasmonic acid pathway (Pieterse *et al.*, 2012). However, the more we understand the complexity of immune responses, the more we realize that both MAMP- and DAMP-responses are intricately connected, using the same core machinery leading to very similar outputs (Tang *et al.*, 2017). DAMP-triggered immunity is now often described as a means to amplify MAMP-induced responses, especially for secondary danger signals like AtPeps or systemin. MAMPs and DAMPs were postulated to accumulate until a threshold is attained, upon which leading to the induction of immune responses (Gust *et al.*, 2017).

Recently, our work showed that damage is required for gating the induction of MTI in the differentiated part of the root (Zhou *et al.*, 2020), strengthening the idea that both types of signal should contribute to determine where and when immune responses occur.

6.1.1. ATPEP SIGNALLING REINFORCES MAMP-TRIGGERED IMMUNITY THROUGH THE ETHYLENE PATHWAY

AtPep signalling plays a preponderant role in the amplification of MAMP-triggered immunity. Indeed, flg22 and elf18 treatment induce a massive transcription of the precursors *PROPEP2* and *PROPEP3* (Huffaker *et al.*, 2006). Although their activation and secretion are not fully understood, AtPep2 and AtPep3 then activate PEPR1 and PEPR2 receptors and amplify the immune responses. Moreover, *PROPEPs* expression is promoted by SA, JA and ethylene signalling (Liu *et al.*, 2013).

Ethylene biosynthesis relies on the conversion of S-adenosyl-methionine (SAM) in 1-amino-cyclopropane-1-carboxylic acid (ACC) by the rate-limiting enzyme ACS (ACC SYNTHASE). ACC is then oxidatively cleaved by ACC oxidases to form ethylene. Ethylene is perceived by and inactivates its cognate receptor ETR1, which in turn leads to the deactivation of the kinase inhibitor CTR1. This derepresses the downstream target EIN2, which signals through the EIN3/EILs transcription factors families (Adie *et al.*, 2007).

Interestingly, MAMP and AtPep immune responses are linked by the ethylene signalling pathway (Liu *et al.*, 2013; Tintor *et al.*, 2013). Flg22 was shown to directly induce ethylene synthesis by MPK3/6-mediated phosphorylation and stabilization of ACS2 and ACS6 (Han *et al.*, 2010; Liu and Zhang, 2004). Moreover, MPK3/6 also activate the transcription factor WRKY33, which increases *ACS2/6* transcription (Li *et al.*, 2012) and interacts with several members of the ETHYLENE RESPONSE FACTOR family such as ERF6 and ERF104 (Bethke *et al.*, 2009; Meng *et al.*, 2013). Ethylene signalling then enhances the transcription of *PROPEP1* and *PROPEP2*. Elf18 induction of *PROPEP2* was shown to be reduced in *ein2* mutant, indicating its dependency to ethylene, whereas elf18-driven *PROPEP3* was independent (Tintor *et al.*, 2013). Ethylene-driven immune responses are also compromised in the *pepr1/pepr2* mutant (Liu *et al.*, 2013).

PEPR1 activation also triggers the production of ethylene, which could further enhance MTI. Ethylene is indeed required for both constitutive and flg22-induced *FLS2* expression. Interestingly, EFR receptor expression is not modulated by ethylene (Boutrot *et al.*, 2010; Mersmann *et al.*, 2010; Tintor *et al.*, 2013).

6.1.2. RATIONAL OF THE STUDY

Previous studies support that damage responses are particularly important in roots and rely on ethylene signalling. Indeed, AtPep1 treatment induces a very strong induction of several immune transcriptional read-outs in roots, and particularly markers of ethylene signalling such as *ACS6* and *PR4/HEL* (Bertini *et al.*, 2012; Poncini *et al.*, 2017). Moreover, our group showed that single-cell ablation on seedling roots induces locally *ACS6* and *PR4* transcriptional reporters, as well as ROS and calcium signalling. However, read-outs for SA or JA signalling were surprisingly non-responsive (Marhavý *et al.*, 2019). We also observed that *FLS2* expression was locally increased after cell ablation (Zhou *et al.*, 2020), suggesting a possible correlation between wounding, ethylene signalling and MTI.

To investigate the link between MAMP, ethylene and Atpep1 pathways, we compared flg22 and Atpep1 responses, as well as their dependency on ethylene. However, this project started before we actually demonstrated that *FLS2* induction at damage sites was independent of ethylene and cannot be mimicked by DAMPs (Zhou *et al.*, 2020), and that *PEPR1/2* were not responsible for the single-cell damage-induced ethylene signalling

(Marhavý *et al.*, 2019). Although this chapter is mainly composed of exploratory works and preliminary data, it can complete our map of immune responses and deepen our understanding of MTI at cellular resolution. Moreover, it highlights the difference in ethylene dependency between AtPep1 and flg22-triggered immune responses in the roots.

6.2. RESULTS

6.2.1. FLG22 AND ATPEP1 INDUCE IMMUNE AND ETHYLENE RESPONSES WITH DIFFERENT PATTERNS

To investigate the link between flg22 and AtPep1-triggered immunity in the root, I first characterized their respective immune response patterns using our set of fluorescently labelled transcriptional markers. AtPep3 was also used in some experiments. Similar analyses were previously carried out by Poncini *et al.* (2017). However, since different experimental setups can greatly influence stress markers, I wanted to repeat their experiments in our growth conditions and to describe the immune patterns with a true cellular resolution rather than looking globally at root zones. I selected read-outs reported to respond strongly to flg22, *i.e.* *PER5*, *MYB51*, *WRKY11*, *ZAT12*, as well as ethylene responsive reporters *PR4* and *ACS6*.

As previously described, I observed that flg22 induces immune responses mostly in the elongation zone (Millet *et al.*, 2010; Poncini *et al.*, 2017; Zhou *et al.*, 2020). The flg22-driven expression of *PER5* and *MYB51* was extensively characterized in Chapter 2 and 3 (Emonet *et al.*, 2020; Zhou *et al.*, 2020) and will not be further described here. The *WRKY11* transcription factor is constitutively expressed in all tissues, although stronger signal can be observed in the epidermis, the differentiated stele and the root cap cells (Fig.1A). Flg22 slightly induces *WRKY11* in the epidermis and cortex of the elongation zone. *ZAT12* is involved in oxidative stress response and is constitutively expressed in all tissues (Fig.1B). However, in my hands, it was unresponsive to flg22, which contradicts Poncini and colleagues' data (2017).

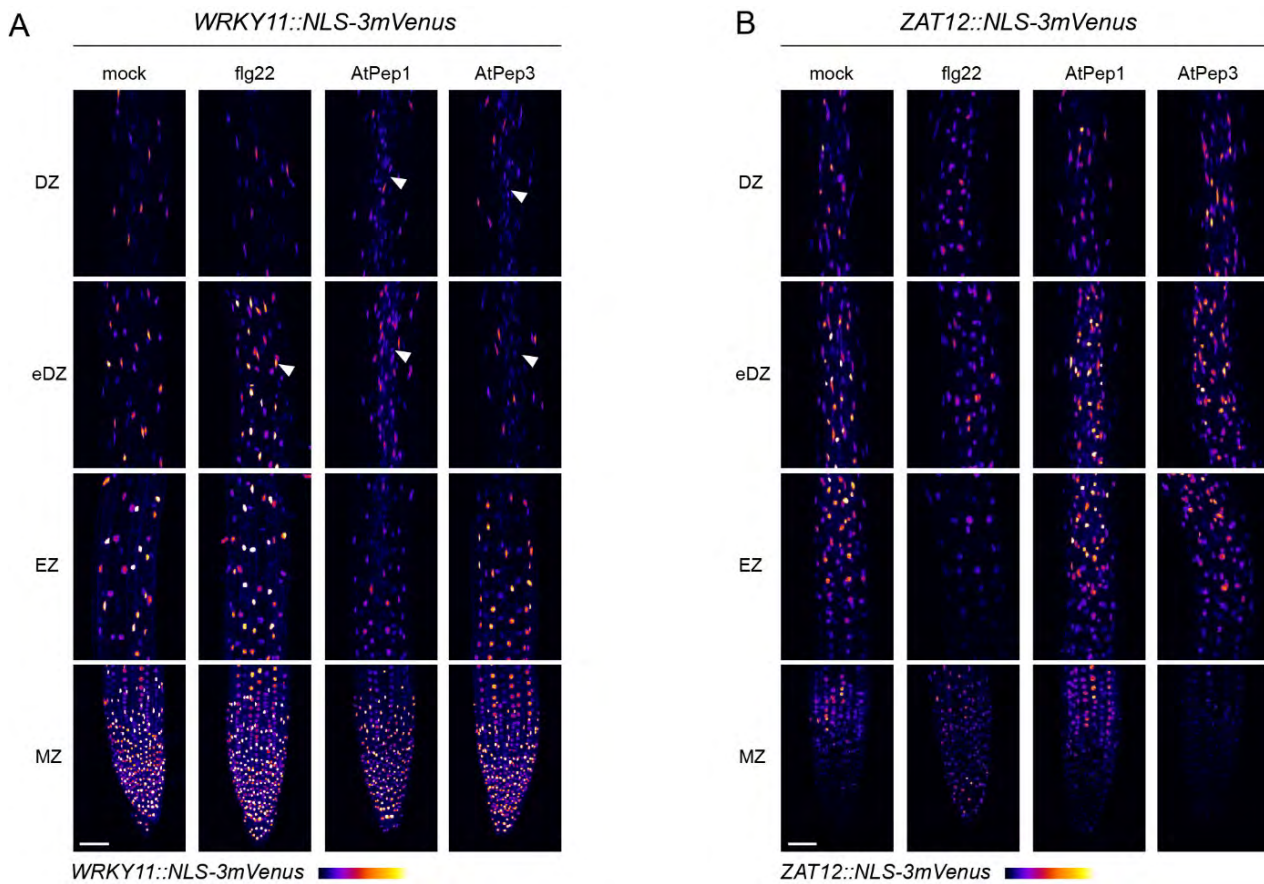


Figure 1: flg22 and AtPeps induce MTI and ethylene markers with different expression patterns

Expression patterns of *WRKY11::NLS-3mVenus* (A) and *ZAT12::NLS-3mVenus* (B) (Fire LUT) in response to 1 μ M flg22, 1 μ M AtPep1 or 1 μ M AtPep3.

(A) Flg22 induces weakly *WRKY11* in the early DZ, mostly in epidermis. AtPeps increase *WRKY11* expression principally in the stele of the DZ. White arrowheads, increased *WRKY11* signal.

(B) None of the treatments significantly affects *ZAT12* marker gene.

Seedlings were treated for 24 h in liquid medium. Settings are identical between samples. MZ, meristematic zone; EZ, elongation zone, eDZ, early differentiated zone (= 10 cells after the onset of elongation); DZ, differentiated zone (20 or 30 cells after the onset of elongation). Scale bar, 50 μ m.

By contrast to flg22, I noticed that AtPep1 induces a much broader expression of immune read-outs, that were generally no longer restricted to the elongation zone. Moreover, the strength of induction was greater than that for flg22, confirming previous data (Poncini *et al.*, 2017). AtPep1 induces *MYB51* in the epidermis and cortex of the meristem, in all tissues in the elongation zone, and the induction is principally restricted to the stele in the differentiated regions (Fig.4B). AtPep1-driven *PER5* pattern was surprisingly restricted to the elongation zone, but in all tissues (Fig.4A). However, some weak signal can be found in the differentiated stele (data not shown). AtPep1 and AtPep3

induce *WRKY11* mostly in the elongating and differentiated stele (Fig.1A). Finally, *ZAT12* was not induced by AtPep1 nor AtPep3 (Fig.1B).

The difference between flg22 and AtPep1 responses was even more pronounced for ethylene markers. *PR4* was constitutively expressed in the root cap cells and the differentiated endodermis (Fig.2A). Some weak signal could sometimes be observed in the elongating and differentiated epidermis and cortex (not shown). *PR4* constitutive expression was very sensitive to experimental conditions, leading to variable induction upon flg22 treatment: *PR4* signal increases in root cap cells and sometimes appears earlier in the endodermal cell compared to control treatment, but the effect was not robust across experiments. In contrast, AtPep1 strongly activates *PR4* in the endodermis and cortex of the differentiated zone, and to a lesser extent in the elongating epidermis (Fig.2A). However, Poncini *et al.* (2017) observed a severe AtPep1-dependent induction of *PR4* in all tissues of the elongation zone and in the differentiated endodermis, while flg22 triggered *PR4* mostly in root cap cells. *ACS6* is constitutively expressed in the differentiated stele and some faint signal can be observed in epidermal and cortical cells (Fig.2B). Flg22 treatment hardly increases *ACS6* expression in the vasculature (Fig.2b'). However, AtPep1 and AtPep3 drastically increase *ACS6* expression, confirming previous reports (Marhavý *et al.*, 2019; Poncini *et al.*, 2017).

Taken together, I noticed that flg22 induces MTI responses mostly in the elongation zone, principally in the epidermis, which correlates with the restricted expression of *FLS2* and the non-responsiveness of the stele described previously (Beck *et al.*, 2014; Emonet *et al.*, 2020; Millet *et al.*, 2010; Zhou *et al.*, 2020). Surprisingly, although ethylene signalling should be induced by flg22 (Bethke *et al.*, 2009; Li *et al.*, 2012; Meng *et al.*, 2013), flg22 only mildly induces ethylene transcriptional read-outs. By contrast, AtPep1 induces particularly severe MTI and ethylene responses in the differentiated stele, where *PEPR1* and *PEPR2* are strongly expressed (Ortiz-Morea *et al.*, 2016; Safaeizadeh and Boller, 2019).

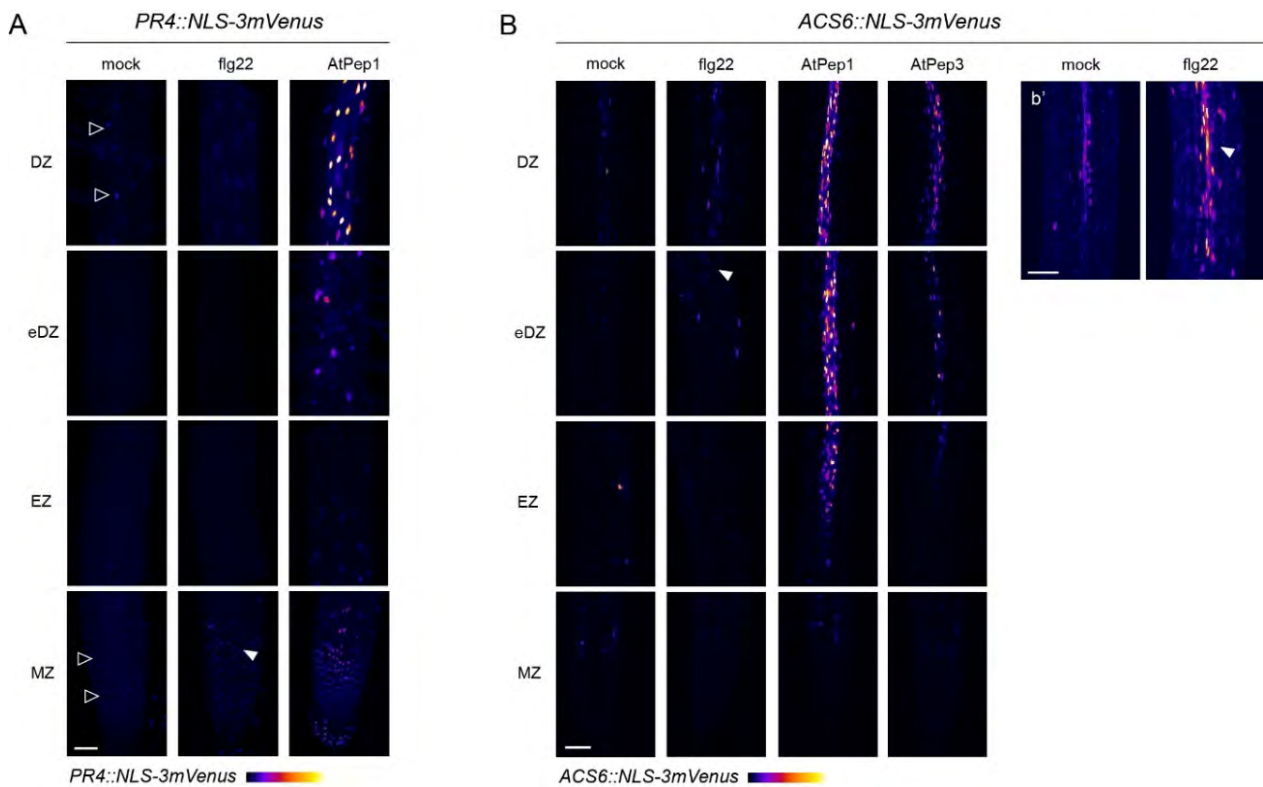


Figure 2: flg22 and AtPeps induce MTI and ethylene markers with different expression patterns

Expression patterns of *PR4::NLS-3mVenus* (A) and *ACS6::NLS-3mVenus* (B) (Fire LUT) in response to 1 μ M flg22, 1 μ M AtPep1 or 1 μ M AtPep3.

(A) AtPep1 strongly induces *PR4* reporter in the endodermis. Black arrowheads, constitutive signal, white arrowhead, weak induction of *PR4* by flg22 in MZ.

(B) Flg22 induces *ACS6* only faintly in the differentiated stele, see close up view of DZ in (b') with increased exposure. AtPeps trigger *ACS6* activation strongly in the stele (EZ and DZ). AtPep3 have weaker effect than AtPep1. White arrowhead, weak induction of *ACS6* by flg22 in DZ.

Seedlings were treated for 24 h in liquid medium. Settings are identical between samples. MZ, meristematic zone; EZ, elongation zone, eDZ, early differentiated zone (= 10 cells after the onset of elongation); DZ, differentiated zone (20 or 30 cells after the onset of elongation). Scale bar, 50 μ m.

6.2.2. ETHYLENE SIGNALLING IS INVOLVED IN FLG22-DRIVEN *PER5* INDUCTION

Flg22-induced ethylene is a common feature of immune responses above ground. To assess whether MTI transcriptional read-outs are dependent on ethylene production in the root, I assessed *PER5* induction after treatments with a combination of flg22 and the ethylene inhibitor AgNO₃. Silver ions can replace a copper co-factor in the ETR1 receptor, which modifies the binding site for ethylene and prevents ethylene sensing (McDaniel and Binder, 2012; Rodríguez et al., 1999).

The inhibition of ethylene perception slightly reduces flg22-mediated induction of *PER5* marker, suggesting that ethylene might be partially required for *PER5* transcriptional induction (Fig.3). Zhou *et al.* (2020) previously showed that *PER5* and *FRK1* induction was reduced after flg22 treatment in the *etr1-1* and *ein2-1* mutants. Moreover, treatment with the ethylene inhibitor 2-aminoethoxyvinyl glycine (AVG) almost completely abolishes *FRK1* induction (Zhou *et al.*, 2020). AVG directly inhibits the ACC SYNTHASE enzymes involved in ethylene biosynthesis (McDaniel and Binder, 2012; Rodríguez *et al.*, 1999). Similarly, it was reported that flg22-mediated induction of *MYB51*, *CYP71A12* and *WRKY11* read-outs was reduced in the *ein2-1* mutant, suggesting they are also partially dependent on ethylene (Millet *et al.*, 2010).

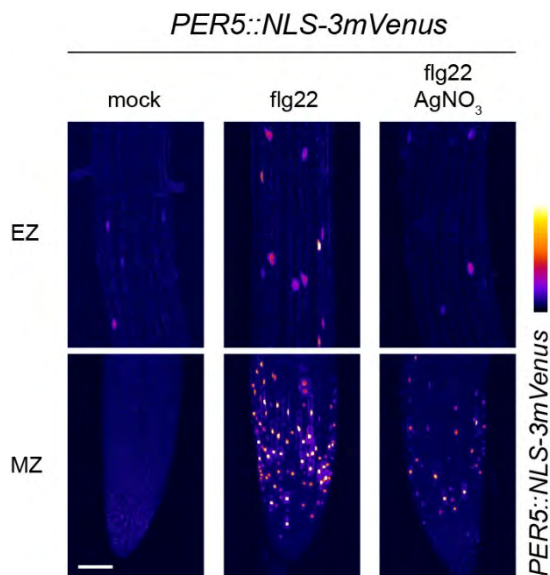


Figure 3: Inhibition of ethylene signalling modulates flg22-dependent *PER5* expression

Inhibition of ethylene perception reduces flg22-dependent expression of *PER5::NLS-3mVenus* (Fire LUT). Maximum projection of z-stacks of seedlings treated on plate, for 24 h in total, with 2 μM AgNO_3 and 6 h with 1 μM flg22.

MZ, meristematic zone; EZ, elongation zone. Scale bar, 50 μm .

6.2.3. INHIBITION OF ETHYLENE SIGNALLING INCREASES RESPONSE TO ATPEP1 IN THE STELE

I then investigated the ethylene dependency of AtPep1-mediated responses. Similarly, I treated seedlings with AtPep1 and AVG or AgNO_3 and analysed the expression patterns of *PER5* and *MYB51*. Since AtPep1 enhances the expression of *ACS6*, suggesting that the ethylene pathway might be involved in root immune responses, I expected to observe decreased *PER5* and *MYB51* transcriptional read-outs. Surprisingly, I noticed a slight increase of *PER5* expression, particularly in the elongating stele (Fig.4A). *MYB51* response was more variable, but generally, after the co-treatment, *MYB51* expression tends to increase in the vascular tissues and slightly decrease in the epidermis (Fig.4B). Therefore, ethylene might have opposite effect depending on cell-types.

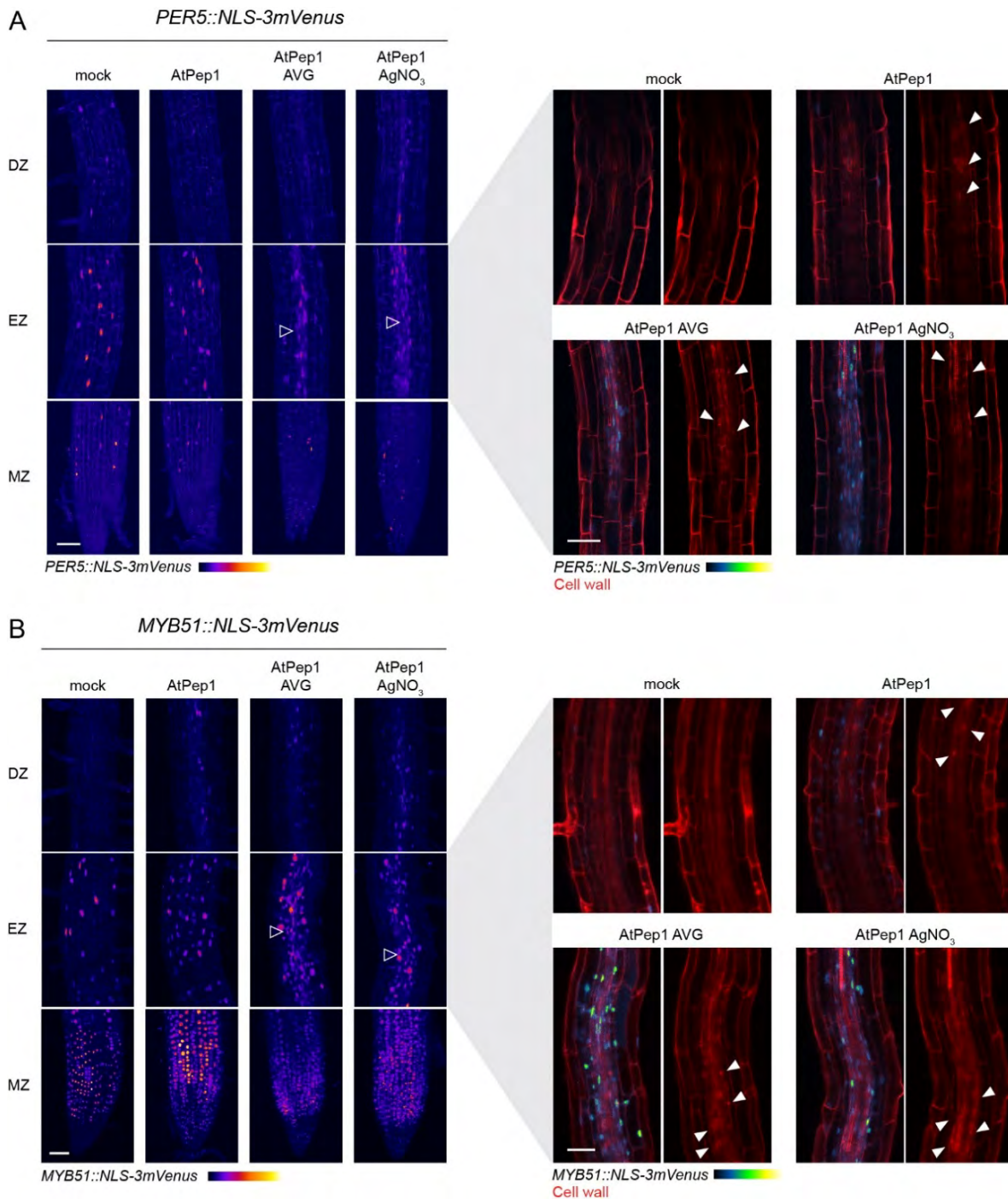


Figure 4: Inhibition of ethylene signalling modulates AtPep1-dependent *PER5* and *MYB51* expression

Inhibition of ethylene perception increases AtPep1-dependent expression of *PER5::NLS-3mVenus* (A) and *MYB51::NLS-3mVenus* (B) (Fire LUT) in the stele (black arrowheads). Maximum projection of z-stacks of seedlings treated on plates for 24 h in total, with 2 μM AgNO_3 /AVG and 6 h with 1 μM AtPep1. Right panels show longitudinal section views (5-slices maximum projection) of pictures taken in EZ. Cell walls are stained with PI staining (red), transcriptional read-outs are in green (GreenFireBlue LUT). White arrows point at unequal PI staining in response to AtPep1. MZ, meristematic zone; EZ, elongation zone; DZ, differentiated zone (20 cells after the onset of elongation). Scale bar, 50 μm .

As a side note, AtPep1 might also influence the structure of the vascular cell wall (Fig.4A, 4B, right panels). I noticed an increase in propidium iodide staining in the stele of the elongation zone. Some cell corners are indeed more strongly stained than in control conditions. Interestingly, PI accumulates in lignified tissues over time (Kian Hematy, *personal communication*). Moreover, AtPep1 treatment was reported to induce lignin deposition in the stele of *Arabidopsis* seedlings (Engelsdorf *et al.*, 2018). The increased PI staining that we observed must therefore be due to lignin deposition. Moreover, this irregular staining seems to increase when roots were co-treated with ethylene inhibitors. Since lignin deposition was generally correlated with *PER5* induction (Emonet *et al.*, 2020), it can be hypothesized that ethylene suppresses or competes with AtPep1-driven lignin deposition.

6.2.4. ACC INDUCES *MYB51* BUT HAD WEAK OR NO EFFECT ON *PER5* AND *WRKY11* EXPRESSION

To better understand the effect of ethylene on MTI markers, I analysed *PER5*, *MYB51* and *WRKY11* expression after ACC treatment. *MYB51* promoter was strongly induced by ACC in the epidermis, particularly in dividing and elongating regions (Fig.S1A). By contrast, treatment with ACC had no effect on *WRKY11* expression (Fig.S1B) but induced *PER5* only in sporadic epidermal cells of the early differentiating zone and was, therefore, not sufficient to mirror flg22 treatment (Fig.S1C). Therefore, although some downstream responses overlap between ACC and flg22 signalling, both treatments have clear specificities.

The absence of response of *WRKY11* and the mild increase in *PER5* signal suggest that ethylene does not mirror flg22- and AtPep1-mediated transcriptional read-outs. By contrast, ethylene is sufficient to activate *MYB51* in the absence of flg22 or AtPep1. However, these results seemingly contradict the enhancement of *PER5* and *MYB51* signal observed in the stele after AtPep1 and ethylene inhibitors treatments. These data might be reconciled if we consider that ethylene is only able to suppress *PER5* and *MYB51* expression driven by AtPep1, but not their constitutive expression. It could be informative to test the combined impact of ACC and AtPep1 to confirm the stele-specific inhibitory effect of ethylene.

6.2.5. *PR4* IS PARTIALLY DEPENDENT OF ETHYLENE SIGNALLING

I also monitored the ethylene-dependency of the AtPep1-driven induction of *PR4* (Fig.S1D). Ethylene signalling inhibition tends to slightly decrease Atpep1-driven *PR4* expression in the early differentiated zone, *i.e.* *PR4* signal appears further from the root tip. *PR4* induction is therefore not fully dependent on ethylene signalling as a response to AtPep1. Indeed, ethylene and jasmonic acid act synergistically for the expression of several defence-related genes including *PR4* (Adie *et al.*, 2007; Bertini *et al.*, 2003; Potter *et al.*, 1993). However, I could show that *PR4* is strongly induced by ACC treatment, and that co-treatment with AgNO₃ impairs this process (Fig.S1E).

6.3. DISCUSSION

Using immune transcriptional read-outs, I characterized in parallel the effect of flg22 and AtPep1. Their patterns of responses appeared to be very different, restricted to the elongation zone for flg22 and extending to the differentiated zone for AtPep1, as previously reported (Millet *et al.*, 2010; Poncini *et al.*, 2017). Since PRRs have a strong impact on the localization of immune responses (Emonet *et al.*, 2020; Zhou *et al.*, 2020), the difference observed between flg22 and AtPep1-responses is likely due to the distinct expression patterns of *FLS2* and *PEPR1/2*. *PEPR2* is restricted to the stele and *PEPR1* is ubiquitous (Ortiz-Morea *et al.*, 2016), which could reflect the broad expression of AtPep1 immune responses. Similarly, AtPep1 strongly induces *FRK1* in the stele (Zhou *et al.*, 2020).

Interestingly, flg22-responses are very different: we indeed showed that the vasculature was insensitive to flg22, even in presence of ectopic *FLS2* expression. Flg22 could only induce *MYB51* in the pericycle cells when *FLS2* was expressed in the endodermis, indicating it was the consequence of non-cell autonomous signalling (Emonet *et al.*, 2020). It will be very interesting to test whether the immune responses induced by AtPep1 are free from this vasculature-specific suppression, or whether they originated from a signal transmitted by adjacent tissues. Indeed, the strongly cell-autonomous *PER5* marker is not induced by AtPep1 in the differentiated vasculature, which tends to support the fact that AtPep1 induces *MYB51* and *WRKY11* expression non-cell autonomously. However, if the first case proves to be true, it will be an elegant way for the plant to protect itself against xylem-invading pathogens, like many cell-wall degrading bacteria or fungi (Digonnet *et al.*, 2012; Eynck *et al.*, 2007), while staying unresponsive to harmless endophytes that would only display MAMPs (Wyrsh *et al.*, 2015).

Flg22-responses must involve ethylene signalling, as shown by the reduced induction of *PER5* and *FRK1* after ethylene inhibition (this work; Zhou *et al.*, 2020). Moreover, *MYB51*, *WRKY11* and *CYP71A12* are partially dependent on ethylene, while callose deposition in response to flg22 is completely abolished in *etr1-3*, *ein2-1* and *ein3-1* mutants (Millet *et al.*, 2010). However, in my hands, flg22-mediated induction of *ACS6* and *PR4* was very weak. Ethylene markers could be specific to the differentiated zone and might not be induced in the younger part of the roots. Indeed, even AtPep1 treatment fails to

strongly induce *ACS6* and *PR4* in the meristematic zone. Other *ACS* genes might be involved in the tip of the root. Indeed, *ACS2* is upregulated by *flg22* and is expressed in the root elongation and meristematic zone (Li *et al.*, 2012; Tsuchisaka and Theologis, 2004). *ACS8* is also constitutively expressed in the root cap cells (Tsuchisaka and Theologis, 2004). Alternatively, ethylene produced in the differentiated zone in response to *flg22* could influence immune responses in the root tip by non-cell autonomous signalling.

AtPep1 should also induce the production of ethylene, as seen by the strong induction of *ACS6* and *PR4* markers. However, the opposite effect of ethylene in the central and peripheral tissues observed for *AtPep1*-responses was at first surprising. An opposing effect in the epidermis and the stele of the roots was also observed for brassinosteroid (BR) signalling. Vragović *et al.* (2015), using ribosomal pulldown and *BR1* ectopic expression, showed that BRs induced a delay in differentiation in outer root tissues, but early differentiation in the central cylinder. The same methods could be used to investigate the tissue-specific ethylene dependency of *AtPep1*-responses, since there is so far not enough data to conclude the exact role of ethylene production in response to *AtPep1*.

If proven, the negative effect of ethylene on *MYB51* and *PER5* expression in the stele could function as a regulatory loop to avoid overactivation of MTI in response to *AtPeps*. We previously suggested that roots keep their defences low, particularly in the early vasculature, to avoid deleterious consequences on growth (Emonet *et al.*, 2020). Such a mechanism of upregulation of an inhibitor was previously reported for *FLS2*. *Flg22* perception induces the activation of *SITE-1 PROTEASE (S1P)* that cleaves RALF propeptides to suppress innate immunity (Stegmann *et al.*, 2017). Interestingly, the negative effect of ethylene on stelar immune markers was not observed in response to *flg22*, suggesting *AtPep1* induces a specific response. It would be worth to test whether *PER5* expression and lignification can be differentially modulated by ethylene, depending on their induction by *AtPep1* or *flg22*. For example, one of the differences between *AtPep1* and *flg22* signalling, in leaves, is the requirement for jasmonate perception. Indeed, *coi1-1* and *coi1-16* mutants, lacking the *COI1 (CORONATINE-INSENSITIVE 1)* jasmonic acid receptor, are compromised in *AtPep1*-dependent ethylene production but still synthesize ethylene in response to *flg22* (Flury *et al.*, 2013; Holmes *et al.*, 2018).

Increased expression of *MYB51* and *PER5* in the stele due to AtPep1 treatment and ethylene inhibition could be due to defective endodermal barriers. Indeed, our group observed that Casparian strip integrity was compromised in the endodermal-specific *etr1* mutant (*CASP1::etr1-1*) (Feng Zhou, *personal communication*). The dominant negative *etr1-1* mutation renders plants insensitive to ethylene, which mirrors the AgNO₃ inhibitory effect. In this regard, AgNO₃ and AVG treatments might have increased the root permeability to AtPep1 and cause stronger induction of *MYB51* and *PER5* in the stele. However, I could not observe an AtPep1-dependent increase of *PER5* expression in the stele of the *sgn3-3* mutant, despite its compromised endodermal barriers (Fig.S2, preliminary data). Moreover, AVG treatment does not seem to affect PI permeability in previous data (Zhou *et al.*, 2020; Fig.S5D). This should refute this hypothesis, although more comprehensive analyses must be carried out to confirm these results.

Overall, we showed that, although flg22 and AtPep1 induce very similar downstream signalling cascades, their responses do not spatially overlap in the root. Whether this is due entirely to PRR expression patterns or to other regulatory mechanisms still needs to be elucidated. We also described the dependency of MAMP- and DAMP-responses on ethylene signalling. However, the observed effects were often weak and variable, so that further experiments should be realized before drawing any conclusions. Nevertheless, our preliminary experiments highlighted ethylene as a potential tissue-specific modulator of MAMP- and DAMP-triggered immunity.

6.4. MATERIAL AND METHODS

6.4.1. PLANT MATERIAL AND GROWTH CONDITIONS

All experiments used *A. thaliana* ecotype Columbia Col-0. Reporter lines are characterised in Poncini *et al.* (2017). Seeds were surface-sterilized, stratified and germinated as described previously (Emonet *et al.*, 2020).

6.4.2. ELICITOR AND INHIBITOR TREATMENTS

Elicitors and chemicals used, as well as elicitor treatments, were previously described in Chapter 2, section 2.5.1. For combined treatments with ethylene inhibitors, seedlings were transferred on ½ MS plates containing AVG or AgNO₃ to the indicated concentration, then elicitor treatment was carried out following the “combined method” previously described. Timing of treatments is described in figure legends.

6.4.3. MICROSCOPY ANALYSIS

Imaging was carried out on a Zeiss LSM700 or a Leica SP8 inverted confocal scanning microscope. Pictures were taken with a 63x water immersion objective (SP8) or 40x water immersion objective (SP8 and LSM700). For marker visualisation, the excitation and detection windows were set as follows: on LSM700, mVenus/PI (488nm, 500-530nm and 600-670nm); on SP8, mVenus/PI (514nm, 510-530nm, 600-670nm, sequential scan). Images were processed with the Fiji software.

6.5. LITERATURE

- Adie, B., Chico, J.M., Rubio-Somoza, I., and Solano, R. (2007). Modulation of Plant Defenses by Ethylene. *J. Plant Growth Regul.* *26*, 160–177.
- Beck, M., Wyrsh, I., Strutt, J., Wimalasekera, R., Webb, A., Boller, T., and Robatzek, S. (2014). Expression patterns of FLAGELLIN SENSING 2 map to bacterial entry sites in plant shoots and roots. *J. Exp. Bot.* *65*, 6487–6498.
- Bertini, L., Leonardi, L., Caporale, C., Tucci, M., Cascone, N., Di Bernardino, I., Buonocore, V., and Caruso, C. (2003). Pathogen-responsive wheat *PR4* genes are induced by activators of systemic acquired resistance and wounding. *Plant Sci.* *164*, 1067–1078.
- Bertini, L., Proietti, S., Aleandri, M.P., Mondello, F., Sandini, S., Caporale, C., and Caruso, C. (2012). Modular structure of HEL protein from *Arabidopsis* reveals new potential functions for PR-4 proteins. *Biol. Chem.* *393*, 1533–1546.
- Bethke, G., Unthan, T., Uhrig, J.F., Pöschl, Y., Gust, A.A., Scheel, D., and Lee, J. (2009). Flg22 regulates the release of an ethylene response factor substrate from MAP kinase 6 in *Arabidopsis thaliana* via ethylene signaling. *Proc. Natl. Acad. Sci.* *106*, 8067–8072.
- Boutrot, F., Segonzac, C., Chang, K.N., Qiao, H., Ecker, J.R., Zipfel, C., and Rathjen, J.P. (2010). Direct transcriptional control of the *Arabidopsis* immune receptor FLS2 by the ethylene-dependent transcription factors EIN3 and EIL1. *Proc. Natl. Acad. Sci.* *107*, 14502–14507.
- Digonnet, C., Martinez, Y., Denancé, N., Chasseray, M., Dabos, P., Ranocha, P., Marco, Y., Jauneau, A., and Goffner, D. (2012). Deciphering the route of *Ralstonia solanacearum* colonization in *Arabidopsis thaliana* roots during a compatible interaction: focus at the plant cell wall. *Planta* *236*, 1419–1431.
- Emonet, A., Zhou, F., Vacheron, J., Heiman, C.M., Tendon, V.D., Ma, K.-W., Schulze-Lefert, P., Keel, C., and Geldner, N. (2020). Spatially Restricted Immune Responses Allow for Root Meristematic Activity During Bacterial Colonisation. *BioRxiv* 2020.08.03.233817.
- Engelsdorf, T., Gigli-Bisceglia, N., Veerabagu, M., McKenna, J.F., Vaahtera, L., Augstein, F., Van der Does, D., Zipfel, C., and Hamann, T. (2018). The plant cell wall integrity maintenance and immune signaling systems cooperate to control stress responses in *Arabidopsis thaliana*. *Sci. Signal.* *11*, eaao3070.
- Eynck, C., Koopmann, B., Grunewaldt-Stoecker, G., Karlovsky, P., and Tiedemann, A. von (2007). Differential interactions of *Verticillium longisporum* and *V. dahliae* with *Brassica napus* detected with molecular and histological techniques. *Eur. J. Plant Pathol.* *118*, 259–274.
- Flury, P., Klauser, D., Schulze, B., Boller, T., and Bartels, S. (2013). The Anticipation of Danger: Microbe-Associated Molecular Pattern Perception Enhances AtPep-Triggered Oxidative Burst. *Plant Physiol.* *161*, 2023–2035.
- Gust, A.A., Pruitt, R., and Nürnberger, T. (2017). Sensing Danger: Key to Activating Plant Immunity. *Trends Plant Sci.* *22*, 779–791.
- Han, L., Li, G.-J., Yang, K.-Y., Mao, G., Wang, R., Liu, Y., and Zhang, S. (2010). Mitogen-activated protein kinase 3 and 6 regulate *Botrytis cinerea*-induced ethylene production in *Arabidopsis*. *Plant J.* *64*, 114–127.
- Holmes, D.R., Grubb, L.E., and Monaghan, J. (2018). The jasmonate receptor COI1 is required for AtPep1-induced immune responses in *Arabidopsis thaliana*. *BMC Res. Notes* *11*, 555.
- Huffaker, A., Pearce, G., and Ryan, C.A. (2006). An endogenous peptide signal in *Arabidopsis* activates components of the innate immune response. *Proc. Natl. Acad. Sci.* *103*, 10098–10103.

- Li, G., Meng, X., Wang, R., Mao, G., Han, L., Liu, Y., and Zhang, S. (2012). Dual-Level Regulation of ACC Synthase Activity by MPK3/MPK6 Cascade and Its Downstream WRKY Transcription Factor during Ethylene Induction in *Arabidopsis*. *PLoS Genet.* *8*, e1002767.
- Liu, Y., and Zhang, S. (2004). Phosphorylation of 1-Aminocyclopropane-1-Carboxylic Acid Synthase by MPK6, a Stress-Responsive Mitogen-Activated Protein Kinase, Induces Ethylene Biosynthesis in *Arabidopsis*. *Plant Cell* *16*, 3386–3399.
- Liu, Z., Wu, Y., Yang, F., Zhang, Y., Chen, S., Xie, Q., Tian, X., and Zhou, J.-M. (2013). BIK1 interacts with PEPRs to mediate ethylene-induced immunity. *Proc. Natl. Acad. Sci.* *110*, 6205–6210.
- Marhavý, P., Kurenda, A., Siddique, S., Dénervaud Tendon, V., Zhou, F., Holbein, J., Hasan, M.S., Grundler, F.M., Farmer, E.E., and Geldner, N. (2019). Single-cell damage elicits regional, nematode-restricting ethylene responses in roots. *EMBO J.* *38*, e100972.
- McDaniel, B.K., and Binder, B.M. (2012). Ethylene Receptor 1 (ETR1) Is Sufficient and Has the Predominant Role in Mediating Inhibition of Ethylene Responses by Silver in *Arabidopsis thaliana*. *J. Biol. Chem.* *287*, 26094–26103.
- Meng, X., Xu, J., He, Y., Yang, K.-Y., Mordorski, B., Liu, Y., and Zhang, S. (2013). Phosphorylation of an ERF Transcription Factor by *Arabidopsis* MPK3/MPK6 Regulates Plant Defense Gene Induction and Fungal Resistance. *Plant Cell* *25*, 1126–1142.
- Mersmann, S., Bourdais, G., Rietz, S., and Robatzek, S. (2010). Ethylene Signaling Regulates Accumulation of the FLS2 Receptor and Is Required for the Oxidative Burst Contributing to Plant Immunity. *Plant Physiol.* *154*, 391–400.
- Millet, Y.A., Danna, C.H., Clay, N.K., Songnuan, W., Simon, M.D., Werck-Reichhart, D., and Ausubel, F.M. (2010). Innate Immune Responses Activated in *Arabidopsis* Roots by Microbe-Associated Molecular Patterns. *Plant Cell* *22*, 973–990.
- Ortiz-Morea, F.A., Savatin, D.V., Dejonghe, W., Kumar, R., Luo, Y., Adamowski, M., Begin, J.V. den, Dressano, K., Oliveira, G.P. de, Zhao, X., *et al.* (2016). Danger-associated peptide signaling in *Arabidopsis* requires clathrin. *Proc. Natl. Acad. Sci.* *113*, 11028–11033.
- Pieterse, C.M.J., Van der Does, D., Zamioudis, C., Leon-Reyes, A., and Van Wees, S.C.M. (2012). Hormonal Modulation of Plant Immunity. *Annu. Rev. Cell Dev. Biol.* *28*, 489–521.
- Poncini, L., Wyrsh, I., Tendon, V.D., Vorley, T., Boller, T., Geldner, N., Métraux, J.-P., and Lehmann, S. (2017). In roots of *Arabidopsis thaliana*, the damage-associated molecular pattern AtPep1 is a stronger elicitor of immune signalling than flg22 or the chitin heptamer. *PLoS ONE* *12*, e0185808.
- Potter, S., Uknes, S., Lawton, K., Winter, A.M., Chandler, D., DiMaio, J., Novitzky, R., Ward, E., and Ryals, J. (1993). Regulation of a hevein-like gene in *Arabidopsis*. *MPMI-Mol. Plant Microbe Interact.* *6*, 680–685.
- Rodríguez, F.I., Esch, J.J., Hall, A.E., Binder, B.M., Schaller, G.E., and Bleecker, A.B. (1999). A Copper Cofactor for the Ethylene Receptor ETR1 from *Arabidopsis*. *Science* *283*, 996–998.
- Safaeizadeh, M., and Boller, T. (2019). Differential and tissue-specific activation pattern of the AtPROPEP and AtPEPR genes in response to biotic and abiotic stress in *Arabidopsis thaliana*. *Plant Signal. Behav.* *14*, e1590094.
- Stegmann, M., Monaghan, J., Smakowska-Luzan, E., Rovenich, H., Lehner, A., Holton, N., Belkhadir, Y., and Zipfel, C. (2017). The receptor kinase FER is a RALF-regulated scaffold controlling plant immune signaling. *Science* *355*, 287–289.
- Tang, D., Wang, G., and Zhou, J.-M. (2017). Receptor Kinases in Plant-Pathogen Interactions: More Than Pattern Recognition. *Plant Cell* *29*, 618–637.

- Tintor, N., Ross, A., Kanehara, K., Yamada, K., Fan, L., Kemmerling, B., Nürnberger, T., Tsuda, K., and Saijo, Y. (2013). Layered pattern receptor signaling via ethylene and endogenous elicitor peptides during *Arabidopsis* immunity to bacterial infection. *Proc. Natl. Acad. Sci.* *110*, 6211–6216.
- Tsuchisaka, A., and Theologis, A. (2004). Unique and Overlapping Expression Patterns among the *Arabidopsis* 1-Amino-Cyclopropane-1-Carboxylate Synthase Gene Family Members. *Plant Physiol.* *136*, 2982–3000.
- Vragović, K., Sela, A., Friedlander-Shani, L., Fridman, Y., Hacham, Y., Holland, N., Bartom, E., Mockler, T.C., and Savaldi-Goldstein, S. (2015). Translatome analyses capture of opposing tissue-specific brassinosteroid signals orchestrating root meristem differentiation. *Proc. Natl. Acad. Sci.* *112*, 923–928.
- Wyrsh, I., Domínguez-Ferreras, A., Geldner, N., and Boller, T. (2015). Tissue-specific FLAGELLIN-SENSING 2 (FLS2) expression in roots restores immune responses in *Arabidopsis fls2* mutants. *New Phytol.* *206*, 774–784.
- Zhou, F., Emonet, A., Dénervaud Tendon, V., Marhavy, P., Wu, D., Lahaye, T., and Geldner, N. (2020). Co-occurrence of Damage and Microbial Patterns Controls Localized Immune Responses in Roots. *Cell* *180*, 440-453.e18.

6.6. SUPPLEMENTAL FIGURES

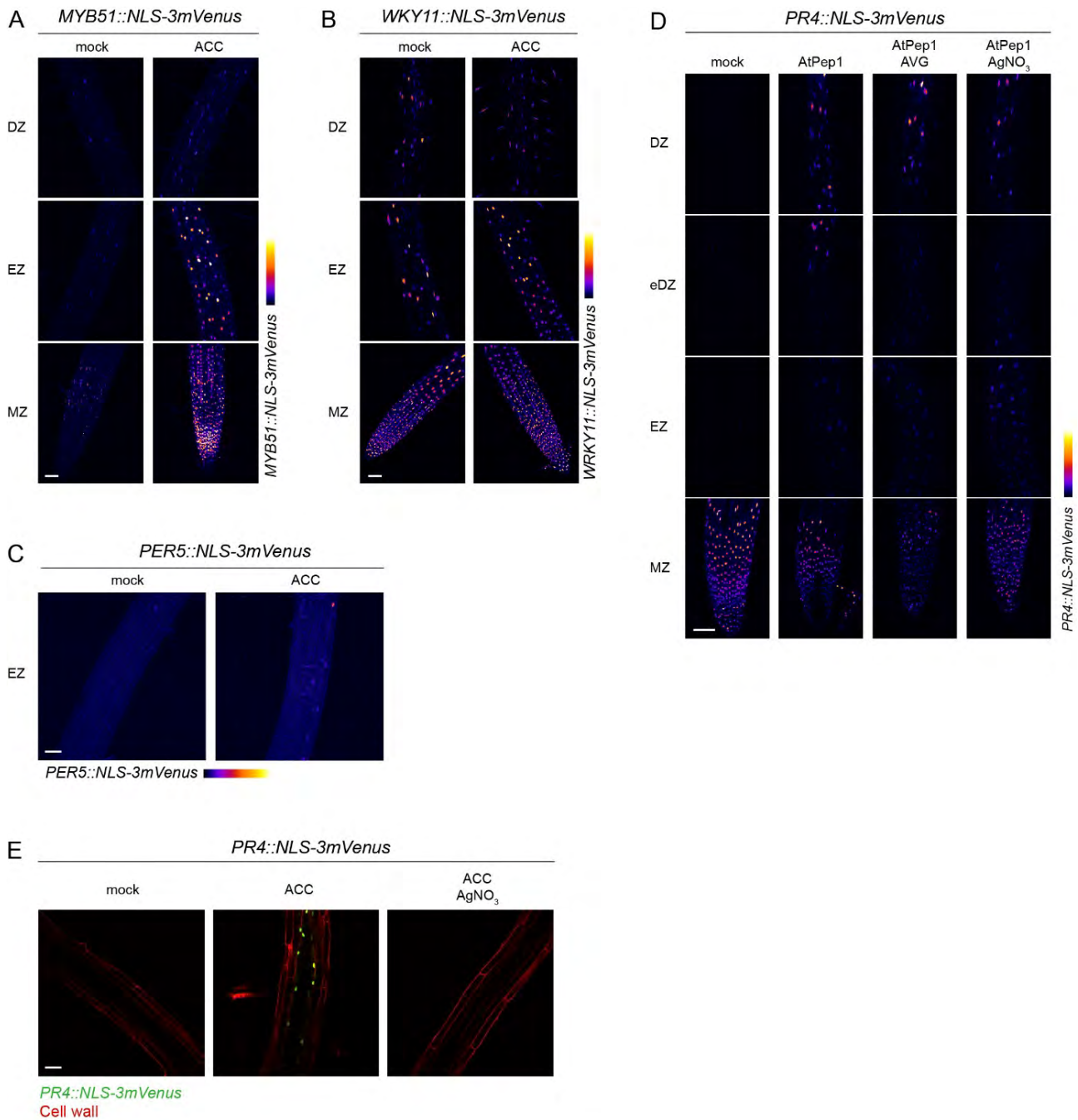


Figure S1: Ethylene induces only specific MTI transcriptional read-outs

(A-C) ACC treatment induces *MYB51::NLS-3mVenus* (A) in all regions of the roots. (B) *WRKY11::NLS-3mVenus* and (C) *PER5::NLS-3mVenus* are not or faintly induced by ethylene treatment, respectively. Maximum projections of z-stack images of seedlings treated on plate for 24 h with 5 μ M ACC. Settings are identical between samples.

(D) Inhibition of ethylene perception inconsistently reduced AtPep1-dependent expression of *PR4::NLS-3mVenus* (Fire LUT). Induction of *PR4* in the stele seems to appear later after treatment with inhibitors (eDZ). Maximum projections of z-stack images of seedlings with combined 24 h treatment with 2 μ M AgNO₃ /AVG and 1 μ M AtPep1.

(E) 5 μ M ACC treatment induces strongly *PR4::NLS-3mVenus* transcription in the endodermis. The effect is inhibited by 2 μ M AgNO₃ treatment. Picture taken in DZ.

MZ, meristematic zone; EZ, elongation zone, eDZ, early differentiated zone (= 10 cells after the onset of elongation); DZ, differentiated zone (20 or 30 cells after the onset of elongation). Scale bar, 50 μ m.

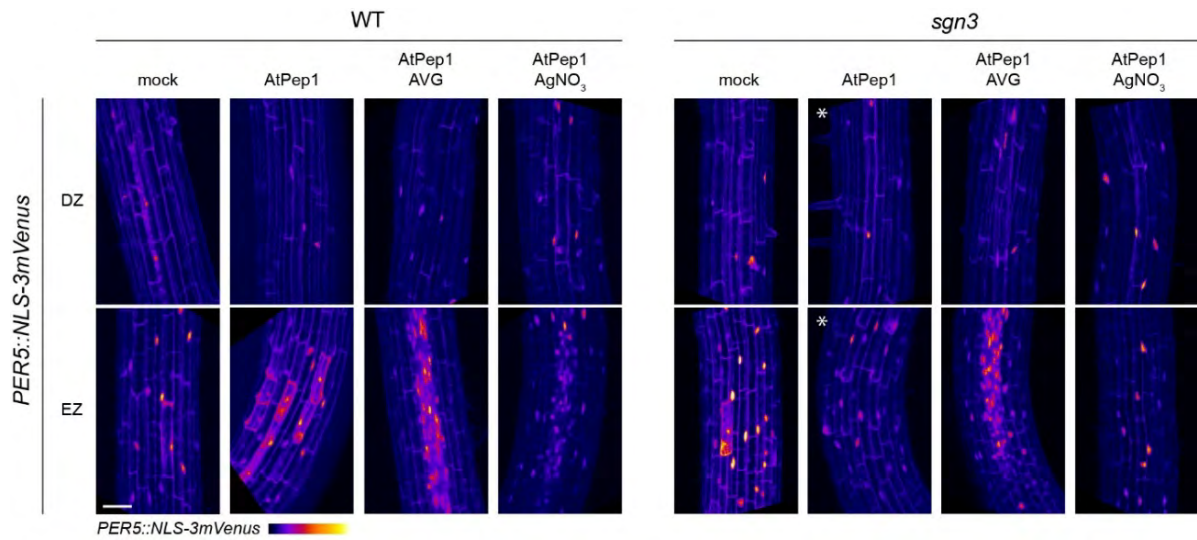


Figure S2: *sgn3* mutants does not affect the ethylene-dependent response to AtPep1

Preliminary experiment (one replicate) showing that combined treatment with AtPep1 and ethylene inhibitors increases *PER5::NLS-3mVenus* (Fire LUT) expression in the stele of the EZ both in WT and *sgn3* mutants. Despite the endodermis being permeable to AtPep1 in *sgn3*, note the absence of response in the stele (star). Maximum projections of z-stack images of seedlings treated on plate, for 24 h in total, with 2 μ M AgNO₃/AVG and with 1 μ M AtPep1 for 8 h. MZ, meristematic zone; EZ, elongation zone. Scale bar, 50 μ m.

7 COMPARISON OF CIF2- AND FLG22-INDUCED LIGNIFICATION OF THE ENDODERMIS

7.1. CONTRIBUTIONS

The project described in this chapter was carried out in collaboration with Yan Ma and Damien De Bellis. Here are our respective contributions. Electron microscopy pictures were done by Damien De Bellis, who fixed and prepared samples, which I had previously treated. Preliminary image analysis was done by Damien. Transcriptomic analysis was designed together with Yan Ma. I did preliminary assays while the actual experiment and RNA extraction was done together with Yan. The Genome Technology Facility (GTF) carried out the library preparation, the sequencing and the first steps of bioinformatics analysis. I did preliminary qPCR assays on selected genes. Bioinformatic analyses and graphical displays were made by Yan. Analysis and discussion of the results was done together with Yan.

I generated CRISPR mutants and carried out all confocal imaging (lignin deposition in *CASP1::FLS2-GFP fls2* lines, fluorescent transcriptional read-outs, *etc.*) and their subsequent analyses. Satoshi Fujita and Robertas Ursache designed and provided the triple gRNA CRISPR system vectors.

7.2. INTRODUCTION

7.2.1. LIGNIN IN CASPARIAN STRIP AND ECTOPIC COMPENSATORY LIGNIN

One of the features of root endodermis is the Casparian strip (CS), a finely localized ring-like impregnation of its cell wall which forms an apoplastic diffusion barrier between the outer tissues and the central cylinder (Caspary, 1865; Geldner, 2013). Though the exact composition of the CS was a long-standing debate, it has now been clearly demonstrated that it is made of lignin (Naseer *et al.*, 2012). CASPARIAN STRIP DOMAIN PROTEINS 1-5 (CASPs) are transmembrane domain proteins highly important for the precise localization of the CS and define a plasma membrane region called the Casparian Strip Domain (CSD) (Roppolo *et al.*, 2011). These proteins are thought to form a scaffold for lignin polymerizing proteins such as PEROXIDASE 64 (PRX64), the dirigent protein ESB1 (ENHANCED SUBERIN 1) and the NADPH oxidase RBOHF (RESPIRATORY BURST OXIDASE PROTEIN F) (Barbosa *et al.*, 2019; Hosmani *et al.*, 2013; Lee *et al.*, 2013).

Lignin is essentially composed of an intricate polymer of cinnamyl alcohols, also called monolignols, derived from the phenylpropanoid pathway. Their polymerisation occurs in the apoplast and is thought to be a spontaneous process. However, such oxidative coupling requires the dehydrogenation of monolignols, forming resonance-stabilized radicals. This mechanism can be catalysed by peroxidases or laccases, depending on the cell types (Barbosa *et al.*, 2019). Deposition of the CS lignin requires enzymes precisely localized at the CSD. Five peroxidases, including PRX64, were recently shown to be necessary for CS lignification, since their quintuple mutant (*prx3, 9, 39, 72, 64*) completely lacks CS (Rojas-Murcia *et al.*, 2020). Surprisingly, a nonuple mutant for laccases (*lac1, 3, 5, 7, 8, 9, 12, 13, 16*) does not cause any defects in the CS, despite their expression in the endodermis and the localisation of LAC1, 3, 5 and 13 at the CSD (Rojas-Murcia *et al.*, 2020). Peroxidases requires H₂O₂ for their activity, which is provided by the oxidation of oxygen in superoxide by NADPH oxidases (NOX) followed by dismutation by superoxide dismutases (SOD). CS lignification was shown to rely mainly on the NADPH oxidase RBOHF (Lee *et al.*, 2013). In addition, the putative manganese SOD MSD2 is also implicated (Rojas-Murcia, 2019).

Mutations in genes required for CS deposition cause various phenotypes, from intermittent strips described as “string-of-pearls” in *casp1* and *esb1* mutants (Hosmani *et*

al., 2013; Roppolo *et al.*, 2011) to delayed formation of the CS in *prx64* and *rboh1* (Lee *et al.*, 2013). Interestingly, these mutants not only show defects in the formation of the Casparian strip, but also induce compensatory lignin deposition at the corners of the endodermis. This phenomenon is also observed in *myb36*, a mutant of the transcription factor required for Casparian strip formation, which completely lacks CS (Kamiya *et al.*, 2015). In addition to compensatory lignin, *casp1 casp3*, *esb1*, *rboh1* and *myb36* mutants also show increased deposition of suberin lamellae below the primary cell wall (Fujita *et al.*, 2020; Hosmani *et al.*, 2013).

7.2.2. COMPENSATORY LIGNIN IS DEPENDENT ON THE SCHENGEN PATHWAY

This compensatory lignin was recently shown to be dependent of a receptor/peptide signalling pathway (SCHENGEN pathway) whose function ensures the proper sealing of the CS during root development. Plants with dysfunctional SGN3 (SCHENGEN3, also called GASSH01 - GS01) LRR-receptor kinase display intermittent CS and CASP1, without inducing any compensatory mechanisms (Pfister *et al.*, 2014). Moreover, *sgn3* mutation can abolish the ectopic lignin and suberin deposition observed in *casp1 casp3* and *esb1* mutants. SGN3 was identified in a screen for apoplastic permeability of the CS with three other mutants named *schengen 1*, *2* and *4* in tribute to the Schengen area of free movement. While SGN4 was actually allelic to RBOHF, SGN1 encodes a receptor like kinase (RLK) and SGN2 encodes the TPST tyrosylprotein sulfotransferase (Alassimone *et al.*, 2010; Doblaz *et al.*, 2017; Lee *et al.*, 2013; Pfister *et al.*, 2014). Moreover, TPST was shown to sulphate the small peptide ligands CIF1 and CIF2 (CASPARIAN STRIP INTEGRITY FACTOR 1 and 2) of the receptor SGN3, a process necessary to increase the peptide activity, which otherwise reduces the SGN3 signalling significantly. Indeed, *cif1 cif2* double mutant phenocopies *sgn3*, indicating that CIF1 and CIF2 function in the same pathway.

The SGN3 pathway monitors the integrity of CS by assessing its ability to block apoplastic diffusion from within the stele (Fig.1) (Alassimone *et al.*, 2016; Doblaz *et al.*, 2017; Fujita *et al.*, 2020; Pfister *et al.*, 2014). In wild-type plants, CIF2 and CIF1 peptides are produced in the stele and diffuse through the gaps of the developing Casparian strip to reach the SGN3-SGN1 receptor complex situated on the outer side of the CSD (Fig.1A)(Doblaz *et al.*, 2017). SGN3 is localised as a ring slightly broader than the CSD. However, its

downstream receptor-like kinase target, SGN1, is polarly localized to the cortex-facing plasma membrane and excluded from the CSD. The SGN3 receptor and the SGN1 kinase only co-localized at a very restricted region at the outer border of the CS (Alassimone *et al.*, 2016; Fujita *et al.*, 2020). Therefore, CIF1/2 peptides will only induce the SGN3/SGN1 signalling module as long as the CS is interrupted (Fig.1A). The signalling events then lead to lignin deposition that can seal the gaps of the immature Casparian strip. Once the CS is sealed, the CIF1/2 peptides can no longer diffuse and activate the receptors, halting the signalling (Fig.1B). When the integrity of the CS is impaired, the CIF peptides are not blocked and SGN3 is continuously stimulated, leading to compensatory lignin deposition in endodermal corners. Similarly, when plants are exogenously treated with CIF1/2 peptides, the SGN1/SGN3 module is constantly activated, inducing ROS production at the outer edge of the CSD, which diffuse to the cell corners (Fig.1C). This leads to polymerisation of monolignols and strong lignification of the cortex-endodermal corners (Fig.1D) (Doblas *et al.*, 2017; Fujita *et al.*, 2020).

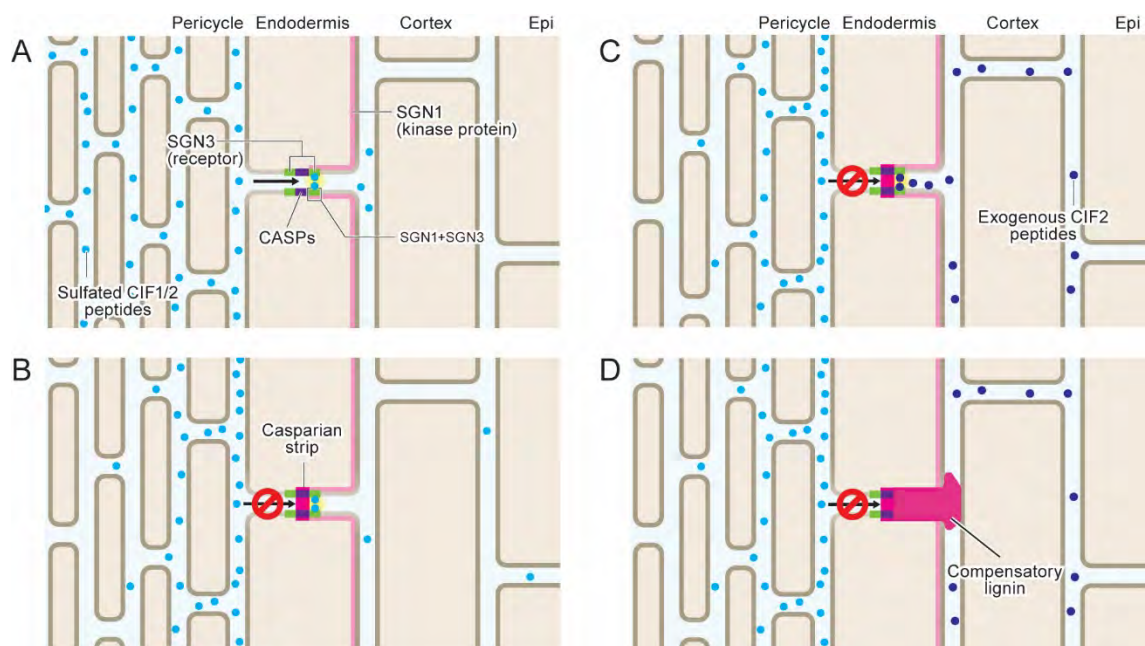


Figure 1: The SCHENGEN pathway ensures CS integrity.

Scheme representing four states of the SCHENGEN pathway. (A) CS formation in early differentiating zone. CIF1/2 peptides diffuse from the stele through the gaps of the developing CS and bind to the SGN3/SGN1 complex at the outer side of the CSD. This results in (B) CS sealing and halting of CIF1/2 peptides. The SCHENGEN pathway is no longer activated. In case of exogenous CIF2 treatment (C), the peptide stimulates the SGN3/SGN1 complex at the outer side of the CS, which leads to (D) compensatory lignin deposition at the cell corners. Modified illustration from Hiroko Uchida.

7.2.3. SIMILARITY BETWEEN MTI AND SCHENGEN PATHWAYS

Interestingly, downstream components of the SCHENGEN pathway are analogues to MAMP-triggered immune signalling (Alassimone *et al.*, 2016; Fujita *et al.*, 2020). Firstly, SGN3 is an LRR receptor protein whose closest homologues are the receptors PEPR1 and PEPR2, recognizing AtPeps (Creff *et al.*). Moreover, SGN3 requires SERK1 and SERK3/BAK1 as co-receptors for its activation (Okuda *et al.*, 2020). BAK1 is also a co-receptor for the LRR-RK FLS2, EFR, PEPR1 and PEPR2 (Chinchilla *et al.*, 2007; Heese *et al.*, 2007; Schulze *et al.*, 2010). SGN3 interacts and phosphorylates SGN1, which belongs to the RLCK VII subfamily, whose many members, like BIK1, associate and function with PRRs (Alassimone *et al.*, 2016; Ranf *et al.*, 2014). SGN1 in turn phosphorylates both NADPH oxidases RBOHF and RBOHD (Fujita *et al.*, 2020). By comparison, BIK1 induces the phosphorylation of RBOHD downstream of FLS2 signalling (Kadota *et al.*, 2014; Li *et al.*, 2014). After endogenous activation by CIF1/2, RBOHF and RBOHD produce very localized H₂O₂ that can be visualized by electron microscopy at the outer side of the CSD (Lee *et al.*, 2013). However, when plants are exogenously treated with CIF2, ROS production extends until the first endodermal-cortex corner (Fujita *et al.*, 2020). ROS is also produced in response to MAMPs, though its cellular localization remained unexplored. Finally, both SCHENGEN and MTI pathways induce the phosphorylation of MAPK3 and MAPK6. MAPK phosphorylation occurs independently of NADPH oxidases for MTI signalling, which seems to also be the case for the SCHENGEN pathway (Fujita *et al.*, 2020; Xu *et al.*, 2013).

RNA profiling of CIF2 responses also revealed the induction of genes related to defence responses in addition to the more expected increased in suberin and lignin biosynthesis genes (Fujita *et al.*, 2020). Interestingly, the transcription factor MYB15, which is involved in pathogen- and flg22-induced lignification (Chezem *et al.*, 2017), is also strongly induced after CIF2 treatment (Fujita *et al.*, 2020). Taken together, the parallels between CIF2- and MAMPs-induced lignification are particularly striking and lead to the idea that the SCHENGEN pathway might be a neofunctionalization of the more evolutionary ancient MTI pathway into a developmental process, regulating barriers formation (Fujita *et al.*, 2020).

Lignin deposition is also observed in response to pathogens and flg22 in leaves and seedlings of *A. thaliana* (Ch.1; Chezem *et al.*, 2017; Lee *et al.*, 2019). However, flg22-driven lignification is not naturally observed in roots but can be obtained after ectopic overexpression of *FLS2* in these tissues (Emonet *et al.*, 2020). Interestingly, this induced lignification mostly occurs at cell corners, a phenomenon that resembles CIF2-induced lignin deposition. Whether the immunity-related lignification mechanism is equivalent to the one observed in a developmental context is still unclear, but current evidence suggests that they share a common basis. Interestingly, in addition to the involvement of MYB15 transcription factors for both flg22- and CIF2-induced lignin deposition, pathogen-mediated lignification in the leaves depends on *CASP-LIKE PROTEINS L1D1* and *L4D1* (*CASPL1D1* and *CASPL4D1*). This suggests that this deposition of lignin possibly uses an analogous mechanism to the Casparian strip formation (Lee *et al.*, 2019). Although *CASP1-5* are not required for compensatory lignin formation (I. Barbosa, *personal communication*), it is probable that some of their *CASPLs* homologues could be involved. Whether flg22 and CIF2 induce a common pathway for lignification or trigger their own specific signalling is so far unknown.

7.2.4. THE ENDODERMIS AS A MODEL TO STUDY SPECIFICITY

How to compare pathways without being influenced by the identity of the different tissues in which they occur? The ectopic expression of *FLS2* in the endodermis, using the specific endodermal promoter *CASP1* to drive *FLS2* in a *fls2* mutant background, can bypass such limitation. Indeed, *CASP1::FLS2* line deposits lignin only at the endodermal cell corner in a cell-autonomous fashion (Emonet *et al.*, 2020), allowing the direct comparison of lignin deposition triggered by two distinct inputs in the same cell type.

Since CIF2 and flg22 pathways share many components including co-receptor, RBOHD and MAPKs, we wanted to investigate whether these developmental and biotic signals induce a common “lignin deposition program”. In addition, using the endodermis as a model cell type provides a powerful tool to elucidate how specificity can be achieved by different inputs despite the convergence of their signalling cascade. Indeed, the SCHENGEN pathway is also required for endodermal-specific fusion of *CASP1* into a ring around the endodermis, a process which is not expected to occur as a MTI response (Pfister *et al.*, 2014).

Moreover, it is easier to compare both pathways in the endodermis, where all signalling components are present, than to reproduce the SCHENGEN pathway in another cell type. Drapek *et al.* (2018) previously generated a CS in the subepidermis layer of *WER::SHR* lines treated with CIF2, but the barrier was not completely functional. Here, we compared compensatory lignification driven by CIF2 treatment with flg22-mediated lignification using specific endodermal expression of *CASP1::FLS2* in *fls2* background.

7.3. RESULTS

7.3.1. LIGNIN DEPOSITION IN RESPONSE TO CIF2 AND FLG22 HAVE UNMATCHING PATTERNS

Corner lignin deposition after CIF2 or flg22 treatments might look similar at first sight, but a careful comparison was necessary to determine if both outputs were indeed identical. I took advantage of the *CASP1::FLS2* line and analyse its cell wall modifications side by side with wild-type plants after CIF2 or flg22 treatments. Results show differences of lignin deposition patterns induced by CIF2 and flg22 ligands. In regions closer to the root tip (15 cells after the onset of elongation), both treatments induced lignification restricted to the endodermis-cortex corners (Fig.2A, left panel). However, at a later stage (20 cells), flg22-driven lignification expands beyond the corners into the cell boundary between endodermis and cortex (Fig.2A, right panel). It could be noted that, although the concentrations of both peptides were identical, flg22-induced responses were consistently stronger. Moreover, flg22 does not induce lignin deposition in wild-type roots, confirming previous data (Chezem *et al.*, 2017; Emonet *et al.*, 2020).

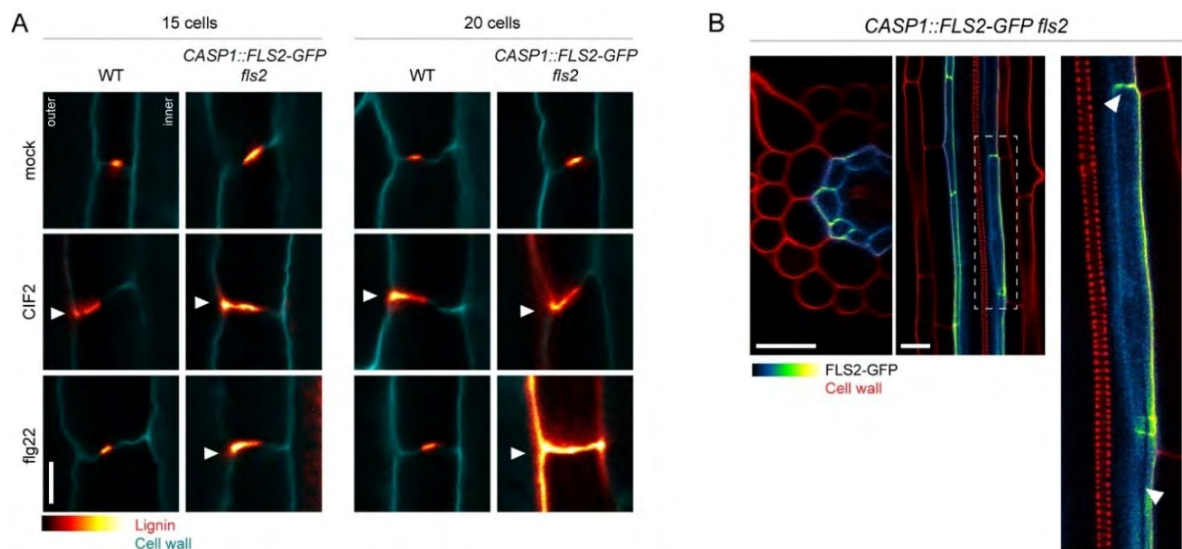


Figure 2: CIF2- and flg22-induced lignin in *CASP1::FLS2-GFP fls2* differ in location

(A) Lignin accumulation patterns at endodermis, view as median position at 15 and 20 cells after the onset of elongation, with 1 μ M CIF2, 1 μ M flg22 or mock treatment. Lignin accumulates at outer corners after CIF2 treatment in both genotypes and after flg22 treatment in *CASP1::FLS2-GFP fls2* only. Note that flg22 can induce lignin all along the outer border of the endodermis. Lignin and cellulosic cell walls are stained with Basic Fuchsin (RedHot LUT) and Calcofluor White (cyan), respectively. White arrowheads indicate sites of excess lignification on the cortex-facing (outer) side. “Inner” designates the stele-facing endodermal side, “outer”, the cortex-facing side. Scale bar, 5 μ m.

(B) *CASP1*-driven FLS2-GFP localizes all around the plasma membrane of the endodermis and is excluded from the CSD (white arrowheads). Transversal and longitudinal views of *CASP1::FLS2-GFP fls2* line. FLS2-GFP (GreenFireBlue LUT) is co-visualized with PI-stained cell wall (red). Picture on the right is a zoomed in view from the selection in dashed box. Scale bars, 25 μ m.

In contrast to the native SGN3 receptor, *CASP1::FLS2* is not restrictively localized around the CSD, but can be found all around the plasma membrane of the endodermis (Fig.2B). This could explain why the pattern of lignin deposition is broader in response to flg22. Pericycle-endodermal boundaries are not lignified in the early differentiated regions, though the FLS2 receptor is expressed on both sides. Since flg22 is blocked by the mature Casparian strip, the peptide cannot penetrate to the inside of the endodermis, justifying the polarity of lignin deposition I observed (Fig.2A).

7.3.2. ROS PRODUCTION COINCIDES WITH LIGNIN DEPOSITION PATTERN IN *CASP1::FLS2*

To further characterize the difference between flg22- and CIF2-induced lignification, I assessed H₂O₂ production using ROS-triggered cerium precipitation, followed by visualisation via transmission electron microscopy (TEM). According to previous work from our lab, CIF2-induced lignification in wild-type plants goes hand in hand with restricted local ROS production at the cortical side of the CSD until the endodermal-endodermal-cortex cell corner (see Fig.4 by Fujita *et al.*, 2020). By contrast, flg22 treatment on *CASP1::FLS2* induces ROS production in the same sites (Fig.3A, 3C), but also in the endodermal-cortex cell walls (Fig.3A, 3B). ROS were nevertheless not uniformly produced in the whole endodermal-cortex boundary. Notably, ROS also accumulate at the next closest endodermal-cortex-cortex corner (Fig.3A, 3D). It should be noted that, in contrast to CIF2 treatment (Fujita *et al.*, 2020), the Casparian strip domain is not extended after flg22 treatment (Fig.3C). As a side note, we could observe that in some samples, ROS staining displays a diffused pattern (Fig.3D, left panel), but in others, it forms a sharp line close to the plasma membrane, maybe due to the restriction of its diffusion by the newly formed lignin layer (Fig.3D, right panel). Overall, ROS production localization matches the pattern of lignification observed with fuchsin staining. Flg22-induced ROS production is less localized than the CIF2-induced one and extends to the endodermal-cortex side.

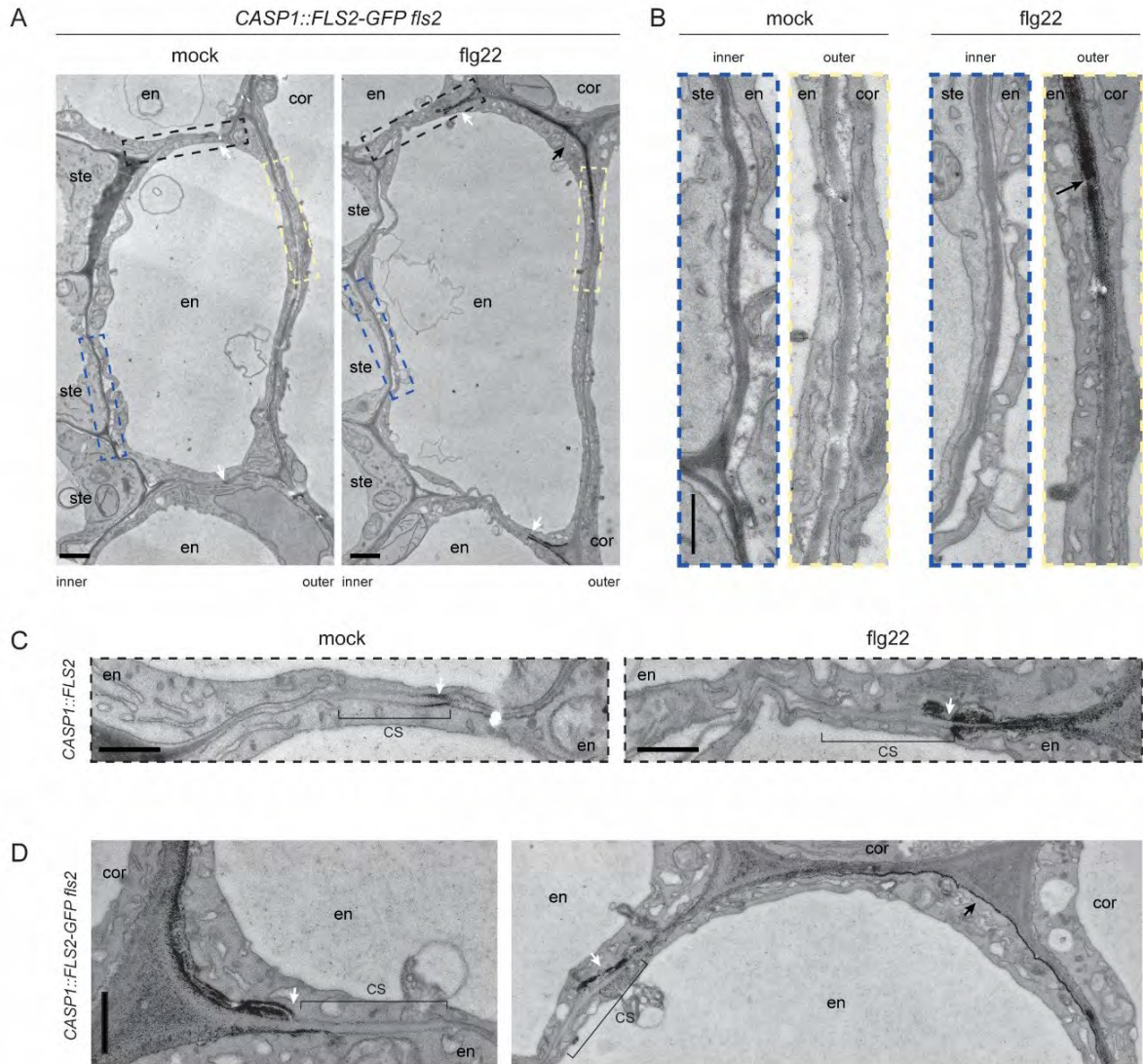


Figure 3: ROS production is diffuse and less localized in *CASP1::FLS2-GFP fls2*

(A) Overview of endodermal cells in *CASP1::FLS2-GFP fls2* after 24h treatment with 1 μ M flg22. Boxes in dotted lines correspond to the zoom-in regions in (B) (blue and yellow boxes) and in (C) (black boxes). Scale bar, 1 μ m.

(B) *In situ* H₂O₂ detection on inner and outer border of the endodermis. Scale bar, 500 nm.

(C) *In situ* H₂O₂ detection at Casparian strips after treatment with 1 μ M flg22. Scale bar, 500 nm.

(D) Specific examples of ROS production after flg22 treatment in *CASP1::FLS2-GFP fls2*. Scale bar, 500 nm.

White arrows indicate ROS production sites at the Casparian strip, black arrows, ROS production outside of the CS domain; brackets, Casparian strips (CS); cor, cortex; en, endodermis; ste, stele.

7.3.3. *RBOHF*, *RBOHD* AND *MYB15* ARE IMPLICATED IN FLG22-DRIVEN LIGNIN DEPOSITION

Lignin cellular localisation is generally affected by the localisation of the polymerizing enzymes. Since flg22-induced lignin was not as precisely localized as the SCHENGEN-dependent compensatory lignin, I investigated whether different NADPHs were involved in this process.

I used the CRISPR-Cas9 system (Ursache, Fujita *et al.*, manuscript in preparation) to generate single mutants of *RBOHF*, *RBOHF*, *MYB15* and *RBOHA* in *CASP1::FLS2-GFP fls2* background. All four genes were shown to be induced in transcriptomic data obtained from CIF2-treated seedlings (Fujita *et al.*, 2020). The list of the different mutant alleles obtained by CRISPR (Fig.S1, Table S2) and their predicted effect on proteins (Table S3) can be found in Section 7.7. Large deletions were found easily in *rboha* and *myb15* and were conserved from T1 to T2 generation. In contrast, the CRISPR-induced deletions in *rbohd* and *rboh* were often lost at T2 generation. Nevertheless, CRISPR-driven mutagenesis worked well enough for me to obtain single point mutations or few base-pair deletions. All experiments related to Figure 4 were done in *CASP1::FLS2 fls2* background.

Flg22-driven lignification was generally slightly reduced in *rbohd* and in *rboh* compared to wild type, especially at 15 cells after the start of elongation. At 20 cells, the difference was less visible. By contrast, lignin deposition induced by flg22 was identical to wild-type lines in *rboha* mutant (Fig.4A, S2A for 2nd independent allele). As negative controls, *rboha*, *rbohd* and *rboh* in *fls2* background were insensitive to flg22 treatment and had identical phenotypes to the corresponding mutants in *CASP1::FLS2* background (Fig.S3). *RBOHD* is described as the main player in the signalling cascade of the MAMP-triggered immunity (Zhang *et al.*, 2007). It is interesting to note that in the endodermis, *RBOHD* is not fully required and that other NOXs, probably *RBOHF*, can take over its role. It will be particularly important to assess lignin content of the double mutant *rboh rbohd* in *CASP1::FLS2 fls2* background to confirm their redundancy.

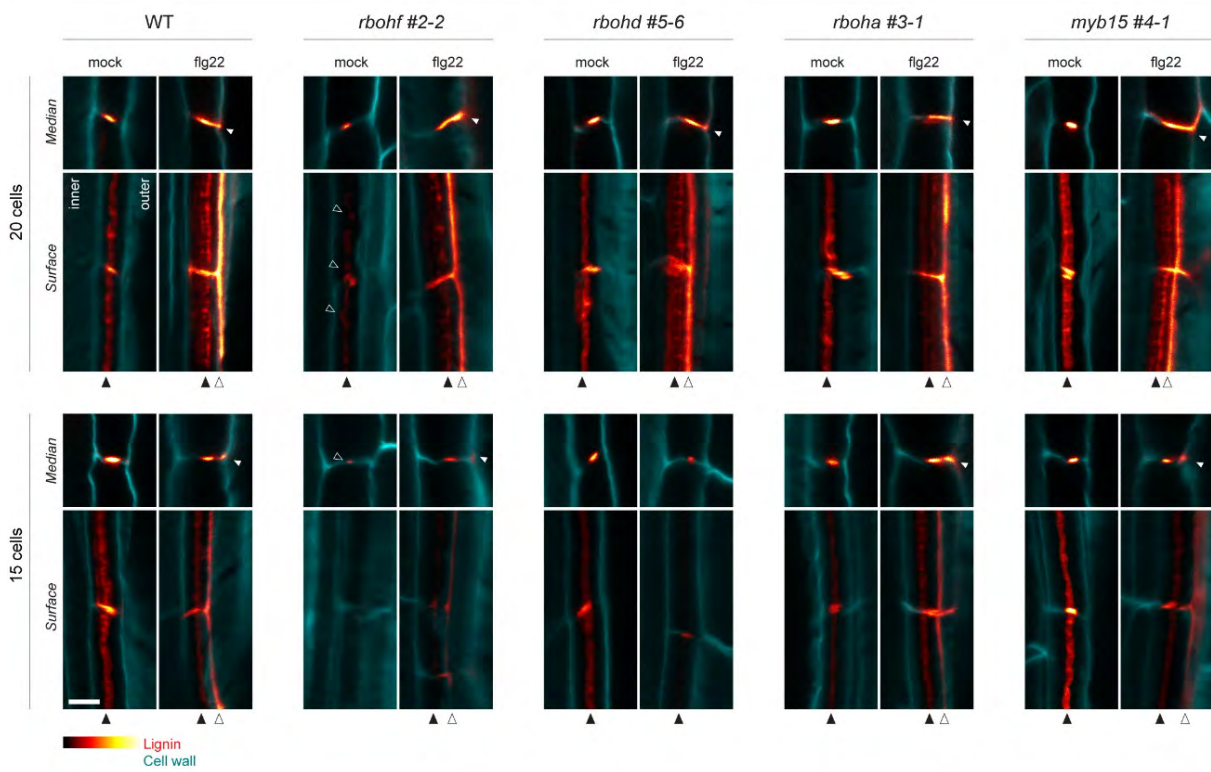
Mutations in *rbohd* and *rboha* did not impact the CS, starting around 8-10 cells after the onset of elongation. However, *rboh* mutants in both *CASP1::FLS2 fls2* and *fls2* background had delayed CS formation with mock treatment (CS starts roughly around 15-20 cells)(Fig.4A, S2A). Indeed, at 15 cells after the start of elongation, wild-type plants already possess a fused Casparian strip, while *rboh* displayed a dotted CS or no lignin at all (Fig.4A). This replicates the phenotype observed for *rboh-2* single mutant in Col-0 wild-type background (Lee *et al.*, 2013). Interestingly, treatment with flg22 could partially rescue the delayed CS phenotype in *CASP1::FLS2 fls2 rboh* and triggers compensatory lignin (Fig.4A, B, S2A). Fig.4A (2nd bottom panel) shows that flg22 induced patch-like accumulation

of lignin at the CSD already at 15 cells after the onset of elongation. With variability between replicates, these patches seem to fuse around 20 cells or later and form a CS that resembles wild type, and can have an identical (Fig.4B) or weaker lignin deposition intensity (Fig.4A, S2). However, this CS is not regular and presents some holes in the centre (Fig.4A, B). This “ladder” phenotype was previously seen in *esb1* and *casp 5x* mutants (Hosmani *et al.*, 2013, I. Barbosa, *personal communication*). It is also observed in response to flg22 in wild type, *rboh*d, *rboh*a and *myb15* mutants (Fig. 4A, S2) and might be simply correlated to strong induction of compensatory lignin. Indeed, in contrast to *esb1*, which displays an abnormal CS structure by electron microscopy, lignin deposition induced by flg22 at the CS looks similar to CIF2-response (Fig.3C) (Fujita *et al.*, 2020; Hosmani *et al.*, 2013). This “ladder” phenotype might be due to different affinities of Basic Fuchsin staining for freshly deposited and older lignin. Nevertheless, *rboh*f tends to display a lignin pattern which looks bulkier than other mutants (Fig.4B). It would be crucial to analyse the permeability phenotype by propidium iodide assay in these conditions to assess if the barrier function can be restored. Overall, *RBOHF* is required for the proper formation of the CS, but might be partially replaced by the activation of other NOXs through the flg22-triggered immunity pathway.

In addition, though *myb15* mutants were able to lignify in response to flg22, the strength of the Basic Fuchsin signal was slightly lower compared to wild-type plants, with some variation depending on replicates (compare Fig.4A, Fig.S2A and Fig.S2B). Interestingly, *MYB15* is also strongly induced after CIF2-treatment (Fujita *et al.*, 2020), and compared to Col-0, *myb15* mutant shows a decreased ectopic lignin deposition after CIF2 treatment (Yan Ma, *personal communication*). *MYB15* is therefore important for lignification in root and shoot of *A. thaliana* (Chezem *et al.*, 2017; Lee *et al.*, 2019).

In summary, both CIF2 and flg22-induced lignin deposition seems to rely on a common basis involving *RBOHF*, *RBOHD* and *MYB15*, despite their slightly different localisation.

A

CASP1::FLS2-GFP *fls2*

B

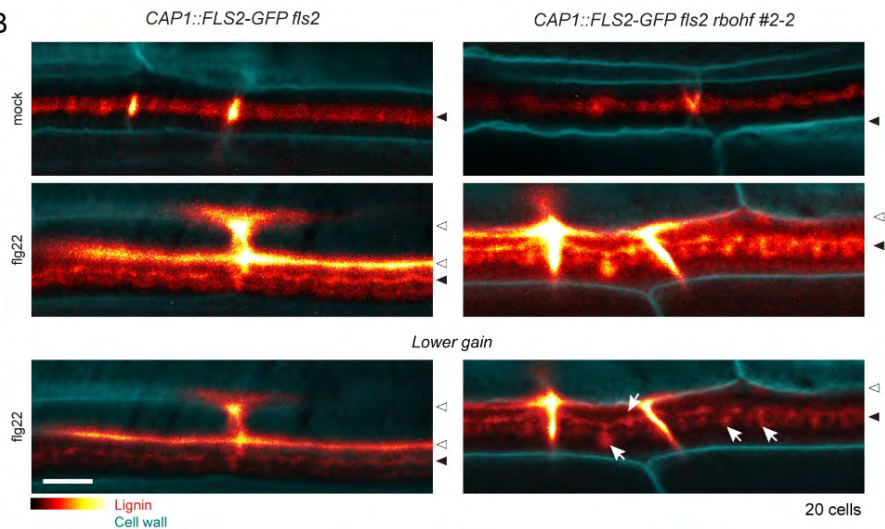


Figure 4: *RBOHD*, *RBOHF* and *MYB15* are required but not sufficient for flg22-induced lignification

(A) Lignin accumulation in WT, *rbohD*, *rbohF*, *rbohA* and *myb15* single mutants, in *CASP1::FLS2-GFP fls2* background, with 1 μ M flg22 or mock treatment for 24 h. Pictures are shown as surface and median views at 15 and 20 cells after the onset of elongation. Lignin and cell walls are stained with Basic Fuchsin (RedHot LUT) and Calcofluor White (cyan), respectively. One independent line is presented by mutant, see Figure S2 for other independent lines and Figure S3 for controls in *fls2* background.

(B) Zoom in on lignin patterns in *CASP1::FLS2-GFP fls2* and *CASP1::FLS2-GFP fls2 rbohF* lines in response to flg22 at 20 cells after the onset of elongation. Images of flg22 treatment are duplicated with lower gain to visualise bulky deposition of lignin (white arrows).

Black arrowheads, CS lignin; white arrowheads, compensatory lignin. Scale bars, 5 μ m.

7.3.4. COMPARISON OF MTI AND SCHENGEN UPSTREAM PATHWAYS

CIF2 INDUCES DEFENCE MARKERS IN THE ENDODERMIS

To confirm the capacity of the SCHENGEN pathway to induce genes involved in immunity (Fujita *et al.*, 2020), I subjected *PER5::NLS-3mV* and *MYB51::NLS-3mV* lines to CIF2 treatment. *PER5* expression was increased in the cortex and endodermal cells of the differentiated zones (Fig.5A). Similarly, *MYB51* was also induced by CIF2 treatment in the differentiated cortex, endodermis and pericycle cells (Fig.5B). The SGN3 receptor was previously shown to localize at the plasma membrane of endodermal and cortex cells (Pfister *et al.*, 2014), explaining why only such tissues induce *PER5* cell-specific markers. In contrast, the non-cell autonomous *MYB51* marker has, as expected, a broader pattern of induction (Fig.5B) (Emonet *et al.*, 2020). This corroborates the finding that CIF2 can induce many defence-related genes, as shown in the early time points of the transcriptomic analysis of CIF2-induced responses carried out in our group (Fujita *et al.*, 2020)

FLG22 DOES NOT AFFECT MARKERS OF THE SCHENGEN PATHWAY IN WILD-TYPE

BACKGROUND

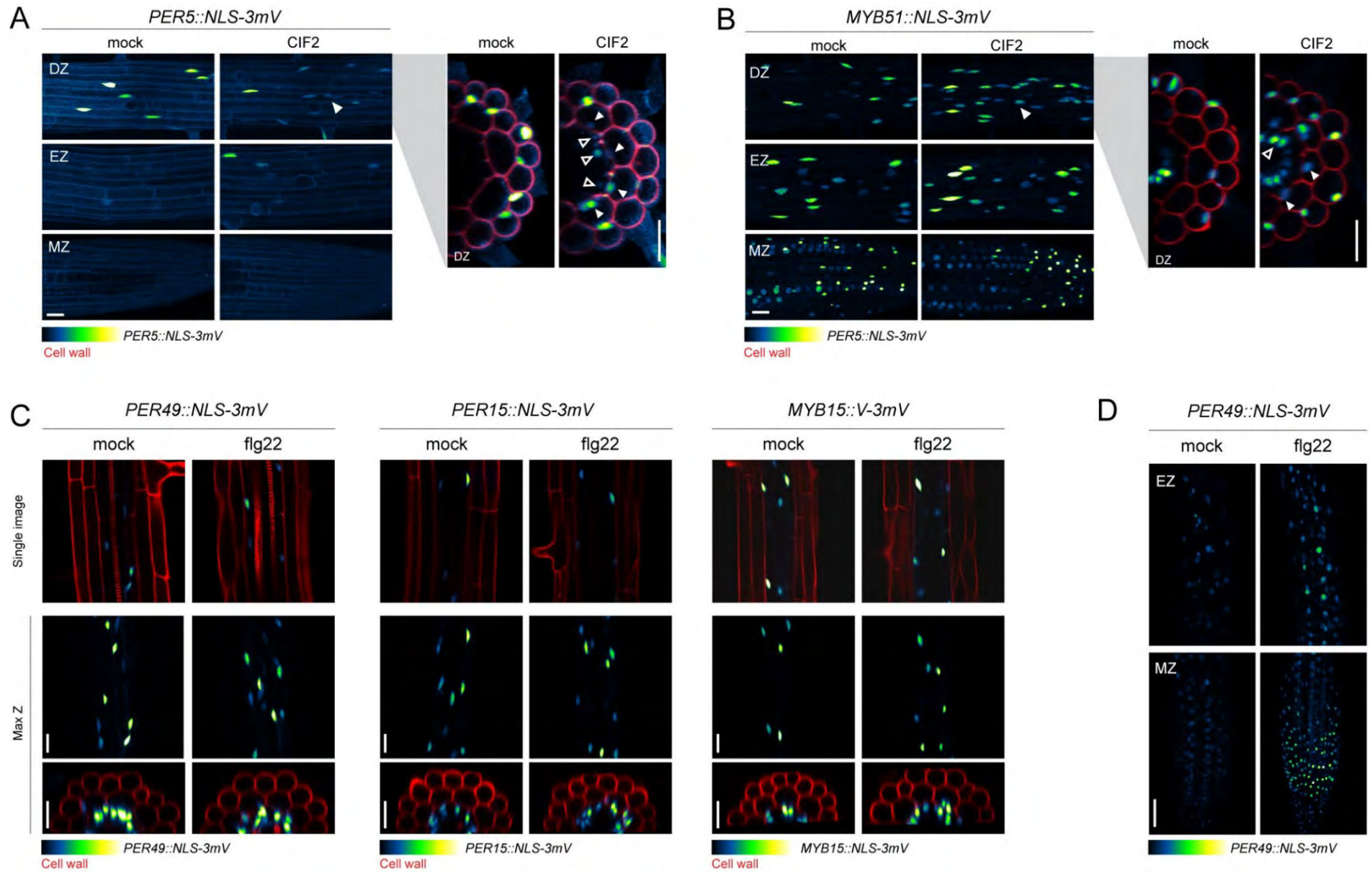
I assessed whether *flg22* treatment could induce markers of the SCHENGEN pathway. Our recently published transcriptomic analysis of CIF2-induced responses underlined a set of strongly induced genes that were related to lignin production. Therefore, I tested *PER15* (*PEROXIDASE 15*), *PER49* (*PEROXIDASE 49*) and *MYB15* transcriptional read-outs generated previously in our lab in wild-type background (Andersen, *unpublished*).

Figure 5 (next page): CIF2 induces immune transcriptional read-outs but *flg22* has almost no impact on SCHENGEN markers in wild-type plants.

(A-B) CIF2 treatment induces *PER5::NLS-3mVenus* (A) and *MYB51::NLS-3mVenus* (B) in the differentiated cortex and stele of wild-type plants. Maximum projection of *PER5* and *MYB51* signal (GreenFireBlue LUT) in meristematic (MZ), elongation (EZ) and differentiated (DZ) zones. Maximal projection of transverse sections views is provided for the DZ, cell walls are stained with PI (red). (A) White arrowheads, cortex cells with *PER5* signal, black arrowheads, endodermal cells with *PER5* signal. (B) White arrowheads, cortex cells with *MYB51* signal, black arrowheads, pericycle cells with *PER5* signal. Scale bar, 25 μ m.

(C) *Flg22* treatment does not affect markers of the SCHENGEN pathway such as *PER49::*, *PER15::* and *MYB15::NLS-3mVenus* (GreenFireBlue LUT). Single pictures and maximum projections of normal and transverse section views of markers in response to 1 μ M *flg22* in the differentiated zone. Cell walls are stained with PI (red). Scale bar, 25 μ m.

(D) *PER49::NLS-3mVenus* marker (GreenFireBlue LUT) responds to *flg22* in the EZ and the MZ in 3 out of 8 independent lines. Scale bar, 50 μ m.



These three SCHENGEN markers were constitutively expressed in the endodermis, but none of them was reproducibly induced upon flg22 treatment (Fig.5C). Only a weak *PER49* induction could be observed in the meristematic and elongation zones in three out of eight independent T2 lines (Fig.5D). This suggests that SCHENGEN markers are either independent of flg22, or only endodermis specific. Flg22-responses, when elicited in wild-type plants, only affect the elongation zone and do not cause lignification (Emonet *et al.*, 2020; Millet *et al.*, 2010; Poncini *et al.*, 2017; Zhou *et al.*, 2020), which could explain the absence of SCHENGEN marker responses. It would be interesting to transform them in *CASP1::FLS2* background, where the MTI pathway is strongly induced by flg22 in the endodermis and where lignin can be deposited. In that case, SCHENGEN markers of lignification should have more chance to be activated.

7.3.5. FLG22 AND CIF2 INDUCES VERY SIMILAR TRANSCRIPTOMIC CHANGES

To compare flg22 and CIF2 transcriptional responses, we then performed a transcriptomic analysis reproducing the time frame and experimental conditions of the SCHENGEN-RNaseq profiling previously done in our lab (Fujita *et al.*, 2020). Briefly, we used two plates of densely sown seedlings per genotype (*CASP1::FLS2* and *fls2*), per treatment (mock and 1 μ M flg22) and per time points (30 min, 120 min and 480 min) and carried out the experiment in triplicate on three different days. A flg22 peptide concentration of 1 μ M was used instead of 100 nM since it induced lignin deposition more representative of the pattern we usually saw (data not shown). Five-day old seedlings grown on mesh were transferred at time point zero in parallel onto fresh mock or 1 μ M flg22-containing plates, then roots were harvested and snap frozen after 30 min, 120 min or 480 min. Extracted RNA was sent to the Genome Technology Facility (GTF) who carried out the library preparation and RNA sequencing with a procedure identical to Fujita *et al.* (2020).

Before sending RNA for sequencing, I quickly assessed the expression level of a set of markers genes for MTI and SCHENGEN pathways using real-time polymerase chain reactions (qPCR) (Fig.S4). I observed that both *PER5* and *MYB51* markers were strongly induced by flg22 at 30 min after flg22 treatment, whereas *FRK1* was expressed slightly later, at the 120 min time point. In contrast, the commonly used *PR1* (*PATHOGENESIS-RELATED*

GENE 1) defence marker was unaffected by flg22, which was consistent with the absence of *PR1* induction by salicylic acid and flg22 in *Arabidopsis* roots (Marhavý *et al.*, 2019; Poncini *et al.*, 2017). Like MTI markers, *PER15*, *PER49* and *MYB15* expressions were highly upregulated upon flg22 treatment, with fold changes ranging between 20 to 150 (Fig. S4). As for CIF2 treatment, *MYB15* was induced at early time points (30 min and 120 min) while *PER15* and *PER49* were upregulated later. In contrast to wild-type plants (Fig.5C, D), flg22 clearly induces SCHENGEN markers in *CASP1::FLS2* background. As a side note, it would be interesting to test if *PER15*, *PER49* and *MYB15* are also upregulated downstream of the FLS2 pathway in other tissues, using *prom::FLS2* lines.

Preliminary RNAseq analysis was carried out by the Genome Technology Facility (GTF). We obtained 1317 genes differentially expressed comparing mock and flg22 treatments in all genotypes and time points using a standard cut-off (adjusted P-value ≤ 0.05 AND $\log_{2}FC \geq 1$ or $\log_{2}FC \leq -1$). PCA analysis revealed that samples were clustered by time points (Fig.S5A). Within each time point, flg22-treated *CASP1::FLS2* samples diverged from the respective mock treatment, as well as from both treatments on *fls2* (Fig.S5B, 30 min; Fig.S5C, 120 min, Fig.S5D, 480 min). We then compared our dataset to RNAseq data obtained by Fujita *et al.* (2020) (analysis done by Y.Ma). Consistent with our qPCR data, we observed that flg22-induced transcripts patterns were highly similar to the ones obtained after CIF2 treatment (Fig.6). Genes usually activated by the SCHENGEN pathway, such as laccases (Fig.6B), peroxidases (Fig.6D) and suberin-related genes (Fig.6C), were induced after both CIF2 and flg22 treatments. This indicates that both CIF2 and flg22 responses share some common outputs. In contrast, *CASP* genes were only significantly induced (or inhibited for *CASP5*) after CIF2 treatments (Fig.6A), suggesting that unique genes for each pathway can also be found.

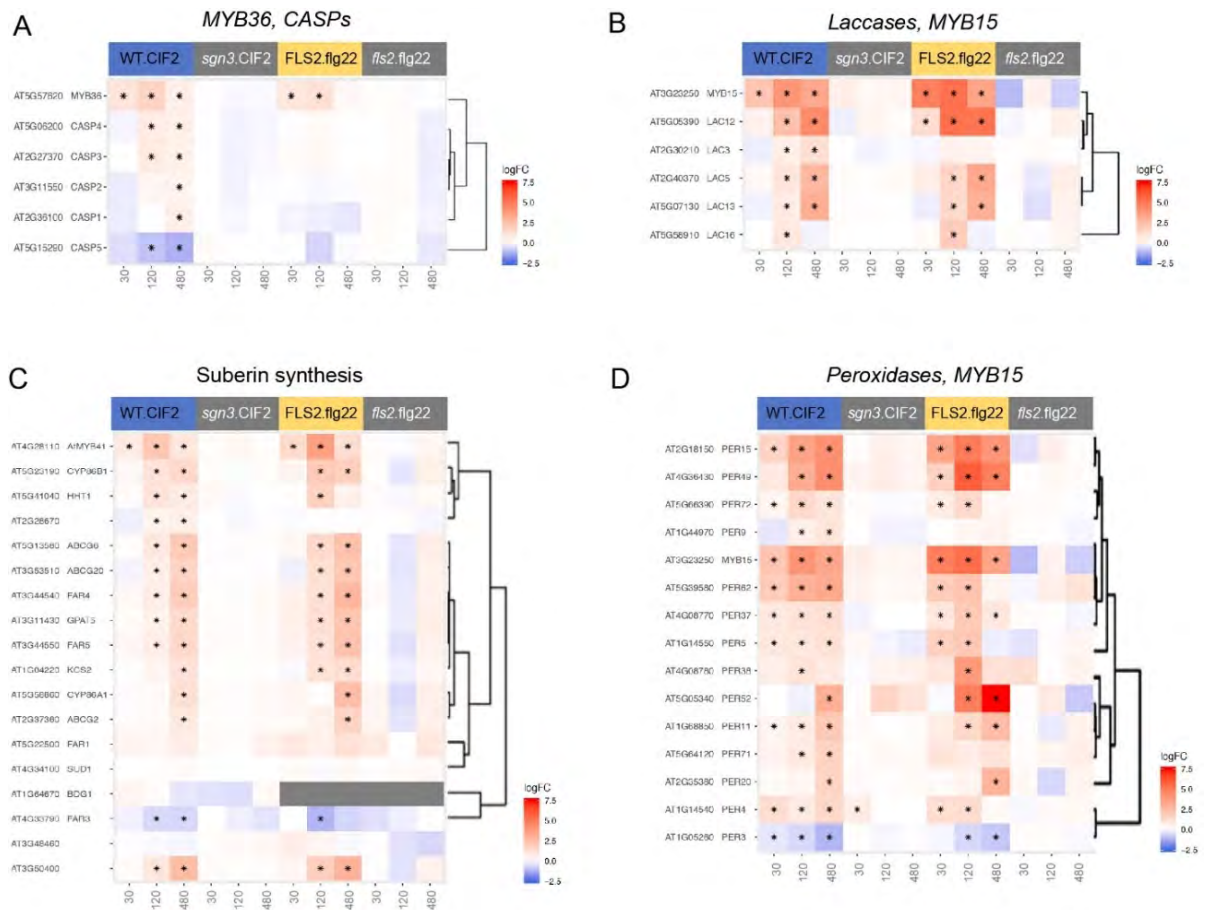


Figure 6: Comparative expression profiles of the “usual suspects” involved in lignification and suberisation of the endodermis in response in CIF2 vs flg22 (heat maps made by Yan Ma).

Comparison of fold changes of selected genes ($P < 0.05$ and $\log_2(\text{fold change}) \geq 1$ or ≤ -1 in at least one time point in one genotype) involved in Casparian strip formation and lignification, such as *CASPs* (A), laccases (B) and peroxidases (D); or in suberisation (C). Fold changes in response to 100 nM CIF2 treatment on WT (blue label) or *sgn3* (grey label) plants are compared to fold changes in response to 1 μM flg22 treatment on *CASP1::FLS2-GFP fls2* (yellow label) or *fls2* (grey label) plants, at indicated time points (30, 120, 480 minutes). Degree of the fold changes is indicated by a colour code. Significant differences are shown by stars.

Though a significant proportion of differentially expressed genes were common to both pathways, many were identified for a particular time point as specific to one or the other treatment. However, a gene categorized as specific to the flg22 pathway in an early time point could become common or specific to CIF2 at a later time point. In addition, common genes were generally transcribed more strongly for flg22 than for CIF2 treatment. This might be due to the stronger concentration used for flg22 (1 μM) compared to CIF2 (100 nM), but also to the stronger expression of *CASP1::FLS2* compared to *SGN3* (Emonet *et al.*, 2020; Pfister *et al.*, 2014). As a general observation, flg22-responses peaked earlier than CIF2-responses and their amplitude was stronger, which made it difficult to identify unique

response markers for each pathway. Therefore, several methods were used to normalize and compare the two datasets, and to minimize bias, which permitted the identification of common or specific gene sets for both pathways (analysis done by Y.Ma).

With this process, Y.Ma identified the top 10% of most differentially expressed genes after CIF2 or flg22 treatments and went back to the original data to compare their logFC in WT or *sgn3* in response to CIF2 (blue and grey label) and in *CASP1::FLS2* and *fls2* in response to flg22 (yellow or light grey label), for individual time points (Fig.7A-D). Here we present the top 20 candidate genes that are preferentially up- or down-regulated after CIF2 treatment (Fig.7A, B) and after flg22 treatment (Fig.7C, D). The uniquely CIF2-induced genes include several WRKY transcription factors (WRKY41, WRKY30, WRKY71) and some peroxidases (PER62, PER71). Interestingly, many *SWEET* genes (*SWEET 1*, *SWEET3*, *SWEET11*, *SWEET12*) were also specifically downregulated after CIF2 treatments. On the other hand, flg22-specific markers encompass many receptors (e.g. cysteine-rich RLK CRK31 or G-type lectin S-receptor-like serine/threonine-protein kinase), some being described as disease resistance proteins (TIR-NBS-LRR and TIR-NBS class). Ethylene-related genes (ERF105) and oxidative enzymes (PER52, PER38, CYP715A1, LAC1) were also induced more strongly after flg22 treatment than after CIF2. This analysis also allowed to pinpoint genes that were upregulated in one treatment and downregulated in the other, providing good candidates for pathway-specific markers. It is interesting to note that different peroxidases and laccases are specifically induced in each pathway, in addition to the other common ones. It would be relevant to test whether they also harbour distinct localisation patterns, which could explain the more restricted lignin deposition induced by CIF2. Taken together, our transcriptomic analysis allowed us to identify not only a strong overlap between CIF2 and flg22 responses, but also many specific response markers for each pathway.

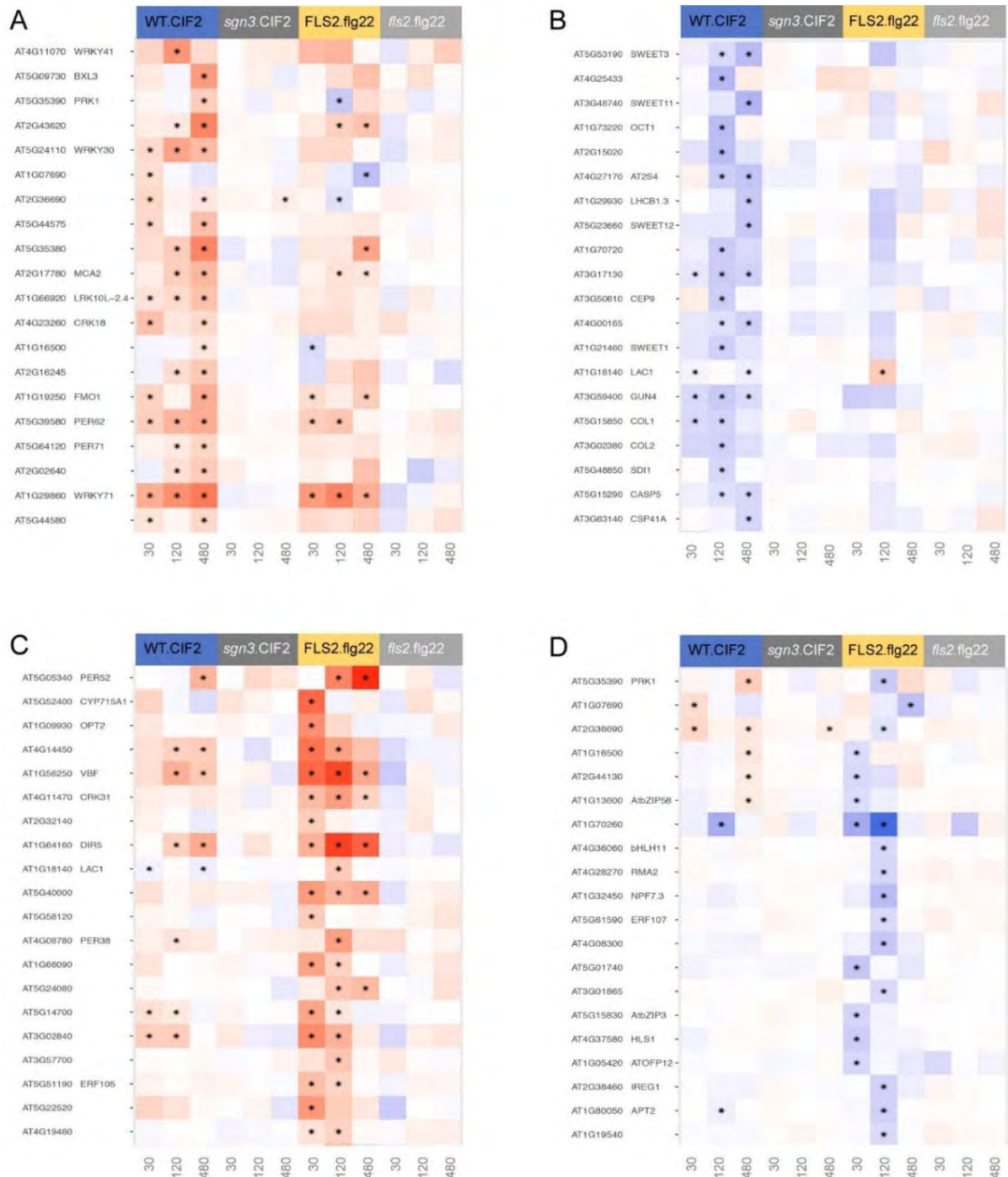


Figure 7: Specific genes induced by CIF2 and flg22 (heat map made by Yan Ma)

(A) Top 20 genes specifically upregulated in response to CIF2 treatment.

(B) Top 20 genes specifically downregulated by CIF2 treatment.

(C) Top 20 genes specifically upregulated by flg22 treatment.

(D) Top 20 genes specifically downregulated by flg22 treatment.

Genes selected among the ones with $P < 0.05$ and $\log_2(\text{fold change}) \geq 1$ or ≤ -1 in at least one time point in one genotype. Fold changes in response to CIF2 treatment on WT (blue label) or *sgn3* (grey label) plants are compared to fold changes in response to flg22 treatment on *CASP1::FLS2-GFP fls2* (yellow label) or *fls2* (light grey label) plants, at indicated time points. Degree of the fold changes is indicated by a colour code. Significant differences are shown by stars.

7.4. DISCUSSION

7.4.1. MTI AND SCHENGEN PATHWAYS TRIGGER A COMMON STRESS-INDUCED SIGNALLING MODULE

Our analysis revealed that the lignin deposition pattern induced by immune responses shares many features with the developmental lignin deployed by the SCHENGEN pathway to seal the Casparian strip. Indeed, CIF2 and flg22, when applied exogenously, induce surprisingly similar lignin deposition at cell corners. In wild-type condition, SCHENGEN-driven lignification is however restricted at the CSD to fuse the patches of the nascent Casparian strip (Doblas *et al.*, 2017). Remarkably, it is only in stressful conditions, for instance in several previously described mutants in which the CS integrity is impaired (Barberon, 2016), that the CIF2-driven lignin localization is most comparable to the flg22-response. This might suggest that the developmental SCHENGEN pathway is more related to stress responses than expected.

Indeed, MTI and SCHENGEN pathways induce lignin deposition with analogous mechanisms. They both trigger ROS production and rely on the redundant use of *RBOHF* and *RBOHD* (this work; Fujita *et al.*, 2020). Although flg22 triggers immune responses predominantly through *RBOHD* (Zhang *et al.*, 2007), it still induced lignification in the *rbohhd* single mutant (Fig.4). This suggests that flg22 signalling uses NADPH oxidases other than *RBOHD* in the endodermis. It would be interesting to test whether flg22-induced lignification also depends on both *RBOHF* and *RBOHD* in other root tissues (e.g. epidermis, stele...), by introducing specific *prom::FLS2* constructs in the *rbohhd* and *rbohfh* single and double mutant backgrounds. Moreover, like the SCHENGEN pathway, flg22 also induces suberin deposition in the endodermis of *CASP1::FLS2* (Ch.2; Emonet *et al.*, 2020). However, suberin deposition is not occurring outside of the endodermis, even in lines expressing *FLS2* in the epidermis or the stele. Taken together, this supports a model where the MTI pathway can branch on the endodermis-specific SCHENGEN signalling, using *RBOHF* and inducing suberin deposition.

The RNAseq profiling of both treatments further supports the similarity of MTI and SCHENGEN pathways. Indeed, most of the very strongly induced genes were common to both treatments and encompass many lignification-related genes, such as laccases,

peroxidases or *MYB15* (Chezem *et al.*, 2017; Fujita *et al.*, 2020; Lee *et al.*, 2013; Rojas-Murcia *et al.*, 2020), and suberisation-related genes like *MYB41* or *GPAT* genes (Barberon, 2016; Barberon *et al.*, 2016; Beisson *et al.*, 2007; Kosma *et al.*, 2014). Moreover, many defence-related genes were also induced by both treatments (*PER5*, *MYB51*, *FRK1*), which could be confirmed by qPCR and MAMP-response fluorescent reporters. This strong similarity suggests that MTI and SCHENGEN pathways might induce a common “defence and stress-related cell wall modification” module.

It is therefore tempting to speculate that developmental processes such as the Casparian strip integrity control have evolved from neofunctionalization of defence and stress-related signalling to induce lignin deposition. Plants start to interact with other microorganisms long before land colonization and the appearance of structural lignin, such as vasculature. Even streptophyte algae host a microbiome encompassing beneficial and potentially pathogenic bacteria (Knack *et al.*, 2015). Interestingly, streptophyte algae were reported to contain lignin-like components that may be used for cell-wall strengthening in response to pathogens (Delwiche *et al.*, 1989; Sørensen *et al.*, 2011; Vries *et al.*, 2018). Genes involved in the phenylpropanoid pathway are also induced in the liverwort *Marchantia polymorpha* in response to oomycete infection (Carella *et al.*, 2019). Therefore, immunity and stress-induced lignification evolved long before the appearance of roots and their Casparian strip. Given the close homology of the SGN3 receptor to the PEPR1 and PEPR2 receptors, the regulation of compensatory lignin deposition by the SCHENGEN pathway might be derived from MTI. Indeed, stimulation of PEPR1 and PEPR2 by their ligand AtPep1 induces strong lignin deposition in the root, particularly in the stele where both receptors are expressed (Engelsdorf *et al.*, 2018). Endogenous DAMPs are often considered as phytochemicals due to their autocrine and paracrine abilities, and can be seen as immunomodulatory hormones rather than elicitors (Gust *et al.*, 2017). CIF2 peptide could potentially originate from such phytochemicals. One could imagine that the evolution might have taken advantage of an ancestral stress-response pathway to tune it as a highly specific integrity-sensing signalling process.

7.4.2. SPECIFIC LOCALISATION OF SCHENGEN AND IMMUNE RESPONSES

Despite their strong similarities, the SCHENGEN pathway and the endodermal-specific MTI signalling displayed some specific outcomes, notably regarding the precise localisation of lignin deposition. Although both pathways induce lignification of the endodermis, *flg22*-triggered lignin extends further than the first endodermal-cortex corner in *CASP1::FLS2*, and could reach the next corner as well as the cortex-endodermal cell wall. H_2O_2 production was also following the same pattern.

Interestingly, several examples show that local deposition of lignin is dependent of the strict localisation of ROS production (Barbosa *et al.*, 2019). Most peroxidases, laccases, SOD and NADPH oxidases so far shown to be involved in CS formation are found within the CSD (Lee *et al.*, 2013; Rojas-Murcia *et al.*, 2020). Endogenous CIF2-induced lignin is also precisely localized at the interplay of SGN3, SGN1 and RBOHF (Alassimone *et al.*, 2016; Doblaz *et al.*, 2017; Fujita *et al.*, 2020). Other developmental lignin depositions involve co-localisation of polymerising enzymes. In protoxylem, LAC4 and LAC17 are targeted to the spiral patterned secondary cell wall of tracheary elements, where they are required for local lignin deposition (Schuetz *et al.*, 2014). Therefore, the difference in lignin patterns that we observed between *flg22* and CIF2 treatment must be due to the distinct localisation of ROS production. Our transcriptomic analysis revealed a number of peroxidases and laccases preferentially induced by CIF2 or *flg22* that could specifically influence ROS production.

However, CIF2 and *flg22* lignification partly relies on RBOHD, localised all around the plasma membrane. This suggests that ROS production site is not determined by the localisation of NADPH oxidases alone, but rather by their local activation by LRR receptors. Indeed, SGN3 is precisely restricted around the CSD (Fujita *et al.*, 2020; Pfister *et al.*, 2014) while *CASP1*-driven FLS2 is localized non-specifically at the plasma membrane (Beck *et al.*, 2014; Emonet *et al.*, 2020; Wyrsh *et al.*, 2015). ROS produced at the CSD will likely diffuse no further than the first endodermal corner, explaining the more contained lignin deposition induced by CIF2. This underlines the importance of the receptor complexes localisation for determining lignin patterns.

Given that SGN3 is closely associated with the CASPs proteins, it can be asked whether FLS2 also requires a scaffold to form a lignin polymerizing complex. Lee *et al.* (2019)

observed that the *amiCASPL1D1* and *caspl1d4* single and double mutants had reduced lignin deposition in response to avirulent pathogens and were consequently more susceptible. Lignin deposition in the abscission zone is also correlated with the induction of *CASPLs* genes, though their involvement is not yet characterized (Lee *et al.*, 2018). Interestingly, five *CASPL* genes (1B1, 1B2, 1C1, 1C2 and 1D2) are induced in response to flg22 and CIF2 in our transcriptomic analyses, generally at the later time point (Fig.S6). No specificity can be clearly inferred from these data, but *CASPL1C1* appears to be preferentially induced by CIF2. Therefore, it could be worth assessing *CASPLs* expression and localisation patterns and compare their responses to CIF2 and flg22 peptides. For example, *CASPL1B1*, driven by the *CASP1* promoter, was shown to localize all around the plasma membrane but accumulated slightly at the CSD (Roppolo *et al.*, 2014). However, expressed under their endogenous promoter, *CASPL1B1* and *CASPL1B2* were correlated with cells producing suberin, though a clear role in suberin deposition could not be demonstrated (Champeyroux *et al.*, 2019). Since both CIF2 and flg22 increase suberisation of the endodermis (Emonet *et al.*, 2020), *CASPLs* upregulation could be also involved in that process. Little is known about *CASPLs* functions, but they are probably involved in cell wall modification related to stress.

7.4.3. SPECIFICITY AT THE HEART OF THE ENDODERMIS

Although both CIF2 and flg22 treatments activate an overlapping “stress module” transcriptional machinery, we also found preferences for specific genes in one or the other pathway. In that sense, even if both receptor complexes activate some of the same downstream targets, such as MAPK3/6 and RBOHF/D (Fujita *et al.*, 2020), they might somehow activate different responses. Although only a few genes displayed opposite behaviours in response to CIF2 or flg22, we found a number of genes that were responsive to both pathways but with a strength of induction/repression that was different between CIF2 and flg22. A possible explanation could be that, despite both peptide-receptor complexes can induce the same actors, their respective affinities for specific downstream components might be slightly different, which would cause quantitatively different responses. Therefore, despite a very strong conservation of downstream components between both the immune and the SCHENGEN pathways, their different roles might be achieved by subtle different outputs.

It would be interesting to use either, specific genes with opposite responses to flg22 and CIF2, or genes with large difference in induction, to design ratio-metric markers for MTI vs SCHENGEN pathways. These markers would enable us to visualise and determine whether an endodermal cell is in “defence mode” or in “developmental mode” and provide a readout of specificity. This work is currently carried out by Y.Ma. We could then easily assess the status of the endodermis and investigate what could influence it. It would be informative to alter common or specific components of one or the other pathway and assess whether they control the status of the cell. For example, MAPK3 and 6 are involved in numerous functions, but how they trigger distinct outputs remains elusive (Andreasson and Ellis, 2010; Suarez Rodriguez *et al.*, 2010). Being able to visualize *in vivo* how targeted mutations of MAPKs can affect the ability of the endodermis to induce CIF2- or flg22-specific responses, would greatly enhance our understanding of specificity control.

Moreover, the SCHENGEN pathway is not only involved in sealing the CS, but also plays a role in the actual formation of the CS. Indeed, CASP1 proteins localized correctly but failed to fuse in the *sgn3* mutant, so that the CS stays in the form of a string-of-pearl (Pfister *et al.*, 2014). Moreover, *CASPs* genes are induced specifically by CIF2 but are not affected by flg22. EM visualisation of the CS after CIF2 treatment also highlights an extension of the CS, which is not observed after flg22 treatment (Fujita *et al.*, 2020). There are therefore several cues indicating that at least part of the SCHENGEN pathway has a developmental outcome that is not found in response to flg22. Whether these responses depend on the CIF2-specific candidate genes identified in our transcriptomic analysis must be investigated.

Interestingly, the induction of “immune lignin” by FLS2 activation could partly rescue the CS delay in *rbohF* mutant, suggesting that the MTI pathway might be able to compensate the role of the SCHENGEN pathway in the CS formation. It is particularly surprising that FLS2, which is even excluded from the CSD (Fig.2B), can produce lignin that is deposited at the CS. It is possible that ROS produced downstream of FLS2 by RBOHD is sufficiently close to the CS to make up for the malfunction of RBOHF. It would be therefore very interesting to induce this flg22-dependent lignin deposition in other CS mutants, such as *casp1* or *esb1*, and see if these genes are required for the partial rescue of CS formation in *rbohF*. The Casparian strip is completely missing in *prx3*, 9, 39, 72, 64 (*prx 5x*) but the

quintuple mutant still displays compensatory lignin, which is dependent on *CIF1* and *CIF2*. (Rojas-Murcia *et al.*, 2020). I would predict that flg22-driven lignification would not be able to rescue the CS in the *cif1 cif2 prx 5x* mutant and that flg22 would only induce compensatory lignin deposition. However, it would be essential to assess whether the other functions of the SCHENGEN pathways can be carried out by flg22-induced lignification, notably by introducing *CASP1::CASP1-GFP* in the *sgn3 CASP1::FLS2 fls2* background and to assay CASP domain integrity.

Taken together, *CIF2* and flg22 responses will prove useful to understand how specificity is achieved inside a single cell using the endodermis as a model system. Moreover, comparison of the two signalling mechanisms may provide new insight on the evolution of developmental pathways in general and on the formation of the Casparian strip in particular.

7.5. MATERIAL AND METHODS

If not specified, plant material, chemicals, methods and statistical analyses were identical to the ones used in Emonet *et al.* (2020) and Chapter 3, Section 3.5.

7.5.1. PLANT MATERIAL

CRISPR mutants *rboh*f, *rboh*d, *rboh*a and *myb15* were generated by CRISPR Cas-9 system in both *fls2* and *CASP1::FLS2-3myc-GFP fls2* backgrounds as described further. *PER15::NLS-3mVenus*, *PER49::NLS-3mVenus* and *MYB15::NLS-3mVenus* were generated in our lab by Tonni G. Andersen (*unpublished*).

7.5.2. GENERATION OF CRISPR LINES

Plasmids for CRISPR-Cas9 mediated mutations were generated using Gateway and Golden-Gate cloning systems. I used a protocol established in our lab for three sgRNA cloning based on a set of Gateway binary vectors for *Agrobacterium*-mediated transformation generated in Prof. Holger Puchta's group (Fauser *et al.*, 2014) and modified for FASTRed selection (Ursache, Fujita *et al.*, *unpublished*). Three 20nt-protospacer sequences for each targeted gene were designed using Benchling and CRISPR-P software (Fig.S1 and Table S1). Protospacers were chosen targeting the first two exons of the gene of interest. In order to obtain deletions that could be visualised by PCR amplification, each sgRNA was separated from the next one by around 100 to 600 base pairs.

The protospacer sequences were obtained by oligo annealing then ligated into the three vectors pRU41, pRU42 and pRU43 previously linearized with the BbsI restriction enzyme. They contain respectively the *Arabidopsis* promoter pU6, pU3 and pU6 upstream of the insertion site for the protospacer sequence. Assembly of the three sgRNAs-containing vectors was obtained by Golden-Gate reaction with the pEntry (L1-BSaI-L2) vector pSF278. The entry vector obtained was then combined by single Gateway LR reaction to the destination vector *pUBQ::CAS9-FR* containing the *spCas9* endonuclease gene from *Streptococcus pyogenes* and a selective marker based on the fluorescence-accumulating seed technology (FAST) expressing the seed-oil body protein OLE1 tagged with the red fluorescent protein RFP (Shimada *et al.*, 2010).

Generated expression vectors were then transformed in *fls2* mutant and *CASP1::FLS2-GFP fls2* line by floral dipping method with *Agrobacterium tumefaciens* GV3101 strains.

7.5.3. gDNA EXTRACTION AND SELECTION OF CRISPR-CAS9 INDUCED MUTANTS

Plants expressing the CRISPR-Cas9 constructs were selected by hand-picking red-fluorescent T1 seeds under a Leica MZ16 stereomicroscope. Leaf samples from 2- or 3-week-old plants were collected and gDNA extracted by cetyltrimethylammonium bromide (CTAB) protocol routinely used in our lab.

T1 plants were first screened for large deletion by PCR amplification of targeted regions (see primers list in Table S1). Samples harbouring deletions were sequenced with the Illumina-Sanger method. Since only a few lines had a deletion, I kept around 20 lines (1 to 27) for genotyping at T2. T2 seeds were then screened against the presence of the CRISPR-Cas9 cassette (pick black seeds) to avoid further mutation. gDNA extraction and PCR amplification were performed before Sanger sequencing on a selection of lines. Eight seedlings were sequenced by line in order to find homozygous mutations.

7.5.4. ELICITOR TREATMENT

CIF2 peptide (DYGHSSPKPKLVPPFKLIPN) were ordered from EZBioLab and synthesized from the Protein & Peptide Chemistry Facility of the University of Lausanne, respectively. For comparison of CIF2 and flg22 responses, five-day-old seedlings were treated for 24 h on ½ MS agar plates containing 1µM of CIF2 or flg22 peptides. If not specified, flg22 treatment was performed as previously described (Emonet *et al.*, 2020).

7.5.5. H₂O₂ PRODUCTION *IN SITU* ANALYSIS USING TRANSMISSION ELECTRON MICROSCOPY

Detection of H₂O₂ production in the endodermis was done by cerium chloride method as described previously (Fujita *et al.*, 2020). Briefly, four-day-old seedlings were grown on ½ MS small petri dishes (5.5 cm diameter), then 1.5 ml of ½ MS solution with or without 1 µM flg22 was gently poured over the seedlings and incubated 24 hours horizontally. After treatment, seedlings were incubated in 50 mM MOPS pH7.2 buffer including 10 mM CeCl₃ for 30 min, then washed twice in MOPS buffer for 5 min and fixed for 1 h in 2.5% glutaraldehyde (EMS, Hatfield, PA) in 100 mM phosphate buffer (pH 7.4) at

room temperature. Post-fixation of seedlings was done in osmium tetroxide 1% (EMS) with 1.5% potassium ferrocyanide (Sigma, St. Louis, MO) in phosphate buffer for 1 h at room temperature. Subsequently, samples were rinsed twice in deionised water, and dehydrated in ethanol solution (Sigma) at gradient concentrations (30% 40 min; 50% 40 min; 70% 40 min; two times (100% 1 h). Infiltration with Spurr resin (EMS) was performed at gradient concentrations [Spurr 33% in ethanol, 4 h; Spurr 66% in ethanol, 4 h; Spurr two times (100% 8 h)]. Finally, the resin was polymerized for 48 h at 60°C in an oven. Ultrathin 50 nm thick sections were cut transversally at 1 ± 0.1 mm from the root tip on a Leica Ultracut (Leica Microsystems GmbH, Vienna, Austria) and placed on a copper slot grid 2×1 mm (EMS) coated with polystyrene film (Sigma). Micrographs were taken with the FEI CM100 (FEI, Eindhoven, The Netherlands) transmission electron microscope at an acceleration voltage of 80 kV and $11,000 \times$ magnification (pixel size of 1.851 nm, panoramic of 17×17 pictures), exposure time of 800 ms, using a TVIPS TemCamF416 digital camera (TVIPS GmbH, Gauting, Germany) and the software EM-MENU 4.0 (TVIPS GmbH, Gauting, Germany). Same beam intensity was used for all pictures, which were panoramic aligned with the software IMOD (Kremer *et al.*, 1996).

7.5.6. SAMPLE PREPARATION FOR RNAseq ANALYSIS

For each sample, two $\frac{1}{2}$ MS agar plates were sown with 100 ml (in total) of *fls2* or *CASP1::FLS2-GFP fls2* seeds, on a sterile mesh. In total, 36 plates by genotypes were prepared, for a total of three replicates (12 plates by replicates and by genotypes). *CASP1::FLS2-GFP fls2* and *fls2* lines (12 plates each) were grown for 5 days, then transferred quickly, always both treatments in parallel, onto fresh medium containing $1 \mu\text{M}$ flg22 or mock. After 30 min, 120 min and 480 min incubations, roots were cut off and quickly collected, then immediately frozen in liquid nitrogen. Three replicates were realized on three different days. RNA was extracted with a TRIzol-adapted ReliaPrep RNA extraction kit (Promega).

7.5.7. RNAseq LIBRARY PREPARATION AND SEQUENCING

Libraries were prepared by the Genome Technology Facility (GTF), following the exact same protocol than Fujita *et al.* (2020). Briefly, RNA quality control was performed on a Fragment Analyzer (Advanced Analytical Technologies, Inc., Ankeny, IA, USA). 1,000 ng of

total RNA was used to prepare RNA-seq libraries with the Illumina TruSeq Stranded mRNA reagents (Illumina; San Diego, California, USA) on a Sciclone liquid handling robot (PerkinElmer; Waltham, Massachusetts, USA) using a PerkinElmer-developed automated script. The resulting library was used for cluster generation with the Illumina TruSeq SR Cluster Kit v4 reagents and sequenced on the Illumina HiSeq 2500 using TruSeq SBS Kit v4 reagents. The Illumina Pipeline Software version 2.20 was used to process sequencing data.

7.5.8. RNAseq DATA PROCESSING AND ANALYSIS

Lausanne Genomic Technologies Facility performed the data processing using their in-house RNA-seq pipeline, as described in Fujita *et al.* (2020). Briefly, purity-filtered read trimming for adapters and low-quality sequences was done with Cutadapt (v. 1.8) (Martin, 2011) and removal of reads matching ribosomal RNA sequences with fastq_screen (v. 0.11.1). Low complexity reads were filtered with reaper (v. 15-065)(Davis *et al.*, 2013). Cleaned reads were aligned against *A.thaliana* TAIR10 genome using STAR (v. 2.5.3a) (Dobin *et al.*, 2013) and read counts per gene locus were obtained with htseqcount (v. 0.9.1) (Anders *et al.*, 2015) using *A. thaliana* TAIR10 Ensembl 39 gene annotation. RSeQC (v. 2.3.7; Wang *et al.*, 2012) was used to evaluate the quality of the data alignment.

Statistical analysis was performed for genes in R (3.5.3). Genes with low counts were filtered out according to the rule of one count per million (cpm) in at least one sample. Library sizes were scaled using TMM normalization and log-transformed into counts per million or CPM (EdgeR package version 3.24.3; Robinson *et al.*, 2010). Data was corrected for the experimental batch effect using removeBatchEffect function (limma).

Statistical quality controls were performed through pairwise sample correlations, clustering and sample PCA using batch corrected normalized data. Differential expression was computed with limma-trend approach (Ritchie *et al.*, 2015) by fitting all samples into one linear model. The experimental batch factor was added to the model. Moderated t-test was used for each pairwise comparisons treated vs untreated per time point. Differential expression of untreated *CASP1::FLS2-GFP fls2* vs *fls2* per time point was assessed by moderated F-test. The adjusted p-value is computed by the Benjamini-Hochberg method, controlling for false discovery rate (FDR or adj.P.Val).

RNAseq results were compared to data from Fujita *et al.* (2020). Interaction tables were generated for each time point of Fujita's RNAseq data using the same statistical model and significance was tested using moderated F-test for each time point independently. Interaction lists were then compared, and, for each time point, genes were considered significant if the adjusted P-value was equal or below 0.05 and the log₂ fold (log₂FC) change was ≥ 1 in any comparison. Genes responsive in control genotypes were excluded. Candidates were compared with their original log₂FC at all time points with all controls. Heatmaps were constructed using ggplot2 package in R.

7.5.9. qPCR

RNA samples from RNAseq analysis were reverse transcribed with PrimeScript RT Master Mix (Takara), following manufacturer's instructions. The MESA BLUE SYBR Green kit (Eurogentech) was used to performed qPCR on an Applied Biosystems QuantStudio3 thermocycler. All transcripts were normalized to Clathrin adaptor complexes medium subunit family protein (AT4G24550) expression. Primers are listed in Table S1.

7.6. LITERATURE

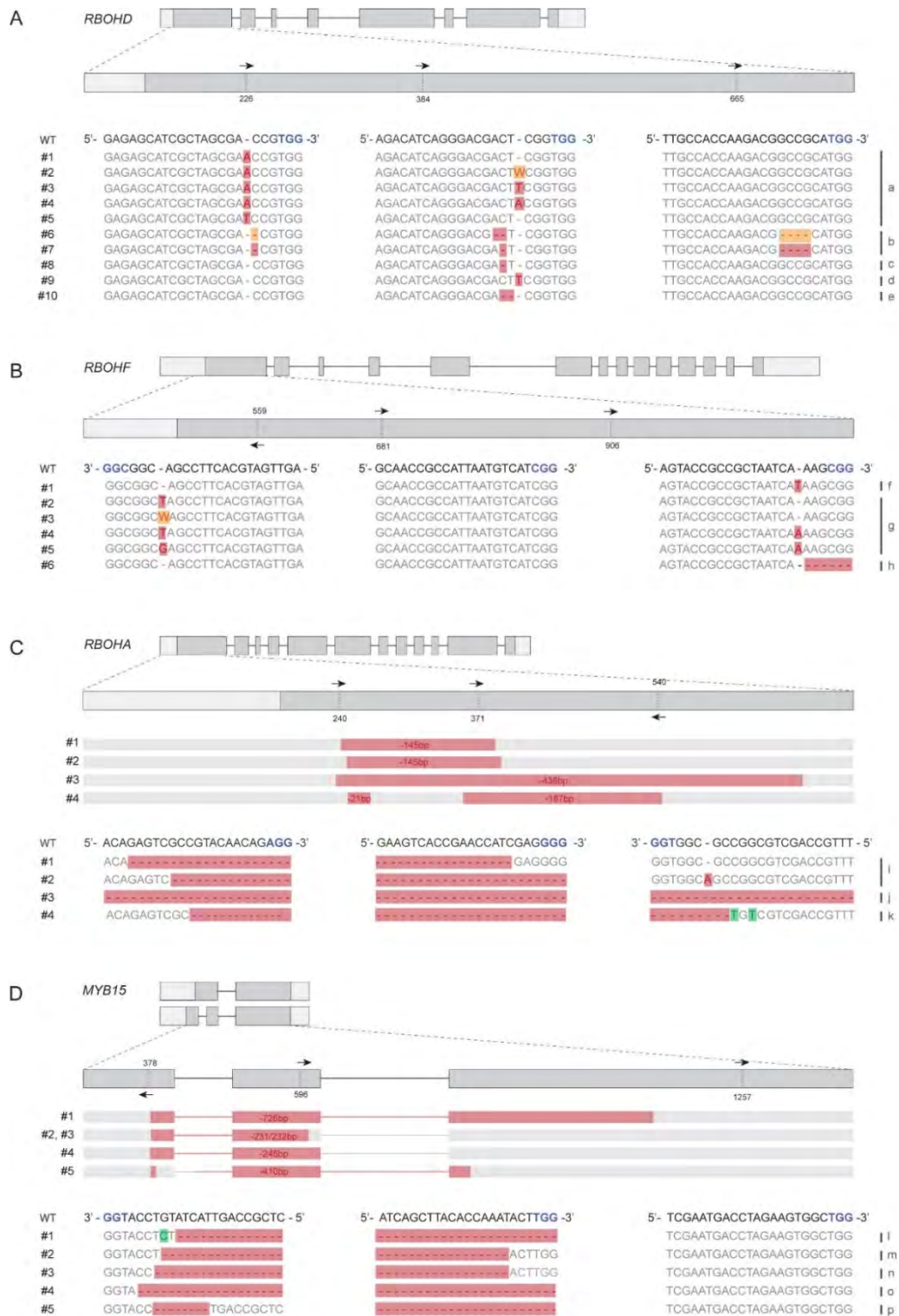
- Alassimone, J., Naseer, S., and Geldner, N. (2010). A developmental framework for endodermal differentiation and polarity. *Proc. Natl. Acad. Sci.* *107*, 5214–5219.
- Alassimone, J., Fujita, S., Doblas, V.G., Dop, M. van, Barberon, M., Kalmbach, L., Vermeer, J.E.M., Rojas-Murcia, N., Santuari, L., Hardtke, C.S., *et al.* (2016). Polarly localized kinase SGN1 is required for Casparian strip integrity and positioning. *Nat. Plants* *2*, 1–10.
- Anders, S., Pyl, P.T., and Huber, W. (2015). HTSeq—a Python framework to work with high-throughput sequencing data. *Bioinformatics* *31*, 166–169.
- Andreasson, E., and Ellis, B. (2010). Convergence and specificity in the *Arabidopsis* MAPK nexus. *Trends Plant Sci.* *15*, 106–113.
- Barberon, M. (2017). The endodermis as a checkpoint for nutrients. *New Phytol.* *213*, 1604–1610.
- Barberon, M., Vermeer, J.E.M., De Bellis, D., Wang, P., Naseer, S., Andersen, T.G., Humbel, B.M., Nawrath, C., Takano, J., Salt, D.E., *et al.* (2016). Adaptation of Root Function by Nutrient-Induced Plasticity of Endodermal Differentiation. *Cell.* *164*, 447 – 459.
- Barbosa, I.C.R., Rojas-Murcia, N., and Geldner, N. (2019). The Casparian strip—one ring to bring cell biology to lignification? *Curr. Opin. Biotechnol.* *56*, 121–129.
- Beck, M., Wyrsh, I., Strutt, J., Wimalasekera, R., Webb, A., Boller, T., and Robatzek, S. (2014). Expression patterns of FLAGELLIN SENSING 2 map to bacterial entry sites in plant shoots and roots. *J. Exp. Bot.* *65*, 6487–6498.
- Beisson, F., Li, Y., Bonaventure, G., Pollard, M., and Ohlrogge, J.B. (2007). The Acyltransferase GPAT5 Is Required for the Synthesis of Suberin in Seed Coat and Root of *Arabidopsis*. *Plant Cell* *19*, 351–368.
- Casparry, R. (1865). Bemerkungen über die Schutzscheide und die Bildung des Stammes und der Wurzel. *Jb Wiss Bot* *4*, 101.
- Champeyroux, C., Bellati, J., Barberon, M., Rofidal, V., Maurel, C., and Santoni, V. (2019). Regulation of a plant aquaporin by a Casparian strip membrane domain protein-like. *Plant Cell Environ.* *42*, 1788–1801.
- Chezem, W.R., Memon, A., Li, F.-S., Weng, J.-K., and Clay, N.K. (2017). SG2-type R2R3-MYB transcription factor MYB15 controls defense-induced lignification and basal immunity in *Arabidopsis*. *The Plant Cell* *29*, 1907–1926.
- Chinchilla, D., Zipfel, C., Robatzek, S., Kemmerling, B., Nürnberger, T., Jones, J.D.G., Felix, G., and Boller, T. (2007). A flagellin-induced complex of the receptor FLS2 and BAK1 initiates plant defence. *Nature* *448*, 497–500.
- Creff, A., Brocard, L., Joubès, J., Taconnat, L., Doll, N.M., Marsollier, A.-C., Pascal, S., Galletti, R., Boeuf, S., and Moussu, S. (2019). A stress-response-related inter-compartmental signalling pathway regulates embryonic cuticle integrity in *Arabidopsis*. *PLoS Genet.* *15*, e1007847.
- Davis, M.P., van Dongen, S., Abreu-Goodger, C., Bartonicek, N., and Enright, A.J. (2013). Kraken: a set of tools for quality control and analysis of high-throughput sequence data. *Methods* *63*, 41–49.
- Delwiche, C.F., Graham, L.E., and Thomson, N. (1989). Lignin-Like Compounds and Sporopollenin Coleochaete, an Algal Model for Land Plant Ancestry. *Science* *245*, 399–401.
- Dobin, A., Davis, C.A., Schlesinger, F., Drenkow, J., Zaleski, C., Jha, S., Batut, P., Chaisson, M., and Gingeras, T.R. (2013). STAR: ultrafast universal RNA-seq aligner. *Bioinformatics* *29*, 15–21.

- Doblas, V.G., Smakowska-Luzan, E., Fujita, S., Alassimone, J., Barberon, M., Madalinski, M., Belkhadir, Y., and Geldner, N. (2017). Root diffusion barrier control by a vasculature-derived peptide binding to the SGN3 receptor. *Science* 355, 280–284.
- Drapek, C., Sparks, E.E., Marhavy, P., Taylor, I., Andersen, T.G., Hennacy, J.H., Geldner, N., and Benfey, P.N. (2018). Minimum requirements for changing and maintaining endodermis cell identity in the *Arabidopsis* root. *Nat. Plants* 4, 586–595.
- Emonet, A., Zhou, F., Vacheron, J., Heiman, C.M., Tendon, V.D., Ma, K.-W., Schulze-Lefert, P., Keel, C., and Geldner, N. (2020). Spatially Restricted Immune Responses Allow for Root Meristematic Activity During Bacterial Colonisation. *BioRxiv* 2020.08.03.233817.
- Engelsdorf, T., Gigli-Bisceglia, N., Veerabagu, M., McKenna, J.F., Vaahtera, L., Augstein, F., Van der Does, D., Zipfel, C., and Hamann, T. (2018). The plant cell wall integrity maintenance and immune signaling systems cooperate to control stress responses in *Arabidopsis thaliana*. *Sci. Signal.* 11, eaao3070.
- Fausser, F., Schiml, S., and Puchta, H. (2014). Both CRISPR/Cas-based nucleases and nickases can be used efficiently for genome engineering in *Arabidopsis thaliana*. *Plant J.* 79, 348–359.
- Fujita, S., De Bellis, D., Edel, K.H., Köster, P., Andersen, T.G., Schmid-Siegert, E., Dénervaud Tendon, V., Pfister, A., Marhavý, P., Ursache, R., *et al.* (2020). SCHENGEN receptor module drives localized ROS production and lignification in plant roots. *EMBO J.* 9, e103894.
- Geldner, N. (2013). The Endodermis. *Annu. Rev. Plant Biol.* 64, 531–558.
- Gust, A.A., Pruitt, R., and Nürnberger, T. (2017). Sensing Danger: Key to Activating Plant Immunity. *Trends Plant Sci.* 22, 779–791.
- Heese, A., Hann, D.R., Gimenez-Ibanez, S., Jones, A.M.E., He, K., Li, J., Schroeder, J.I., Peck, S.C., and Rathjen, J.P. (2007). The receptor-like kinase SERK3/BAK1 is a central regulator of innate immunity in plants. *Proc. Natl. Acad. Sci. U. S. A.* 104, 12217–12222.
- Hosmani, P.S., Kamiya, T., Danku, J., Naseer, S., Geldner, N., Guerinot, M.L., and Salt, D.E. (2013). Dirigent domain-containing protein is part of the machinery required for formation of the lignin-based Casparian strip in the root. *Proc. Natl. Acad. Sci.* 110, 14498–14503.
- Kadota, Y., Sklenar, J., Derbyshire, P., Stransfeld, L., Asai, S., Ntoukakis, V., Jones, J.D., Shirasu, K., Menke, F., Jones, A., *et al.* (2014). Direct Regulation of the NADPH Oxidase RBOHD by the PRR-Associated Kinase BIK1 during Plant Immunity. *Mol. Cell* 54, 43–55.
- Kamiya, T., Borghi, M., Wang, P., Danku, J.M.C., Kalmbach, L., Hosmani, P.S., Naseer, S., Fujiwara, T., Geldner, N., and Salt, D.E. (2015). The MYB36 transcription factor orchestrates Casparian strip formation. *Proc. Natl. Acad. Sci.* 112, 10533–10538.
- Knack, J.J., Wilcox, L.W., Delaux, P.-M., Ané, J.-M., Piotrowski, M.J., Cook, M.E., Graham, J.M., and Graham, L.E. (2015). Microbiomes of Streptophyte Algae and Bryophytes Suggest That a Functional Suite of Microbiota Fostered Plant Colonization of Land. *Int. J. Plant Sci.* 176, 405–420.
- Kosma, D.K., Murmu, J., Razeq, F.M., Santos, P., Bourgault, R., Molina, I., and Rowland, O. (2014). AtMYB41 activates ectopic suberin synthesis and assembly in multiple plant species and cell types. *Plant J.* 80, 216–229.
- Kremer, J.R., Mastrorarde, D.N., and McIntosh, J.R. (1996). Computer visualization of three-dimensional image data using IMOD. *J. Struct. Biol.* 116, 71–76.
- Kurihara, D., Mizuta, Y., Sato, Y., and Higashiyama, T. (2015). ClearSee: a rapid optical clearing reagent for whole-plant fluorescence imaging. *Development* 142, 4168–4179.

- Lee, M.-H., Jeon, H.S., Kim, S.H., Chung, J.H., Roppolo, D., Lee, H.-J., Cho, H.J., Tobimatsu, Y., Ralph, J., and Park, O.K. (2019). Lignin-based barrier restricts pathogens to the infection site and confers resistance in plants. *EMBO J.* *38*, e101948.
- Lee, Y., Rubio, M.C., Alassimone, J., and Geldner, N. (2013). A Mechanism for Localized Lignin Deposition in the Endodermis. *Cell* *153*, 402–412.
- Lee, Y., Yoon, T.H., Lee, J., Jeon, S.Y., Lee, J.H., Lee, M.K., Chen, H., Yun, J., Oh, S.Y., Wen, X., *et al.* (2018). A Lignin Molecular Brace Controls Precision Processing of Cell Walls Critical for Surface Integrity in *Arabidopsis*. *Cell* *173*, 1468–1480.e9.
- Li, L., Li, M., Yu, L., Zhou, Z., Liang, X., Liu, Z., Cai, G., Gao, L., Zhang, X., Wang, Y., *et al.* (2014). The FLS2-Associated Kinase BIK1 Directly Phosphorylates the NADPH Oxidase RbohD to Control Plant Immunity. *Cell Host Microbe* *15*, 329–338.
- Marhavý, P., Kurenda, A., Siddique, S., Dénervaud Tendon, V., Zhou, F., Holbein, J., Hasan, M.S., Grundler, F.M., Farmer, E.E., and Geldner, N. (2019). Single-cell damage elicits regional, nematode-restricting ethylene responses in roots. *EMBO J.* *38*, e100972.
- Martin, M. (2011). Cutadapt removes adapter sequences from high-throughput sequencing reads. *EMBnet J.* *17*, 10–12.
- Millet, Y.A., Danna, C.H., Clay, N.K., Songnuan, W., Simon, M.D., Werck-Reichhart, D., and Ausubel, F.M. (2010). Innate Immune Responses Activated in *Arabidopsis* Roots by Microbe-Associated Molecular Patterns. *Plant Cell* *22*, 973–990.
- Naseer, S., Lee, Y., Lapierre, C., Franke, R., Nawrath, C., and Geldner, N. (2012). Casparian strip diffusion barrier in *Arabidopsis* is made of a lignin polymer without suberin. *Proc. Natl. Acad. Sci.* *109*, 10101–10106.
- Okuda, S., Fujita, S., Moretti, A., Hohmann, U., Doblas, V.G., Ma, Y., Pfister, A., Brandt, B., Geldner, N., and Hothorn, M. (2020). Molecular mechanism for the recognition of sequence-divergent CIF peptides by the plant receptor kinases GSO1/SGN3 and GSO2. *Proc. Natl. Acad. Sci.* *117*, 2693–2703.
- Pfister, A., Barberon, M., Alassimone, J., Kalmbach, L., Lee, Y., Vermeer, J.E., Yamazaki, M., Li, G., Maurel, C., Takano, J., *et al.* (2014). A receptor-like kinase mutant with absent endodermal diffusion barrier displays selective nutrient homeostasis defects. *ELife* *3*, e03115.
- Poncini, L., Wyrsh, I., Tendon, V.D., Vorley, T., Boller, T., Geldner, N., Métraux, J.-P., and Lehmann, S. (2017). In roots of *Arabidopsis thaliana*, the damage-associated molecular pattern AtPep1 is a stronger elicitor of immune signalling than flg22 or the chitin heptamer. *PLOS ONE* *12*, e0185808.
- Ranf, S., Eschen-Lippold, L., Fröhlich, K., Westphal, L., Scheel, D., and Lee, J. (2014). Microbe-associated molecular pattern-induced calcium signaling requires the receptor-like cytoplasmic kinases, PBL1 and BIK1. *BMC Plant Biol.* *14*, 374.
- Robinson, M.D., McCarthy, D.J., and Smyth, G.K. (2010). edgeR: a Bioconductor package for differential expression analysis of digital gene expression data. *Bioinformatics* *26*, 139–140.
- Rojas-Murcia, N. (2019). Elucidating the machinery for lignification of the Casparian strip. University of Lausanne.
- Rojas-Murcia, N., Hematy, K., Lee, Y., Emonet, A., Ursache, R., Fujita, S., Bellis, D.D., and Geldner, N. (2020). High-order mutants reveal an essential requirement for peroxidases but not laccases in Casparian strip lignification. *BioRxiv* 2020.06.17.154617.

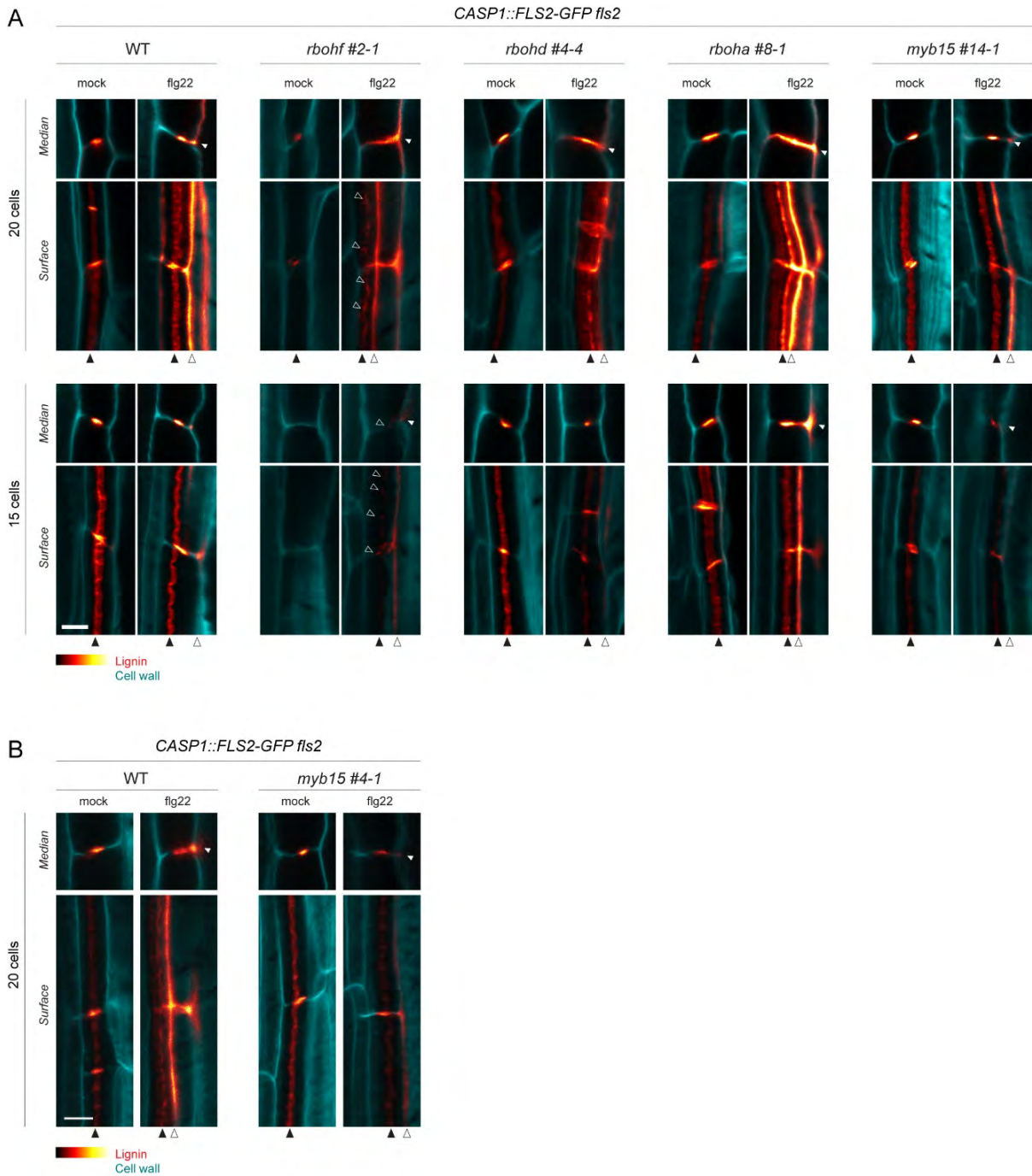
- Roppolo, D., De Rybel, B., Tendon, V.D., Pfister, A., Alassimone, J., Vermeer, J.E.M., Yamazaki, M., Stierhof, Y.-D., Beeckman, T., and Geldner, N. (2011). A novel protein family mediates Casparian strip formation in the endodermis. *Nature* *473*, 380–383.
- Roppolo, D., Boeckmann, B., Pfister, A., Boutet, E., Rubio, M.C., Dénervaud-Tendon, V., Vermeer, J.E.M., Gheyselinck, J., Xenarios, I., and Geldner, N. (2014). Functional and Evolutionary Analysis of the CASPARIAN STRIP MEMBRANE DOMAIN PROTEIN Family. *Plant Physiol.* *165*, 1709–1722.
- Shimada, T.L., Shimada, T., and Hara-Nishimura, I. (2010). A rapid and non-destructive screenable marker, FAST, for identifying transformed seeds of *Arabidopsis thaliana*. *Plant J.* *61*, 519–528.
- Schuetz, M., Benske, A., Smith, R.A., Watanabe, Y., Tobimatsu, Y., Ralph, J., Demura, T., Ellis, B., and Samuels, A.L. (2014). Laccases Direct Lignification in the Discrete Secondary Cell Wall Domains of Protoxylem. *Plant Physiol.* *166*, 798–807.
- Schulze, B., Mentzel, T., Jehle, A.K., Mueller, K., Beeler, S., Boller, T., Felix, G., and Chinchilla, D. (2010). Rapid Heteromerization and Phosphorylation of Ligand-activated Plant Transmembrane Receptors and Their Associated Kinase BAK1. *J. Biol. Chem.* *285*, 9444–9451.
- Sørensen, I., Pettolino, F.A., Bacic, A., Ralph, J., Lu, F., O'Neill, M.A., Fei, Z., Rose, J.K.C., Domozych, D.S., and Willats, W.G.T. (2011). The charophycean green algae provide insights into the early origins of plant cell walls. *Plant J.* *68*, 201–211.
- Suarez Rodriguez, M.C., Petersen, M., and Mundy, J. (2010). Mitogen-Activated Protein Kinase Signaling in Plants. *Annu. Rev. Plant Biol.* *61*, 621–649.
- Ursache, R., Andersen, T.G., Marhavý, P., and Geldner, N. (2018). A protocol for combining fluorescent proteins with histological stains for diverse cell wall components. *Plant J.* *93*, 399–412.
- Vries, S. de, Vries, J. de, Dahlen, J.K. von, Gould, S.B., Archibald, J.M., Rose, L.E., and Slamovits, C.H. (2018). On plant defense signaling networks and early land plant evolution. *Commun. Integr. Biol.* *11*, 1–14.
- Wang, L., Wang, S., and Li, W. (2012). RSeQC: quality control of RNA-seq experiments. *Bioinformatics* *28*, 2184–2185.
- Wyrsh, I., Domínguez-Ferreras, A., Geldner, N., and Boller, T. (2015). Tissue-specific FLAGELLIN-SENSING 2 (FLS2) expression in roots restores immune responses in *Arabidopsis fls2* mutants. *New Phytol.* *206*, 774–784.
- Xu, J., Xie, J., Yan, C., Zou, X., Ren, D., and Zhang, S. (2013). A chemical genetic approach demonstrates that MPK3/MPK6 activation and NADPH oxidase-mediated oxidative burst are two independent signaling events in plant immunity. *Plant J.* *77*, 222–234.
- Zhang, J., Shao, F., Li, Y., Cui, H., Chen, L., Li, H., Zou, Y., Long, C., Lan, L., Chai, J., *et al.* (2007). A *Pseudomonas syringae* Effector Inactivates MAPKs to Suppress PAMP-Induced Immunity in Plants. *Cell Host Microbe* *1*, 175–185.
- Zhou, F., Emonet, A., Dénervaud Tendon, V., Marhavy, P., Wu, D., Lahaye, T., and Geldner, N. (2020). Co-incidence of Damage and Microbial Patterns Controls Localized Immune Responses in Roots. *Cell* *180*, 440-453.e18.

7.7. SUPPLEMENTAL FIGURES AND TABLES



Supplemental Figure 1: CRISPR alleles and mutations

Alleles identified for *rbohD* (A), *rbohF* (B), *rboHA* (C) and *myb15* (D) in *fls2* and *CASP1::FLS2-GFP fls2* background. Gene structures are represented with the three sgRNA sequences (black arrows, numbers represent base pairs after transcriptional start). PAM sites are displayed in blue. See Table S1 for correspondence of allele numbers with mutant lines. Vertical lines with letters correspond to different types of proteins obtained from mutations (see Table S2). All genes are at the same scale. Red, homozygous insertions or deletions; orange, heterozygous insertions or deletions; green; base mismatches.

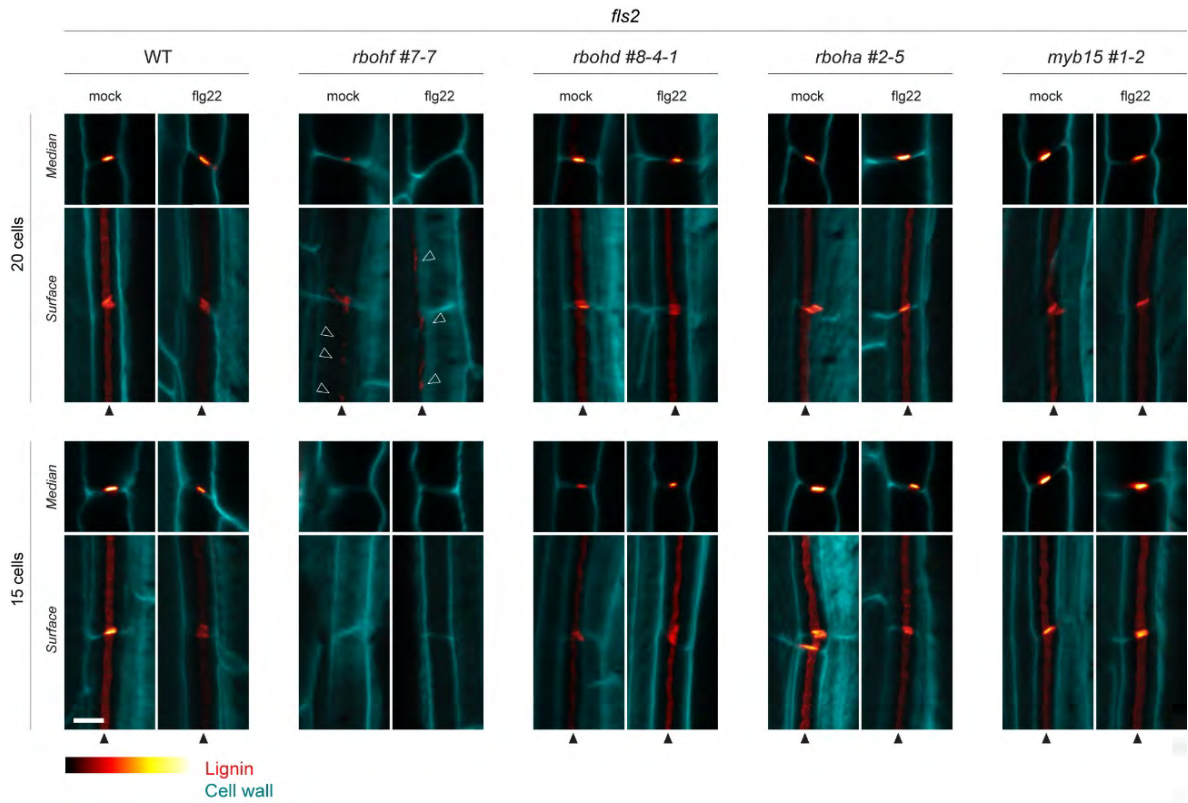


Supplemental Figure 2: Independent alleles for CRISPR *rboh*f, *rboh*d, *rboh*a and *myb15*

(A) Supplementary alleles completing Fig.4. Lignin accumulation in WT, *rboh*d, *rboh*f, *rboh*a and *myb15* single mutants in *CASP1::FLS2-GFP fls2* background, with or without 1 μ M flg22 treatment.

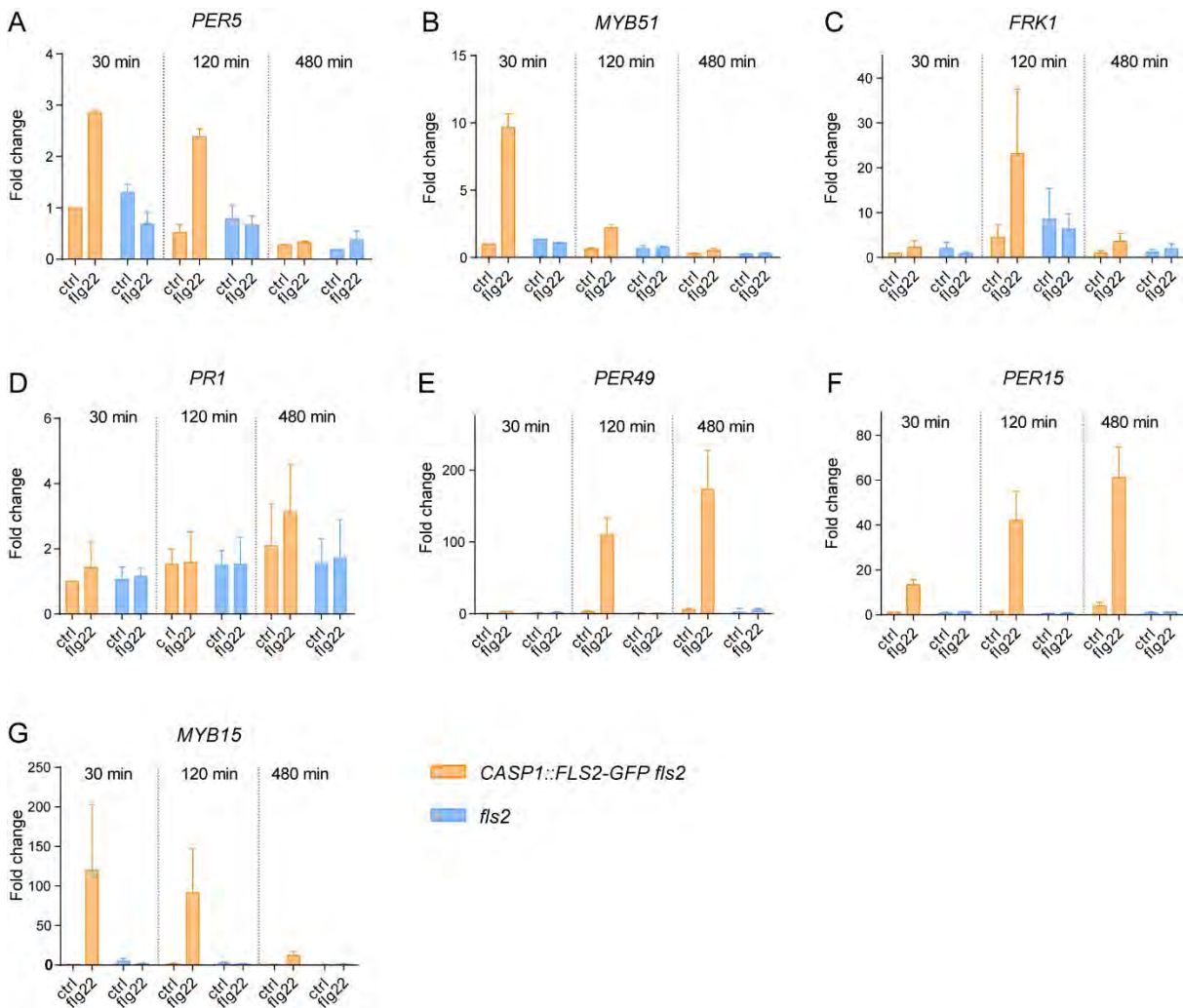
(B) Lignin accumulation in WT and *myb15* single mutants, in *CASP1::FLS2-GFP fls2* background, with or without 1 μ M flg22 treatment. Replicate showing clear reduction in lignin deposition in response to flg22 treatment.

Pictures are shown as surface or median views 15 or 20 cells after the onset of elongation. Lignin and cell walls are stained with Basic Fuchsin (red) and Calcofluor White (cyan), respectively. White arrowheads, corner lignification; black arrowheads, lignin deposition at CS. Scale bar, 5 μ M.



Supplemental Figure 3: Controls in *fls2* background for CRISPR-induced *rbohF*, *rbohD*, *rbohA* and *myb15* mutants

Lignin accumulation in WT, *rbohD*, *rbohF*, *rbohA* and *myb15* single mutants, in *fls2* background as control of Fig.5A, with or without 1 μ M flg22 treatment. Pictures are shown as surface and median views 15 or 20 cells after the onset of elongation. Lignin and cell walls are stained with Basic Fuchsin (red) and Calcofluor White (cyan), respectively. Black arrowheads, lignin deposition at CS. Scale bar, 5 μ M.



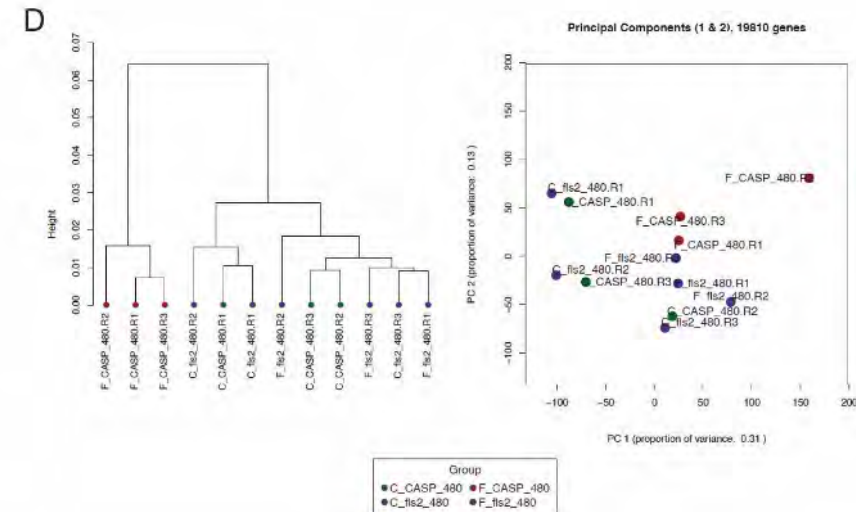
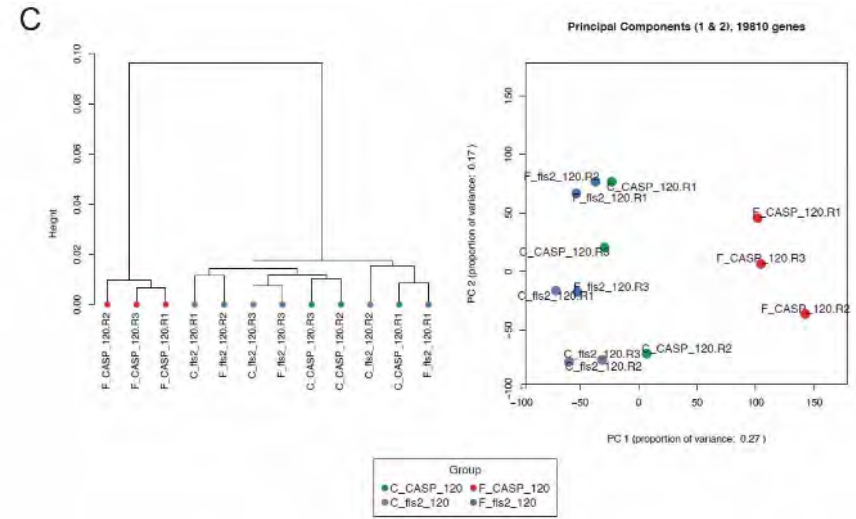
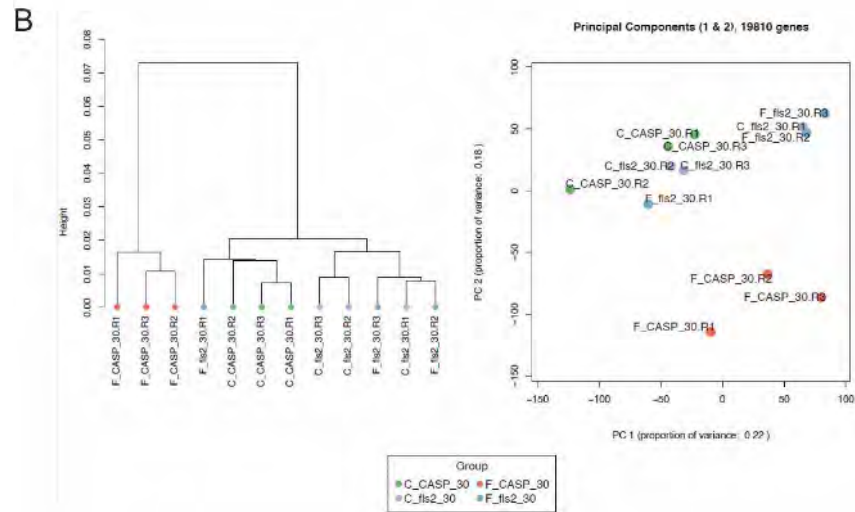
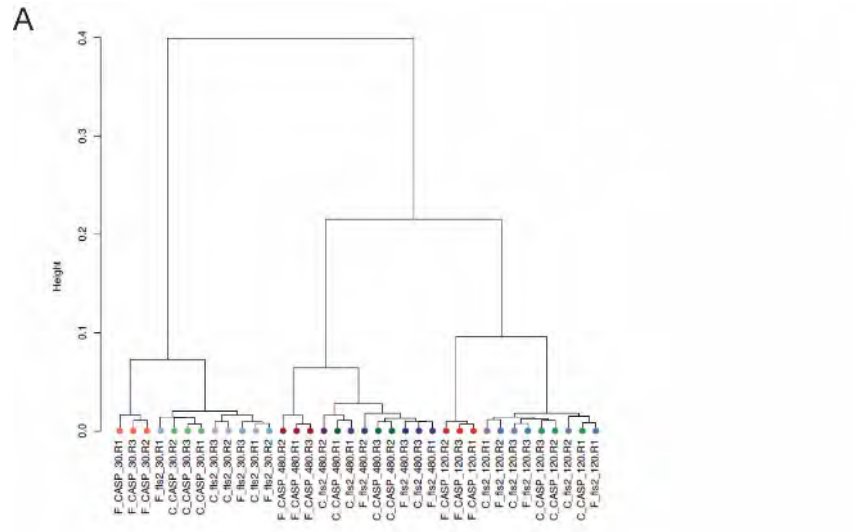
Supplemental Figure 4: Flg22 induces transcription of immune and SCHENGEN markers genes

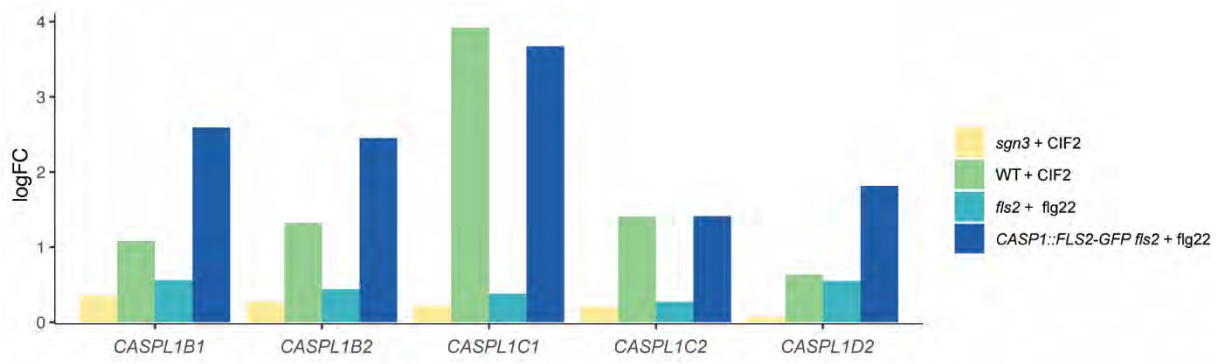
qPCR analyses on samples collected from RNAseq experiments. *CASP1::FLS2-GFP fls2* and *fls2* mutant lines were treated for 30 min, 120 min and 480 min with 1 μ M flg22 or mock as control. Immune markers *PER5* (A), *MYB51* (B) and *FRK1* (C) as well as SCHENGEN markers *PER49* (E), *PER15* (F) and *MYB15*(G) are induced by flg22 treatment. Note that the *PR1* immune marker gene (D) is unaffected.

Supplemental Figure 5 (next page): Transcriptomic data of flg22-treated *CASP1::FLS2-GFP fls2* and *fls2* cluster according to time points and treatments

(A) PCA analysis of all batch corrected RNAseq samples all time points confounded. Analysis includes all genes (19810 genes) with $P < 0.05$ and $\log_2(\text{fold change}) \geq 1$ or ≤ -1 in at least one time point in one genotype. Samples separate by time points then by treatment, flg22-treated *CASP1::FLS2-GFP fls2* clusters away from other samples.

(B-D) PCA analysis of batch-corrected samples taken at the 30min (A), 120min (B) or 480min (C) time points shows a clear separation of flg22-treated *CASP1::FLS2-GFP fls2* from other samples (*fls2* treated with mock or flg22, *CASP1::FLS2-GFP fls2* treated with mock). Figures generated by the Genome Technology Facility (GTF)





Supplemental Figure 6: *CASPL* genes are induced by CIF2 and flg22 treatment

Fold change inductions of *CASPL1B1*, *CASPL1B2*, *CASPL1C1*, *CASPL1C2* and *CASPL1D2* in *sgn3* and wild-type lines in response to CIF2 treatment, in *fls2* and *CASP1::FLS2-GFP fls2* lines in response to flg22 treatment. Data extracted from transcriptomic analyses.

Supplemental Table 1: Primer list

Code	Name	Sequence (5'-3')	Description	F/R
oAE104	oAE104_rbohff_1_F	ATTGAGTACCGCCGCTAATCAAAG	CRISPR <i>rbohff</i> sgRNA_1 fw	F
oAE105	oAE105_rbohff_1_R	AAACCTTTGATTAGCGGCGGTACT	CRISPR <i>rbohff</i> sgRNA_1 rv	R
oAE106	oAE106_rbohff_2_F	GTCAGTTGATGCCTCCGACGG	CRISPR <i>rbohff</i> sgRNA_2 fw	F
oAE107	oAE107_rbohff_2_R	AAACCCGTCGGAAGTGCATCAACT	CRISPR <i>rbohff</i> sgRNA_2 rv	R
oAE108	oAE108_rbohff_3_F	ATTGGCAACCGCCATTAATGTCAT	CRISPR <i>rbohff</i> sgRNA_3 fw	F
oAE109	oAE109_rbohff_3_R	AAACATGACATTAATGGCGGTTGC	CRISPR <i>rbohff</i> sgRNA_3 rv	R
oAE110	oAE110_rbohhd_1_F	ATTGTTGCCACCAAGACGGCCGCA	CRISPR <i>rbohhd</i> sgRNA_1 fw	F
oAE111	oAE111_rbohhd_1_R	AAACTGCGGCCGTCTTGGTGGCAA	CRISPR <i>rbohhd</i> sgRNA_1 rv	R
oAE112	oAE112_rbohhd_2_F	GTCAGACATCAGGACGACTCGG	CRISPR <i>rbohhd</i> sgRNA_2 fw	F
oAE113	oAE113_rbohhd_2_R	AAACCCGAGTCGTCCCTGATGTCT	CRISPR <i>rbohhd</i> sgRNA_2 rv	R
oAE114	oAE114_rbohhd_3_F	ATTGGAGAGCATCGTAGCGACCG	CRISPR <i>rbohhd</i> sgRNA_3 fw	F
oAE115	oAE115_rbohhd_3_R	AAACCGTGCCTAGCGATGCTCTC	CRISPR <i>rbohhd</i> sgRNA_3 rv	R
oAE116	oAE116_rboha_1_F	ATTGGAAGTACCGAACCATCGAG	CRISPR <i>rboha</i> sgRNA_1 fw	F
oAE117	oAE117_rboha_1_R	AAACCTCGATGGTTCGGTGACTTC	CRISPR <i>rboha</i> sgRNA_1 rv	R
oAE118	oAE118_rboha_2_F	GTCACAGAGTCGCGGTACAACAG	CRISPR <i>rboha</i> sgRNA_2 fw	F
oAE119	oAE119_rboha_2_R	AAACCTGTTGTACGGCGACTCTGT	CRISPR <i>rboha</i> sgRNA_2 rv	R
oAE120	oAE120_rboha_3_F	ATTGTTTGCCAGCTGCGGCCGCGG	CRISPR <i>rboha</i> sgRNA_3 fw	F
oAE121	oAE121_rboha_3_R	AAACCCGCGGCCGAGCTGGCAAA	CRISPR <i>rboha</i> sgRNA_3 rv	R
oAE122	oAE122_myb15_1_F	ATTGCTGCCAGTTACTATGTCCA	CRISPR <i>myb15</i> sgRNA_1 fw	F
oAE123	oAE123_myb15_1_R	AAACTGGACATAGTAACTGGCGAG	CRISPR <i>myb15</i> sgRNA_1 rv	R
oAE124	oAE124_myb15_2_F	GTCATCAGCTTACACCAATACT	CRISPR <i>myb15</i> sgRNA_2 fw	F
oAE125	oAE125_myb15_2_R	AAACAGTATTTGGTGTAAGCTGAT	CRISPR <i>myb15</i> sgRNA_2 rv	R
oAE126	oAE126_myb15_3_F	ATTGTCGAATGACCTAGAAGTGGC	CRISPR <i>myb15</i> sgRNA_3 fw	F
oAE127	oAE127_myb15_3_R	AAACGCCACTTCTAGGTCATTCGA	CRISPR <i>myb15</i> sgRNA_3 rv	R
oAE128	oAE128_rbohff_gen_F	AAGCAGAGAGTTTACAGCGCG	Genotyping CRISPR <i>rbohff</i>	F
oAE129	oAE129_rbohff_gen_R	GCATTGAGCGAAATCGGAGCG	Genotyping CRISPR <i>rbohff</i>	R
oAE130	oAE130_rbohhd_gen_F	ACTCGGACACCAACTCGGACAC	Genotyping CRISPR <i>rbohhd</i>	F
oAE131	oAE131_rbohhd_gen_R	ACCTCTTCTCTGTTACTCGCCATC	Genotyping CRISPR <i>rbohhd</i>	R
oAE132	oAE132_rboha_gen_F	ACCAGAGTTGATGATGAATCGAAGTG	Genotyping CRISPR <i>rboha</i>	F
oAE133	oAE133_rboha_gen_R	AGCAGCATATTCATCAGCTTGTCTCC	Genotyping CRISPR <i>rboha</i>	R
oAE134	oAE134_myb15_gen_F	AGAGCTCCATGCTGTGAGAAGATGG	Genotyping CRISPR <i>myb15</i>	F
oAE135	oAE135_myb15_gen_R	ATCGAACCAAGAAGTCCATCTCACTGTC	Genotyping CRISPR <i>myb15</i>	R
oAE150	oAE150_rbohhd_gen2_F	CTGTGGTTTTCTTGCCAAATCTAGTGAG	Genotyping CRISPR <i>rbohhd</i> - for 1st gRNA	F
oYMa13	oYMa13_PER49_qPCR_F	AGTGCGCAAATCAGGAAGAAT	qPCR <i>PER49</i> (AT4G36430)	F
oYMa14	oYMa14_PER49_qPCR_R	CACAACGCAAATAACACGAAATAAA	qPCR <i>PER49</i> (AT4G36430)	R
oYMa15	oYMa15_MYB15_qPCR_F	AGCCCTCCCTAAGCAAGC	qPCR <i>MYB15</i> (AT3G23250)	F
oYMa16	oYMa16_MYB15_qPCR_R	GTTATCGTTCTCCAGGCA	qPCR <i>MYB15</i> (AT3G23250)	R
oYMa17	oYMa17_PER5_qPCR_F	GAGCACACACCATAGGACAA	qPCR <i>PER5</i> (AT1G14550)	F
oYMa18	oYMa18_PER5_qPCR_R	CAGATTACCATCACCTCCCAC	qPCR <i>PER5</i> (AT1G14550)	R
oYMa19	oYMa19_MYB51_qPCR_F	GGTGAAGGTGGATGGCGAA	qPCR <i>MYB51</i> (AT1G18570)	F
oYMa20	oYMa20_MYB51_qPCR_R	TGAAGGGCGTGAAGAGAGATG	qPCR <i>MYB51</i> (AT1G18570)	R
oYMa21	oYMa21_FRK1_qPCR_F	GCCAACGGAGACATTAGAG	qPCR <i>FRK1</i> (AT2G19190)	F
oYMa22	oYMa22_FRK1_qPCR_R	CCATAACGACCTGACTCATC	qPCR <i>FRK1</i> (AT2G19190)	R
oYMa23	oYMa23_PR1_qPCR_F	CTCTGTAGGTGCTCTTGTCTTCC	qPCR <i>PR1</i> (AT2G14610)	F
oYMa24	oYMa24_PR1_qPCR_R	GCAACCTCTCGTCCCCT	qPCR <i>PR1</i> (AT2G14610)	R
oYL558	YL558_PER15_qPCR-1_S	ACAACCAAGGTCTCGATCTCAC	qPCR <i>PER15</i> (AT2G18150)	F
oYL559	YL559_PER15_qPCR-1_AS	CAAGTTAGCAGCGTAGGATTGC	qPCR <i>PER15</i> (AT2G18150)	R
oMB78	oMB78_Clathrin_QPCR_F	AGCATACACTGCGTGCAAAG	qPCR Clathrin (AT4G24550)	F
oMB79	oMB79_Clathrin_QPCR_R	TCGCCTGTGCACATATCTC	qPCR Clathrin (AT4G24550)	R

F, forward primer; R, reverse primer

Supplemental Table 2: Correspondence CRISPR alleles and line numbers

CRISPR Mutant	Background	Line number	Allele number ^a	Chimeric product ^b	Reference code ^c
<i>rboh</i> d	<i>CASP1::FLS2-GFP fls2</i>	#4-2	#2 (biallelic #1 and #3)	a	AE185
<i>rboh</i> d	<i>CASP1::FLS2-GFP fls2</i>	#4-2-3	#4	a	AE186
<i>rboh</i> d	<i>CASP1::FLS2-GFP fls2</i>	#4-2-4	#3	a	AE187
<i>rboh</i> d	<i>CASP1::FLS2-GFP fls2</i>	#4-4	#6 (biallelic #7 and #8)	b/c	AE188
<i>rboh</i> d	<i>CASP1::FLS2-GFP fls2</i>	#4-4-7	#8	c	AE189
<i>rboh</i> d	<i>CASP1::FLS2-GFP fls2</i>	#4-4-x ^d	#7	b	AE190
<i>rboh</i> d	<i>CASP1::FLS2-GFP fls2</i>	#5-6	biallelic #1 and #9	a	AE191
<i>rboh</i> d	<i>CASP1::FLS2-GFP fls2</i>	#5-6-4	#9	d	AE192
<i>rboh</i> d	<i>CASP1::FLS2-GFP fls2</i>	#5-6-x ^d	#1	a	AE193
<i>rboh</i> d	<i>fls2</i>	#8-4-1	#1	a	AE194
<i>rboh</i> d	<i>fls2</i>	#8-6-1	#9	d	AE195
<i>rboh</i> d	<i>fls2</i>	#8-6-5	#5	a	AE196
<i>rboh</i> d	<i>fls2</i>	#8-7-2	#10	e	AE197
<i>rboh</i> f	<i>CASP1::FLS2-GFP fls2</i>	#2-1	#1	f	AE198
<i>rboh</i> f	<i>CASP1::FLS2-GFP fls2</i>	#2-2	#2	g	AE199
<i>rboh</i> f	<i>CASP1::FLS2-GFP fls2</i>	#3-6	#3	g	AE200
<i>rboh</i> f	<i>fls2</i>	#2-3	#2	g	AE201
<i>rboh</i> f	<i>fls2</i>	#3-1	#6	h	AE202
<i>rboh</i> f	<i>fls2</i>	#7-5	#5	g	AE203
<i>rboh</i> f	<i>fls2</i>	#7-7	#4	g	AE204
<i>rbo</i> ha	<i>CASP1::FLS2-GFP fls2</i>	#3-1	#1	i	AE205
<i>rbo</i> ha	<i>CASP1::FLS2-GFP fls2</i>	#8-1	#4	k	AE206
<i>rbo</i> ha	<i>fls2</i>	#2-5	#2	i	AE207
<i>rbo</i> ha	<i>fls2</i>	#7-1	#3	j	AE208
<i>myb</i> 15	<i>CASP1::FLS2-GFP fls2</i>	#4-1	#1	l	AE209
<i>myb</i> 15	<i>CASP1::FLS2-GFP fls2</i>	#4-8	#2	m	AE210
<i>myb</i> 15	<i>CASP1::FLS2-GFP fls2</i>	#14-1	#3	n	AE211
<i>myb</i> 15	<i>fls2</i>	#1-1	#4	o	AE212
<i>myb</i> 15	<i>fls2</i>	#1-2	#5	p	AE213

^a Refers to Fig.S1

^b Chimeric products described in Table S3

^c Seed stock reference number

^d Homozygous line in selection

Lines in grey were analysed in this thesis

Supplemental Table 3: CRISPR mutation effects on proteins RBOHF, RBOHD, RBOHA and MYB15

Gene	Product	Description	Frameshift	Chimeric product
<i>RBOHD</i>	a	early stop codon 255bp after TSS	out of frame	39 amino acids protein product
	b	early stop codon 483bp after TSS	out of frame	80 amino acids protein product
	c	early stop codon 464bp after TSS	out of frame	107 amino acids protein product
	d	early stop codon 414bp after TSS	out of frame	91 amino acids protein product
	e	early stop codon 585bp after TSS	out of frame	148 amino acids protein product
<i>RBOHF</i>	f	early stop codon 1013bp after TSS	out of frame	174 amino acids protein product
	g	early stop codon 590bp after TSS	out of frame	33 amino acids protein product
	h	6bp deletion (starting 923bp after TSS)	in frame	144 th and 145 th QS amino acids replaced by H
<i>RBOHA</i>	i	145bp deletion (starting 242bp after TSS) causes early stop codon 459bp after transcription start	out of frame	43 amino acids chimeric product
	j	438bp deletion (starting 238bp after TSS)	in frame	chimeric protein lacking 146 amino acids has three mutated amino acids (RYY->SCL)
	k	21 bp deletion (starting 250bp after TSS), 187bp deletion (starting at 358bp after TSS), cause early stop codon at position 588 after TSS	in frame then out of frame	chimeric protein of 65 amino acids 2 nd splicing variant loses TSS site
<i>MYB15</i>	l	726bp deletion (384bp after TSS), remove splicing sites, cause early stop codon 1267bp after TSS	in frame	chimeric protein of 86 amino acids 2 nd splicing variant loses TSS site
	m	231bp deletion (388bp after TSS), remove 1st splicing sites, loses sequence 2nd splicing site, causes early stop codon 622bp after TSS	in frame	chimeric protein of 36 amino acids 2 nd splicing variant loses TSS site
	n	232bp deletion (381bp after TSS), remove 1st splicing sites	in frame with end of second exon	chimeric protein lacking 51 amino acids 2 nd splicing variant loses TSS site
	o	245bp deletion (379bp after TSS), remove 1st splicing site, lose 2nd splicing site, cause early stop codon 642bp after TSS	out of frame	chimeric protein of 39 amino acids 2 nd splicing variant loses TSS site
	p	8 bp deletion (381bp after TSS) and 410bp deletion (443bp after TSS), cause early stop codon 405bp after TSS	out of frame	chimeric protein of 38 amino acids 2 nd splicing variant loses TSS site

TSS, Transcription Start Site; bp, base pair.

8 CONCLUDING REMARKS AND PERSPECTIVES

The analysis of MAMP-triggered immunity using cellular resolution methods opened new perspectives for understanding the plant-microbiota interactions and highlighted the crucial importance of spatially targeted defences. This work investigates different aspects of the intricate links between rhizosphere microorganisms and plant immunity: from the fine characterisation of tissue-specific immune responses to the broader impact of FLS2-dependent MTI on the microbiome structure, making a detour via the connection between the immune and developmental facets of lignification. This chapter hopes to provide a broader context to the content of this thesis and emphasizes future perspectives.

8.1. THE LOCAL COMPONENT OF IMMUNITY

As discussed previously, the soil is a very heterogenous environment, in terms of both substrate nature and biodiversity. Roots also have a complex structure, made of different cell-types with distinct functions and features. It is therefore no wonder that immune responses are highly intricate and variable. Immunity has long been studied at a global scale, mostly focusing on the final output of single plant-pathogen interactions. Thus, the local component of immune responses has been overlooked, although it could provide valuable information to understand and reconstruct mechanisms observed at a global scale.

In line with recent publications, we provide evidence that each tissue has a specific immune response characterized by the activation of its own set of transcriptional read-outs. How this specification is regulated is so far unknown. Hormonal control could be involved in the local regulation of responses, since we noticed tissue-specific dependency to ethylene. Moreover, immune signalling might branch out to cell-specific developmental pathways. For instance, suberin lamellae are a well-known feature of the endodermis, and flg22-induced suberisation was only observed in this same tissue. Interestingly, an analysis of tissue-specific transcriptomic responses to flagellin was carried out for the epidermis, the cortex and the periderm, and highlighted the connection between cell identity and tissue-specific immunity networks (Rich-Griffin *et al.*, 2020). Tissue-specific or single-cell transcriptomic approaches could be used to establish cell-type specific immune markers. Understanding which genes are activated in which tissue could decipher whether cell types

have specific roles in immune responses. For example, biosynthesis of the phytoalexins coumarin and camalexin is thought to occur in cortex and phloem, respectively, based on the expression of regulatory or biosynthetic genes and could represent tissue-specific functions (Koprivova *et al.*, 2019; Schmid *et al.*, 2014; Stringlis *et al.*, 2019a). Different cells might after all be partly specialized for defences.

Immune responsiveness is also variable across the root and specific regions have different competency to induce immune responses. This is partly because of their propensity to express PRR receptors, but also due to their intrinsic properties. We indeed report that the central meristem was refractory to the induction of flg22-responses, calling the dogma of strict cell autonomy of immune responses into question. It is tempting to speculate that this feature might be specific to meristematic tissues, which may favour growth over defence. Similarly, we could suggest that super-competent tissues might surround and protect refractory cell-types. It would be particularly interesting to assess tissue competencies in other organs, like apical meristems. Leaves also display variation in the expression pattern of *FLS2* (Beck *et al.*, 2014). Since we showed that defence competency is not always correlated with receptor expression, it would be informative to look for other non- or weak-responsive zones. Moreover, little is known about MTI responses in flowers and seed pods. Recently, Lee *et al.* (2018) observed that cutin protects the abscission zone of flower against pathogens. One could imagine that expression of defences might be particularly well regulated in a context where new organs are developing while surface integrity is disturbed. Coming back to the root, we also do not know if the defence compartmentation observed in *A. thaliana* is conserved across developmental stages or across species. Since microorganisms interact with plants even before the colonization of land, it would be worth assessing defence expression patterns in more archaic species, from the *Bryophyta* division for example. Indeed, it is unknown whether the propensity to restrict immune responses is conserved in primitive root structures.

The absence of response in root meristem expressing *FLS2* is compelling in the sense that it was not caused by the absence of Pattern Recognition Receptors, but rather by a potential inhibition of MTI responses. However, we do not understand how the meristem avoids immune responses. Downstream components of MTI signalling are usually

ubiquitously expressed, but it would be worth confirming that all of them are actually found in the meristem. Meristem-specific transcriptome profiling could help deciphering whether part of the pathway is still induced or whether the inhibition is total. Moreover, the suppression of MTI responses might occur at a very early step, since we observed that meristematic pericycle cells, refractory to FLS2, can still induce weak responses when stimulated by non-cell autonomous signalling. Several inhibitors such as BIR1/2, ANX1/2 or RALF23 are known to regulate the FLS2/BAK1 complex formation and could be strongly activated in the meristem. Reversely, stabilization of the complex could be impaired if stimulating components such as FER, IOS1 or LRG1 were inactivated or missing (see Chapter 1). It would be interesting to assess their expression level in the meristem and to generate tissue-specific KO mutants by CRISPR (Decaestecker *et al.*, 2019). Recycling of FLS2 was also shown to be crucial to sustain a strong immune response and might be impaired in the meristem (Mersmann *et al.*, 2010; Robatzek *et al.*, 2006). Finally, immune responses in the root tip might be inhibited by antagonistic auxin and brassinosteroid signalings, which are important for meristem development (Naseem *et al.*, 2015; Wang, 2012). BRZ1 was indeed shown to suppress FLS2 signalling, and is activated in the central zone of the meristem (Jaillais and Vert, 2016).

Cellular resolution coupled to tissue-specific expression of PRRs also allowed us to distinguish purely local responses, such as *PER5*, *FRK1* activation or lignin and suberin deposition, from non-cell autonomous responses at small scale (*MYB51*) or on longer distance (calcium signalling) (Emonet *et al.*, 2020; Zhou *et al.*, 2020). This opens new possibilities to investigate the mechanisms of signal propagation. We could now assess whether calcium and ROS signals are responsible of the regional induction of *MYB51*, using inhibitors and mutants. For example, to test the implication of *RBOHD* in non-cell autonomous signalling, we could complement the *rbohD* mutant with cell-type-specific *RBOHD*, e.g. *PRP3::RBOHD*. By inducing flg22 responses only in these cells expressing *RBOHD*, using *PRP3::FLS2* background for example, we could monitor whether the induction of *MYB51* is still occurring in neighbouring tissues. Calcium/ROS waves are thought to propagate through plasmodesmata (Choi *et al.*, 2016). We could now test their implication using callose-mediated plasmodesmata closure with the inducible *icals3m* vector system (Sevilem *et al.*, 2013).

Increased resolution for immune responses will reveal its full potential only if combined with the development of precise microbial tracking strategies. Indeed, we observed that current genomic methods are not suitable to detect local changes in the microbiome. Very little is known about what governs the spatial organisation of the microbiota along the root. Indeed, only a couple of infection strategies of some specific pathogens and random examples of commensal colonization sites have been described so far (see Chapter 1). Improving techniques to follow bacterial colonization promises to help understanding what type of bacteria colonizes which part of the root, or how dynamic is the structure of the community in space and time. These methods would also permit to dissect the bidirectional interactions between plant and bacteria. Preliminary experiments indeed showed that endodermal damage attracts strongly *Pseudomonas protegens* CHA0 bacteria, probably because of nutrient leakage (Feng Zhou, *personal communication*). However, whether these colonizers stay at the wounded locus even in presence of a strong immune response is not known. Similarly, it would be interesting to test if bacteria are also attracted around passage cells, which were reported to channel nutrient fluxes towards the stele (Andersen *et al.*, 2018). Some of these questions will be soon investigated in our group, where we plan to characterize microbiota root colonization using labelled bacteria combined to gnotobiotic systems, assessing interactions with single bacteria or small synthetic bacterial communities to visualize what is actually happening at the root surface.

8.2. REGULATION OF MTI RESPONSES IN THE ROOT IS HIGHLY DYNAMIC

The induction of immune responses is tissue-dependent, but is also highly dynamic and can be modulated by both plants and their microbiota. We indeed showed that immune responses are usually restricted to the elongation zone but can be gated in the differentiated zone by damages or the development of lateral roots. This allows the plant to reduce considerably the unwanted activation of defence in response to harmless bacteria. However, the link between damage and *FLS2* expression is still unexplained. Since DAMPs alone could not reproduce laser ablation, we suggested the involvement of a mechanical signal. Moreover, cortex cell surrounding the primordia have increased sensitivity to flg22 (Zhou *et al.*, 2020). This may not depend on cell damage since lateral root emergence usually

causes only mechanical constraints (Vilches-Barro and Maizel, 2015). It would be interesting to test whether *FLS2* induction can be dependent on the cell wall integrity system pathway (Rui and Dinneny, 2020). Plant mechano-sensors such as the Ca²⁺-permeable stretch-sensitive channel MCA1 involved in touch-sensing and cell wall damage responses could be implicated (Denness *et al.*, 2011; Nakagawa *et al.*, 2007).

This work also highlighted that MTI responses can be largely affected by bacteria. We observed that many rhizosphere commensals evade flg22 detection, while some others induce immune transcriptional read-outs but prevent root growth inhibition. Whether this absence of response is due to direct MAMP signalling suppression, modification of environmental pH, LPS or biofilm formation needs to be further investigated. Nevertheless, the use of super-competent plants as the *WER::FLS2* line will be advantageous to isolate responses induced by native bacterial MAMPs. As previously discussed, these lines could be used to reconstitute bacterial MAMP repertoires and validate sequence-based predictions of MAMP detectability. The group of Prof. Jeffery Dangl is now using *WER::FLS2* high sensitivity to screen flg22 variants for RGI induction. Interestingly, most bacterial epitopes recognized as MAMPs are either intracellular or buried inside proteins (Albert *et al.*, 2020; Buscaill *et al.*, 2019). Super-competent lines might be useful to investigate how and when MAMPs are released, a process so far elusive. Finally, the strong root growth inhibition induced by flg22 on *WER::FLS2* makes this line a very powerful tool to easily screen numerous bacterial strains. This feature was used by the group of Prof. Paul Schulze-Lefert to select bacteria that suppress flg22-induced root growth inhibition (Ma *et al.*, 2020).

Manipulation of MTI by bacteria must also be considered in the broader context of the microbial community. Indeed, we observed that even highly sensitive plants as *WER::FLS2* line develop as wild-type when grown with complex bacterial communities (non-sterile natural soil or SynCom), suggesting the microbiota suppresses immune responses. We previously discussed how individual bacteria could inhibit MTI responses. However, in a microbial assemblage, bacteria not only combine their individual effects, but they also potentiate or counteract the contribution of other species. For example, it was recently shown that the *Variovorax* genus degrades auxin produced by other members of the rhizosphere community and suppresses the root growth inhibition associated with their

colonization (Finkel *et al.*, 2020). Similarly, bacteria suppressive of flg22-mediated root growth inhibition have a dominant effect on non-suppressive bacteria (Ma *et al.*, 2020). Bacteria were also shown to compete or inhibit other bacterial strains, or fungi and oomycetes (Durán *et al.*, 2018; Helfrich *et al.*, 2018; Teixeira *et al.*, 2019). This will affect the constitution of the microbiome community and the final plant growth. Although we did not observe significant changes in the composition of the *WER::FLS2* rhizosphere, it would be interesting to investigate smaller communities, or even tripartite interactions. These reductionist approaches might ease the analysis of bacterial responses to localized defences.

8.3. MAMP-TRIGGERED IMMUNE RESPONSES INFLUENCE PLANT DEVELOPMENT

Immunity is traditionally associated to plant development by the concept of the growth-defence trade-off. This was illustrated in this work by the ability of *WER::FLS2* line to tip the balance in favour of defence, leading to meristem collapse. However, the molecular mechanisms behind this process was not elucidated.

Meristem collapse, including cell swelling and lignin deposition, was surprisingly reminiscent of the morphological changes observed upon activation of the cell wall integrity (CWI) system. Indeed, inhibition of cellulase by isoxaben (ISX) treatment or knock-out mutant of *CESA* (*CELLULOSE SYNTHASE A*) genes induced a similar phenotype (Cano-Delgado *et al.*, 2000; Caño-Delgado *et al.*, 2003; Ellis *et al.*, 2002; Hématy *et al.*, 2007). However, Engelsdorf and colleagues (2018) suggest that pattern-triggered immunity pathway and CWI signalling act independently to induce stress responses, even if CWI signalling can compensate the loss of AtPep-triggered responses. The altered development induced by flg22 in *WER::FLS2* might therefore be a general stress response. Similarity can be found in PTI and CWI pathways. Thus, cell swelling is, in both cases, not caused by lignification. Indeed, treatment with ISX and the lignin synthesis inhibitor AIP triggers cell swelling without lignin deposition (Caño-Delgado *et al.*, 2003; Ellis *et al.*, 2002). It might be interesting to finely compare MTI and CWI effects to assess whether flg22-driven

lignification and meristem collapse are independent of the activation of the CWI system. It should be noted that cell swelling was particularly evident in the elongation zone. It is therefore tempting to speculate that sustained cell growth is required for the swelling phenotype. Indeed, other tissue-specific *prom::FLS2* lines, even if they induce strong immune responses and lignin deposition, do not alter cell morphology. Ethylene was previously shown to inhibit root cell elongation by up-regulation of auxin synthesis (Swarup *et al.*, 2007). It would be worth investigating whether ethylene, potentially produced by the induction of MTI, could explain the cell swelling and meristem collapse observed in *WER::FLS2*.

This work also highlighted that MTI responses can drastically affect the cell wall composition. We provided strong evidence that *flg22* induces lignin deposition in roots, when *FLS2* receptor is ectopically overexpressed. In addition, we also observed that endodermal-specific immune responses trigger suberin deposition (Emonet *et al.*, 2020). As previously discussed, the induction of cell wall modification in the endodermis was particularly similar to the compensatory lignin induced by the SCHENGEN pathway, which prompted us to do a comparative analysis of *flg22*- and *CIF2*-induced responses. Such project is currently carried out in our lab by Yan Ma. One of the most interesting questions is whether the induction of MTI responses could replace the SCHENGEN pathway and complement the *sgn3* mutation. Yan Ma is now expressing *FLS2* under the *SGN3* promoter, in the *sgn3 fls2* background. To properly mimic the SCHENGEN pathway, it would be ideal to express the *flg22* peptide from the inside of the central cylinder, using a stele-specific inducible promoter. *Flg22* was in the past successfully expressed in plant cells, indicating the feasibility of the process (Wyrsh, 2015). This would be a fantastic way to demonstrate that very specific responses induced by developmental problems could have easily evolved from general stress signalling through tinkering the precise positioning of its different components.

8.4. FINAL REMARK

MAMP-triggered immunity is the core of defence responses against plant threats and proved to be a successful strategy for plants to thrive. However, the more we study its components and signalling cascades, the more we realize the complexity and interplays of these pathways. Roots, readily accessible and simple to image, are an advantageous model to investigate the local facet of MTI. The various approaches used in this thesis illustrate how high-resolution immune markers, tissue-dependent expression of PRRs, single-cell laser ablation and inoculation with fluorescently labelled bacteria can improve our understanding of microbiome-induced immune responses. Cell-type specific analyses promise to shed light on the hidden world of the rhizosphere.

8.5. LITERATURE

- Albert, I., Hua, C., Nürnberger, T., Pruitt, R.N., and Zhang, L. (2020). Surface Sensor Systems in Plant Immunity. *Plant Physiol.* *182*, 1582–1596.
- Andersen, T.G., Naseer, S., Ursache, R., Wybouw, B., Smet, W., De Rybel, B., Vermeer, J.E.M., and Geldner, N. (2018). Diffusible repression of cytokinin signalling produces endodermal symmetry and passage cells. *Nature* *555*, 529–533.
- Beck, M., Wyrsh, I., Strutt, J., Wimalasekera, R., Webb, A., Boller, T., and Robatzek, S. (2014). Expression patterns of FLAGELLIN SENSING 2 map to bacterial entry sites in plant shoots and roots. *J. Exp. Bot.* *65*, 6487–6498.
- Buscaill, P., Chandrasekar, B., Sanguankiattichai, N., Kourelis, J., Kaschani, F., Thomas, E.L., Morimoto, K., Kaiser, M., Preston, G.M., and Ichinose, Y. (2019). Glycosidase and glycan polymorphism control hydrolytic release of immunogenic flagellin peptides. *PLANT Sci.* *364*, eaav0748.
- Caño-Delgado, A., Penfield, S., Smith, C., Catley, M., and Bevan, M. (2003). Reduced cellulose synthesis invokes lignification and defense responses in *Arabidopsis thaliana*. *Plant J.* *34*, 351–362.
- Cano-Delgado, A.I., Metzloff, K., and Bevan, M.W. (2000). The eli1 mutation reveals a link between cell expansion and secondary cell wall formation in *Arabidopsis thaliana*. *Development* *127*, 3395–3405.
- Choi, W.-G., Hilleary, R., Swanson, S.J., Kim, S.-H., and Gilroy, S. (2016). Rapid, Long-Distance Electrical and Calcium Signaling in Plants. *Annu. Rev. Plant Biol.* *67*, 287–307.
- Decaestecker, W., Buono, R.A., Pfeiffer, M.L., Vangheluwe, N., Jourquin, J., Karimi, M., Isterdael, G.V., Beeckman, T., Nowack, M.K., and Jacobs, T.B. (2019). CRISPR-TSKO: A Technique for Efficient Mutagenesis in Specific Cell Types, Tissues, or Organs in *Arabidopsis*. *Plant Cell* *31*, 2868–2887.
- Denness, L., McKenna, J.F., Segonzac, C., Wormit, A., Madhou, P., Bennett, M., Mansfield, J., Zipfel, C., and Hamann, T. (2011). Cell Wall Damage-Induced Lignin Biosynthesis Is Regulated by a Reactive Oxygen Species- and Jasmonic Acid-Dependent Process in *Arabidopsis*. *Plant Physiol.* *156*, 1364–1374.
- Durán, P., Thiergart, T., Garrido-Oter, R., Agler, M., Kemen, E., Schulze-Lefert, P., and Hacquard, S. (2018). Microbial Interkingdom Interactions in Roots Promote *Arabidopsis* Survival. *Cell* *175*, 973-983.e14.
- Ellis, C., Karafyllidis, I., Wasternack, C., and Turner, J.G. (2002). The *Arabidopsis* Mutant *cev1* Links Cell Wall Signaling to Jasmonate and Ethylene Responses. *Plant Cell* *14*, 1557–1566.
- Emonet, A., Zhou, F., Vacheron, J., Heiman, C.M., Tendon, V.D., Ma, K.-W., Schulze-Lefert, P., Keel, C., and Geldner, N. (2020). Spatially Restricted Immune Responses Allow for Root Meristematic Activity During Bacterial Colonisation. *BioRxiv* 2020.08.03.233817.
- Engelsdorf, T., Gigli-Bisceglia, N., Veerabagu, M., McKenna, J.F., Vaahtera, L., Augstein, F., Van der Does, D., Zipfel, C., and Hamann, T. (2018). The plant cell wall integrity maintenance and immune signaling systems cooperate to control stress responses in *Arabidopsis thaliana*. *Sci. Signal.* *11*, eaao3070.
- Finkel, O.M., Salas-González, I., Castrillo, G., Conway, J.M., Law, T.F., Teixeira, P.J.P.L., Wilson, E.D., Fitzpatrick, C.R., Jones, C.D., and Dangl, J.L. (2020). A single bacterial genus maintains root development in a complex microbiome. *BioRxiv* 645655.
- Helfrich, E.J.N., Vogel, C.M., Ueoka, R., Schäfer, M., Ryffel, F., Müller, D.B., Probst, S., Kreuzer, M., Piel, J., and Vorholt, J.A. (2018). Bipartite interactions, antibiotic production and biosynthetic potential of the *Arabidopsis* leaf microbiome. *Nat. Microbiol.* *3*, 909–919.

- Hématy, K., Sado, P.-E., Van Tuinen, A., Rochange, S., Desnos, T., Balzergue, S., Pelletier, S., Renou, J.-P., and Höfte, H. (2007). A Receptor-like Kinase Mediates the Response of *Arabidopsis* Cells to the Inhibition of Cellulose Synthesis. *Curr. Biol.* *17*, 922–931.
- Jaillais, Y., and Vert, G. (2016). Brassinosteroid signaling and BRI1 dynamics went underground. *Curr. Opin. Plant Biol.* *33*, 92–100.
- Koprivova, A., Schuck, S., Jacoby, R.P., Klinkhammer, I., Welter, B., Leson, L., Martyn, A., Nauen, J., Grabenhorst, N., Mandelkow, J.F., et al. (2019). Root-specific camalexin biosynthesis controls the plant growth-promoting effects of multiple bacterial strains. *Proc. Natl. Acad. Sci.* *116*, 15735–15744.
- Lee, Y., Yoon, T.H., Lee, J., Jeon, S.Y., Lee, J.H., Lee, M.K., Chen, H., Yun, J., Oh, S.Y., Wen, X., et al. (2018). A Lignin Molecular Brace Controls Precision Processing of Cell Walls Critical for Surface Integrity in *Arabidopsis*. *Cell* *173*, 1468–1480.e9.
- Ma K., Niu Y., Jia Y., Ordon J., Copeland C., Emonet A., Geldner N., Guan R., Stolze S. C., Nakagami H., Garrido Oter R., Schulze-Lefert P. (10 September 2020). Coordination of microbe-host homeostasis via a crosstalk with plant innate immunity. PREPRINT (Version 1) available at Research Square. DOI:10.21203/rs.3.rs-69445/v1
- Mersmann, S., Bourdais, G., Rietz, S., and Robatzek, S. (2010). Ethylene Signaling Regulates Accumulation of the FLS2 Receptor and Is Required for the Oxidative Burst Contributing to Plant Immunity. *Plant Physiol.* *154*, 391–400.
- Nakagawa, Y., Katagiri, T., Shinozaki, K., Qi, Z., Tatsumi, H., Furuichi, T., Kishigami, A., Sokabe, M., Kojima, I., Sato, S., et al. (2007). *Arabidopsis* plasma membrane protein crucial for Ca²⁺ influx and touch sensing in roots. *Proc. Natl. Acad. Sci.* *104*, 3639–3644.
- Naseem, M., Kaldorf, M., and Dandekar, T. (2015). The nexus between growth and defence signalling: auxin and cytokinin modulate plant immune response pathways. *J. Exp. Bot.* *66*, 4885–4896.
- Rich-Griffin, C., Eichmann, R., Reitz, M.U., Hermann, S., Woolley-Allen, K., Brown, P.E., Wiwatdirekkul, K., Esteban, E., Pasha, A., Kogel, K.-H., et al. (2020). Regulation of Cell Type-Specific Immunity Networks in *Arabidopsis* Roots. *Plant Cell*. tpc.00154.2020.
- Robatzek, S., Chinchilla, D., and Boller, T. (2006). Ligand-induced endocytosis of the pattern recognition receptor FLS2 in *Arabidopsis*. *Genes Dev.* *20*, 537–542.
- Rui, Y., and Dinneny, J.R. (2020). A wall with integrity: surveillance and maintenance of the plant cell wall under stress. *New Phytol.* *225*, 1428–1439.
- Schmid, N.B., Giehl, R.F.H., Döll, S., Mock, H.-P., Strehmel, N., Scheel, D., Kong, X., Hider, R.C., and Wirén, N. von (2014). Feruloyl-CoA 6'-Hydroxylase1-Dependent Coumarins Mediate Iron Acquisition from Alkaline Substrates in *Arabidopsis*. *Plant Physiol.* *164*, 160–172.
- Sevilem, I., Miyashima, S., and Helariutta, Y. (2013). Cell-to-cell communication via plasmodesmata in vascular plants. *Cell Adhes. Migr.* *7*, 27–32.
- Stringlis, I.A., de Jonge, R., and Pieterse, C.M.J. (2019). The Age of Coumarins in Plant–Microbe Interactions. *Plant Cell Physiol.* *60*, 1405–1419.
- Swarup, R., Perry, P., Hagenbeek, D., Straeten, D.V.D., Beemster, G.T.S., Sandberg, G., Bhalerao, R., Ljung, K., and Bennett, M.J. (2007). Ethylene Upregulates Auxin Biosynthesis in *Arabidopsis* Seedlings to Enhance Inhibition of Root Cell Elongation. *Plant Cell* *19*, 2186–2196.
- Teixeira, P.J.P., Colaianni, N.R., Fitzpatrick, C.R., and Dangl, J.L. (2019). Beyond pathogens: microbiota interactions with the plant immune system. *Curr. Opin. Microbiol.* *49*, 7–17.

- Vilches-Barro, A., and Maizel, A. (2015). Talking through walls: mechanisms of lateral root emergence in *Arabidopsis thaliana*. *Curr. Opin. Plant Biol.* 23, 31–38.
- Wang, Z.-Y. (2012). Brassinosteroids modulate plant immunity at multiple levels. *Proc. Natl. Acad. Sci.* 109, 7–8.
- Wyrsh, I. (2015). Immune signaling in *Arabidopsis thaliana* upon perception of bacterial and viral molecular patterns with a special emphasis on roots. Thesis. University_of_Basel.
- Zhou, F., Emonet, A., Dénervaud Tendon, V., Marhavy, P., Wu, D., Lahaye, T., and Geldner, N. (2020). Co-occurrence of Damage and Microbial Patterns Controls Localized Immune Responses in Roots. *Cell* 180, 440-453.e18.

ACKNOWLEDGEMENTS

I would first like to thank my PhD committee constituting of the president Prof. Antoine Guisan and the scientific experts Prof. Cyril Zipfel and Prof. Edward E. Farmer, for taking the time to read and evaluate my PhD thesis and for their valuable inputs and expertise.

My deepest gratitude goes to Prof. Niko Geldner for offering me the opportunity to do my PhD in his group and for believing in me. I thank him for his endless support, his enthusiasm and his trust throughout this project and for the invaluable scientific discussions we had during the last five years, his advice and expertise that made this work possible. I thank him for taking the time to share his passion and knowledge.

Many thanks go to our collaborators, Prof. Christoph Keel, Jordan Vacheron and Clara Heiman, for insightful discussions and providing us with their favourite pet bacteria. I also want to thank Prof. Schulze-Lefert for hosting me in his lab for two months and let me enter the fascinating world of the microbiome. A special thank to Ka-Wai Ma who taught me many new techniques. Thanks also for their critical comments and inputs.

This project would have not been successful with the help of many colleagues. I am grateful to Feng Zhou for our close collaboration on many projects and as my cell ablation guru, Yan Ma for being my buddy and expert in transcriptomics, Damien De Bellis for revealing the unseen by electron microscopy analysis, Artan Graf and Yasmine Genolet for their incredible patience and assiduity to determine the identity of more than 32'000 cells.

I also want to especially thank all past and present members of the Prof. Geldner's research team for their critical advice, creativity, support and scientific discussion, and for creating a pleasant and stimulating work atmosphere. In particular, I wish to thank Yuree Lee for supervising me at my very beginning as a Master student, Robertas Ursache and Satoshi Fujita for their innumerable cloning and technical advice, Feng Zhou, Tonni G. Andersen, Yan Ma and Inês C. R. Barbosa for their excellent suggestions and helpful discussion and Marie Barberon for her wise advice and constant support. Also, a big thank you to Inês Barbosa, Yan Ma and Kian Hématy for correcting parts of this thesis. I want to thank all members of the Prof. Geldner's group for their everyday help, the time we spent

together and the good memories we created. In addition to the ones cited above, this include Joop E. M. Vermeer, Sadaf Naseer, Enrique Neumann, Frédéric Brun, Deborah Mühlemann, Lothar Kalmbach, Valérie Dénervaud-Tendon, Catherine Schwab, Sarra Ammar, Giti Ghazi Soltani, Alexandre Pfister, Verónica Gonzáles Doblás, Nelson Rojas-Murcia, Peter Marhavy, , Andreas Kolbeck, Anaxi Houbaert, Isabelle Flückiger, Damien De Bellis. Also, many thanks to Marine, Shaoline, Kelly and Yasmine for their help with seed harvesting and experiments.

I also wish to thank all members of our Department of Plant Molecular Biology (DBMV) for scientific exchanges and technical assistance. I would like to specially acknowledge Elia Stahl and Steven Moussu, for comments and proof-reading of this thesis, Alice Berhin, Sebastian Augustin, Pauline Anne, Nasim Fahaarani Zayas and Raphaël Groux for their constructive comments and suggestions. I also thank Blaise Tissot for the management of our culture rooms, Laurence Cienciala and Debora Zoia for all the administrative work.

During these five years, I came across a number of people outside of the University of Lausanne who helped me and contributed to our projects. This include Ines Wyrsh, Prof. Thomas Boller and Prof. Jean-Pierre Métraux for providing starting material and participating in the design of the project, Prof. Corné Pieterse from Utrecht University for sharing bacterial strains and advice, Matthieu Platre in San Diego for our unexpected epistolary scientific discussions, Ruben Garrido-Otter, Rui Guan, Paloma Duran and Nathan Vannier from Prof. Paul Schulze-Lefert's department in Cologne for their help with microbiome analysis design, computational work and technical assistance.

Finally, I would like to thank the many friends these five years in Lausanne has brought me and who made this experience so unique: Inês Barbosa, Yan Ma, Octavia Roman, Alice Berhin, Marie Barberon, Tonni Andersen, Steven Moussu, Robertas Ursache, Colleen Drapek, Debora Zoia and Amandine Masson, and so many others.

Doing my PhD in my own country, I had the chance to have my family and my dearest friends close. I want to thank them for supporting me and for cheering me up these last years. Thanks to Elisa, Manon, Clara and Noémie for all these fun times together. Finally, I am so grateful to Arnaud, who has always been there for me all these years.